



# University of HUDDERSFIELD

## University of Huddersfield Repository

Wormald, Richard

Environmental Limits of Methanogenesis and Sulphate Reduction

### Original Citation

Wormald, Richard (2019) Environmental Limits of Methanogenesis and Sulphate Reduction. Doctoral thesis, University of Huddersfield.

This version is available at <http://eprints.hud.ac.uk/id/eprint/35063/>

The University Repository is a digital collection of the research output of the University, available on Open Access. Copyright and Moral Rights for the items on this site are retained by the individual author and/or other copyright owners. Users may access full items free of charge; copies of full text items generally can be reproduced, displayed or performed and given to third parties in any format or medium for personal research or study, educational or not-for-profit purposes without prior permission or charge, provided:

- The authors, title and full bibliographic details is credited in any copy;
- A hyperlink and/or URL is included for the original metadata page; and
- The content is not changed in any way.

For more information, including our policy and submission procedure, please contact the Repository Team at: [E.mailbox@hud.ac.uk](mailto:E.mailbox@hud.ac.uk).

<http://eprints.hud.ac.uk/>

# **Environmental Limits of Methanogenesis and Sulphate Reduction**

Richard Matthew Wormald, BSc (Hons)

*University of*  
**HUDDERSFIELD**

*A thesis submitted to the University of Huddersfield in the partial  
fulfilment of the requirements for the degree of Doctor of Philosophy*

**Department of Biological and Geographical Sciences**

**March 2019**

*This work was funded by Radioactive Waste Management limited.*



## Copyright Statement

- i. The author of this thesis (including any appendices and/ or schedules to this thesis) owns any copyright in it (the “Copyright”) and s/he has given The University of Huddersfield the right to use such Copyright for any administrative, promotional, educational and/or teaching purposes.
- ii. Copies of this thesis, either in full or in extracts, may be made only in accordance with the regulations of the University Library. Details of these regulations may be obtained from the Librarian. Details of these regulations may be obtained from the Librarian. This page must form part of any such copies made.
- iii. The ownership of any patents, designs, trademarks and any and all other intellectual property rights except for the Copyright (the “Intellectual Property Rights”) and any reproductions of copyright works, for example graphs and tables (“Reproductions”), which may be described in this thesis, may not be owned by the author and may be owned by third parties. Such Intellectual Property Rights and Reproductions cannot and must not be made available for use without permission of the owner(s) of the relevant Intellectual Property Rights and/or Reproductions.

## **Acknowledgements**

I would like to express my profound gratitude to my supervisor Prof. Paul Humphreys, who has offered me endless support, guidance and time not only during my PhD but also throughout my undergraduate studies. I will always be grateful for the many opportunities Paul has given me. I would like to sincerely thank Dr. Simon Rout, Dr. Christopher Charles and Dr. Emma Ransom-Jones for their limitless help and time spent interpreting data, offering feedback and keeping lab work entertaining. Many thanks to my placement student Harry Mitchell who was a great asset in the lab and to my colleague Kim Patel for a memorable trip to Denmark and for lending an ear when I needed to have a moan. I would also like to thank Dr. Gage Ashton for helping me analyse the thermal properties of sediment samples and Dr. Jeremy Hopwood for his assistance with the geochemical modelling. I would finally like to thank my family and friends, who have supported me throughout the good and bad times and were always there when I needed them.

# Abstract

The current proposed strategy for the disposal of intermediate-level radioactive waste (ILW) within the United Kingdom is through emplacement within a deep underground facility, termed a geological disposal facility (GDF). Anaerobic and highly alkaline ( $10.0 < \text{pH} < 13$ ) conditions are expected to prevail within the near-field of a GDF, which will result in the chemical degradation of cellulose-bearing ILW. Isosaccharinic acids (ISA) and volatile fatty acids (VFA) are the major products of alkaline cellulose hydrolysis and their generation within an ILW-GDF will result in a range of organic carbon sources being present. The potential for these carbon sources to provide the substrates for methanogenesis and sulphate reduction under near-field conditions holds importance within a GDF. The generation of biogases such as  $^{14}\text{CH}_4$  from  $^{14}\text{C}$ -bearing waste could facilitate the transfer of radionuclides to the biosphere. The production of corrosive sulphide by colonising microorganisms could impact the integrity of engineered barriers used to prevent the transfer of radioelements to the biosphere.

The potential for methanogens and sulphate-reducing bacteria (SRB) to be active under ILW-GDF conditions is poorly understood. The work outlined in this thesis utilised anaerobic sediments from anthropogenic analogue sites to demonstrate the activity of methanogens and SRB under near-field conditions. The alkaline leachates generated in these sites result in high pore-water pH values equivalent with those expected to dominate an ILW-GDF (pH 11.0-13.0). In spite of these conditions, the incubation of cellulose *in situ* allowed a range of active microbial processes to be identified, including cellulose degradation by *Fibrobacter* species, sulphate-reduction by *Desulfobacter* and hydrogenotrophic methanogenesis by members of the order *Methanomicrobiales*. The formation of hydrophobic extracellular polymeric substances (EPS) and production of metabolic acids *in situ* facilitated microbial survival within these extreme environments.

Microcosms operating under methanogenic conditions at pH 10.0-11.0 developed from these alkaline sediments demonstrated high hydrogen consumption rates and were dominated by alkaliphilic *Methanobacterium* and *Methanoculleus* genera. Acetate was unable to be utilised as substrate by the associated methanogen communities under these conditions, however high acetate consumption rates were observed in pH 7.0-8.0 microcosms where the acetoclastic lineages *Methanosarcina* became more important. Sub-cultures of the alkaline methanogenic microcosms demonstrated the ability to utilise precipitated calcium carbonates as the sole carbon source for hydrogenotrophic metabolism at pH 10.0. Alkaliphilic *Desulfonatronum* biofilms grown on stainless steel surfaces developed from the alkaline sediment communities were capable of dissimilatory sulphate reduction at pH 11.0 using the products of alkaline cellulose degradation as the sole carbon and energy source. The sulphide produced by these biofilms induced the corrosion of stainless steel at pH 11.0 within 3 months.

The results outlined here suggest the colonisation of an ILW-GDF by methanogens will result in a population dependent on the hydrogenotrophic pathway, with acetate-derived methanogenesis being inhibited under these conditions. Furthermore, biofilms formed within the near-field facilitate the corrosion of steel materials by alkaliphilic SRB and enable microbial survival through the production of low pH niches. These findings can inform future safety assessments and gas generation modelling studies used to predict ILW-GDF performance.

# Contents

1.0	Introduction.....	19
1.1	Overview.....	20
1.2	Radioactive waste disposal.....	20
1.2.1	Low level waste.....	20
1.2.2	Intermediate level waste.....	21
1.2.3	High level waste.....	21
1.2.4	Near-field conditions.....	21
1.2.5	Alkaline cellulose degradation under near-field conditions.....	24
1.3	Microbial processes relevant to the disposal of ILW.....	25
1.3.1	Fermentation.....	25
1.3.2	Methanogenesis.....	27
1.3.3	Sulphate reduction.....	35
1.4	Microbial survival under ILW-GDF conditions.....	38
1.4.1	Natural alkaline sites.....	40
1.4.2	Anthropogenic alkaline sites.....	41
1.4.3	Biofilms.....	42
1.5	Summary of chapter.....	44
2.0	Methods for the analysis of environmental microbiology.....	45
2.1	Overview.....	46
2.2	Culturing techniques.....	46
2.3	Nucleic acid techniques.....	47
2.3.1	Amplicon sequencing.....	48
2.3.2	Next generation techniques.....	49
2.3.3	Microbial 16S community analysis.....	50
2.4	Microscopic techniques.....	51
2.5	Summary of chapter.....	52
3.0	Aims and objectives.....	53
3.1	Background.....	54
3.2	Primary research goals.....	55
3.3	Research impacts.....	55
4.0	Experimental Methodologies.....	56
4.1	General Reagents.....	57

4.2 Culture Media .....	57
4.2.1 Mineral Media.....	57
4.2.2 Synthesis of cellulose degradation products (CDP).....	59
4.3 Liquid sample preparation .....	59
4.4 Analytical Methodologies .....	59
4.4.1 High performance anion exchange chromatography with pulsed.....	59
amperometric detection (HPAEC-PAD).....	59
4.4.2 Gas chromatography .....	60
4.4.3 Determination of dissolved organic and inorganic carbon .....	61
4.4.4 Ion chromatography .....	61
4.5 Environmental sample analysis.....	61
4.5.1 Extraction of volatile fatty acids .....	61
4.5.2 Metal analysis of pore waters via inductively coupled plasma mass spectrometry.....	62
4.5.3 Thermal gravimetric analysis.....	62
4.5.4 Simultaneous thermogravimetry mass spectrometry (TG-MS).....	62
4.5.5 pH determination .....	63
4.6 Dissolved sulphide determination.....	63
4.7 X-ray diffraction .....	63
4.8 Surface area analysis.....	63
4.9 PHREEQC analysis .....	64
4.10 Microscopy techniques .....	65
4.10.1 Sample preparation .....	65
4.10.2 Scanning electron microscopy and elemental analysis.....	65
4.10.3 Confocal laser scanning microscopy .....	65
4.10.4 Atomic force microscopy.....	66
4.10.5 Alicona microscopy .....	67
4.10.6 Light microscopy .....	67
4.11 Molecular Biology .....	67
4.11.1 Extraction and purification of nucleic acids .....	67
4.11.2 Polymerase chain reaction (PCR) .....	70
4.11.3 cDNA synthesis .....	71
4.11.4 Microbial community analysis via Illumina MiSeq platform.....	72
4.11.5 Microbial community BioProject accession numbers .....	72
4.12 Site investigations .....	74
4.12.1 Cotton preparation .....	74

4.12.2	Sampling site investigations .....	75
4.13	Microcosm investigations .....	81
4.13.1	Batch fed microcosms .....	81
4.13.2	Batch microcosms .....	82
4.13.3	CDC biofilm reactors .....	84
4.13.4	Calculation of rates .....	84
4.13.5	Preparation of NRVB .....	91
4.14	Micro profiling .....	91
4.14.1	pH profiling .....	91
4.14.2	Redox profiles .....	92
4.14.3	Hydrogen profiles .....	92
4.15	Statistical analysis and data processing .....	92
5.0	Investigation of Anthropogenic Alkaline Sites .....	94
5.1	Rationale .....	95
5.2	Site Geochemistry .....	96
5.2.1	Chemical Analysis .....	96
5.2.2	Metal Analysis .....	101
5.2.3	Thermogravimetric Analysis .....	104
5.2.4	Thermogravimetric Analysis coupled with Mass Spectrometry .....	107
5.3	Microbial Community Analysis .....	109
5.3.1	DNA Sequencing .....	109
5.3.2	cDNA Sequencing .....	124
5.4	Microscopy .....	132
5.4.1	Scanning Electron Microscopy .....	132
5.4.3	Confocal Laser Scanning Microscopy .....	135
5.5	Conclusions .....	137
6.0	Investigating the Utilisation of Methanogenic Pathways at High pH .....	139
6.1	Rationale .....	140
6.2	CDP-fed Microcosms .....	141
6.2.1	Control Site Microcosms .....	141
6.2.2	Lime Site Microcosms .....	149
6.3	H <sub>2</sub> /CO <sub>2</sub> and Acetate-fed Microcosms .....	157
6.3.1	Control Site Microcosms .....	157
6.3.2	Lime Site Microcosms .....	163
6.4	Inhibition Studies .....	170

6.4.1 Control Site Microcosms .....	170
6.4.2 Lime Site Microcosms .....	173
6.5 Old Lime and Steel Enrichments at pH 7.0 and 10.0.....	175
6.5.1 Old Lime Microcosms at pH 10.0.....	175
6.5.2 Old Lime Microcosms at pH 7.0.....	179
6.5.3 Steel Microcosms at pH 7.0 and 10.0 .....	183
6.6 Conclusions.....	188
7.0 Calcium Carbonate as a Potential Substrate for Hydrogenotrophic Methanogenesis at High pH.....	190
7.1 Rationale .....	191
7.2 Reactor Chemistry .....	192
7.2.1 Headspace Gas Analysis .....	192
7.2.2 Dissolved Inorganic Carbon Analysis .....	194
7.2.3 Surface Area Testing.....	196
7.2.4 Volatile Fatty Acid Analysis.....	198
7.2.5 pH.....	199
7.2.5 PHREEQC Modelling.....	200
7.3 Archaeal Community Analysis .....	201
7.4 Carbonation Analysis.....	205
7.4.1 Phenolphthalein Staining .....	205
7.4.2 SEM .....	206
7.4.3 XRD .....	209
7.5 Imaging .....	211
7.5.1 5-Colour CLSM .....	211
7.5.2 FISH.....	214
7.6 Conclusions.....	215
8.0 Development of Sulphate-reducing and Methanogenic Biofilms on Steel Surfaces under Alkaline Conditions .....	217
8.1 Rationale .....	218
8.2 Results and Discussion .....	218
8.2.1 CDC Biofilm Reactor Bulk Chemistry .....	218
8.2.2 Biofilm Micro-profiling.....	222
8.2.3 Biofilm Characterisation.....	229
8.2.4 Microbial Community Analysis.....	239
8.2.5 Steel Surface Characterisation .....	250

8.3 Conclusions.....	261
9.0 Concluding Remarks.....	262
References.....	278
Supplementary Information .....	303

Word count excluding appendices and references – 45,199

## List of Figures

Figure 1.1. Illustration of a geological disposal facility.....	18
Figure 1.2. Multiple barriers used for ILW disposal.....	18
Figure 1.3. The evolving pH values within the near-field of an ILW-GDF.....	19
Figure 1.4. The fermentation of sugars by difference bacteria results in varied fermentation end-products.....	21
Figure 1.5. Proposed models of hydrogenotrophic and acetoclastic pathways in methanogenesis.....	27
Figure 1.6. The pathways for anaerobic degradation of organic matter to methane.....	29
Figure 1.7. Internal and external pH values in neutralophilic and alkaliphilic bacteria.....	34
Figure 4.1. Map and grid references for the various sampling sites employed throughout the period of study.....	70
Figure 4.2. Photographs of the New Lime sites.....	71
Figure 4.3. Photographs of the Old Lime sites.....	72
Figure 4.4. Photographs of the Steel sites.....	73
Figure 4.5. Photographs of the Control site.....	74
Figure 4.6. Batch-fed microcosm diagram.....	80
Figure 4.7. Batch microcosms for pH adaption study.....	81
Figure 4.8. Work flow for pH adapt study using neutral-pH sediments from the control site.....	82
Figure 4.9. Work flow for pH adapt study using alkaline sediments from sites B, H and T.....	83
Figure 4.10. Batch microcosms for calcium carbonate investigations.....	84
Figure 4.11. CDC biofilm reactor diagram.....	85
Figure 4.12. Micro-profiling of steel coupons diagram.....	88
Figure 5.1. Comparison of dissolved organic and inorganic carbon within the sediments from various anthropogenic alkaline sites.....	94
Figure 5.2. The dissolved organic and inorganic carbon content of the sediments plotted against the age of the New Lime, Old Lime and Steel sites.....	95
Figure 5.3. Metal analysis of the pore-waters from various anthropogenic sites.....	97
Figure 5.4. Sodium and magnesium concentrations in the pore-waters of various anthropogenic sites.....	98
Figure 5.5. Thermal analysis of sediment samples acquired from the Steel site SC.....	100

Figure 5.6. Thermal gravimetric analysis coupled to mass spectrometry of soil samples from anthropogenic alkaline sites.....	102
Figure 5.7. Phylum-level composition of background sediments and alkaline sediments...	105
Figure 5.8. Principal components analysis of background sediments and alkaline sediments at the phylum level.....	106
Figure 5.9. Heat maps comparing background and alkaline sediment communities at the phylum level from the Control, New Lime, Old Lime and Steel sites.....	107
Figure 5.10. Genus-level composition of methanogens within the alkaline sediments from various anthropogenic alkaline sites, alongside the neutral-pH control site.....	111
Figure 5.11. Proportion of methanogenic pathways in the alkaline sediments from various anthropogenic alkaline sites and correlation between levels of dissolved organic/inorganic carbon and proportion of acetoclastic/hydrogenotrophic methanogens.....	112
Figure 5.12. Genus-level composition of sulphate reducing bacteria in the background and alkaline sediments. Also shown in principal components analysis showing the differences between background and alkaline SRB communities at the genus level.....	115
Figure 5.13. Phylum-level composition of alkaline sediments and cotton samples from various anthropogenic alongside principal components analysis of the sediments vs the cotton samples.....	118
Figure 5.14. Genus-level methanogen community composition of alkaline sediments and cotton samples. Also showing PCA comparing genus-level methanogen communities within cotton samples and alkaline sediments.....	120
Figure 5.15. Proportion of acetoclastic, hydrogenotrophic, methylotrophic and metabolically diverse methanogens within the alkaline sediments and cotton samples.....	121
Figure 5.16. Genus-level composition of sulphate reducing bacteria within the alkaline sediments and cotton samples, alongside principal components analysis comparing the SRB sediment and cotton communities.....	123
Figure 5.17. Scanning electron micrographs of cotton samples retrieved from various anthropogenic alkaline sites after 3 months incubation.....	125
Figure 5.18. SEM-EDS of cotton samples showing elemental composition of the biofilm materials.....	126
Figure 5.19. CLSM investigation of cellulose cotton samples.....	128
Figure 6.1. ISA concentrations within microcosms employing neutral-pH Canal sediments.....	134
Figure 6.2. Rate of $\alpha$ , $\beta$ and X-ISA degradation within CDP-fed microcosms employing neutral-pH Canal sediments between pH 7.0-10.0.....	135
Figure 6.3. Acetate concentrations and removal rates within CDP-fed microcosms employing neutral-pH Canal sediments.....	137

Figure 6.4. Methane quantities and production rates within CDP-fed microcosms employing neutral-pH sediments.....	138
Figure 6.5. Genus-level methanogen community and proportion of acetoclastic/hydrogenotrophic methanogens within CDP-fed microcosms employing neutral-pH sediments.....	140
Figure 6.6. Acetate removal rates and proportion of reads attributed to the genus <i>Methanosarcina</i> within pH 7.0-10.0 CDP-fed microcosms employing the neutral-pH sediments.....	141
Figure 6.7. ISA degradation within microcosms employing alkaline sediments from lime sites B, H and T.....	143
Figure 6.8. Comparison of ISA degradation rates between microcosms employing neutral-pH sediments (control) and alkaline sediments (lime).....	144
Figure 6.9. Acetate concentrations between pH 7.0-11.0 within CDP-fed microcosms employing the alkaline lime sediments.....	145
Figure 6.10. Methane quantities within CDP-fed microcosms employing alkaline sediments from the lime sites between pH 7.0-11.0.....	146
Figure 6.11. Genus level methanogen community composition and proportion of hydrogenotrophic/acetoclastic methanogens within CDP-fed microcosms employing alkaline sediments from the lime sites.....	148
Figure 6.12. Hydrogen, acetate and methane quantities within microcosms employing control site sediments between pH 7.0-10.0.....	152
Figure 6.13. Acetate and hydrogen consumption rates within microcosms employing neutral-pH sediments between pH 7.0-10.0.....	153
Figure 6.14. Genus-level methanogen composition and proportion of acetoclastic and hydrogenotrophic genera within H <sub>2</sub> /CO <sub>2</sub> -fed and acetate-fed microcosms between pH 7.0-10.0.....	154
Figure 6.15. Hydrogen, acetate and methane quantities within microcosms employing lime site sediments between pH 7.0-11.0.....	157
Figure 6.16. Acetate and hydrogen consumption rates within microcosms employing alkaline lime sediments between pH 7.0-11.0.....	158
Figure 6.17. Measured and theoretical methane generation quantites within pH 7.0 and 8.0 acetate-fed microcosms employing the alkaline sediments from the lime sites.....	158
Figure 6.18. Genus-level methanogen composition and proportion of acetoclastic/hydrogenotrophic species within H <sub>2</sub> /CO <sub>2</sub> -fed and acetate-fed microcosms between pH 7.0-11.0.....	161
Figure 6.19. Methane, acetate and hydrogen quantites within pH 7.0 and 10.0 microcosms employing the control sediments in the presence (+CH <sub>3</sub> F) and absence (-CH <sub>3</sub> F) of methyl fluoride.....	164

Figure 6.20. Percentage of methane derived from acetate and H <sub>2</sub> /CO <sub>2</sub> at pH 7.0 and 10.0 within microcosms employing control site sediments.....	165
Figure 6.21. Methane, acetate and hydrogen quantities within pH 7.0 and 10.0 microcosms employing the alkaline sediments in the presence (+CH <sub>3</sub> F) and absence (-CH <sub>3</sub> F) of methyl fluoride.....	166
Figure 6.22. Microcosm chemistry in acetate-fed and H <sub>2</sub> /CO <sub>2</sub> -fed Old Lime microcosms at pH 10.0.....	169
Figure 6.23. Genus-level methanogen composition of H <sub>2</sub> /CO <sub>2</sub> -fed microcosms operating at pH 10.0 employing the Old Lime sediments.....	170
Figure 4.24. Microcosm chemistry within acetate-fed and H <sub>2</sub> /CO <sub>2</sub> -fed microcosms operating at pH 7.0 employing the Old Lime sediments.....	173
Figure 6.25. Genus-level composition of acetate-fed and H <sub>2</sub> /CO <sub>2</sub> -fed microcosms employing the Old Lime sediments at pH 7.0.....	174
Figure 6.26. Acetate and hydrogen consumption rates within microcosms employing the Old Lime sediments at pH 7.0 and 10.0.....	175
Figure 6.27. Chemistry within acetate-fed and H <sub>2</sub> /CO <sub>2</sub> -fed microcosms employing the Steel sediments at pH 7.0 and 10.0.....	176
Figure 6.28. Measured and theoretical methane production within pH 7.0 acetate-fed microcosms employing the Steel sediments.....	177
Figure 6.29. Genus-level composition of methanogen enrichment cultures at pH 7.0 and 10.0.....	178
Figure 6.30. Average percentage of 16S rRNA gene reads attributed to the acetoclastic genus <i>Methanosarcina</i> within pH 7.0 and 10.0 methanogenic microcosms employing the Steel sediments.....	179
Figure 7.1. Headspace gas analysis of calcite-supplemented microcosms.....	185
Figure 7.2. Hydrogen consumption and methane generation rates of microcosms containing calcium carbonates.....	186
Figure 7.3. Dissolved inorganic carbon concentrations within pH 10.0 microcosms supplemented with calcium carbonates.....	188
Figure 7.4. Volatile fatty acid analysis of calcite microcosms.....	191
Figure 7.5. Bulk pH of calcite-supplemented microcosms.....	192
Figure 7.5. PHREEQC modelling of dissolved inorganic carbon at various pH values.....	193
Figure 7.6. Archaeal community analysis of calcite microcosms.....	196
Figure 7.7. PCA of archaeal communities from calcite-amended microcosms.....	197
Figure 7.8. Carbonation analysis of NRVB via phenolphthalein staining.....	198
Figure 7.9. SEM investigation of NRVB.....	199

Figure 7.10. EDS investigation of inner and outer NRVB surfaces.....	200
Figure 7.11. SEM investigation of biotic NRVB after incubation under methanogenic conditions.....	201
Figure 7.12. XRD patterns of CaCO <sub>3</sub> powder, marble chips and NRVB.....	202
Figure 7.13. CLSM investigation of biofilm materials taken from NRVB reactors.....	204
Figure 7.14. CLSM investigation of biotic NRVB.....	205
Figure 7.15. FISH investigation of biotic materials attached to NRVB.....	206
Figure 8.1. Bulk liquid pH of CDC biofilm reactors.....	212
Figure 8.2. CDC biofilm reactor bulk chemistry under sulphate-reducing and methanogenic conditions at pH 11.0.....	213
Figure 8.3. pH profiles of sulphate-reducing biofilm at pH 11.0.....	215
Figure 8.4. H <sub>2</sub> profiles of sulphate-reducing and methanogenic biofilm at pH 11.0.....	218
Figure 8.5. Redox profiles of sulphate-reducing and methanogenic biofilm at pH 11.0.....	220
Figure 8.6. SEM investigation of sulphate-reducing biofilm.....	222
Figure 8.7. SEM investigation of methanogenic biofilm.....	223
Figure 8.8. 5-colour CLSM investigation of sulphate-reducing biofilm.....	225
Figure 8.9. 5-colour CLSM investigation of methanogenic biofilm.....	226
Figure 8.10. 5-colour CLSM investigation of sulphate-reducing and methanogenic biofilms.....	227
Figure 8.11. 5-colour CLSM investigation of sulphate-reducing biofilm.....	228
Figure 8.12. 5-colour CLSM investigation of methanogenic biofilm.....	229
Figure 8.13. 5-colour CLSM investigation of sulphate-reducing biofilm.....	230
Figure 8.14 Phylum-level community analysis of methanogenic and sulphate-reducing biofilms and bulk liquid at pH 11.0.....	234
Figure 8.15. Genus-level community analysis of methanogenic and sulphate-reducing biofilms and bulk liquid at pH 11.0.....	235
Figure 8.16. Rarefaction and rank abundance curves of biofilms and bulk communities under sulphate-reducing and methanogenic conditions.....	236
Figure 8.17. Principle components analysis and heat-map of steel disk biofilm and bulk liquid communities.....	238
Figure 8.16. FISH investigation of sulphate-reducing biofilms.....	240
Figure 8.17. FISH investigation of sulphate-reducing biofilms.....	241
Figure 8.18. Steel surface characterisation.....	243

Figure 8.19. Steel surface characterisation.....	245
Figure 8.20. Steel surface characterisation of grade 304 biotic steel surfaces via Alicona...	247
Figure 8.21. Steel surface characterisation of grade 316 biotic steel surfaces via Alicona...	248
Figure 8.22. Steel surface characterisation of grade 304 abiotic positive controls via Alicona.....	249
Figure 8.23. Steel surface characterisation of grade 316 abiotic positive controls via Alicona.....	250
Figure 8.24. Steel surface characterisation of grade 304 abiotic negative controls via Alicona.....	251
Figure 8.25. Steel surface characterisation of grade 316 abiotic negative controls via Alicona.....	252
Figure 9.1. The disposal of cellulose within the near-field of an ILW-GDF will result in the generation of ISA and VFA's through alkaline hydrolysis pathways. The fermentation of these cellulose degradation products provides the substrates for downstream methanogenic and sulphate-reducing processes. Sulphate-rich inflowing ground-water could saturate the facility post-closure, leading to the development of sulphate-reducing and methanogenic conditions within the near-field.....	256
Figure 9.2. Evolution of pH within the near-field of an ILW-GDF.....	259
Figure 9.3. Hydrogen and acetate consumption rates under far-field and near-field conditions when employing canal sediments or alkali-adapted lime sediments.....	263
Figure 9.4. CO <sub>2</sub> availability under far-field and near-field conditions within a closed system as determined through geochemical modelling using PHREEQC.....	266
Figure 9.5. Characterisation of abiotic control stainless steel surfaces, together with biotic surfaces before and after removal of biofilm materials.....	269

## List of Tables

Table 4.1 Mineral media composition per litre.....	52
Table 4.2 Carbonate/bicarbonate buffer composition per litre.....	52
Table 4.3 Trace element solution composition per litre.....	52
Table 4.4. PHREEQC modelling input data (x = 7, 8, 9, 10, 11 and 12).....	58
Table 4.5. Properties of the stains used for visualisation of biofilm materials.....	60
Table 4.6. Details of oligonucleotide FISH probes.....	60
Table 4.7. Primers used for the amplification of the 16S rRNA gene and microbial community analysis.....	65
Table 4.8. Microbial community BioProject accession numbers.....	66
Table 4.9. Composition of NRVB.....	86
Table 5.1 Chemical analysis of sediment samples.....	93
Table 5.2. Composition of sediment samples from various anthropogenic alkaline sites obtained through TGA.....	99
Table 6.1 Alpha, beta and xylo-ISA degradation rates within microcosms employing neutral-pH Canal sediments between pH 7.0-10.0.....	135
Table 7.1. Surface area testing.....	189
Table 7.2. Dissolved inorganic carbon species at various pH values based on PHREEQC geochemical modelling.....	193
Table 8.1. ISA degradation rate constants.....	212
Table 8.2. Alpha diversity statistics of biofilms and bulk communities under sulphate-reducing and methanogenic conditions.....	237

## List of Abbreviations

- ACE – Abundance coverage based estimator
- ATP – Adenosine triphosphate
- BLAST – Basic local alignment search tool
- cDNA – Complementary deoxyribose nucleic acid
- CDP - Cellulose degradation products
- ConA - Concanavalin A, tetramethylrhodamine conjugate
- CLSM – Confocal scanning electron microscopy
- CTAB - Cetyl-trimethylammonium bromide
- DIC – Dissolved inorganic carbon
- DNA – Deoxyribose nucleic acid
- DNase – Deoxyribonuclease
- dNTPs - Nucleoside triphosphates
- EDS - Electron dispersive X-ray spectroscopy
- EDTA - Ethylenediaminetetraacetic acid
- EPS - Exopolymeric substances
- FISH - Fluorescence *in situ* hybridisation
- FITc - Fluorescein isothiocyanate
- gDNA – Genomic deoxyribose nucleic acid
- GDF – Geological disposal facility
- GC – Gas chromatography
- HLW – High level waste
- HPAEC-PAD - High performance anion exchange chromatography with pulsed amperometric detection
- IC – Ion chromatography
- ILW – Intermediate level waste
- ILW-GDF - Intermediate level waste geological disposal facility
- ISA - Isosaccharinic acid
- LLW – Low level waste
- MIC – Microbially induced corrosion

MPN – Most probable number  
NDA – Nuclear Decommissioning Authority  
NCBI – National Centre for Biotechnology Information  
NRVB – Nirex reference vault backfill  
OTU – Operational taxonomic unit  
PBS - Phosphate buffered saline  
PCA – Principal components analysis  
PCR – Polymerase chain reaction  
RDP – Ribosomal database project  
RNA – Ribose nucleic acid  
RNase – Ribonuclease  
rRNA – Ribosomal RNA  
SAO – Syntrophic acetate oxidation  
SAOB – Syntrophic acetate oxidising bacteria  
SDS-PAGE - Sodium dodecyl sulfate polyacrylamide gel electrophoresis  
SEM - Scanning electron microscopy  
SRB – Sulphate reducing bacteria  
TAEB - Tris-acetate EDTA buffer  
TC - Total carbon  
TEA – Terminal electron acceptor  
TGA - Thermal gravimetric analysis  
TG-MS - Simultaneous thermogravimetry mass spectrometry  
TIC – Total inorganic carbon  
TOC – Total organic carbon  
Tris-HCl - Trizma® hydrochloride  
UK – United Kingdom  
VFA – Volatile fatty acid  
XISA – Xylo isosaccharinic acid

# 1.0 Introduction

## **1.1 Overview**

One current option for the disposal of higher activity radioactive waste within the United Kingdom (UK) is via geological disposal within a deep underground facility, termed a geological disposal facility (GDF). This disposal concept employs a multiple barrier system in order to retain the radioelements within the facilities near-field and prevent their release to the biosphere. Both intermediate and high level wastes are destined for storage within a GDF, however only the intermediate-level fraction contains a range of cellulosic materials. Within a GDF backfilled with cement, a high pH, anoxic and chemically reducing environment is predicted to form within the near-field. Under these conditions any cellulose materials present will chemically degrade to a range of cellulose degradation products (CDP), the predominant components of which include isosaccharinic acids (ISA) and volatile fatty acids (VFA). Both of these components have the potential to provide a carbon source for microbial metabolism through processes such as fermentation and anaerobic respiration linked to terminal electron acceptors (TEA). Since the microbial colonisation of a GDF is possible, microbial activity could impact the long-term performance of such a facility via the production of biogas and corrosive species such as sulphide. This chapter will discuss the various aspects of a GDF with respect to the disposal of radioactive wastes, the important microbial processes likely to occur within such a facility will be explored and the potential for microbial survival under the extreme conditions of an ILW-GDF will be deliberated.

## **1.2 Radioactive waste disposal**

Radioactive materials are used for a range of purposes in the UK, including power generation, the treatment of medical illnesses and for use in military research. Waste is generated as a by-product of these processes and can be categorised based on its level of thermal and radioactive output. 4.7 million cubic meters of the UK's radioactive waste inventory in 2016 was composed of low level waste (90.5 %), intermediate level waste (9.4 %) and high level waste (0.03 %) (1), which are briefly discussed below.

### **1.2.1 Low level waste**

Low level waste (LLW) is generally composed of plastic, paper, cardboard, soil, rubble and metal (2), whose radioactive content does not exceed 4 GBq (gigabecquerels) per tonne of alpha activity and 12 GBq per tonne of beta or gamma activity (2). Currently LLW is disposed

of via incineration, recycling or it is disposed of within concrete-lined vaults within steel containers. Since the radioactive emissions generated by LLW fall below the limits for emplacement within a GDF, the disposal strategy for this type of waste does not rely on saturated alkaline conditions (1), instead the cellulose portion of LLW undergoes microbial degradation as opposed to alkaline chemical hydrolysis (3).

### **1.2.2 Intermediate level waste**

The radioactive emissions generated by intermediate level waste (ILW) exceed the upper boundaries for LLW classification and it is therefore destined for storage within a GDF. As of 2016, 449,000 m<sup>3</sup> of the UK's radioactive waste inventory was designated ILW (1), which contains a significant proportion of cellulosic materials such as wood, paper and cloth. ILW also contains a range of other organic and inorganic materials generated from the operation and decommissioning of facilities, including various forms of steel reactor components, graphite moderator blocks and concrete from the dismantling of power stations, along with sludges arising from liquid treatment effluents (4, 5).

### **1.2.3 High level waste**

Any of the UK's radioactive waste inventory that requires cooling due to its radioactivity is classified as high level waste (HLW). HLW is initially produced as a nitric acid solution that is subsequently vitrified into a solid glass and due to its high radioactivity levels requires long time frames for these levels to reduce through natural decay processes (6). HLW contains no cellulosic materials and will be stored separately from the ILW and LLW fractions (6).

### **1.2.4 Near-field conditions**

According to current UK government policies, higher activity wastes (ILW and HLW) are to be disposed of indefinitely within a GDF. This facility can be up to 1000 m below ground (Figure 1.1), although the current siting of such a facility is yet to be decided (7). A GDF will comprise both surface and underground facilities, where the surface facility will receive the waste and transport it to the underground facility where it will be isolated from the biosphere indefinitely using a multiple barrier system (Figure 1.2) (6). The waste will initially be compacted into 500 L stainless steel containers within a cement grout matrix which will form the first physical barrier between the waste and biosphere. The steel waste containers will contain vents to allow for the release of gases which are likely to be produced through corrosion

processes and minimise the potential for pressurisation events (6). The second barrier that contributes to the containment of radioelements is through chemical conditioning with the use of an appropriate backfilling material (Figure 1.2). Nirex reference vault backfill (NRVB) is one potential material used to backfill the waste containers within the facility and is primarily considered within this thesis, although clay-based backfilling materials could be employed (6). NRVB is a cement-based grout composed of Ordinary Portland Cement, lime and limestone flour. The high pH values produced by the backfilling material enhances sorption of the radioelements to the backfill surface and therefore supports radioelement retention (8). Inundating groundwater is expected to saturate the facility post-closure which will result in a highly alkaline environment via the formation of soluble metal hydroxides (6). During the early post-closure period, the bulk pH values of the near-field are predicted to be as high as pH 13.5 due to the dissolution of metal hydroxides (6) (Figure 1.3). During the evolution of the facility, interactions between the backfilling material and inflowing groundwater are expected to maintain a bulk pH of 12.5 through the generation of hydroxyl ions ( $\text{OH}^-$ ) and the dissolution of Portlandite (6) (Figure 1.3). During the late post-closure period, the bulk pH is expected to reduce to values between pH 10.0-12.5 due to the dissolution of cement hydration products, such as calcium silicate hydrate (Figure 1.3) (9). Anaerobic conditions are expected to develop through the removal of oxygen due to the corrosion of steel materials present, such as the steel waste canisters (6, 10).

The third and final barrier is that of the host rock, which provides geological containment of the waste (Figure 1.3). Gases and heat are expected to be generated during the disposal process, therefore the host rock is required to be capable of heat conduction to prevent significant rises in temperature, but also requires gas dispersal properties that prevent the facility from mechanical failure due to pressurisation (5). The host rock is also required to have a number of geochemical and mechanical properties that help to retain the waste, including properties that slow the movement of radionuclides in groundwater via sorption onto mineral surfaces (11). The use of high strength rock (such as metamorphic rock or crystalline igneous rock) is necessary so that its properties show little fluctuation over the long time scales expected of an operational GDF (6).

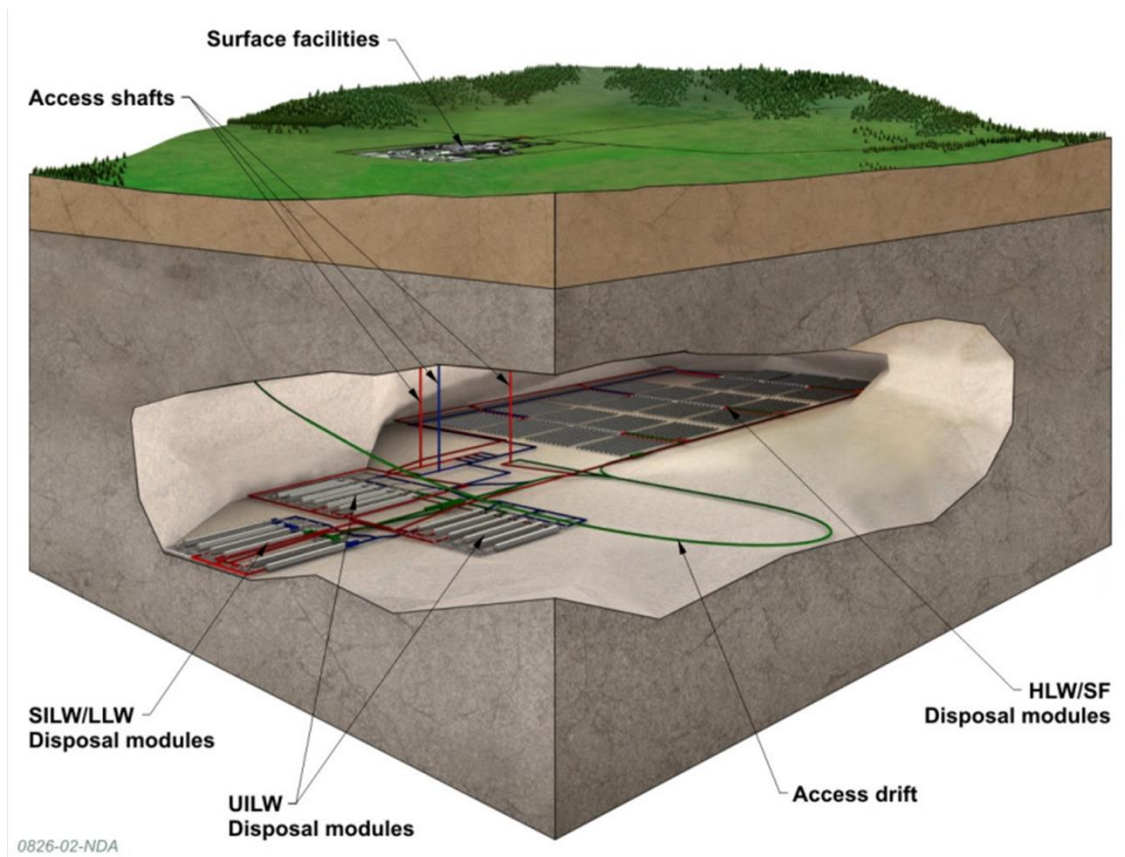


**Figure 1.1. Illustration of a geological disposal facility.** A geological disposal facility represents one potential option for the disposal of higher activity radioactive waste within the UK, whereby the wastes will be stored indefinitely within a deep underground facility as illustrated above. Taken from (7).

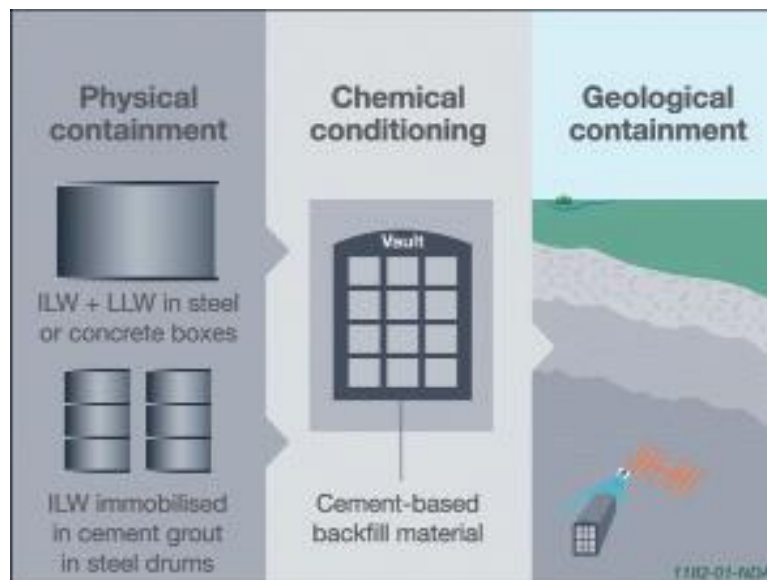


**Figure 1.2 Multiple barriers used for ILW disposal.** Radioelements will be contained within a geological disposal facility using physical, chemical and geological barriers in order to prevent their release to the biosphere. Taken from (7)

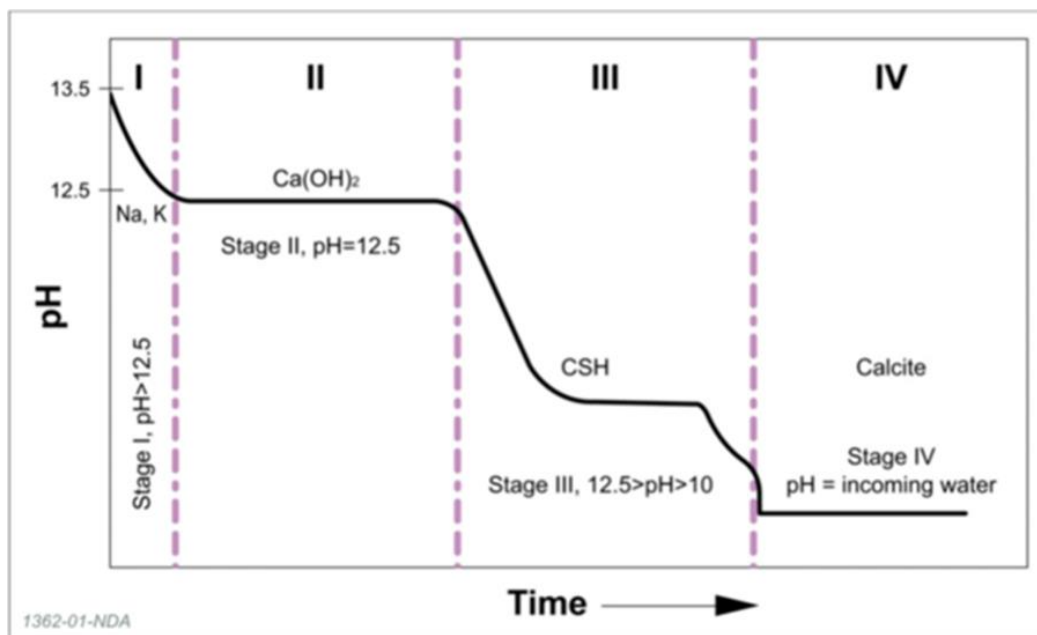


**Figure 1.3. The evolving pH values within the near-field of an ILW-GDF.** During the early post-closure period, the near-field of a cementitious GDF will be  $>12.5$ . Over time the pH is expected to drop to between  $12.5-10.0$ . Taken from (6).

### 1.2.5 Alkaline cellulose degradation under near-field conditions

A range of cellulosic materials will be present within the near-field of an ILW-GDF. Materials such as cotton and wood are composed of cellulose, hemicellulose and lignin polymers (12). Under the anoxic, alkaline conditions expected within the near-field of an ILW-GDF (Section 1.2.4), cellulose and hemicellulose are susceptible to chemical degradation via the peeling reaction (13-15). Alkaline chemical hydrolysis is expected to contribute to the majority of cellulose degradation within an ILW-GDF, rather than via radiolysis pathways (6). The major products of alkaline cellulose degradation are the alpha and beta forms of isosaccharinic acid (ISA), along with a range of lower abundance small chained organic acids, including acetic, formic, propionic and lactic acid (14). The generation of alpha and beta ISA has particular importance within a GDF because of their ability to complex and thereby change the mobility of radionuclides (13). ISA is capable of forming soluble complexes with a range of radioelements under alkaline conditions, including plutonium (16), uranium (17) and nickel (18). The increased mobility of radioelements complexed with ISA could make them more likely to reach the biosphere. Furthermore, the bio-degradation of ISA by colonising microorganisms could impact the long term performance of a GDF due to the removal of these complexants.

### **1.3 Microbial processes relevant to the disposal of ILW**

The generation of ISA and VFA's via the alkaline hydrolysis of cellulose-bearing ILW could provide a carbon source for microbial metabolism. Microbial colonisation of a GDF during the facilities construction phase or from the subterranean biosphere is possible (6), and due to the anoxic, chemically reducing conditions expected to develop within the near-field, microbial processes such as fermentation and anaerobic respiration linked to terminal electron acceptors (TEA) are likely to be important. The presence of organic molecules within an ILW-GDF arising from the chemical degradation of cellulose provides a range of electron donors for the respiration of electron acceptors by microorganisms. The generation of hydrogen within a GDF through corrosion processes could lead to the establishment of methanogenic conditions (10). Furthermore, some UK ground-waters are rich in sulphates (19) which could lead to the development of sulphate-reducing conditions following saturation of the facility. Methanogenesis and sulphate-reduction could impact the ability of a GDF at retaining radionuclides due to the production of methane and sulphide. Additionally, fermentation processes could provide a further source of electron donors for downstream anaerobic respiration via the production of fermentation end products.

#### **1.3.1 Fermentation**

Unlike aerobic and anaerobic respiratory processes where high energy TEA's are utilised for oxidative phosphorylation via the electron transport chain, fermentation processes rely on the synthesis of adenosine triphosphate (ATP) through substrate level phosphorylation (20). Fermentative organisms are metabolically versatile and are able to degrade a range of organic polymers, including polysaccharides, protein, DNA and lipids, with the use of extracellular enzymes (20). The resulting monomeric units, such as sugars (hexoses, pentoses, tetroses), amino acids and organic acids are consequently degraded by fermenters to various fermentation end-products, including VFA's, alcohols and gases such as hydrogen and carbon dioxide (Figure 1.4) (20, 21). The products of fermentation therefore provide substrates for downstream respiratory processes, such as methanogenesis and sulphate-reduction.

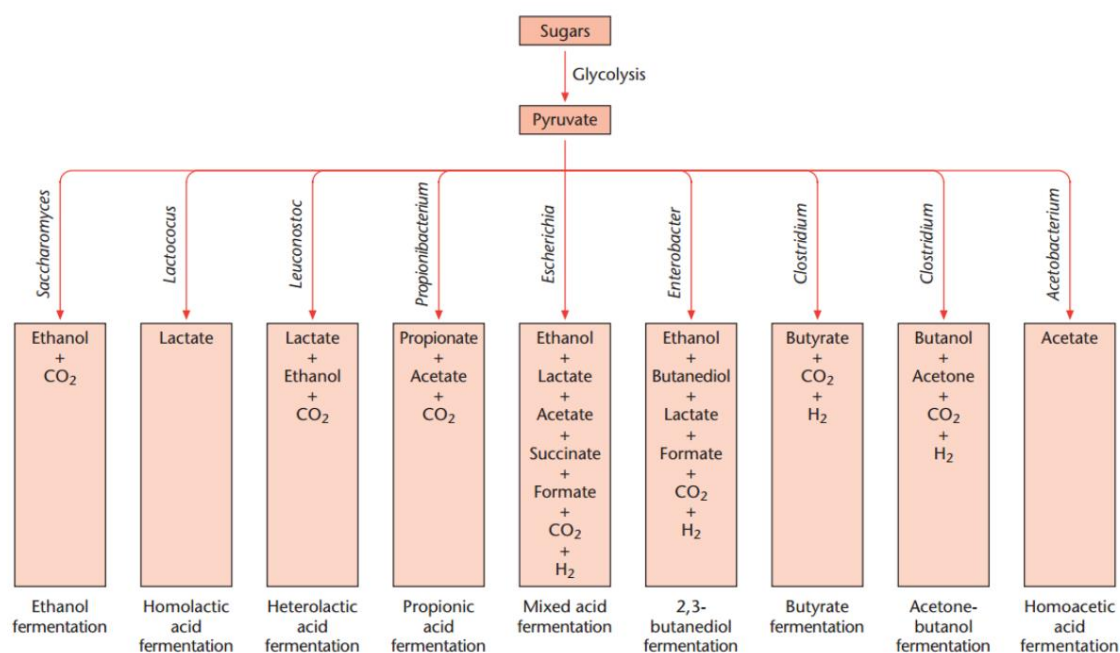


**Figure 1.4. The fermentation of sugars by different bacteria results in varied fermentation end products.** The products of sugar fermentation by bacteria results in the generation of fermentation end-products that can be used downstream by anaerobic microbial processes. Taken from (20).

### 1.3.1.1 Microbial degradation of isosaccharinic acids

The ability of microorganisms to degrade ISA through fermentation pathways under conditions expected of an ILW-GDF have been studied extensively. Microorganisms from neutral-pH canal sediments have been shown to be capable of degrading the alpha and beta forms of ISA through fermentation pathways under iron reducing, sulphate reducing and methanogenic conditions at neutral pH (22). The same microorganisms were able to degrade ISA under ILW-GDF conditions up to pH 10.0 with the products of ISA fermentation able to support methanogenesis at this pH, although ISA degradation rates decreased significantly under these conditions (23). Further microcosm experiments showed the fermentation of ISA up to pH 11.0 was possible when employing alkaline sediments from an anthropogenic lime-contaminated site, an ability that was attributed to the increased adaptation of the microorganisms within this site (24). The fermentation of ISA to acetate, hydrogen and carbon dioxide at pH 11.0 within these microcosms resulted in the generation of methane at this pH, with hydrogenotrophic methanogenesis apparently dominating under these conditions, evidently due to the accumulation of acetate and dominance of the genus *Methanobacterium* (a strictly hydrogenotrophic genus) within the archaeal community (24). Further microcosm based

studies showed the bio-degradation of ISA at pH 10.0 under nitrate reducing, iron reducing and sulphate reducing conditions was possible using alkaline sediments from the legacy lime working site near Buxton, UK (25). The metabolism of ISA at pH 10.0 in these microcosms was able to support nitrate and iron reducing processes, however no sulphate reduction was observed (25).

### 1.3.2 Methanogenesis

Methanogenesis is exclusively performed by anaerobic archaea of the phylum *Euryarchaeota*. The largest source of biogenic methane on Earth is generated by methanogens (26), which is an important part of the global carbon cycle. Carbon-14, which has a half-life of 5,730 years, is expected to be an important radionuclide within an ILW-GDF (6). The production of carbon-14 bearing gases, such as methane ( $^{14}\text{CH}_4$ ), could negatively impact the performance of a GDF through the transfer of radionuclides to the biosphere. Methanogens are only capable of using a limited number of substrates for growth and in the wider environment these organisms rely on the activity of fermenters and syntrophic acetate oxidising bacteria (SAOB) to provide the substrates for methanogenesis. Methanogens are ubiquitous in nature and have been detected in a wide range of environments, including wetlands, landfills, hydrothermal vents, ruminants, termites and rice paddy fields (26, 27). Only seven orders of methanogens have currently been classified, namely the *Methanobacteriales*, *Methanocellales*, *Methanococcales*, *Methanomassiliicoccales*, *Methanomicrobiales*, *Methanopyrales* and *Methanosarcinales* (27-29). Methanogenesis can proceed via three well defined pathways depending on the substrates utilised, these include the hydrogenotrophic pathway (using  $\text{H}_2/\text{CO}_2$ ), the acetoclastic pathway (using acetate) and the methylotrophic pathway (using methylated compounds) (29). The relative contribution of these substrates to methane generation under alkaline conditions is currently not well understood.

#### 1.3.2.1 The hydrogenotrophic pathway

The hydrogenotrophic pathway is thought to be the ancestral form of methane production (30), since it is found in almost all orders of methanogens, except for the *Methanomassiliicoccales*. The equation and associated Gibbs free energy for hydrogenotrophic methane generation is shown below:



$$\Delta G^\circ = -135 \text{ kJ/mol} \quad (32)$$

During hydrogenotrophic methanogenesis, hydrogen gas is used as an electron donor for the reduction of carbon dioxide to methane for ATP synthesis via the electron transport chain. In anaerobic environments  $\text{H}_2$  is a common compound, where it is often present in low concentrations and undergoes a fast turnover (33, 34). The maintenance of low  $\text{H}_2$  concentrations is necessary for the degradation of fatty acids and alcohols by syntrophic bacteria, a process which generates  $\text{H}_2$  for downstream consumption by hydrogen-consuming methanogens (35). In the absence of TEA's other than  $\text{CO}_2$ , hydrogen can only be consumed by methanogens or homoacetogenic bacteria (35). The equation and associated Gibbs free energy for homoacetogenesis is shown below:



$$\Delta G^\circ = -95 \text{ kJ/mol} \quad (36)$$

The relative contribution of the hydrogenotrophic pathway to methane production appears to vary depending on the environment studied. Since 4 moles of  $\text{H}_2$  are required to produce 1 mole of methane (as shown in the above equation) and only 1 mole of acetate is used to generate 1 mole of methane (Section 1.3.2.2), it is theorised that  $\text{H}_2/\text{CO}_2$ -derived methane can only contribute 33 % of the total methane formed during the anaerobic degradation of organic matter (32) (Figure 1.6). This claim has been substantiated in a number of studies.  $\text{H}_2/\text{CO}_2$ -derived methane accounted for 36-46 % of the total methane produced in sediments from Lake Mendota, USA (37). The hydrogenotrophic pathway was responsible for 15-39 % of the methane produced in the sediments of Lake Washington, USA (38) and 17-37 % in flooded rice fields in the Po valley, Italy (39). However, within some environments the hydrogenotrophic pathway contributes to a lesser degree, particularly within marine environments due to competition with hydrogen-consuming sulphate reducing bacteria (40). Methanogenesis in these environments is reliant on non-competitive substrates that are utilised in the methylotrophic pathway, such as trimethylamine (41). The reduced contribution of  $\text{H}_2/\text{CO}_2$ -derived methane can also be a result of an increased contribution of homoacetogenesis, as seen within the acidic sediments from Knaack Lake, USA (42). Additionally, the contribution of  $\text{H}_2/\text{CO}_2$ -derived methane can be temperature sensitive, with studies on rice fields seeing a shift towards acetate-dependent methane generation as the temperature lowered from 30 °C to 15 °C (34, 43).

Within some environments however, the hydrogenotrophic pathway can contribute to a higher degree than is theorised (i.e. more than ~33 %). As much as 100 % of the methane generated in an acidic peat bog in Washington, USA, was a result of the hydrogenotrophic pathway (44) and similar values were recorded in the bottom sediments of Lake Baikal, Russia (45). H<sub>2</sub>/CO<sub>2</sub>-dependent methanogenesis contributed between 74-86 % of the total methane produced in low sulphate microbial mats (46) and in the sediments of a stratified eutrophic lake (47). However, the reason for an increased contribution of H<sub>2</sub>/CO<sub>2</sub>-derived methane in these environments is not well understood. Additional sources of hydrogen (besides fermentation and syntrophic acetate oxidation) which could result in a higher contribution of hydrogenotrophic methanogenesis are currently undescribed, except for in Lake Kivu, Africa, where a geological input of H<sub>2</sub> provides the methanogens in this environment with a surplus of the substrate (48).

### 1.3.2.2 *The acetoclastic pathway*

Although the dominant source of biogenic methane within the atmosphere is thought to be derived from acetate (49), only one order of methanogens (the Methanosarcinales) and two genera (*Methanosarcina* and *Methanosaeta*) are capable of acetoclastic methanogenesis (50, 51). The equation and associated Gibbs free energy for acetoclastic methane generation is shown below:



$$\Delta G^\circ = -36 \text{ kJ/mol} \quad (32)$$

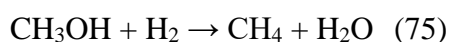
The acetoclastic pathway is performed exclusively by members of the order Methanosarcinales via the activation of acetate to acetyl-coenzyme A (acetyl-CoA), from which the methyl group is reduced to methane using electrons derived from the oxidation of the carbonyl group to CO<sub>2</sub> (52). Whilst the acetyl-CoA synthetase pathway is used by the genus *Methanosaeta* (53), the genus *Methanosarcina* use a different pathway consisting of acetate kinase (AckA) and phosphoacetyl transferase (Pta) (54). The higher acetate half-saturation coefficients of the AckA/Pta pathway enzymes compared with the acetyl-CoA synthetase pathway gives the *Methanosarcina* an advantage over *Methanosaeta* under high acetate concentrations (>1 mM) (55). In contrast, the *Methanosaeta* tend to dominate in environments with low acetate concentrations (<1 mM) due to their higher affinity for the substrate (56-58), although *Methanosaeta* have demonstrated competitiveness under elevated acetate concentrations in animal wastewater treatment systems (59).

Members of the *Methanosarcina* predominantly use acetate for methanogenesis, however a number of species are metabolically diverse and capable of utilising multiple methanogenic pathways for ATP synthesis. The ability of *Methanosarcina* species to metabolise and grow on various methanogenic substrates has been studied through the isolation and characterisation of pure cultures from a range of environments. Neutrophilic *Methanosarcina mazei*, *Methanosarcina siciliae*, *Methanosarcina horonobensis* and *Methanosarcina acetivorans* have been isolated from anaerobic digesters, marine sediments and groundwater samples, with all of these species able to utilise acetate and methylated compounds (methanol, dimethylamine, trimethylamine, dimethylsulfide), but not H<sub>2</sub>/CO<sub>2</sub> for growth and methanogenesis (60-63). Thermophilic strains of *Methanosarcina* have been isolated from anaerobic sludge digesters operating at 55 °C, all of which were capable of growth between pH 5.5-8.0 on acetate and methylated compounds, but were unable to use H<sub>2</sub>/CO<sub>2</sub> (64). *Methanosarcina vacuolata* isolated from wetland soil is the only known member of the *Methanosarcina* incapable of growth on acetate, instead methanol, methylamines and H<sub>2</sub>/CO<sub>2</sub> are used (65). Additionally, a number of species have been identified that are able to grow using all known methanogenic substrates (H<sub>2</sub>/CO<sub>2</sub>, methylated compounds and acetate), including *Methanosarcina spelaei* isolated from a sulphurous lake in Romania (66), *Methanosarcina soligelidi* isolated from permafrost-affected soil (67) and *Methanosarcina barkeri* (68), all of which demonstrate optimum growth under neutral-pH conditions. In contrast to the metabolically diverse genus *Methanosarcina*, all known members of the genus *Methanosaeta* are strictly acetoclastic and are unable to use methylated compounds or H<sub>2</sub>/CO<sub>2</sub> for growth and methanogenesis. The limited number of *Methanosaeta* species studied in pure culture all demonstrate optimum growth under neutral-pH conditions (69-71). In fact, no alkaliphilic methanogens capable of acetoclastic methanogenesis in pure culture could be found in the literature.

### **1.3.2.3 The methylotrophic pathway**

Hydrogenotrophic and acetoclastic methanogenesis are widely regarded as the predominant pathways to biogenic methane production globally, however sulphate reduction can thermodynamically inhibit both of these pathways. In sulphate-rich environments methanogens can circumvent the competition for substrates with the use of non-competitive methylated compounds, such as methanol, methylamines and methyl sulphides (40). The significance of this is illustrated by studies investigating marine sediments of the Western Mediterranean Sea, where the methylotrophic pathway accounted for as much as 98 % of the total methane

production in the sulphate-rich zones (72). In the deeper zones where sulphate was absent, the hydrogenotrophic pathway dominated (72). The quantity and age of the organic matter present can also govern the extent of methanogenesis in these environments, where acetate-dependent methane production only became important in the organic-rich zones (72). The simultaneous operation of methanogenic and sulphate reducing processes in salt marsh sediments was facilitated by the use of methylated compounds (40). The methylotrophic pathway was also recently recognised to be the dominant methanogenic pathway in the highly saline sediments of Orca Basin in the Gulf of Mexico (73), and also appears to be important in alkaline soda lakes (74). The equation and associated Gibbs free energy for methane generation from methanol using hydrogen as electron donor is shown below:



$$\Delta G^\circ = -112.5 \text{ kJ/mol} \quad (75)$$

### ***1.3.2.3 Energy conservation in cytochrome-containing methanogens***

Methanogens can also be classified into two groups based on the presence or absence of cytochromes, with the Methanosarcinales being the only order to possess cytochromes (50), and consequently the only methanogens capable of using all three methanogenic pathways. Methanogens lacking cytochromes only use  $\text{H}_2$  (and sometimes formate) as electron donors for the reduction of  $\text{CO}_2$  to methane via the hydrogenotrophic pathway. Since the free energy change is very low during acetoclastic methane generation ( $\Delta G^\circ = -36 \text{ kJ/mol}$ ), acetate-consuming methanogens require an efficient energy conserving mechanism to cope with this thermodynamic limitation. The synthesis of ATP by these organisms is accomplished via interactions between ion translocating enzymes and ATP synthases. It has long been established that the membrane-bound methyltransferase (Mtr) enzyme catalyses the transfer of methyl groups coupled with the extrusion of  $\text{Na}^+$  ions out of the cell for electron transfer and ATP synthesis in all types of methanogens (76-78) (Figure 1.5AB). However, analysis of ion transport in membrane vesicles and the use of ATP hydrolysis assays it was recently revealed that the membrane-bound enzyme  $\text{A}_1\text{A}_0$  ATP synthase from *Methanosarcina acetivorans* translocates both  $\text{Na}^+$  and  $\text{H}^+$  ions simultaneously to generate an electrochemical gradient for ATP synthesis (79) (Figure 1.5B). The use of  $\text{Na}^+/\text{H}^+$  antiporters in *Methanosarcina acetivorans* is thought to aid in optimisation of the ATP synthase by adjusting the ratio of  $\text{Na}^+$  and  $\text{H}^+$  ions (80). This unique energy conserving strategy employed by cytochrome-containing methanogens could have important implications under alkaline conditions, where the

availability of  $H^+$  ions will be extremely limited and therefore the establishment of electrochemical gradients required for ATP synthesis in these organisms may prove difficult.

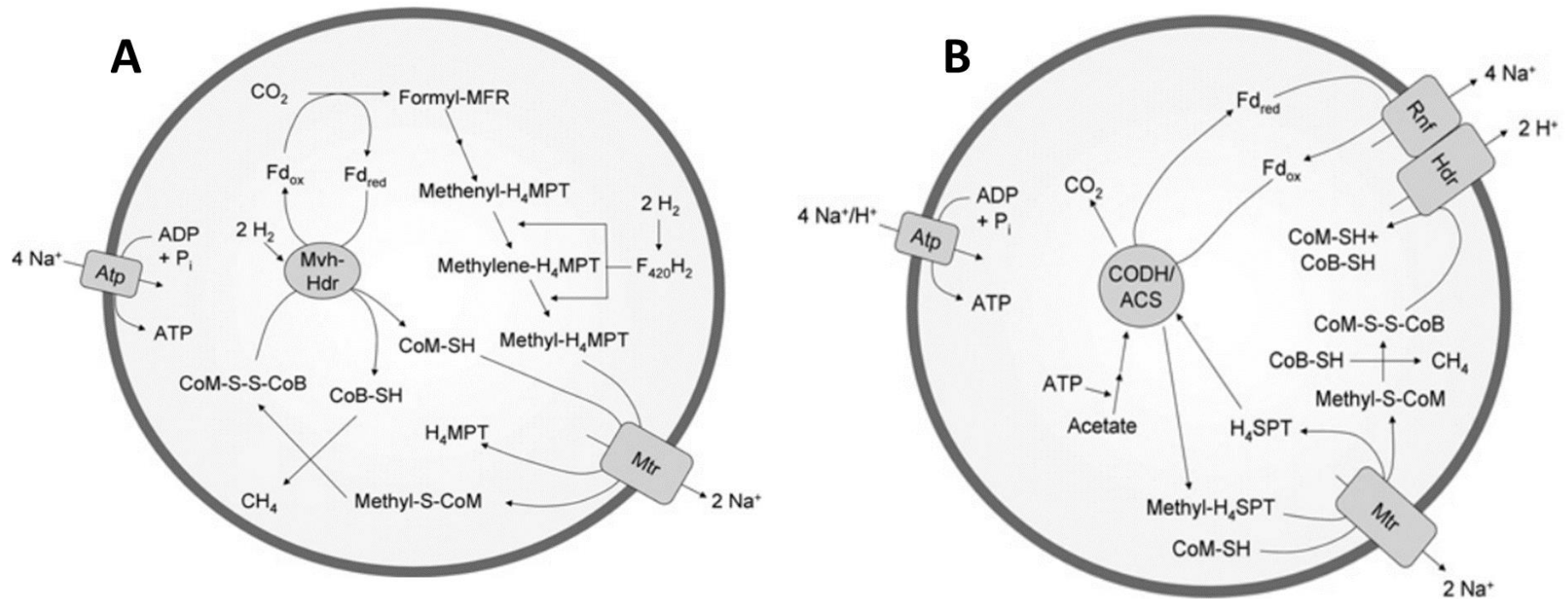


**Figure 1.5. Proposed models of hydrogenotrophic and acetoclastic pathways in methanogenesis.** [A] Hydrogenotrophic methane generation without cytochromes, using  $\text{Na}^+$ -dependent ATP synthases to establish electrochemical gradients, [B] acetoclastic methane generation with cytochromes, using ATP synthases that simultaneously translocate  $\text{Na}^+$  and  $\text{H}^+$  across the membrane for the establishment of electrochemical gradients and ATP synthesis. Taken from (81)

#### 1.3.2.4 Methanogenesis in extreme environments

Environmental factors such as temperature, salinity and organic matter content can have a significant impact on methanogenesis (82-86). For example, microcosm experiments using arctic sediments were dominated by the strictly hydrogenotrophic family *Methanoregulaceae* at low temperatures (5 °C), whereas incubations at increased temperatures (30 °C) saw an increase in the acetoclastic lineages *Methanosarcinaceae* and *Methanosaetaceae* (82). Other studies have shown that an input of organic matter in the form of rice straw can stimulate acetoclastic methane generation due to changes in soil microbial community structure (86). However, there is a scarcity of information regarding the influence pH has on the composition and functioning of methanogenic communities, particularly under alkaline conditions. The vast majority of studies relating to methane generation at high pH have focused on soda lake environments, which demonstrate highly saline and alkaline *in situ* conditions (74, 87). Incubations using sediments from the Big Soda Lake in Nevada, USA, demonstrated a clear preference for the methylotrophic pathway, with methane production stimulated in enrichments with methanol and trimethylamine but not in microcosms supplied with H<sub>2</sub>/CO<sub>2</sub> and acetate (74). Investigations into the soda lake sediments of Kulunda Steppe in Siberia revealed the presence of all three methanogenic pathways functioning between a pH range of 8.0-10.5 (87). The salt concentration within these microcosms appeared to influence the methanogenic activity, with an increased contribution of methylotrophic methanogenesis under highly saline conditions (87). The investigation of Kulunda Steppe sediments is the only report of acetoclastic methanogenesis operating under alkaline conditions (pH 9.5) present in the literature, although the authors did make a note of the difficulties culturing these acetate-metabolising methanogens due to very slow growth rates (10 mM acetate conversion in 3 months) (87).

Methanogens have been successfully cultured from deep subsurface and thermophilic environments previously, indicating their presence within the subterranean biosphere and tolerance to increased temperatures. Pure cultures of the thermophilic and hydrogenotrophic species *Methanocaldococcus jannaschii* and *Methanopyrus kandleri* were isolated from smoker chimneys at a depth of 2600 m and 2000 m respectively (88, 89). A number of strictly hydrogenotrophic methanogens of the genus *Methanobacterium* have been isolated from low salt alkaline lakes in Egypt (90), all of which were capable of growth up to pH 10.0 in pure

culture. An alkaliphilic hydrogenotroph *Methanocalculus* has been isolated from soda lake sediments which was able to grow between pH 8.0 – 10.2 in pure culture (91).

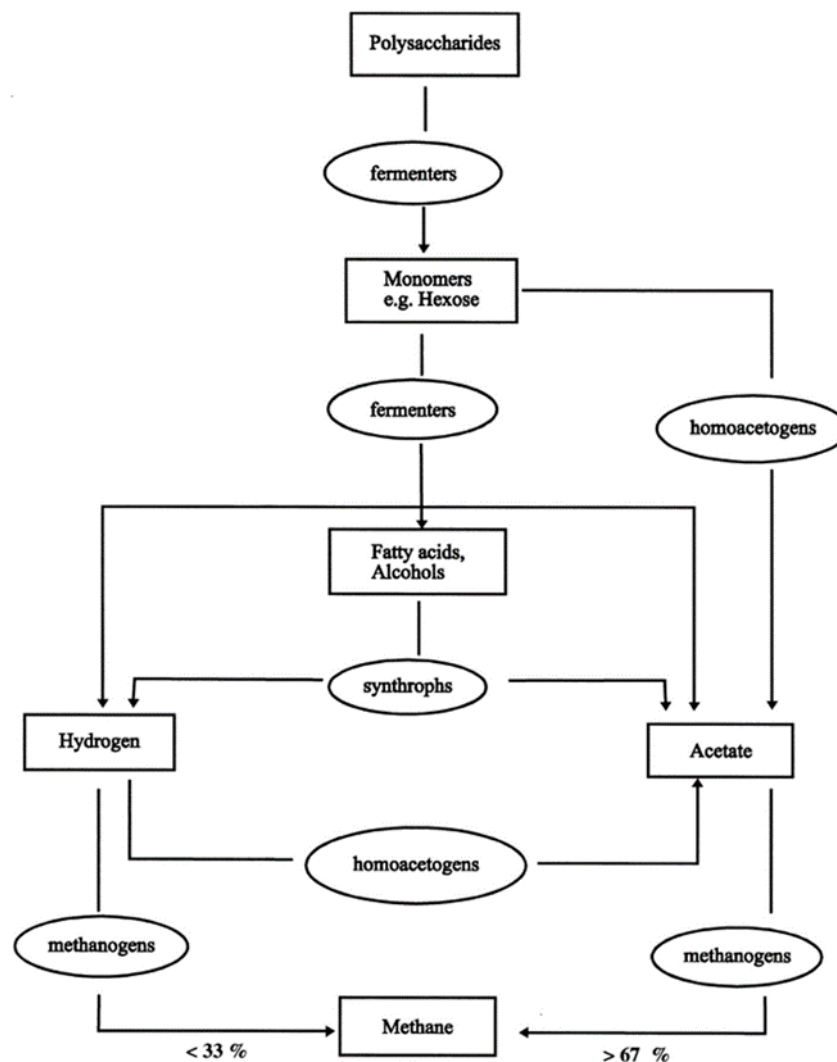


**Figure 1.6. The pathways for anaerobic degradation of organic matter to methane.**

Taken from (32).

### 1.3.3 Sulphate reduction

Dissimilatory sulphate reducing bacteria (SRB) are a metabolically diverse group of anaerobic microorganisms that play an important role in the global carbon and sulphur cycles. SRB traditionally use sulphate as the terminal electron acceptor (TEA) and are able to use a wide range of electron donors, including hydrogen and various organic compounds (92). Some SRB have demonstrated growth without sulphate, and can instead use nitrate as TEA and have even demonstrated autotrophic growth using H<sub>2</sub> and CO<sub>2</sub> (93, 94). This metabolic flexibility has allowed SRB to become widespread in nature and their importance within marine environments

and anaerobic digesters are well documented (95-97). Sulphide is produced as an end product of dissimilatory sulphate reduction, which is highly corrosive and contributes to microbially-induced corrosion (MIC). Although a range of microorganisms have been implicated in bio-corrosion processes, including acetogenic bacteria (98), nitrate reducers (99) and even methanogens (100, 101), the most widespread and economically relevant MIC processes are mediated by SRB.

### ***1.3.3.1 Corrosion of metal by sulphate reducing bacteria***

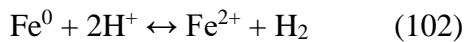
Iron corrosion is an electrochemical process (except for instances of mechanical stress), where metal oxidation is coupled to the reduction of a suitable oxidant. The tendency of iron to give off electrons is central to the corrosion process:



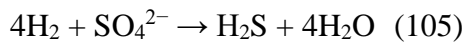
In anaerobic environments, the protons from dissociated water provide the most common electron acceptors for iron oxidation, which are reduced to molecular hydrogen:



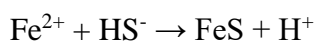
The above two reactions are stoichiometrically coupled and yield the following net reaction:

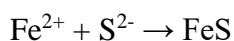


Proton availability will be extremely limited under alkaline conditions and therefore from a purely chemical point of view, iron corrosion could be insignificant under these conditions. However, the above statement changes in the presence of microorganisms, where metabolic products, such as organic acids or sulphide can dramatically enhance corrosion kinetics (95, 103, 104). SRB are capable of using molecular hydrogen as an electron donor for the reduction of sulphate and production of hydrogen sulphide:



Under alkaline conditions, hydrogen sulphide ( $\text{H}_2\text{S}$ ) produced by SRB will be present as  $\text{HS}^-$  or  $\text{S}^{2-}$  and both of these chemical species are known to react with metallic iron and thereby produce the characteristic iron sulphide corrosion product:





The generation of iron sulphide can actually help protect against corrosion in a process known as passivation, whereby a film of iron sulphide on the metal surface prevents the diffusion of iron ions into the bulk liquid (106, 107). Additionally, the production of stainless steel from the alloying of iron with active metals, such as nickel, chromium and molybdenum can improve corrosion resistance. Since corrosion processes within a GDF are an important safety consideration, the ability of SRB to survive at high pH and corrode materials relevant to ILW disposal is an important area of research. The integrity of engineered barriers used to limit the travel of radioelements to the biosphere within a GDF (such as the stainless steel waste canisters) could be compromised by the corrosive activity of SRB. The bio-corrosion of metals by SRB has been studied extensively. For example biofilm growth by *Desulfovibrio desulfuricans* and *Desulfovibrio fairfieldensis* resulted in the corrosion of endodontic files within 32 days, indicated by the cracks formed on the materials surface as visualised by scanning electron microscopy (SEM) and the formation of sulphur-containing minerals within the biofilm matrix measured with SEM coupled with energy-dispersive X-ray spectrometry (EDS) (108). The corrosion of stainless steel was observed during the growth of *Desulfovibrio desulfuricans* where the formation and morphology of corrosion pits were analysed using atomic force microscopy (AFM) (109). Furthermore SRB were able to induce the corrosion of carbon steel in artificial seawater, with corrosion processes evaluated using electrochemical impedance spectroscopy (EIS) and surface characterisation undertaken using SEM and SEM-EDS (110). Although bio-corrosion of metals by SRB under neutral pH conditions is well described, little information is available regarding this process under alkaline conditions.

### ***1.3.3.2 Sulphate reduction under extreme conditions***

All known dissimilatory SRB belong to the  $\beta$ -Proteobacteria, Clostridia, Nitrospirae, Thermodesulfobiaceae, Thermodesulfobacteria, Crenarchaeota and Euryarchaeota lineages and have been detected and cultured from a range of extreme environments. Alkaline soda lakes have been well studied in terms of alkaliphilic SRB with reports of high sulphate reducing rates at pH 10.7 in Lake Tanatar sediments (111). Non-alkaliphilic SRB cultured from a Danish heating plant have demonstrated growth and sulphide production up to pH 9.3 in planktonic culture and up to pH 10.2 in biofilms (112). Pure cultures of alkaliphilic *Thermodesulfovibrio* were isolated from an aquifer system at a depth of 2,000 m and were capable of growth up to pH 10.5, using formate, pyruvate and lactate as electron donors (113). Novel strains of

*Desulfonatronum* have been isolated from alkaline brackish lakes in Siberia, Russia, with some of these strains able to grow up to pH 10.5 in pure culture and use hydrogen as electron donor (114). However, studies employing sediments from a proposed ILW-GDF analogue site at Buxton, UK showed very little sulphate reducing activity between pH 10.0 – 12.0 using acetate and lactate as electron donor (115).

Sulphate can be present in both natural and anthropogenic water systems. The natural sources of sulphate can be produced through atmospheric deposition, the dissolution of sulphate minerals or the oxidation of sulphide minerals (116). Sources of sulphate can also be present through anthropogenic contamination, as seen from the operation of coal mines, phosphate refineries and power plants (117, 118). Sulphide produced by SRB can be toxic to microorganisms due to its ability to react with metal ions and the functional groups of enzymes used for electron transport (119). Additionally, sulphide production can lead to the precipitation of essential trace metals as metal sulphides, which can negatively affect cell growth. The speciation of sulphide is highly dependent on the pH. Previous studies have shown that H<sub>2</sub>S is the most toxic form of sulphide due to the increased membrane permeability of this uncharged molecule (120, 121). Therefore, the growth of SRB at high pH could be advantageous due to the formation of HS<sup>-</sup> and S<sup>2-</sup> sulphide species, which are less membrane permeable than H<sub>2</sub>S and can be tolerated at higher concentrations (122).

#### **1.4 Microbial survival under ILW-GDF conditions**

The anaerobic, chemically reducing and highly alkaline conditions expected to develop within an ILW-GDF are likely to stunt microbial activity considerably, particularly within the early post-closure period when pH values of >13.0 are expected. However, the pH values of an ILW-GDF are expected to reduce during the evolution of the facility to between pH 10.0-12.5, and furthermore a number of microorganisms have adapted mechanisms to survive extreme environmental conditions. These organisms are termed extremophiles and have a number of structural, physiological and metabolic adaptations that enable them to function well under extreme conditions. A number of alkaliphilic organisms have demonstrated the ability to grow above pH 10.0 in pure culture (123, 124) and the upper pH limits for microbial growth can increase with the formation of biofilm (112, 125). One particular adaptation utilised by alkaliphiles is the ability to maintain cytoplasmic pH homeostasis to allow for normal function of enzymes and metabolic processes. *Bacillus pseudofirmus* OF4 has been extensively studied due to its ability to grow between pH 7.5 – 11.4 (126). A common ability of alkaliphilic

organisms is the ability to maintain an intracellular pH value lower than the external pH value. *Bacillus pseudofirmus* OF4 for example maintains a cytoplasmic pH of 8.2 when the external pH is 10.5 and this ability is observed in other bacteria, including *Bacillus halodurans* C-125, *Bacillus alcalophilus* and *Spirulina platensis* (127-129). In fact, obligate alkaliphiles grow better under alkaline conditions and growth is stunted under more neutral-pH conditions, which was observed in *Bacillus pseudofirmus* OF4 which has a doubling time of 54 minutes at pH 7.5 and a doubling time of 38 minutes when grown between pH 8.5-10.5 (123). The primary mechanism for maintenance of cytoplasmic pH homeostasis used by alkaliphiles is through uptake of H<sup>+</sup> using membrane-bound Na<sup>+</sup>/H<sup>+</sup> antiporters. These antiporters extrude Na<sup>+</sup> and uptake H<sup>+</sup> into the cell which is allowed to accumulate within the cytoplasm. A lesser number of Na<sup>+</sup> ions are extruded compared with H<sup>+</sup> ions taken up, therefore the net positive charge is present within the cell with each turnover of the antiporter (130).

Additional strategies are used by alkaliphiles that complement the use of Na<sup>+</sup>/H<sup>+</sup> antiporters. Some bacteria upregulate deaminases which produce cytoplasmic acids (131). Teichuronopeptides are secondary cell wall polymers that play an important role in maintaining cytoplasmic pH homeostasis in alkaliphiles (127). Metabolic acids produced within the cytoplasm during fermentation processes could help to maintain cytoplasmic pH homeostasis in *Bacillus* species (131, 132). Acidic lipids and teichuronic acids incorporated into the cell walls could further enable adaptation to alkaline environments by alkaliphiles (127, 133).

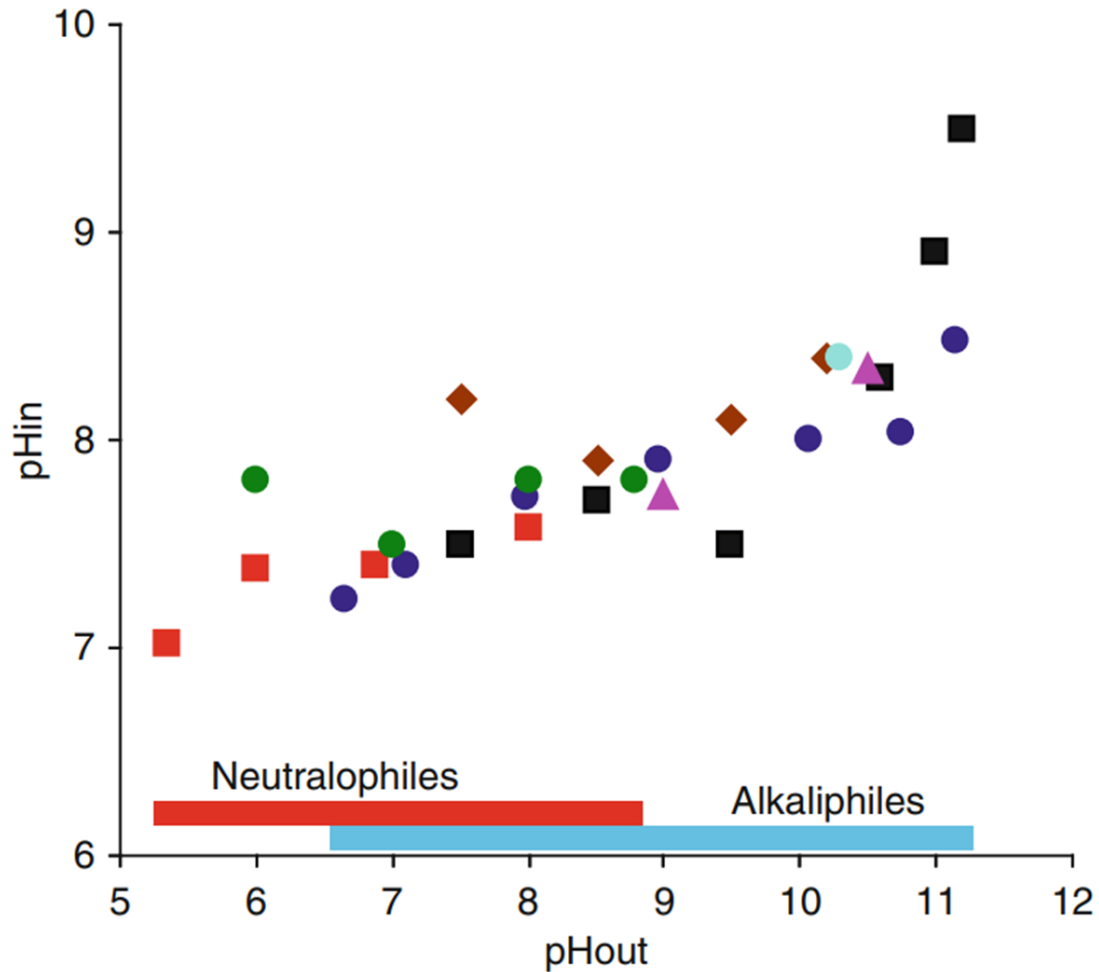


**Figure 1.7. Internal and external pH values in neutralophilic and alkaliphilic bacteria.**

The internal cytoplasmic pH of alkaliphiles is maintained at a lower value than the external pH, a mechanism by which alkaliphilic organisms can grow at higher pH values. Taken from (134).

#### 1.4.1 Natural alkaline sites

A range of alkaline environments are present throughout the world that have analogous conditions to those likely to be experienced within an ILW-GDF. These sites enable the study of microbial and chemical processes under ILW-GDF conditions. The alkalinity of these sites can develop through natural evaporation processes or due to the local geochemistry of the rock formations in these regions (135-137). Soda lakes are one example of a natural alkaline site that develop highly alkaline waters (pH 8.0-12.0) due to the presence of carbonate as the dominant anion. In some cases these sites can also demonstrate highly saline conditions due to the presence of NaCl (138). A high degree of microbial diversity has been revealed within the

sediments and waters of soda lakes despite the harsh environmental conditions present (139). Methanogenic and sulphate reducing processes have also been detected in these environments (140, 141). Another example of naturally occurring alkaline environments are ophiolites composed of mafic and ultramafic rock which generate high *in situ* pH values due to serpentinisation processes (142). An example of this is in the Troodos Mountains, Cyprus, where *in situ* pH values up to 11.9 have been observed (143). A range of microbial processes were present within the site, including nitrogen fixation by *Paenibacillus* species, hydrogen oxidation by *Hydrogenophaga* species and iron reducing processes within microcosms employing samples taken from the site (143). A wide range of bacteria have been detected in other ophiolite systems around the globe, including Del Puerto in California (144), Oman (144) and the Leka complex in Norway (135). Studies investigating the microbial diversity at the Maqarin site in Jordan revealed a clear dominance of Proteobacteria phylum which were present between  $10^3$  and  $10^5$  cells mL<sup>-1</sup> water (145). The alkalinity of this site has been attributed to interactions with naturally occurring cement materials present in the site, as opposed to alteration of ultramafic materials due to serpentinisation observed within other ophiolite complexes (146).

#### **1.4.2 Anthropogenic alkaline sites**

In contrast to naturally occurring alkaline sites, the formation of high pH environments can also result from anthropogenic contamination, such as through the deposition of lime and steel production waste (147, 148). The contaminating materials can in some cases be rich in heavy metals, such as chromium, arsenic and copper, which are toxic to microbes (149, 150). The contamination of these sites with anthropogenic wastes can lead to a reduction in microbial diversity, however the ability of the local microbial community to adapt and evolve can lead to their survival under these conditions (151). The adaptation of microbial communities has been observed at a site contaminated with tannery waste, where chromium resistant organisms were isolated (152). Additionally, acid-tolerant communities developed within an acid mine drainage site (153).

A lime-contaminated site near Buxton, UK, has been investigated due to its analogy with some aspects of ILW disposal (154). The materials deposited at this site include lime, calcined limestone and coal ash. As rain water percolates through these wastes, an alkaline leachate is generated which forms a calcium carbonate tufa as it comes into contact with atmospheric carbon dioxide and *in situ* pH values as high as 13.0 have been observed (154). A number of

previously unclassified bacteria relating to the Comamonadaceae, Bacteroidetes and Firmicutes lineages have been detected within the sediments from this site (154). ISA has been detected at this site *in situ* due to the alkaline hydrolysis of cellulosic materials, and sediments from this site demonstrated the ability to degrade all three forms of ISA in microcosm studies (24). Additionally, ISA degradation under sulphate reducing, iron reducing and methanogenic conditions has been demonstrated over a range of pH values using sediments from this site (23, 155, 156). Furthermore sediments from this site have demonstrated nitrate, iron and sulphate reduction under alkaline conditions using acetate and lactate as electron donors (115). Despite *in situ* pH values of >13.0 being recorded in this site, a diverse and active microbial community was detected via Illumina MiSeq, with the dominant phyla present being the Firmicutes, Proteobacteria and Bacteroidetes, with a low abundance of methanogenic archaea (157).

### **1.4.3 Biofilms**

Biofilms are composed of polymicrobial communities lodged in self-produced extracellular polymeric substances (EPS). The formation of biofilms by microorganisms allows for microbial adhesion and growth on almost any surface and has proven to be a particularly successful form of life on earth in both agreeable and extreme environments (158-162). The internal biofilm environment is often heterogeneous and can differ significantly to the external environment (163). This is largely due to the microbial production and consumption of metabolic products within the biofilm, together with the limited diffusion of chemical species through the EPS matrix (164). The biofilm matrix offers a protective barrier from the external environment and has been shown to provide microbes with increased resistance to a range of environmental stresses, including desiccation, predation and extreme shifts in pH and temperature (165). An example of this was revealed within acid mine drainage biofilms, where the associated microorganisms were shown to secrete proteins with a high isoelectric point which increased the pH buffering capacity of the internal biofilm environment (166). Recent studies have shown that biofilms can facilitate survival under ILW-GDF conditions through the production of low pH microsites within the internal biofilm surface (125). The acidic properties of the EPS components and the production of metabolic acids enabled the microbes within these biofilms limited survival up to pH 13.0 (125).

The formation of biofilm by microorganisms is undertaken using a number of steps. Firstly, planktonic cells must adhere to a surface prior to the formation of the structured biofilm architecture. This is initially achieved using cellular appendages, such as flagella and pili, and

is a form of reversible attachment (167). The cellular surface proteins, such as SadB or LapA, along with the production of EPS enhances the irreversible attachment to a surface, whereby the cell commits to a biofilm mode of existence (168, 169). The transition between reversible and irreversible surface attachment appears to be mediated by intracellular secondary messengers, such as cyclic adenosine monophosphate (cAMP), which are produced in response to environmental conditions (170). Following the irreversible attachment to a surface, cells begin to proliferate and (along with the production of EPS) develop micro-colonies. The EPS components can account for >90 % of the dry mass in mature biofilms (158). The individual EPS components can include a range of biopolymers, such as proteins, polysaccharides, lipids and nucleic acids, and these components are responsible for a wide range of functions within the biofilm. These functions include facilitating attachment to biotic and abiotic surfaces (171), enabling the binding of enzymes to the biofilm matrix (172), aiding horizontal gene transfer (173) and providing resistance to desiccation and other environmental stresses, such as antimicrobial agents and oxidation (165, 174). Additionally, the EPS matrix allows metabolic products to accumulate and provides a carbon and nitrogen source for microbial metabolism (175, 176). The biofilm matrix is stabilised via interactions between the different functional EPS components (177). Quorum sensing signalling molecules are retained within the biofilm, therefore EPS production enhances cell-cell communication and nutrient uptake (178). Since cells exist in close proximity to one another within the biofilm, this allows syntrophic interactions to take place, such as interspecies hydrogen transfer between fermenters and methanogens (179).

Microbial cells are capable of returning to a planktonic form of life following the maturation of the biofilm. Cells can disperse from the biofilm passively, for example due to physical shearing forces, or can actively disperse by responding to environmental stimuli, such as temperature or oxidation (180). Genes involved in EPS production are downregulated, whilst genes involved in cell motility and EPS degradation are upregulated in actively dispersing cells (180). These dispersed cells are able to seed new environments where the process of biofilm formation can begin again.

## 1.5 Summary of chapter

The UK currently has a relatively large inventory of radioactive waste arising from a long nuclear legacy. One potential strategy for disposing of the higher activity wastes (ILW and HLW) is that of a GDF, which employs a multiple barrier system in order to retain the radioelements within the facilities near field and prevent their release to the biosphere. These barriers include physical containment of the waste in stainless steel canisters, chemical containment within an appropriate backfilling material (e.g. NRVB) and geological containment within the host rock. Anaerobic and highly alkaline conditions are expected to prevail within the facilities near field, which will result in the chemical degradation of cellulose-bearing ILW to a range of cellulose degradation products. ISA and VFA's will constitute the majority of the products formed from the alkaline hydrolysis of cellulose, and these products could provide a carbon source for fermentative and anaerobic respiratory microbial processes. Since the predominant TEA's within a GDF are likely to include CO<sub>2</sub> and possibly sulphate, methanogenesis and sulphate reduction could be important processes within this environment. Active methanogenic and sulphate reducing processes may impact the ability of a GDF at retaining the waste through biogas and sulphide production. Since diverse microbial populations have demonstrated the ability to colonise and grow within a range of anaerobic and highly alkaline natural and anthropogenic environments across the planet, this suggests the conditions of a GDF could provide a niche site for a variety of specialist organisms, such as anaerobic alkaliphiles and ISA degrading bacteria. The survival of microbes under extreme conditions can also be facilitated through the formation of biofilms, a mode of existence that allows for microbial durability at the thermodynamic limits of life.

## **2.0 Methods for the analysis of environmental microbiology**

## **2.1 Overview**

A range of techniques are available that allow the effective characterisation of natural and model microbial systems. The cultivation and isolation of microorganisms from environments that are analogous to aspects of radioactive waste disposal can provide information that may help to predict the effect of microbial processes on GDF performance. Culturing techniques allow microbial processes to be studied in the laboratory where the conditions of interest can be simulated and studied. An array of molecular techniques have been developed that utilise the conserved 16S rRNA gene for the purpose of analysing and describing microbial communities. Additionally, a variety of microscopic techniques can be utilised to provide a greater insight into the functioning of a microbial system. The following chapter discusses some of the current methods that allow microbial systems to be effectively characterised.

## **2.2 Culturing techniques**

One important technique for the study of environmental microbiology involves the direct culturing of microorganisms from an environmental sample using solid or liquid media. The culture conditions imposed on the samples, such as temperature, pH, carbon source and O<sub>2</sub> concentration, will dictate the types of microorganisms that grow (181). The establishment of microcosms is an effective way to simulate the conditions of interest, and these systems can be developed using pure or mixed cultures and operated with great flexibility. The system can be sealed and operated in a batch process, where the chemistry is allowed to develop, or microcosms can be batch-fed, where nutrients are continuously supplied to the system and waste is removed. The production and consumption of metabolic products can be analysed when employing microcosms, which can provide information regarding the metabolic capabilities of the population within a given environmental site. Batch microcosms have been used previously to determine the sulphate reducing rates in acid mine drainage sites (182). The methanogenic activity of soda lakes sediments has been studied with the use of microcosms, where methane generation and substrate consumption could be measured using gas chromatography (183). Batch microcosms have been used to estimate gas production under conditions simulating LLW disposal (184). Batch-fed systems have been employed previously to provide ISA degradation rates under ILW-GDF conditions using both neutral-pH and alkaline sediments (23, 24). Previous authors have also used enrichment cultures to analyse iron reduction processes in sediments from leachate ponds in California, USA, which resulted

in the isolation of a novel alkaliphilic iron reducer, *Alkaliphilus metalliredigens* (185). Since enrichment cultures induce a selection bias towards a particular type of organism depending on the conditions employed, this direct culturing method does not necessarily reflect the microbial processes ongoing *in situ*. Techniques such as Most Probable Number (MPN) can be used to estimate the number of viable organisms within an environmental sample with the use of serial dilutions and the detection of biochemical markers to assess microbial growth. MPN techniques have been used to study the viable organisms present within a number of disposal sites across the world (186-188). Microorganisms can also be isolated from environmental samples using serial dilutions, streak plating techniques and selective media. The characterisation of pure cultures can help to provide specific reaction rates and optimum culture conditions for a particular organism. The optimum culture conditions for a vast array of microorganisms are now available in the literature and the environmental conditions of a particular site can be simulated in the laboratory to some extent. However, a large proportion of environmental microorganisms remain uncultured and some prove extremely difficult to isolate (181, 189), therefore direct culturing techniques when used alone can misrepresent the true microbial diversity of an environment. A number of nucleic acid methods and microscopic techniques have been developed that can provide a more detailed analysis of microbial systems, especially when combined with the direct culturing approaches described above.

### **2.3 Nucleic acid techniques**

The extraction and sequencing of nucleic acids from environmental samples and laboratory cultures can be used to provide genetic information regarding the associated microbial consortium. For example, DNA sequencing can reveal the genes present in a sample and RNA sequencing can describe the genes that are actively being transcribed under the conditions studied. A variety of DNA/RNA extraction methods are available and the procedure generally begins with the lysing of cells using chemical and/or physical abrasion, followed by further chemical treatment in order to purify the nucleic acids via the removal of cell debris and contaminants. Methods developed by Griffiths et al., (190) allow for the co-extraction of DNA and RNA from environmental samples within relatively quick timeframes and yield nucleic acids of high purity. A number of commercial kits are also available, such as the DNeasy PowerSoil Kit for use with soil materials and the DNeasy UltraClean Microbial Kit for use with pure cultures, that are tailored to a specific sample type and drastically speed up the process (191). The extraction procedure can prove troublesome in samples with low biomass

or in environmental samples where the pH or the presence of clay minerals and humic acids can interfere (190, 192). Purified DNA or RNA can be sequenced in its entirety as seen within the emerging field of genomics and transcriptomics, or specific regions of the nucleic acids can be targeted for analysis using techniques such as polymerase chain reaction (PCR).

### **2.3.1 Amplicon sequencing**

Following the extraction and purification of genomic DNA (gDNA) or generation of complementary DNA (cDNA) from RNA extracts, PCR can be employed to amplify a specific region of interest. This technique uses a DNA polymerase isolated from *Thermus aquaticus* (193) together with oligonucleotide primers that are complimentary to the 3' ends of the sense and antisense DNA strands within the region of interest. The region of interest is amplified exponentially by subjecting the reaction to heating and cooling cycles in the presence of deoxynucleoside triphosphates (dNTPs) (194), which takes advantage of the thermophilic properties of the DNA polymerase. The 16S rRNA gene is a common target for amplification by PCR within microbial-based studies as it is a highly conserved sequence between prokaryotic species and undergoes very slow evolutionary changes. Consequently, phylogenetic relationships can be constructed based on the comparison of 16S rRNA gene sequences between different microorganisms. Since environmental samples and mixed population microcosms are likely to contain a diverse microbial population composed of different species, the extraction of gDNA from such a sample is likely to result in the presence of multiple different 16S rRNA gene copies.

Following the amplification of the 16S rRNA gene using PCR, techniques such as denaturing gradient gel electrophoresis (DGGE) have been used previously to describe the diversity of microorganisms in a range of environments, including soils (195), paper pulp wastewater (196) and marine environments (197). DGGE separates the PCR products based on their differences in G-C content, with products of low G-C content having hindered mobility through the gel over an increasing chemical gradient. The separated fragments can be excised from the gel and sequenced for downstream comparisons of the 16S rRNA gene. Cloning techniques can also be applied to the amplified DNA fragments in order to obtain a single gene sequence from a mixture of different sequences. This involves the ligation of PCR products to a vector which is then transformed into competent *Escherichia coli* cells. Since one *E.coli* cell is only capable of taking up one plasmid, colonies that have been successfully transformed should only contain multiple copies of the same PCR product (197). The plasmid can then be extracted and the PCR

fragment sequenced to allow for the assignment of phylogeny with the use of databases and search tools, such as the NCBI Basic Local Alignment Search Tool (BLAST). The use of cloning and sequencing techniques has allowed for the characterisation of microbial communities within deep crystalline bedrock, a site which has relevance to the disposal of radioactive waste (198). Uncultured microbial species within environmental samples can be identified using cloning and sequencing strategies (199). Other authors have used this strategy to investigate the microbial community within pH 11.0 ISA degrading microcosms developed from lime contaminated sediments (24). It is important to note that PCR and cloning techniques are subject to bias and error due to the production of chimeras (200), the formation of heteroduplex molecules (201) and Taq polymerase errors (202). Additionally, the primers used for PCR can be biased towards certain microbial species which can result in a large proportion of unamplified DNA and the misrepresentation of a microbiome (203).

### **2.3.2 Next generation techniques**

A range of high throughput techniques are now available that allow for an even more detailed analysis of microbial systems through the generation of millions of copies of 16S rRNA gene sequences. The development of platforms such as Illumina HiSeq has allowed for the sequencing of (meta-) genomes and (meta-) transcriptomes from environmental samples, pure cultures and mixed cultures, which provides a more in-depth description of the genes present and active under the conditions studied. Metabolic pathways can be reconstructed based on the information generated from (meta-) genomes and (meta-) transcriptomes (204) and the sequencing of nucleic acids in their entirety avoids the bias associated with PCR techniques and direct plate counting methods (205). Since many microorganisms are capable of dormancy through processes such as sporulation (206), their detection within an environment based on DNA sequencing may not represent an active community profile. The generation and sequencing of cDNA from 16s rRNA (instead of rDNA) can give an insight into the actively metabolising microbial population within an environment. This approach has been used previously and significant differences were revealed between 16S rRNA and rDNA libraries of microbial communities within the alkaline sediments of Lake Magadi, Kenya (207). The use of metagenomics has been used to uncover the presence of previously undescribed phylogenetic groups in soda lakes (208, 209), and whole-genome sequences can be assembled from metagenomes which can help to elucidate the physiology and ecology of uncultured taxa within an environment (210).

### 2.3.3 Microbial 16S community analysis

Microbial community analysis using next generation sequencing approaches via the 16S rRNA gene can generate large data sets with up to millions of individual sequences. The statistical analysis of these sequences can be undertaken with the use of specialised bioinformatics software packages, such as CLcommunity provided by the sequencing company ChunLab (Korea). Databases, such as EzTaxon or the Ribosomal Database Project can be utilised in order to assign phylogeny to the 16S rRNA gene sequences generated using next generation technologies (211, 212). This is initially achieved by aligning sequences with a reference, such as the Silva reference alignment (213). The aligned sequences can then be compared using search tools, such as the BLAST algorithm (214) and sequence similarity can then be compared with known previously-sequenced microorganisms using different taxonomic levels and confidence intervals (212). Chimeric sequences can be analysed with the use of algorithms, such as UCHIME (215). Sequences can be further assembled into operational taxonomic units (OTUs) based on their sequence similarity to other known organisms, with previous authors using a 95 % confidence interval to group communities within an ISA degrading microcosm operating at pH 9.0 (157). The grouped OTUs can be further analysed using alpha and beta diversity statistics.

Alpha diversity statistics represent the microbial diversity and species richness of an individual sample, whereas beta diversity statistics can be used to analyse the differences between multiple samples. The alpha diversity statistics such as Chao1 and Abundance-based Coverage Estimator (ACE) can be used to determine whether sufficient sequencing depth was achieved during the analysis (216, 217). Chao1 and ACE statistics generate rarefaction curves that plot the number of OTUs against the number of sequence reads and as the number of species left to find reaches saturation, the curve plateaus, indicating sufficient sequencing depth was achieved during sampling. An alternative method for representing how effectively the microbial communities have been sampled is with the use of Rank Abundance curves. This involves ordering the species data along the x-axis from most to least abundant, with the y-axis showing the abundance of each species. Within microbially diverse environments where a high number of species are present, the Rank Abundance curves generally show a sharp initial peak representing a small number of abundant species, which then trails off due to the presence of a large number of species with relatively low abundance (218). The Shannon diversity index can also be used as a quantitative measure that accounts for both abundance and species richness

(219). Alpha diversity statistics have been used previously to determine whether the availability of nutrients has changed the microbial diversity of a site (220).

## 2.4 Microscopic techniques

Microbial systems can be directly visualised with the use of microscopic techniques which enable a greater insight into the system being studied. The high resolution and magnification of instruments such as scanning electron microscopes (SEM) has allowed individual microbial cells and complex biofilm communities to be studied in detail. For example the complex 3D structure of *Pseudomonas fluorescens* biofilms was elucidated using SEM which provides morphological clues for the identification of biofilms *in vivo* (221). SEM can provide information regarding the thickness and heterogeneity of biofilms (222). It has been shown that different strains of *Histophilus somni* produce biofilms with different morphologies that can contain either filamentous structures or mound-shaped colonies embedded in extracellular polymers (223), therefore investigating biofilms with SEM can provide information regarding the associated microbial community. Techniques such as atomic force microscopy (AFM) can be used in conjunction with SEM to characterise the morphological changes of abiotic surfaces brought about by the activity of biofilms. For example, the corrosion pits and crevice attack on 2205 duplex stainless steel by pure cultures of *Desulfovibrio desulfuricans* was visualised using SEM and AFM (224). The elemental composition of microbial systems can be studied by coupling SEM with energy-dispersive X-ray spectroscopy (EDS). SEM-EDS techniques have been employed previously to reveal the bio-mineralisation of gold by *Ralstonia metallidurans* biofilms (225) and to identify the presence of sulphur-containing corrosion products within sulphate reducing biofilms produced by *Desulfovibrio vulgaris* on carbon steel (226).

Microscopy can also be combined with the use of fluorescent stains, a technique that enables the visualisation of individual types of microorganisms or biofilm components within a mixture. Stains which take advantage of the permeability of cell membranes can be used to distinguish between alive and dead cells. For example the combined use of SYTO 9 and propidium iodide stains allowed previous authors to identify the viable cells within spent fuel ponds (227), whereby propidium iodide can only bind to cells with compromised cell membranes. Fluorescent stains have been used to visualise the individual components of biofilms, with previous authors able to observe the polysaccharide, protein, extracellular DNA and lipid fractions of the EPS aggregates simultaneously (228). The composition of the EPS components can give an indication of biofilm functional properties and determine how the EPS

components interact with one another. The use of confocal scanning laser microscopy (CLSM) coupled with fluorescent stains enables the construction of high resolution 3D images of biofilms. CLSM has been used previously to visualise the extracellular components of *Salmonella enterica* biofilms over various stages of growth (229). Oligonucleotide probes that are complimentary to microbial DNA sequences can be ligated with fluorochromes and hybridised to specific cells in a process known as fluorescence *in situ* hybridisation (FISH). The hybridised probes can then be visualised using CLSM based on the fluorochromes specific absorption and emission spectra. FISH has been used by previous authors to distinguish between different microbial groups within coral tissues (230) and to characterise the microbial community of Siberian tundra soil (231).

## **2.5 Summary of chapter**

The development of microcosms from environmental samples provides a means by which microbial processes can be investigated under conditions similar to those expected within an ILW-GDF. The isolation of microorganisms and the characterisation of pure cultures can help to expand our understanding of the microbial processes ongoing within an environment. The development of methods relying on the sequencing of nucleic acids from an environmental sample or laboratory culture has helped to reveal the true microbial diversity of these ecosystems. Microscopic techniques aid with the investigation of microbial systems by allowing their visualisation.

## **3.0 Aims and objectives**

### 3.1 Background

The extent to which microbial activity can proceed in and around a geological disposal facility (GDF) can have a significant impact on the transport of radionuclides, particularly carbon-14. The expected evolution of the near field of an ILW disposal facility and the associated alkaline disturbed zone will have a profound impact on the associated microbial activity. The predicted pH of >12.5 for thousands of years are above that normally associated with even the most extreme alkaliphiles (6). The upper pH limits for microbial activity is a contentious subject, with pH 12.0 being proposed as an upper limit due to the inability of bacteria to maintain the required internal pH of 10.0. However, reports of microbial activity above this value do exist (232, 233). Generally speaking, pure culture investigations provide lower maximum pH values than environmental observations, suggesting that microsites and biofilms may have an important role in attenuating the impact of environmental pH values. Of the microbial processes potentially associated with a GDF, sulphate reduction and methanogenesis are key processes, since they both lead to the complete mineralisation of organic materials such as cellulose degradation products and are able to oxidise molecular hydrogen. The presence of sulphate in many UK ground-waters emphasises the relevance of sulphate reduction (234), whilst methanogenesis has a key role in the transport of carbon-14 due to the generation of highly mobile 14-methane ( $^{14}\text{CH}_4$ ).

The proposed PhD will investigate the maximum pH that sulphate reduction and methanogenesis can proceed under conditions consistent with the near field and associated alkaline disturbed zone of a GDF. Until recently the general consensus has been that carbonates and calcite are not a form of inorganic carbon accessible to microbes. However, recent research focussed on serpentinising systems has demonstrated that aerobic, hydrogen-consuming bacteria operating at pH 11.0 are able to utilise calcite directly (235), potentially by forming low pH microsites on the calcite surface. There have also been some limited investigations of methanogens utilising calcite at neutral-pH (236), showing that methane generation employing calcite as a source of inorganic carbon was possible at a reduced rate.

The proposed research will build on current work on CDP degradation and CDP-fed biofilms where alkaliphilic methanogenic and sulphate reducing systems have been established. Micro-pH probes will be employed to determine the difference between the bulk pH and that experienced within the internal biofilm surface. The proposed research will provide an upper pH boundary for two important biogeochemical processes under conditions relevant to the

cementitious GDF. The data generated may be utilised directly or indirectly by relevant modelling studies and enable a better prediction of gas generation within a GDF.

### **3.2 Primary research questions**

- Can methanogens access precipitated carbonates to drive methane generation?
- Can methanogenic biofilms be established on the surface of cementitious materials?
- Can methanogenic and sulphate reducing biofilms induce the corrosion of stainless steel under ILW-GDF conditions?
- What are the upper pH limits for methanogenesis and sulphate reduction?

### **3.3 Research impacts**

- Provide the upper pH limits for methanogens and sulphate reducing bacteria under simulated near-field conditions, even when biofilms are considered.
- Provide the rates of reaction for methanogenic and sulphate reducing processes that are consistent with model input parameters.
- Underpin current assumptions regarding the impact of carbonation on methanogenesis or provide an alternative conceptual model for future modelling studies.
- Consolidate aspects of the science base on which assumptions regarding gas generation and associated transport processes are based.

### **3.4 Research Objectives**

- Determine the upper pH limits for methanogenesis and examine the primary methanogenic pathways utilised under alkaline conditions, using alkali-adapted communities from anthropogenic alkaline sites as inoculum.
- Determine the potential for sulphate-reducing communities to corrode stainless steel under alkaline conditions using CDP as the sole carbon and energy source
- Determine the potential for calcium carbonate to be used as substrate for hydrogenotrophic methanogenesis under alkaline conditions.

# 4.0 Experimental Methodologies

## 4.1 General Reagents

Unless indicated otherwise all reagents used for the following experimental methodologies were purchased from either Sigma-Aldrich Co. Ltd (Gillingham, Dorset, UK), Fisher Scientific UK (Loughborough, Leicestershire, UK) or LabM Limited (Haywood, Lancashire, UK).

## 4.2 Culture Media

### 4.2.1 Mineral Media

Mineral media was prepared as described previously (237) with the following amendments. The reagents listed in Table 4.1 and Table 4.2, except for disodium sulphide nonahydrate ( $\text{Na}_2\text{S}\cdot 9\text{H}_2\text{O}$ ), were mixed with 500 mL of ultra-pure water in a 500 mL Schott bottle. The solution was purged with  $\text{N}_2$  for approximately 20 minutes, followed by the addition of  $\text{Na}_2\text{S}\cdot 9\text{H}_2\text{O}$  whilst maintaining the nitrogen purging for a further 10 minutes. The pH of the media for alkaline microcosms (pH 9.0-11.0) was achieved using the appropriate amounts of sodium bicarbonate and sodium carbonate buffers as listed in Table 4.2. The pH was measured and if necessary adjusted using 2 M sodium hydroxide and 2 M hydrochloric acid whilst purging with  $\text{N}_2$ . The solution was autoclaved under a nitrogen headspace at 121°C for 20 minutes, then allowed to cool under a  $\text{H}_2/\text{N}_2$  (10:90) headspace by which point the oxygen indicator (resazurin) had turned clear, indicating the media was chemically reducing. Bicarbonate/carbonate buffers were not used for the calcium carbonate amended microcosms, instead the pH was adjusted as desired using 2 M sodium hydroxide and 2 M hydrochloric acid.

**Table 4.1 Mineral media composition per litre**

Reagent	Chemical Formula	Concentration (g/L)
Potassium dihydrogen phosphate	$\text{KH}_2\text{PO}_4$	0.270
Disodium hydrogen phosphate dodecahydrate	$\text{Na}_2\text{HPO}_4 \cdot 12\text{H}_2\text{O}$	1.120
Ammonium chloride	$\text{NH}_4\text{Cl}$	0.530
Calcium chloride dihydrate	$\text{CaCl}_2 \cdot 2\text{H}_2\text{O}$	0.075
Magnesium chloride hexahydrate	$\text{MgCl}_2 \cdot 6\text{H}_2\text{O}$	0.100
Iron(II) chloride tetrahydrate	$\text{FeCl}_2 \cdot 4\text{H}_2\text{O}$	0.020
Resazurin (oxygen indicator)	$\text{C}_{12}\text{H}_7\text{NO}_4$	0.001
Disodium sulphide nonahydrate	$\text{Na}_2\text{S} \cdot 9\text{H}_2\text{O}$	0.500
10ml Trace elements solution	See Table 4.3	See Table 4.3

**Table 4.2 Carbonate/bicarbonate buffer composition per litre**

Reagent	Chemical Formula	Concentration at pH 9.0 (g/L)	Concentration at pH 10.0 (g/L)	Concentration at pH 11.0 (g/L)
Sodium carbonate	$\text{Na}_2\text{CO}_3$	2.86	17.16	25.76
Sodium bicarbonate	$\text{NaHCO}_3$	7.56	3.36	0.84

**Table 4.3 Trace element solution composition per litre**

Reagent	Chemical Formula	Concentration (g/L)
Manganese chloride tetrahydrate	$\text{MnCl}_2 \cdot 4\text{H}_2\text{O}$	0.050
Boric acid	$\text{H}_3\text{BO}_3$	0.005
Zinc chloride	$\text{ZnCl}_2$	0.005
Copper chloride	$\text{CuCl}_2$	0.003
Disodium molybdate dihydrate	$\text{Na}_2\text{MoO}_4 \cdot 2\text{H}_2\text{O}$	0.001
Cobalt chloride hexahydrate	$\text{CoCl}_2 \cdot 6\text{H}_2\text{O}$	0.100
Nickel chloride hexahydrate	$\text{NiCl}_2 \cdot 6\text{H}_2\text{O}$	0.010
Disodium selenite	$\text{Na}_2\text{SeO}_3$	0.005
Disodium tungstate	$\text{Na}_2\text{WO}_4 \cdot 2\text{H}_2\text{O}$	0.002

#### **4.2.2 Synthesis of cellulose degradation products (CDP)**

Cellulose degradation products (CDP) were synthesised as described previously (22). 1.8 L of 0.1 M sodium hydroxide and 10 g/L calcium hydroxide was purged with N<sub>2</sub> inside a pressure vessel for 20 minutes prior to the addition of 200g of laboratory tissue (Pristine Paper Hygiene, UK). The vessel was sealed and the headspace was purged with N<sub>2</sub> for a further 30 minutes to remove oxygen, followed by incubation at 80°C for 30 days. After the incubation the resulting solution was filtered through a 0.22 µm filter unit (Millipore, UK) within an oxygen-free glovebox that had been purged with nitrogen for approximately 20 minutes. The filtrate was stored in the dark at 4 °C within autoclaved and nitrogen purged Schott bottles.

#### **4.3 Liquid sample preparation**

Unless stated otherwise, microcosm liquid or environmental sample liquid requiring analysis were transferred to sterile Eppendorf tubes (1.5 mL) or Falcon tubes (50 mL) prior to centrifugation at 8000 RPM for 10 minutes to pellet the solids. The supernatant was filtered through a 0.45 µm syringe filter (Millipore, UK) into sterile tubes and stored at -20 °C for long term storage if necessary prior to analysis.

#### **4.4 Analytical Methodologies**

##### **4.4.1 High performance anion exchange chromatography with pulsed amperometric detection (HPAEC-PAD)**

A Dionex 3000 or 5000 ion chromatography system employing HPAEC-PAD was used to detect and quantify the alpha, beta and xylo forms of isosaccharinic acid (ISA) as described previously (24). 50 mM NaOH was used as an isocratic mobile phase with a flow rate of 0.5 mL/min and the injected analyte (10µL) was separated using a Dionex CarboPac PA20 column (250 mm length, 3 mm internal diameter, 6 µm particle size with a 10 Å pore size). The column was regenerated between the analyses of each sample via the elution of 200 mM sodium hydroxide for 20 minutes. Before analysis D-ribonic acid was added to each sample as an internal standard to a final concentration of 40 ppm. Calibration curves were used for the quantification of ISA after preparing pure forms of alpha, beta and xylo isosaccharinic acid as

described previously (238, 239). Chromatograms were integrated and processed using the Chromeleon 7.0 software package.

#### **4.4.2 Gas chromatography**

##### ***4.4.2.1 Volatile fatty acid analysis***

A HP GC6890 (Hewlett Packard, UK) gas chromatograph fitted with an auto-sampler was used for the detection and quantification of volatile fatty acids (VFA) as described previously (24). Samples were acidified prior to analysis by the addition of 85% phosphoric acid (10% v/v) followed by injection of 1µL acidified sample into the system. Helium was used as carrier gas which passed the sample through a HPFFAP column (30 m x 0.535 mm x 1.00 µm; Agilent Technologies, UK). A flame ionisation detector using a hydrogen/compressed air blend was used to detect VFA's under the following conditions: initial temperature of 95 °C for 2 minutes, followed by an increase to 140 °C at a ramp rate of 10 °C min<sup>-1</sup> with no hold, followed by a second ramp to 200 °C at a ramp rate of 40 °C min<sup>-1</sup> with a hold of 10 minutes, falling to a post run temperature of 50 °C. A standard mix of VFA's (Supelco analytical, US) was used to identify and quantify VFA's within the samples and the Chemstation software package (Agilent Technologies, UK) was used to process chromatograms.

##### ***4.4.2.2 Headspace gas analysis***

The headspace gas composition of microcosms was analysed using an Agilent GC6850 equipped with HP-PLOT/Q column with particle traps (35 m x 0.32 mm x 20 µm, Agilent Technologies, UK). Pressure lock syringes were used to remove 100 µL of headspace gas prior to injection into the column using nitrogen as carrier gas. Gas species were detected using a thermal conductivity detector operating under the following conditions: initial temperature of 60 °C for 2 minutes, followed by an increase to 120 °C at a ramp rate of 30 °C min<sup>-1</sup> with a detector temperature of 250 °C. A handheld digital manometer (TPI, UK) was used to measure the gas headspace pressure and gases were quantified using standards of known concentration along with the ideal gas law shown in Equation 4.1.

#### **Equation 4.1. The ideal gas law.**

$$PV = nRT$$

P = Pressure (bar),

V = Volume (L),

n = Moles of gas (mol),

R = Universal gas constant (8.314 L bar K<sup>-1</sup> mol<sup>-1</sup>),

T = temperature of gas (K)

#### **4.4.3 Determination of dissolved organic and inorganic carbon**

Dissolved organic carbon (DOC) and dissolved inorganic carbon (DIC) concentrations were determined with a Shimadzu TOC5000A (Shimadzu, Japan) employing nitrogen as carrier gas at a rate of 150 mL min<sup>-1</sup>. Prior to analysis samples were filtered through a 0.45 µm syringe filter (Millipore, UK) and diluted 10-fold in ultrapure water if sample volumes were insufficient for analysis or concentrations were above the limits of detection. Total carbon (TC) was quantified against a standard curve of potassium hydrogen phthalate in ultrapure water and dissolved inorganic carbon (DIC) was quantified against a standard curve of sodium carbonate and sodium bicarbonate in ultrapure water. The dissolved organic carbon (DOC) was calculated from the difference between total carbon and dissolved inorganic carbon as per the following equation: TC – DIC = DOC.

#### **4.4.4 Ion chromatography**

##### ***4.4.4.1 Sulphate, nitrate and chloride quantification***

Sulphate, nitrate and chloride analysis was carried out by ion chromatography employing a Thermofisher ICS-5000, Dionex IonPac AS14 column. 10 µl samples were injected into the system which used a 3.5 mM Na<sub>2</sub>CO<sub>3</sub>/ 1.0 mM NaHCO<sub>3</sub> eluent at a flow rate of 1.2 mL/min. Analytes were detected via conductivity detection following suppression by Dionex AERS in auto-suppression recycle mode.

#### **4.5 Environmental sample analysis**

##### **4.5.1 Extraction of volatile fatty acids**

Extractable VFA's were determined from environmental sediment samples by the addition of 1g of sample to 10 mL of 85 % (v/v) phosphoric acid, followed by vortexing and incubating at room temperature for 24 hours. The resulting mixture was centrifuged for 10 minutes at 8000

RPM and the concentration of VFA's in the supernatant was determined via gas chromatography as described in Section 4.4.2.1.

#### **4.5.2 Metal analysis of pore waters via inductively coupled plasma mass spectrometry**

Pore-waters retrieved from the sampling sites were filtered through a 0.45 µm filter (Millipore, UK) and diluted 100-fold in ultrapure water containing trace-metal concentrated nitric acid (10 % v/v). Inductively coupled plasma mass spectrometry (ICP-MS) was used to measure the dissolved metals using an Agilent 7900 ICP-MS in Spectrum Analysis acquisition mode. Mixed element stock solutions (CCS-2, CCS-4 and CCS-6, Inorganic Ventures) were prepared to a final concentration of 100 ppb in ultrapure water and trace-metal concentrated nitric acid (10 % v/v) to generate a calibration curve. The stock solution contained the following elements: Ag, Al, As, Au, Ba, Be, Bi, Ca, Cd, Co, Cr, Cs, Cu, Fe, Ga, Hg, In, Ir, K, Li, Mg, Mn, Na, Ni, Pb, Pd, Pt, Rb, Rh, Ru, Se, Sr, Tl, V and Zn. Additionally a blank solution containing ultrapure water and the trace-metal nitric acid (10 % v/v) was run alongside as a negative control.

#### **4.5.3 Thermal gravimetric analysis**

In order to determine the levels of free-water, organic content and inorganic content of environmental sediment samples, thermal gravimetric analysis (TGA) was carried out using a TGA 1 (Mettler Toledo). Samples were heated over a defined temperature range and the associated mass losses were recorded. Samples (wet weight) were transferred to 70 µl alumina crucibles and heated at 10 °C min<sup>-1</sup>, from 25 °C to 1000 °C under a nitrogen atmosphere. Sample sizes varied from 14.8 mg to 37.0 mg of material. Mass losses were recorded using the STARE software package.

#### **4.5.4 Simultaneous thermogravimetry mass spectrometry (TG-MS)**

Thermal gravimetric analysis coupled to mass spectrometry (TG-MS) was used to further investigate the sediment samples. This technique gathers additional information compared with TGA, since the gases released from the samples can be measured as it is heated. Samples were analysed using a Mettler Toledo TGA/SDTA851e thermobalance. Temperature calibration was achieved following the manufacturer's recommendations using the SDTA melting point signal for indium and aluminium (calibration standard purity, 99.999%). Prior to TG-MS analysis, all samples were dried for 24 hours at 110 °C to remove excess water. The samples were then ground and passed through a sieve to ensure all particles were less than 100 µm in size. Each

sample was weighed to approximately 10 mg and placed within alumina crucibles and subjected to a temperature ramp of 10 °C min<sup>-1</sup> from 30 to 800 °C. The sample was kept under an atmosphere of dry air flowing at 70 mL min<sup>-1</sup>. The evolved gas products were analysed online using a Hiden HPR20 quadrupole mass spectrometer coupled to the thermobalance through a custom made interface. The products were transferred to the mass spectrometer through a heated silica capillary line. Ionisation of gaseous products were made through electron ionisation and detected using a Faraday detector. Selected ion monitoring was acquired at an interval of 200 ms per scan for the 44 Da signal assigned to the release of CO<sub>2</sub>.

#### **4.5.5 pH determination**

The pH of liquid media, microcosm fluid and liquid environmental samples were determined using a portable handheld pH meter with electrodes (Mettler Toledo, UK), calibrated using pH 4.0, 7.0 and 10.0 buffers. The pH of sediment samples and solid environmental samples were measured using standard methods as per BS ISO10390:2005 (240).

#### **4.6 Dissolved sulphide determination**

A micro ion electrode (LIS-146AGSCM, Lazar research laboratories Inc, US) together with a handheld mV unit were used to determine the concentration of dissolved sulphide against a standard curve of sodium sulphide nonahydrate.

#### **4.7 X-ray diffraction**

X-ray powder diffraction (XRD) was carried out using a D2 PHASER X-ray diffractometer (Bruker). Samples were dried at 80 °C for 24 hours, prior to being homogenised using a pestle and mortar, then transferred to the sample holder and scanned for 3 minutes. Diffraction patterns were monitored and processed using DIFFRAC Measurement Centre V4.

#### **4.8 Surface area analysis**

Surface area analysis of the various forms of calcium carbonate was performed using a micromeritics ASAP 2020 surface analyser. Samples were powdered by mechanical grinding. The powdered samples were dried prior to analysis by holding them isothermally for 24 hours at approximately 110 °C. Each sample was then allowed to cool to room temperature and stored in glass wrapped in parafilm to prevent further moisture reuptake. Each sample was weighed directly *in situ* using the instruments analysis cells, a fixed volume reducing insert was added

to assist with the analysis. All three samples were degassed under the following conditions; 60 minutes at 90 °C, under high vacuum, then 600 minutes at 250 °C, under high vacuum. Each sample was then back filled using nitrogen. Samples were left on the degas stage and transferred directly to the analysis stage immediately before analysis to prevent minimal contact with the atmosphere. The BET surface area measurements were taken at relative pressure ( $P/P^0$ ) measurements between 0.06 and 0.24.

#### 4.9 PHREEQC analysis

Geochemical modelling was undertaken to determine the concentration of total calcium and dissolved inorganic carbon (DIC) using the PHREEQC program after equilibration with calcite between pH 7.0 – 12.0. The modified minteqplus database was used under the conditions outlined in Table 4.4, which is an ion speciation and solubility database.

**Table 4.4. PHREEQC modelling input data (x = 7, 8, 9, 10, 11 and 12)**

```
SOLUTION 1
    temp      25
    pH        x
    pe        4
    redox     pe
    units     mmol/kgw
    density   1
    B         1.6 uMol/kgw
    Ca        0.05
    Cl        14.34
    Cu(2)     0.4 uMol/kgw
    Fe(2)     0.05
    K         1.98
    Mg        0.49
    Mn(2)     29.5 uMol/kgw
    N(-3)     9.9
    Na        6.27
    Ni        1.2 uMol/kgw
    P         5.11
    Se(4)     0.12 umol/kgw
    Zn        6.4 umol/kgw
    -water    1 # kg
EQUILIBRIUM_PHASES 1
    Calcite   0 10
```

## **4.10 Microscopy techniques**

### **4.10.1 Sample preparation**

Unless stated otherwise, biological samples were fixed in 4% paraformaldehyde in PBS at 4°C for 24 hours. Samples were centrifuged at 8000 RPM for 5 minutes and the pellet was washed with PBS twice to remove paraformaldehyde. Samples were subsequently stored at -20 °C until use in a storage buffer composed of 250 mL of 96% ethanol (v/v), 140 mL ultrapure water and 10 mL of 1 M TRIS-HCl (pH 7.5).

### **4.10.2 Scanning electron microscopy and elemental analysis**

A Quanta FEG 250 (FEI, USA) microscope with an electron dispersive X-ray spectroscopy (EDS) was used for the analysis of samples via scanning electron microscopy. Samples were dehydrated prior to analysis using a series of ethanol dilutions between 25, 50, 75 and 100% for 2 minutes on each step. Samples were then sputter coated via a gold palladium plasma (CA7625 Polaron, Quorum Technologies Ltd, UK).

### **4.10.3 Confocal laser scanning microscopy**

Confocal laser scanning microscopy (CLSM) of samples was performed either at the Bioimaging facility at the University of Huddersfield, UK, or at the Bioimaging Centre at Leeds University, UK. A Zeiss LSM880 inverted confocal microscope was used for the imaging and images were processed using Zen 2.1 software (Zeiss Microscopy).

#### ***4.10.3.1 Five colour biofilm imaging***

Extracellular polymeric substances (EPS) were stained and visualised using previously described methods (228). Nile red was used for the visualisation of lipids and hydrophobic sites.  $\alpha$ -mannopyranosyl and  $\alpha$ -glucopyranosyl sugars were visualised with Concanavalin A, Tetramethylrhodamine Conjugate (ConA). Protein was visualised using FITC.  $\beta$ -1,4 and  $\beta$ -1,3 polysaccharides were visualised using calcofluor white. Total cells and extracellular DNA was visualised using Syto 63. Table 4.5 shows the concentration, staining times and absorption/emission spectra for each component. Negative controls were performed on

materials not exposed to stains to indicate auto-fluorescence and samples were kept hydrated throughout the procedure.

**Table 4.5. Properties of the stains used for visualisation of biofilm materials**

Stain	Concentration	Time (minutes)	Excitation (nm)	Emission (nm)
Calcofluor white	30 mg L <sup>-1</sup>	30	400	410 - 480
ConA	25 mg L <sup>-1</sup>	30	543	550 - 600
FITc	100 mg L <sup>-1</sup>	60	488	500 - 550
Nile red	0.6 mg L <sup>-1</sup>	10	514	625 - 700
Syto 63	2µM	30	633	650 - 700

#### 4.10.3.2 Fluorescence *in situ* hybridisation

Fluorescence *in situ* hybridisation (FISH) was performed using previously described methods (230). The buffer used for the hybridisation was composed of 0.9 M NaCl, 0.01 % SDS, 0.01 M TrisHCl (pH 7.2) and 35 % formamide, with all probes used at a final concentration of 5 ng/µL. The hybridisation was conducted at 46 °C for 1.5 hours, followed by a 10 minute wash in a buffer composed of 0.08 M NaCl, 0.01 % SDS and 0.01 M Tris-HCl (pH 7.2) at 46 °C. The details of each probe is shown in Table 4.6, with all probes manufactured by MWG operons. Negative controls were performed on materials not exposed to stains to indicate auto-fluorescence.

**Table 4.6. Details of oligonucleotide FISH probes**

Probe	Target	Oligonucleotide sequence 5' → 3'	Fluorochrome	Excitation (nm)	Emission (nm)	Reference
<b>ARC915</b>	Archaea	GTGCTCCCCGCCAATTCCT	CY3	548	561	(241)
<b>EUB338</b>	Eubacteria	GCTGCCTCCCGTAGGAGT	FAM	494	519	(241)
<b>LGC354</b>	Firmicutes	TGGAAGATTCCTACTGC	FITC	494	519	(242)
<b>Delta495</b>	Deltaproteobacteria	AGTTAGCCGGTGCTTCCT	ATTO 425	439	485	(243)
<b>Bac303</b>	Bacteroidetes	CCAATGTGGGGGACCTT	ATTO 610	616	633	(244)

#### 4.10.4 Atomic force microscopy

Atomic force microscopy (AFM) was carried out using a Dimension® Icon™ Scanning Probe Microscope (Bruker) with ScanAsyst. A triangular probe was used (SCANASYST-AIR,

Bruker) with the following specifications: resonant frequency 70 kHz, spring constant 0.4 N/m, length 115  $\mu\text{m}$ , width 25  $\mu\text{m}$ . The software package NanoScope Analysis (Bruker) was used for image processing.

#### **4.10.5 Alicona microscopy**

3D surface characterisation of steel coupons was carried out using an Alicona EdgeMaster G4 instrument at 100x magnification. The instrument uses focus variation and has a vertical resolution of 10 nm. Alicona software was used to process the images and Replica mode was applied when viewing replicated steel surfaces.

##### ***4.10.5.1 Replication of steel surfaces***

The surfaces of steel coupons was replicated using Microset 202 (Microset, UK), which is a high resolution (50 nm) replication compound. The material was prepared to the manufacturer's instructions, then applied to the steel surface and allowed to set for 5 minutes, before being removed and visualised using Alicona instruments (Section 4.10.5).

#### **4.10.6 Light microscopy**

Images of the phenolphthalein-stained NRVB surfaces were taken using a VHX-6000 series digital microscope (Keyence). The Keyence software package was used to process the images.

### **4.11 Molecular Biology**

#### **4.11.1 Extraction and purification of nucleic acids**

##### ***4.11.1.1 DNA/RNA co-extraction method***

A modified version of the Griffiths method (190) was used to extract genomic DNA and RNA from microcosms and environmental samples. Liquid samples (50 mL) were centrifuged at 5000 RPM for 30 minutes to pellet the biological material. Approximately 45 mL of supernatant was discarded and the pellet was re-suspended in the remaining supernatant volume. 0.5 mL of the re-suspended pellet fluid was added to a glass bead tube containing 0.1 mm glass beads (Cambio, UK) along with 0.5 mL of cetyl-trimethylammonium bromide (CTAB), 0.5 mL of phenol chloroform isoamyl alcohol (25:24:1) and 0.1 mL of  $\beta$ -mercaptoethanol (RNase inhibitor). If the sample was solid approximately 0.5 g of material

was added to the bead tube in the same fashion as liquid samples. CTAB was prepared by mixing 10 % (w/v) cetyl-trimethylammonium bromide in 0.7 M sodium chloride and 240 mM phosphate buffer, followed by diluting 50:50 in 240 mM phosphate buffer (pH 8.0). The bead tube was homogenised using a BeadBlaster™ 24 at 5.5 m/s for 60 seconds followed by centrifuging the tube at 13,000 RPM for 5 minutes. Following the centrifugation the upper layer of supernatant (approximately 450 µL) was removed and added to an Eppendorf tube (1.5 mL) containing an equal volume of chloroform/isoamyl alcohol (24:1), followed by vortexing the mixture for 30 seconds. The tube was centrifuged at 13,000 RPM for 5 minutes and the upper layer of supernatant (approximately 450 µL) was removed and added to a fresh Eppendorf tube as described above. Different methods were applied to precipitate RNA and DNA. For DNA the supernatant acquired in the previous step was mixed with two volumes of 30 % (w/v) polyethylene glycol-6000 in 1.6 M sodium chloride and incubated for 24 hours at 4 °C. If RNA was required then the supernatant was instead mixed with two volumes of ice cold molecular grade absolute ethanol together with 1/10<sup>th</sup> the volume of DNA suspension of 3 M sodium acetate and incubated at -20 °C for 2 hours. The shorter incubation times and lower temperatures used for the precipitation of RNA was employed to reduce the risk of RNA degradation. Following the incubation period tubes were centrifuged at 13,000 RPM for 20 minutes and the complete volume of supernatant was discarded. The pellet was washed with 200 µL ice cold molecular grade absolute ethanol and centrifuged for 5 minutes at 13,000 RPM. The ethanol was then removed and the pellet allowed to air dry for 10 minutes or until visibly dry, followed by re-suspending the pellet in DNase/RNase free ultra-pure water. Reagents were made DNase/RNase free by incubating overnight at 37 °C with 0.1 % diethylpyrocarbonate followed by autoclaving at 121 °C for 20 minutes.

#### ***4.11.1.2 Extraction of DNA using MO-BIO PowerSoil® kit***

DNA from calcium carbonate microcosms and alkaline sediment samples was extracted using the PowerSoil® DNA extraction kit (MO-BIO, US) to the manufacturer's instructions. This extraction method includes steps for the removal of humic substances and calcium ions which appeared to interfering with purification of nucleic acids using the Griffiths method outlined above. For the calcium carbonate reactors the microcosm fluid was first passed through a 0.45 µm filter. The filter paper was retained and cut into pieces using sterile scissors. Approximately 0.25 g of filter paper or 0.25 g of sediment sample (wet weight) was added to the PowerBead tube, together with 60 µL of solution C1 (lysis solution), followed by vortexing and

homogenising using a BeadBlaster™ 24 at 5.5 m/s for 60 seconds. The tubes were centrifuged at 10,000 RPM for 60 seconds, followed by transferring the supernatant to a clean 2 mL Eppendorf tube. 250 µL of solution C2 was added to the tube, followed by incubation at 4 °C for 5 minutes to remove humic substances. Tubes were centrifuged for 60 seconds at 10,000 RPM, followed by transferring the supernatant to a clean 2 mL Eppendorf tube. 200 µL of solution C3 was added to the tube and incubated for 5 minutes at 4 °C. Tubes were centrifuged at 10,000 RPM for 60 seconds and the supernatant was mixed with 1.2 mL of solution C4 in a fresh collection tube, followed by centrifugation at 10,000 RPM for 60 seconds through a silica membrane column. Solution C5 was added to wash the filter via centrifugation for 60 seconds at 10,000 RPM. After all ethanol had been removed from the filter, 30 µL of solution C6 was applied to the membrane and the purified DNA was eluted via centrifugation at 10,000 RPM for 60 seconds.

#### ***4.11.1.3 Purification of RNA***

The DNase I kit (Invitrogen™) was used to enzymatically digest the DNA from the mixture of RNA/DNA (extracted using the Griffiths method outlined above) in order to isolate the RNA. Briefly, the sample of RNA/DNA was made up to a volume of 8 mL using DNase/RNase free water, followed by the addition of 1 mL 10X reaction buffer (provided) and 1 mL DNase I (1 unit mL<sup>-1</sup>). The sample was mixed gently via pipetting and incubated for 15 minutes at room temperature. DNase was removed and RNA was purified using the RNeasy MinElute Cleanup Kit (Qiagen) as per the manufacturer's instructions.

#### ***4.11.1.4 Quantification of nucleic acids***

Nucleic acids were quantified using either a Jenway Genova nano spectrophotometer (Bibby Scientific, UK) or using a Qubit™ 4 fluorometer. For spectrophotometric quantification samples (1 µL) were exposed to UV light at 260 nm and the purity ratios of the sample was determined based on the extinction coefficient for DNA and RNA. For fluorometric quantification the Qubit™ dsDNA HS Assay Kit or Qubit™ RNA HS Assay Kit was used to the manufacturers instructions.

#### ***4.11.1.5 Visualisation of nucleic acids***

Gel electrophoresis was employed to visualise genomic DNA and RNA via the use of 1 % agarose gels prepared in tris-acetate EDTA buffer (TAEB). The 1 % agarose solution prepared

in TAE buffer was melted by microwaving, to which 1  $\mu\text{L}$  of SYBR® safe stain was added before pouring the solution into plastic moulds and being allowed to set at room temperature. After setting the gel was immersed in TAE buffer and genomic DNA/RNA (5  $\mu\text{L}$ ) was mixed with 1  $\mu\text{L}$  of 5X loading dye (BioLone, UK) by pipetting, followed by inserting the mixture into each well along with a 1-10 kb ladder (Hyperladder 1kb, BioLone, UK). The gel was subjected to electrophoresis at 100 V for 60 minutes then visualised under UV light prior to recording the image using the BioDoc-It® 210 imaging system (UVP LLC, US).

#### **4.11.2 Polymerase chain reaction (PCR)**

##### ***4.11.2.1 Hot start PCR for 16S rRNA gene amplification***

A hot start PCR method was employed to reduce the chance of primer dimer formation and non-specific amplification. MyTaq™ HS red mix (BioLone, UK) was used to generate PCR products for analysis via the Illumina MiSeq platform, which contained the reaction buffer, dNTPs, magnesium and Taq polymerase. The reaction was generically composed of the MyTaq™ HS red mix (25  $\mu\text{L}$ ), template genomic DNA/cDNA (10-100 ng), together with forward and reverse primers (2  $\mu\text{L}$  of each at 20  $\mu\text{M}$ ) and topped up to a final reaction volume of 50  $\mu\text{L}$  using DNase/RNase free water. Reaction tubes were placed into a thermocycler and run under the following conditions: initial denaturation at 95 °C for 1 minute, followed by 30 cycles of denaturation at 95 °C for 15 seconds, annealing at 60 °C for 30 seconds, extension at 72 °C for 15 seconds followed by a final extension at 72 °C for 2 minutes. Following the thermocycler run the samples were maintained at 4 °C before use in downstream applications. Positive controls for the PCR reactions used genomic DNA extracted from *Pseudomonas aeruginosa* cultured in the laboratory and *Methanobacterium bryantii* (DSMZ 863), with negative controls run without genomic DNA. The visualisation of PCR products was undertaken via electrophoresis on 2 % agarose gels for 45 minutes at 100 V.

**Table 4.7. Primers used for the amplification of the 16S rRNA gene and microbial community analysis**

Primer	Target	Sequence 5' → 3'	16S region	Reference
<b>341f</b>	Eubacteria & Archaea	TCGTCGGCAGCGTCAGATGTGTATAAGAGACAG CCTACGGGNGGCWGCAG	V4	(245)
<b>805r</b>		GTCTCGTGGGCTCGGAGATGTGTATAAGAGACA G GACTACHVGGGTATCTAATCC	V4	
<b>519f</b>	Archaea	TCGTCGGCAGCGTCAGATGTGTATAAGAGACAG CAGCCGCCGCGGTAA	V4	(246)
<b>958r</b>		GTCTCGTGGGCTCGGAGATGTGTATAAGAGACA GYCCGGCGTTGAMTCCAATT	V4	(247)

#### **4.11.2.2 Purification of PCR products**

The Qiaquick PCR purification kit (Qiagen, UK) was used to purify PCR products for downstream applications by following the manufacturer's instructions. Briefly, the PCR products were bound to a silica membrane via centrifugation at 10,000 RPM after conversion to a salt via the addition of 5 volumes of buffer (supplied) and 10 µL of 3 M sodium acetate. The bound PCR products were cleaned of redundant materials (primers, polymerases) using an ethanol-based wash buffer, prior to eluting from the column using RNase/DNase free water and centrifugation.

#### **4.11.2.3 Primer synthesis**

All primers were synthesised commercially by MWG Operons and prepared to a final stock concentration of 100 pmol/µL using the instructions on the synthesis report.

#### **4.11.3 cDNA synthesis**

cDNA was generated from isolated RNA using the Tetro cDNA Synthesis Kit (Bioline, UK). Briefly, between 10-100 ng of RNA was added to 1 µL random hexamer mix, 1 µL 10 mM dNTPs, 1 µL Tetro reverse transcriptase (200 U µL<sup>-1</sup>), 4 µL 5x RT buffer and 1 µL RiboSafe RNase inhibitor with a final volume of 200 µL achieved using RNase/DNase grade water. Samples were then incubated at 25 °C for 10 minutes, followed by heating for 30 minutes at 45

°C. The reaction was terminated by incubating the samples for 5 minutes at 85 °C. Samples were then stored until use at -20 °C.

#### 4.11.4 Microbial community analysis via Illumina MiSeq platform

The MiSeq nano platform (Illumina, USA) was used for the sequencing of PCR products and genomic DNA using the commercial service provided by ChunLab (South Korea). The pipeline for sequencing began with the generation of PCR amplicons from genomic DNA followed by the barcoding of these amplicons via an index PCR technique. The PCR amplicons were run via the MiSeq nano platform at 250bp paired ends after being purified and quantified. PandaSeq was used to merge paired ends (248) and the UCHIME algorithm was used to identify and remove chimeric sequences (215). The EzTaxon database was used to assign sequence phylogeny (211) and CD-HIT-EST used to perform OTU clustering at a 95 % confidence interval (249). The CLcommunity software suite (ChunLab, South Korea) was used to assign alpha diversity statistics, rank abundance curves and Rarefaction curves.

##### 4.11.4.1 Additional bioinformatics analysis

Heat-maps and principal components analysis (PCA) was undertaken using ClustVis (250).

#### 4.11.5 Microbial community BioProject accession numbers

**Figure 4.8. Microbial community BioProject accession numbers**

Sample	BioProject Accession	BioSample Accession
Buxton Background	PRJNA524631	SAMN11037403
Horton Background		SAMN11037404
Tarmac Background		SAMN11037405
LK Background		SAMN11037406
Canal Background		SAMN11037407
ConsettWetland Background		SAMN11037408
ConsettStream Background		SAMN11037409
Redcar Background		SAMN11037410
Scunthorpe Background		SAMN11037411
Buxton Alkaline		SAMN11044315
Horton Alkaline		SAMN11044316
Tarmac Alkaline		SAMN11044317
LK Alkaline		SAMN11044318
Canal Alkaline		SAMN11044319
ConsettWetland Alkaline		SAMN11044320

ConsettStream Alkaline		SAMN11044321
Redcarb Alkaline		SAMN11044322
Scunthorpe Alkaline		SAMN11044323
Buxton Cotton		SAMN11044324
Horton Cotton		SAMN11044325
Tarmac Cotton		SAMN11044326
ConsettWetland Cotton		SAMN11044327
ConsettStream Cotton		SAMN11044328
Redcar Cotton		SAMN11044329
Scunthorpe Cotton		SAMN11044330
Canal pH 7 CDP	PRJNA525260	SAMN11044343
Buxton pH 7 CDP		SAMN11044344
Tarmac pH 7 CDP		SAMN11044345
Horton pH 9 CDP		SAMN11044346
Canal pH 8 CDP		SAMN11044347
Buxton pH 8 CDP		SAMN11044348
Tarmac pH 8 CDP		SAMN11044349
Horton pH 10 CDP		SAMN11044350
Canal pH 9 CDP		SAMN11044355
Buxton pH 9 CDP		SAMN11044356
Tarmac pH 9 CDP		SAMN11044357
Horton pH 11 CDP		SAMN11044358
Canal pH 10 CDP		SAMN11044359
Buxton pH 10 CDP		SAMN11044360
Tarmac pH 10 CDP		SAMN11044361
Canal pH 7 H2		SAMN11044362
Buxton pH 7 H2		SAMN11044363
Tarmac pH 8 H2		SAMN11044364
Horton pH 9 H2		SAMN11044365
Canal pH 8 H2		SAMN11044366
Buxton pH 8 H2		SAMN11044367
Tarmac pH 9 H2		SAMN11044368
Horton pH 10 H2		SAMN11044369
Canal pH 9 H2		SAMN11044370
Buxton pH 9 H2		SAMN11044371
Tarmac pH 10 H2		SAMN11044372
Horton pH 11 H2		SAMN11044373
Canal pH 10 H2		SAMN11044374
Buxton pH 10 H2		SAMN11044375
Tarmac pH 8 ACE		SAMN11044376
Canal pH 7 ACE		SAMN11044377
Buxton pH 7 ACE		SAMN11044378
Canal pH 8 ACE		SAMN11044379
Canal pH 9 ACE		SAMN11044380
LK pH 7		SAMN11044382
Con Wet pH 7		SAMN11044383
Con Stream pH 7		SAMN11044384
Redcar pH 7		SAMN11044385

Scunthorpe pH 7		SAMN11044386
LK pH 10		SAMN11044387
Con Wet pH 10		SAMN11044388
Con Stream pH 10		SAMN11044389
Redcar pH 10		SAMN11044390
Scunthorpe pH 10		SAMN11044391
304BF CDP	PRJNA524633	SAMN11044394
316BF CDP		SAMN11044395
Bulk CDP		SAMN11044396
304BF CDP+SO4		SAMN11044397
316BF CDP+SO4		SAMN11044398
Bulk CDP+SO4		SAMN11044399
Bux CaCO3 Powder	PRJNA525266	SAMN11044400
Hor CaCO3 Powder		SAMN11044401
Tar CaCO3 Powder		SAMN11044402
LK CaCO3 Powder		SAMN11044403
Conwet CaCO3 Powder		SAMN11044404
ConStream CaCO3 Powder		SAMN11044405
Redcar CaCO3 Powder		SAMN11044406
Scun CaCO3 Powder		SAMN11044407
Bux Marble		SAMN11044408
Hor Marble		SAMN11044409
Tar Marble		SAMN11044410
LK Marble		SAMN11044411
Conwet Marble		SAMN11044412
Constream Marble		SAMN11044413
Redcar Marble		SAMN11044414
Scun Marble		SAMN11044415
NRVB 1		SAMN11044416
NRVB 2		SAMN11044417
NRVB 3		SAMN11044418

## 4.12 Site investigations

### 4.12.1 Cotton preparation

Prior to incubation within the anthropogenic alkaline sites and neutral-pH controls sites cotton fabric samples were first saponified using NaOH, and any impurities were emulsified using an alkali stable phosphate ester detergent. The fabric was bleached via treatment with NaOH and phosphonate stabilised H<sub>2</sub>O<sub>2</sub>. The cotton was neutralised under acetic acid, before being rinsed and autoclaved at 121 °C for 20 minutes.

#### 4.12.2 Sampling site investigations

A total of 13 sampling sites were investigated during the period of study. These sites varied from lime-contaminated environments, steel slag sites and ancient lime field kilns, which were investigated along with a neutral-pH uncontaminated site acting as a control. The newest of the lime-contaminated environments included the Buxton site (Site B), the Horton quarry site (Site H) and the Tarmac quarry site (Site T). The older lime sites were associated with five ancient lime field kilns (Sites LK1-5). The steel slag sites included the Consett wetlands (Site CW), the Consett stream (Site CS), the Redcar site (Site RC) and the Scunthorpe site (Site SC). The Huddersfield canal was used as a control (Site C). Sediment cores were retrieved from all of these sites using a hand corer (dia. 2.2 cm) at a depth of approximately 0.5 m from saturated areas. The retrieved sediment cores were placed within Falcon tubes (50 mL) which were filled to maximum capacity with the associated pore waters to eliminate the atmosphere, then transported to the laboratory within 3 hours. Any samples that were not used immediately were stored at -80 °C until use. VFA species, sulphate, nitrate, chloride and metal concentrations of the samples were analysed using methods described in Section 4.5.

After extracting the sediment cores, cellulose samples were incubated within the resulting boreholes, except for within the ancient lime field kiln sites (Sites LK1-5). This was achieved by inserting an inert plastic liner into each borehole containing holes in the lower section to allow for colonisation of the cotton. A mesh bag filled with approximately 5 g of sterile cotton and 5 g sterile sand was placed at the bottom of the borehole and incubated for approximately 3 months. At least triplicate boreholes were generated within each site for analysis of the intra-site variation. The pH of the associated pore waters was recorded *in situ* using a portable pH meter and calibrated electrodes (Mettler Toledo, UK). Pore waters from each site were extracted before emplacement of the cellulose samples, with VFA species, sulphate, nitrate, chloride and metal concentrations analysed as described above. Cotton from each borehole was prepared for microscopic analysis via CLSM and SEM as described in Section 4.7.1. A map and the grid references for the sampling sites employed during the period of study are shown in Figure 4.1 and photographs of these sites are shown in Figures 4.2-4.5.

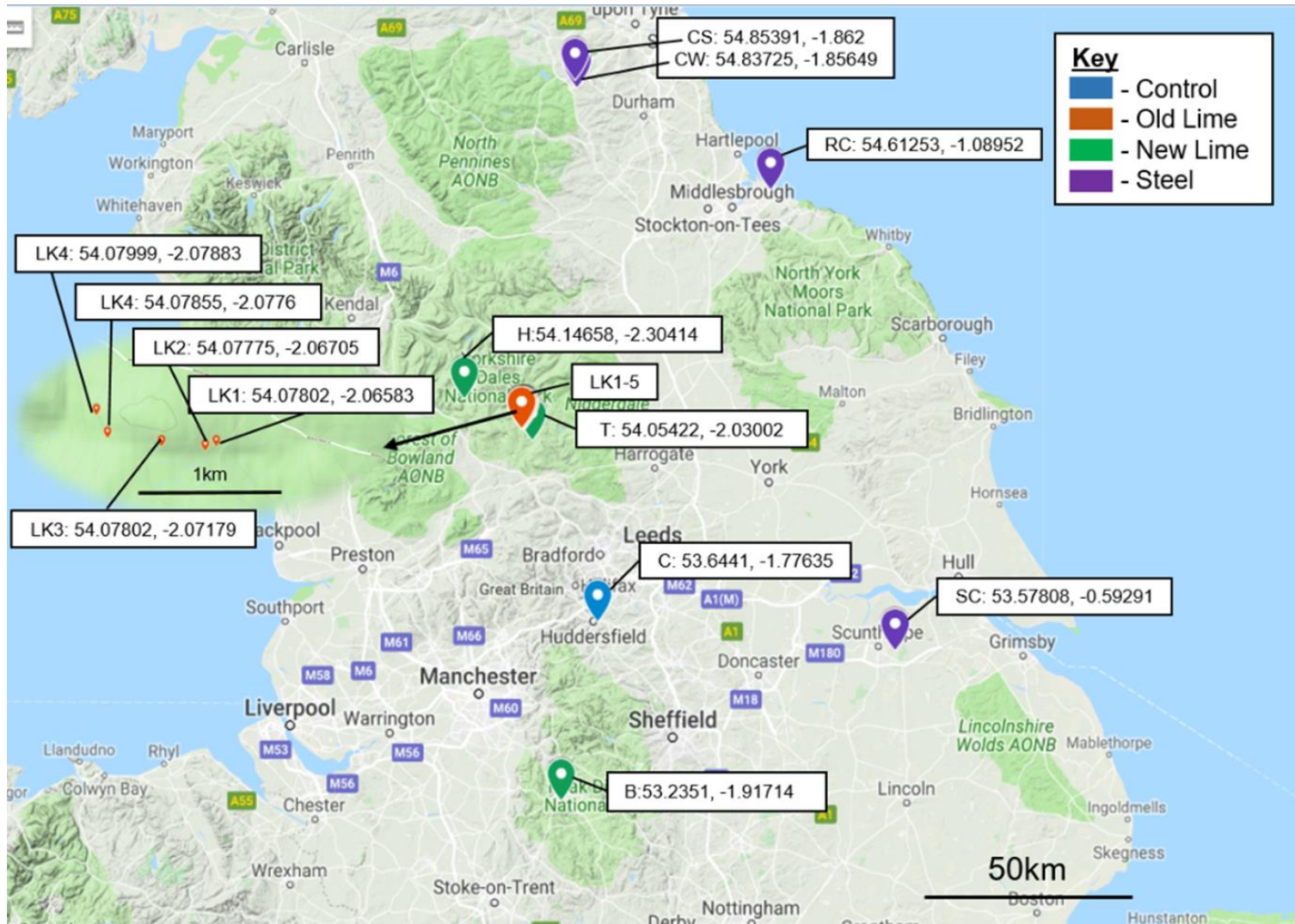
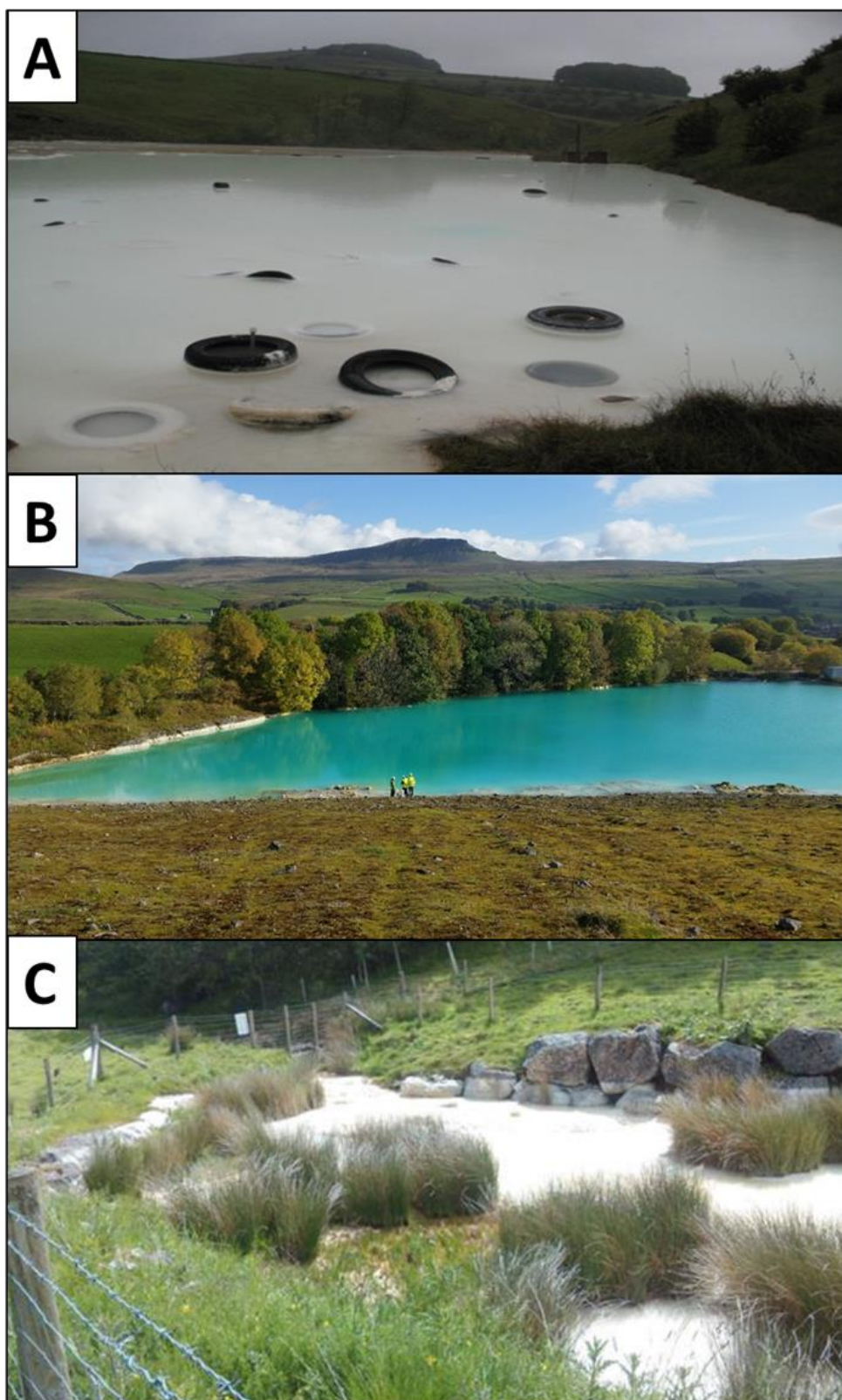


Figure 4.1. Map and grid references for the various sampling sites employed throughout the period of study.



**Figure 4.2. Photographs of the New Lime sites.** The New Lime sites had highly alkaline waters and sediments, along with tufa deposits. Organic materials were present and in contact with the alkaline waters. [A] Buxton (Site-B), [B] Horton-in-Ribblesdale (Site-H), [C] Tarmac quarry (Site-T).



**Figure 4.3. Photographs of the Old Lime sites.** The Old Lime sites had mildly alkaline sediments and were unsaturated during sampling. [A] Ancient field lime kiln (Site LK5), [B] lime kiln bowl (Site LK4).

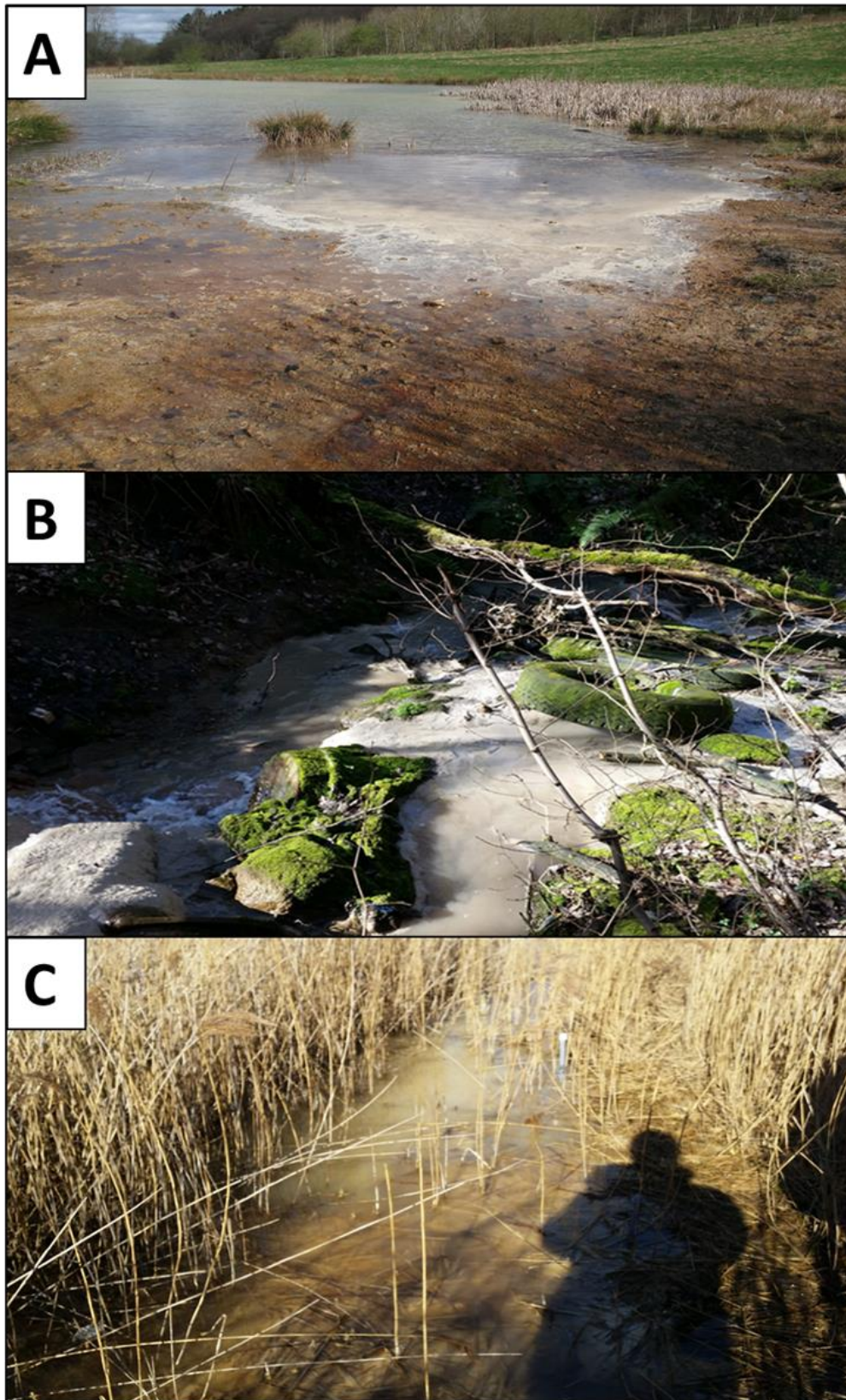


**Figure 4.4. Photographs of Steel sites.** The Steel sites had highly alkaline waters and sediments and in some cases tufa deposits. Organic materials were present and in contact with the alkaline waters. [A] Consett Wetlands (Site CW), [B] Consett Stream (Site CS), [C] Redcar (Site RC).



**Figure 4.5. Photographs of Control site.** The Control site (site C) had neutral-pH waters and sediments surrounded by organic materials.

## 4.13 Microcosm investigations

### 4.13.1 Batch fed microcosms

Microcosms were developed under sulphate-reducing and methanogenic conditions using approximately 10 % (w/v) of sediment sample from the sites described in Section 4.12 as inoculum. These microcosms were operating at pH 10.0 and 25 °C on a 2-weekly waste/feed cycle. The growth media was comprised of 10% CDP (v/v) (Section 4.2.2) and 90 % mineral media (Section 4.2.1). For microcosms operating under sulphate-reducing conditions the mineral media was amended with Na<sub>2</sub>SO<sub>4</sub> (1 g/L). The microcosms were purged with N<sub>2</sub> during the waste/feed procedure and liquid/gas samples were withdraw from the reactors for analysis as described previously. A typical batch-fed microcosm is shown in Figure 4.6.

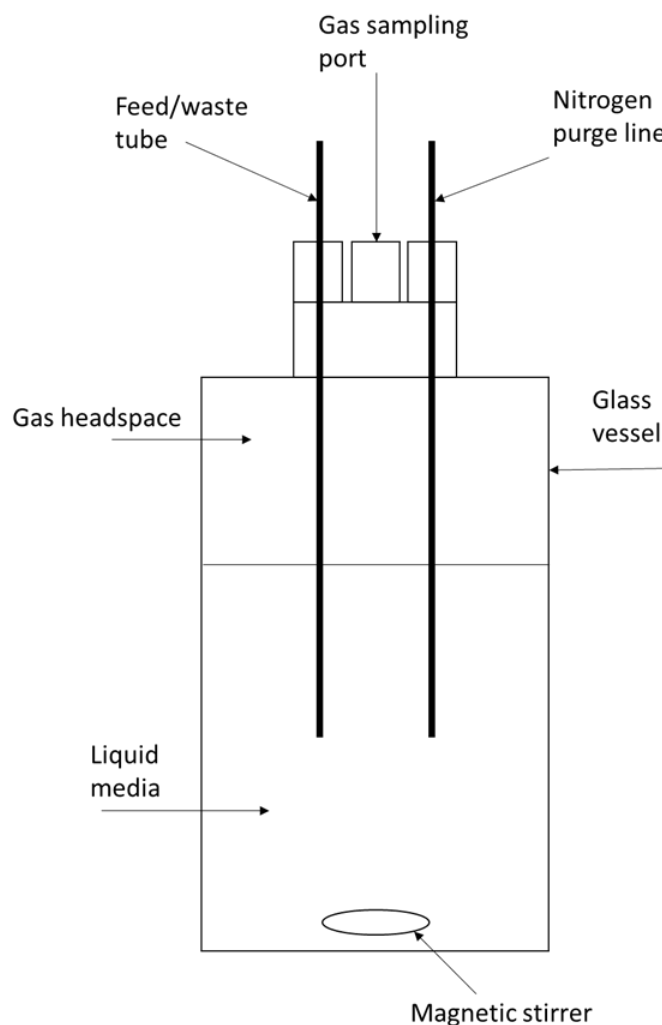


**Figure 4.6. Batch-fed microcosm diagram**

## 4.13.2 Batch microcosms

### 4.13.2.1 pH adaption study

To investigate the upper pH limits for methanogenesis and to determine the methanogenic pathways being utilised over a range of pH values, the sediment samples retrieved from the alkaline sites B, H, T and control site C were used to develop fermentative (CDP-fed), hydrogenotrophic ( $H_2/CO_2$ -fed) and acetoclastic (acetate-fed) methanogen enrichment cultures. For  $H_2/CO_2$ -fed microcosms, Wheaton bottles (100 mL) were left open inside an anaerobic chamber (DW Scientific) and allowed to reach equilibrium with the chambers atmosphere, with gas composition of  $H_2/CO_2/N_2$  (10:10:80) at 1.4 atm for 24 hours. The mineral media (Section 4.2.1) was dispensed (45 mL) into the vessels within the chamber and a butyl rubber septum and aluminium crimp top was used to seal the vessel, followed by autoclaving at 121 °C for 20 minutes. For CDP-fed, acetate-fed and negative control microcosms the same procedure was followed, however Wheaton bottles were purged for 15 minutes with  $N_2$  by fitting a nitrogen line through the post box of the anaerobic chamber, prior to autoclaving and inoculating. The mineral media used for acetate-fed microcosms was amended with sodium acetate, giving a final concentration of 30 mM acetate. CDP was added to the CDP-fed microcosms after autoclaving to a final concentration of 10 % (v/v), using degassed syringes and needles inside the anaerobic chamber. Figure 4.7 shows a diagram of the  $H_2/CO_2$ -fed, acetate-fed and CDP-fed batch microcosms used for the pH adaption study.

In order to inoculate the culture vessels, approximately 5 g of sediment sample was mixed with 5 mL of sterile mineral media inside a Falcon tube (50 mL) under a nitrogen atmosphere, followed by inoculating the Wheaton bottles with the resulting slurry (5 mL) using degassed syringes and needles. CDP was used as substrate for the initial inoculation (Figure 4.7C) due to its ability to provide  $H_2/CO_2$  and acetate through fermentation pathways (22-24). The alkaline site microcosms (sites B, H, T) were initiated at pH 10.0 and the neutral-pH sediments (site C) were initiated at pH 7.0. Culture vessels were incubated for 2 weeks in the dark at 25 °C, with headspace gas, VFA's and ISA quantities monitored throughout the incubation using previously described methods. Microcosms that were positive for headspace methane were sub-cultured three times into the same media (after the 2 week incubation) in order to remove redundant TEA's and organic materials present in the sediments. Sub-cultures of these were subsequently generated between pH 7.0-12.0 using either  $H_2/CO_2$ , acetate or CDP as substrate (Figure 4.7) and monitored as described above. A workflow of the pH adaption study using the

neutral-pH and alkaline sediments is shown in Figure 4.7 and 4.8. DNA was extracted from all active methanogenic reactors for microbial community analysis as described in Section 4.11.

#### ***4.13.2.2 Additional methanogenic enrichment cultures***

Further sampling sites were investigated for their methanogenic potential, namely the Steel sites (CW, CS, RC, SC) and Old Lime sites (LK1-5) described in Section 4.9.2. H<sub>2</sub>/CO<sub>2</sub>-fed and acetate-fed microcosms were established from these sediments as described in Section 2.13.2.1, however these were only tested at pH 7.0 and 10.0 due to time constraints.

#### ***4.13.2.3 Calcium carbonate microcosms***

In order to determine whether calcium carbonate could be used as a carbon source for hydrogenotrophic methanogenesis at high pH, microcosms were developed where the CO<sub>2</sub> being supplied in the growth media was replaced with either calcium carbonate powder, marble chips or pre-carbonated NRVB. The microcosms developed from the New Lime, Old Lime and Steel sites fed with H<sub>2</sub>/CO<sub>2</sub> and operating at pH 10.0 described previously were used as inoculum for this study. This was achieved as described in Section 4.13.2.1, however the anaerobic chamber used for this study (BugBox Anaerobic Workstation) had a gas composition of H<sub>2</sub>/N<sub>2</sub> (10:90). Culture vessels were amended with either calcium carbonate powder (10 % w/v), marble chips (10 % w/v) or NRVB chips (10 % w/v). Low concentrations of dissolved inorganic carbon (<20 ppm) were detected within the original sub-cultures due to carry-over from the carbonate buffered systems, therefore further sub-cultures (1:10 dilution) were generated after a 6 week incubation in order to restrict all carbon sources to the solid phase of culture bottles at the start of the experiment. Negative controls contained a 100 % nitrogen headspace. Abiotic controls were run alongside the test reactors without the addition of inoculum to test hydrogen leakage during headspace gas sampling. The culture bottles were incubated at 25 °C for 6 weeks, with liquid and gas samples routinely removed with degassed syringes and needles to monitor pH, VFA's, headspace gas composition and DIC concentrations. A diagram of the calcium carbonate microcosms is shown in Figure 4.10.

#### ***4.13.2.4 Inhibition studies***

Methyl fluoride (CH<sub>3</sub>F) was used to inhibit acetoclastic methanogenesis, which was injected into the headspace of culture bottles with pressure-lock syringes to a final concentration of 1

% (v/v) as described previously (251). This was achieved firstly by filling sealed Wheaton bottles (100 mL) with methyl fluoride (Fluorochem) from a gas cylinder using an inlet and outlet gassing line which pierced through the rubber septum of the vessel. The pressure within the Wheaton bottles containing 100 % CH<sub>3</sub>F was measured using a digital handheld manometer (TPI, UK), with a pressure of 1 atm inferring 1 mL was injected into the headspace of biotic microcosm vessels to reach a final concentration of 1 % (v/v).

#### **4.13.3 CDC biofilm reactors**

CDC biofilm reactors (Figure 4.11) were employed to develop methanogenic and sulphate-reducing biofilms on steel surfaces at pH 11.0. The batch-fed microcosms described in Section 2.13.1 operating under sulphate-reducing conditions employing site B sediments was used as inoculum for this study. Grade 304 and 316 steel coupons were fitted into the holder rods of the reactor and immersed in 400 mL of mineral media (methanogenic conditions) or mineral media amended with 1 g/L Na<sub>2</sub>SO<sub>4</sub> (sulphate-reducing conditions) and 50 mL CDP under a constant stream of nitrogen. The vessel was sealed whilst maintaining nitrogen purging through the inlet and outlet tubes, followed by inoculation (50 mL) using degassed syringes. The reactor was maintained on a two-weekly waste/feed cycle (10 % volume) for 3 months using the same media, as described in Section 4.13.1. Liquid and gas samples were removed for analysis through the sampling tubing using degassed syringes. After the incubation steel coupons were removed aseptically for analysis via SEM, CLSM and microbiome analysis. Biofilm materials were removed from a proportion of the coupons using a diluted nitric acid (10 % v/v) wash for surface characterisation. Abiotic negative control microcosms were run alongside as per the biotic reactors without the addition of inoculum. Abiotic positive control microcosms were also run alongside, which contained a high dissolved sulphide concentration (5 g/L) using Na<sub>2</sub>S.9H<sub>2</sub>O.

##### ***4.13.3.1 Steel coupons***

Grade 304 and 316 steel coupons (13 mm dia. x 1 mm thick) used in the CDC biofilm reactors were ordered from SYSPAL, UK. Coupons were autoclaved prior to use within the microcosm experiments.

#### **4.13.4 Calculation of rates**

#### 4.13.4.1 ISA degradation rates

The half-life ( $t_{1/2}$ ) first order reaction rates for ISA were calculated using Equation 4.1:

$$Cx = C_0 e^{-kt}$$

**Equation 4.1.**  $Cx$  = ISA final concentration,  $C_0$  = ISA initial concentration,  $k$  = first order rate constant and  $t$  = time.

#### 4.13.4.2 Methane generation rates

Methane generation rates were calculated using Equation 4.2:

$$(Mx - M_0) / t$$

**Equation 4.2.**  $Mx$  = final methane quantity,  $M_0$  = initial methane quantity,  $t$  = time

#### 4.13.4.3 Acetate and hydrogen consumption rates

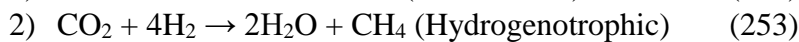
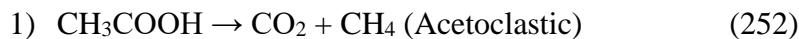
Acetate and hydrogen consumption rates were calculated using Equation 4.3:

$$(Q_0 - Qx) / t$$

**Equation 4.3.**  $Q_0$  = initial quantity,  $Qx$  = final quantity,  $t$  = time

#### 4.13.4.4 Theoretical methane generation

Theoretical methane values were calculated using the following balance equations for acetoclastic and hydrogenotrophic methanogenesis:



Therefore 1 mole of acetate is converted to 1 mole of methane during acetoclastic methanogenesis, in contrast 1 mole of hydrogen is converted to 0.25 moles of methane during hydrogenotrophic methane generation. Theoretical methane values assume any acetate or hydrogen consumed are converted to methane. 1 mole of acetate removed from a microcosm by microbial action should in theory equate to the generation of 1 mole of methane within the same vessel.

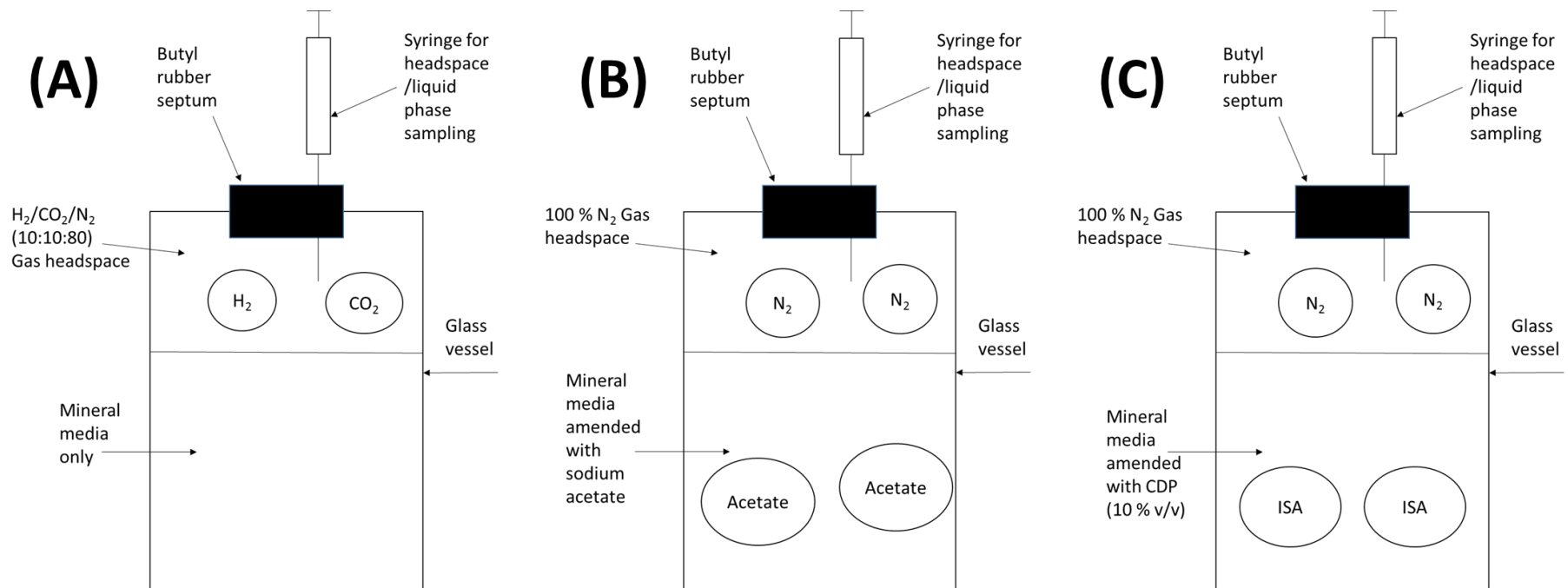


**Figure 4.7. Batch microcosms for pH adaption study.** [A] H<sub>2</sub>/CO<sub>2</sub>-fed microcosms, [B] acetate-fed microcosms, [C] CDP-fed microcosms. Negative control microcosms contained a 100 % nitrogen headspace with mineral media only in the liquid phase.

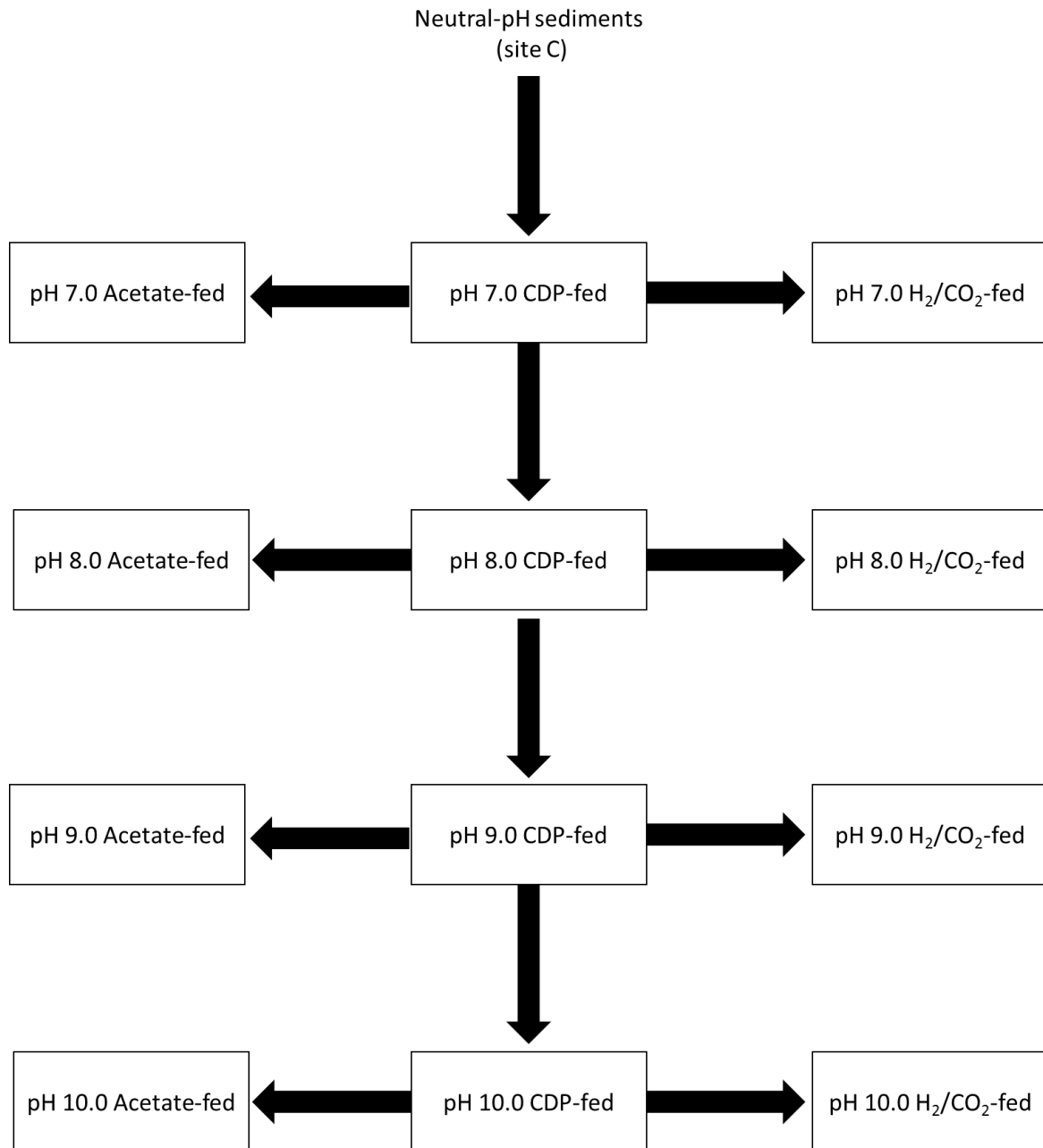


**Figure 4.8. Work flow for pH adapt study using neutral-pH sediments from the control site.** The workflow continued up to pH 11.0 and 12.0 (not shown), or until no methanogenesis could be detected.

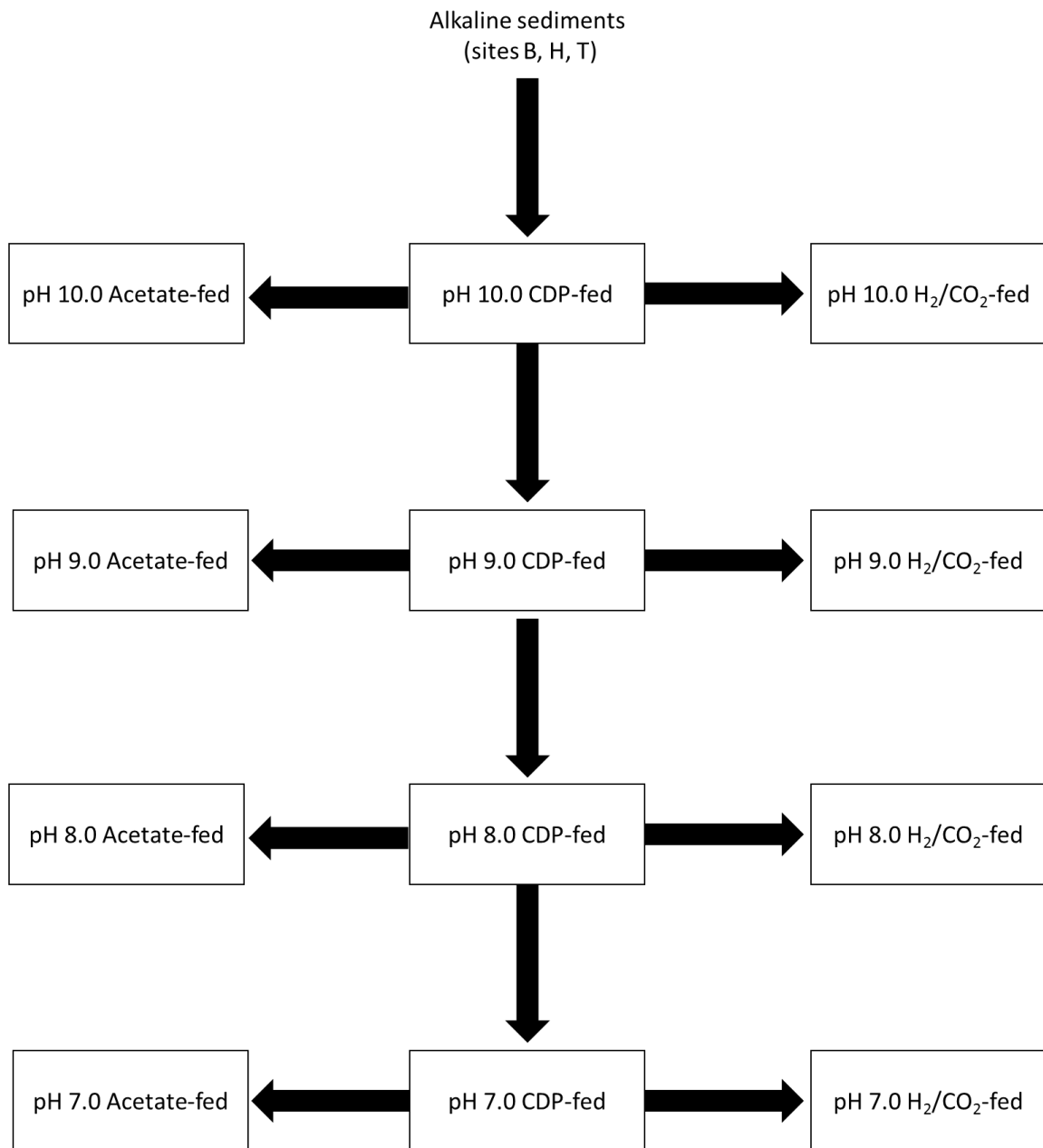


**Figure 4.9. Work flow for pH adapt study using alkaline sediments from sites B, H and T.** pH 10.0 microcosms were also sub-cultured into pH 11.0 and 12.0 microcosms fed with CDP, H<sub>2</sub>/CO<sub>2</sub> and acetate (not shown).

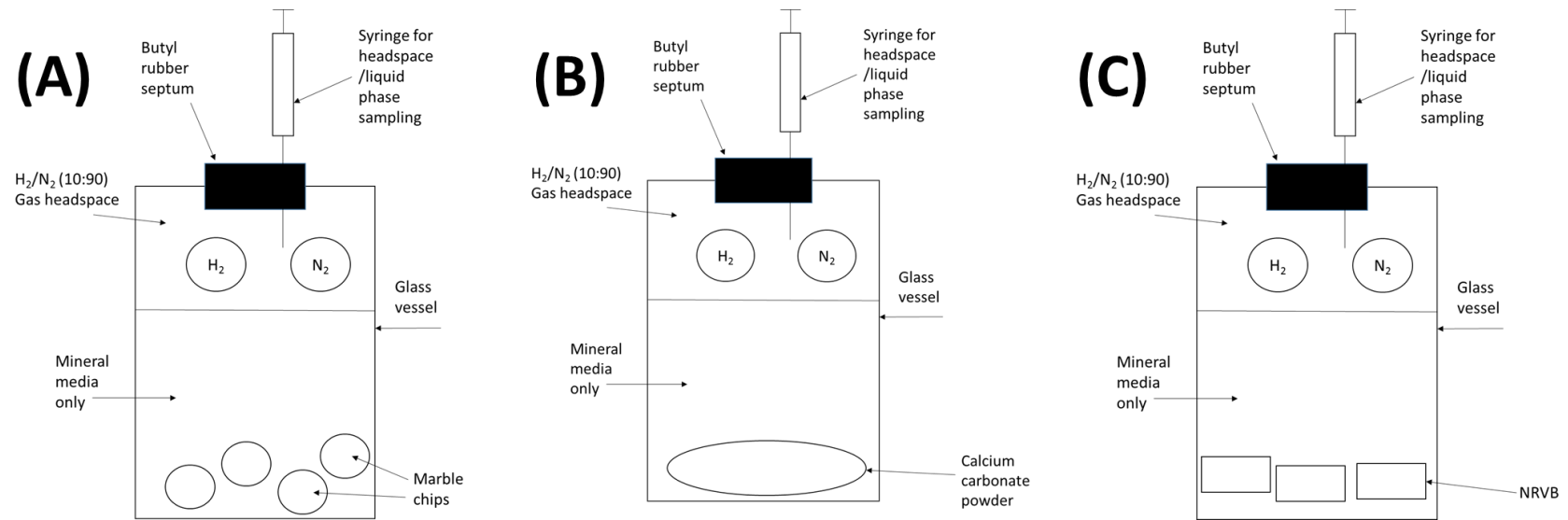


**Figure 4.10. Batch microcosms for calcium carbonate investigations.** [A] Microcosms amended with marble chips [B] microcosms amended with calcium carbonate powder, [C] microcosms amended with NRVB. Negative controls had 100 % nitrogen headspace.

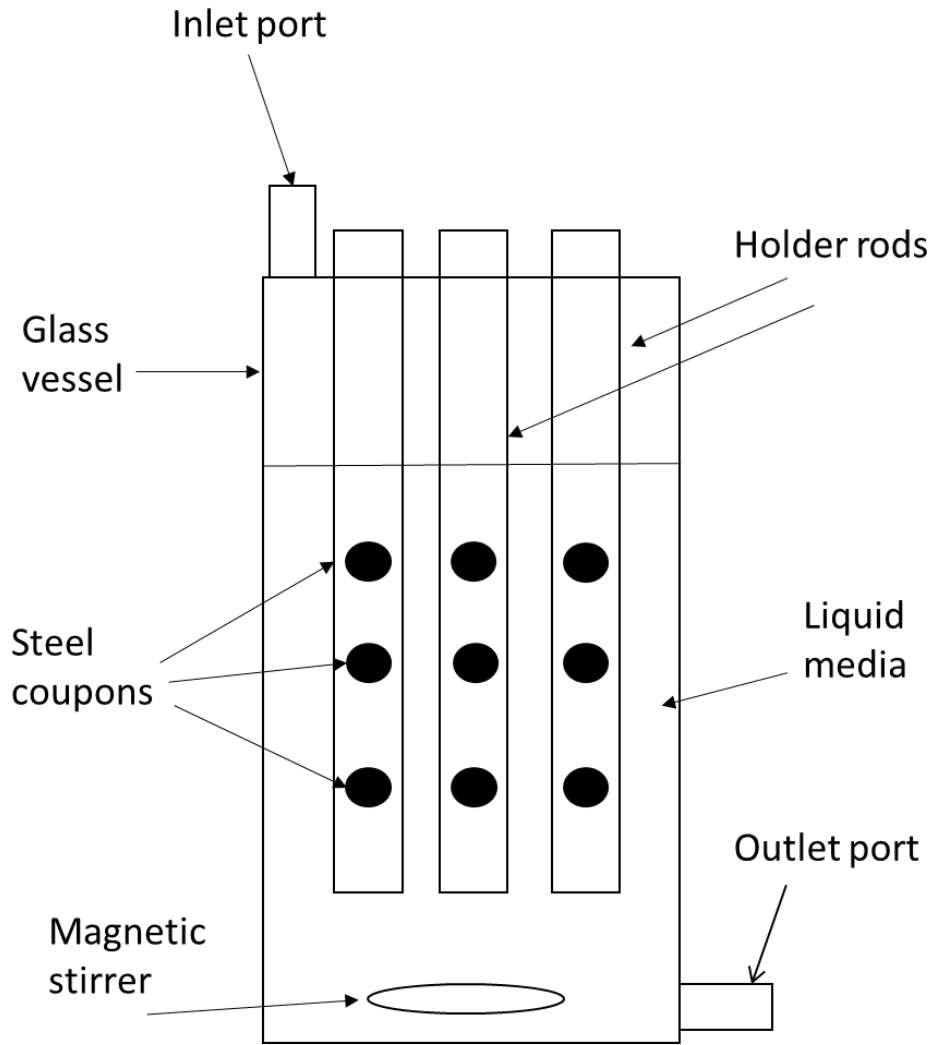


**Figure 4.11. CDC biofilm reactor diagram**

#### 4.13.5 Preparation of NRVB

Nirex reference vault backfill (NRVB) was prepared using previously described methods (9). The components listed in Table 4.8 were mixed and then allowed to set within circular moulds (dia. 1 cm) under a nitrogen atmosphere. The solidified NRVB chips were then incubated under a 10 % CO<sub>2</sub> atmosphere for 4 weeks at 25 °C prior to use within the microcosm experiments. A proportion of the NRVB chips were maintained under nitrogen as negative controls for carbonation analysis.

**Table 4.9. Composition of NRVB**

Component	Mass (g)
Lime	300
Limestone flour	990
Portland cement	900
Water	1230

##### *4.13.5.1 Carbonation analysis of NRVB*

NRVB surfaces were analysed for evidence of carbonation via staining with a phenolphthalein ethanol solution (1 % v/v) (254). The solution was added directly to the surface of NRVB, with pink areas indicating alkaline zones and colourless areas representing low pH zones. Colourless areas is an indicator of carbonation due to the production of carbonic acid.

#### 4.14 Micro profiling

##### 4.14.1 pH profiling

pH profiles of the sulphate-reducing and methanogenic biofilms developed on the steel coupons was performed using a micromanipulator (Unisense, Denmark) attached to a motor (Unisense, Denmark). A pH electrode (dia. 10 µm) and external reference electrode (Unisense, Denmark) was connected to a multi-channel pH meter and calibrated against pH 4.0, 7.0 and 10.0 buffers. The steel coupons along with 20 mL of the liquid reactor fluid were removed from reactors under nitrogen and placed within Falcon tubes (50 mL) that had been prepared as follows: 100 mL of mineral media pH 11.0 (Section 4.2.1) was amended with Agar No. 2

Bacteriological (1% w/v) and heated by microwaving until the Agar had melted, followed by pouring 20 mL into the Falcon tubes under a nitrogen atmosphere and allowing to set at 25 °C. The solidified media at the bottom of the Falcon tube provided a raised support for the steel coupon to allow the electrode ease of access to the steel coupon. The sealed Falcon tube containing the steel coupon and reactor fluid was transferred into a gas bag on a stand that was constantly purging with nitrogen, before being opened and profiled. Control profiles were taken through pH 11.0 agar. All data was recorded using the SensorTrace suite (Unisense, Denmark). A diagram of the experiment set-up is shown in Figure 4.12.

#### **4.14.2 Redox profiles**

Redox profiles of methanogenic and sulphate-reducing biofilms on the steel coupons was undertaken as described previously (Section 4.11.1 and Figure 4.12) using redox electrodes (dia. 20 µm) along with an external reference electrode (Unisense, Denmark). The redox electrode was calibrated using pH buffer solutions saturated with quinhydrone as per the manufacturer's instructions.

#### **4.14.3 Hydrogen profiles**

Hydrogen profiles of methanogenic and sulphate-reducing biofilms on the steel coupons was undertaken as described in Section 4.11.1 and Figure 4.12 using hydrogen microsensors (dia. 20 µm) (Unisense, Denmark). The hydrogen microsensors were calibrated to the manufacturer's instructions using a calibration chamber (Unisense, Denmark). Briefly, a gas mixture containing 5 % H<sub>2</sub> and 95 % N<sub>2</sub> was bubbled through water in the calibration chamber for 5 minutes at a rate of 5 L min<sup>-1</sup> to saturate the water and obtain a hydrogen partial pressure of 0.05 atm. Given the solubility of H<sub>2</sub> (805 µmol/L/atm) the hydrogen-saturated water equates to a final hydrogen concentration of 40.25 µM. Unsaturated water was used as a zero reading. Hydrogen profiles of the biofilms was then undertaken as described above.

### **4.15 Statistical analysis and data processing**

Unless otherwise stated all data was processed in Microsoft Exel and statistical analysis was undertaken using SPSS.

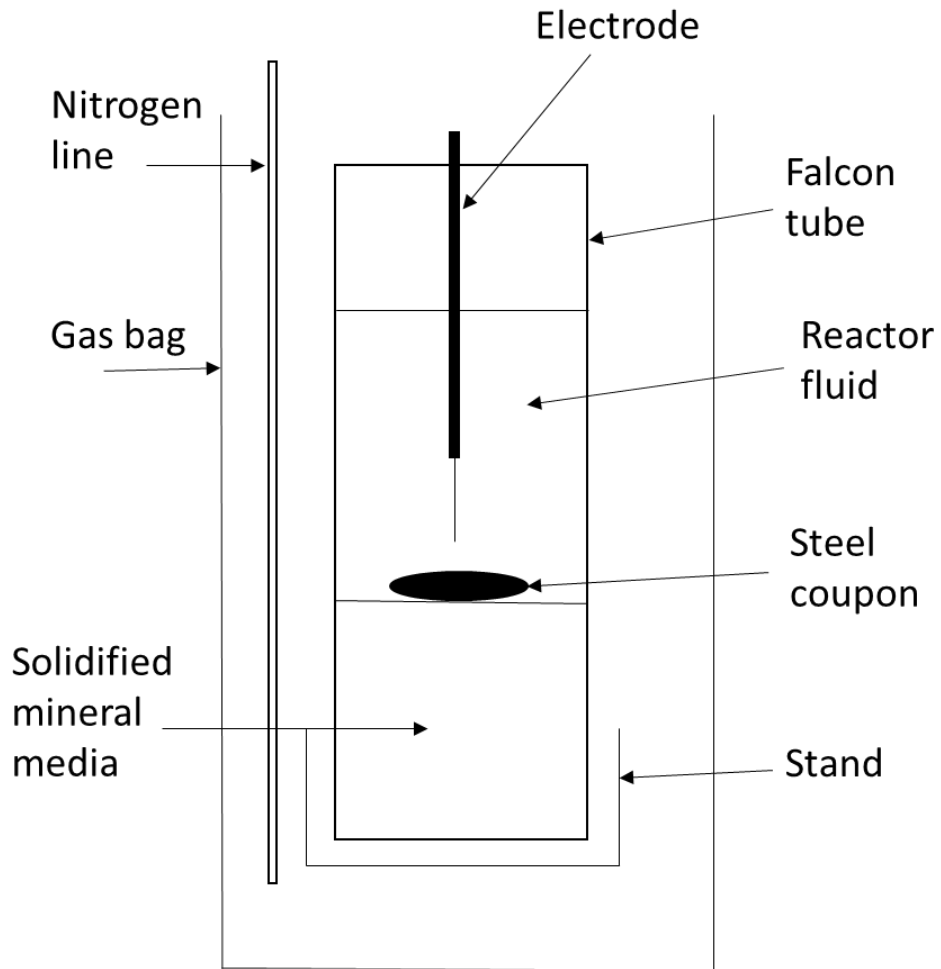


**Figure 4.12. Micro-profiling of steel coupons diagram**

## **5.0 Investigation of Anthropogenic Alkaline Sites**

## 5.1 Rationale

A number of high pH anthropogenic sites are present within the UK that enable the study of alkali-tolerant and alkaliphilic microbial processes. As described in Chapter 1, the presence of alkaline environments can be a result of natural processes, as seen within soda lakes and hot springs, whereas others may arise due to anthropogenic contamination (138, 255-257). A range of environments exist that involve the disposal of wastes associated with the historical manufacture of lime (CaO) and steel (258, 259). Lime manufacture in the UK dates back to the Roman period (260), with a range of historical sites in northern England originating from the 17th to the 20th century (258, 261). The high pH values associated with these sites results from the generation of alkaline leachates due to interactions between the contaminating materials and localised water sources, such as rainwater or streams (154, 262). Highly alkaline environments resulting from the generation of calcium hydroxides have been the focus of a number of recent studies due to their analogy to the conditions likely to be experienced within the cementitious disposal concept for the UK's intermediate level radioactive waste inventory (24, 143, 263). These sites consequently offer an excellent opportunity to study microbial processes under ILW-GDF conditions and provide a source of organisms that can be cultivated and studied in the laboratory.

The data outlined in this first chapter of work aims to provide information regarding the microbial diversity of these alkaline environments, with emphasis on the methanogenic and sulphate reducing populations where possible. The presence of fermentative, methanogenic and sulphate reducing organisms in these sites could underpin the ability of these microbes to grow under ILW-GDF conditions. Sediment cores and pore-waters were retrieved from the anoxic zones in the near subsurface (~1 m) of these sites and cotton samples were incubated within the resulting boreholes to provide a cellulosic substrate for microbial colonisation and biofilm formation. DNA was extracted from the sediment samples and RNA was isolated from the cotton samples prior to the generation of cDNA to demonstrate an active community profile via 16S rRNA gene sequencing. The geochemistry of these sites was investigated using methods such as TGA, TGA-MS, IEC and ICP-MS to determine the impact these properties may have on the associated microbial communities. Additionally, fluorescent microscopic techniques and SEM were employed to visualise the formation of biofilm on the incubated cotton samples. To supplement the study a neutral-pH control site was also sampled for comparisons with the alkaline environments.

## 5.2 Site Geochemistry

### 5.2.1 Chemical Analysis

The chemical properties of the sampling sites are summarised in Table 5.1. Replicate *in situ* pH values were recorded from the pore-waters of each site to determine the intra-site and inter-site variation. The New Lime sites were highly alkaline, with an average pore-water pH of 13.2 ( $\pm 0.3$ ,  $n=3$ ), 12.5 ( $\pm 0.3$ ,  $n=3$ ) and 11.2 ( $\pm 0.3$ ,  $n=3$ ) for sites B, H and T respectively. The Steel sites also demonstrated highly alkaline *in situ* pH values of 11.7 ( $\pm 0.2$ ,  $n=4$ ), 11.4 ( $\pm 0.3$ ,  $n=3$ ), 12.3 ( $\pm 0.1$ ,  $n=5$ ) and 11.3 ( $\pm 0.2$ ,  $n=3$ ) in sites CW, CS, RC and SC respectively. However, it is important to note that the Steel sites are subjected to significant seasonal pH changes and when sampled towards the end of summer these sites demonstrated more neutral *in situ* pH values. The pore-water pH values of the Old Lime sites could not be analysed *in situ* as the site was too dry during sampling, with the Control site demonstrating neutral-pH pore-waters of 6.9 ( $\pm 0.0$ ,  $n=2$ ). The pH values recorded for the New Lime and Steel sites were higher than those reported for natural soda lake and ophiolite alkaline environments studied previously (138, 144), suggesting the microbial populations within these environments could be more adapted to surviving under alkaline conditions.

Interestingly, the pH values of the sediment samples were lower than those recorded for the *in situ* pore-waters, suggesting the microorganisms within these sites could be surviving in lower pH niches within the sediments. For the New Lime sites, the average pH of the sediments was 12.5 ( $\pm 0.4$ ,  $n=3$ ), 11.7 ( $\pm 0.3$ ,  $n=3$ ) and 10.5 ( $\pm 0.4$ ,  $n=3$ ) for sites B, H and T respectively. For the Steel sites the average sediment pH was 11.0 ( $\pm 0.1$ ,  $n=4$ ), 10.1 ( $\pm 0.4$ ,  $n=3$ ), 12.1 ( $\pm 0.3$ ,  $n=5$ ) and 9.5 ( $\pm 0.3$ ,  $n=3$ ) within sites CW, CS, RC and SC respectively. Although the pore-water pH could not be evaluated for the Old Lime sites, the sediments from these sites demonstrated near-neutral pH conditions, with average pH values of 7.6 ( $\pm 0.2$ ,  $n=5$ ) recorded across the five ancient lime field kilns (site LK). The pH of the sediments from the Control site were the same as those recorded for the pore-waters (pH 6.9  $\pm 0.0$ ,  $n=2$ ).

The dissolved organic carbon (DOC) and dissolved inorganic carbon (DIC) quantities within the sediments from each site was analysed. The DOC and DIC levels varied significantly across the sampling sites, however similarities were observed within replicates from the Control, New Lime, Old Lime and Steel sites (Figure 5.1). The highest DOC levels were detected in the Steel site sediments, with an average quantity of 3764.2 ( $\pm 193.2$ ,  $n=4$ ), 4077.2 ( $\pm 176.7$ ,  $n=3$ ), 2311.5

( $\pm 375.7$ ,  $n=5$ ) and  $2336.5 (\pm 185.1, n=3) \mu\text{g g}^{-1}$  across sites CW, CS, RC and SC respectively. Lowest levels of dissolved organics were detected in the sediments from the Old Lime sites, with an average value of  $103.4 (\pm 49.7, n=5) \mu\text{g g}^{-1}$  across the five ancient lime field kilns (site LK). DOC quantities within the New Lime sediments fitted in between the Steel site and Old Lime site values, with an average quantity of  $839.7 (\pm 128.3, n=3)$ ,  $1039.2 (\pm 252.8, n=3)$  and  $1261.8 (\pm 51.6, n=3) \mu\text{g g}^{-1}$  across sites B, H and T respectively. The determination of DOC across these sites suggests the steel-contaminated environments were the richest in terms of dissolved organic content, which could impact the associated microbial community structure by providing extra sources of organic carbon for metabolism (264). Previous studies have found a close correlation between DOC levels and the abundance of *Betaproteobacteria* and *Gammaproteobacteria* lineages (265). Within the present study there appeared to be a link between the age of the sampling sites and the levels of DOC, where the younger sites demonstrated higher levels of DOC compared with the older sites (Figure 5.2A). This could be linked to the death of peripheral vegetation that is unable to recover due to the alkaline conditions imposed in these sites for longer time periods.

DIC quantities also varied across the sampling sites, although similarities were observed within the New Lime, Old Lime, Steel and Control sites (Table 5.1 and Figure 5.1). Highest DIC levels were detected in the Old Lime sites, with average values of  $881.5 (\pm 51.9, n=5) \mu\text{g g}^{-1}$  across the five ancient lime kiln sediments (site LK). Steel sites had the lowest DIC levels, with an average of  $61.0 (\pm 41.1, n=4)$ ,  $50.8 (\pm 38.5, n=3)$ ,  $51.7 (\pm 44.3, n=5)$  and  $64.5 (\pm 42.7, n=3) \mu\text{g g}^{-1}$  within sites CW, CS, RC and SC respectively. New Lime sediments had average DIC levels of  $468.3 (\pm 99.3, n=3)$ ,  $243.8 (\pm 32.9, n=3)$  and  $306.2 (\pm 18.2, n=3) \mu\text{g g}^{-1}$  within sites B, H and T respectively. The high dissolved inorganic carbon levels detected in the lime-contaminated environments are likely to be due to the presence of calcium carbonates which dominate these sites (262). In similar fashion to the DOC levels, a link between the age of the site and the level of DIC was observed, but in this case the older sites generally had higher levels of DIC compared with the younger sites (Figure 5.2B).

Acetate was detected within the sediments from all sites except the steel site SC, with highest levels found within the neutral-pH Control site (Table 5.1). No acetate could be detected in any of the pore-water samples and no volatile fatty acids (VFA's) other than acetate were detected in the sediments from these sites. The detection of acetate within the sediments potentially suggests fermentation or homoacetogenic pathways were active in these environments despite the highly alkaline conditions, which indicates electron donors for downstream anaerobic

respiratory pathways were also available. The presence of acetate within these sites could also be due to the alkaline hydrolysis of cellulosic materials as opposed to the biotic generation of acetate through microbial action (14). Sulphate was detected within the sediments from all sites except the steel site SC, with elevated levels observed in the Steel site CS, indicating the potential for sulphate-reduction processes to be available in these environments. The alkaline leachates in the steel slag sites were historically treated with sulphuric acids for remediation purposes (266), which explains the increased levels of sulphate in site CS. Chloride was detected in all sites except site C and CS, with highest concentrations of nitrate detected in the Old Lime sites LK1-5 (Table 5.1). Chloride concentrations have been shown to impact microbial community structure previously (267), however the values recorded for this study are lower than those reported here.

**Table 5.1 Chemical analysis of sediment samples.** Chemical properties of the sampling sites, including the uncontaminated Control site (C), New Lime sites (B, H, T), Old Lime sites (LK) and Steel sites (CW, CS, RC, SC). Error ( $\pm$ ) represents standard deviation.

Site	pH		Dissolved Carbon ( $\mu\text{g g}^{-1}$ )		Acetate ( $\mu\text{g g}^{-1}$ )	Chloride ( $\mu\text{g g}^{-1}$ )	Sulphate ( $\mu\text{g g}^{-1}$ )	Nitrate ( $\mu\text{g g}^{-1}$ )	Approximate Age (years)
	<i>In situ</i>	Sediments	Organic	Inorganic					
C	6.9 ( $\pm 0.0$ )	6.9 ( $\pm 0.0$ )	2147.5 ( $\pm 14.2$ )	73.6 ( $\pm 22.6$ )	17.0 ( $\pm 5.9$ )	N/D	11.2 ( $\pm 3.6$ )	6.3 ( $\pm 1.2$ )	N/A
B	13.2 ( $\pm 0.3$ )	12.5 ( $\pm 0.4$ )	839.7 ( $\pm 128.3$ )	468.3 ( $\pm 99.3$ )	2.5 ( $\pm 1.7$ )	58.8 ( $\pm 5.5$ )	28.1 ( $\pm 3.9$ )	23.6 ( $\pm 7.3$ )	150
H	12.5 ( $\pm 0.3$ )	11.7 ( $\pm 0.3$ )	1039.2 ( $\pm 252.8$ )	243.8 ( $\pm 32.9$ )	9.3 ( $\pm 2.5$ )	13.7 ( $\pm 2.0$ )	12.9 ( $\pm 3.8$ )	133.6 ( $\pm 14.6$ )	50-75
T	11.2 ( $\pm 0.3$ )	10.5 ( $\pm 0.4$ )	1261.8 ( $\pm 51.6$ )	306.2 ( $\pm 18.2$ )	1.7 ( $\pm 1.3$ )	43.6 ( $\pm 3.7$ )	19.5 ( $\pm 0.03$ )	N/D	25-30
LK	NT	7.6 ( $\pm 0.2$ )	103.4 ( $\pm 49.7$ )	881.5 ( $\pm 51.9$ )	2.9 ( $\pm 1.8$ )	22.0 ( $\pm 9.4$ )	17.9 ( $\pm 6.8$ )	86.5 ( $\pm 14.8$ )	200-500
CW	11.7 ( $\pm 0.2$ )	11.0 ( $\pm 0.1$ )	3764.2 ( $\pm 193.2$ )	61.0 ( $\pm 41.1$ )	2.4 ( $\pm 1.1$ )	16.2 ( $\pm 11.4$ )	36.8 ( $\pm 17.5$ )	N/D	5-30
CS	11.4 ( $\pm 0.3$ )	10.1 ( $\pm 0.4$ )	4077.2 ( $\pm 176.7$ )	50.8 ( $\pm 38.5$ )	1.4 ( $\pm 0.1$ )	41.7 ( $\pm 11.0$ )	280.8 ( $\pm 79.8$ )	N/D	5-30
RC	12.8 ( $\pm 0.1$ )	12.1 ( $\pm 0.3$ )	2311.5 ( $\pm 375.7$ )	51.7 ( $\pm 44.3$ )	2.2 ( $\pm 1.2$ )	124.8 ( $\pm 56.9$ )	94.0 ( $\pm 33.6$ )	0.4 ( $\pm 0.7$ )	5-30
SC	11.3 ( $\pm 0.2$ )	9.5 ( $\pm 0.3$ )	2336.5 ( $\pm 185.1$ )	64.5 ( $\pm 42.7$ )	N/D	N/D	N/D	N/D	5-30

N/T – Not Tested, N/D – Not Detected, N/A – Not Applicable

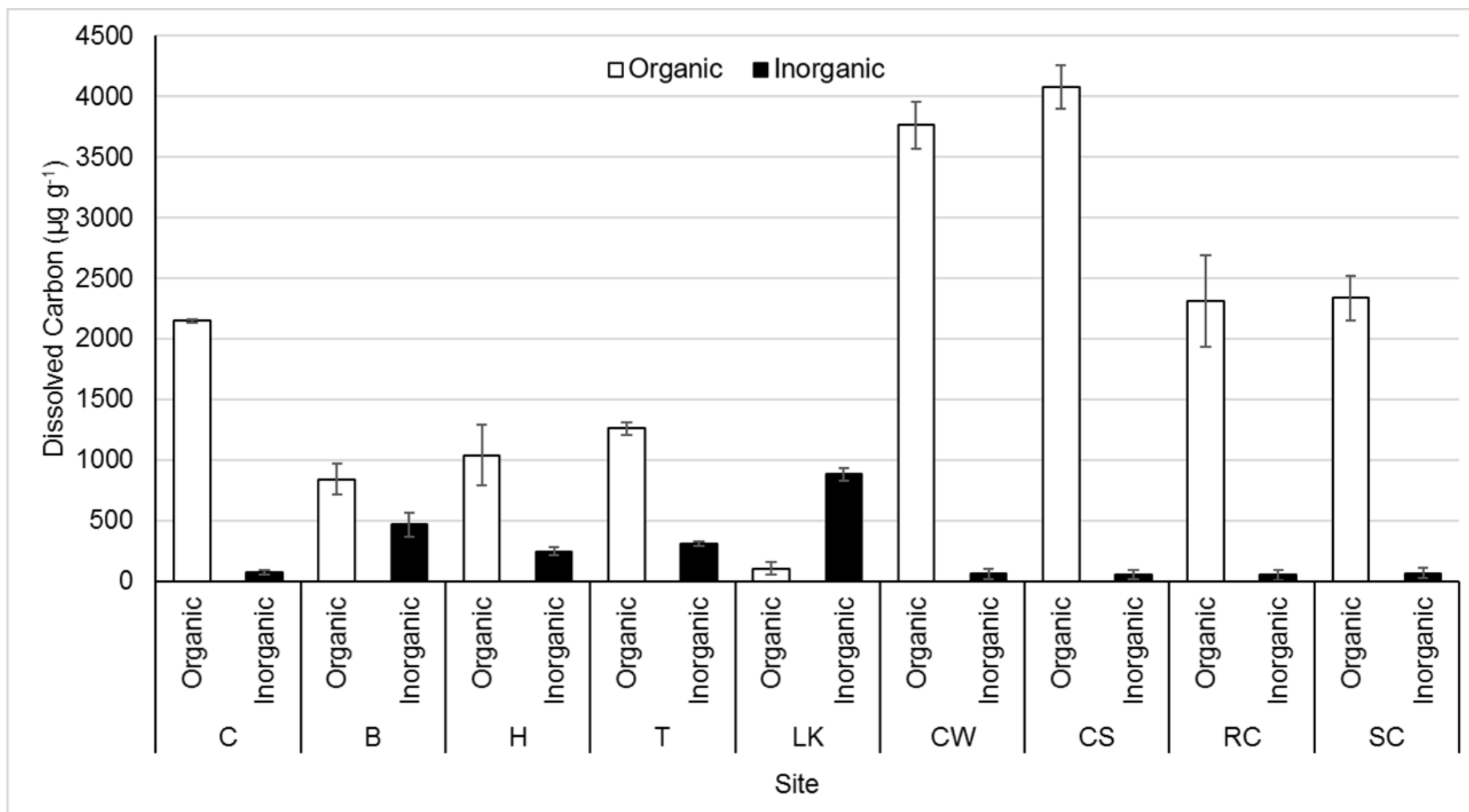


**Figure 5.1. Comparison of dissolved organic and inorganic carbon within the sediments from various anthropogenic alkaline sites.** Highest levels of dissolved organic carbon were detected in the Steel sites, with the lowest observed in the Old Lime sites. Highest dissolved inorganic carbon levels were present in the Old Lime sites and lowest quantities were detected in the Steel Sites. Error bars represent standard deviation.

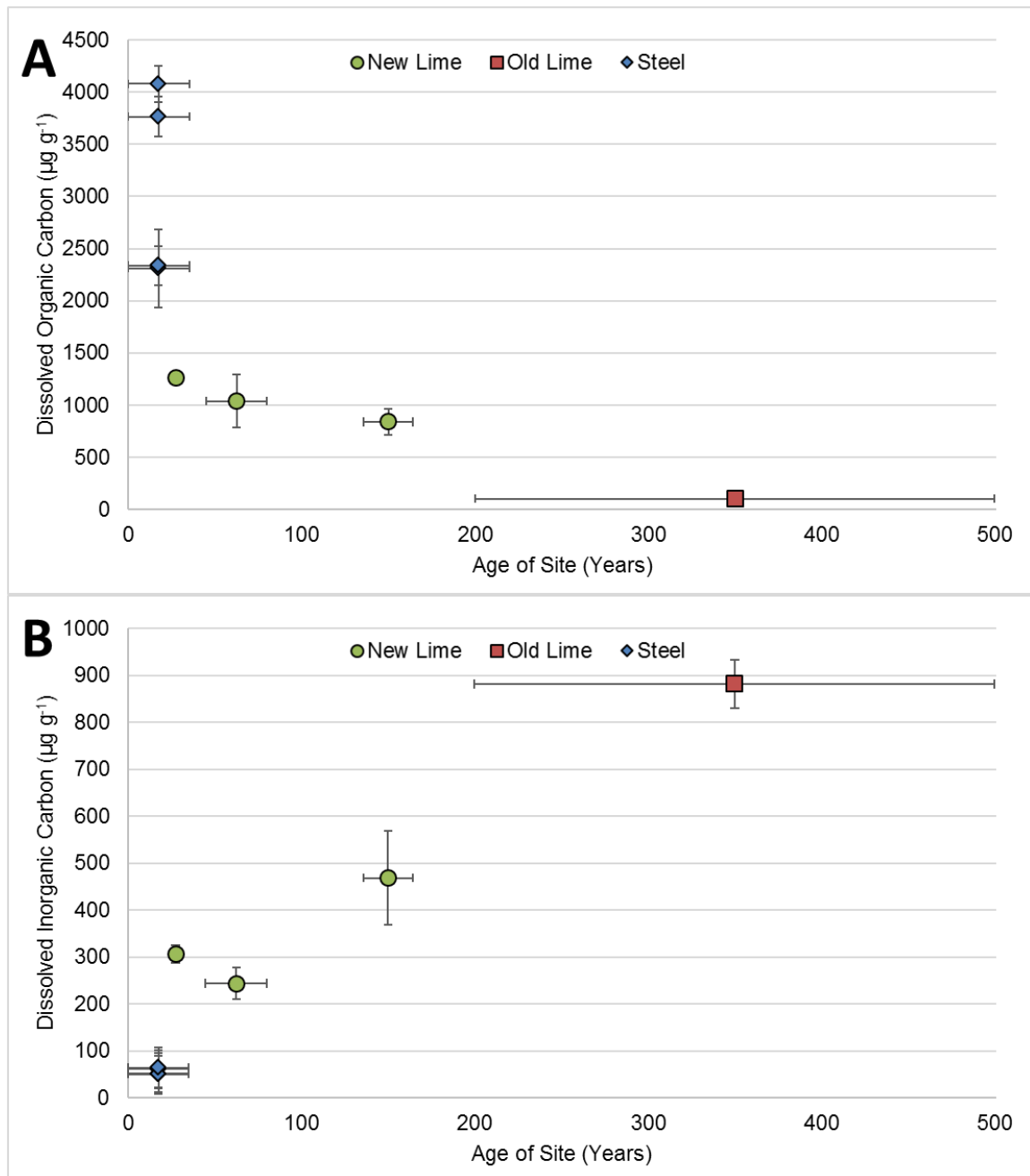


**Figure 5.2. The dissolved organic and inorganic carbon content of the sediments plotted against the age of the New Lime, Old Lime and Steel sites. [A] Dissolved organic carbon levels versus age, [B] dissolved inorganic carbon levels versus age. As the age of the site increases, the levels of dissolved organic carbon decreases and dissolved inorganic carbon increases. Error bars represent standard deviation.**

### 5.2.2 Metal Analysis

The concentration of metals within the pore-waters extracted from the New Lime (B, H, T), Steel (CW, CS, RC, SC) and Control (C) sites was analysed via ICP-MS (Figure 5.3). Metal analysis of the Old Lime sites (LK) could not be undertaken as the site was too dry to obtain

pore-waters. Elevated levels of aluminium, copper and barium were detected in the pore-waters of the New Lime site H, giving a concentration of 35.0 (n=1), 6.2 (n=1) and 6.0 (n=1) ppm respectively (Figure 5.3). Highest levels of iron and manganese were detected in the pore-waters of the Steel site SC, with concentrations of 19.7 ( $\pm 3.4$ , n=2) and 5.9 ( $\pm 0.9$ , n=2) ppm respectively (Figure 5.3). The Steel site CS had the highest concentrations of lithium and strontium, giving concentrations of 5.7 (n=1) and 30 (n=1) ppm respectively. The Control site (C) had the lowest total quantities of metals present and only aluminium and manganese gave significant values, suggesting this site was less impacted by contamination. However, heavy metals Cadmium, Arsenic, Lead, Zinc and Chromium, which can be toxic to microorganisms (268), were absent at levels above background readings. It is possible these heavy metals are present in the solid-phase deposits, since they have been detected in a number of steel slag sites in the UK previously (266).

Sodium concentrations were highest within the pore-waters from Steel sites SC, RC and CS, giving concentrations of 1403.3 ( $\pm 32.3$ , n=2), 630 (n=1) and 260 (n=1) ppm respectively (Figure 5.4), suggesting these sites may be impacted by salinity, but to a much lesser degree than is observed within saline lakes where sodium concentrations can reach saturated levels (269). Previous studies have suggested sodium content can be an important driver of microbial community composition in soils (270) and methylotrophic methanogenesis seems to be important within soda lake environments where *in situ* sodium concentrations are high (73). Therefore, the detection of sodium within the pore-waters of the Steel sites could impact the associated methanogen community. Previous authors investigating the microbial community structure along a metal pollution gradient found that pH and organic matter content was a more important driver of microbial community structure than the presence of toxic metals (271).

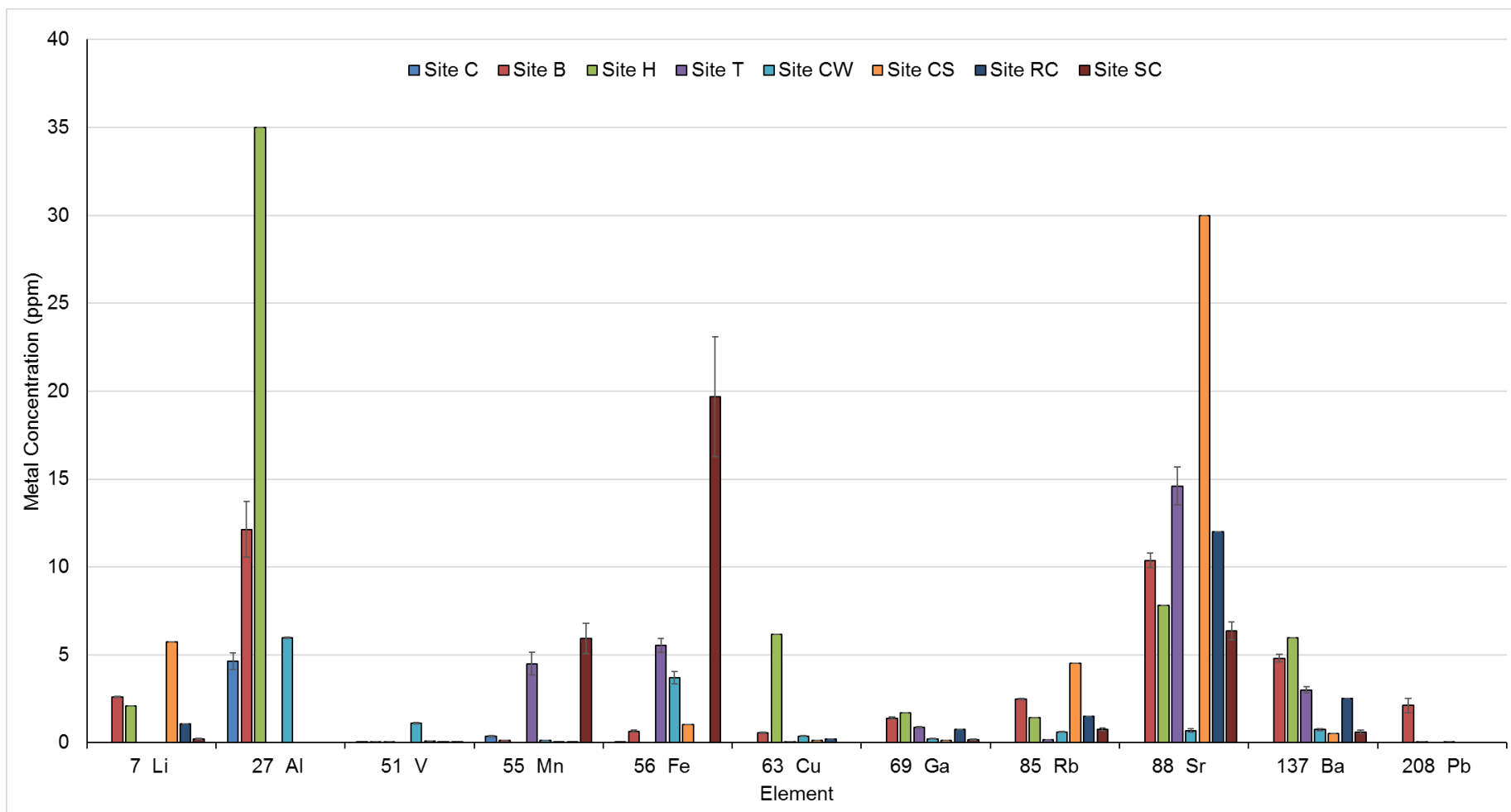


**Figure 5.3. Metal analysis of the pore-waters from various anthropogenic sites. Error bars represent standard deviation.**

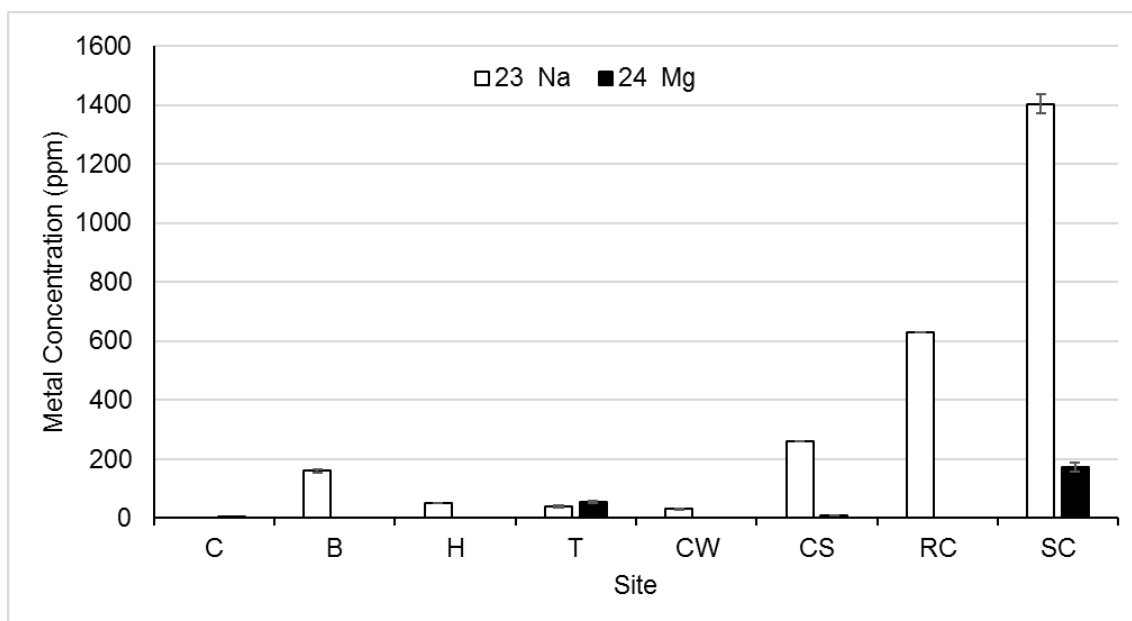


**Figure 5.4. Sodium and magnesium concentrations in the pore-waters of various anthropogenic sites. Error bars represent standard deviation.**

### 5.2.3 Thermogravimetric Analysis

TGA is a thermoanalytical technique used to monitor the stability of materials by recording changes in mass as a function of temperature. As material degrades under the influence of heating, mass losses are observed as any gaseous products are released. The loss of gaseous products gives characteristic steps in profiles known as thermograms (272). TGA was carried out on the sediment samples extracted from the anthropogenic alkaline sites. The aim of these experiments was to compare the various levels of free water, assumed organic content and inorganic content across the sampling sites, through comparisons of mass losses over specified temperatures ranges. At least duplicate experiments were performed wherever possible.

Thermograms are presented in Figure 5.5 and Figures S5.1 - S5.4. All samples analysed exhibited an initial mass loss from the onset of heating which varied between 19.7% and 68.8%. This has been attributed to the dehydration of the soil both in terms of removal of excessive water and potential hydrate drying which typically concluded by 130 °C and returned to a stable baseline. The second mass loss stage is observed over a range of 150 to 650 °C. The broad range is likely to be comprised of several overlapping mass loss events, which is assumed to be due to the decomposition of organic material (273). Due to the inert atmosphere mass loss processes are pyrolytic and organic decompositions observed on the TGA are broadened

through being starved of oxygen. The final mass loss stage, above 650 °C has been assigned to the decomposition of inorganic matter present. Typical types of inorganics that could decompose are carbonates which yield CO<sub>2</sub> to form the corresponding oxide. Since the sites studied here are calcium dominated (274), it is likely that CaCO<sub>3</sub> is decomposing to CaO in the final mass loss event. The remainder of the material is deemed thermally stable up to 1000 °C.

The mass losses recorded for all the samples tested are given in Table 5.2, which demonstrated good reproducibility across replicates, however the table highlights large differences between the sediments taken from different sites. The levels of solid organic material within the sediments from all sites were very similar, although the New Lime site B sediments had slightly elevated levels (4.4 %) compared with the Steel site CS, which had the lowest quantities of solid organics (1.8 %). However, the percentage of inorganic material within the sediments varied significantly across the sampling sites. The highest levels of solid inorganic materials were detected in the New Lime site T sediments (35.3 %) and lowest levels detected in the Steel site SC (4.1 %). The sediments from the Steel sites CS and RC also had elevated levels of solid inorganic material present, which represented 20.1 % and 21.2 % of the total material respectively.

**Table 5.2. Composition of sediment samples from various anthropogenic alkaline sites obtained through TGA.** Shows percentage of water, organic material, inorganic material and remaining ash based on mass loss after exposure to increasing temperatures (25-1000 °C). Percentage errors are calculated from duplicate experiments.

Site	Water (%)	Organic (%)	Inorganic (%)	Total Loss (%)	Remaining Ash (%)
<b>B</b>	67.4 (±2.0)	4.4 (±0.1)	8.3 (±0.04)	80.1 (±2.2)	19.9 (±2.2)
<b>H</b>	52.1 (±2.8)	2.4 (±0.5)	13.5 (±0.3)	68.1 (±3.0)	31.9 (±3.0)
<b>T</b>	33.1 (±0.3)	2.7 (±0.2)	35.3 (±0.0)	71.1 (±0.07)	28.9 (±0.07)
<b>CW</b>	55.2 (±0.7)	2.0 (±0.007)	9.0 (±0.0)	66.2 (±0.7)	33.8 (±0.7)
<b>CS</b>	43.1 (±13.6)	1.8 (±0.5)	20.1 (±6.0)	65.0 (±7.1)	35.0 (±7.1)
<b>RC</b>	41.6 (±1.5)	2.2 (±0.2)	21.2 (±0.4)	65.0 (±1.4)	35.0 (±1.4)
<b>SC</b>	25.9 (±5.6)	3.7 (±0.2)	4.1 (±1.7)	33.7 (±4.1)	66.3 (±4.1)

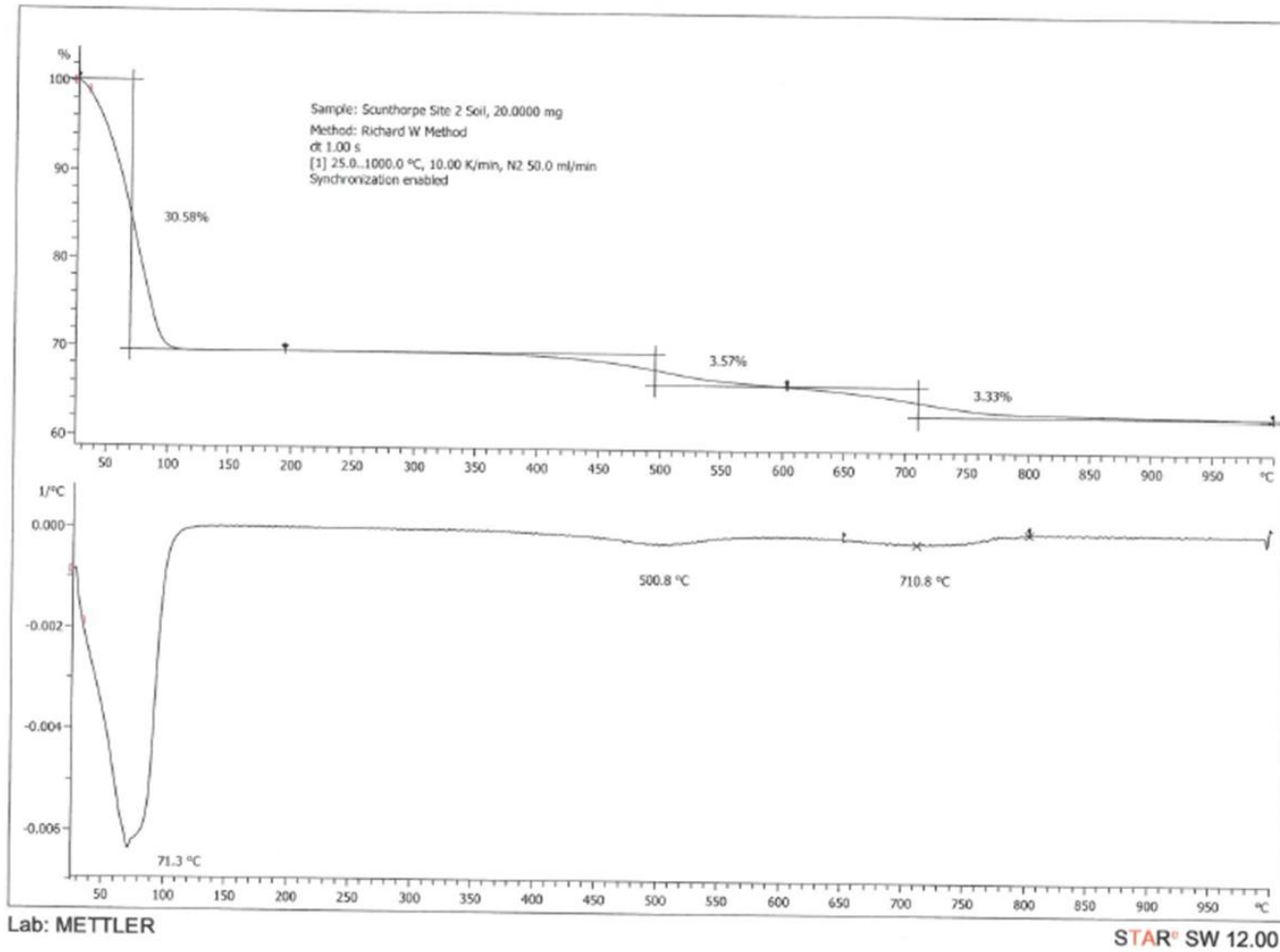


**Figure 5.5. Thermal analysis of sediment samples acquired from the Steel site SC.** Showing mass loss of the sediments with increasing temperature, indicating water loss (25-130 °C), organic content loss (130-650 °C) and inorganic content loss (>650°C). The remaining ash is thermally stable up to 1000°C.

#### 5.2.4 Thermogravimetric Analysis coupled with Mass Spectrometry

TGA-MS methods were also applied to the sediment samples in order to identify the chemical species present during the mass losses observed in the previous TGA runs mentioned in Section 5.3.3. For these experiments samples were dried and sieved to eliminate large particulates (stones and plant matter) and excessive surface moisture that could obscure the measurements. To aid with resolution between the organic and inorganic mass losses, the atmosphere was changed to an oxidative one to ensure complete oxidation of the sample. The generation of CO<sub>2</sub> due to the degradation of organic and inorganic material was measured via mass spectrometry and adds confidence to the measurements outlined in Section 5.3.3.

The neutral-pH uncontaminated Control sediments were predominantly composed of organic material, indicated by the significant increase in the amount of observed CO<sub>2</sub> between 200 and 400 °C that coincided with a large mass loss (Figure 5.6A), with very little CO<sub>2</sub> generation and mass loss observed at >600 °C. In contrast, the alkaline sediment samples were largely composed of inorganic material indicated by the generation of CO<sub>2</sub> at temperatures above 600 °C and consequent mass losses (Figure 5.6B-H), although the Steel site CS was more comparable with the Control samples and was richer in organic material (Figure 5.6F). Differences were observed between New Lime and Steel samples, with site B and T (New Lime) being heavily composed of inorganic material (Figure 5.6BD) and sites CW, CS, RC and SC (Steel) containing a higher proportion of organics (Figure 5.6E-H). Although TGA has been used to analyse the properties of soil samples previously (273, 275), little is known about the impact these properties may have on the associated microbial communities. The extremely low levels of organic material within the sediments from the lime-contaminated sites (particularly sites B and T) could infer that the associated microbial community will have a limited amount of organic matter for fermentation processes which could have an impact on downstream anaerobic respiratory processes. This fact could also give autotrophic processes, such as hydrogenotrophic methanogenesis, an advantage in this environment due to the increased levels of inorganic carbon present. Further work is required to confirm the identity of the species present in both organic and inorganic phases. Instruments such as FTIR, XRD, along with a history of the area from where the sample was extracted will provide better identity for the unknown compounds present in the soil. Further analysis of these samples is beyond the scope of this project.

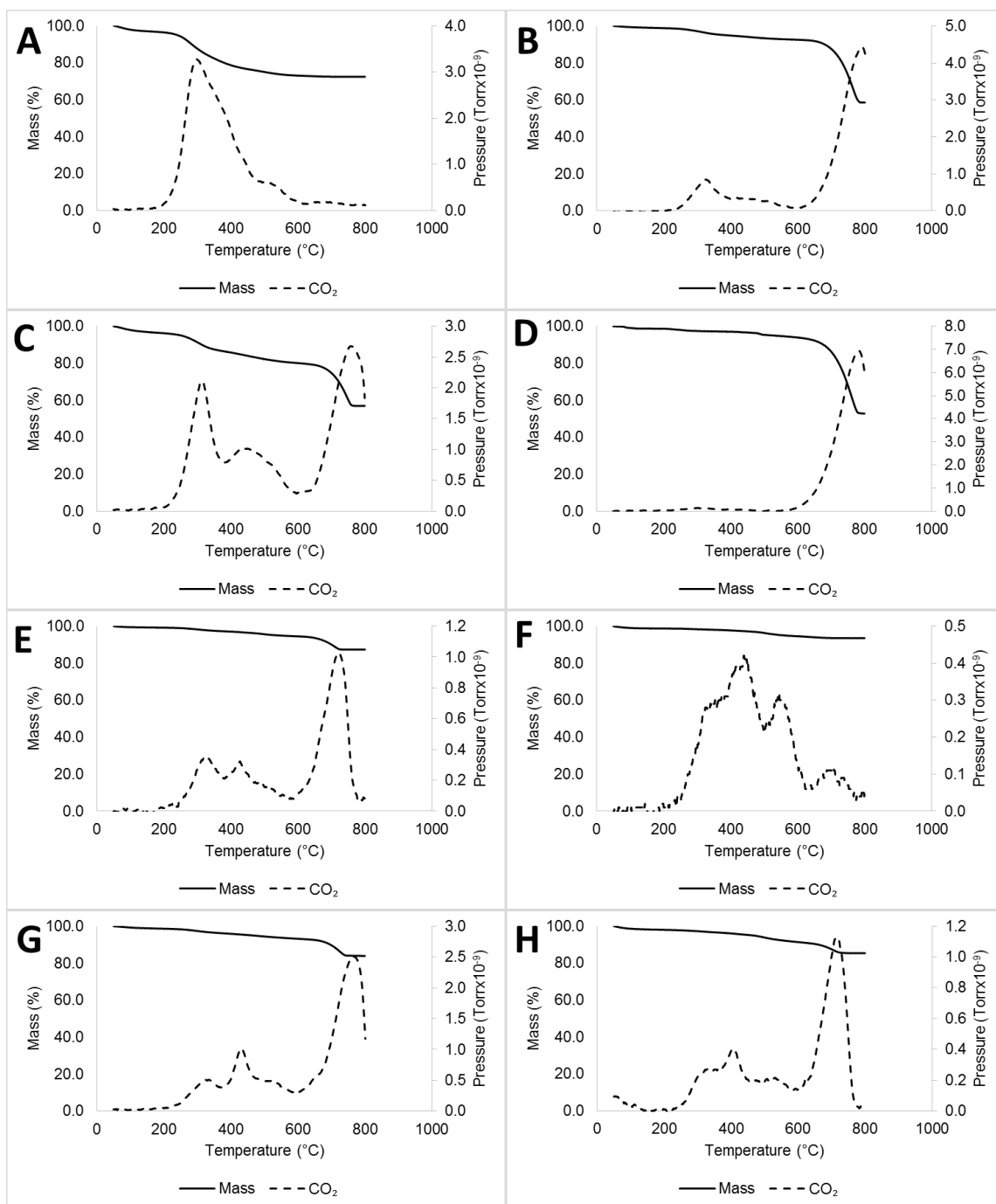


**Figure 5.6. Thermal gravimetric analysis coupled to mass spectrometry of soil samples from anthropogenic alkaline sites. [A] Uncontaminated Control site C, [B] Site B, [C] Site H, [D] Site T, [E] Site CW, [F] Site CS, [G] Site RC, [H] Site SC.**

## 5.3 Microbial Community Analysis

### 5.3.1 DNA Sequencing

#### 5.3.1.1 Phylum-level composition of background and alkaline sediments

Background sediments from non-contaminated regions of the sites which were not impacted by alkaline conditions were selected for microbiome analysis for a comparison with the contaminated (alkaline) regions. These background sediments had the same parent soil material as the contaminated regions but were not in contact with the alkaline leachates. Total gDNA was extracted from the background and alkaline sediments for analysis of the 16S rRNA genes via the Illumina MiSeq platform. The background sediment communities from the New Lime, Old Lime, Steel and Control sites had a very similar composition at the phylum taxonomic level (Figure 5.7), with all samples dominated by Proteobacteria, Bacteroidetes, Actinobacteria and Acidobacteria lineages. These phyla have been implicated as the dominant microbes in a wide-range of neutral-pH environments previously, including cave sediments (276), freshwater sediments (277) and intertidal sediments (278). Members of the Firmicutes were under-represented in the background samples and could only be detected with any significance from the Old Lime sites (LK) and Steel sites (CW, RC and SC) where they were present in low abundance (Figure 5.7). Alongside the dominant phyla discussed above, small percentages of 16S rRNA gene reads were attributed to the Chloroflexi, Gemmatimonadetes, Nitrospirae and Planctomycetes lineages within all background sediment samples (Figure 5.7).

Despite the highly alkaline *in situ* conditions (Section 5.3.1), microbial community analysis of the contaminated alkaline sediments revealed a diverse microbial population at the phylum taxonomic level (Figure 5.8). In similar fashion to the background samples, the Proteobacteria phylum dominated in the alkaline sediments, however a noticeable increase in the percentage of 16S rRNA gene reads attributed to the Firmicutes and Bacteroidetes lineages was observed (Figure 5.8). The increased abundance of Firmicutes and Bacteroidetes resulted in a decrease in the percentage of Acidobacteria 16S rRNA gene reads within the alkaline sediments (Figure 5.8). Both Proteobacteria and Firmicutes lineages have been observed to dominate highly alkaline (pH 10.8) and saline ponds in Poland previously (279). Firmicutes lineages have been detected in alkaline ISA-degrading microcosms previously where they contributed to fermentation processes (23, 24). The detection of fermentative species within the alkaline sediments suggests fermentation end-products are available for consumption by methanogenic

or sulphate reducing communities within these environments. The increased detection of the Firmicutes phylum within the alkaline sediments could be attributed to their ability to form spores (280), which could be advantageous to their survival within these environments.

Principal components analysis (PCA) was carried out on the background and alkaline sediment communities at the phylum level with a 95 % confidence interval to ascertain the statistical differences between the populations within these environments. The background sediments from the New Lime, Old Lime and Control sites clustered very closely together (Figure 5.9A), indicating the background communities were very similar at the phylum level regardless of the sampling site, although Steel site background sediments had a much wider distribution. The similarities observed across the non-contaminated background microbiomes is perhaps expected given that these samples were taken from geographically comparable environments in the North of England. The phylum-level composition of the alkaline sediments from New Lime, Old Lime and Steel sites were significantly different when compared with the neutral-pH Control sediments (Figure 5.9B), suggesting that pH was an important environmental factor driving microbial community structure in these sites. Significant differences were also revealed between the communities within the contaminated regions and the background regions of these sites (Figure 5.9C), where background communities clustered very closely together and the contaminated regions had a much wider distribution. The differences between individual phyla within the background and alkaline sediments was further analysed with the use of heat maps. The heat maps confirmed the increased abundance of Firmicutes lineages within the alkaline sediments compared to the background sediments (Figure 5.10). Additionally, members of the Tenericutes, Bathyarchaeota, Fusobacteria and Euryarchaeota phyla increased in abundance within the alkaline contaminated sediments (Figure 5.10), particularly within the Steel sites, where increased levels of organic materials were detected (Section 5.3.1 and 5.3.4). Since the methanogen-containing phylum Euryarchaeota increased in abundance within the contaminated regions of some of these sites, this could suggest methanogens were more prevalent within the alkaline zones.

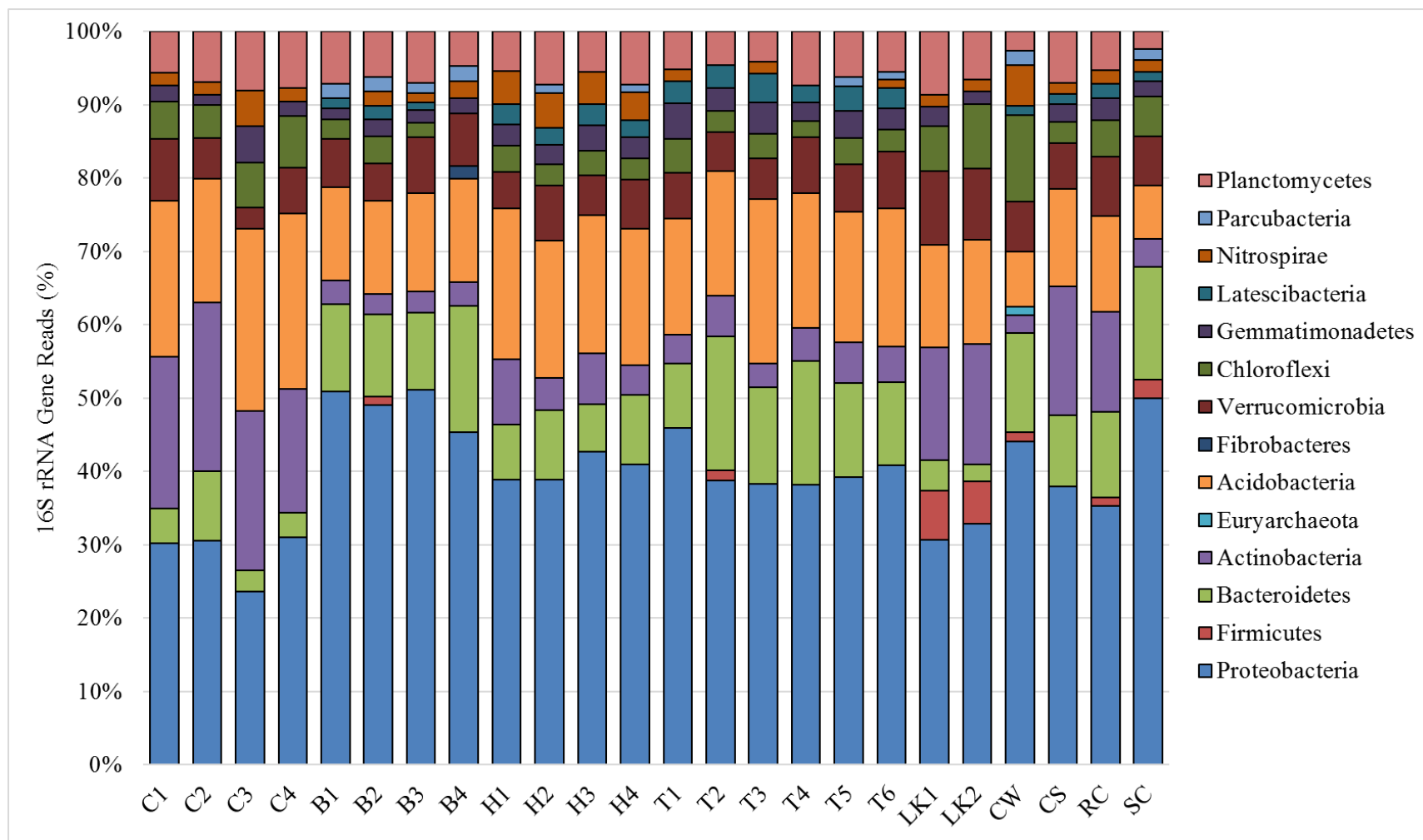


**Figure 5.7. Phylum-level composition of background sediments.** Shows phylum-level composition of background sediments from Control (site C), New Lime (sites B, H, T), Old Lime (sites LK) and Steel (sites CW, CS, RC, SC).

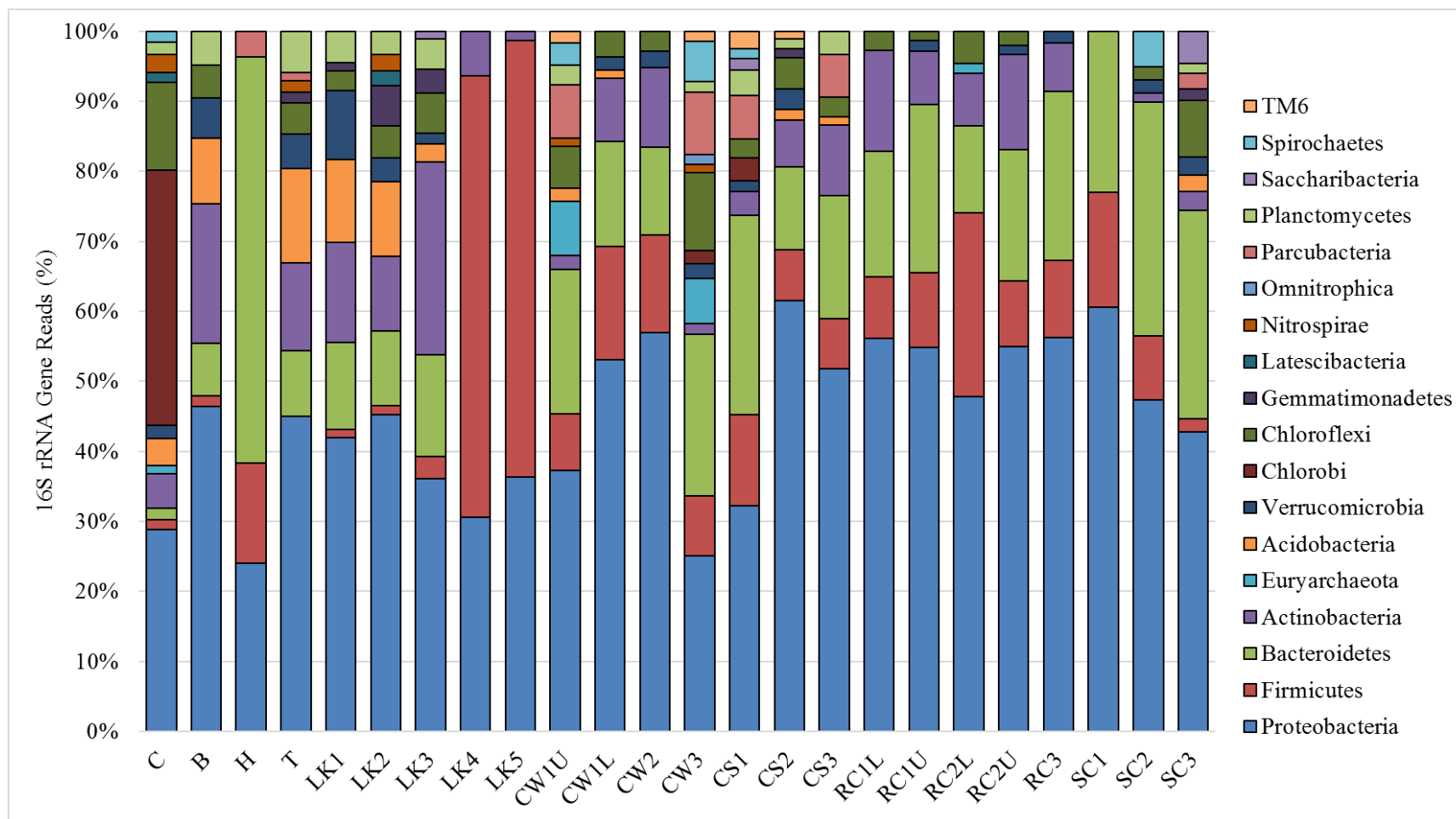


**Figure 5.8. Phylum-level composition of alkaline contaminated sediments.** Shows phylum-level composition of the alkaline contaminated sediments from Control (site C), New Lime (sites B, H, T), Old Lime (sites LK) and Steel (sites CW, CS, RC, SC).

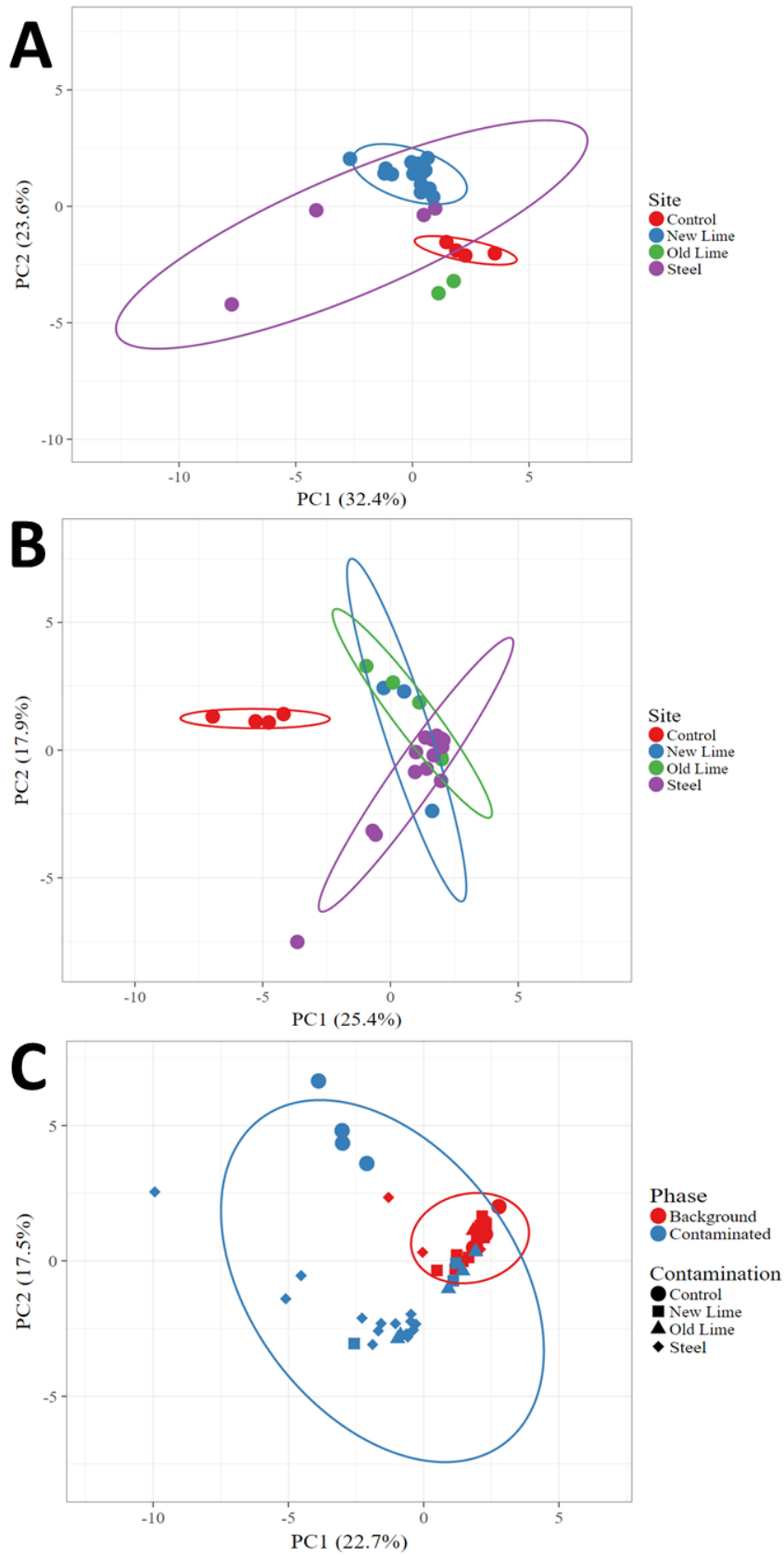


**Figure 5.9. Principal components analysis of background sediments and alkaline sediments at the phylum level. [A] PCA of background sediments, [B] PCA of alkaline sediments, [C] PCA of background and alkaline sediments together.**

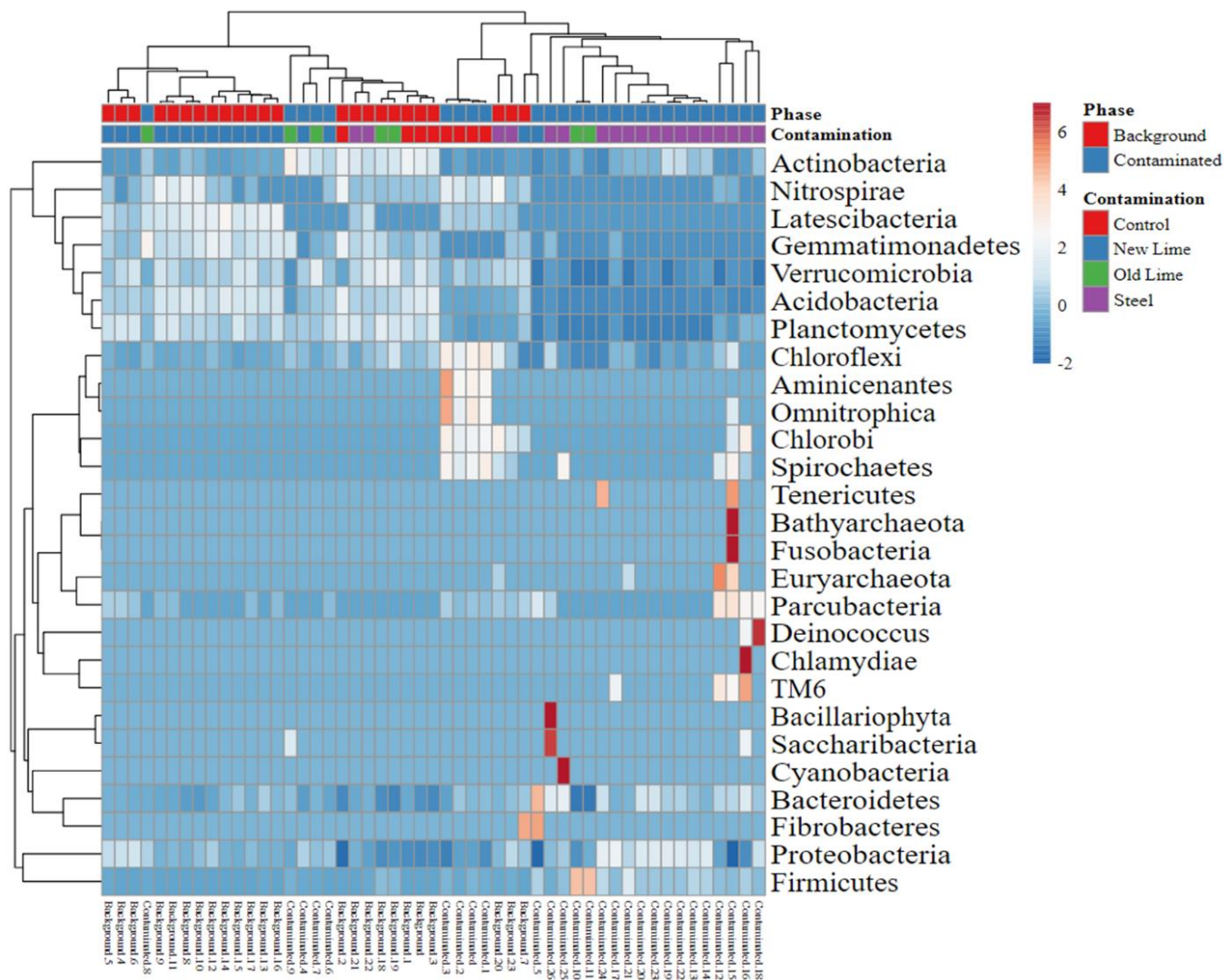


**Figure 5.10.** Heat maps comparing background and alkaline sediment communities at the phylum level from the Control, New Lime, Old Lime and Steel sites.

### 5.3.1.2 Genus-level bacterial composition of the alkaline sediments

The dominant genera within the alkaline sediments were analysed in more detail, since phylum-level analysis can only provide a limited amount of information regarding the microbial community. Within the New Lime sites the genera *Terrimicrobium* and *Bradyrhizobium* dominated the site B contaminated sediments, and represented 2.6 % and 1.8 % of the total 16S rRNA gene reads respectively (Table S5.1). The genus *Methyloceanibacter* also appeared to be important within the alkaline site B sediments, where they represented 1.2 % of the total 16S rRNA gene reads. The genus *Methyloceanibacter* are capable of oxidising methane as the sole carbon and energy source (281), which suggests methane was being generated *in situ* within this site. The nitrate-reducing bacterium *Geofilum* and hydrogen-oxidising bacterium *Hydrogenophaga* dominated the site H alkaline sediments, representing 20.6 % and 3.9 % of the total 16S rRNA gene reads respectively (Table S5.2). The detection of *Hydrogenophaga* species within the alkaline sediments from site H suggests hydrogen is available in this environment for use within anaerobic respiratory processes (282). Additionally, alkali-tolerant species of the genus *Geofilum* have demonstrated growth up to pH 9.8 in pure culture previously (283). *Azonexus* was an important genus in the alkaline sediments of site H and represented 1.6 % of the total 16S rRNA gene reads (Table S5.2), with alkali-tolerant members of this genus being isolated previously from lime-contaminated environments that were capable of nitrate reduction (284). Significant quantities of nitrate were detected in this site (Table 5.1) which could give the nitrate-reducing *Azonexus* genera a survival advantage in this environment. None of the dominant genera within the site T alkaline sediments could be identified with confidence, since the majority of detected species had <90 % 16S rRNA gene sequence similarity to any previously sequenced microbes (Table S5.3).

The genus *Hydrogenophaga* also dominated within all of the Steel site alkaline sediments, where they represented 4.2 %, 5.6 % and 2.4 % of the total 16S rRNA gene reads at sites CW, CS and SC respectively (Tables S5.4, S5.5 and S5.7). The degradation of cellulose and cellulose degradation products (CDP) within these environments appears to result in the generation of hydrogen which can be subsequently utilised by hydrogenotrophic microorganisms, evidenced by the abundance of Proteobacteria in these sites, and in particular *Hydrogenophaga* species. *Hydrogenophaga* species have been detected in a number of natural alkaline environments previously, including the Leka Ophiolite complex in Norway and the Allas Springs in Cyprus (135, 143). The genus *Shewanella* was the dominant genus within the

alkaline sediments of the Steel site RC and represented 10.7 % of the total 16S rRNA gene reads (Table S5.6). Reports of alkaliphilic members of this genus are present in the literature, including *Shewanella chilikensis* which is capable of growth up to pH 10.0 in pure culture (285). Additionally, *Shewanella oneidensis* is capable of hydrogen sulphide production, which suggests sulphidogenic processes could be ongoing within the Steel site RC. The genus *Methylothermobacter* was detected within the Steel site CS alkaline sediments and represented 1.3 % of the total 16S rRNA gene reads (Table S5.5). The species *Methylothermobacter mobilis* is capable of utilising methylamines as sole carbon and nitrogen source (286), therefore the detection of this genus within the Steel sites suggests methylamines were available for consumption by methylotrophic methanogens. The sulphur-reducing bacterium *Desulfuromonas* was an important genus within the alkaline sediments from the Steel site SC and represented 2.8 % of the total 16S rRNA gene reads (Table S5.7). Species relating to this genus have demonstrated hydrogen sulphide production (287), suggesting sulphidogenic processes were ongoing in this site. Additionally, the dissimilatory sulphate reducing bacterium *Desulfomicrobium* represented 1.2 % of the total 16S rRNA gene reads within the Steel site SC (Table S5.7) (288), suggesting further sulphidogenic processes were present in this site which again has been attributed to the treatment of these leachates with sulphuric acid resulting in the generation of metal sulphates (266).

#### **5.3.1.3 Genus-level archaeal composition of the alkaline sediments**

The percentage of 16S rRNA gene reads attributed to the methanogen-containing phylum Euryarchaeota was <1.0 % within all sites, except for the Steel site CW, where they represented 3.0 % of the total 16S rRNA gene reads and no methanogens could be detected in the alkaline sediments of the New Lime site H and Steel site SC (Figure 5.11). This suggests the methanogen population represented only a minority of the overall microbial community in these environments. However, in the sites where methanogens could be detected a diverse community was present, where a total of 23 different genera were identified (Figure 5.11). The New Lime (B and T) and Old Lime (LK) sites were the least diverse in terms of methanogens, where the strictly hydrogenotrophic genera *Methanobacterium* and *Methanothermococcus* dominated. The genus *Methanobacterium* represented 66.7 %, 19.4 % and 80.8 % of the total archaea 16S rRNA gene reads in sites B, T and LK respectively (Figure 5.11). In contrast, the Steel sites and Control site which contained higher levels of organics had a highly diverse methanogen community composed of genera capable of all three methanogenic pathways (Figure 5.11). The strictly acetoclastic genus *Methanosaeta* dominated the neutral-pH Control

site and was also present with varying abundance in the Steel sites. *Methanosaeta* represented 58.8 %, 50.2 %, 25.9 % and 19.2 % of the total methanogen 16S rRNA gene reads in sites C, CW, CS and RC respectively (Figure 5.11). The metabolically diverse genus *Methanosarcina*, which have the potential to use all three methanogenic pathways, represented 1.2 %, 3.3 %, 37.9 % and 52.1 % of the total methanogen 16S rRNA gene reads in sites C, CW, CS and RC respectively (Figure 5.11). Methylophilic methanogens, including *Methanomassiliicoccus* and *Methanomethylovorans* were only present in the Control site and to a lesser extent in the Steel sites. The genus *Methanomassiliicoccus* represented 13.2 %, 12.7 % and 4.9 % of the total methanogen 16S rRNA gene reads in sites C, CW and CS respectively (Figure 5.11), with the genus *Methanomethylovorans* representing <1 % of the reads in the same sites.

The percentage of acetoclastic, hydrogenotrophic, methylophilic and metabolically diverse methanogens was calculated based on the percentage of 16S rRNA gene reads for these organisms (Figure 5.12A). These calculations suggest the Control site and Steel sites were composed of methanogenic communities capable of all three methanogenic pathways (Figure 5.12A). In contrast, the New Lime and Old Lime alkaline sediments only harboured hydrogenotrophic methanogens. The lack of acetoclastic methanogen lineages within the New Lime and Old Lime sites correlated weakly with the levels of DOC in these sites, where the sites with higher levels of DOC generally contained a higher proportion of acetoclasts ( $R^2 = 0.4247$ ) (Figure 5.12B). A weak correlation was also observed based on the proportion of hydrogenotrophs and levels of DIC, where an increase in DIC generally saw an increase in hydrogenotrophic species ( $R^2 = 0.5853$ ) (Figure 5.12C). Increased levels of DIC in these sites could provide autotrophic processes with an advantage and result in the domination of hydrogenotrophic methanogens, since these organisms are able to metabolise inorganic forms of carbon, such as  $\text{CO}_2$  and  $\text{HCO}_3^-$  (75). Previous studies have observed a link between organic carbon levels and acetoclastic methanogenesis, for example acetate-dependent methane generation only became important in the organic-rich zones of marine sediments (72), and the addition of organic carbon in the form of rice straw stimulated acetate-derived methanogenesis through changes in the bacterial community structure in microcosm experiments (86). However, the similarities observed between the neutral-pH Control site and Steel site methanogen communities could also be a result of the seasonal pH variation observed within the Steel sites, which demonstrate neutral-pH *in situ* conditions during the late summer seasons. Therefore, the establishment of acetoclastic methanogen communities within these sites could be negatively influenced by alkaline conditions.

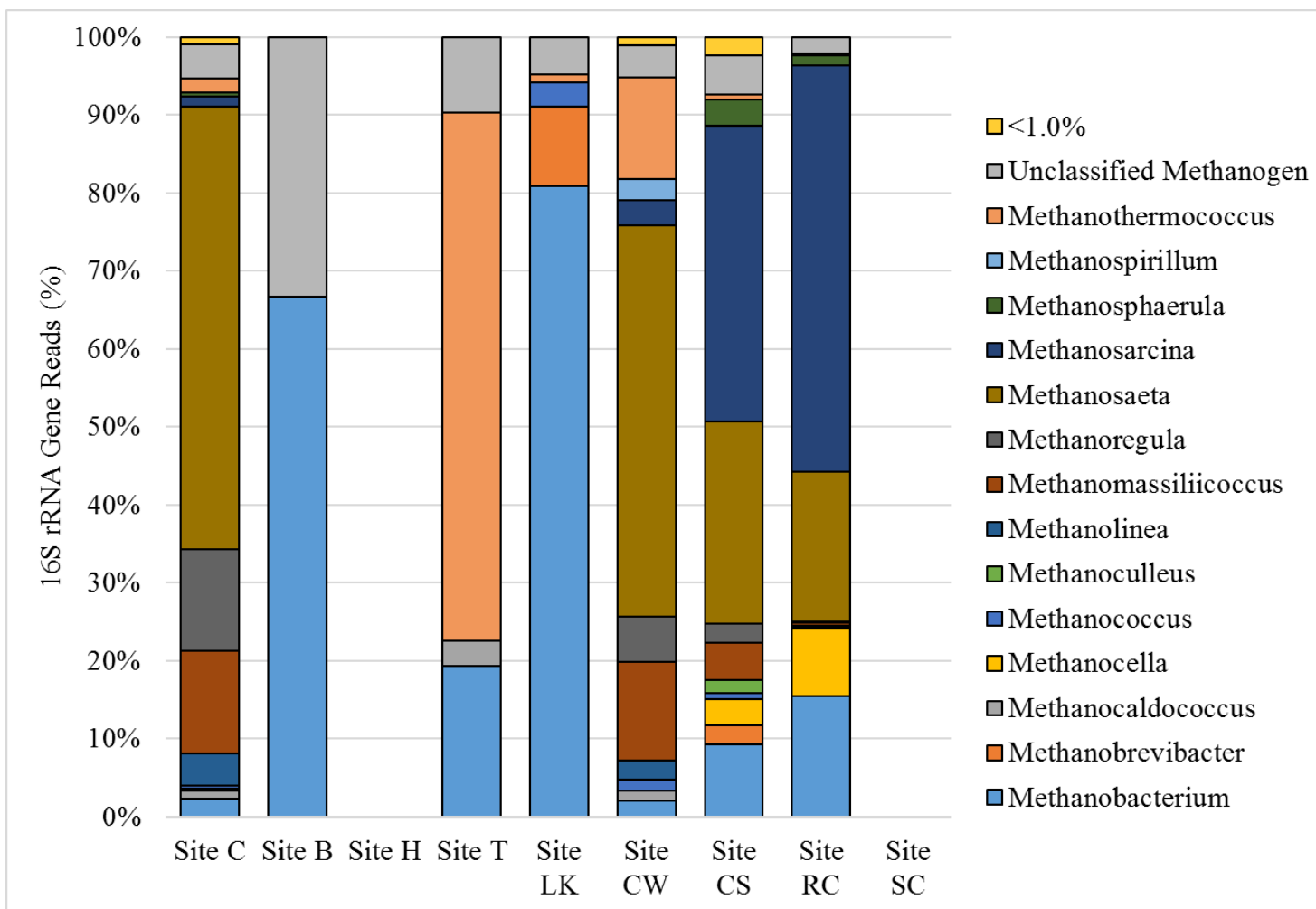


**Figure 5.11. Genus-level composition of methanogens within the alkaline sediments from various anthropogenic alkaline sites, alongside the neutral-pH control site.** Shows genus-level composition of methanogens within Control (site C), New Lime (sites B, H, T), Old Lime (site LK) and Steel (sites CW, CS, RC, SC).

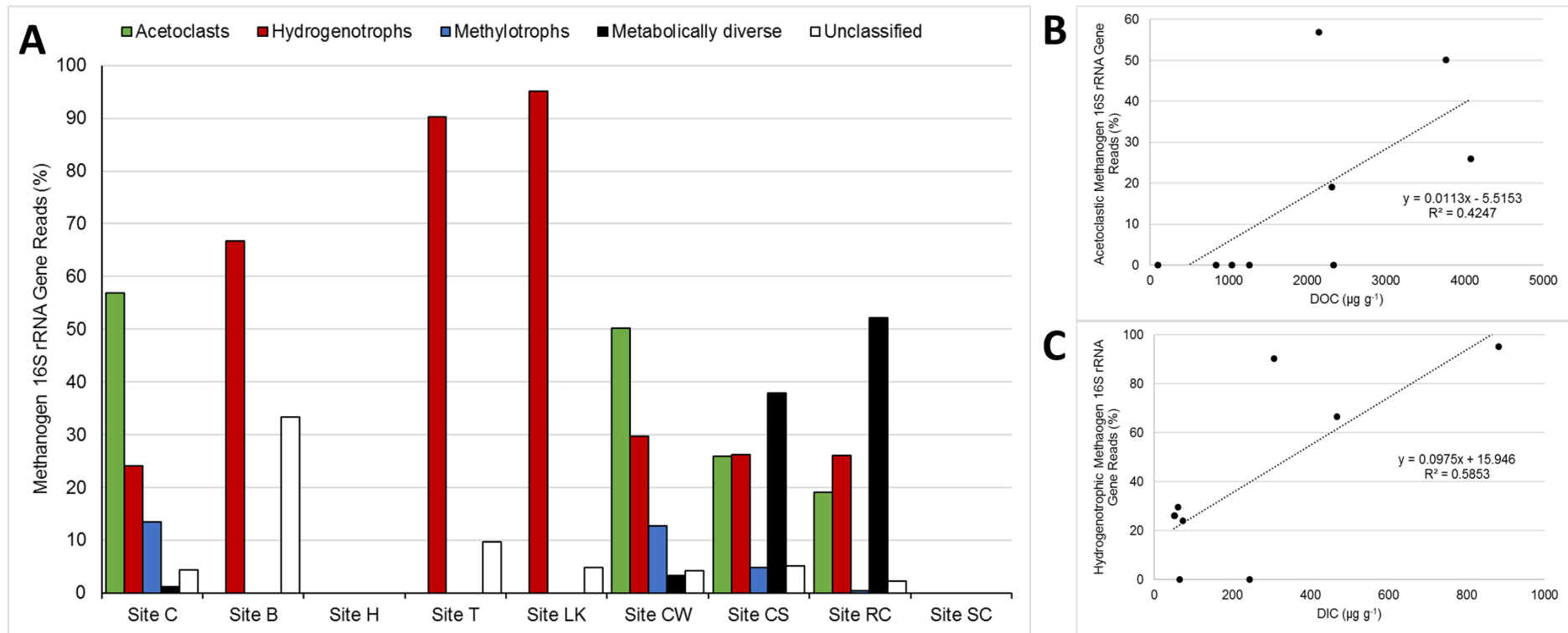


**Figure 5.12. Proportion of methanogenic pathways in the alkaline sediments from various anthropogenic alkaline sites based on 16S rRNA gene counts and correlation between levels of dissolved organic/inorganic carbon and proportion of acetoclastic/hydrogenotrophic methanogens.** [A] Methanogens capable of all three pathways were detected in the Control site and Steel sites (CW, CS, RC) and only hydrogenotrophic genera could be identified within the New Lime and Old Lime sites (B, H, T, LK). [B and C] The levels of DOC and DIC correlated weakly with the proportion of acetoclastic and hydrogenotrophic methanogen 16S rRNA gene reads.

#### 5.3.1.4 Diversity of sulphate reducing bacteria in background and alkaline sediments

The genus-level composition of SRB within the background and contaminated soils were analysed in order to highlight any differences between the neutral and alkaline regions of the sites (Figure 5.13). The average percentage of 16S rRNA gene reads attributed to SRB within the background samples from Control, New Lime, Old Lime and Steel sites was  $8.6 \times 10^{-3}$  % ( $\pm 0.01$  n=4), 0.020% ( $\pm 0.01$  n=14), 0.051% ( $\pm 0.04$  n=2) and 1.43% ( $\pm 1.38$  n=4) respectively, suggesting SRB were the less abundant members of the total bacterial community within the background soils. Interestingly, the total percentage of 16S rRNA gene reads attributed to SRB increased within the contaminated regions to 2.72% ( $\pm 0.23$  n=4), 0.05% ( $\pm 0.02$  n=3), 0.03% ( $\pm 0.02$  n=5) and 1.70% ( $\pm 2.13$  n=15) within Control, New Lime, Old Lime and Steel sites respectively. This potentially suggests more SRB were present in the alkaline contaminated regions of the sites compared to the neutral-pH background areas, however many SRB are spore-formers (289-291) and DNA sequencing does not represent an active community profile which could be obscuring this finding. The increased abundance of SRB detected within the Steel sites could be a result of the increased DOC levels in these sites as described in Section 5.3.1 and high organic content of the soil measured via TGA-MS in Section 5.3.4. SRB are capable of utilising a wide-range of organic electron donors, including acetate, lactate, propionate and free amino acids (292-294). High DOC and organic soil content could indicate that a wider range of electron donors are present and thereby increase SRB numbers in that environment. The increased detection of the Firmicutes within the contaminated sediments (Section 5.4.1, Figure 5.13) could also be resulting in higher numbers of SRB through syntrophic interactions, since many species of Firmicutes are capable of fermentative metabolism (280).

The majority of SRB 16S rRNA gene reads could not be identified with confidence at the genus-level (Figure 5.13), particularly within the background samples, potentially suggesting the sites studied here contain novel SRB that could be targeted for future studies. Within the background samples no clear correlation between sampling sites and SRB could be found. Background samples from Control, New Lime and Old Lime sites were particularly sparse in terms of SRB 16S reads. However, Steel site background soils were rich in SRB and 23 different genera were detected, the most important of which included *Desulforhopalus*, *Desulfatiglans*, *Desulfatitalea*, *Desulfobacterium*, *Desulfobulbus*, *Desulfoprunumand* *Desulfuromonas*. Species relating to these genera have been isolated previously from estuaries

(36), marine sediments (37, 38), tidal flat sediment (39), sewage sludge digesters (40), wastewater treatment plants (41) and freshwater sediments (42). Although the majority of SRB within the alkaline sediments could not be identified at the genus level with confidence (Figure 5.14), an even more diverse sulphate reducing community was detected in these environments compared to the background zones, particularly within the Steel sites and Control site where levels of organics were higher. Principal components analysis comparing the genus-level SRB communities in the background and alkaline sediments confirmed their increased diversity in the contaminated zones of the sites (Figure 5.15). The alkaline sediments had a much wider distribution compared with the background sediments, which clustered very closely together. This suggests the contaminating materials deposited in these sites were broadening the diversity of SRB communities at the genus level in these environments. The high pH conditions of these sites could be resulting in the alkaline hydrolysis of organic materials present, thereby releasing soluble forms of organic carbon into these environments and enabling the establishment of an SRB community with a higher diversity.

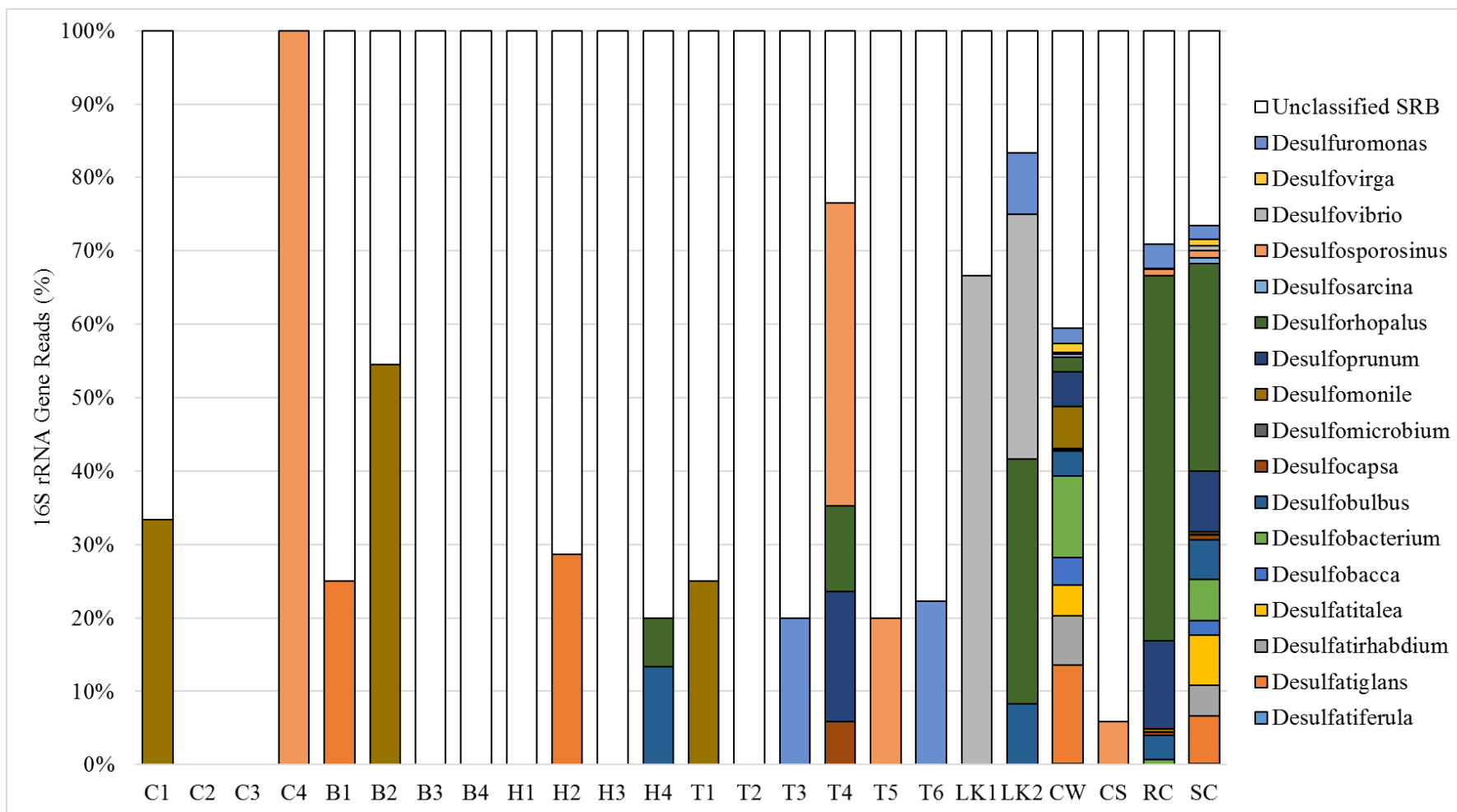


**Figure 5.13. Genus-level composition of sulphate reducing bacteria in the background sediments.** Genus-level composition of SRB in the background sediments from Control (site C), New Lime (sites B, H, T), Old Lime (site LK) and Steel (sites CW, CS, RC, SC).

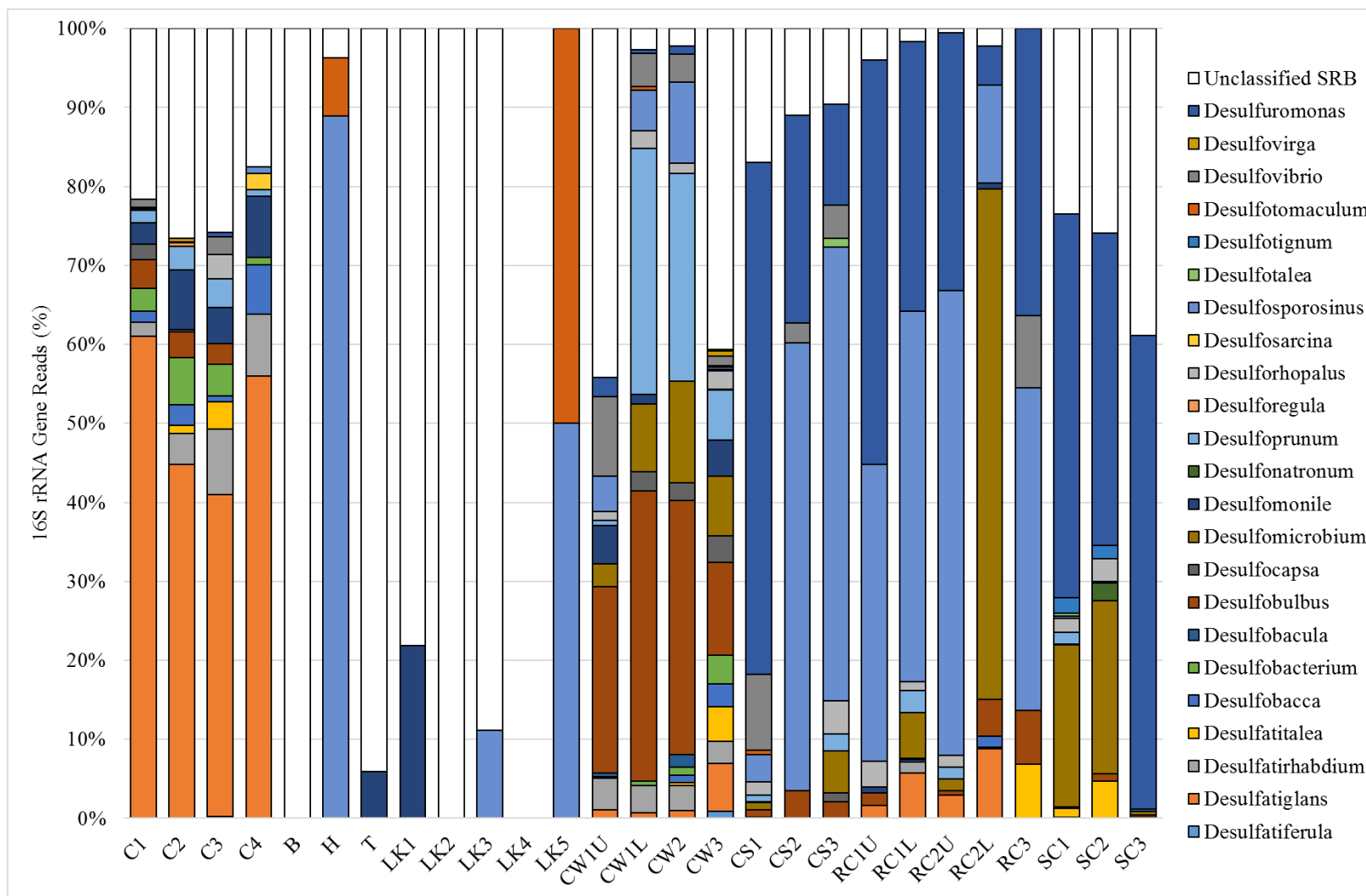


**Figure 5.14. Genus-level composition of sulphate reducing bacteria in the alkaline contaminated sediments.** Genus-level composition of SRB in the alkaline contaminated sediments from Control (site C), New Lime (sites B, H, T), Old Lime (site LK) and Steel (sites CW, CS, RC, SC).

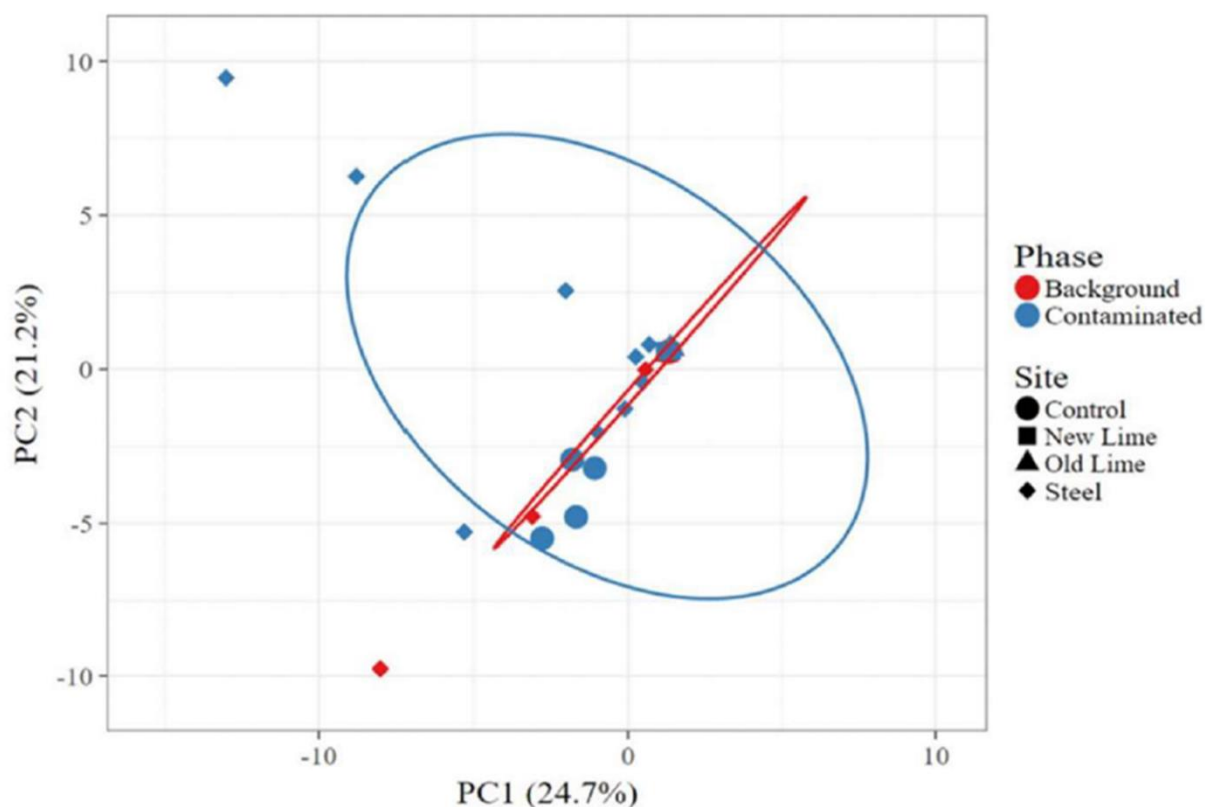


**Figure 5.15. Principal components analysis comparing the genus-level composition of SRB within the background and alkaline sediments, from Control, New Lime, Old Lime and Steel sites.**

### 5.3.2 cDNA Sequencing

Difficulties arise when trying to distinguish between active and dormant microbial populations based on DNA sequencing. It has been estimated that 20-80% of cells in aquatic and terrestrial environments are dormant and do not contribute to biological processes in their surroundings (295). The extraction of RNA from environmental samples, followed by the generation and sequencing of cDNA is a potential approach for providing an active community profile, since only actively metabolising cells are capable of synthesising RNA. RNA was extracted from the incubated cotton samples and used as a template for the generation of cDNA followed by sequencing of the 16S rRNA gene in order to demonstrate an active community profile of these alkaline environments. The Old Lime sites (LK) and Control site are not included in the present data set.

### 5.3.2.1 Phylum-level composition of cotton samples

In similar fashion to the alkaline sediments, the cotton samples were dominated by lineages related to the Proteobacteria phylum (Figure 5.16AB). However, the input of organic carbon in the form of cellulose into these environments resulted in the enrichment of fermentative lineages related to the Firmicutes phylum, which were generally detected in higher proportions on the cotton compared to the alkaline sediments (Figure 5.16AB). Although absent from the alkaline sediment communities, the phylum Fibrobacteres were present in significant proportions on the cotton samples, particularly within the Steel sites (Figure 5.16). The phylum Fibrobacteres represented 4.1 %, 4.4 %, 10.7 % and 18.0 % of the total 16S rRNA gene reads on the cotton from sites T, CW, CS and SC respectively (Figure 5.16). The increased detection of this phylum on the cotton is perhaps not surprising, given these organisms are implicated in cellulose degradation processes (296) and this is the first account of cellulose degradation by the phylum Fibrobacteres under alkaline conditions. The fact that Fibrobacteres lineages were largely absent from the alkaline sediments, yet dominated on the cotton samples suggests the incubation of cotton within these sites resulted in the enrichment of cellulose degrading bacteria, despite the harsh *in situ* pH values observed in these environments.

A small amount of overlap was observed via PCA between alkaline sediments and cotton samples at the phylum level (Figure 5.16C), suggesting a proportion of the phyla within these samples were similar. However, the alkaline sediments were more widely distributed compared with the cotton samples, which clustered more closely together (Figure 5.16C). This suggests the input of cotton into these sites resulted in the enrichment of a narrower niche of organisms, such as the cellulose-degrading lineages Firmicutes and Fibrobacteres.

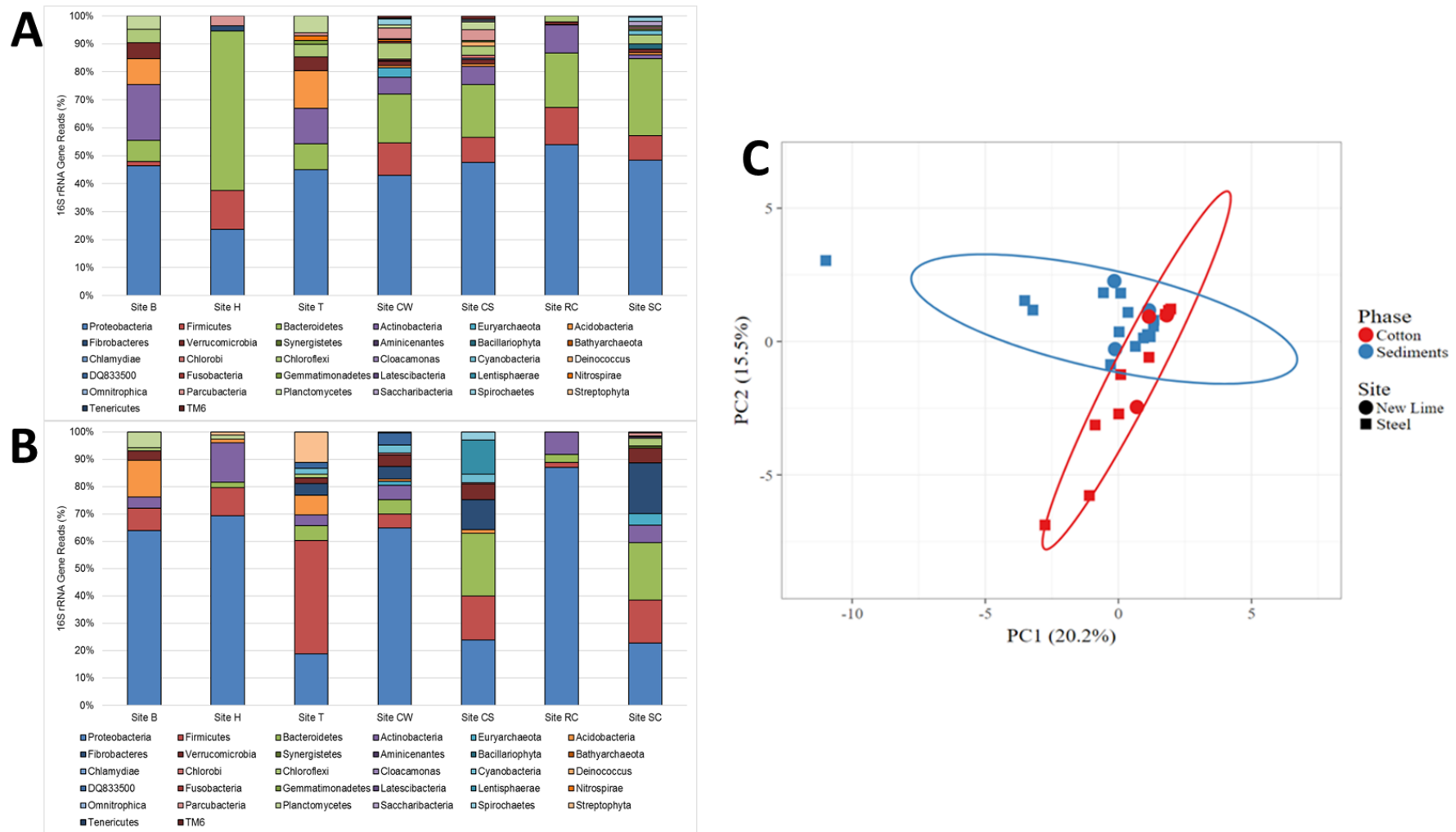


**Figure 5.16. Phylum-level composition of alkaline sediments and cotton samples from various anthropogenic alongside principal components analysis of the sediments vs the cotton samples. [A] Phylum-level composition of alkaline sediments, [B] phylum-level composition of cotton samples, [C] principal components analysis of alkaline sediments and cotton samples.**

### 5.3.2.2 Genus-level archaeal analysis of cotton samples

The methanogen community of the cotton samples based on cDNA sequencing had a different composition compared with the alkaline sediment samples based on DNA sequencing (Figure 5.17AB). In contrast to the alkaline sediments, the strictly hydrogenotrophic genera *Methanoregula*, *Methanoculleus* and *Methanospirillum* dominated the cotton samples at all sites (Figure 5.17AB). The genus *Methanoregula* represented 100 %, 33.3 %, 54.7 %, 72.3 % and 3.3 % of the total methanogen 16S rRNA gene reads from sites B, H, T, CW and CS respectively (Figure 5.17B). The genus *Methanoculleus* dominated the site T cotton samples, where 66.7 % of the total methanogen 16S rRNA gene reads were attributed to this organism (Figure 5.17B). *Methanospirillum* represented 4.7 %, 25.5 %, 91.1 % and 96.7 % of the total methanogen 16S rRNA gene reads from sites T, CW, CS and SC respectively (Figure 5.17B). The strictly acetoclastic genus *Methanosaeta* was only present in low abundance in sites T and CS, representing 17.2 % and 0.3 % of the total methanogen 16S rRNA gene reads respectively (Figure 5.14). The metabolically diverse genus *Methanosarcina* was also present in low abundance in sites T, CW, CS and SC, representing 20.3 %, 1.1 %, 5.3 % and 0.2 % of the total methanogen 16S rRNA gene reads respectively. In similar fashion to the bacterial cotton communities (Section 5.4.2.1) the incubation of cotton within these sites resulted in the enrichment of a narrow niche of archaea. This was illustrated by PCA where the methanogen communities on the cotton clustered very closely together regardless of the sampling site (Figure 5.17C). In contrast, the methanogen communities in the alkaline sediments had a much wider distribution (Figure 5.17C), suggesting the incubated cotton samples were selecting for a specific methanogen population.

Although methanogens capable of utilising all three pathways were detected in the alkaline sediments (Figure 5.18A), the cotton samples were dominated by hydrogenotrophs regardless of the sampling site (Figure 5.18B). The lower abundance of acetoclastic and methylotrophic species detected on the cotton compared with the alkaline sediments based on cDNA sequencing suggests the active methanogen population in these sites are contributing predominantly to hydrogenotrophic methane generation (Figure 5.18AB). The input of a cellulosic substrate into an alkaline environment, as is expected to be the case within an ILW-GDF, resulted in a methanogenic population almost entirely dependent on hydrogenotrophic methanogenesis.

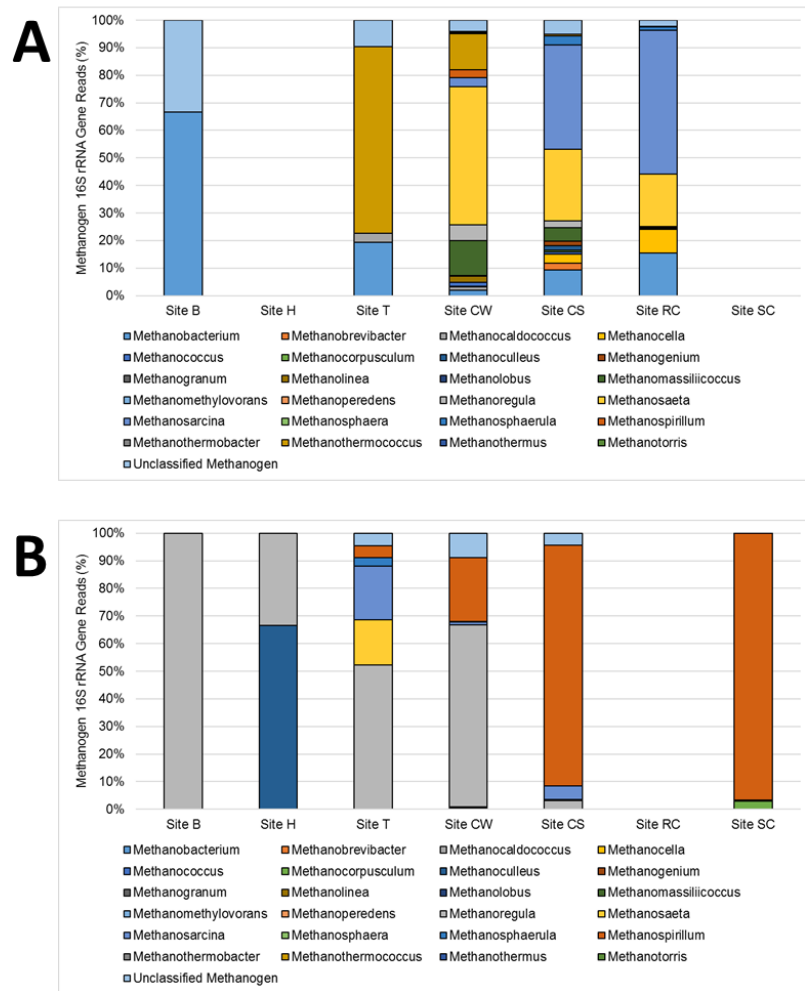


**Figure 5.17. Genus-level methanogen community composition of alkaline sediments and cotton samples. Also showing PCA comparing genus-level methanogen communities within cotton samples and alkaline sediments. [A] Genus-level methanogen composition of alkaline sediments, [B] genus-level methanogen composition of cotton samples, [C] PCA of genus-level methanogen communities from cotton samples and alkaline sediments.**

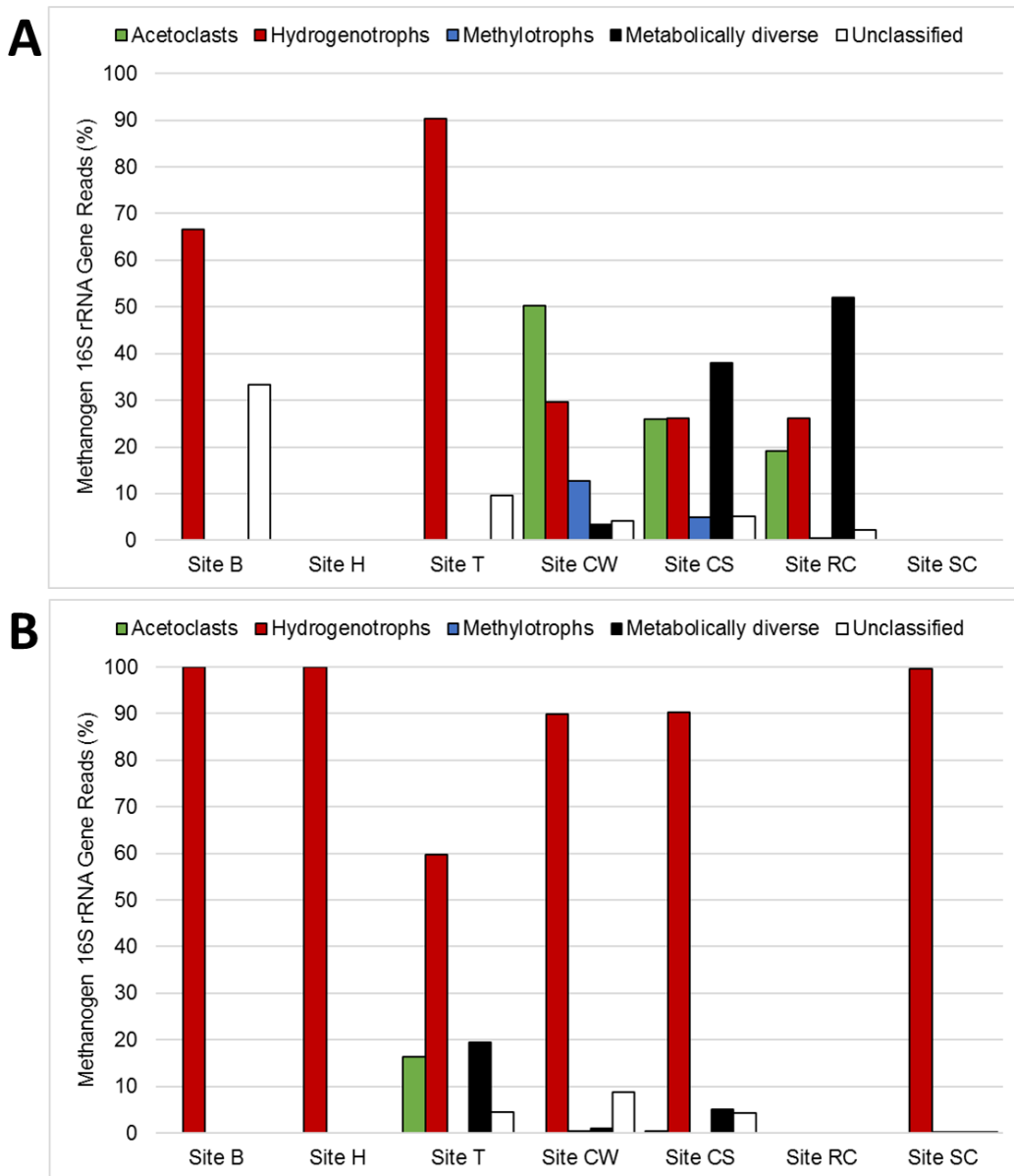


**Figure 5.18. Proportion of acetoclastic, hydrogenotrophic, methylotrophic and metabolically diverse methanogens within the alkaline sediments and cotton samples.**

[A] Methanogenic pathways present within the alkaline sediments, [B] methanogenic pathways present on the cotton samples.

### 5.3.2.3 Diversity of sulphate reducing bacteria on the cotton samples

In addition to the active methanogenic population present on the cotton samples, an active sulphate reducing community was also detected on these samples via cDNA sequencing. Although the percentage of 16S rRNA gene reads attributed to SRB was <1 % within the lime-contaminated sites, the cotton samples taken from Steel sites CS and SC were dominated by SRB, where they represented 19.0 % and 6.0 % of the total 16S rRNA gene reads respectively (Figure 5.19). The elevated levels of sulphate detected in the Steel site CS (Table 5.1) resulted in the dominance of SRB on the cotton in this environment. Within the sites where SRB were abundant, the genera *Desulfobulbus*, *Desulfobacter* and *Desulforhopalus* were the most dominant (Figure 5.19B). The genus *Desulfobulbus* has been implicated in bio-corrosion processes previously (297). Additionally, a number of species relating to the genus *Desulfobacter* have been identified as strictly acetate-oxidising SRB (298), therefore the detection of this genus on the cotton samples suggests sulphate reduction is competing with methanogenesis for acetate. The competition for acetate between SRB and methanogens could explain the lack of acetoclastic methanogens detected on the cotton samples as described in Section 5.4.2.2, and may be resulting in the domination of hydrogenotrophic species in these environments. Previous authors have suggested sulphate reduction can thermodynamically inhibit methanogenesis when sulphate is abundant (72), however these processes can also co-exist in the presence of non-competitive substrates, such as methylamines (40).

As observed with the archaeal community analysis (Section 5.4.2.2), the incubation of cellulose within these sites appeared to select for a more narrow and less diverse sulphate reducing community. This was revealed by PCA, where the SRB communities on the cotton clustered closely together compared with the SRB sediment communities, which generally had a more diverse and wider distribution, even though a small amount of overlap was observed (Figure 5.19C). The use of molecular methods to characterise the methanogenic and sulphate reducing communities in these environments could help to reduce the bias associated with direct culturing methods. However, it is important to note that the communities analysed here were from near-subsurface environments (~1 m deep) and therefore do not represent deep subsurface populations, such as those likely to be encountered within an ILW-GDF, which could be constructed up to 1000 m below ground (6).

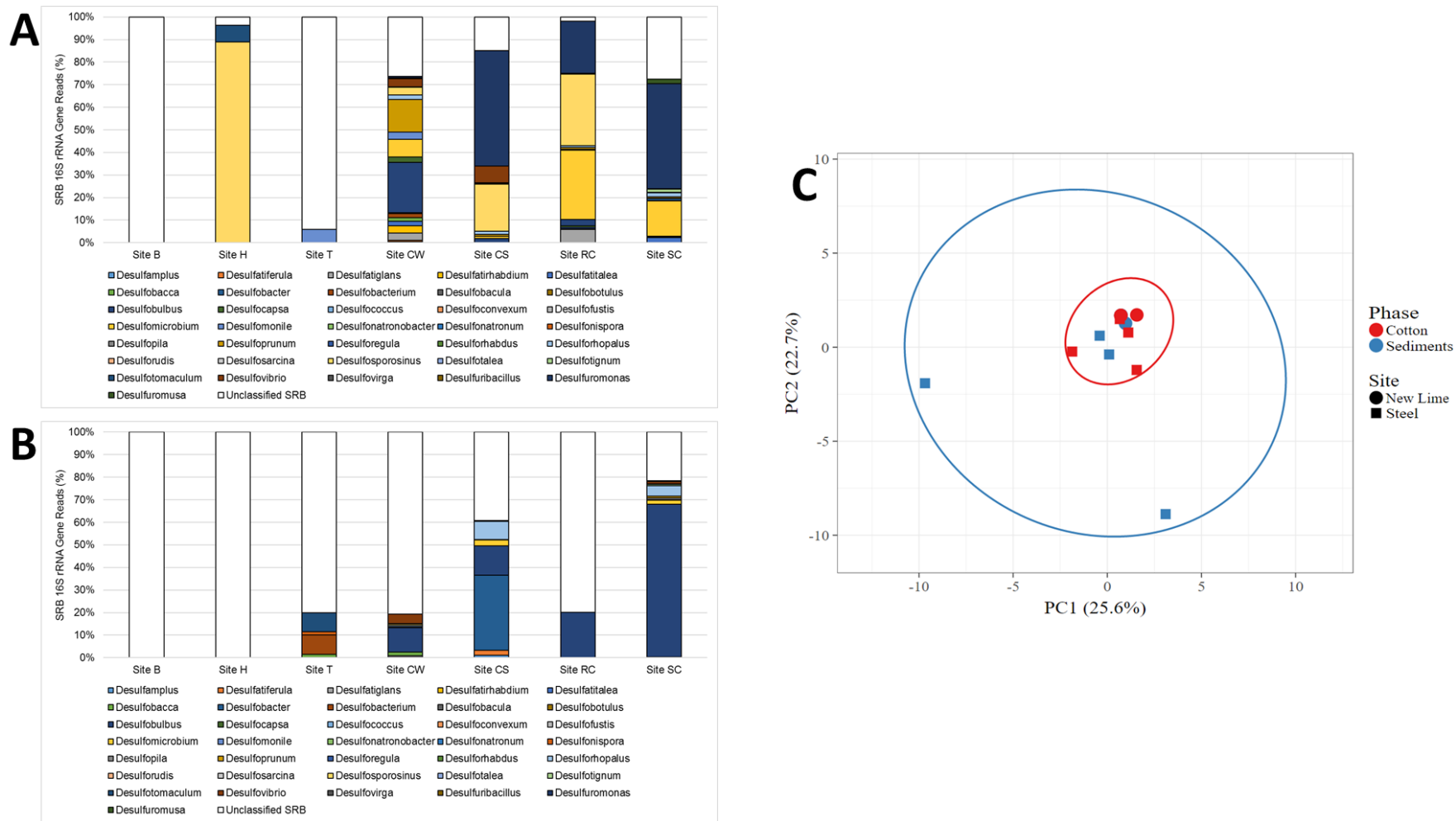


**Figure 5.19. Genus-level composition of sulphate reducing bacteria within the alkaline sediments and cotton samples, alongside principal components analysis comparing the SRB sediment and cotton communities. [A] Genus-level composition of SRB within the alkaline sediments, [B] genus-level composition of SRB on the cotton, [C] principal components analysis comparing the differences between sediment and cotton SRB communities**

## 5.4 Microscopy

### 5.4.1 Scanning Electron Microscopy

The formation of biofilm on the incubated cotton samples was analysed via SEM. All cotton samples were colonised by microbial cells embedded in extracellular polymers when compared with abiotic samples, indicating biofilm was being formed *in situ* within these sites (Figure 5.20). In some cases the cotton fibres appeared to be visually degraded, indicated by the perforated edges of the fibres when compared to abiotic samples (Figure 5.20C). The degradation of the cotton samples could be a result of alkaline cellulose hydrolysis or due to the activity of cellulose-degrading bacteria. Since a significant proportion of bacteria on the cotton samples were cellulose-degraders, including the Fibrobacteres and Firmicutes lineages (Section 5.4.2), it is likely that microbial activity is contributing to cellulose degradation in these environments. Cotton samples taken from the New Lime sites appeared to contain a number of mineral structures that had sharper edges than would be expected from microbial biofilms (Figure 5.20D), potentially suggesting calcium carbonates are being incorporated into the biofilm materials.

SEM-EDS was employed to determine the elemental composition of the biofilms formed on the cotton (Figure 5.21). Calcium, carbon and oxygen were the dominant elements present on all analysed cotton samples compared with abiotic controls, potentially suggesting that calcium carbonate was precipitating on the biofilm surfaces, although SEM-EDS can only provide information regarding individual elements and not compounds. The potential detection of calcium carbonate minerals in the biofilm could provide autotrophic methanogens with substrate for metabolism as described previously under neutral-pH conditions (236). Furthermore, the presence of calcium carbonate in the biofilm could give hydrogenotrophic methanogens an advantage in these environments and result in a lower contribution of acetoclastic methanogenesis, as described in Section 5.3.2.2. Since calcium can co-precipitate with radioelements (299), the precipitation of calcium carbonate has importance when determining the performance of an ILW-GDF (300). The carbonation of NRVB can impact the surface chemistry and porosity of the backfilling material and result in the build-up of gases which could lead to pressurisation issues (6).

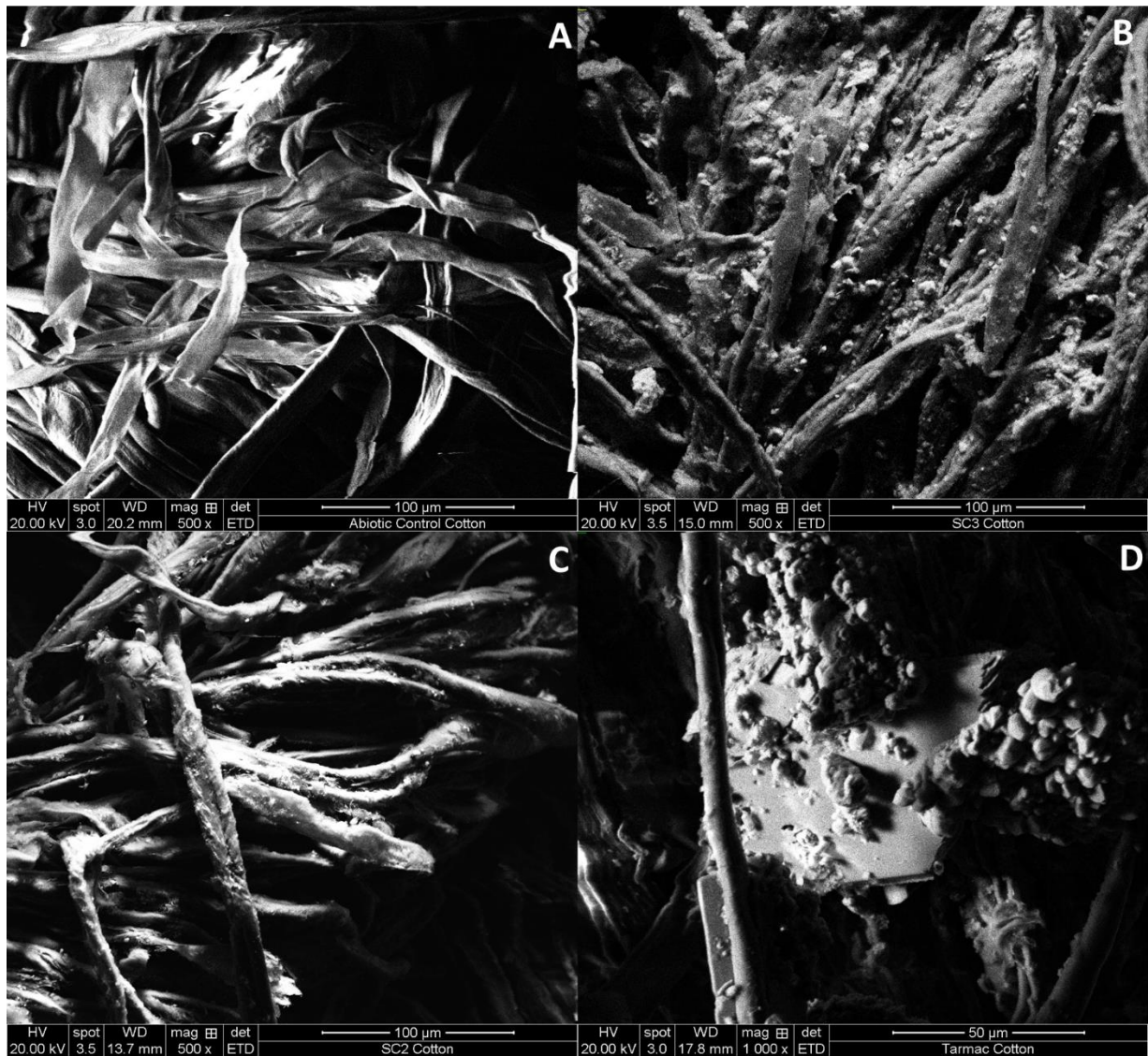


**Figure 5.20. Scanning electron micrographs of cotton samples retrieved from various anthropogenic alkaline sites after 3 months incubation. [A] Abiotic cotton, [B] biotic cotton from the Steel site SC biofilm, [C] biotic cotton from the Steel site SC showing potential degradation, [D] biotic cotton from the New Lime site T, showing potential minerals incorporated into the biofilm.**

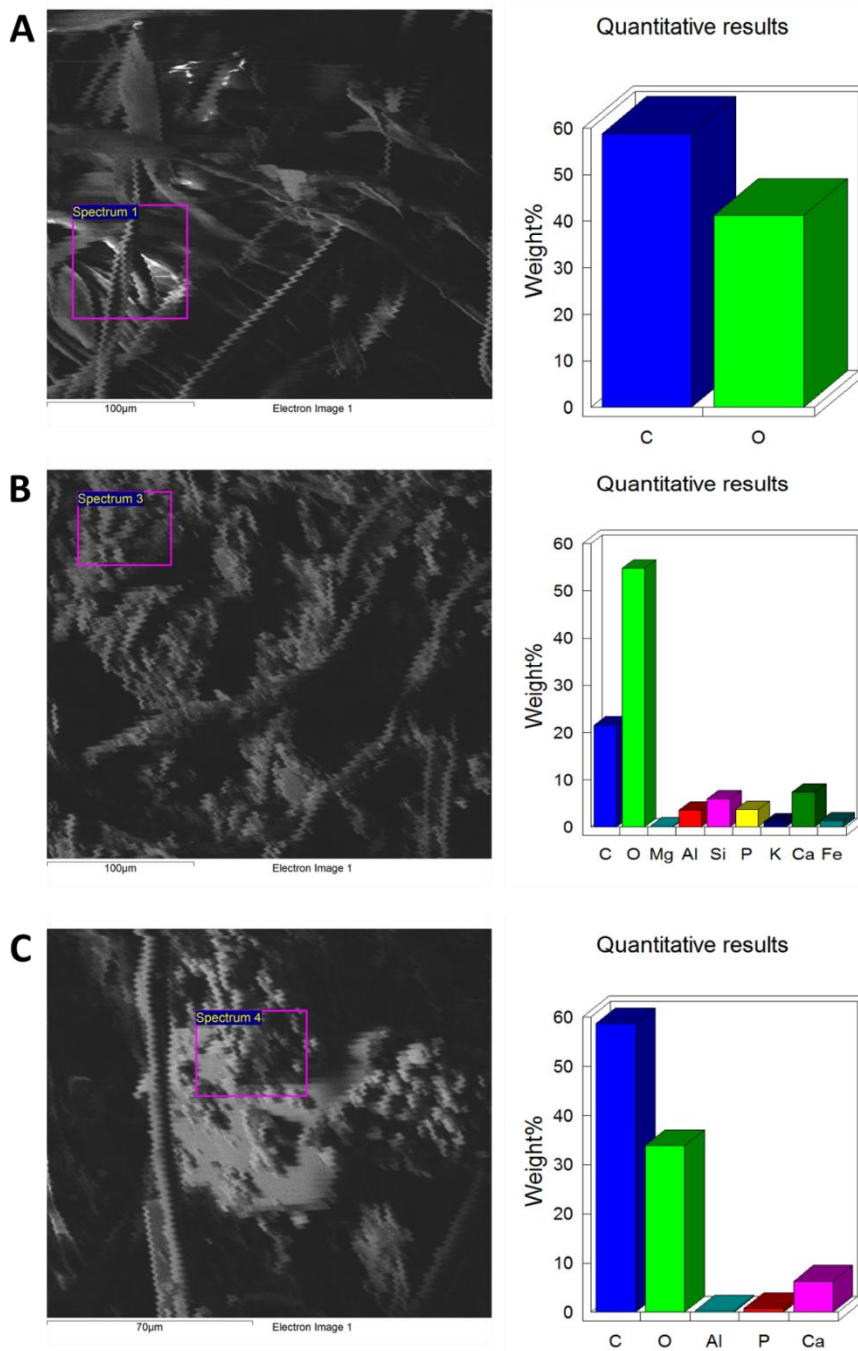


**Figure 5.21. SEM-EDS of cotton samples showing elemental composition of the biofilm materials. [A] Abiotic cotton, [B] biotic cotton from Steel site SC, [C] biotic cotton from New Lime site T.**

### 5.4.3 Confocal Laser Scanning Microscopy

The biofilm materials detected on the cotton samples via SEM were subsequently analysed using fluorescence microscopy with the use of CLSM. Significant auto-fluorescence was observed from the polysaccharide component when viewing the abiotic control cotton and therefore was not included as a potential component of the biofilm matrix (Figure 5.22B). However, a range of EPS components were detected on the biotic cotton samples that were not present on the abiotic samples, including lipids, sugars, protein, eDNA and cells (Figure 5.22C-F). The edges of the cotton fibres in some cases were lined with sugars (Figure 5.22CD), which could indicate cellulose was being degraded to simple monomeric sugar residues by the associated microbial community, such as the Fibrobacteres and Firmicutes lineages and provides a further indication that microbial activity is contributing to the degradation of cellulose, rather than alkaline chemical hydrolysis pathways. Within the sites that contained the highest *in situ* pH values, the biofilm appeared to be predominantly composed of lipids (Figure 5.22EF). The higher lipid content of these biofilms could be contributing to their hydrophobicity, which not only improves microbial attachment to the cotton surface (158), but also reduces the impact of the alkaline pore-waters by reducing wetting (301). The production of lipid-based EPS can also result in the generation of low pH niches due to the presence of acidic phospholipids, such as those produced in alkaliphilic bacteria (133). The negative charge produced by the eDNA component of the biofilms could be resulting in the binding of  $\text{Ca}^{2+}$  ions to the EPS matrix, which can in turn enhance the structural properties of the biofilm as described previously (302).

The formation of biofilm on the cotton suggests the organisms were not surviving under *in situ* pH conditions within these sites. As described previously biofilm formation can facilitate microbial survival through the production of low pH niches that can improve microbial activity (125). Therefore, the methanogenic and sulphate-reducing activity detected in these environments using molecular methods (Section 5.3) may be due to the generation of low pH microsites through biofilm formation and metabolic acid production.

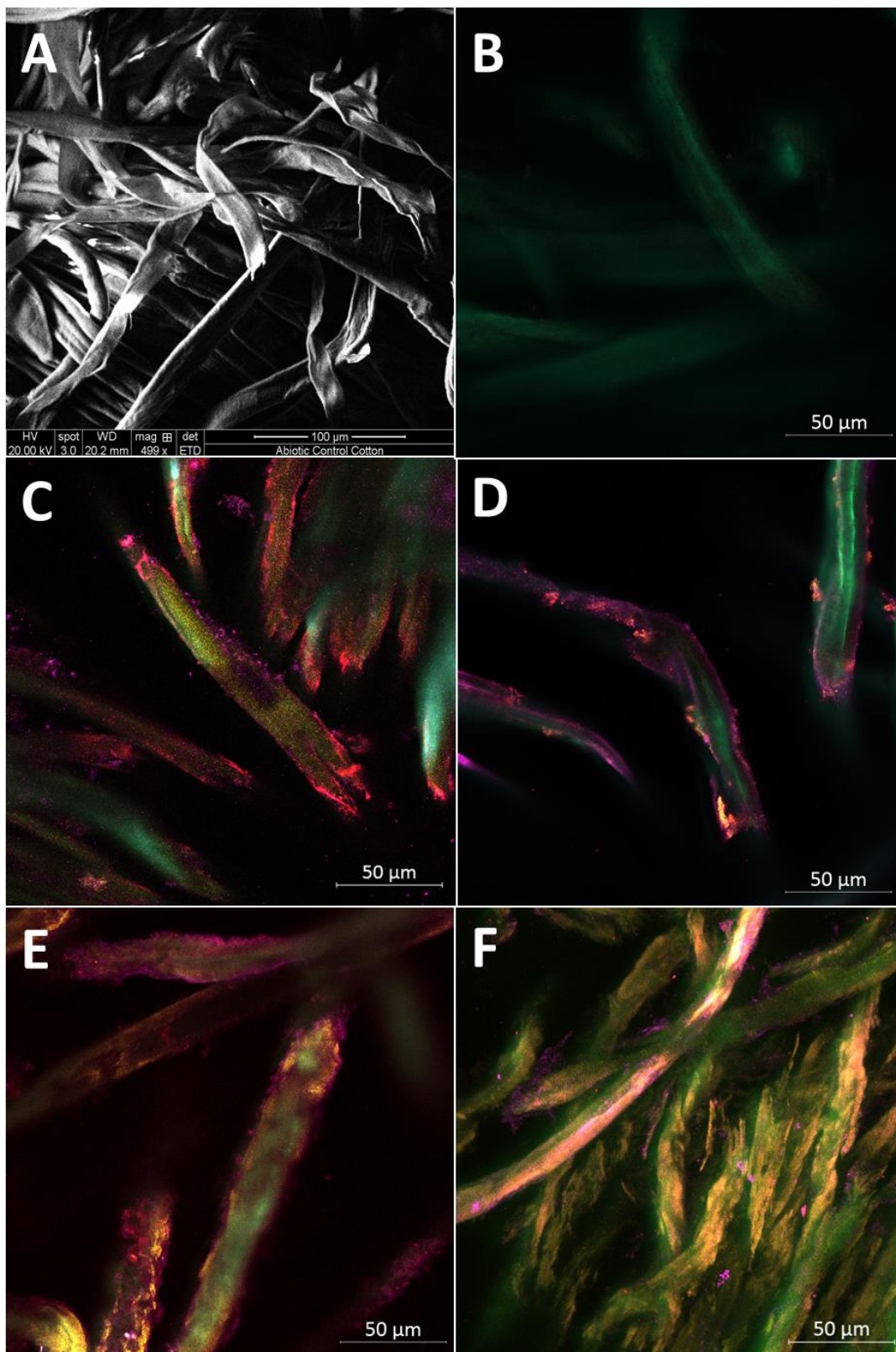


**Figure 5.22. CLSM investigation of cellulose cotton samples.** [A] SEM of abiotic cotton, [B] auto-fluorescence control of abiotic cotton, [C] site CW cotton, [D] site B cotton, [E] site H cotton, [F] site RC cotton. Showing protein (green), lipids and hydrophobic sites (yellow), polysaccharides (blue), cells and extracellular DNA (pink) and sugar residues (red).

## 5.5 Conclusions

Anthropogenic alkaline environments, such as the lime-waste and steel-waste disposal sites studied here, represent some of the least studied systems in terms of microbial diversity, therefore a better understanding of the microbiology in these sites could provide an insight into the evolution of microbial communities within an ILW-GDF. The detection of methanogenic and sulphate reducing communities within these anthropogenic sites using RNA as a template for 16S rRNA gene sequencing underpins the ability of these microbes to survive and grow within an ILW-GDF. The input of cellulose into these sites simulates some aspects of ILW disposal, where cellulosic substrates will be placed within a highly alkaline and anaerobic environment.

A diverse and active anaerobic microbial community was present in these sites despite the extreme environmental conditions, capable of processes including cellulose degradation, fermentation, sulphate reduction and methanogenesis. The detection of cellulose-degrading bacteria based on cDNA sequencing, including lineages relating to the phylum Fibrobacteres, underlines the ability of near-surface and alkali-adapted communities to survive and grow within an ILW-GDF. The degradation of cellulose within these sites through abiotic alkaline hydrolysis and microbial activity provided the substrates for downstream fermentation, sulphate reduction and methanogenesis, where hydrogen appeared to be an important electron donor. Hydrogenotrophic methanogens of the genera *Methanoregula*, *Methanoculleus* and *Methanospirillum* dominated the archaeal communities on the cellulose, and the ubiquitous nature of *Hydrogenophaga* throughout the bacterial communities in these sites further underlines the importance of H<sub>2</sub> within an ILW-GDF. Methanogens capable of all three pathways were detected in the sediments based on DNA sequencing, suggesting the input of cellulose into these sites selected for a methanogen community dependent on H<sub>2</sub>/CO<sub>2</sub>. Alongside methanogenesis, an active sulphate reducing community was detected on the cellulose samples incubated within the organic-rich steel slag sites that demonstrated conditions of lower alkalinity (pH ~11.0). The dominant SRB within these sites were the acetate-utilising *Desulfobacter*, which resulted in a decreased contribution of acetoclastic methanogenesis in these environments.

Statistical differences were revealed between the background and alkaline zones of these sites, where spore-forming and fermentative lineages of the phylum Firmicutes became more abundant in the alkaline-disturbed zones and members of the phylum Acidobacteria reduced in

abundance. Even though pore-water pH values of ~13.0 were detected in some cases, the majority of microbial activity may be ongoing at pH values much lower than this, facilitated by the formation of biofilm and production of metabolic acids, such as acetate. Overall, the data shown in this first chapter of work suggests the products of cellulose degradation can support methanogenic and sulphate reducing processes under environmental conditions when bulk pH values of 11.0-13.0 are observed.

# **6.0 Investigating the Utilisation of Methanogenic Pathways at High pH**

## 6.1 Rationale

This chapter aims to identify the dominant methanogenic pathways utilised at high pH and to identify the upper pH limits for methanogenesis in planktonic culture. As discussed in Chapter 1, the ability of an ILW-GDF at retaining radioelements could be influenced by an active methanogenic community (6). Methane generation has the potential to influence gas volumes and pressures within the near-field of an ILW-GDF and could act as a mechanism by which  $^{14}\text{C}$  can be transported to the biosphere via the production of  $^{14}\text{CH}_4$  (303). The upper pH limits for methanogenesis are not well defined and there is a lack of information available regarding the relative contribution of methanogenic substrates to methane generation under alkaline conditions. The sediment samples retrieved from the alkaline New Lime sites (B, H and T) mentioned in Chapter 5 were used as inoculating materials for the development of methanogenic enrichment cultures between pH 7.0-12.0. Additionally, the Control site (C) was used as a reference. The consumption and generation of methanogenic substrates when fed with CDP,  $\text{H}_2/\text{CO}_2$  or acetate was measured within these microcosms in order to assess pathway utilisation and the methanogen community was described via 16S rRNA gene sequencing. Methyl fluoride ( $\text{CH}_3\text{F}$ ), the selective inhibitor of acetoclastic methanogenesis, was employed to help discriminate between  $\text{H}_2/\text{CO}_2$ -derived and acetate-derived methane generation within these cultures. The study was expanded further to incorporate the Old Lime (LK) and Steel (CW, CS, RC and SC) sediments, which were used to develop hydrogenotrophic ( $\text{H}_2/\text{CO}_2$ -fed) and acetoclastic (acetate-fed) methanogen enrichment cultures at pH 7.0 and 10.0.

## 6.2 CDP-fed Microcosms

### 6.2.1 Control Site Microcosms

#### 6.2.1.1 ISA Degradation

CDP-fed microcosms employing the neutral-pH control sediments were capable of degrading all three forms of ISA between pH 7.0-10.0 (Figure 6.1), with the rate of fermentation reducing significantly at pH 10.0 (Figure 6.1). The rate of  $\alpha$ ,  $\beta$  and X-ISA degradation was calculated between pH 7.0-10.0 (Figure 6.2 and Table 6.1). Within pH 7.0, 8.0, 9.0 and 10.0 microcosms  $\alpha$ -ISA degradation rates were  $2.4 \times 10^{-1}$  ( $\pm 2.7 \times 10^{-2}$ , n=2),  $1.6 \times 10^{-1}$  ( $\pm 9.0 \times 10^{-3}$ , n=2),  $1.3 \times 10^{-1}$  ( $\pm 2.2 \times 10^{-2}$ , n=2) and  $6.1 \times 10^{-3}$  ( $\pm 6.3 \times 10^{-3}$ , n=2) day<sup>-1</sup> respectively.  $\beta$ -ISA degradation rates were  $1.8 \times 10^{-1}$  ( $\pm 9.6 \times 10^{-3}$ , n=2),  $1.5 \times 10^{-1}$  ( $\pm 4.3 \times 10^{-3}$ , n=2),  $1.1 \times 10^{-1}$  ( $\pm 2.5 \times 10^{-4}$ , n=2) and  $1.2 \times 10^{-2}$  ( $\pm 8.6 \times 10^{-3}$ , n=2) day<sup>-1</sup> within pH 7.0, 8.0, 9.0 and 10 microcosms respectively. X-ISA degradation rates within pH 7.0, 8.0, 9.0 and 10.0 microcosms were  $1.2 \times 10^{-1}$  ( $\pm 1.9 \times 10^{-2}$ , n=2),  $1.2 \times 10^{-1}$  ( $\pm 2.6 \times 10^{-3}$ , n=2),  $9.5 \times 10^{-2}$  ( $\pm 2.3 \times 10^{-3}$ , n=2) and  $3.2 \times 10^{-2}$  ( $\pm 5.0 \times 10^{-4}$ , n=2) day<sup>-1</sup> respectively. This suggests the rate of  $\alpha$ ,  $\beta$  and X-ISA degradation decreased as the pH increased. Highest rates of  $\alpha$  and  $\beta$  ISA degradation were present in pH 7.0 microcosms and X-ISA degradation rates were highest in pH 8.0 microcosms. It should perhaps not be surprising that ISA degradation rates were highest under neutral-pH conditions and decreased significantly under alkaline conditions when employing populations from a neutral-pH site. Microcosms employing the same canal sediments as used here have been shown to be capable of ISA fermentation and consequently methanogenesis up to pH 10.0 previously and demonstrated comparable ISA degradation rates to those observed here (23). However, using alkali-adapted communities could increase the rate of ISA degradation under alkaline conditions (24).

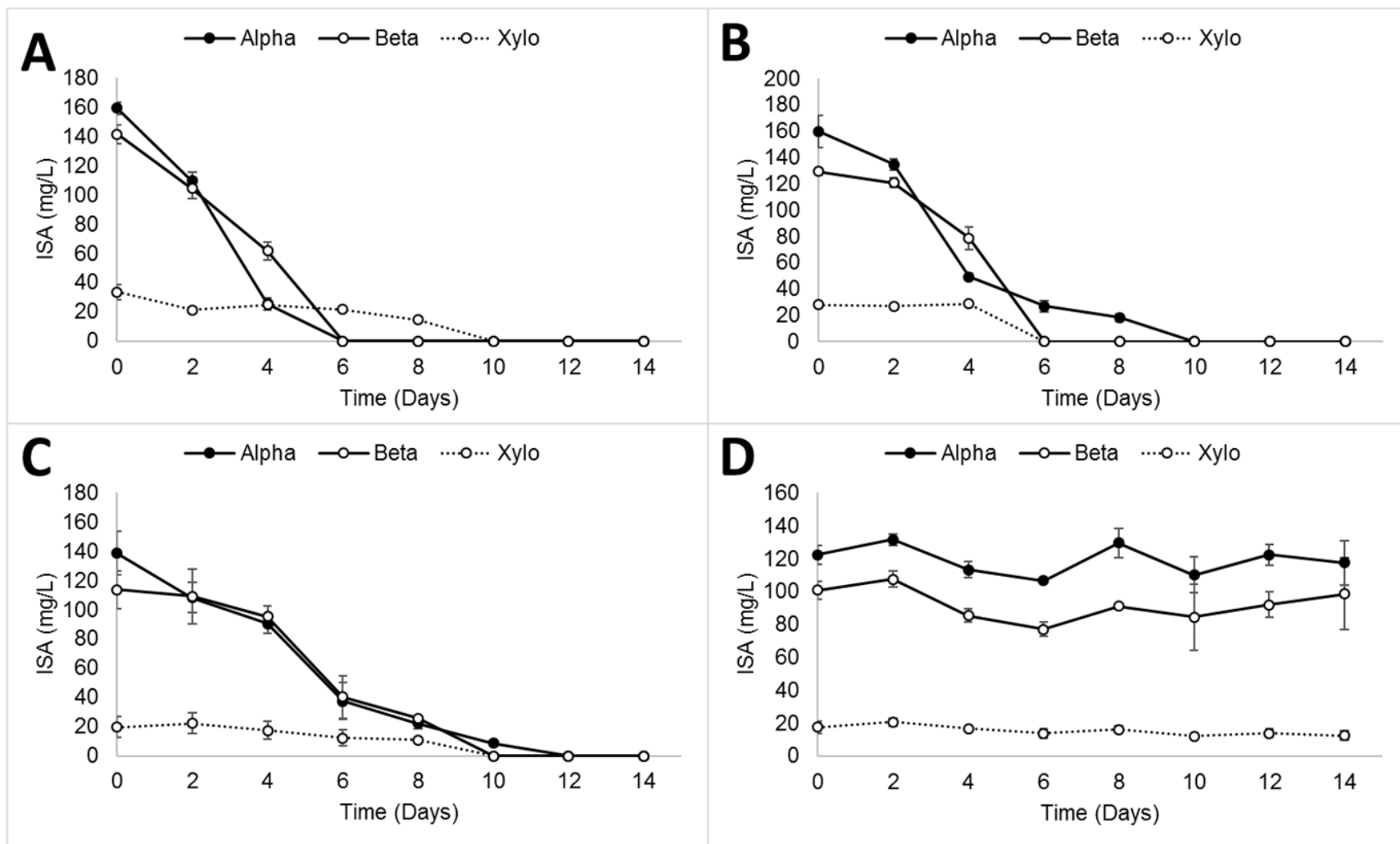


**Figure 6.1. ISA concentrations within microcosms employing neutral-pH Canal sediments. [A] pH 7.0, [B] pH 8.0, [C] pH 9.0, [D] pH 10.0. Error bars represent standard deviation (n=2).**

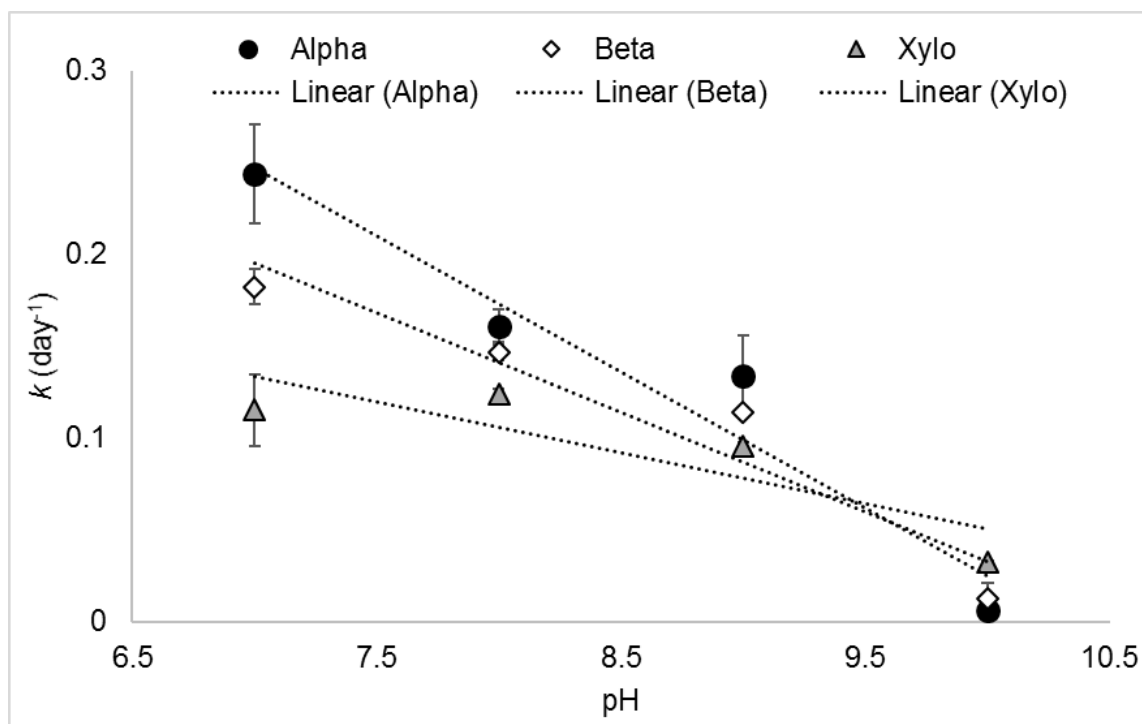


**Figure 6.2. Rate of  $\alpha$ ,  $\beta$  and X-ISA degradation within CDP-fed microcosms employing neutral-pH Canal sediments between pH 7.0-10.0. Error bars represent standard deviation (n=2).**

**Table 6.1 Alpha, beta and xylo-ISA degradation rates within microcosms employing neutral-pH Canal sediments between pH 7.0-10.0. Error represents standard deviation (n=2).**

ISA	pH 7.0	pH 8.0	pH 9.0	pH 10.0
<b>Alpha</b>	$2.4 \times 10^{-1}$ ( $\pm 2.7 \times 10^{-2}$ )	$1.6 \times 10^{-1}$ ( $\pm 9.0 \times 10^{-3}$ )	$1.3 \times 10^{-1}$ ( $\pm 2.2 \times 10^{-2}$ )	$6.1 \times 10^{-3}$ ( $\pm 6.3 \times 10^{-3}$ )
<b>Beta</b>	$1.8 \times 10^{-1}$ ( $\pm 9.6 \times 10^{-3}$ )	$1.5 \times 10^{-1}$ ( $\pm 4.3 \times 10^{-3}$ )	$1.1 \times 10^{-1}$ ( $\pm 2.5 \times 10^{-4}$ )	$1.2 \times 10^{-2}$ ( $\pm 8.6 \times 10^{-3}$ )
<b>Xylo</b>	$1.2 \times 10^{-1}$ ( $\pm 1.9 \times 10^{-2}$ )	$1.2 \times 10^{-1}$ ( $\pm 2.6 \times 10^{-3}$ )	$9.5 \times 10^{-2}$ ( $\pm 2.3 \times 10^{-3}$ )	$3.2 \times 10^{-2}$ ( $\pm 5.0 \times 10^{-4}$ )

The fermentation of ISA to  $H_2/CO_2$  and acetate has the potential to provide both acetoclastic and hydrogenotrophic methanogens with substrate for metabolism (23, 24, 304). All microcosms showed evidence of fermentation, indicated by the generation of acetate alongside the degradation of ISA. Acetate present in the CDP or generated via the fermentation of ISA was completely removed from pH 7.0 and 8.0 microcosms within the 14 day incubation period (Figure 6.3A). Within pH 9.0 microcosms acetate also showed evidence of consumption, although it could still be detected in low concentrations on day 14 (Figure 6.3A). In contrast,

acetate accumulated within pH 10.0 microcosms, likely due to the low rates of ISA fermentation, with no significant acetate consumption detected (Figure 6.3A). In similar fashion to the ISA degradation rates, the rate of acetate removal decreased as the microcosm pH increased ( $R^2=0.9237$ ) (Figure 6.3B). Within pH 7.0, 8.0 and 9.0 microcosms acetate was removed at a rate of 71.9 ( $\pm 1.4$ ,  $n=2$ ), 45.3 ( $\pm 1.4$ ,  $n=2$ ) and 40.0 ( $\pm 1.7$ ,  $n=2$ )  $\mu\text{moles day}^{-1}$ , with no significant acetate removal detected at pH 10.0 (Figure 6.3B). Since no TEA's were available in the growth media and the inoculating sediment materials were gradually removed from these microcosms via sub-culturing, it is assumed any acetate removal is a result of consumption by acetotrophic methanogens or acetate-oxidising bacteria (305).

### ***6.2.1.2 Methane Generation***

Methane was generated in all CDP-fed microcosms between pH 7.0-10.0, however the quantity and rate of methanogenesis differed across microcosms. Within pH 7.0, 8.0, 9.0 and 10.0 microcosms an average of 0.44 ( $\pm 0.03$ ,  $n=2$ ), 0.38 ( $\pm 0.04$ ,  $n=2$ ), 0.24 ( $\pm 0.06$ ,  $n=2$ ) and 0.15 ( $\pm 0.01$ ,  $n=2$ ) mmoles of methane was detected on day 14 of the incubation period respectively (Figure 6.4A). This suggests the methanogenic population was more active under neutral-pH conditions, which is perhaps expected given that these organisms were harvested from neutral-pH sediments. It is perhaps surprising however that methanogenesis was able to proceed up to pH 10.0, and suggests a proportion of methanogens within this neutral-pH site were tolerant to alkaline conditions. Although, the generation of methane at pH 10.0 by neutral-pH soil communities has been observed previously (23). In similar fashion to the acetate and ISA removal rates discussed above, the rate of methane production decreased in a linear fashion ( $R^2=0.9832$ ) as the pH within microcosms was increased (Figure 6.4B). This suggests the lower levels of methane produced at high pH was due to loss of acetate consumption and that the acetate being removed under more neutral-pH conditions was being converted to methane, rather than conversion to  $\text{H}_2$  and  $\text{CO}_2$  via syntrophic acetate oxidation. The ability of neutrophilic microorganisms to adapt to alkaline pH values has importance within an ILW-GDF. The fact that neutrophilic communities within the present study were capable of methane generation at pH 10.0 suggests microorganisms in the far-field of an ILW-GDF could adapt to near-field (alkaline) conditions.

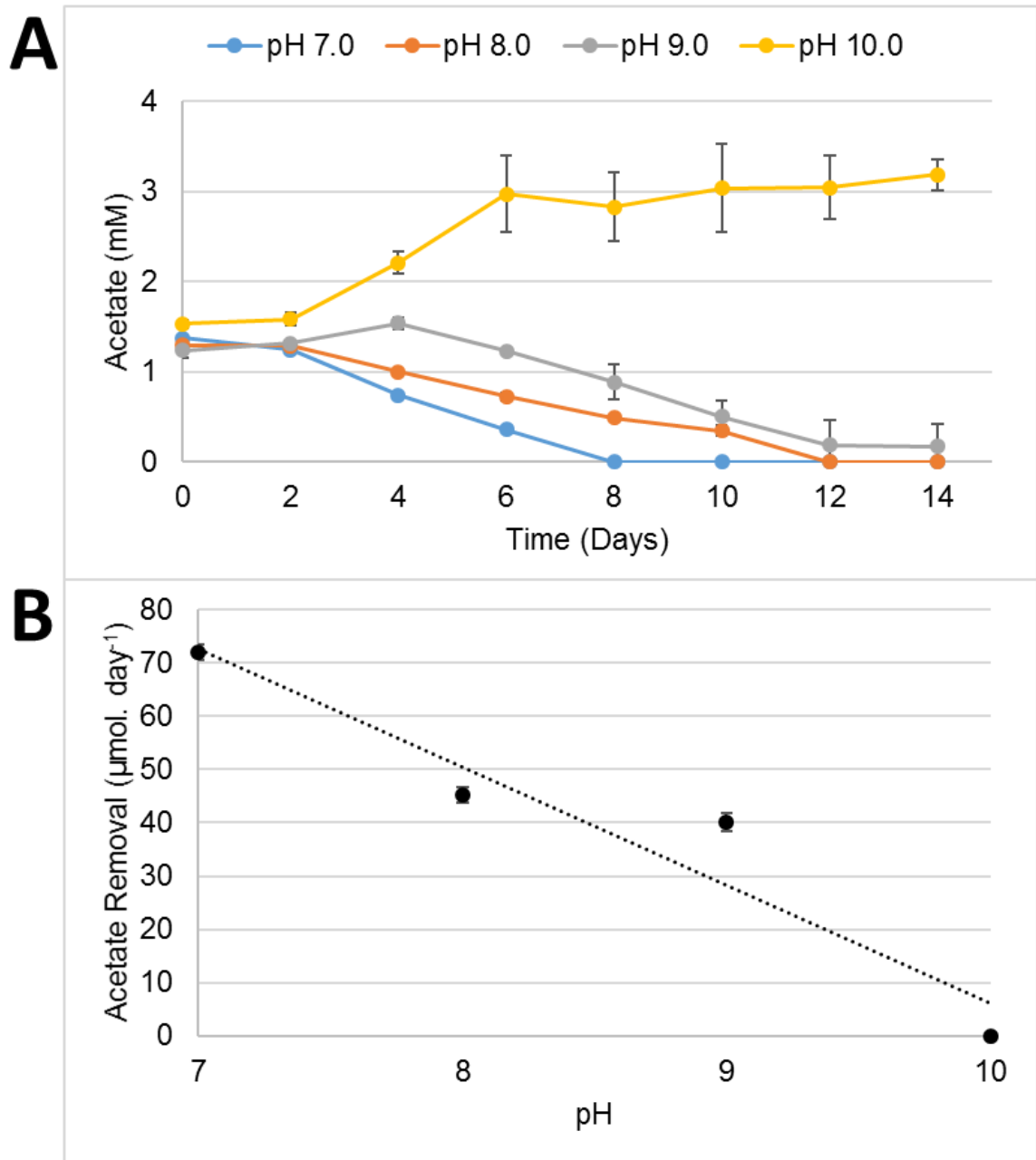


**Figure 6.3. Acetate concentrations and removal rates within CDP-fed microcosms employing neutral-pH Canal sediments.** [A] Acetate concentrations, [B] acetate removal rates. Error bars represent standard deviation (n=2).

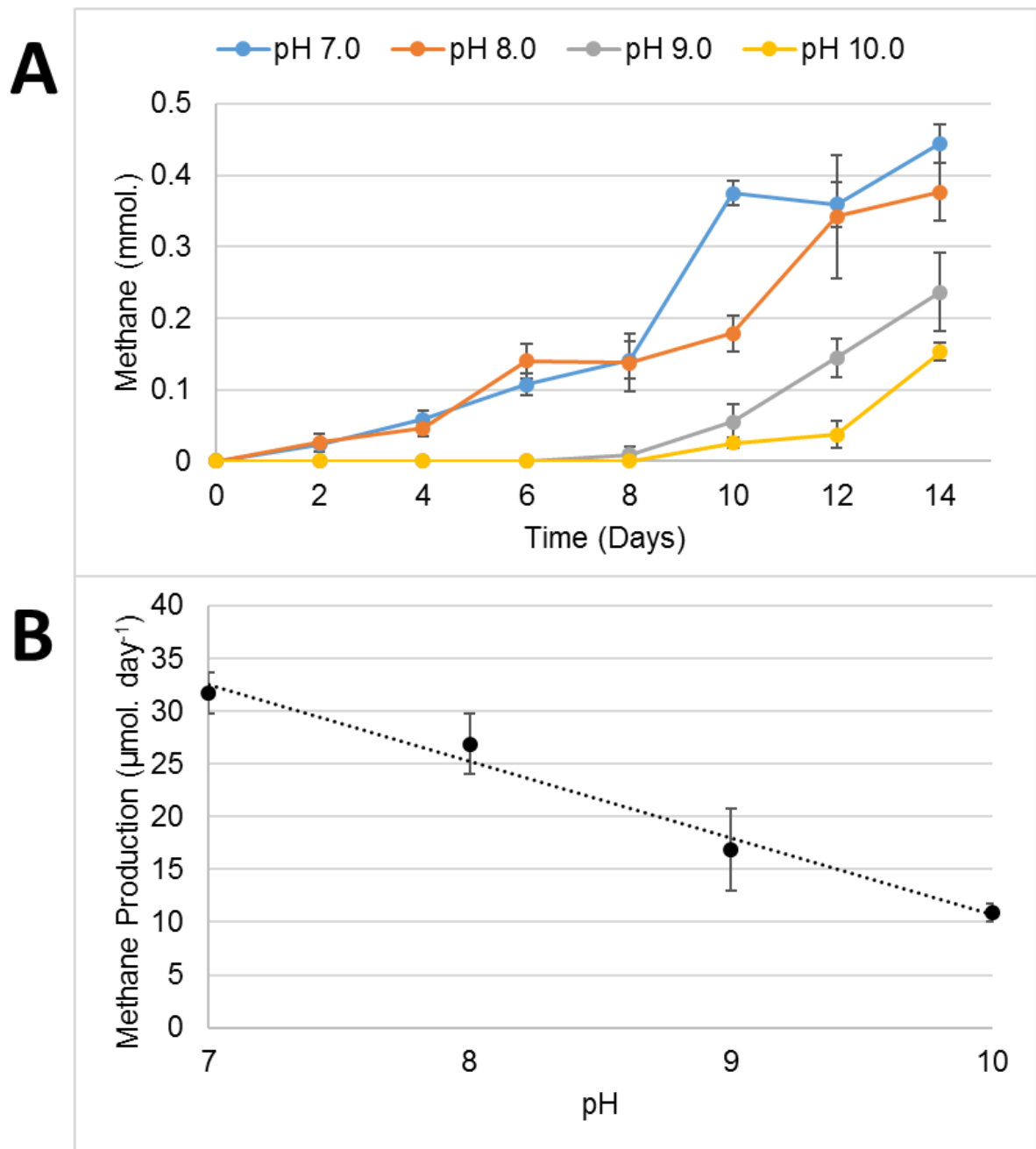


**Figure 6.4. Methane quantities and production rates within CDP-fed microcosms employing neutral-pH sediments. [A] Methane quantities, [B] methane production rates.**

### 6.2.1.3 Methanogen Community

Microbial community analysis of the CDP-fed microcosms employing the neutral-pH sediments that were capable of methane generation was undertaken via 16S rRNA gene sequencing. Within the pH 7.0 and 8.0 microcosms, the strictly hydrogenotrophic *Methanobacterium* and the metabolically diverse *Methanosarcina* were the dominant

methanogenic genera, which were present in roughly equal proportions (Figure 6.5A). Within the pH 9.0 microcosms the percentage of reads attributed to the genus *Methanobacterium* increased to 74.4%, which consequently resulted in a reduced proportion of reads attributed to the genus *Methanosarcina* (23.4%) (Figure 6.5A). Microcosms operating at pH 10.0 were dominated by the genus *Methanobacterium* (99.1%), with the genus *Methanosarcina* representing <1.0% of the total archaea reads (Figure 6.5A).

Although members of the genus *Methanosarcina* have been shown to be capable of participating in all three methanogenic pathways (306), the vast majority of isolated strains relating to this genus are capable of utilising acetate for growth and methanogenesis (61, 62, 307-310). Since the proportion of 16S rRNA gene reads relating to the genus *Methanosarcina* correlated well with the rate of acetate consumption (Figure 6.6) it would seem this genus is contributing to acetoclastic methane generation within these microcosms. The loss of *Methanosarcina* genera within the pH 9.0 and 10.0 microcosms and reduced acetate consumption under these conditions suggests acetate-derived methane was being inhibited at high pH. This suggests the reduced quantities of methane generated within pH 9.0 and 10.0 microcosms is due to inhibition of the acetoclastic pathway. The increased levels of methane generated in pH 7.0 and 8.0 microcosms and the detection of both acetoclastic and hydrogenotrophic methanogens at this pH is therefore a result of two methanogenic pathways being active, in contrast only the hydrogenotrophic pathway appeared to be active at pH 10.0. To the authors knowledge the only member of the *Methanosarcina* in the literature that has been shown to be capable of alkaliphilic growth in pure culture has been isolated from mangrove sediment previously (311), which strictly uses methylated compounds (dimethylsulfide, methanethiol, methanol) for growth and is incapable of using acetate or H<sub>2</sub>/CO<sub>2</sub> for methanogenesis. The fact that alkaliphilic acetate-metabolising *Methanosarcina* are absent from the literature agrees with the community analysis within the present study, where the high pH conditions resulted in a loss of this genus. The absence of the strictly acetoclastic *Methanosaeta* genus within the methanogen community could be explained by their lower maximum growth rates ( $\mu_{max}$ ) and half-saturation coefficients ( $K_s$ ) compared with *Methanosarcina* (55). Therefore high acetate concentrations (>1mM) are expected to result in *Methanosarcina* species as the dominant acetoclastic methanogen (58), which is in line with the present study, where the initial acetate concentrations within the CDP-fed microcosms was 1.4 mM ( $\pm 0.1$ ) (Figure 6.3).

A number of alkaliphilic strains relating to the genus *Methanobacterium*, which dominated in the pH 9.0 and 10.0 microcosms, have been isolated from alkaline lakes previously (312) and were capable of growth up to pH 10.0 in pure culture, all of which strictly use H<sub>2</sub> and CO<sub>2</sub> for methanogenesis. Additionally, a number of neutrophilic strains have been isolated previously from anaerobic digestors (313), ricefields (314) and marine sediments (315) which underlines their ability to maintain a population between pH 7.0-10.0 within the microcosms studied here. All other methanogenic genera that were present represented <1.0% of the total archaeal 16S rRNA gene reads and were therefore considered insignificant. A small proportion of unclassified methanogen reads were also detected within pH 7.0, 8.0, 9.0 and 10.0 microcosms, representing 0.11%, 0.15%, 0.14% and 0.18% of the total archaea 16S rRNA gene reads respectively, suggesting a small proportion of methanogens within these microcosms are potentially novel and undescribed organisms.

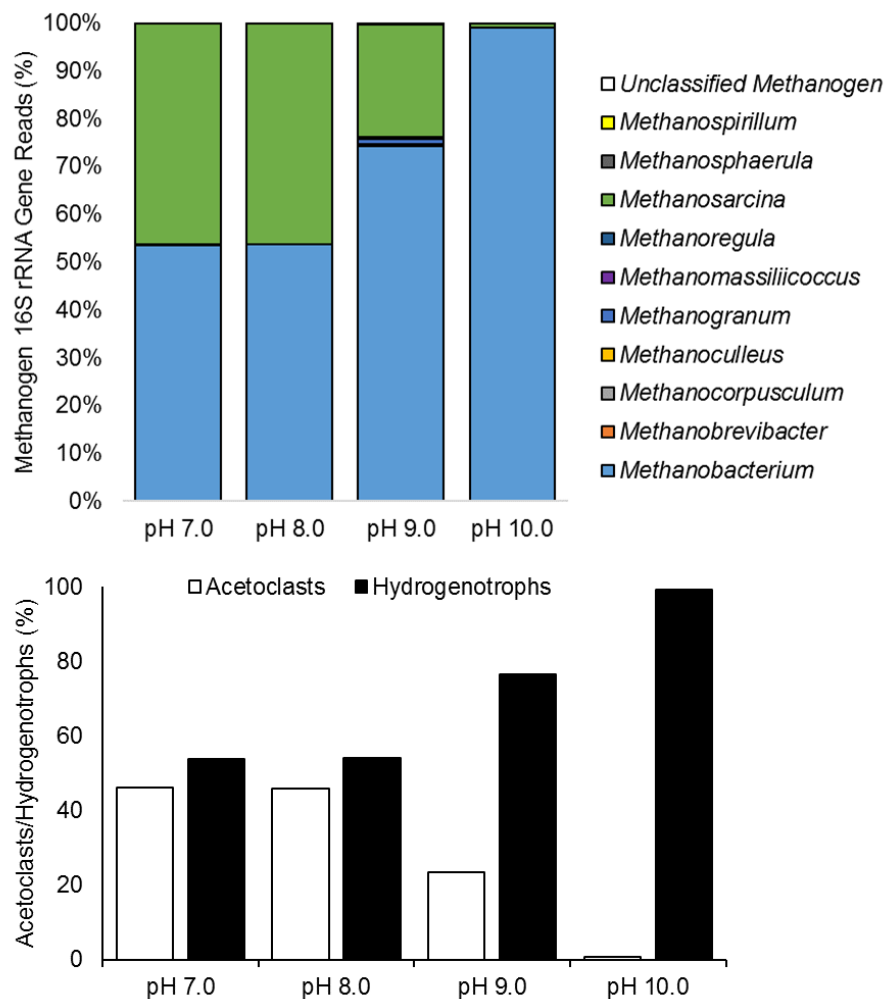


**Figure 6.5. Genus-level methanogen community and proportion of acetoclastic/hydrogenotrophic methanogens within CDP-fed microcosms employing neutral-pH sediments.**

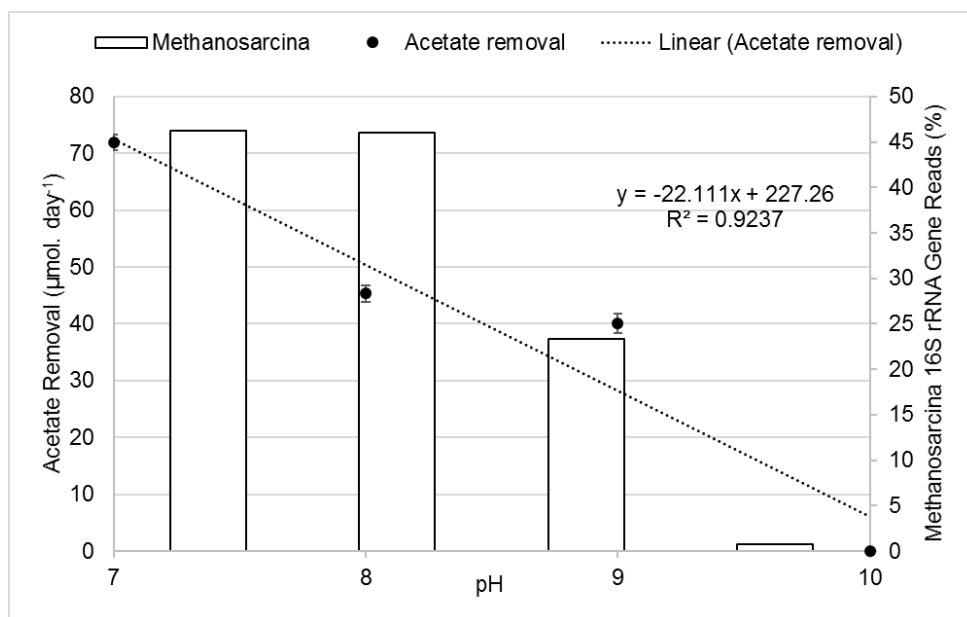


**Figure 6.6. Acetate removal rates and proportion of reads attributed to the genus *Methanosarcina* within pH 7.0-10.0 CDP-fed microcosms employing the neutral-pH sediments.**

## 6.2.2 Lime Site Microcosms

### 6.2.2.1 ISA Degradation

In contrast to the CDP-fed microcosms employing neutral-pH sediments (Section 6.2.1), CDP-fed microcosms employing alkaline sediments from lime sites B, H and T showed evidence of degrading all three forms of ISA between pH 7.0-11.0 (Figure 6.7). On average 487.4 ( $\pm 216.7$ ,  $n=4$ ), 194.2 ( $\pm 92.2$ ,  $n=4$ ), 160.7 ( $\pm 86.9$ ,  $n=6$ ), 65.6 ( $\pm 27.2$ ,  $n=6$ ) and 92.1 ( $\pm 6.6$ ,  $n=2$ )  $\mu\text{g day}^{-1}$  of  $\alpha$ -ISA was removed from pH 7.0, 8.0, 9.0, 10.0 and 11.0 microcosms respectively. On average 329.1 ( $\pm 107.9$ ,  $n=4$ ), 149.6 ( $\pm 46.6$ ,  $n=4$ ), 168.8 ( $\pm 39.8$ ,  $n=6$ ), 91.5 ( $\pm 8.9$ ,  $n=6$ ) and 62.9 ( $\pm 1.0$ ,  $n=2$ )  $\mu\text{g day}^{-1}$  of  $\beta$ -ISA was removed from pH 7.0, 8.0, 9.0, 10.0 and 11.0 microcosms respectively (Figure 6.7). X-ISA was removed at rate of 69.8 ( $\pm 14.7$ ,  $n=4$ ), 78.2 ( $\pm 38.6$ ,  $n=4$ ), 48.2 ( $\pm 28.8$ ,  $n=6$ ), 43.1 ( $\pm 1.9$ ,  $n=6$ ) and 24.5 ( $\pm 6.5$ ,  $n=2$ )  $\mu\text{g day}^{-1}$  within pH 7.0, 8.0, 9.0, 10.0 and 11.0 microcosms respectively (Figure 6.7). In similar fashion to the microcosms employing neutral-pH sediments (Section 6.2.1), ISA degradation rates were higher between pH 7.0-9.0. However ISA removal between pH 10.0-11.0 was higher when employing the alkaline sediments from the lime sites, compared with the neutral-pH sediments (Figure 6.8), suggesting the microbes within these sites have adapted mechanisms to survive and grow in conditions of higher alkalinity. Previous work employing sediments from site B in CDP-fed microcosms at

pH 11.0 have demonstrated comparable ISA degradation rates which also resulted in the generation of methane at this pH (24).

As seen within the control microcosms (Section 6.2.1), acetate was generated as a consequence of ISA degradation (Figure 6.9), suggesting fermentation processes were active. The initial acetate concentration upon inoculation was 2.0 mM ( $\pm 0.1$ , n=4), 1.8 mM ( $\pm 0.1$ , n=4), 1.6 mM ( $\pm 0.07$ , n=6), 1.4 mM ( $\pm 0.05$ , n=6) and 1.6 mM ( $\pm 0.07$ , n=2) within pH 7.0, 8.0, 9.0, 10.0 and 11.0 microcosms respectively (Figure 6.9), with this variation likely to be a result of carry-over during sub-culturing. After the 14 day incubation period, acetate concentrations had increased to 3.2 mM ( $\pm 0.2$ , n=4), 3.3 mM ( $\pm 1.1$ , n=4), 2.8 mM ( $\pm 0.7$ , n=6), 1.9 mM ( $\pm 0.1$ , n=6) and 2.0 mM ( $\pm 0.1$ , n=2) within pH 7.0, 8.0, 9.0, 10.0 and 11.0 microcosms respectively (Figure 6.9). The increased accumulation of acetate between pH 7.0 and 8.0, compared with the pH >9.0 microcosms is likely to be a result of the higher ISA degradation rates observed at these pH values (Figure 6.7F). In contrast to the microcosms employing the neutral-pH sediments (Section 6.2.1), low pH reactors (pH 7.0-8.0) employing the alkaline sediments were unable to demonstrate high acetate consumption rates, with the rate of fermentation appearing to outcompete the rate of acetotrophy. The lack of acetate consumption from lime-site reactors could be due to the absence of acetoclastic species within the inoculating sediments as described in Chapter 5. It is possible the alkaline *in situ* conditions of the sites has resulted in the loss of *Methanosarcina* and *Methanosaeta* species from the sediments, as seen in Section 6.2.1 (Figure 6.5).

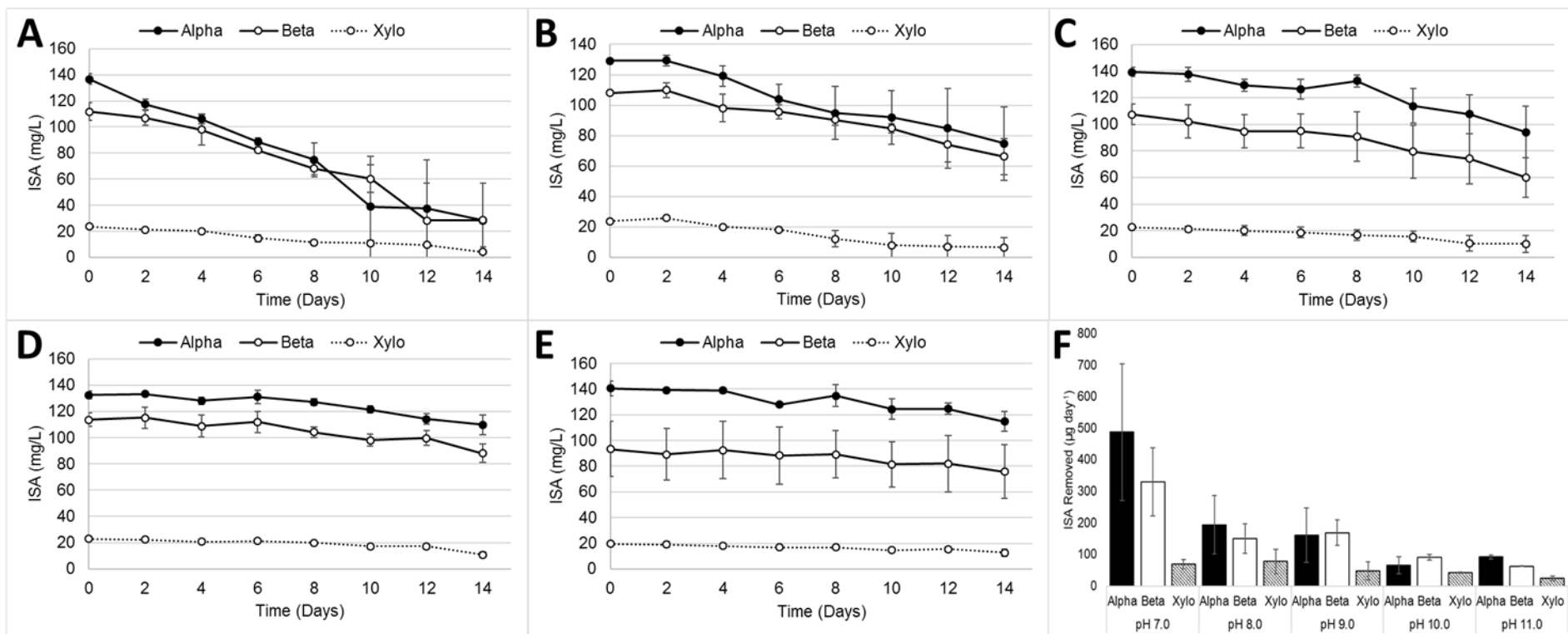


**Figure 6.7.** ISA degradation within microcosms employing alkaline sediments from lime sites B, H and T. [A] pH 7.0, [B] pH 8.0, [C] pH 9.0, [D] pH 10.0, [E] pH 11.0, [F] ISA removal rates. Error bars represent standard deviation (n=6).

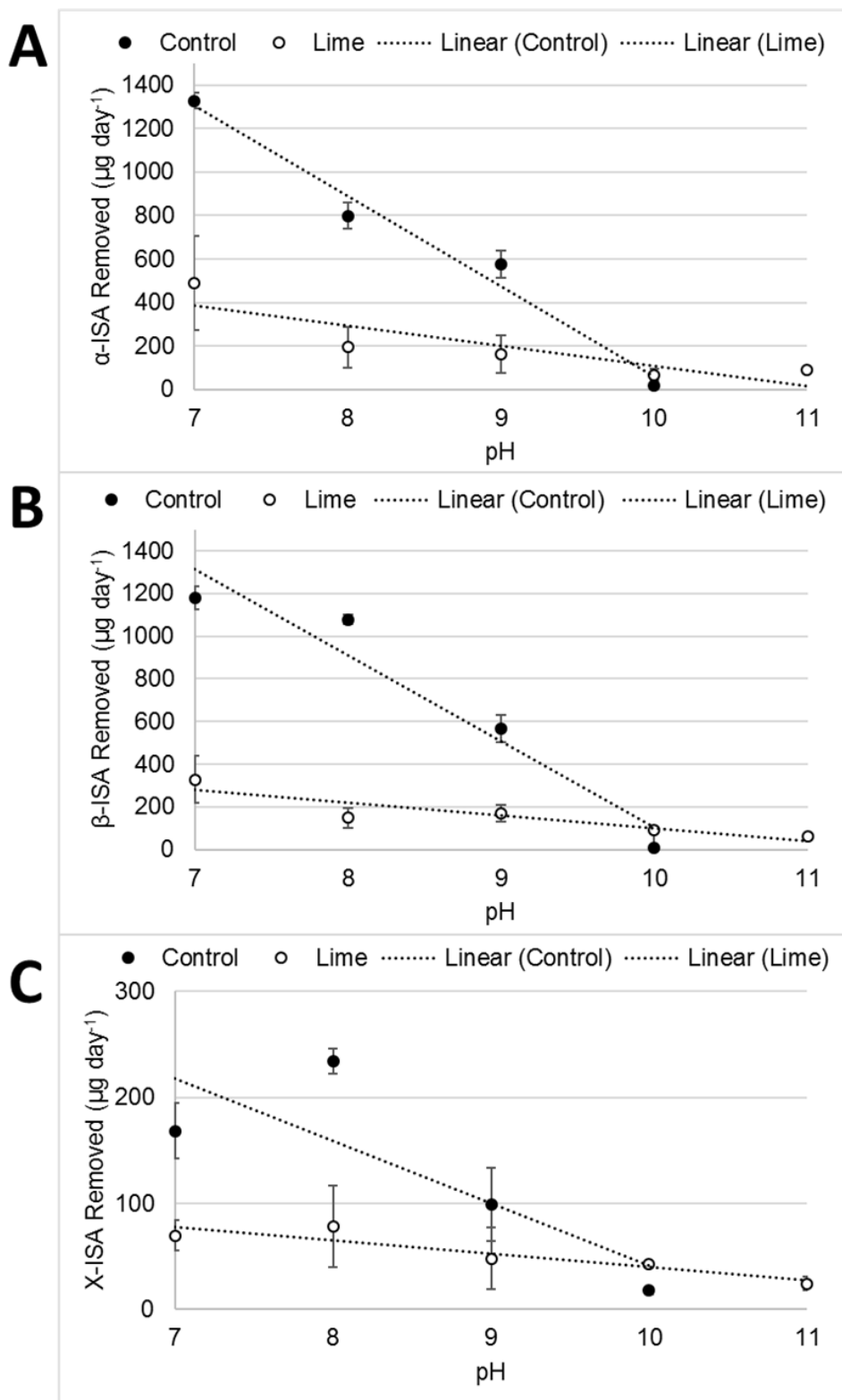


**Figure 6.8. Comparison of ISA degradation rates between microcosms employing neutral-pH sediments (control) and alkaline sediments (lime). [A]  $\alpha$ -ISA, [B]  $\beta$ -ISA, [C] X-ISA. Error bars represent standard deviation (control n=2, lime n=6).**

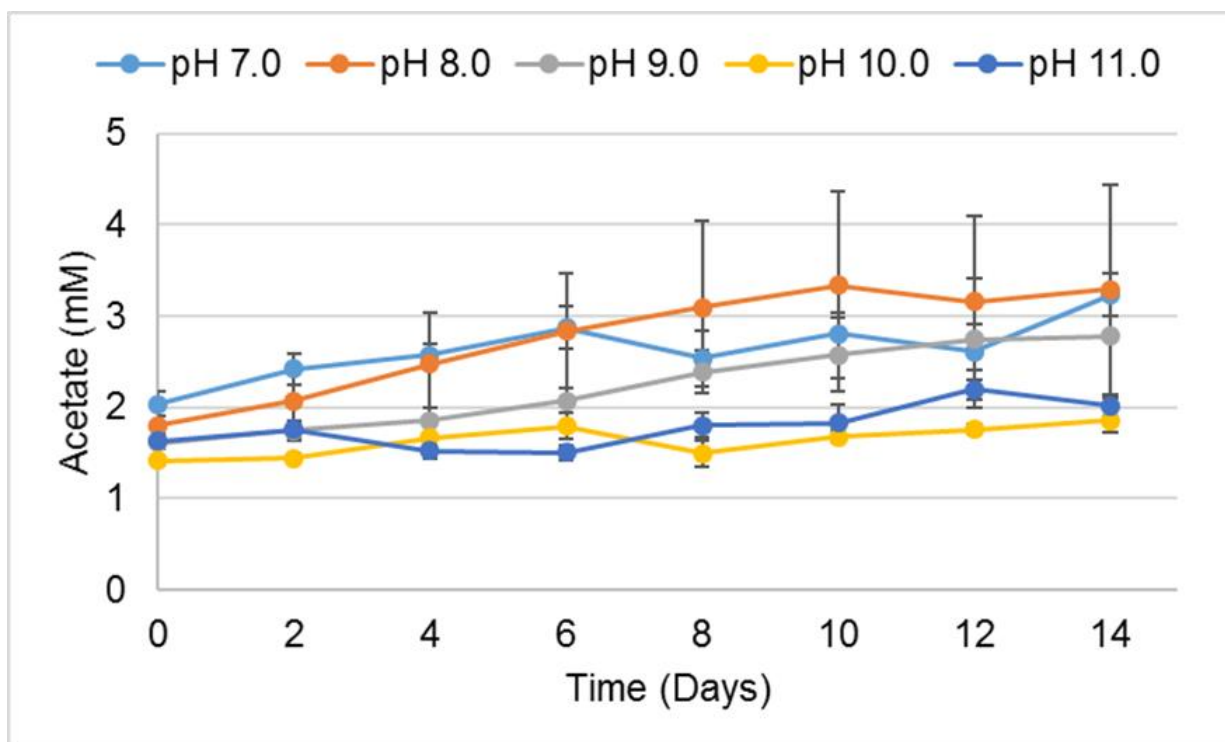


**Figure 6.9. Acetate concentrations between pH 7.0-11.0 within CDP-fed microcosms employing the alkaline lime sediments.** Error bars represent standard deviation (pH 7.0 n=2, pH 8.0 n=4, pH 9.0 n=6, pH 10.0 n=6, pH 11.0 n=2).

#### 6.2.2.2 Methane Generation

CDP-fed microcosms employing the lime sediments were capable of generating methane between pH 7.0-11.0 (Figure 6.10), one pH unit higher than microcosms employing the neutral-pH sediments in Section 6.2.1. On day 14 the average quantity of methane within pH 7.0, 8.0, 9.0, 10.0 and 11.0 microcosms was 0.04 ( $\pm 0.03$ , n=4), 0.13 ( $\pm 0.05$ , n=4), 0.24 ( $\pm 0.02$ , n=6), 0.18 ( $\pm 0.03$ , n=6) and 0.04 ( $\pm 0.03$ , n=2) mmoles respectively (Figure 6.10A). This equates to a methane production rate of 9.4 ( $\pm 1.1$ , n=4), 14.4 ( $\pm 3.2$ , n=4), 17.1 ( $\pm 1.2$ , n=6), 12.6 ( $\pm 2.2$ , n=6) and 9.6 ( $\pm 0.9$ , n=2)  $\mu\text{moles day}^{-1}$  at pH 7.0, 8.0, 9.0, 10.0 and 11.0 respectively (Figure 6.10B), suggesting that under fermentative conditions the methanogen community had an optimum pH of 9.0 for growth, despite the fact that *in situ* pH values of the inoculating sediments was much higher (see Chapter 5). Even though a number of alkaliphilic microorganisms have demonstrated growth above pH 10.0 (123, 124), the optimum growth conditions for many alkaliphiles tends to be pH  $\sim 9.0$ , therefore the methanogen community present in the sediments from these alkaline sites are likely to be surviving in low pH microsites *in situ*, as described in Chapter 5.

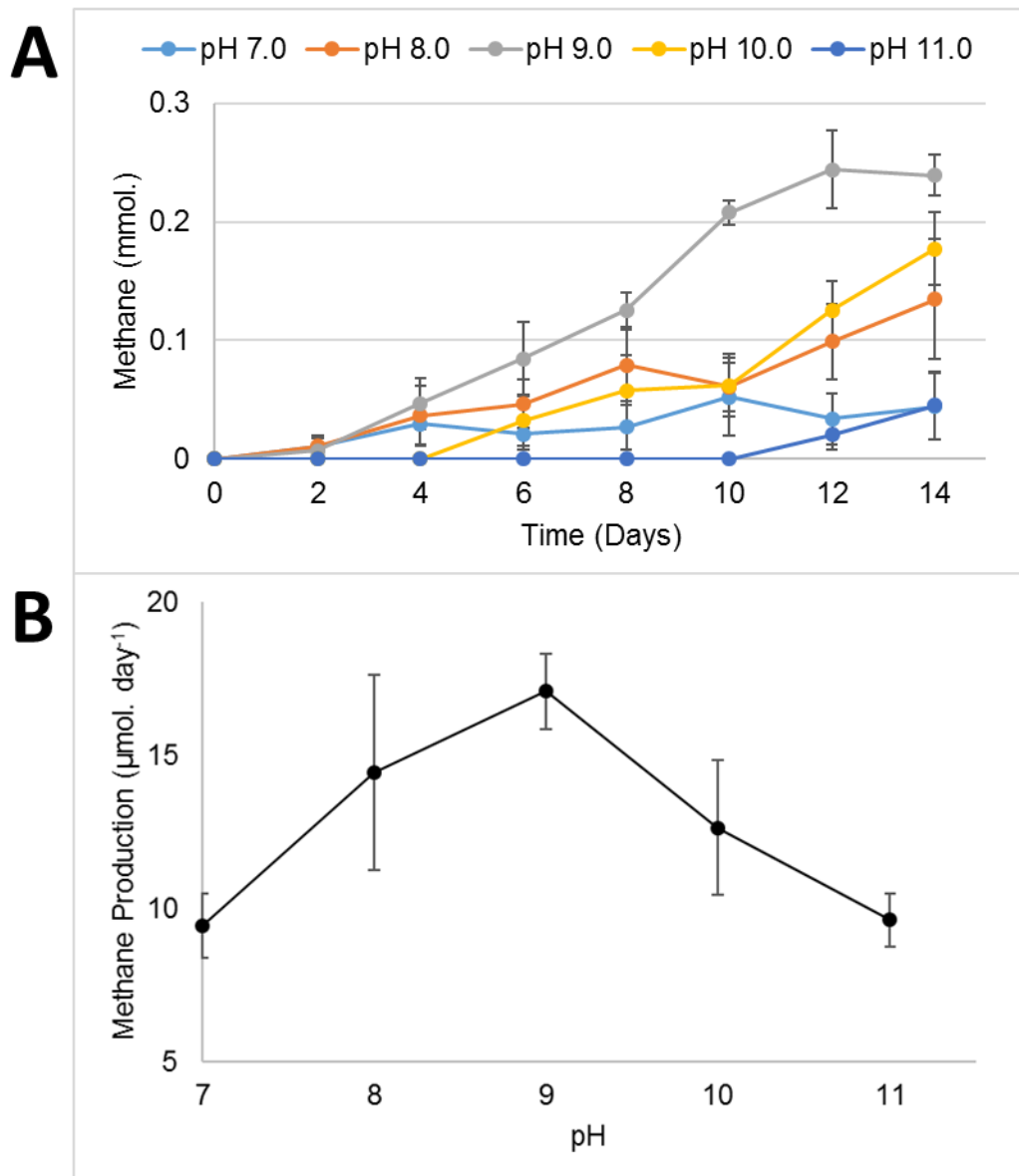


**Figure 6.10. Methane quantities within CDP-fed microcosms employing alkaline sediments from the lime sites between pH 7.0-11.0.** [A] Methane quantities against time between pH 7.0-11.0, [B] rate of methane production between pH 7.0-11.0. Error bars represent standard deviation (pH 7.0 n=2, pH 8.0 n=4, pH 9.0 n=6, pH 10.0 n=6, pH 11.0 n=2).

### 6.2.2.3 Methanogen Community

All methanogenic CDP-fed microcosms were dominated by hydrogenotrophic methanogens of the genus *Methanobacterium* and *Methanoculleus* (Figure 6.11A). Within pH 7.0, 8.0, 9.0, 10.0 and 11.0 microcosms the *Methanobacterium* represented an average of 84.1% ( $\pm 28.0$ ), 49.8% ( $\pm 33.2$ ), 65.9% ( $\pm 33.0$ ), 65.6% ( $\pm 32.0$ ) and 1.1% ( $\pm 0.4$ ) of the total methanogen reads across the three sites (B, H, T) respectively (Figure 6.11A). The genus *Methanoculleus* represented an average of 1.3% ( $\pm 0.4$ ), 22.1% ( $\pm 14.7$ ), 30.3% ( $\pm 29.8$ ), 26.3% ( $\pm 25.1$ ) and 88.1% ( $\pm 29.4$ ) within pH 7.0, 8.0, 9.0, 10.0 and 11.0 microcosms respectively. The lack of methane generation at pH 7.0 and 8.0 within CDP-fed microcosms inoculated with site H sediments and pH 11.0 microcosms employing site T sediments has resulted in high standard deviation across these averages. Since members of the genus *Methanoculleus* were largely absent from microcosms employing the control sediments in Section 6.2.1.3, but dominated in reactors inoculated with the alkaline sediments, this genus of methanogen could be important within lime-contaminated environments. Strains relating to the strictly hydrogenotrophic genus *Methanoculleus* have been isolated previously from a number of environments, including shale formations (316), oil fields (317), wetland soil (318) and paddy field soil (319), although to the authors knowledge no alkaliphilic species have been described to date and therefore their presence within microcosms operating at pH 11.0 could be the first account of this genus surviving under alkaline conditions.

Only a very small percentage of 16S rRNA gene reads could be attributed to the potentially acetate-metabolising genus *Methanosarcina* and strictly acetoclastic genus *Methanosaeta* at all pH values (Figure 6.11). At pH 7.0, 8.0, 9.0, 10.0 and 11.0 the genus *Methanosarcina* represented an average of 0.16% ( $\pm 0.12$ ), 0.0066% ( $\pm 0.0044$ ), 0.71% ( $\pm 0.69$ ), 1.16% ( $\pm 0.57$ ) and 0.78% ( $\pm 0.51$ ) of the total archaea reads across microcosms employing site B, H and T sediments respectively, suggesting this genus was the minority of the overall methanogen population. The genus *Methanosaeta* represented on average 0.0%, 0.15% ( $\pm 0.10$ ), 0.11% ( $\pm 0.11$ ), 0.029% ( $\pm 0.029$ ) and 0.096% ( $\pm 0.064$ ) of the total archaea reads within pH 7.0, 8.0, 9.0, 10.0 and 11.0 microcosms respectively. The very low percentage of reads attributed to methanogens capable of acetate metabolism at all pH values agrees with the chemistry within these microcosms, where acetate quantities increased due to ISA fermentation and showed no signs of degradation (Figure 6.9). Since the genera *Methanosarcina* and *Methanosaeta* could not be detected in the inoculating sediments (Chapter 5), their absence from these microcosms

is perhaps not surprising. This does however suggest that hydrogenotrophic metabolism dominated within all CDP-fed microcosms employing the alkaline sediments irrespective of pH. This adds confidence to the hypothesis that the alkaline *in situ* conditions of these sites is selecting against acetoclastic methanogens, as seen in the microcosms employing the neutral-pH control sediments in Section 6.2.1.

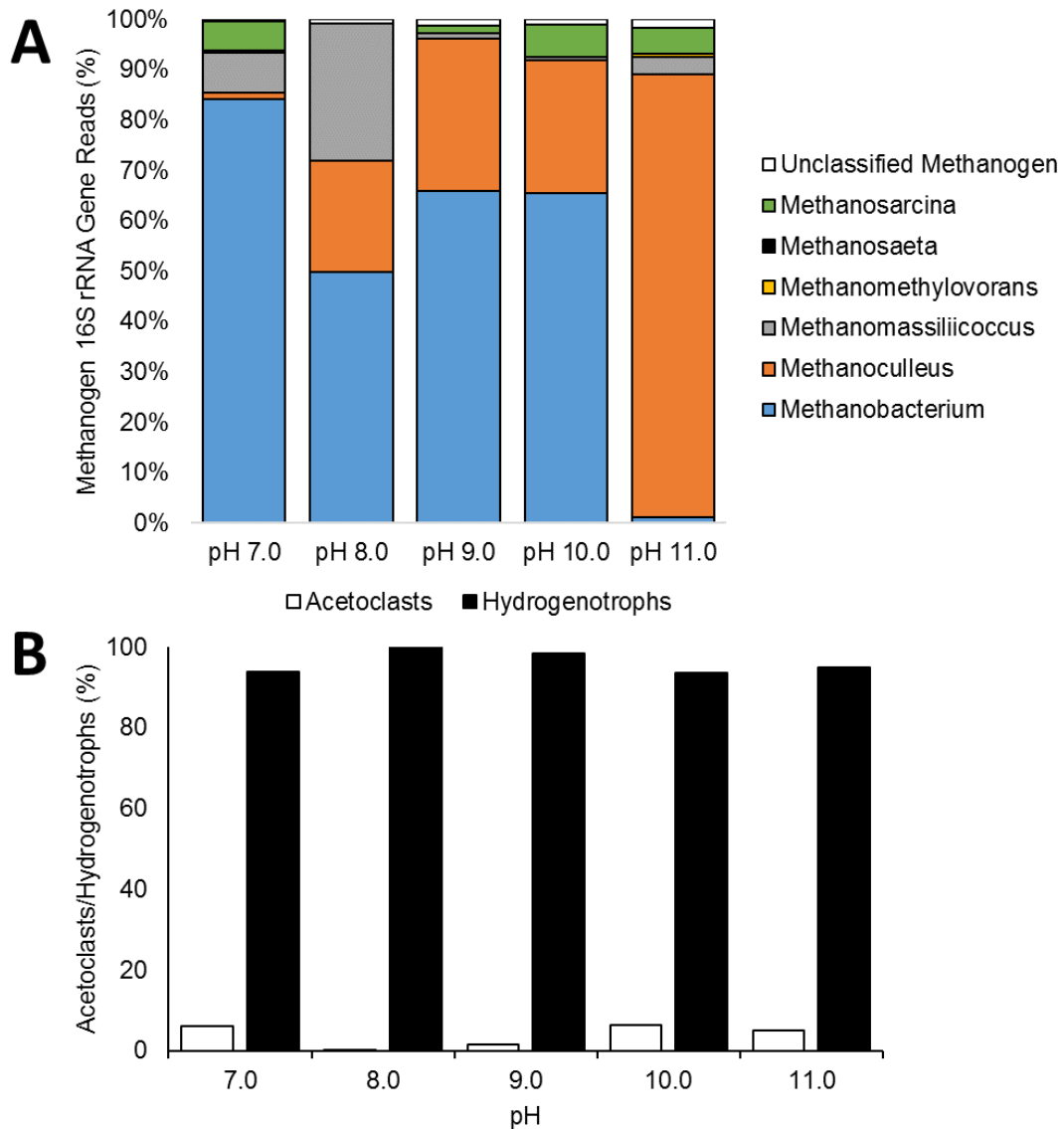


**Figure 6.11. Genus level methanogen community composition and proportion of hydrogenotrophic/acetoclastic methanogens within CDP-fed microcosms employing alkaline sediments from the lime sites.** [A] Genus-level methanogen communities between pH 7.0-11.0, [B] proportion of hydrogenotrophic and acetoclastic methanogens between pH 7.0-11.0.

## 6.3 H<sub>2</sub>/CO<sub>2</sub> and Acetate-fed Microcosms

Since difficulties arise when trying to establish the utilisation of methanogenic substrates under fermentative conditions due to the production of acetate and H<sub>2</sub>/CO<sub>2</sub> which can obscure consumption rates, the ability of the CDP-fed microcosms described in Section 6.2 to generate methane solely from H<sub>2</sub>/CO<sub>2</sub> or acetate supplied in the growth media (in the absence of a fermentation substrate) between pH 7.0-12.0 was investigated. Sub-cultures of the CDP-fed reactors were produced and the quantity of H<sub>2</sub>, acetate and methane was analysed throughout the incubation period. The methanogen communities within any microcosms capable of methanogenesis were described via 16S rRNA gene sequencing.

### 6.3.1 Control Site Microcosms

Microcosms employing the control site sediments fed solely with H<sub>2</sub>/CO<sub>2</sub> were capable of methanogenesis up to pH 10.0, in contrast solely acetate-fed microcosms were only able to generate methane up to pH 9.0 (Figure 6.12), despite extended incubation periods (50 days). Hydrogen consumption rates between pH 7.0-10.0 were 243.3 ( $\pm$ 10.9, n=2), 190.7 ( $\pm$ 23.2, n=2), 121.2 ( $\pm$ 18.4, n=2) and 87.8 ( $\pm$ 19.4, n=2)  $\mu$ moles day<sup>-1</sup> respectively (Figure 6.13) and therefore the rate of hydrogen consumption correlated negatively with the pH of microcosms ( $R^2=0.984$ ). No methane generation or hydrogen consumption was detected in pH 11.0 microcosms fed with H<sub>2</sub>/CO<sub>2</sub>. The rate of acetate consumption also negatively correlated with pH ( $R^2=0.9918$ ) with an average removal rate of 148.7 ( $\pm$ 2.9), 108.3 ( $\pm$ 3.9), 44.9 ( $\pm$ 11.0) and 3.6 ( $\pm$ 0.3)  $\mu$ moles day<sup>-1</sup> between pH 7.0-10.0 respectively (Figure 6.13), with no methane generated in pH 10.0 microcosms fed solely with acetate. The generation of methane solely from acetate up to pH 9.0 but continued methanogenesis from hydrogen up to pH 10.0 agrees with the CDP-fed microcosms in Section 6.2.1, where the same trend was observed.

The methanogen community was analysed via 16S rRNA gene sequencing within H<sub>2</sub>/CO<sub>2</sub>-fed microcosms between pH 7.0-10.0 and acetate-fed reactors between pH 7.0-9.0, since these were the only systems capable of methanogenesis. H<sub>2</sub>/CO<sub>2</sub>-fed microcosms were dominated by the strictly hydrogenotrophic genus *Methanobacteria* which represented 60.7%, 73.7%, 91.0% and 97.1% of the total archaea reads at pH 7.0, 8.0, 9.0 and 10.0 respectively (Figure 6.14). In contrast, acetate-fed microcosms were dominated by the acetoclastic genus *Methanosarcina* which represented 65.1%, 79.3% and 7.1% of the total archaea reads at pH 7.0, 8.0 and 9.0 respectively. In similar fashion to the CDP-fed microcosms (Figure 6.5), the

percentage of reads attributed to the acetoclastic *Methanosarcina* decreased as the pH within the microcosms increased above pH 8.0, suggesting this genus was unable to maintain a significant population under alkaline conditions. The fact that methanogens capable of acetoclastic methanogenesis reduce in number as the pH increases is in agreement with the microcosm chemistry where acetate consumption rates decreased at the higher pH values tested (Figure 6.12). It is interesting to note that a small proportion of hydrogenotrophic methanogen reads were detected within the acetate-fed microcosms and low numbers of potentially acetoclastic species were present within H<sub>2</sub>/CO<sub>2</sub>-fed reactors, which is likely to be a result of ISA carry-over during sub-culturing which led to the generation of undetectable quantities of acetate and H<sub>2</sub>/CO<sub>2</sub> via fermentation pathways. It is also possible that acetate is being fermented to H<sub>2</sub>/CO<sub>2</sub> by syntrophic acetate oxidising bacteria within the acetate-fed microcosms (320) which allowed for hydrogenotrophic populations to develop. Nevertheless, the domination of *Methanosarcina* species within the acetate-fed microcosms and high acetate consumption rates at pH 7.0 and 8.0 verifies the presence of acetoclastic methanogenesis at the lower pH values tested.

The generation of methane has been shown to be sensitive to pH previously under acidic conditions (321), where low pH conditions inhibited both methanogenic pathways and fermentation. Within the present study reduced methane generation rates at pH 10.0 appears to be a result of inhibition of the acetoclastic pathway only, with both hydrogenotrophic methanogenesis and fermentation pathways still active. Therefore the inhibition of methane at pH 10.0 within the present study is not a result of fermentation end product limitations, but rather an inability to metabolise acetate. The degradation of acetate by acetoclastic methanogens begins with its activation to acetyl-coenzyme A (53). As the pH within the microcosms is increased, the dissociated forms of acetate will become more abundant, which could be impairing uptake by cells and result in reduced acetate consumption. Since the charged (dissociated) forms of acetic acid require active transport into the cell (322), an input of energy is required for its conversion to methane. In contrast the uncharged (associated) forms of acetic acid are able to move freely across the cell membrane via simple diffusion which is energetically favourable. This could explain the increased acetate consumption rates (Figure 6.12) under neutral-pH conditions in the present study. Although the electron transport chain of acetoclastic methanogenesis has been studied previously (322, 323), no information in the literature could be found regarding the transport of acetate into the cell and how this transport is affected by acetic acid dissociation, this could therefore be an important area of future

research. The protein acetate kinase (Ack) from *Methanosarcina mazei*, which activates acetate for its transport into the cell, has been shown to have an optimum pH of 6.5-7.0 (322), therefore a significant amount of energy would be required to maintain an intracellular pH at a value close to the enzymes optimum when these cells are growing under alkaline conditions. The fact that reports of alkaliphilic acetate-metabolising methanogens are largely absent from the literature further supports the present studies ascertainment that alkaline conditions impair acetoclastic methanogenesis. A number of methanogens have been enriched and isolated previously from alkaline lake sediments, none of which were capable of utilising acetate and instead used H<sub>2</sub>/CO<sub>2</sub> or methylated compounds for growth (90, 324). Alkaliphilic acetoclastic methanogen enrichment cultures have been successfully developed at pH 9.5 from soda lake sediments previously and were dominated by the strictly acetoclastic *Methanosaeta* (87), however the methanogenic activity in these cultures was extremely low and the activity of these cultures was impaired at pH 10.0.

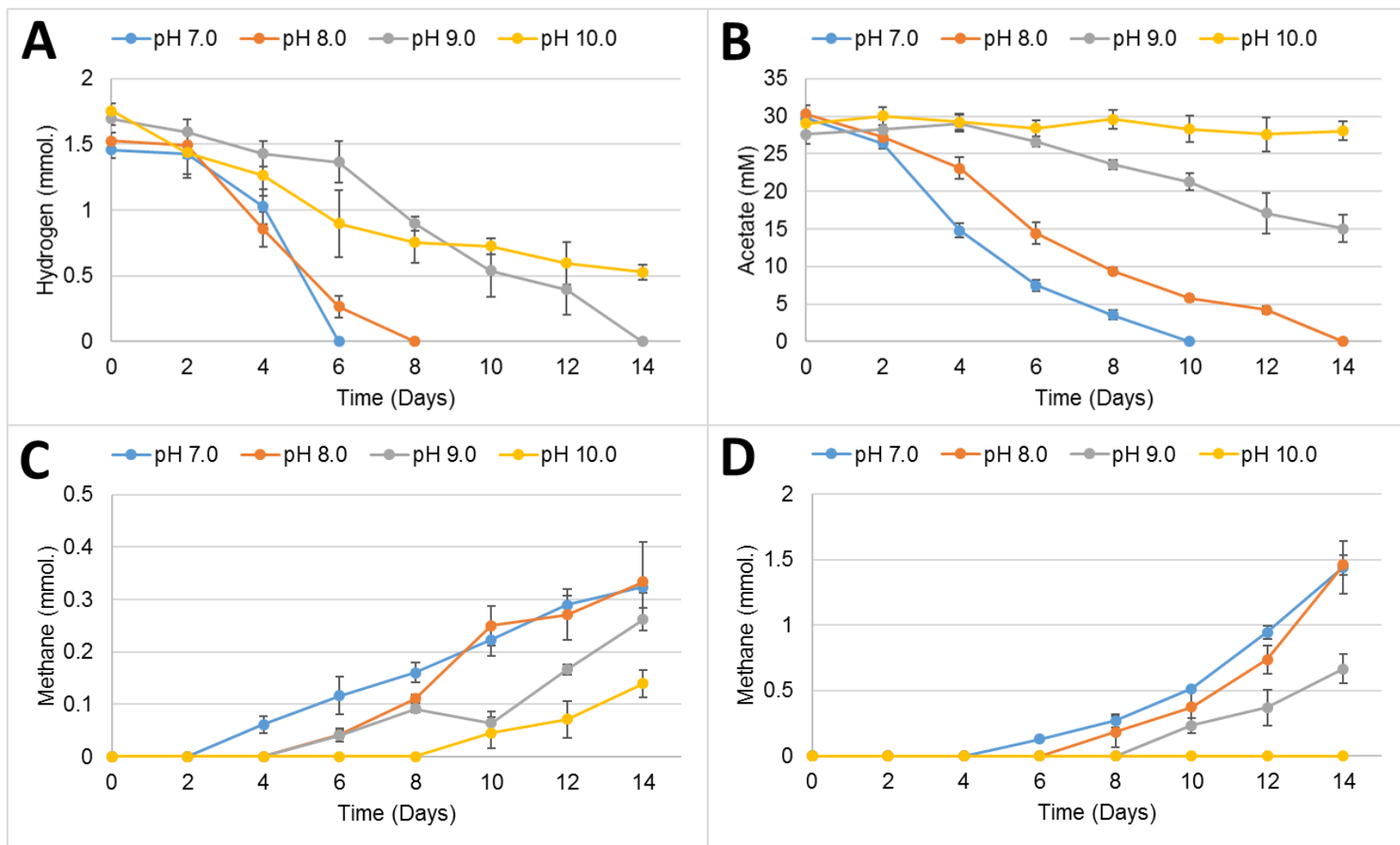


**Figure 6.12. Hydrogen, acetate and methane quantities within microcosms employing control site sediments between pH 7.0-10.0.** [A] Hydrogen quantities between pH 7.0-10.0, [B] acetate concentrations between pH 7.0-10.0, [C] methane generated from H<sub>2</sub>/CO<sub>2</sub>-fed microcosms pH 7.0-10.0, [D] methane generated from acetate-fed microcosms pH 7.0-10.0.

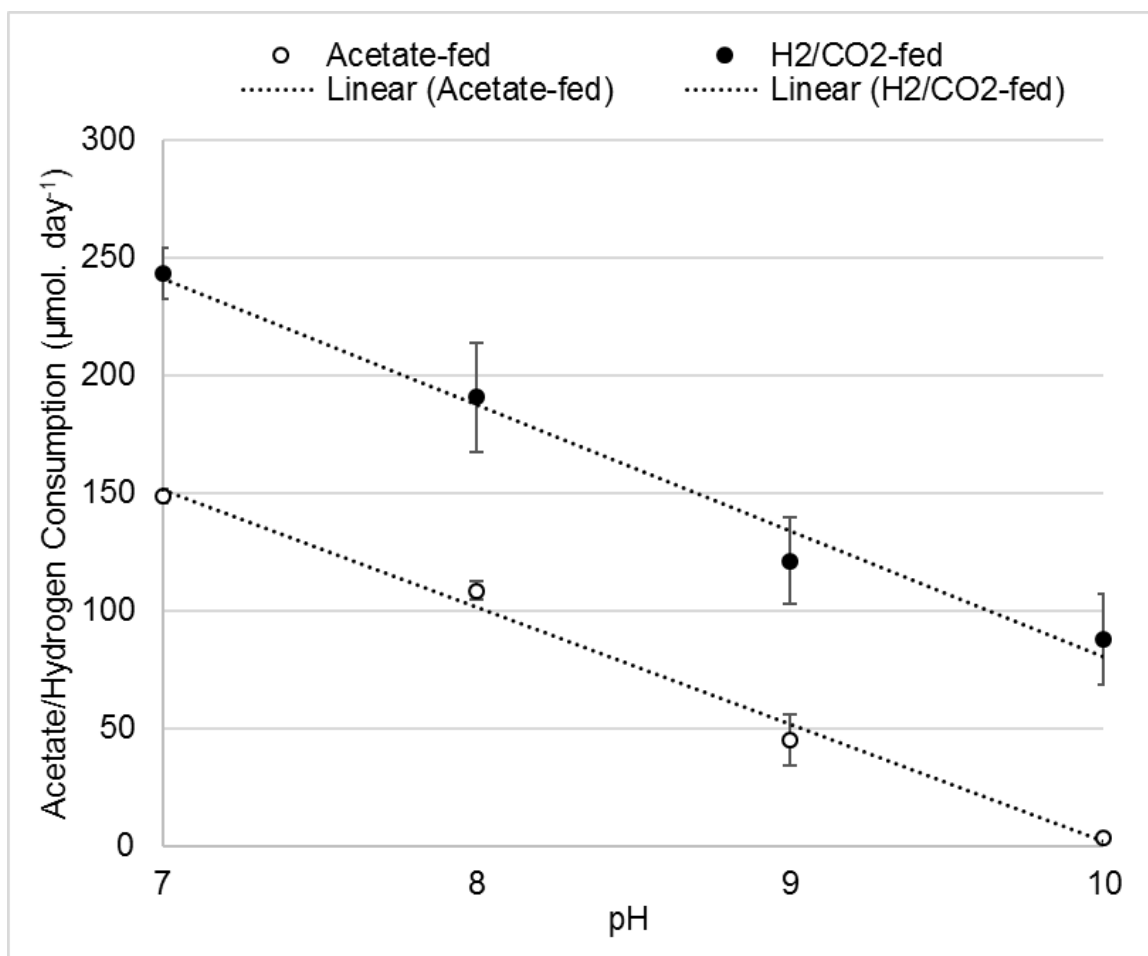


**Figure 6.13. Acetate and hydrogen consumption rates within microcosms employing neutral-pH sediments between pH 7.0-10.0.**

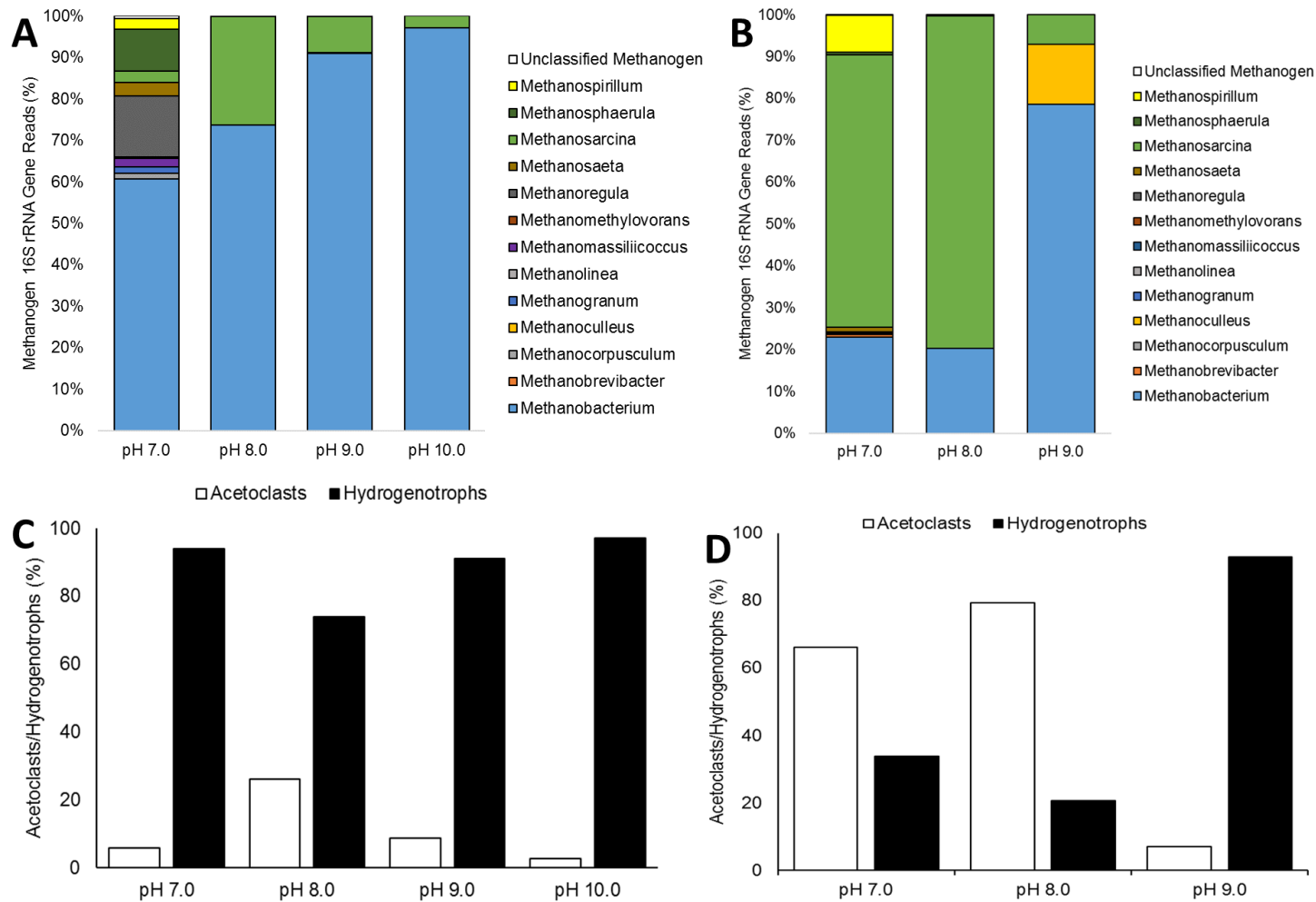


**Figure 6.14. Genus-level methanogen composition and proportion of acetoclastic and hydrogenotrophic genera within H<sub>2</sub>/CO<sub>2</sub>-fed and acetate-fed microcosms between pH 7.0-10.0.** [A] Genus-level composition of H<sub>2</sub>/CO<sub>2</sub>-fed microcosms, [B] genus-level composition of acetate-fed microcosms, [C] proportion of acetoclasts and hydrogenotrophs within H<sub>2</sub>/CO<sub>2</sub>-fed microcosms, [D] proportion of acetoclasts and hydrogenotrophs within acetate-fed microcosms.

### 6.3.2 Lime Site Microcosms

Microcosms employing the alkaline sediments from the lime sites were able to generate methane between pH 7.0-11.0 when fed with H<sub>2</sub>/CO<sub>2</sub>, in contrast acetate-fed microcosms only generated methane at pH 7.0 and 8.0 (Figure 6.15). At pH 9.0 and 10.0 headspace hydrogen was completely removed from H<sub>2</sub>/CO<sub>2</sub>-fed microcosms within the 14 day incubation period (Figure 6.15A). Hydrogen was also consumed within pH 7.0, 8.0 and 11.0 microcosms fed with H<sub>2</sub>/CO<sub>2</sub>, however low quantities of hydrogen were still present within the headspace after 14 days, suggesting the rate of hydrogen consumption slowed down under these conditions. No significant acetotrophy was detected within the acetate-fed microcosms at pH 9.0, 10.0 and 11.0, however the concentration of acetate at pH 7.0 and 8.0 reduced from 29.0 mM ( $\pm 2.8$ ) to 16.3 mM ( $\pm 3.5$ ) and 30.5 mM ( $\pm 2.7$ ) to 16.9 mM ( $\pm 4.4$ ) over the 14 day incubation period respectively (Figure 6.15B). Methane generation rates were highest at pH 9.0 and 10.0, with an average of 0.43 ( $\pm 0.04$ ) and 0.36 ( $\pm 0.04$ ) detected on day 14 respectively (Figure 6.15C). The quantity of methane generated from H<sub>2</sub>/CO<sub>2</sub> by day 14 reduced at pH 7.0, 8.0 and 11.0 to 0.16 ( $\pm 0.02$ ), 0.26 ( $\pm 0.14$ ) and 0.12 ( $\pm 0.06$ ) mmoles respectively (Figure 6.15C), likely due to the lower hydrogen consumption rates under these conditions (Figure 6.15A). Methane could only be detected at pH 7.0 and 8.0 within the acetate-fed microcosms, however only low quantities were detected on day 14 of 0.06 ( $\pm 0.02$ ) and 0.07 ( $\pm 0.04$ ) mmoles respectively (Figure 6.15D).

The rate of acetate and hydrogen consumption was measured for acetate-fed and H<sub>2</sub>/CO<sub>2</sub>-fed microcosms between pH 7.0-11.0 (Figure 6.16). Average hydrogen consumption rates within pH 7.0, 8.0, 9.0, 10.0 and 11.0 microcosms were 90.7 ( $\pm 5.2$ ), 70.9 ( $\pm 17.3$ ), 167.5 ( $\pm 45.3$ ), 133.2 ( $\pm 27.2$ ) and 77.0 ( $\pm 21.3$ )  $\mu\text{moles day}^{-1}$  respectively (Figure 6.16), suggesting the optimum pH for hydrogenotrophic methanogenesis when employing the alkaline sediments was pH 9.0, which is in agreement with the CDP-fed microcosms (Figure 6.10). Since the pH values of the inoculating sediments was much higher than pH 9.0 (see Chapter 5) and no methane could be generated in pH 12.0 microcosms when supplied with CDP, acetate or H<sub>2</sub>/CO<sub>2</sub>, this further suggests the methanogens were surviving in low pH microsites within the sampling sites. Acetate consumption rates within the acetate-fed microcosms were 23.6 ( $\pm 7.6$ ) and 36.4 ( $\pm 14.1$ ) at pH 7.0 and 8.0 respectively (Figure 6.16), with no significant acetate consumption detected at pH 9.0, 10.0 and 11.0 (Figure 6.15B). Stoichiometric calculations of the methanogenic reactors fed with acetate do not correlate well with acetoclastic methanogenesis

(Figure 6.17) and therefore the acetate consumed under these conditions may be a result of other acetate-consuming processes such as syntrophic acetate oxidation (320).

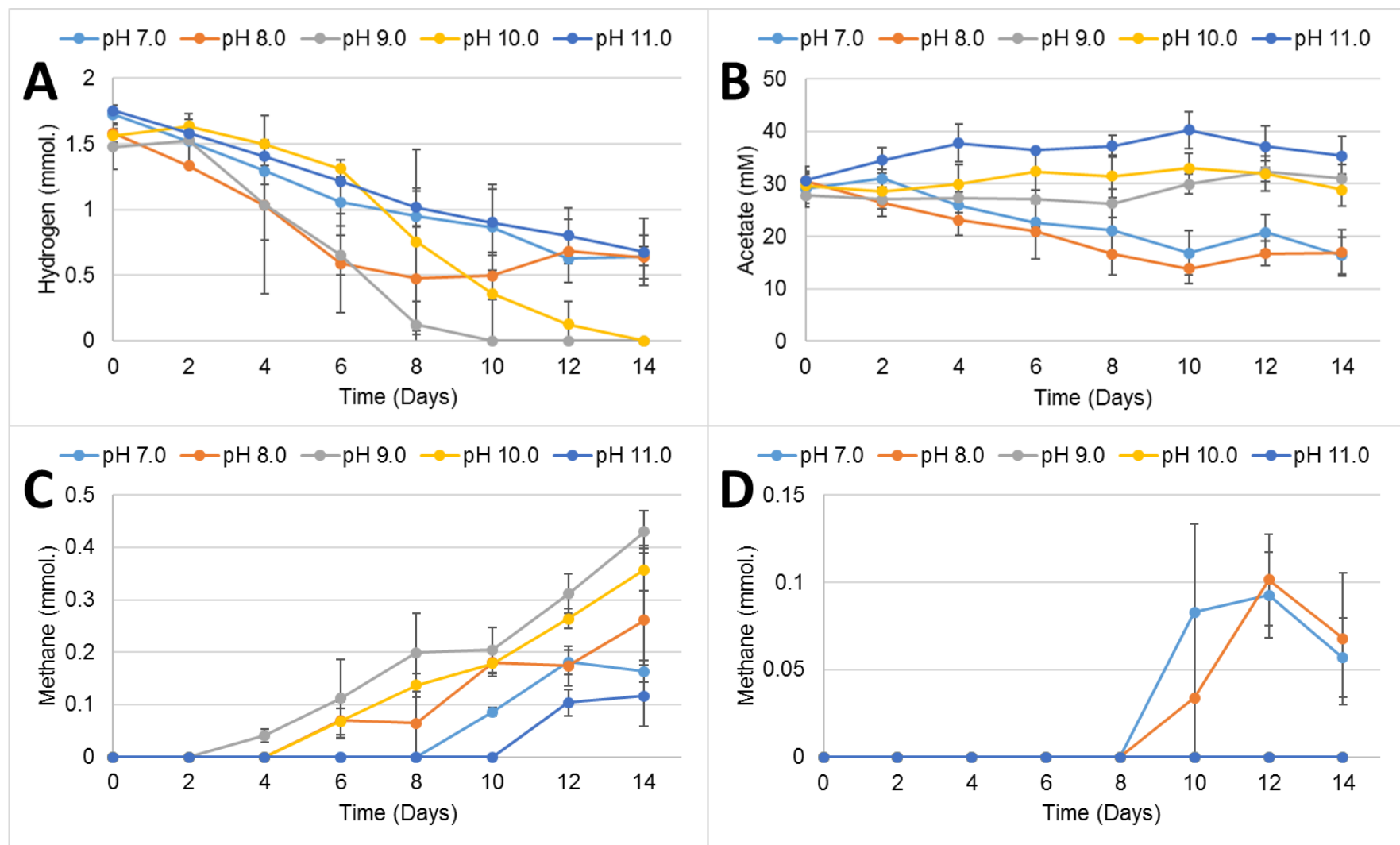


**Figure 6.15. Hydrogen, acetate and methane quantities within microcosms employing lime site sediments between pH 7.0-11.0.** [A] Hydrogen quantities between pH 7.0-11.0, [B] acetate concentrations between pH 7.0-11.0, [C] methane generated from H<sub>2</sub>/CO<sub>2</sub>-fed microcosms pH 7.0-11.0, [D] methane generated from acetate-fed microcosms pH 7.0-11.0.

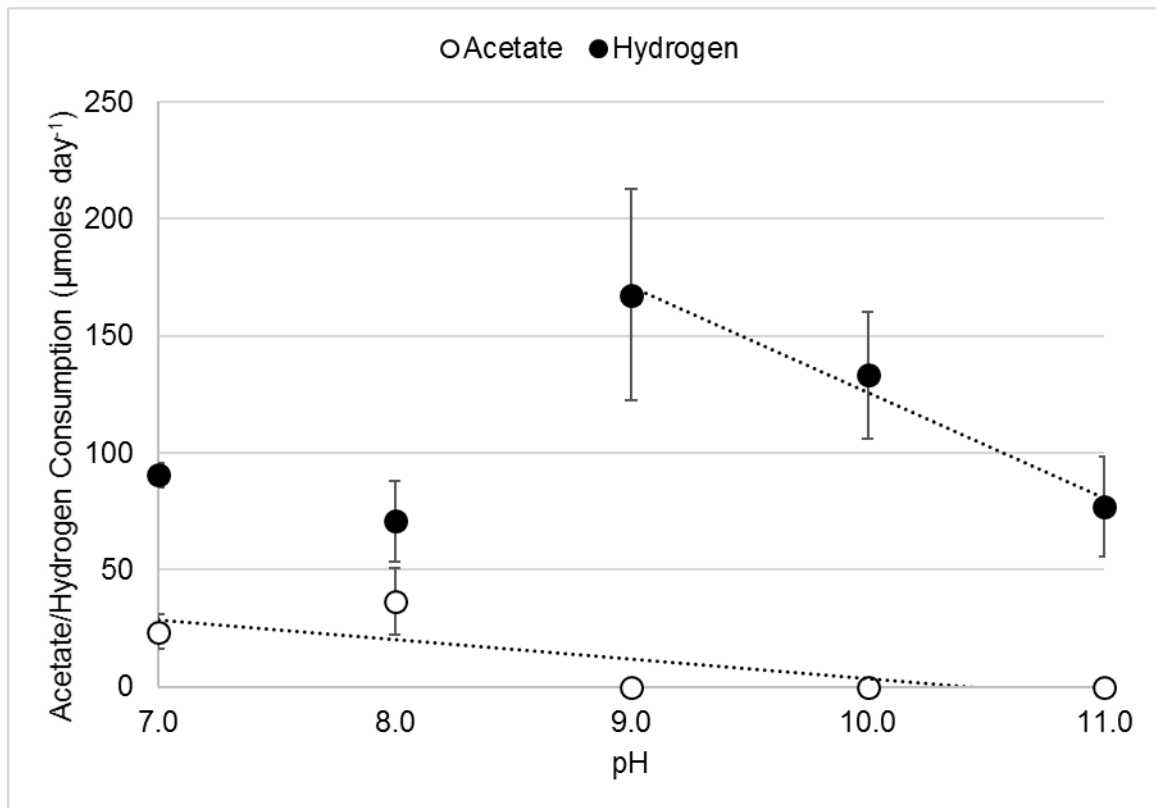


**Figure 6.16. Acetate and hydrogen consumption rates within microcosms employing alkaline lime sediments between pH 7.0-11.0.** The rate of hydrogen consumption increased at pH 9.0. The rate of acetate consumption was only measurable at pH 7.0 and 8.0.

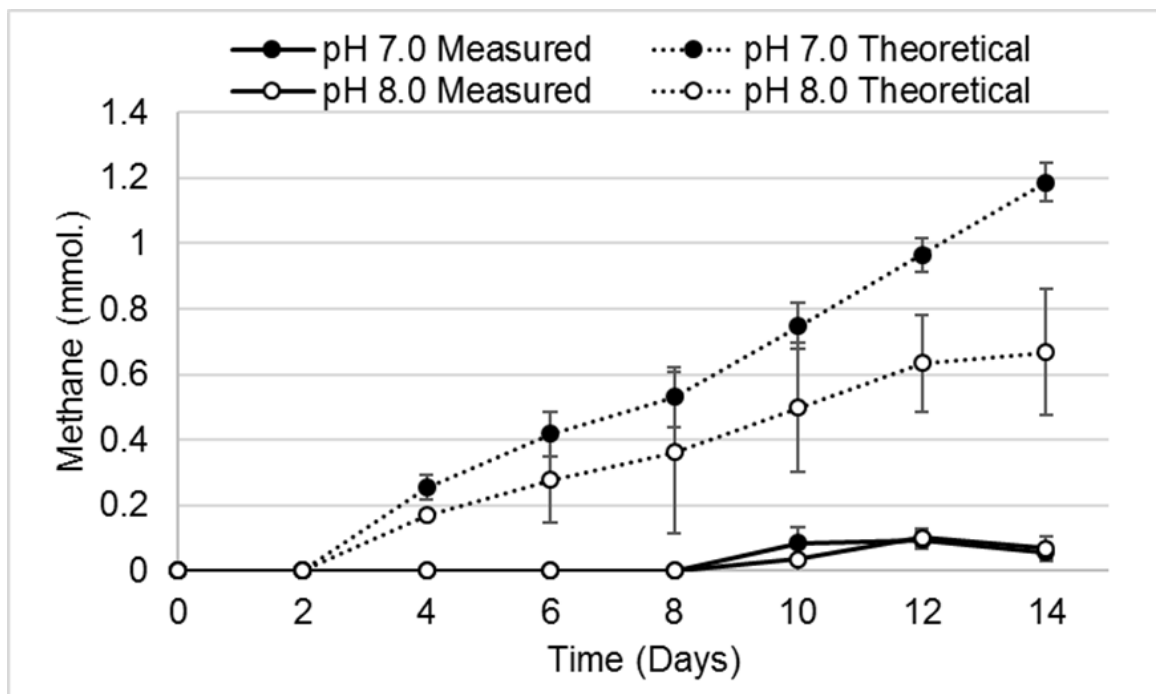


**Figure 6.17. Measured and theoretical methane generation quantities within pH 7.0 and 8.0 acetate-fed microcosms employing the alkaline sediments from the lime sites.**

The methanogen community was analysed within H<sub>2</sub>/CO<sub>2</sub>-fed microcosms between pH 7.0-11.0 and acetate-fed microcosms at pH 7.0 and 8.0, since these were the only reactors that showed evidence of methanogenesis. In similar fashion to the CDP-fed microcosms employing the lime sediments (Section 6.2.2), the strictly hydrogenotrophic genera *Methanobacterium* and *Methanoculleus* dominated in all the H<sub>2</sub>/CO<sub>2</sub>-fed and surprisingly in the acetate-fed reactors (Figure 6.18). At pH 7.0, 8.0, 9.0, 10.0 and 11.0 the genus *Methanobacterium* represented an average of 85.4% ( $\pm 29.5$ ), 93.4% ( $\pm 31.4$ ), 66.1% ( $\pm 33.0$ ), 65.9% ( $\pm 32.9$ ) and 49.3% ( $\pm 32.9$ ) of the total methanogen reads across the lime site reactors fed with H<sub>2</sub>/CO<sub>2</sub> respectively (Figure 6.18A). The genus *Methanoculleus* represented an average of 2.9% ( $\pm 2.0$ ), 5.5% ( $\pm 3.7$ ), 29.9% ( $\pm 29.8$ ), 30.5% ( $\pm 30.5$ ) and 46.9% ( $\pm 30.9$ ) of the total methanogen reads across lime site reactors fed with H<sub>2</sub>/CO<sub>2</sub> at pH 7.0, 8.0, 9.0, 10.0 and 11.0 respectively. 6 other methanogenic genera were detected in the H<sub>2</sub>/CO<sub>2</sub>-fed and acetate-fed microcosms, including *Methanocorpusculum*, *Methanomassiliicoccus*, *Methanomethylovorans*, *Methanoregula*, *Methanosaeta* and *Methanosarcina*, however the percentage of reads attributed to these methanogens was very low (Figure 6.18AB).

Interestingly, only hydrogenotrophic methanogens could be detected with any significance in the acetate-fed reactors employing the lime site sediments (Figure 6.18BD), which supports the chemistry within the microcosms (Figure 6.17), where only very low quantities of methane could be detected which was not stoichiometrically balanced with the amount of acetate consumed. As with the H<sub>2</sub>/CO<sub>2</sub>-fed microcosms, the genera *Methanobacterium* and *Methanoculleus* were the dominant methanogens (Figure 6.18B) and have been discussed in Section 6.2. The lack of acetoclastic methanogenesis from the lime-site microcosms could be a result of the high pH conditions of the sites. Since control microcosms demonstrated high acetate consumption and methane generation at pH 7.0 and 8.0, yet were incapable of this process above pH 9.0, acetoclastic species may have been selected against due to the alkaline *in situ* conditions of the sampling sites. The development of acetoclastic methanogen cultures from the control-site sediments suggests the growth conditions imposed in this study were able to support acetate-dependent methanogenesis and that any lack of acetate metabolism was not a result of the growth media. As discussed in Chapter 5, no acetoclastic methanogens could be detected in the inoculating materials taken from the lime sites prior to the development of enrichment cultures in the laboratory. Furthermore, lime-site reactors were initiated at a pH of 10.0 and gradually decreased to more neutral-pH values, therefore it is possible that acetoclastic species were unable to survive the initial inoculation and were absent when attempting to

culture them under neutral-pH conditions. No methanogens capable of spore formation could be found in the literature which could enable them to survive as dormant cells under alkaline conditions.

The inability of acetoclastic methanogens to grow at high pH within the present study could be linked to energy conservation. The hydrogenotrophic orders of methanogens *Methanobacteriales* and *Methanomicrobiales* that dominated within all of the high pH microcosms lack cytochromes (29, 81). These methanogens synthesise ATP via the establishment of a proton motive force across the membrane using Na<sup>+</sup> ions. In contrast, the metabolically diverse *Methanosarcinales* are the only order of methanogens that contain cytochromes and use a completely different mode of energy generation, namely via the production of an electrochemical proton gradient using H<sup>+</sup> and Na<sup>+</sup> coupled with the reduction of heterodisulfide (29, 323). The availability of H<sup>+</sup> ions decreases as the pH increases which could be inhibiting members of the *Methanosarcinales* from growing under alkaline conditions, as seen within the present study.

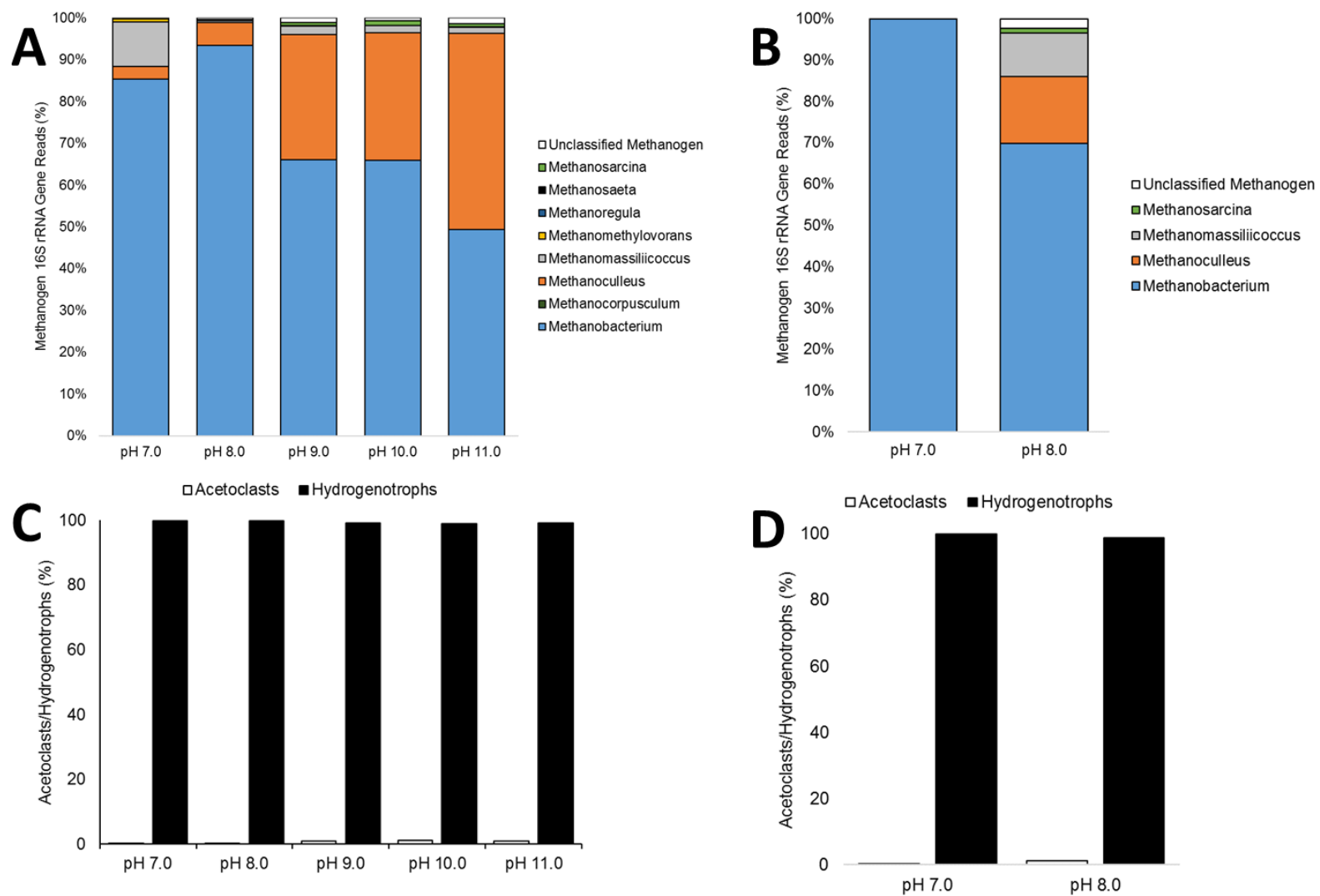


**Figure 6.18. Genus-level methanogen composition and proportion of acetoclastic/hydrogenotrophic species within H<sub>2</sub>/CO<sub>2</sub>-fed and acetate-fed microcosms between pH 7.0-11.0.**

## 6.4 Inhibition Studies

The degradation of acetate under anaerobic conditions in the absence of TEA's can either be a result of conversion to  $H_2/CO_2$  by SAOB (320) or to  $CH_4$  by methanogens (325). Without the use of radio-labelled carbon (305) it is difficult to distinguish the end products of acetate metabolism. However with the use of methyl-fluoride ( $CH_3F$ ), a selective inhibitor of acetoclastic methanogenesis, it is possible to differentiate pathway utilisation by comparing the acetate consumption and methane generation in microcosms treated with  $CH_3F$  and those without treatment (251, 326, 327).  $CH_3F$  has been shown to inhibit pure cultures of acetoclastic *Methanosaeta* and *Methanosarcina*, furthermore in *Methanosarcina barkeri*, which can use both  $H_2/CO_2$  and acetate (328), treatment with  $CH_3F$  only inhibited acetate consumption, whilst hydrogenotrophic methanogenesis remained unaffected (251). Under certain concentrations  $CH_3F$  is also capable of inhibiting acetate-derived methane in defined mixed cultures, whilst having no inhibitory effect on other microbial processes such as SAO (251). Although no acetoclastic methanogenesis was observed at pH 10.0 in Section 4.2 and 4.3, very low percentages of *Methanosarcina* and *Methanosaeta* 16S rRNA gene reads were present within some of these microcosms (Figures 6.6, 6.11, 6.14 and 6.18) and it remains unclear which pathway these organisms are contributing to. Additionally, the consumption of acetate within pH 7.0 and 8.0 microcosms employing the alkaline sediments did not appear to be a result of methanogenesis, since only low quantities of methane were produced, therefore the use of methyl fluoride can help to consolidate this position. The CDP-fed microcosms operating at pH 7.0 and 10.0 discussed in Section 6.2 were used to inoculate further sub-cultures containing both methanogenic substrates ( $H_2/CO_2$  and acetate) supplied in the growth media, both in the presence and absence of  $CH_3F$ .

### 6.4.1 Control Site Microcosms

Methane was generated in pH 7.0 and 10.0 microcosms employing the control site sediments when supplied with both  $H_2/CO_2$  and acetate, in the presence and absence of  $CH_3F$  (Figure 6.19A). However the quantity of methane generation differed significantly between microcosms containing and lacking the inhibitor. By day 14 methane quantities within pH 7.0 microcosms lacking and containing  $CH_3F$  were 1.94 ( $\pm 0.19$ ) and 0.51 ( $\pm 0.14$ ) mmoles respectively (Figure 6.19A). At pH 10.0 methane quantities were 0.39 ( $\pm 0.06$ ) and 0.34 ( $\pm 0.09$ ) mmoles on day 14 in the absence and presence of the inhibitor respectively (Figure 6.19A). These differences are assumed to be due to inhibition of the acetoclastic pathway, which is supported by the fact that acetate consumption was hindered in the presence of  $CH_3F$  at pH 7.0 (Figure 6.19B). Upon inoculation acetate quantities within pH 7.0 microcosms were 1.59

( $\pm 0.07$ ) and 1.46 ( $\pm 0.05$ ) mmoles in the absence and presence of  $\text{CH}_3\text{F}$  respectively (Figure 6.19B). By day 14 the amount of acetate had decreased to 0.39 ( $\pm 0.1$ ) in pH 7.0 microcosms lacking the inhibitor, in contrast microcosms incubated under  $\text{CH}_3\text{F}$  had 1.46 ( $\pm 0.1$ ) mmoles of acetate remaining by the end of the incubation period (Figure 6.19B), suggesting acetate consumption was stunted. Within pH 10.0 microcosms acetate quantities decreased from 1.56 ( $\pm 0.04$ ) mmoles upon inoculation to 1.31 ( $\pm 0.04$ ) by day 14 in the absence of  $\text{CH}_3\text{F}$ , in contrast acetate within pH 10.0 microcosms incubated in the presence of the inhibitor increased from 1.39 ( $\pm 0.03$ ) mmoles on day 0 to 1.74 ( $\pm 0.1$ ) mmoles on day 14 (Figure 6.19B). Since methane quantities within pH 10.0 microcosms were similar in the presence and absence of  $\text{CH}_3\text{F}$  (Figure 6.19A), the very low amounts of acetate consumption observed at pH 10.0 in the absence of the inhibitor must have been a result of SAO, which supports the community analysis undertaken in Section 6.2.1 where hydrogenotrophic methanogens dominated (Figure 6.6). Hydrogen consumption remained largely unaffected by the addition of  $\text{CH}_3\text{F}$  (Figure 6.19C), suggesting that any methane generated in microcosms containing methyl fluoride was derived from hydrogenotrophic metabolism, despite a small amount of lag in the presence of methyl fluoride (Figure 6.19C).

The quantity of methane generated in uninhibited microcosms (total methane) subtracted from the quantity of methane generated in inhibited microcosms (methane from  $\text{H}_2/\text{CO}_2$ ) can be used to determine the amount of acetate-derived methane (326). 73.8% ( $\pm 4.4$ ) of methane within pH 7.0 microcosms was derived from acetate, with the remaining 26.2% ( $\pm 4.4$ ) coming from  $\text{H}_2/\text{CO}_2$  (Figure 6.20). In contrast only 13.3% ( $\pm 9.2$ ) of the methane at pH 10.0 was derived from acetate and 86.7% ( $\pm 9.2$ ) derived from  $\text{H}_2/\text{CO}_2$  (Figure 6.20). This supports the microcosm chemistry and community analysis undertaken in Sections 6.2 and 6.3, which suggested little to no acetoclastic methanogenesis was present at pH 10.0. It is perhaps surprising that the inhibition studies demonstrated as much as 13.3% of methane was being derived from acetate at pH 10.0, however the addition of  $\text{CH}_3\text{F}$  did marginally impact hydrogen consumption rates (Figure 6.19C) which could be obscuring these calculations. Methyl fluoride can also inhibit hydrogenotrophic methanogenesis at concentrations above 1% (v/v) (327). Additionally methyl fluoride does degrade over time (327) and so its inhibitory effects may have worn off towards the end of the incubation period. Nevertheless the inhibitor studies presented here do support the notion that hydrogenotrophic methanogenesis dominates at high pH and the acetoclastic pathway is hindered under alkaline conditions.

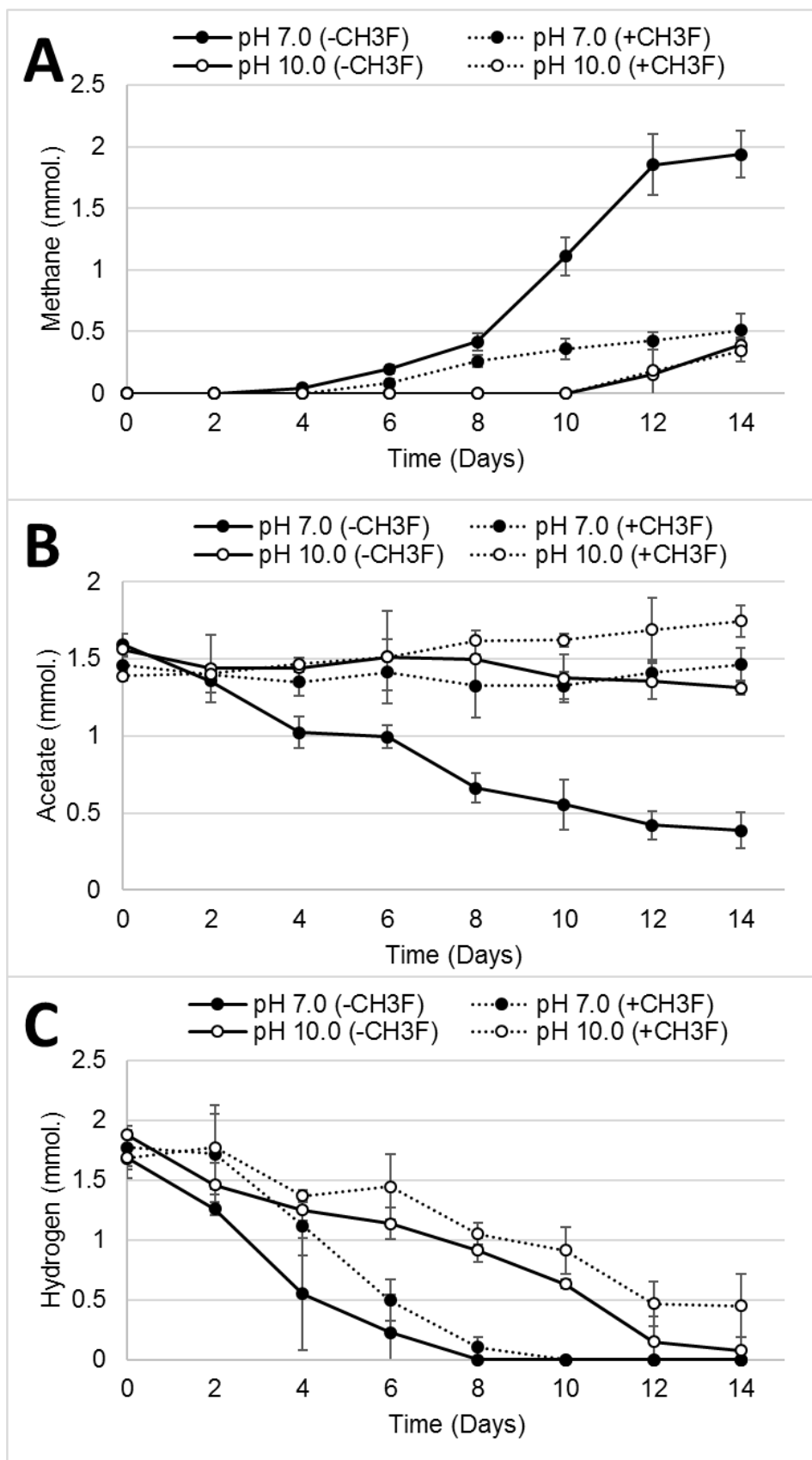


**Figure 6.19. Methane, acetate and hydrogen quantities within pH 7.0 and 10.0 microcosms employing the control sediments in the presence (+CH<sub>3</sub>F) and absence (-CH<sub>3</sub>F) of methyl fluoride.**

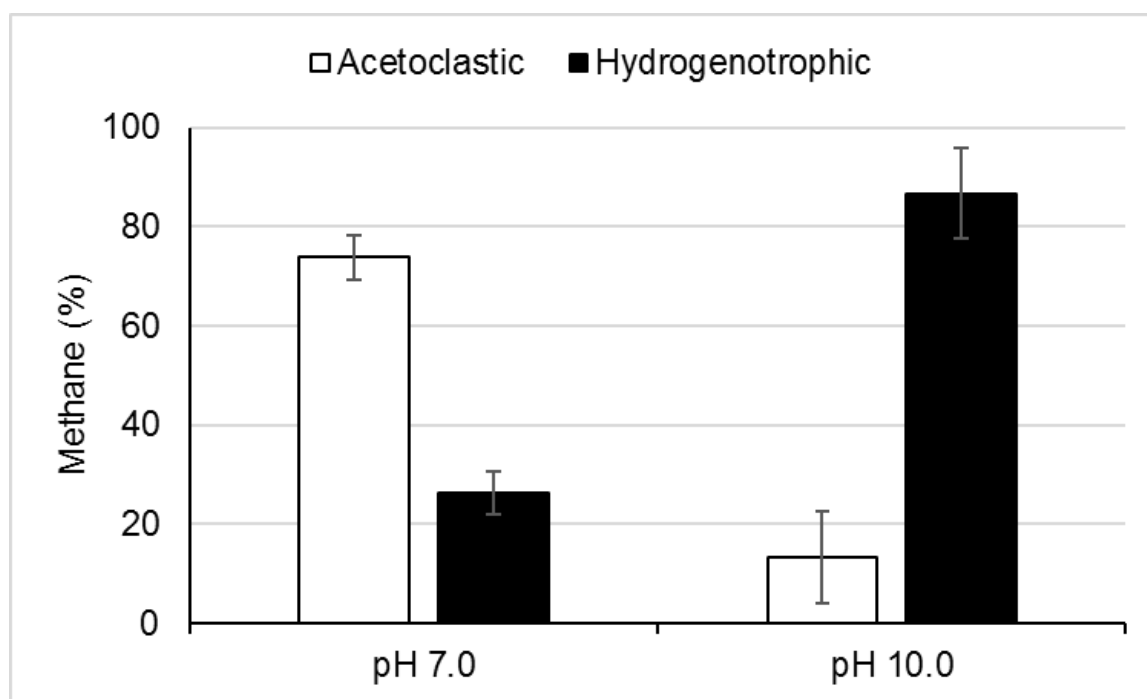


**Figure 6.20. Percentage of methane derived from acetate and H<sub>2</sub>/CO<sub>2</sub> at pH 7.0 and 10.0 within microcosms employing control site sediments.**

#### 6.4.2 Lime Site Microcosms

Microcosms employing the alkaline sediments were able to generate methane at pH 7.0 and 10.0 in the presence and absence of CH<sub>3</sub>F (Figure 6.21A). At pH 7.0 an average of 0.075 (±0.086) and 0.084 (±0.097) mmoles of methane was generated by day 14 in the absence and presence of the inhibitor respectively (Figure 6.21A). Within pH 10.0 microcosms an average of 0.19 (±0.05) and 0.25 (±0.04) mmoles of methane was produced by day 14 in reactors lacking and containing CH<sub>3</sub>F respectively (Figure 6.21A). Hydrogen and acetate consumption was not significantly affected by the addition of methyl fluoride under both pH values tested (Figure 6.21BC). Within pH 7.0 microcosms the average acetate quantities in the absence and presence of CH<sub>3</sub>F upon inoculation were 1.42 (±0.11) and 1.37 (±0.045) respectively. The quantity of acetate within pH 7.0 microcosms reduced to 0.93 (±0.056) and 0.79 (±0.077) mmoles by day 14 in microcosms lacking and containing the inhibitor respectively (Figure 6.21B). Hydrogen quantities reduced throughout the incubation period at pH 7.0 and 10.0 within microcosms containing and lacking CH<sub>3</sub>F at similar rates, suggesting hydrogenotrophic metabolism was unaffected by the addition of the inhibitor (Figure 6.21C). Although the differences were marginal, methane quantities within microcosms containing CH<sub>3</sub>F were slightly elevated compared with reactors lacking the inhibitor, therefore calculating the percentage of methane derived from H<sub>2</sub>/CO<sub>2</sub> yielded values of >100%. Acetate consumption

was evident in both inhibited and uninhibited microcosms, suggesting syntrophic acetate oxidation was present in these reactors. This also confirms the lack of acetoclastic methanogenesis in the pH 7.0 and 8.0 microcosms fed solely with acetate discussed in Section 6.3.2.

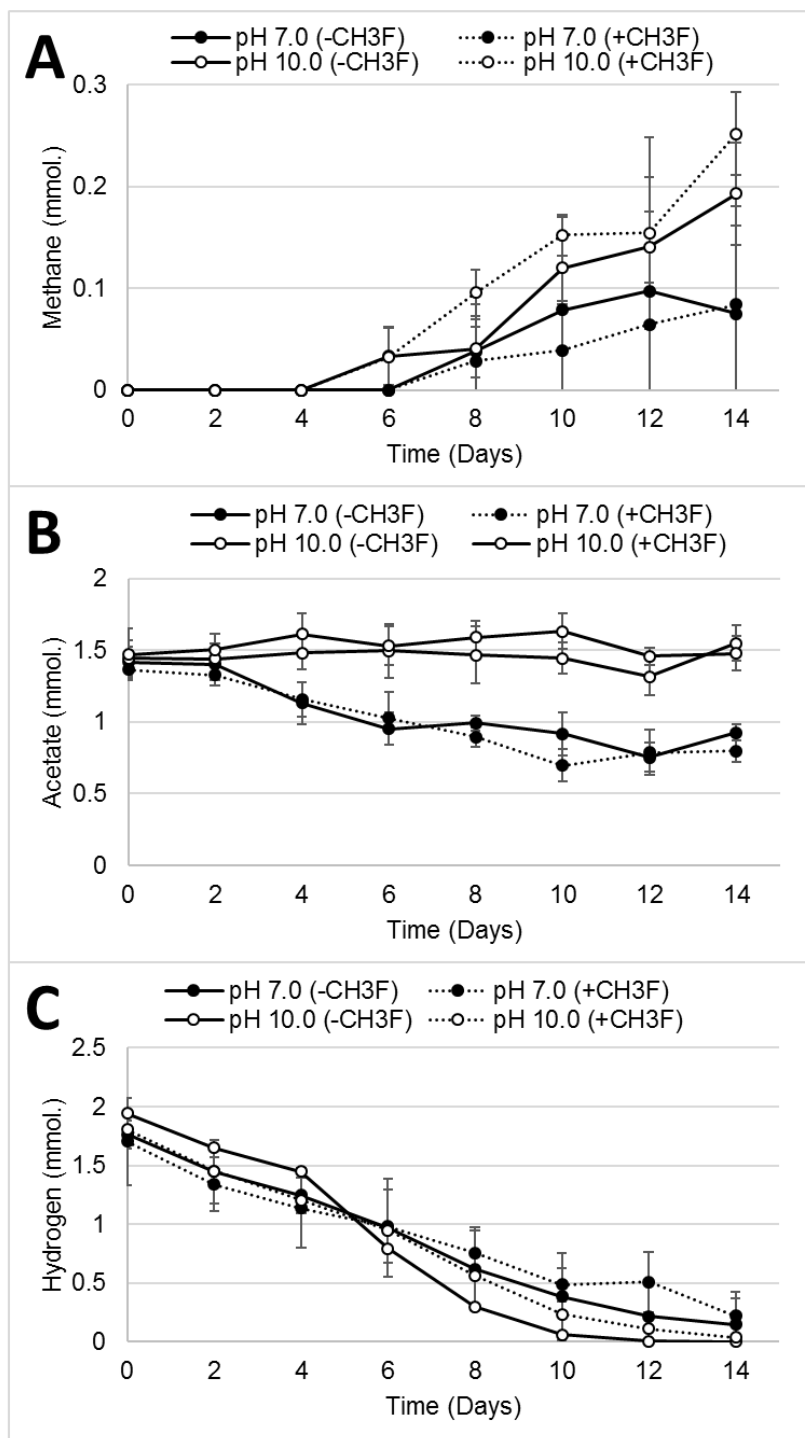


**Figure 6.21. Methane, acetate and hydrogen quantites within pH 7.0 and 10.0 microcosms employing the alkaline sediments in the presence (+CH3F) and absence (-CH3F) of methyl fluoride.**

## 6.5 Old Lime and Steel Enrichments at pH 7.0 and 10.0

Since all the alkaline microcosms ( $\text{pH} \geq 10.0$ ) developed from the Control site and New Lime sites described in Sections 4.2, 4.3 and 4.4 all demonstrated a clear preference for the hydrogenotrophic pathway, the study was expanded to include the Old Lime sites and Steel sites in order to determine whether this trend was ubiquitous to different environments. As discussed in Chapter 5, the Steel site sediments had a comparable methanogen community to the Control site sediments prior to the development of enrichment cultures, where a number of acetoclastic genera were identified. The sediments retrieved from the Old Lime (LK1-5) and Steel sites (CW, CS, RC, SC) were used to develop hydrogenotrophic ( $\text{H}_2/\text{CO}_2$ -fed) and acetoclastic (acetate-fed) enrichment cultures at pH 7.0 and 10.0 after sub-culturing out the inoculating sediments. Substrate consumption and methane generation was measured in these sub-cultures and the methanogen community was analysed in any microcosms positive for methanogenesis using 16S rRNA gene sequencing technologies.

### 6.5.1 Old Lime Microcosms at pH 10.0

The initial acetate quantities within acetate-fed microcosms was 1.83 ( $\pm 0.06$ ,  $n=2$ ), 1.96 ( $\pm 0.06$ ,  $n=2$ ), 1.98 ( $\pm 0.13$ ,  $n=2$ ), 1.84 ( $\pm 0.17$ ,  $n=2$ ) and 1.93 ( $\pm 0.012$ ,  $n=2$ ) mmoles for sites LK1, LK2, LK3, LK4 and LK5 respectively (Figure 6.22A). Following the 56 day incubation period the final acetate quantities within the same microcosms was 2.01 ( $\pm 0.03$ ,  $n=2$ ), 1.98 ( $\pm 0.04$ ,  $n=2$ ), 2.14 ( $\pm 0.26$ ,  $n=2$ ), 1.89 ( $\pm 0.06$ ,  $n=2$ ) and 2.00 ( $\pm 0.097$ ,  $n=2$ ) for sites LK1, LK2, LK3, LK4 and LK5 respectively (Figure 6.22A). This suggests little to no acetate was consumed during the incubation period. To support the lack of measurable acetate consumption, no methane was detected in the acetate-fed microcosms operating at pH 10.0 when employing the Old Lime sediments (Figure 6.22C). In contrast, hydrogen was removed from the headspace of the  $\text{H}_2/\text{CO}_2$ -fed microcosms operating at pH 10.0 employing the Old Lime sediments within 8 weeks (Figure 6.22B), compared with unamended controls, suggesting hydrogen was being consumed via microbial activity. Initial hydrogen quantities within the  $\text{H}_2/\text{CO}_2$ -fed microcosms were 1.97, 1.92, 1.85, 2.04 and 1.85 mmoles for sites LK1, LK2, LK3, LK4 and LK5 respectively (Figure 6.22B). No hydrogen was detected within the headspace of these cultures after 56 days incubation. Methane was detected in the headspace of all  $\text{H}_2/\text{CO}_2$ -fed microcosms operating at pH 10.0 employing the Old Lime sediments (Figure 6.22D). By day 56 average methane quantities were 0.25 ( $\pm 0.19$ ,  $n=2$ ), 0.15 ( $\pm 0.015$ ,  $n=2$ ), 0.09 ( $\pm 0.086$ ,  $n=2$ ), 0.11

( $\pm 0.078$ , n=2) and 0.21 ( $\pm 0.12$ , n=2) mmoles for sites LK1, LK2, LK3, LK4 and LK5 respectively (Figure 6.22D). The methanogen community within the active H<sub>2</sub>/CO<sub>2</sub>-fed microcosms at pH 10.0 were dominated by hydrogenotrophic methanogens of the genus *Methanoculleus*, which represented 99.9 %, 76.0 %, 99.9 %, 91.2 % and 81.9 % of the total archaea reads in sites LK1, LK2, LK3, LK4 and LK5 respectively (Figure 6.23).

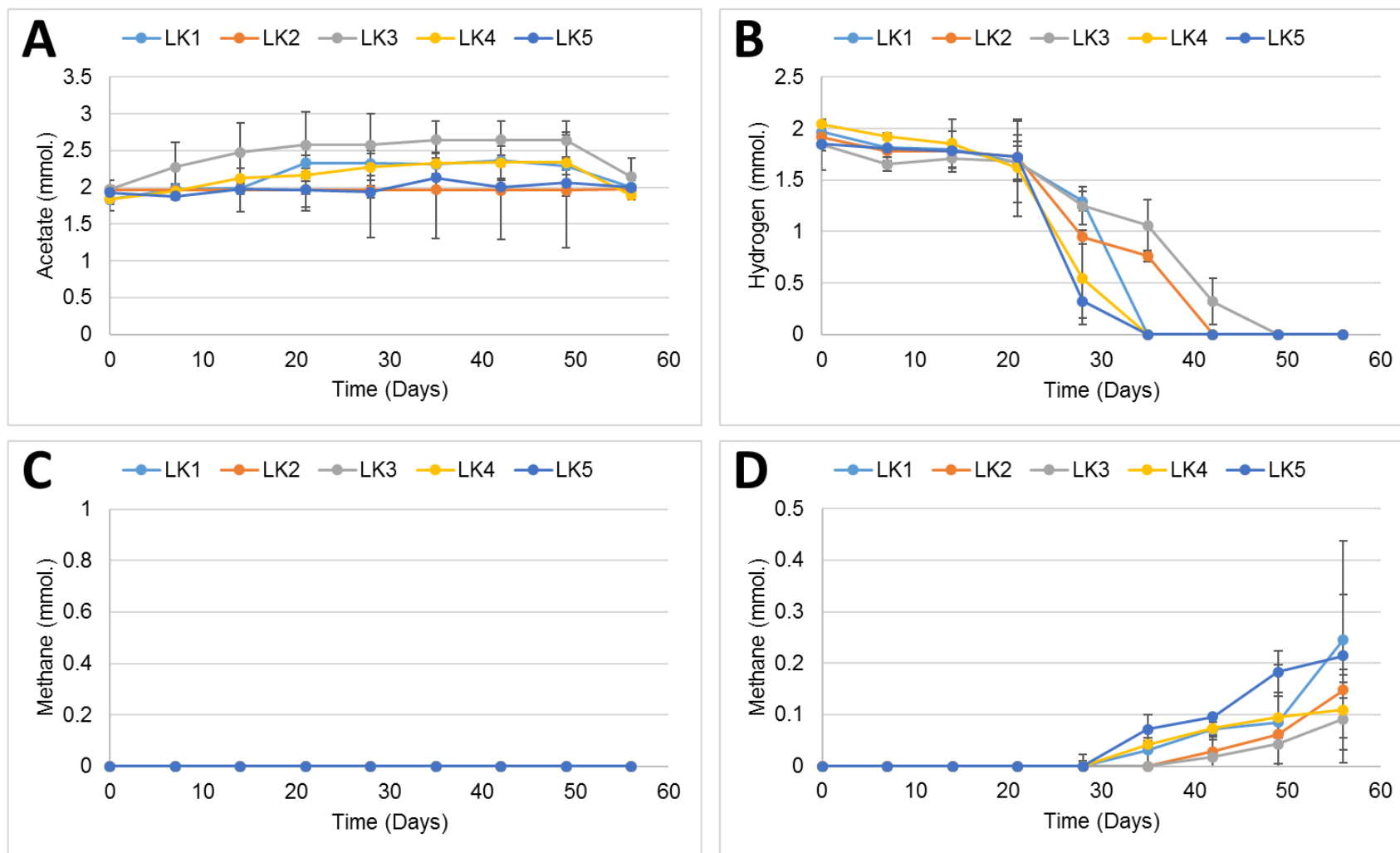


**Figure 6.22. Microcosm chemistry in acetate-fed and H<sub>2</sub>/CO<sub>2</sub>-fed Old Lime microcosms at pH 10.0.** [A] Acetate quantities, [B] hydrogen quantities, [C] methane quantities in acetate-fed microcosms, [D] methane quantities in H<sub>2</sub>/CO<sub>2</sub>-fed microcosms

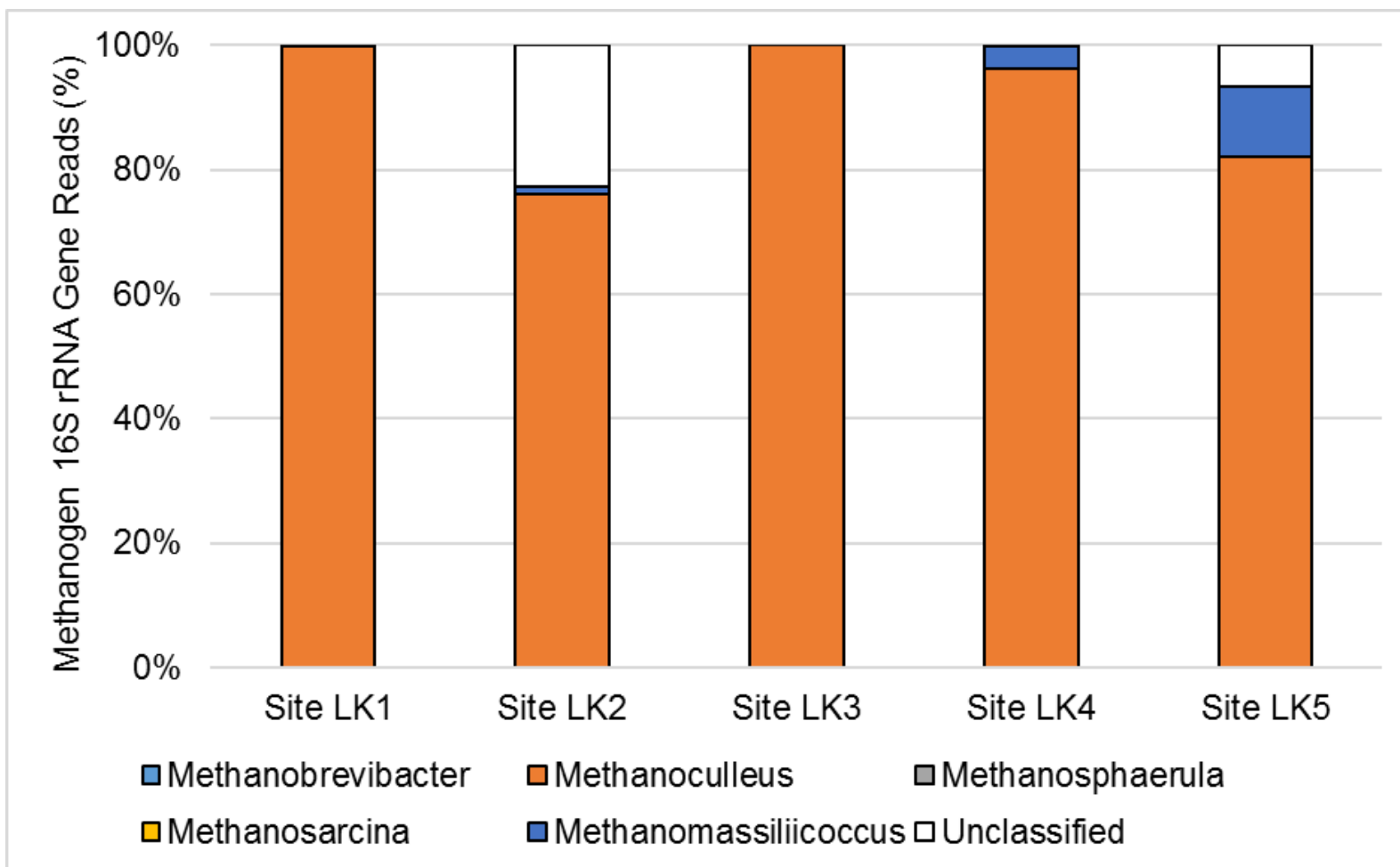


Figure 6.23. Genus-level methanogen composition of H<sub>2</sub>/CO<sub>2</sub>-fed microcosms operating at pH 10.0 employing the Old Lime sediments.

### 6.5.2 Old Lime Microcosms at pH 7.0

In contrast to the pH 10.0 microcosms employing the Old Lime sediments (Section 6.5.1), a number of the pH 7.0 microcosms fed solely with acetate were capable of methanogenesis (Figure 6.24). The initial acetate quantities within the acetate-fed microcosms was 2.78 ( $\pm 0.15$ ,  $n=2$ ), 2.15 ( $\pm 0.39$ ,  $n=2$ ), 2.85 ( $\pm 0.28$ ,  $n=2$ ), 2.26 ( $\pm 0.40$ ,  $n=2$ ) and 2.25 ( $\pm 0.13$ ,  $n=2$ ) mmoles for sites LK1, LK2, LK3, LK4 and LK5 respectively (Figure 6.24A). Within site LK1, LK3 and LK5 microcosms, the final acetate quantities by day 56 were 0.89 ( $\pm 0.59$ ,  $n=2$ ), 0.92 ( $\pm 0.13$ ,  $n=2$ ) and 0.85 ( $\pm 0.71$ ,  $n=2$ ) mmoles respectively, suggesting acetate was being consumed within these reactors (Figure 6.24A). Hydrogen was removed from all H<sub>2</sub>/CO<sub>2</sub>-fed microcosms within the 56 day incubation period (Figure 6.24B). Within the microcosms where acetate showed evidence of consumption, methane was consequently generated (Figure 6.24C), suggesting the acetate in these reactors was being converted to methane. All reactors supplied with H<sub>2</sub>/CO<sub>2</sub> were capable of methanogenesis (Figure 6.24D).

Although acetate-fed pH 7.0 microcosms showed evidence of acetoclastic methanogenesis based on the microcosm chemistry (Figure 6.25), methanogens capable of acetoclastic methanogenesis only represented a minority of the overall population, however the percentage of reads attributed to the metabolically diverse genus *Methanosarcina* did increase compared to pH 10.0 and 7.0 microcosms fed with H<sub>2</sub>/CO<sub>2</sub>. Both acetate-fed and H<sub>2</sub>/CO<sub>2</sub>-fed microcosms were dominated by members of the genus *Methanoculleus*, a strictly hydrogenotrophic methanogen. The ability of these methanogens to maintain a significant population in the absence of supplied H<sub>2</sub>/CO<sub>2</sub> suggests SAO was present in these systems. Within the acetate-fed systems, the potentially acetate-utilising genus *Methanosarcina* represented 23.7 %, 9.5 % and 16.7 % of the total archaea 16S rRNA gene reads within site LK1, LK3 and LK5 microcosms (Figure 6.25A), which does suggest acetoclastic methanogenesis was functioning alongside SAO. In contrast this genus was largely absent from H<sub>2</sub>/CO<sub>2</sub>-fed systems operating at pH 7.0 and 10.0. This suggests the *Methanosarcina* were contributing to acetoclastic methanogenesis at pH 7.0, but were unable to metabolise acetate at pH 10.0. Surprisingly, the genus *Methanomassiliicoccus* was an important part of the archaeal community within pH 7.0 microcosms fed with H<sub>2</sub>/CO<sub>2</sub> (Figure 6.25B). Although the genus *Methanomassiliicoccus* uses hydrogen as electron donor, which explains the high H<sub>2</sub> consumption rates in these systems, this genus uses methanol as TEA and not CO<sub>2</sub> for ATP synthesis (329). Therefore *Methanomassiliicoccus* is likely to be contributing to the methylotrophic pathway in these

reactors, rather than the hydrogenotrophic pathway. Although methanol was not supplied as substrate in these reactors, the increased levels of sediment materials in these microcosms compared to the pH adapt reactors (Section 6.2, 6.3 and 6.4) suggests the inoculating materials contained methylated compounds for use in the methylotrophic pathway.

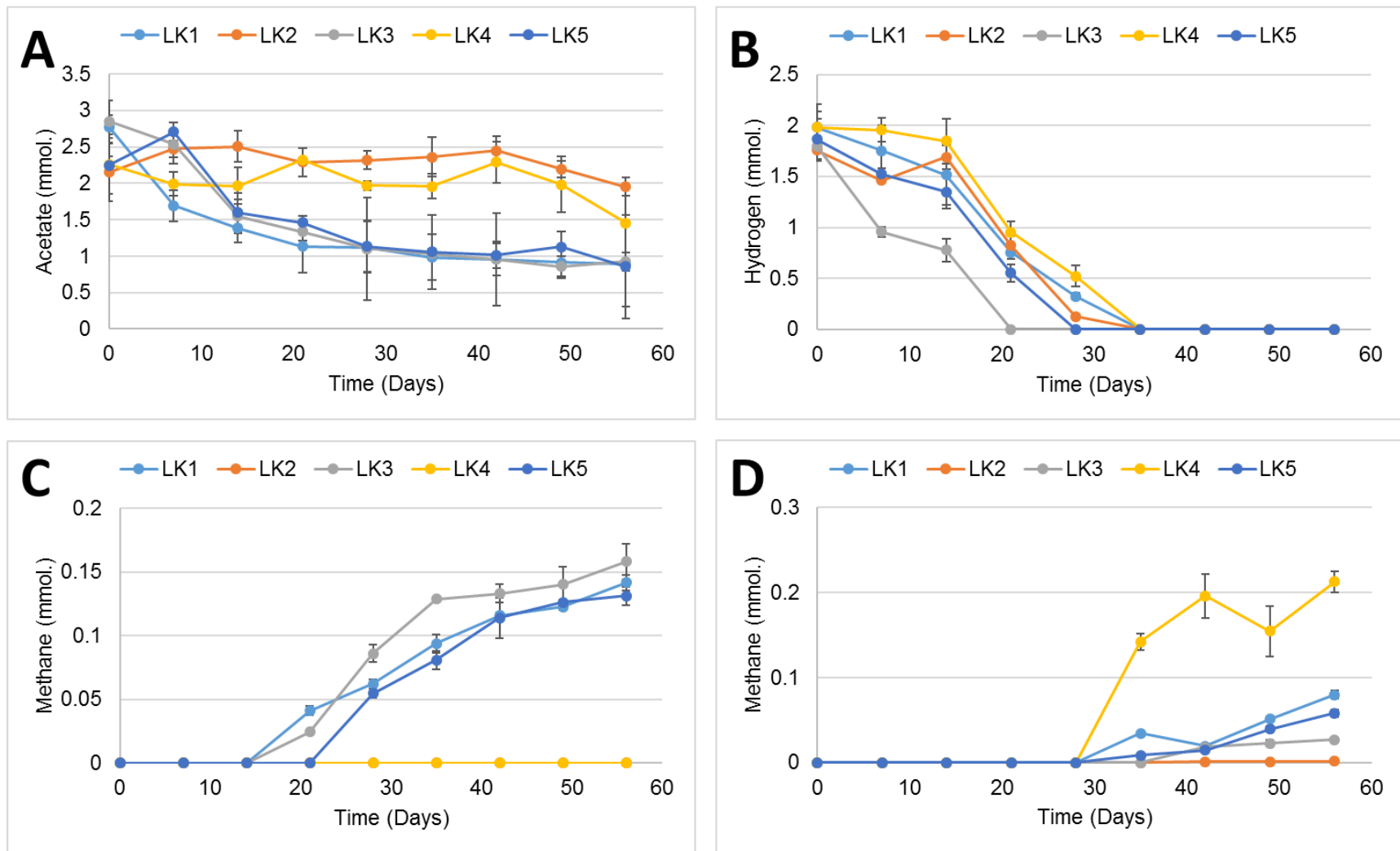


**Figure 4.24. Microcosm chemistry within acetate-fed and H<sub>2</sub>/CO<sub>2</sub>-fed microcosms operating at pH 7.0 employing the Old Lime sediments.** [A] Acetate quantities within acetate-fed microcosms, [B] hydrogen quantities within H<sub>2</sub>/CO<sub>2</sub>-fed microcosms, [C] methane quantities within acetate-fed microcosms, [D] methane quantities within H<sub>2</sub>/CO<sub>2</sub>-fed microcosms. Error bars represent standard deviation (n=2).

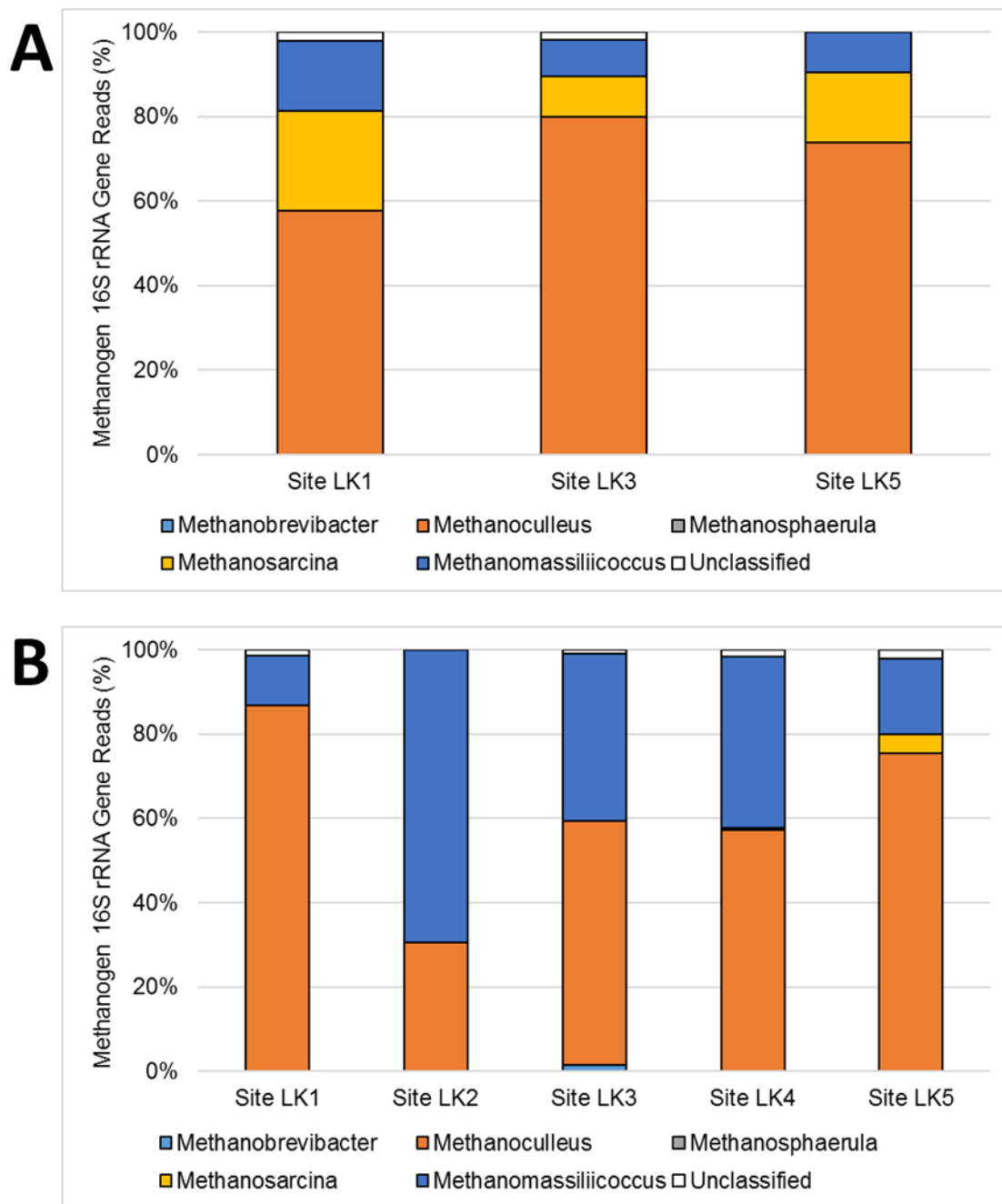


**Figure 6.25. Genus-level composition of acetate-fed and H<sub>2</sub>/CO<sub>2</sub>-fed microcosms employing the Old Lime sediments at pH 7.0. [A] Acetate-fed microcosms, [B] H<sub>2</sub>/CO<sub>2</sub>-fed microcosms.**

At pH 7.0 acetate and hydrogen were consumed at an average rate of 22.2 ( $\pm 5.9$ , n=10) and 63.2 ( $\pm 6.2$ , n=10)  $\mu\text{moles day}^{-1}$  respectively (Figure 6.26). At pH 10 the average consumption rates for acetate and hydrogen were 0.0 ( $\pm 0.0$ , n=10) and 42.2 ( $\pm 8.6$ , n=10)  $\mu\text{moles day}^{-1}$  respectively. This suggests acetate consumption rates were highest under neutral-pH conditions, with no acetate consumption detected at pH 10.0. In contrast, hydrogen was

consumed at both pH 7.0 and 10.0, with lower consumption rates observed under alkaline conditions (Figure 6.26).

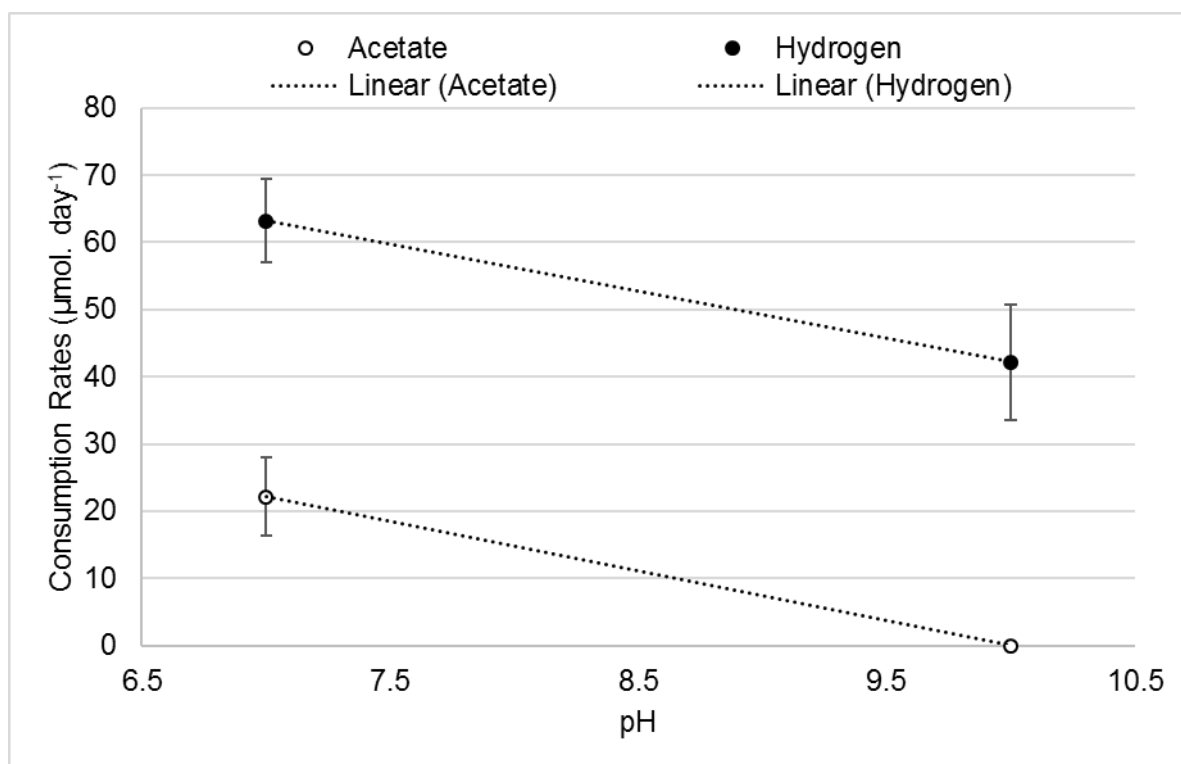


**Figure 6.26. Acetate and hydrogen consumption rates within microcosms employing the Old Lime sediments at pH 7.0 and 10.0.**

### 6.5.3 Steel Microcosms at pH 7.0 and 10.0

In similar fashion to the Old Lime microcosms (Section 6.5.1 and 6.5.2), reactors employing the Steel sediments operating at pH 10.0 were incapable of generating methane when fed solely with acetate, however high acetate-consumption and methane production rates were observed at pH 7.0 (Figure 6.27). Within the acetate-fed microcosms at pH 7.0 and 10.0 the initial acetate quantities across these microcosms was 1.47 ( $\pm 0.09$ ,  $n=10$ ) and 1.41 ( $\pm 0.08$ ,  $n=10$ ) mmoles respectively (Figure 6.27AB). By day 56 the average acetate quantities were 0.07 ( $\pm 0.06$ ,  $n=10$ ) and 1.66 ( $\pm 0.16$ ,  $n=10$ ) mmoles at pH 7.0 and 10.0 respectively (Figure 6.27AB), suggesting the rate of acetotrophy increased significantly under neutral-pH conditions. The consumption of acetate in pH 7.0 microcosms resulted in the generation of high quantities of methane that were stoichiometrically balanced with acetoclastic methanogenesis (Figure 6.28). Both pH 7.0 and 10.0 microcosms were capable of hydrogen consumption and methane production within the 56 day incubation period (Figure 6.27CD).

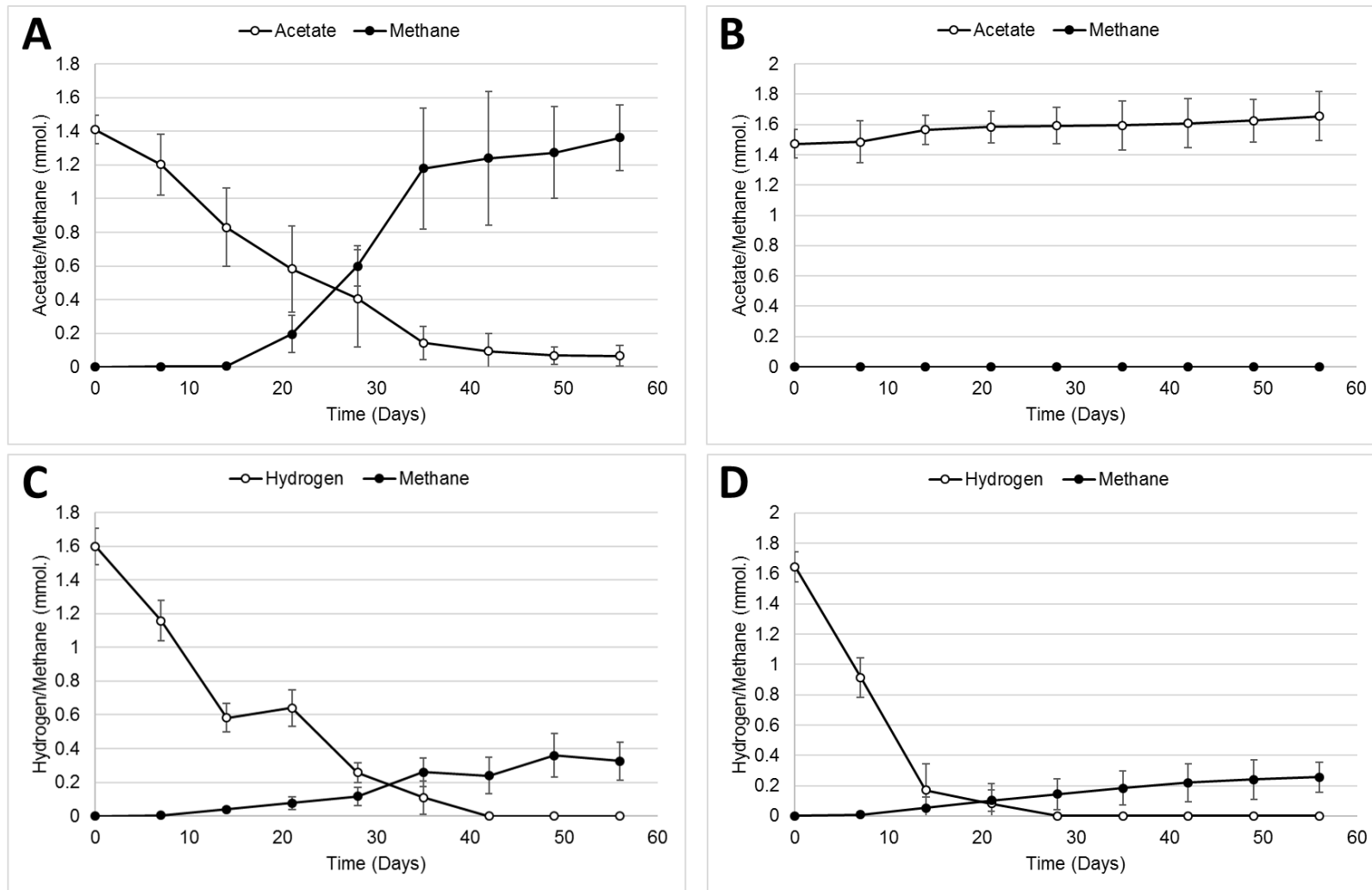


**Figure 6.27. Chemistry within acetate-fed and H<sub>2</sub>/CO<sub>2</sub>-fed microcosms employing the Steel sediments at pH 7.0 and 10.0. [A] Acetate-fed microcosms at pH 7.0, [B] acetate-fed microcosms at pH 10.0, [C] H<sub>2</sub>/CO<sub>2</sub>-fed microcosms at pH 7.0, [D] H<sub>2</sub>/CO<sub>2</sub>-fed microcosms at pH 10.0.**

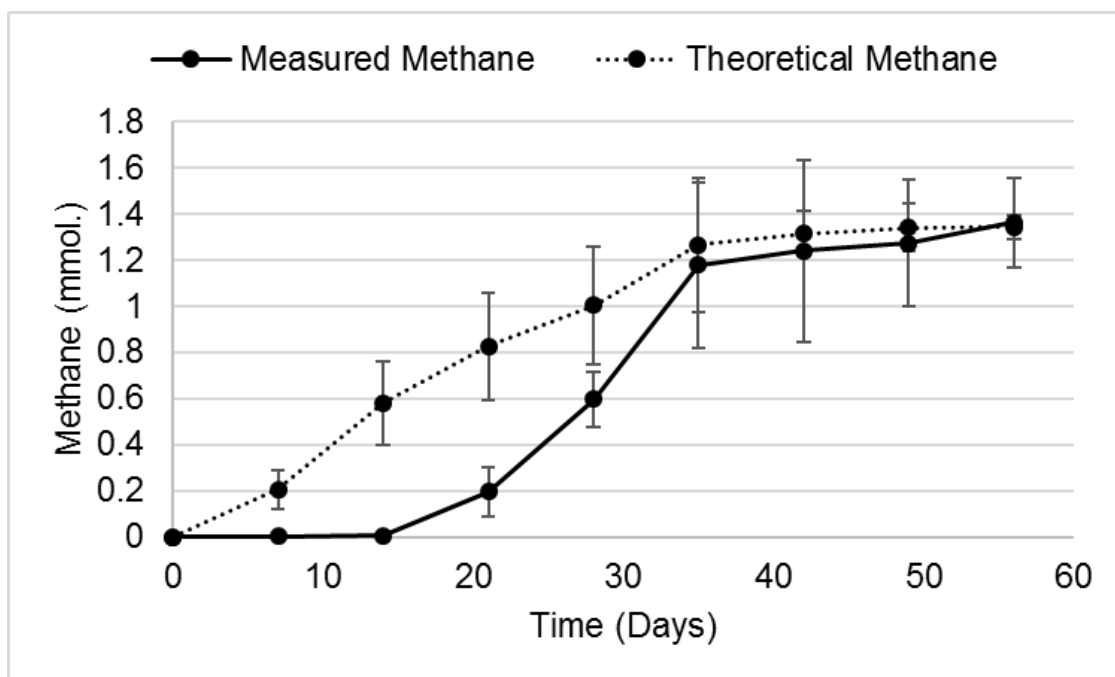


**Figure 6.28. Measured and theoretical methane production within pH 7.0 acetate-fed microcosms employing the Steel sediments.** Error bars represent standard deviation (n=10).

The methanogen community was analysed within pH 7.0 acetate-fed and pH 10.0 H<sub>2</sub>/CO<sub>2</sub>-fed microcosms. The pH 7.0 acetate-fed microcosms were dominated by the acetate-utilising genus *Methanosarcina* across all microcosms, indicating the potential for acetate-dependent methanogenesis to be available in these systems. This adds confidence to the stoichiometric calculations discussed previously (Figure 6.28) which suggested acetoclastic methanogenesis was proceeding under these conditions. In contrast, the pH 10.0 H<sub>2</sub>/CO<sub>2</sub>-fed microcosms were dominated by members of the strictly hydrogenotrophic genus *Methanobacterium*, with the genus *Methanosarcina* only present in low abundance within 2 of the 10 microcosms. Since the genus *Methanosarcina* dominated all of the neutral-pH microcosms, but were unable to generate methane from acetate at pH 10.0 or maintain a population within the H<sub>2</sub>/CO<sub>2</sub>-fed microcosms, this suggests the acetoclastic population in the Steel sediments are neutralophilic. This is in agreement with the Control site microcosms (Section 6.2.1 and 6.3.1) where *Methanosarcina* dominated under neutral-pH conditions when acetate was supplied, but were replaced by *Methanobacterium* genera under alkaline conditions in the presence of both acetate and H<sub>2</sub>/CO<sub>2</sub>. The enrichment cultures developed from the Steel sites had similar methanogenic communities and methane production potentials as the Control site microcosms, which is likely to be due to the similar methanogen communities present in the sediments from these sites (Chapter 5). Both Steel and Control sites harboured methanogens capable of acetoclastic

methanogenesis prior to being cultured in the laboratory. The seasonal pH variation demonstrated by the Steel sites could be resulting in an increased acetoclastic population within these environments (see Chapter 5), which is resulting in their ability to be cultured in the laboratory under neutral-pH conditions.

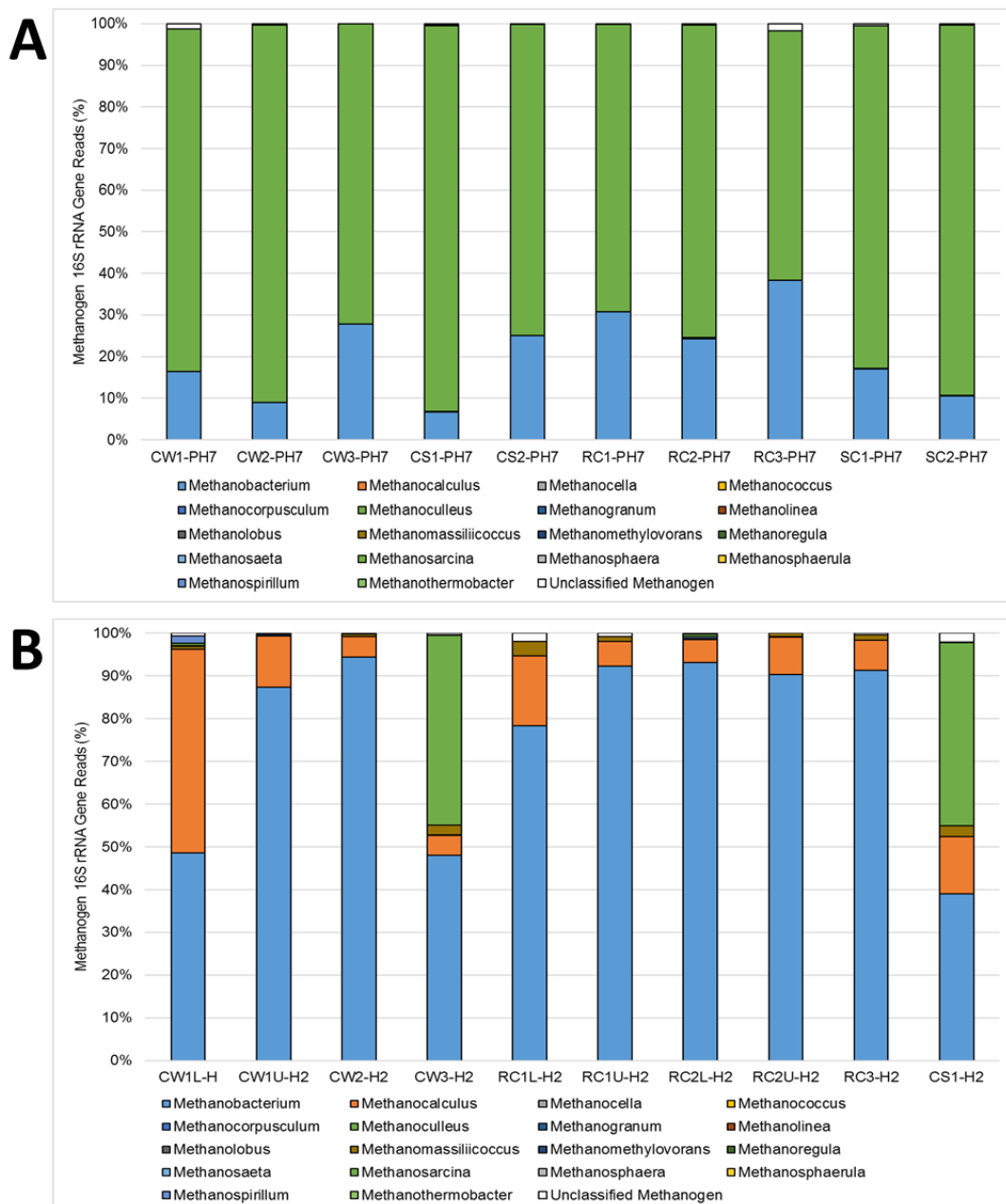


**Figure 6.29. Genus-level composition of methanogen enrichment cultures at pH 7.0 and 10.0.** [A] pH 7.0 genus-level methanogen community, [B] pH 10.0 genus-level methanogen community. At pH 7.0 the acetoclastic *Methanosarcina* dominated, at pH 10.0 the hydrogenotrophic *Methanobacterium* dominated.

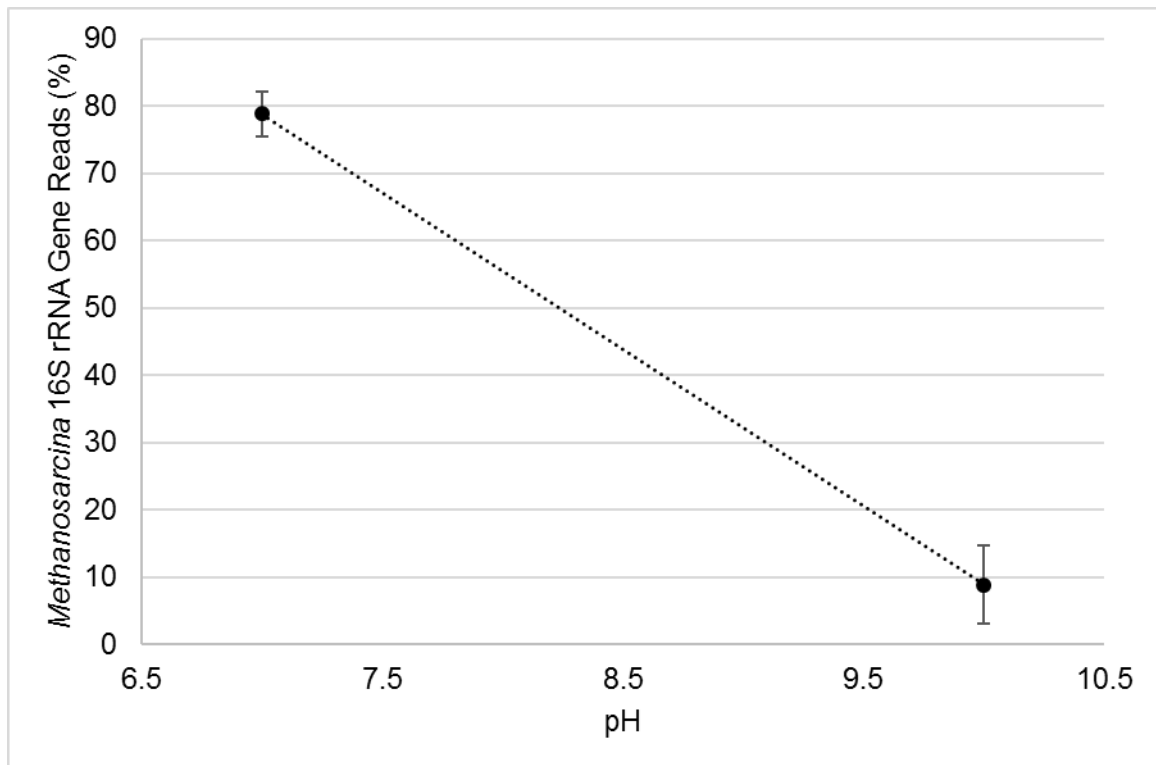


**Figure 6.30. Average percentage of 16S rRNA gene reads attributed to the acetoclastic genus *Methanosarcina* within pH 7.0 and 10.0 methanogenic microcosms employing the Steel sediments. The percentage of reads for *Methanosarcina* increased significantly at pH 7.0 compared with pH 10.0 microcosms.**

## 6.6 Conclusions

The development of methanogen enrichment cultures from neutral-pH and alkaline sediments was undertaken in this study and the utilisation of methanogenic pathways was analysed over a range of pH values. Within the CDP-fed microcosms employing the neutral-pH sediments ISA degradation led to the generation of fermentative conditions which allowed for downstream methanogenesis to take place between pH 7.0-10.0. Highest quantities of methane were generated within pH 7.0 and 8.0 microcosms, where both acetoclastic and hydrogenotrophic methanogens of the genera *Methanosarcina* and *Methanobacterium* were detected. High acetate consumption rates were observed within pH 7.0 and 8.0 microcosms, however the rate of acetate consumption reduced significantly at pH 9.0 and became undetectable at pH 10.0. The acetoclastic population (*Methanosarcina*) was lost as the pH within microcosms was gradually increased which correlated well with the rate of acetate consumption. Although acetate-derived methane was largely absent at pH 10.0, hydrogen-driven methanogenesis was still able to proceed under these conditions. High methane production at pH 7.0 and 8.0 is therefore a result of two methanogenic pathways being active, in contrast only hydrogenotrophic metabolism was present above pH 9.0. Inhibition of the acetoclastic pathway using methyl fluoride confirmed the lack of acetate-derived methane at pH 10.0.

Microcosms employing the alkaline sediments from the lime-contaminated sites (B, H and T) appeared to have a strong preference for hydrogenotrophic metabolism at all pH values. The degradation of ISA within CDP-fed microcosms allowed methanogenesis to proceed between pH 7.0-11.0, one pH unit higher than microcosms employing the neutral-pH sediments. These microcosms were dominated by hydrogenotrophic methanogens of the genera *Methanoculleus* and *Methanobacterium*, however a small proportion of potentially acetoclastic *Methanosarcina* were also present as the minority of the population regardless of pH. Hydrogen consumption and methane production was optimal at pH 9.0 suggesting the methanogenic populations from these sites are alkaliphilic. Methane was generated in pH 7.0 and 8.0 microcosms fed solely with acetate, however stoichiometric calculations and the use of methyl fluoride suggests acetate was being converted to H<sub>2</sub>/CO<sub>2</sub> via syntrophic acetate oxidation, rather than being converted to methane. Further microcosms developed from the Old Lime and Steel sediments demonstrated similar methane production potentials at pH 7.0 and 10.0, where the acetoclastic population (*Methanosarcina*) became more dominant under neutral-pH conditions but was

replaced by a strictly hydrogenotrophic community (*Methanobacterium* and *Methanoculleus*) under alkaline conditions.

The lack of acetoclastic methanogenesis in alkaline (pH >9.0) microcosms could be a result of the high pH conditions of the sites which selected against acetate-consuming methanogens as seen within the microcosms employing the Control sediments. The dissociation of acetic acid under alkaline conditions could be hampering the ability of acetoclastic methanogens to actively transport this substrate into the cell. Additionally, the *Methanosarcinales* are the only order of methanogen to contain cytochromes, which synthesise ATP by simultaneously generating Na<sup>+</sup> and H<sup>+</sup> gradients across the membrane. Since H<sup>+</sup> ions will be extremely limited under alkaline conditions, this could be impeding the ability of cytochrome-containing methanogens to survive and grow at high pH. In contrast, hydrogenotrophic species lack cytochromes and only translocate Na<sup>+</sup> ions for the generation of electrochemical gradients and ATP synthesis, which could give them an advantage when surviving under alkaline conditions.

Overall the data shown here suggests that pH is an important environmental factor affecting biological methane generation. The relative contribution of methanogenic substrates to methane generation within an ILW-GDF is an important consideration for the assessment of the repositories long term safety and performance. The potential for methanogens to be active at alkaline pH values has important implications for the generation of gases within an ILW-GDF. Numerous alkali-tolerant sediment consortiums have been obtained and characterised within this study, all of which have the potential to generate methane from hydrogen and carbon dioxide at high pH. These locally sourced microbial communities showed no ability to generate methane from acetate at pH values expected within the near-field of an ILW-GDF, although acetoclastic methanogenesis was observed under more neutral-pH conditions. The data shown here suggests that the acetoclastic pathway will be unavailable under conditions relevant to the disposal of ILW which in turn reduces the potential for gas generation within a GDF.

# **7.0 Calcium Carbonate as a Potential Substrate for Hydrogenotrophic Methanogenesis at High pH**

## 7.1 Rationale

Methanogens surviving within the near-field of a cementitious repository for ILW may not have access to CO<sub>2</sub> due to alkaline carbonation reactions (6), although significant quantities of highly insoluble calcium carbonates (calcite and aragonite) are likely to be present due to the precipitation of CO<sub>2</sub> at high pH (6). Hydrogen is expected to be generated during the evolution of an ILW-GDF through corrosion processes (6) and potentially via fermentation of the cellulosic materials as described previously (23, 24, 304). To the authors knowledge, the use of highly insoluble carbonates by methanogens has only been studied once previously (236), where pure cultures demonstrated the ability to generate methane via the hydrogenotrophic pathway from both calcium and magnesium carbonate. The work carried out by Kral et al., (2014) concluded that methanogenesis was able to proceed from these highly insoluble carbonates due to the generation of small amounts of carbon dioxide. The CO<sub>2</sub> generated via the reversible reaction of carbonates in solution was enough to drive low rates of methane generation, however these studies were confined to neutral pH values (6.9-8.4), where CO<sub>2</sub> availability will be higher than under alkaline conditions.

The data outlined in this chapter seeks to determine whether the methanogenic populations developed from the alkaline sites in Chapter 6 were able to utilise two types of calcium carbonate (CaCO<sub>3</sub> powder and marble) for hydrogenotrophic methanogenesis at pH 10.0 in the absence of externally supplied CO<sub>2</sub>. Under these conditions CO<sub>2</sub> availability is likely to be extremely limited. Furthermore, the cement-based grout NRVB, which is a potential backfilling material within an ILW-GDF (6), was used to provide an inorganic carbon source for the methanogens after sorption of CO<sub>2</sub> onto its surface. The consumption of hydrogen and generation of methane in microcosms supplied with different forms of calcium carbonate was analysed via gas chromatography. Amplicon sequencing via the Illumina MiSeq platform was used to describe the methanogenic populations. A wide-range of imaging supplemented the study, including SEM, CLSM and FISH which was employed to visualise the methanogen communities growing in association with the carbonate minerals as well as analysing the formation of calcium carbonate on the NRVB surfaces. Geochemical modelling via PHREEQC was performed to determine the availability of CO<sub>2</sub> under the conditions of these experiments. Surface area tests were undertaken to determine the impact this property may have on calcium carbonate solubility and methane generation rates. DIC measurements were taken to observe the movement of inorganic carbon between the solid and liquid phase of cultures.

## 7.2 Reactor Chemistry

### 7.2.1 Headspace Gas Analysis

Microcosms containing a sterile, chemically-reducing mineral media were supplemented with either calcium carbonate powder, marble chips or pre-carbonated NRVB and inoculated under a headspace of either H<sub>2</sub>/N<sub>2</sub> (10:90) (test reactors), H<sub>2</sub>/CO<sub>2</sub>/N<sub>2</sub> (10:10:80) (positive control) or N<sub>2</sub> only (negative control). In order to ensure methanogenesis was not proceeding from fermentation pathways, further negative control microcosms were inoculated under a 100% nitrogen headspace without the addition of supplementary carbon. Abiotic control microcosms containing H<sub>2</sub>/N<sub>2</sub> (10:90) headspace were also run alongside the test experiments to assess hydrogen leakage during headspace gas sampling. The methanogenic reactors described previously (Chapter 6) developed from the New Lime (B, H, T), Old Lime (LK1-5) and Steel sites (CW, CS, RC, SC), which were operating at pH 10.0 and fed with H<sub>2</sub>/CO<sub>2</sub>, were used as inoculum for this study.

Within the test reactors lacking external CO<sub>2</sub>, headspace hydrogen quantities immediately after inoculation were 3.45 mmol. (±0.21), 3.31 mmol. (±0.24) and 3.36 mmol. (±0.046) for microcosms containing calcium carbonate powder, marble chips and pre-carbonated NRVB respectively (Figure 7.1). Over the 42 day incubation period, headspace hydrogen quantities decreased within all test reactors amended with calcite under a H<sub>2</sub>/N<sub>2</sub> headspace compared with abiotic controls (Figure 7.1), indicating hydrogen was being consumed through microbial action. Hydrogen consumption rates were 67.2 (±3.93), 49.9 (±4.78) and 74.4 (±1.56) μmoles day<sup>-1</sup> within microcosms supplemented with CaCO<sub>3</sub> powder, marble chips and pre-carbonated NRVB respectively (Figure 7.2). This indicates reactors supplemented with marble chips demonstrated the lowest rates of hydrogenotrophic metabolism and those containing NRVB had the highest rates. Not all hydrogen was consumed over the 42 day incubation period. Positive control reactors that were supplied with both H<sub>2</sub> and CO<sub>2</sub> in the headspace showed higher rates of hydrogen consumption (244.2 μmoles day<sup>-1</sup> ±7.1) compared with all test reactors where CO<sub>2</sub> was omitted (Figure 7.1), suggesting the addition of CO<sub>2</sub> was enhancing hydrogen consumption rates.

Methane was generated within all test reactors containing CaCO<sub>3</sub> powder, marble chips and pre-carbonated NRVB under a H<sub>2</sub>/N<sub>2</sub> headspace, and in positive controls where CO<sub>2</sub> was supplied in the headspace (Figure 7.1). In contrast, negative controls with 100% nitrogen

headspace were incapable of methane generation, suggesting hydrogen was necessary for methanogenesis to take place and fermentation pathways were absent. Within the test reactors methane quantities reached highest average values on day 42 of 0.36 ( $\pm 0.11$ ), 0.28 ( $\pm 0.16$ ) and 0.69 ( $\pm 0.064$ ) mmoles in microcosms supplemented with CaCO<sub>3</sub> powder, marble chips and pre-carbonated NRVB respectively, with these differences likely to be a result of the varied hydrogen consumption rates (Figure 7.2).

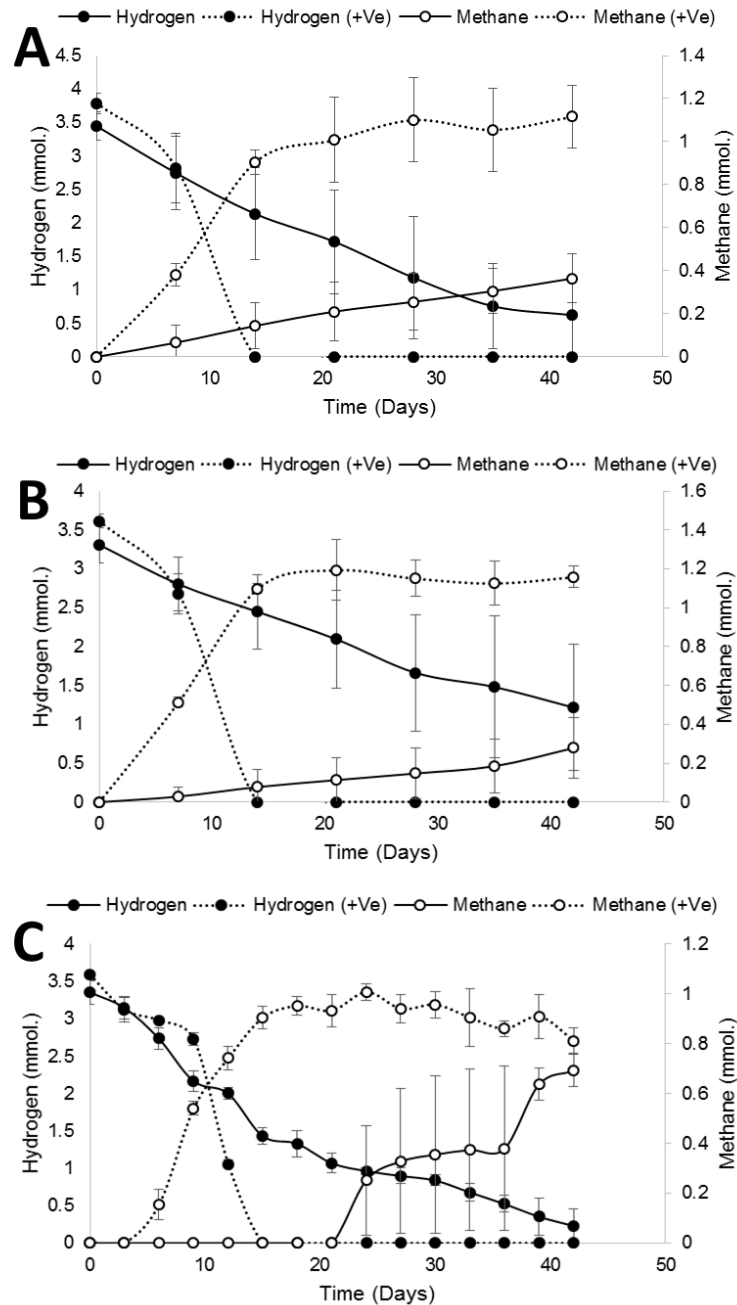


**Figure 7.1. Headspace gas analysis of calcite-supplemented microcosms.** Headspace hydrogen and methane quantities within microcosms supplied with CaCO<sub>3</sub> powder [A], marble chips [B] and pre-carbonated NRVB [C]. Positive controls (+Ve) were supplied with both H<sub>2</sub> and CO<sub>2</sub>. Error bars represent standard deviation (n=24 for [A] and [B], n=3 for [C])

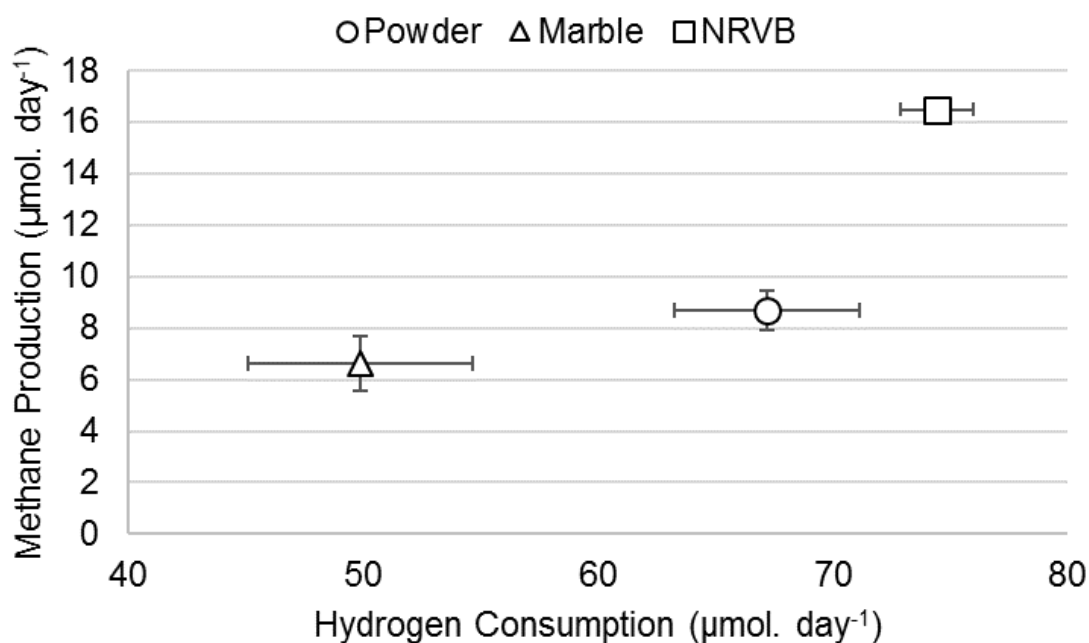
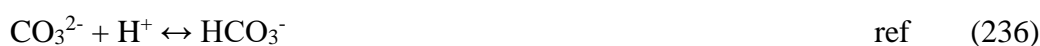


**Figure 7.2. Hydrogen consumption and methane generation rates of microcosms containing calcium carbonates.** Error bars represent standard deviation (Powder n=24, Marble n=24, NRVB n=3).

### 7.2.2 Dissolved Inorganic Carbon Analysis

DIC was analysed within biotic and abiotic microcosms supplemented with CaCO<sub>3</sub> powder, marble chips and pre-carbonated NRVB under a H<sub>2</sub>/N<sub>2</sub> headspace. Upon inoculation no DIC could be detected within inoculated microcosms and abiotic controls (Figure 7.3). Within the abiotic control reactors, DIC concentrations increased throughout the 42 day incubation period and reached highest levels on day 42 of 55.1 (±8.3), 25.2 (±4.2) and 112.5 (±14.2) mg L<sup>-1</sup> within reactors supplemented with CaCO<sub>3</sub> powder, marble chips and pre-carbonated NRVB respectively (Figure 7.3). The steadily increasing concentration of DIC measured within abiotic reactors is assumed to be a result of calcium carbonate dissolution via the following reactions:



DIC also increased initially within the biotic microcosms, however the concentration of inorganic carbon never reached the highest values observed within abiotic reactors, which suggests inorganic carbon was being removed via microbial activity. Within the biotic microcosms supplemented with CaCO<sub>3</sub> powder, highest average DIC values were observed on day 21 of 14.6 ppm ( $\pm 19.2$ ), with the average DIC values decreasing to 4.4 ppm ( $\pm 4.9$ ) by day 42 (Figure 7.3A). Biotic reactors supplemented with marble chips had highest average DIC values of 11.2 ppm ( $\pm 6.5$ ) on day 21, reducing to <2 ppm by day 42 (Figure 7.3B). Average DIC values within biotic microcosms containing NRVB increased to 25.7 ppm ( $\pm 8.2$ ) on day 21, followed by a decrease in concentration to 15.5 ppm ( $\pm 8.5$ ) on day 28 (Figure 7.3C).

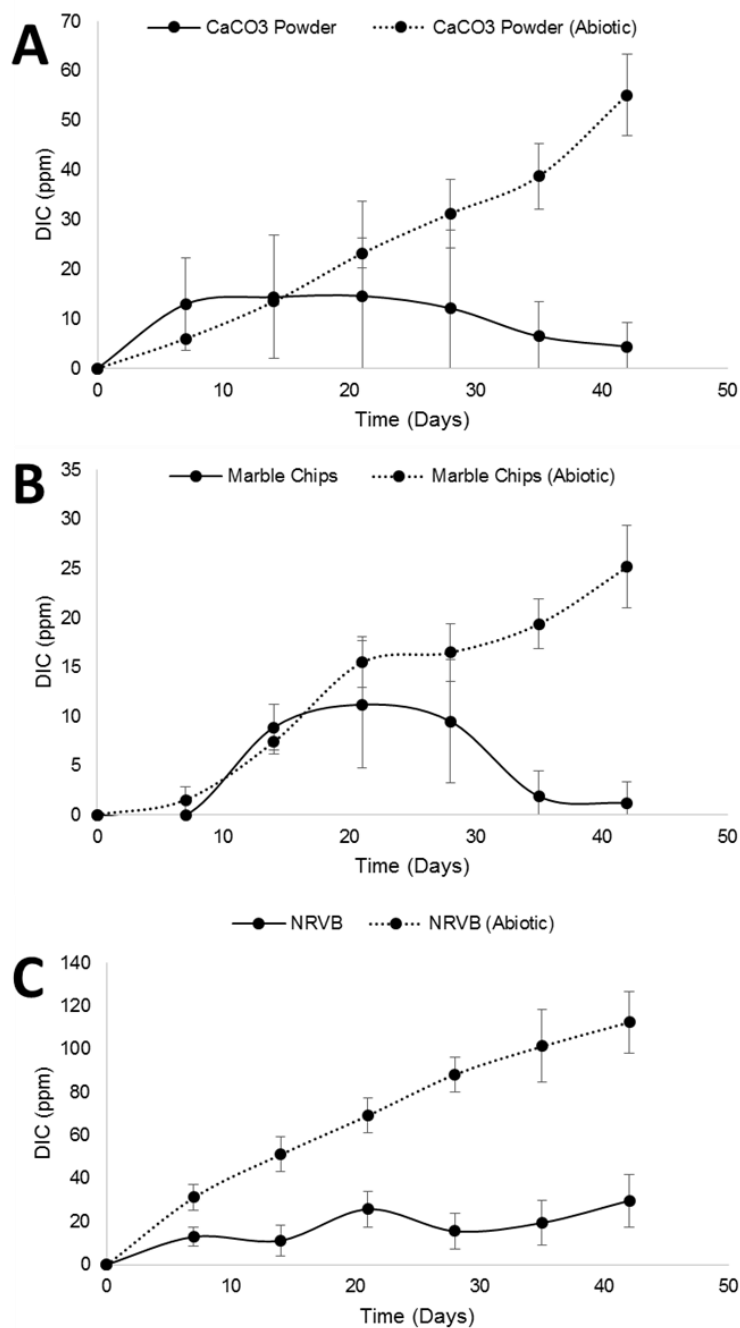


**Figure 7.3. Dissolved inorganic carbon concentrations within pH 10.0 microcosms supplemented with calcium carbonates.** [A] Calcium carbonate powder, [B] marble chips, [C] pre-carbonated NRVB. Also shown is abiotic control reactors under the same conditions.

Error bars represent standard deviation (n=24 for [A] and [B], n=3 for [C]).

### 7.2.3 Surface Area Testing

The surface area of the CaCO<sub>3</sub> powder, marble chips and NRVB used in the microcosm experiments was analysed since this property can impact solubility. NRVB had the highest surface area of 132.6 m<sup>2</sup> g<sup>-1</sup> and the marble chips had the lowest surface area of <3 m<sup>2</sup> g<sup>-1</sup>, with

the CaCO<sub>3</sub> powder fitting in between these two values (3.8 m<sup>2</sup> g<sup>-1</sup>) (Table 7.1). The variation in DIC concentration observed in Section 7.2.2 (Figure 7.3) and hydrogen consumption rates measured in Section 7.2.1 (Figure 7.2) correlates well with the surface area of these minerals, with the highest rates of hydrogen consumption, methane generation and DIC concentration coming from reactors supplemented with NRVB. Lowest hydrogen consumption rates, methane generation and DIC concentrations were observed within reactors supplemented with marble chips, which had the lowest surface area. It is unknown whether the methanogens used in this study are directly using precipitated CaCO<sub>3</sub> as a carbon source for hydrogenotrophic metabolism, or whether these microorganisms are relying on the dissolution of CaCO<sub>3</sub> to HCO<sub>3</sub><sup>-</sup> and CO<sub>2</sub>. However this could be an important area of future research. It is known that autotrophic methanogens are capable of utilising CO<sub>2</sub> and HCO<sub>3</sub><sup>-</sup> as carbon sources (75), however their use of CO<sub>3</sub><sup>2-</sup> and CaCO<sub>3</sub> has not yet been demonstrated. Since the surface area of the mineral impacted the rate of methanogenesis in this study, this provides limited evidence that the methanogens were relying on the generation of bicarbonate and carbon dioxide from the dissolution of calcite in solution. Furthermore, it could be speculated that the bacterial component of the community is altering the chemistry of the calcite surface and thereby releasing soluble inorganic carbon which can be used downstream by autotrophic methanogens. It has been shown previously that alkaliphilic members of the *Betaproteobacteria* are capable of autotrophic growth on calcium carbonate and hydrogen at pH 11.0 under aerobic conditions (235), and there is no reason to believe this process cannot be undertaken by methanogens under the anaerobic conditions employed in this study.

**Table 7.1. Surface area testing.** Shows surface area of marble chips, CaCO<sub>3</sub> powder and pre-carbonated NRVB used during the calcite experiments.

Sample	Mass of sample / g	BET surface area / m <sup>2</sup> g <sup>-1</sup>
Marble Chips	0.3011	< 3
CaCO <sub>3</sub> Powder	0.3017	3.8
NRVB	0.3024	132.6

#### 7.2.4 Volatile Fatty Acid Analysis

Acetate was generated in biotic microcosms supplemented with CaCO<sub>3</sub> powder, marble chips and NRVB under a H<sub>2</sub>/N<sub>2</sub> headspace, with no VFA's detected in abiotic reactors or biotic reactors maintained under 100% nitrogen headspace (Figure 7.4). Highest acetate concentrations were observed on day 42 of 1.65 mM (±0.56), 1.69 mM (±0.81) and 4.65 mM (±1.04) in reactors supplemented with CaCO<sub>3</sub> powder, marble chips and NRVB respectively. Biotic reactors inoculated under a 100% nitrogen headspace showed no evidence of acetogenesis, suggesting acetate generation was dependent on the presence of hydrogen and was independent from fermentation processes. Autotrophic homoacetogenesis is a likely explanation for the generation of acetate, which involves the reduction of CO<sub>2</sub> or HCO<sub>3</sub><sup>-</sup> to acetate using H<sub>2</sub> as electron donor:



It has been suggested previously that hydrogenotrophic methanogens generally outcompete homoacetogens for molecular hydrogen in the absence of TEA's (e.g. sulphate) (332), however in low temperature environments homoacetogens tend to dominate (333, 334). No VFA's other than acetate were detected throughout the incubation period, further suggesting fermentation processes were absent, since other VFA's such as propionic and butyric acids are common fermentation end-products (335). The detection of methane and acetate within the microcosms suggests calcium carbonate and hydrogen are able to support at least two microbial pathways at pH 10.0, namely methanogenesis and homoacetogenesis. Since acetate concentrations continually increased throughout the incubation period (Figure 7.4) and hydrogen was consumed from the headspace (Figure 7.1), methane generation appeared to arise via the hydrogenotrophic pathway in similar fashion to the microcosms described in Chapter 6. However, the generation of acetate could be masking acetate consumption.

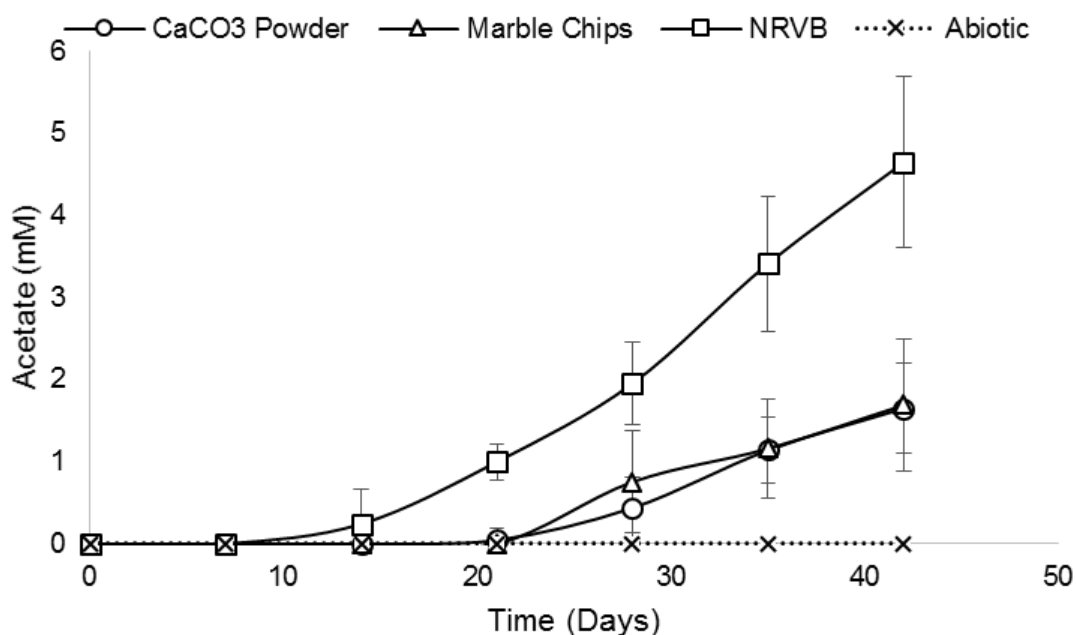


**Figure 7.4. Volatile fatty acid analysis of calcite microcosms.** Acetate concentrations within pH 10.0 microcosms supplemented with CaCO<sub>3</sub> powder, marble chips or pre-carbonated NRVB, alongside abiotic control reactors under the same conditions. Error bars represent standard deviation (Powder n=24, Marble n=24, NRVB n=3).

### 7.2.5 pH

The pH of the microcosms was monitored throughout the 42 day incubation period. Upon inoculation the average pH within microcosms amended with CaCO<sub>3</sub> powder, marble chips and NRVB was 10.04 ( $\pm 0.09$ ), 10.01 ( $\pm 0.05$ ) and 10.02 ( $\pm 0.04$ ) respectively (Figure 7.5). The average pH decreased within the first 7 days to 9.47 ( $\pm 0.2$ ), 9.53 ( $\pm 0.3$ ) and 9.76 ( $\pm 0.08$ ) within reactors supplied with calcium carbonate powder, marble chips and NRVB respectively and was therefore adjusted to pH 10.0 ( $\pm 0.2$ ) with sodium hydroxide. The lowest pH values were detected in reactors amended with marble chips, where the lowest pH of 9.43 ( $\pm 0.32$ ) was observed on day 21. This reduction in pH could be a result of carbonic acid formation via the dissolution of carbonates in solution (see Section 7.2.2), or due to the generation of volatile fatty acids (Figure 7.4).

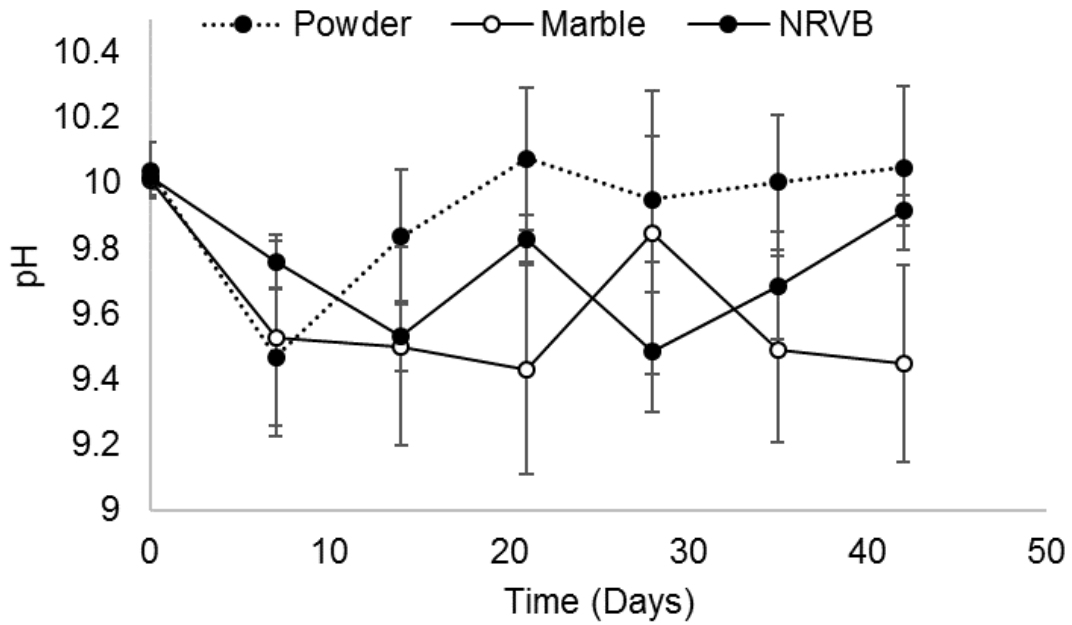


**Figure 7.5. Bulk pH of calcite-supplemented microcosms.** Shows the average pH of microcosms before adjustment to pH 10.0 with 4M NaOH. Error bars represent standard deviation (Powder n=24, Marble n=24, NRVB n=3).

### 7.2.5 PHREEQC Modelling

The availability of inorganic carbon species under the conditions of these experiments between pH 7.0-12.0 was determined via PHREEQC analysis. At pH 10.0 the concentration of  $\text{CO}_2$ ,  $\text{HCO}_3^-$  and  $\text{CO}_3^{2-}$  was calculated to be  $1.1 \times 10^{-3}$  ppm, 4.86 ppm and 3.03 ppm respectively, suggesting  $\text{CO}_2$  concentrations will be relatively low but still available (Figure 7.6, Table 7.2). The dominant carbon species detected in the DIC measurements (Figure 7.3) will therefore be the bicarbonate and carbonate ions under the conditions of these experiments. Since the bulk pH of the microcosms reduced below pH 10.0 at stages of the incubation period (Figure 7.5), this will increase the availability of  $\text{CO}_2$ .

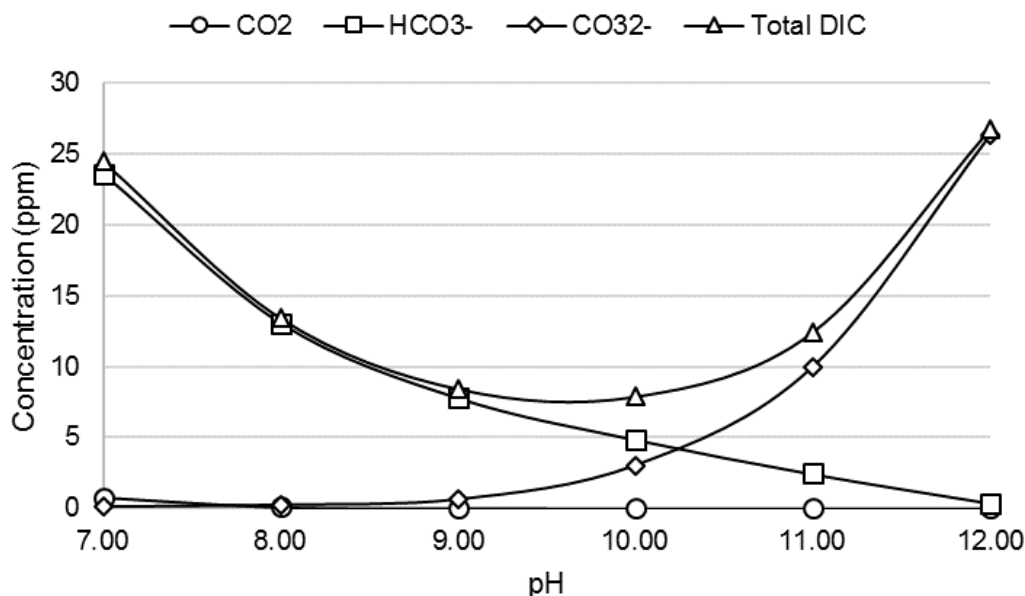


**Figure 7.5. PHREEQC modelling of dissolved inorganic carbon at various pH values.** Showing the concentration of carbon species between pH 7.0-12.0.

**Table 7.2. Dissolved inorganic carbon species at various pH values based on PHREEQC geochemical modelling.** Showing the concentration of carbon species between pH 7.0-12.0.

Initial pH	CO <sub>2</sub> (ppm)	HCO <sub>3</sub> <sup>-</sup> (ppm)	CO <sub>3</sub> <sup>2-</sup> (ppm)	Total DIC (ppm)
7.00	7.9x10 <sup>-1</sup>	23.6	9.9x10 <sup>-2</sup>	24.5
8.00	1.1x10 <sup>-1</sup>	13.1	2.3x10 <sup>-1</sup>	13.4
9.00	1.4x10 <sup>-2</sup>	7.8	6.3x10 <sup>-1</sup>	8.4
10.00	1.1x10 <sup>-3</sup>	4.9	3.03	7.9
11.00	8.2x10 <sup>-5</sup>	2.4	10.01	12.5
12.00	8.1x10 <sup>-7</sup>	3.8x10 <sup>-1</sup>	26.43	26.8

### 7.3 Archaeal Community Analysis

The archaeal community was analysed within all methanogenic microcosms amended with CaCO<sub>3</sub> powder, marble chips and NRVB after DNA extraction and sequencing of the 16S rRNA gene via the Illumina MiSeq platform. The bacterial community could not be analysed due to low DNA yields. All microcosms supplied with CaCO<sub>3</sub> powder were dominated by the genus *Methanobacterium* regardless of which site the microcosm originated from (Figure 7.6A). Pure cultures of this genus have been shown to use hydrogen and carbon dioxide for growth (313, 336, 337) and a number of alkaliphilic strains have been isolated from biogas

plants and alkaline lakes previously (312, 338). Small proportions of reads attributed to the genera *Methanosarcina*, *Methanoculleus* and *Methanomassiliicoccus* were also detected within microcosms originating from the Lime sites (B, H, T, LK1-5) when supplemented with CaCO<sub>3</sub> powder (Figure 7.6A). Although members of the *Methanosarcina* are capable of acetoclastic and methylotrophic methanogenesis (51, 339), they have also been shown to use H<sub>2</sub>/CO<sub>2</sub> for growth (340), making them extremely versatile methanogens. Although acetate was generated and present within microcosms, no acetate consumption was detected, suggesting the *Methanosarcina* here were contributing to hydrogenotrophic methane generation. *Methanoculleus* species are strictly hydrogenotrophic (318, 319, 329) and have been identified in a range of environments, including wetland soil (318), paddy field soil (319) and oil fields (341), however no alkaliphilic species have been identified to date. The genus *Methanocalculus* was only detectable in microcosms originating from the Steel sites (CW, CS, RC, SC) which is an important methanogen within saline environments (342), with a number of alkaliphilic species being isolated from alkaline soda lakes previously (91, 343).

The majority of microcosms supplemented with marble chips had a similar methanogen community compared with reactors amended with CaCO<sub>3</sub> powder, however the percentage of reads attributed to the genera *Methanosarcina*, *Methanoculleus* and *Methanomassiliicoccus* increased within microcosms originating from the Lime sites (Figure 7.6B). Surprisingly a small percentage of reads attributed to the potentially acetoclastic genus *Methanosaeta* were also detected within microcosms supplemented with marble chips originating from site H (11.4%) and site T (1.9%), which could indicate the acetoclastic pathway was also active, even though no acetate consumption was observed and therefore substrate utilisation was minimal. The genus *Methanosaeta* was only detectable in 2 of the 12 reactors containing marble chips and could not be detected in any microcosms containing CaCO<sub>3</sub> powder or NRVB, suggesting acetoclasts were the minority of the overall methanogenic population and hydrogenotrophic methanogens dominated. The significant change in methanogen populations in lime-site reactors containing marble chips compared with those containing CaCO<sub>3</sub> powder could not be accounted for, however the pH of reactors containing marble chips underwent significant changes during the incubation due to the low buffering capacity of the media, which could be promoting the growth of acetoclastic methanogens as seen in the pH adaption study in Chapter 6.

Triplicate microcosms amended with NRVB had a very similar methanogen community (Figure 7.6C), dominated by *Methanosarcina*, *Methanoculleus* and *Methanomassiliicoccus* genera. All these genera have been discussed above.

The differences in archaea community between microcosms amended with CaCO<sub>3</sub> powder, marble chips and NRVB was analysed via PCA (Figure 7.7). Microcosms containing CaCO<sub>3</sub> powder and NRVB clustered very close together, however reactors amended with marble chips had a much wider distribution of methanogens (Figure 7.7). Marble and NRVB are not pure forms of calcite (CaCO<sub>3</sub>) and contain other minerals such as pyrite (FeS<sub>2</sub>) which could be improving the growth rate of *Methanosarcina*, *Methanoculleus* and *Methanomassiliicoccus* species. The activity of *Methanosarcina* and *Methanoculleus* has been shown to be influenced by trace elements previously (344) and iron is a very important metal for enzymatic pathways in methanogenesis (345). Although trace elements were supplied to the growth media, the marble chips and NRVB may be providing *Methanosarcina*, *Methanoculleus* and *Methanomassiliicoccus* species with growth factors that were not included in the media, however further work is required to substantiate this.

Previous studies have shown that high bicarbonate concentrations can negatively impact acetoclastic methanogenesis and reduce numbers of Methanosarcinales (346), which are the only order of methanogens capable of acetate metabolism (52). Since PHREEQC analysis suggests the dominant carbon species present at pH 10.0 are the bicarbonate and carbonate ions (Figure 7.5), this could be leading to an inhibition of acetoclastic methane generation. Microcosms supplied with marble chips demonstrated the lowest DIC concentrations due to the minerals low surface area (Table 7.1), leading to lower amounts of bicarbonate and carbonate ions in solution compared with the CaCO<sub>3</sub> powder and NRVB, which could explain the detection of the genus *Methanosaeta* within these reactors. However it has recently been suggested that *Methanosaeta* are also capable of hydrogenotrophic metabolism via direct interspecies electron transfer (347). This notion agrees with the chemistry within microcosms where no acetate consumption was observed and therefore the detection of *Methanosaeta* genera within the marble chip amended microcosms could still be a result of their ability to generate methane via the hydrogenotrophic pathway.

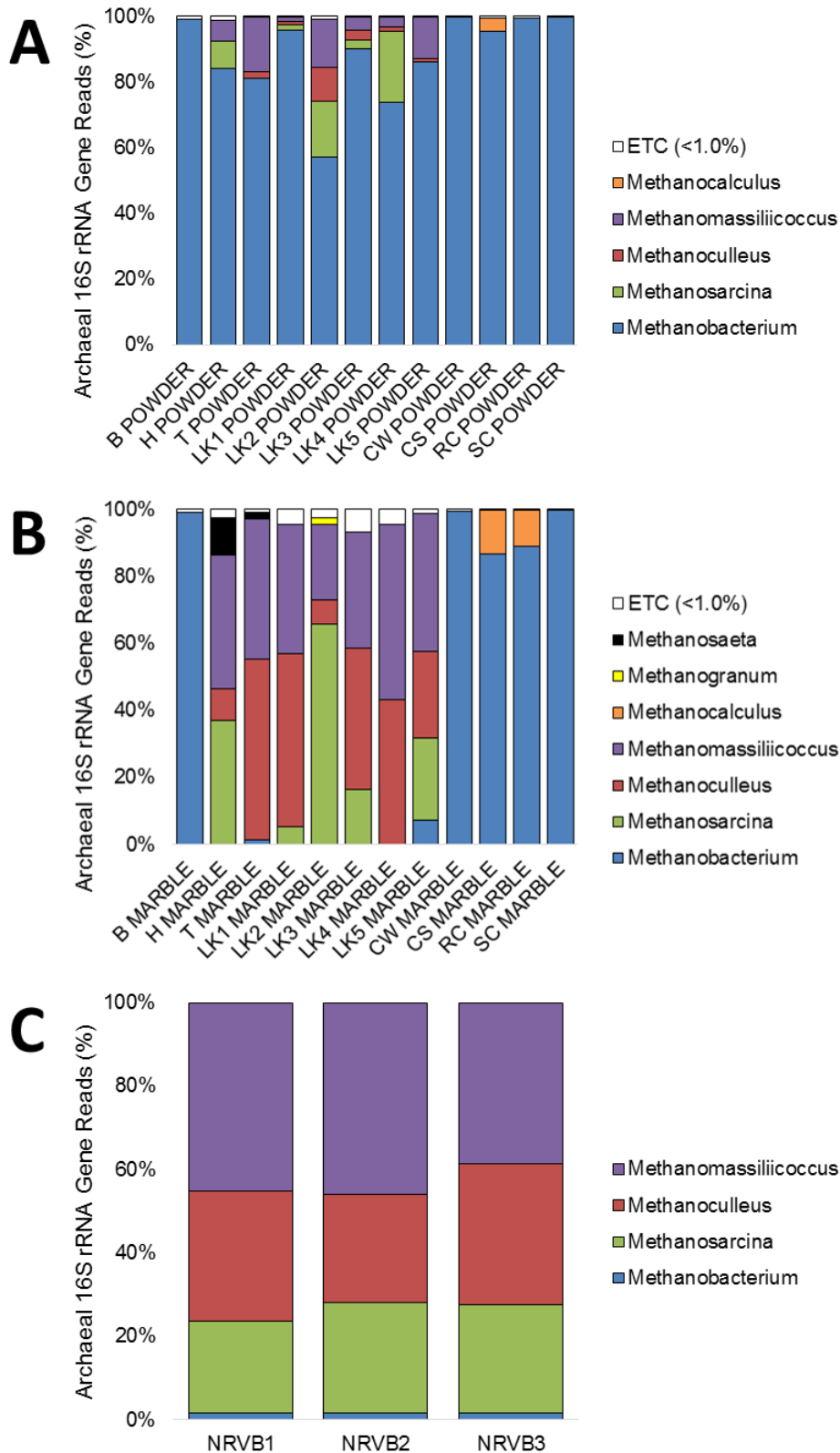


**Figure 7.6. Archaeal community analysis of calcite microcosms.** Genus-level archaeal community within pH 10.0 microcosms supplemented with  $\text{CaCO}_3$  powder [A], marble chips [B] or pre-carbonated NRVB [C].

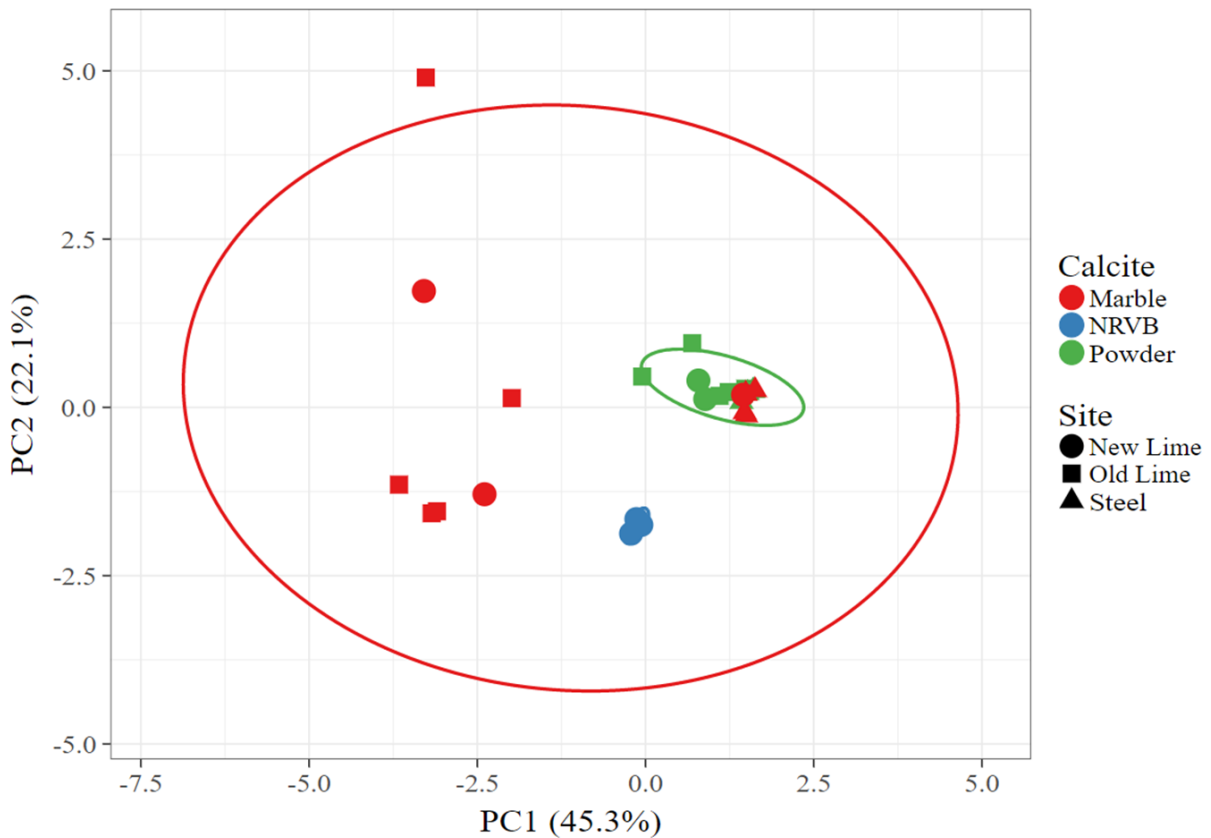


**Figure 7.7. PCA of archaeal communities from calcite-amended microcosms.**

## 7.4 Carbonation Analysis

### 7.4.1 Phenolphthalein Staining

The NRVB incubated under CO<sub>2</sub> used in the microcosm experiments was tested for evidence of carbonation via phenolphthalein staining which indicates high pH (pink) and low pH (white) areas (Figure 7.8). Low pH areas are an indication of carbonation due to the formation of carbonic acid (348). The surface of NRVB maintained under nitrogen was basic (Figure 7.8A) signified by its pink colour after staining. In contrast NRVB incubated under an atmosphere of CO<sub>2</sub> had a lower pH surface indicated by the colourless stain (Figure 7.8B). The inner surfaces of the NRVB remained alkaline however (Figure 7.8CD), suggesting CO<sub>2</sub> was unable to penetrate into the inner surfaces of the NRVB during the incubation.

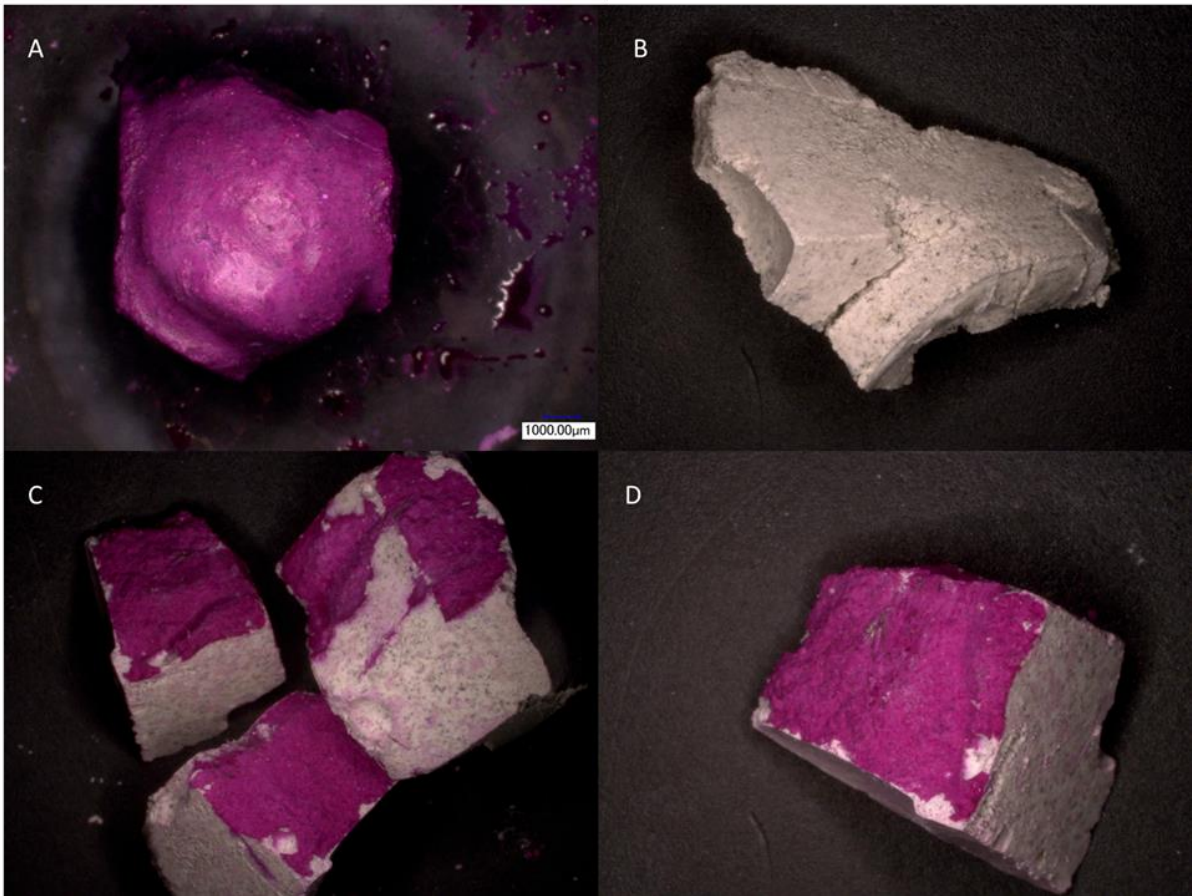


**Figure 7.8. Carbonation analysis of NRVB via phenolphthalein staining.** [A] Outer surface of NRVB incubated under nitrogen, [B] outer surface of NRVB incubated under CO<sub>2</sub>, [C and D] inner surfaces of NRVB incubated under CO<sub>2</sub>.

#### 7.4.2 SEM

The morphology of the inner and outer abiotic NRVB surfaces was analysed via SEM after incubation under CO<sub>2</sub>. Outer surfaces had more sharp needle-like crystalline structures compared with inner surfaces (Figure 7.9). The needle-like structures observed on the outer surfaces had a similar morphology to aragonite (349), with inner surfaces having a similar morphology to calcite (349). EDS of these surfaces suggested calcium, carbon and oxygen were present in high quantities (Figure 6.10), potentially indicating the presence of aragonite or calcite.

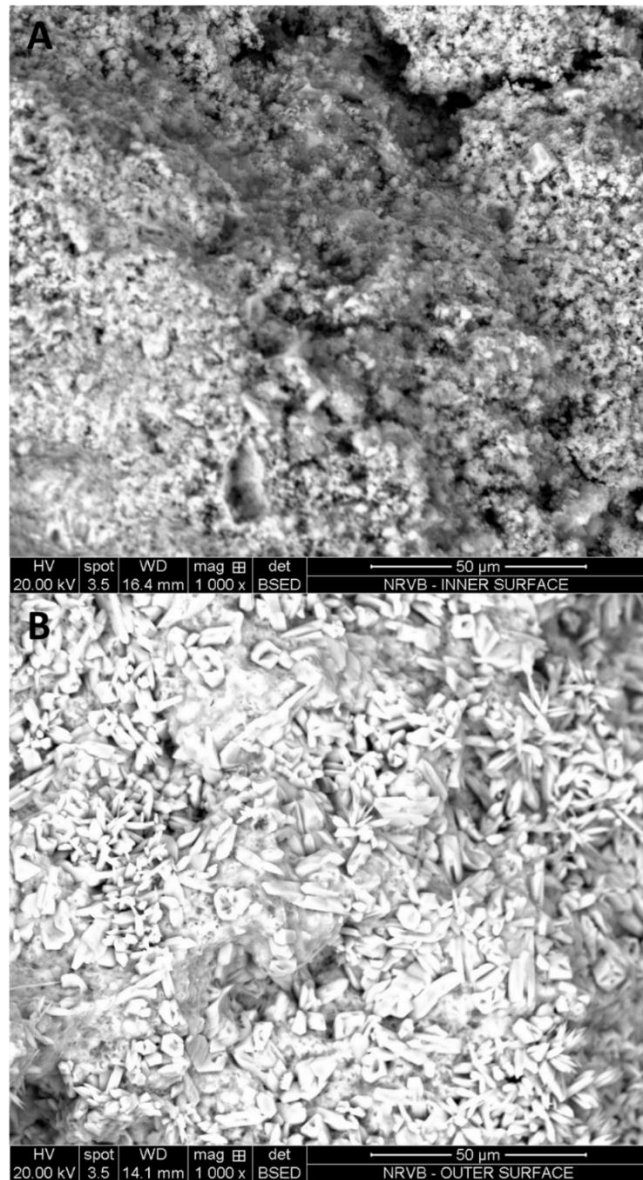


**Figure 7.9. SEM investigation of NRVB.** Scanning electron micrographs of inner [A] and outer [B] surface of pre-carbonated NRVB used during the microcosm experiments.

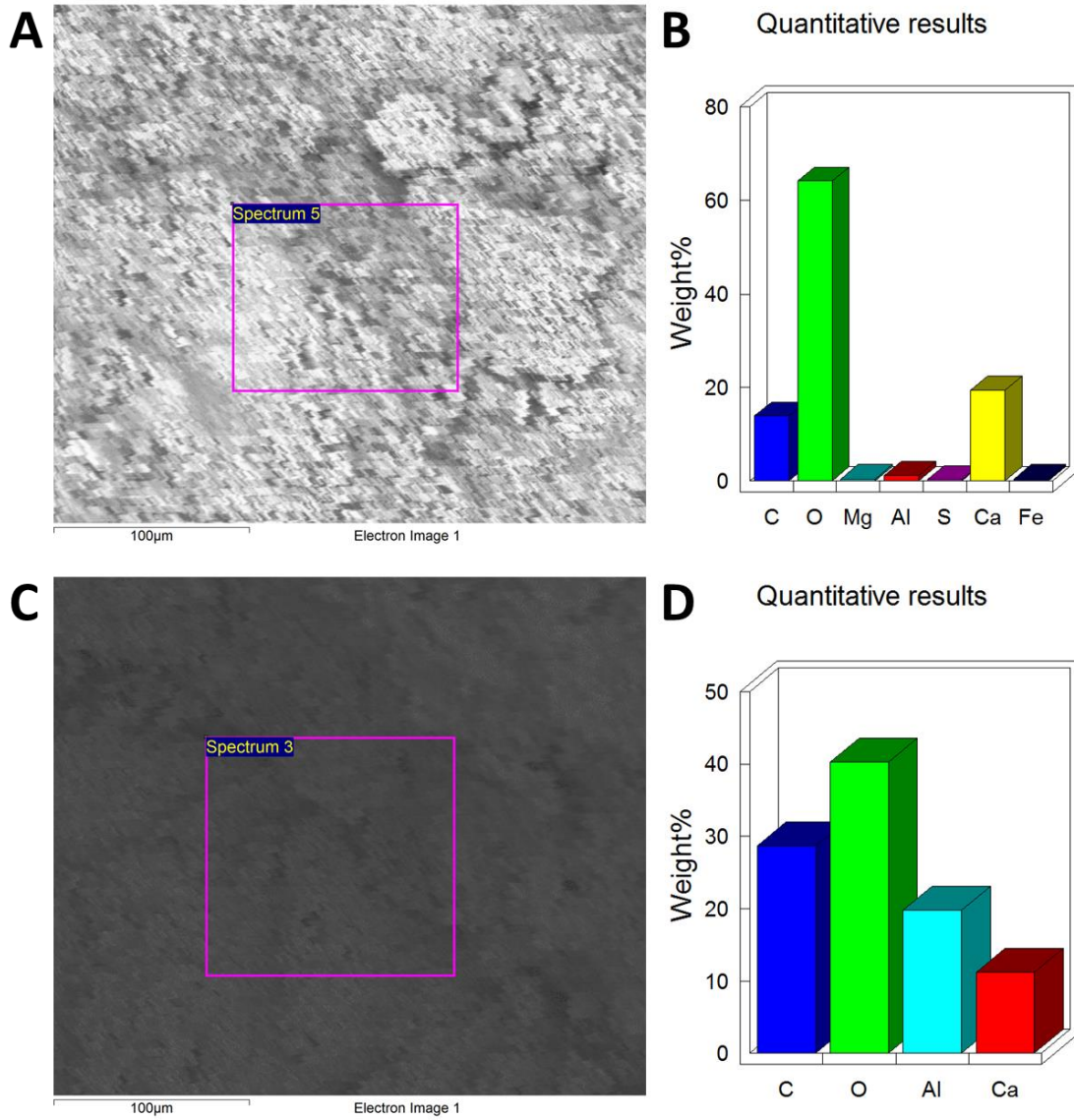


**Figure 7.10. EDS investigation of inner and outer NRVB surfaces.** [A] SEM of inner NRVB surface, [B] EDS of inner NRVB surface, [C] SEM of outer NRVB surface, [D] EDS of outer NRVB surface.

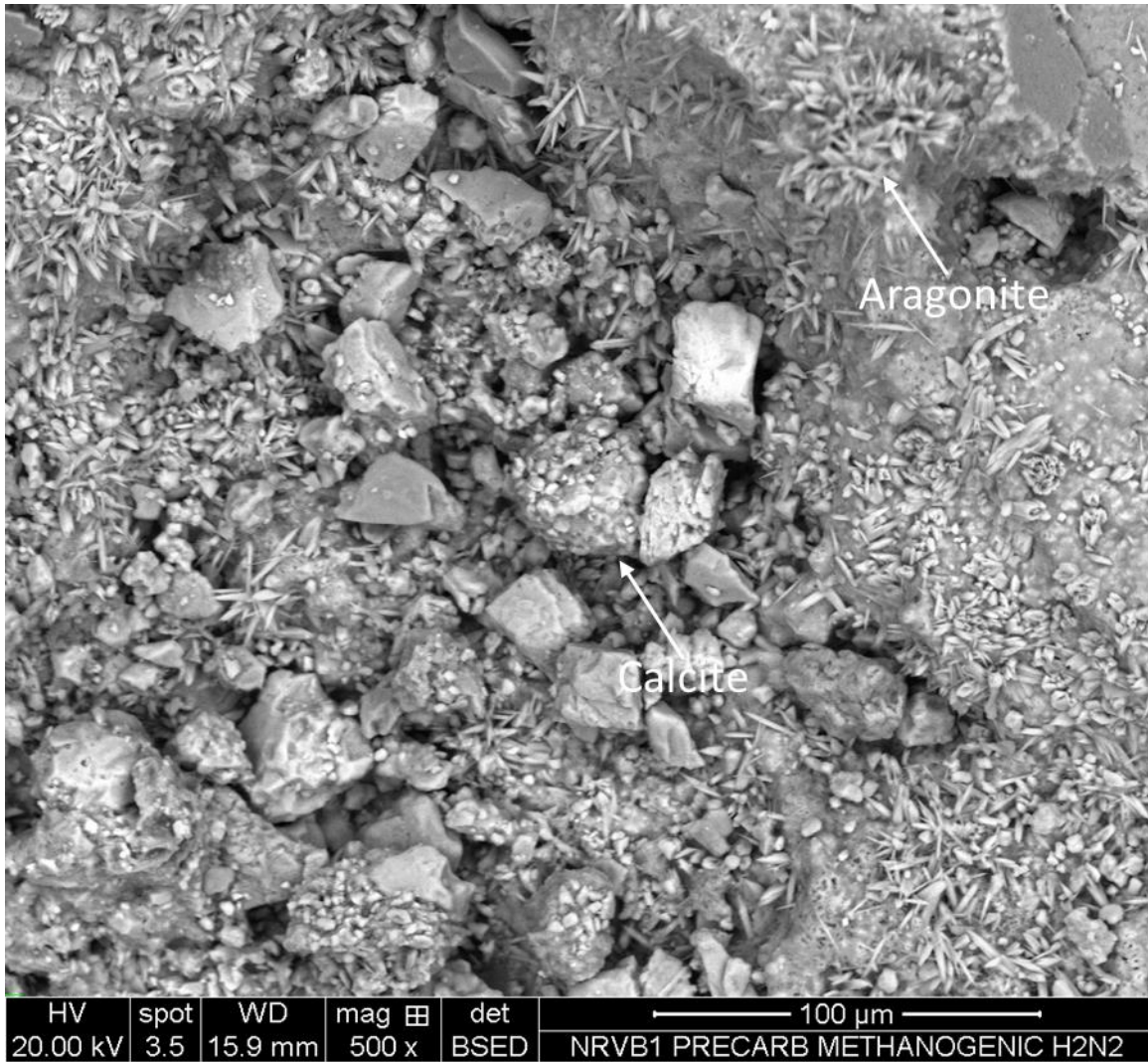


**Figure 7.11. SEM investigation of biotic NRVB after incubation under methanogenic conditions.** Shows potential aragonite and calcite minerals.

### 7.4.3 XRD

XRD patterns of the inner and outer NRVB surfaces were very similar when compared with the  $\text{CaCO}_3$  powder (Figure 6.12), suggesting calcium carbonate was present on both the inner and outer layer of the NRVB. However, the marble chips had a different XRD pattern, presumably due to the presence of other minerals, such as quartz, pyrite and graphite.

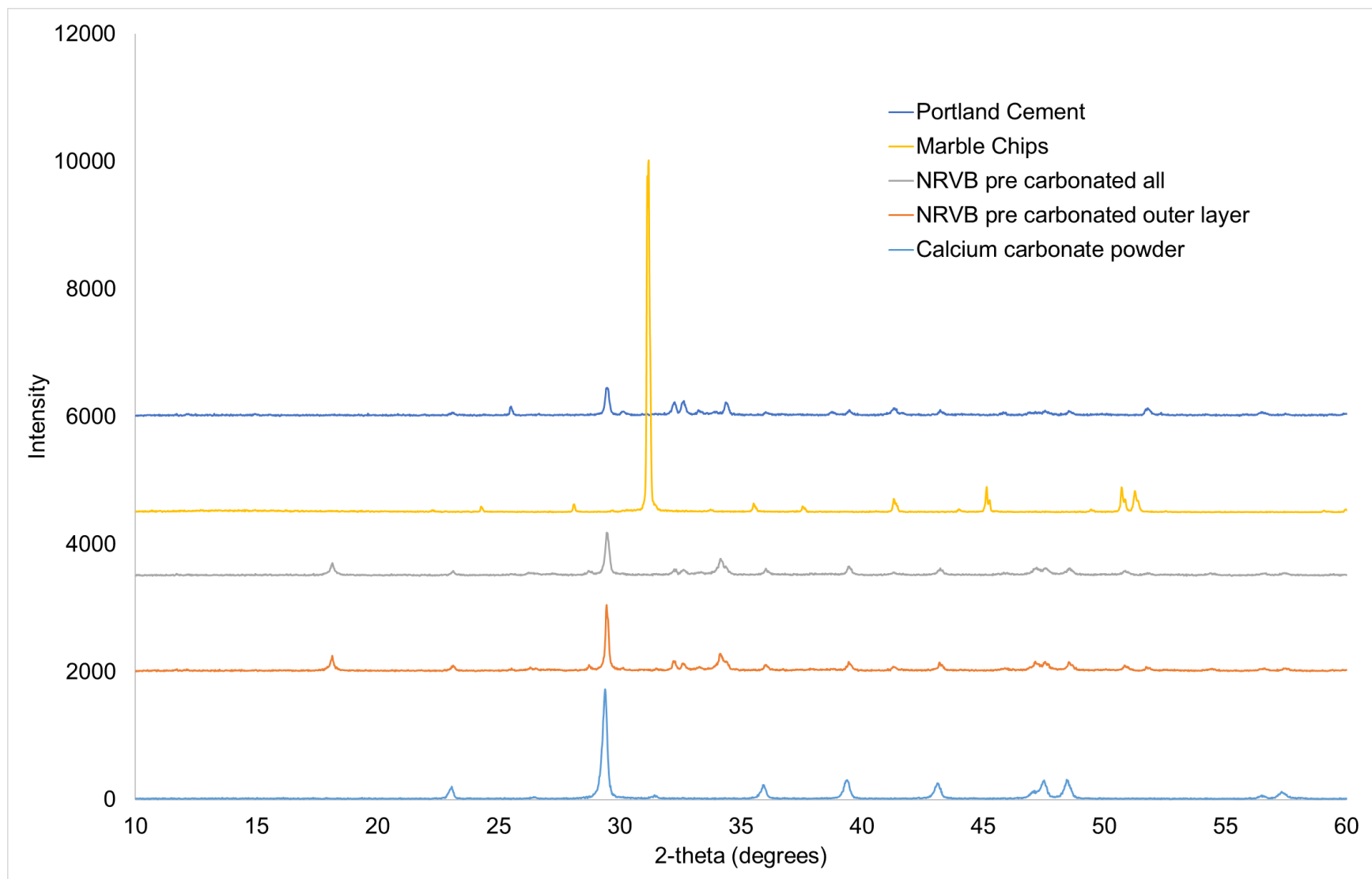


Figure 7.12. XRD patterns of CaCO<sub>3</sub> powder, marble chips and NRVB.

## 7.5 Imaging

### 7.5.1 5-Colour CLSM

Suspected biofilm materials were removed from the NRVB surfaces after incubation in the microcosm experiments and viewed via CLSM to analyse any organic components present. A range of organic polymers were detected within the suspected biofilm materials, including lipids, sugars, proteins, eDNA and cells (Figure 7.13). The homoacetogen *Clostridium ljungdahlii* and the methanogens *Methanobrevibacter smithii*, *Methanosphaera stadtmanae*, *Methanosarcina mazei* have all been shown to be capable of biofilm formation previously (350, 351).

Filamentous eDNA scaffolding was detected within the biofilm materials attached to the NRVB (Figures 7.13BD), which have a similar appearance and width to eDNA produced by *Pseudomonas* species observed previously (352). This eDNA framework is likely to be contributing to the stability and structure of the biofilm as described previously (353, 354). The eDNA component of biofilms has been shown to promote acidification of the local environment (355), which could be resulting in a pH reduction of the outer NRVB surface as described in Section 7.4.1 (Figure 7.8) and a lower bulk pH as described in Section 7.2.5 (Figure 7.5). This could also offer acetoclastic species with a niche site for improved growth as seen in the pH adaption study in Chapter 6. Furthermore, this could also explain the increased detection of *Methanosarcina* genera within the NRVB and marble chip amended reactors (Figure 7.6).

Organic biofilm materials were also detected on the surfaces of the NRVB when directly viewed via CLSM (Figure 7.14). This suggests microorganisms were growing in close association with the NRVB, where carbonate minerals were detected (Section 7.4). It could be speculated that microorganisms aggregating on the surface of the calcite minerals are reducing the pH of the local environment via the generation of a proton gradient, thereby releasing soluble carbonates which convert to bicarbonate (due to the lower pH niche) which become available for autotrophic metabolism, however more work is required to substantiate this claim. The detection of organic polymers and biofilm materials in these microcosms despite the lack of organic carbon present in the growth media suggests autotrophic metabolism alone supported the development of biofilm on the calcite surfaces. The formation of biofilm by

autotrophs could further support downstream processes by bacteria, such as those capable of metabolising proteins (356).

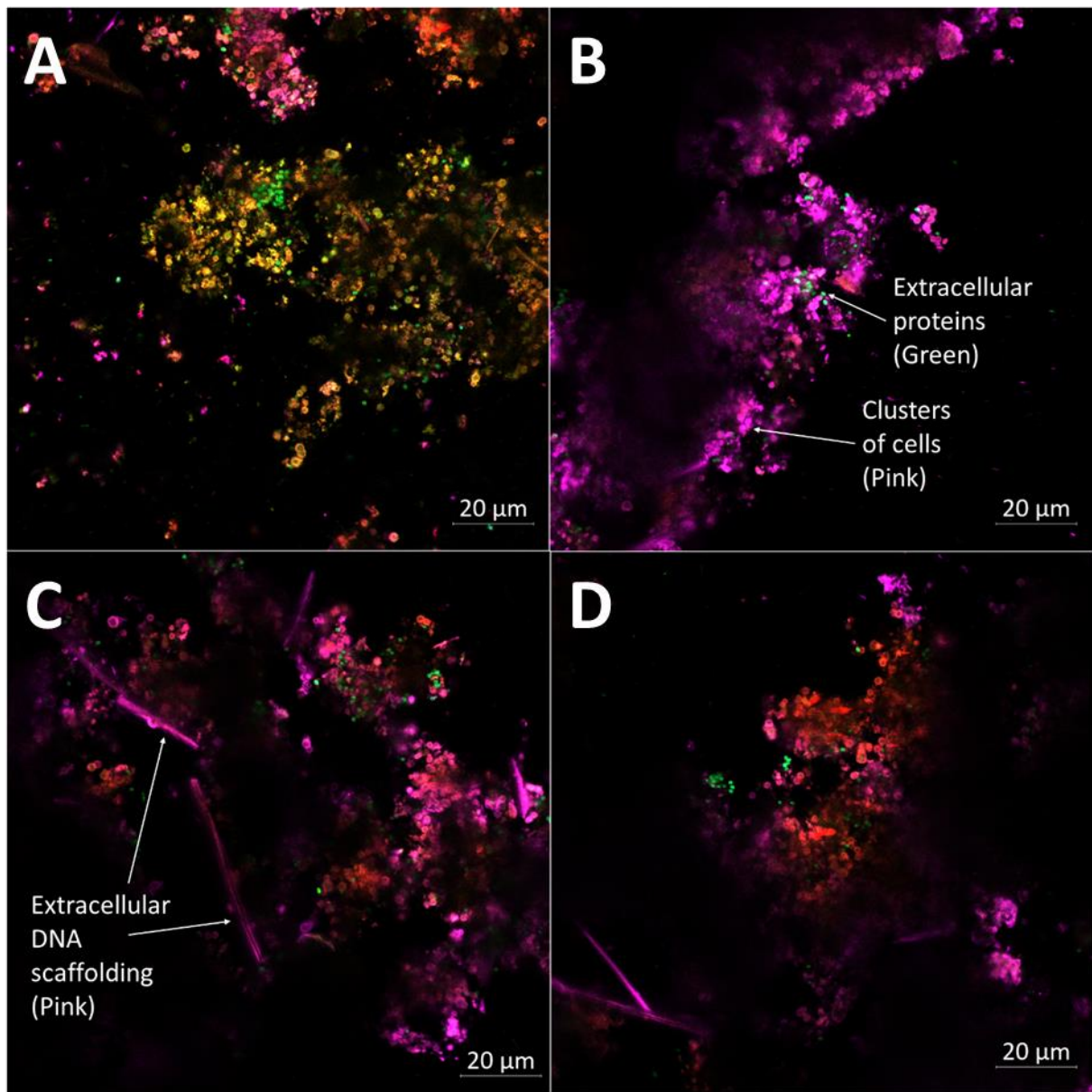


**Figure 7.13. CLSM investigation of biofilm materials taken from NRVB reactors.** 5-colour confocal scanning laser microscopy images of methanogenic biofilm taken from the surface of NRVB. Yellow – lipids, red – sugars, green – protein, pink – eDNA and cells.

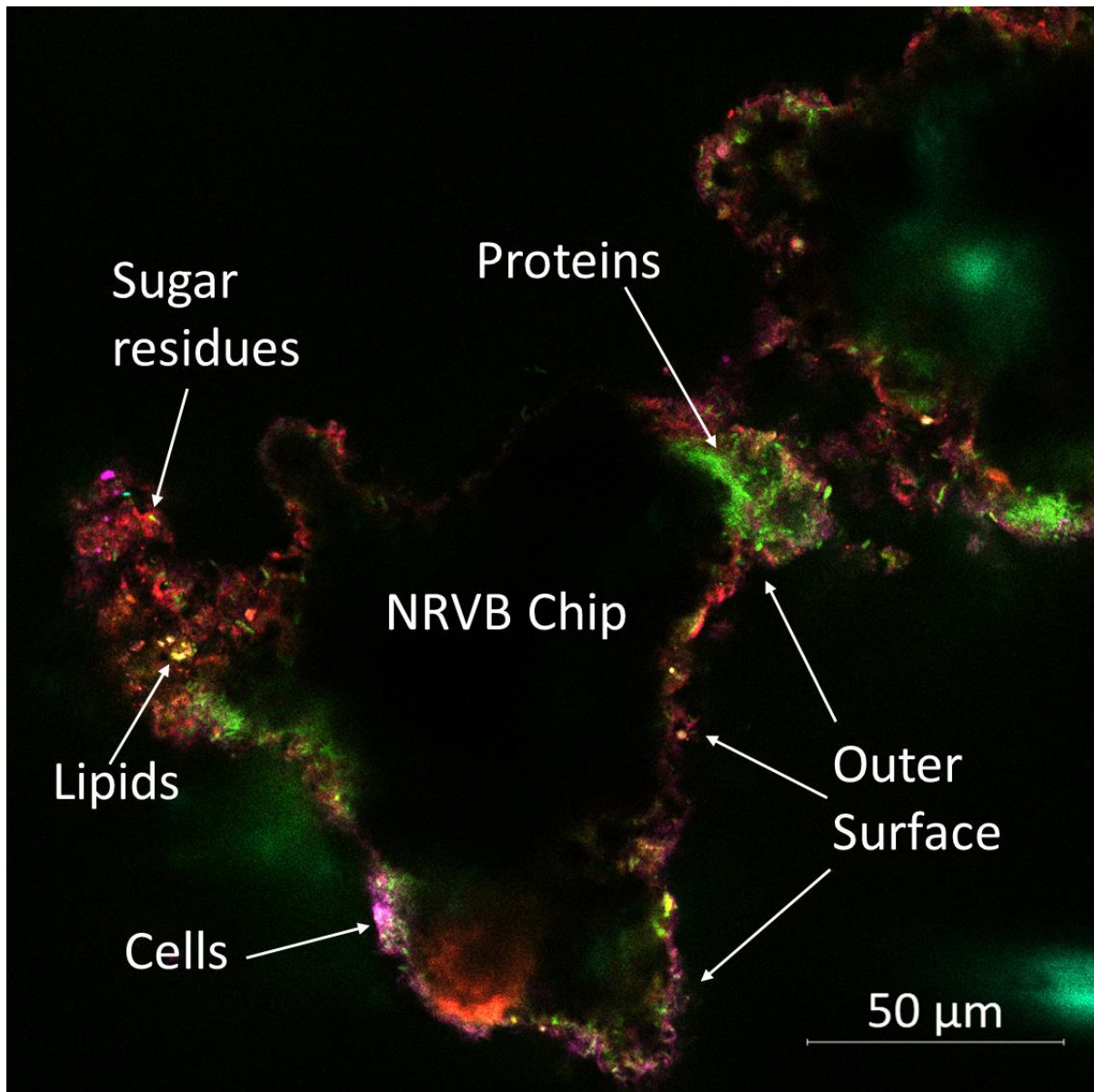


**Figure 7.14. CLSM investigation of biotic NRVB.** 5-colour confocal scanning laser microscopic image of NRVB chip with biofilm formed on the surface. Showing protein (green), lipids and hydrophobic sites (yellow), sugars (red), polysaccharides (blue) together with cells and extracellular DNA (pink).

### 7.5.2 FISH

FISH was carried out in order to visualise the presence of archaea and bacteria within the biofilm materials attached to the NRVB surfaces. Although the probe used was universal to all archaea, only methanogenic archaea could be identified within the microbial community in Section 7.3 (Figure 7.6). FISH confirmed the presence of methanogenic archaea within the aggregates formed on the NRVB surface (Figure 7.15). A significant proportion of Eubacteria were also detected on the NRVB surfaces.

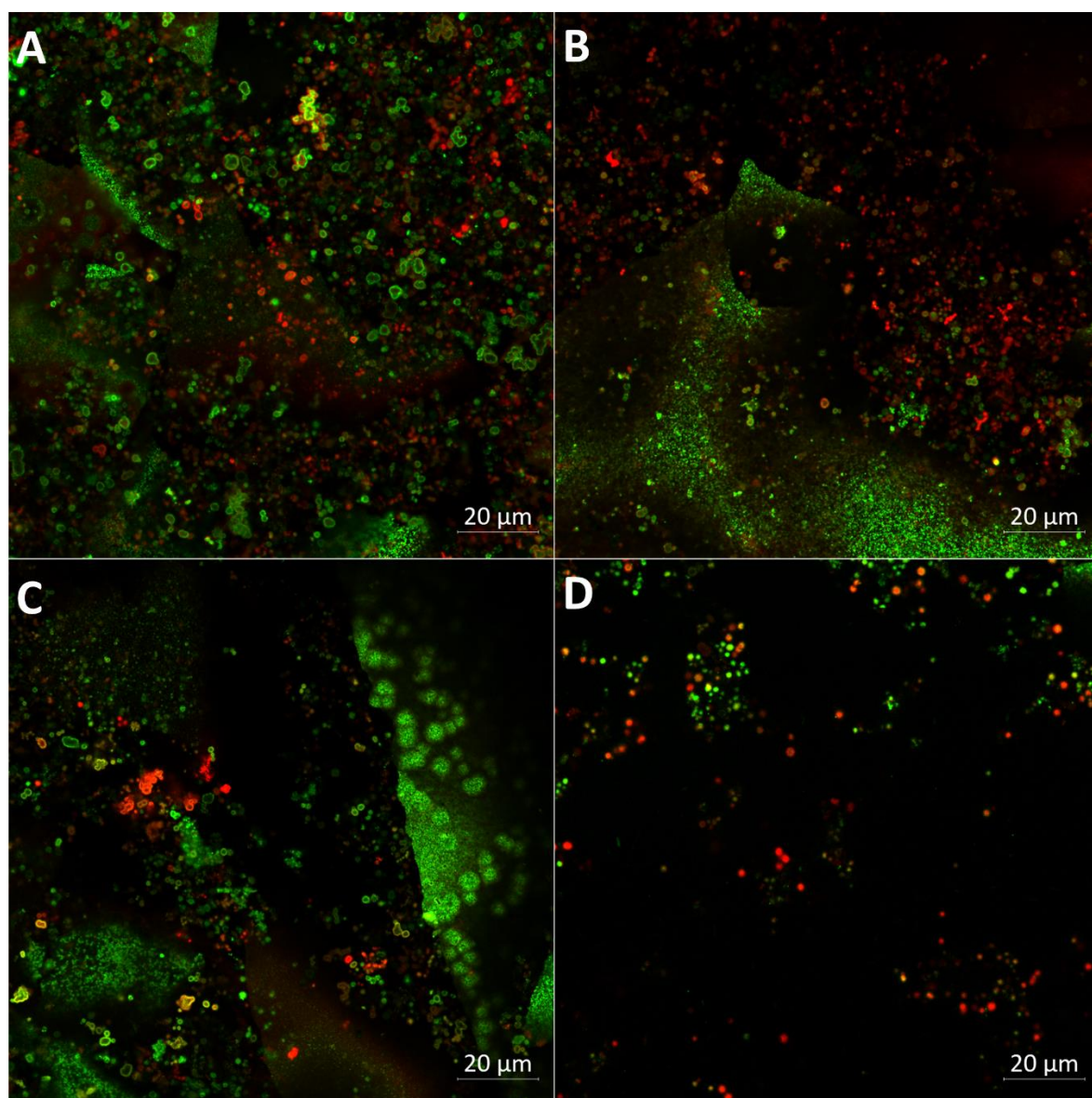


**Figure 7.15. FISH investigation of biotic materials attached to NRVB.** Fluorescence *in situ* hybridisation images of methanogenic biofilm taken from the surface of NRVB. Biofilm materials removed from NRVB surfaces are shown [A-C], alongside biofilm materials diluted in sterile media [D]. Green – Eubacteria, Red – Archaea.

## 7.6 Conclusions

Mixed cultures of methanogens harvested from near-surface alkaline sediments were capable of generating methane using highly insoluble calcium carbonate as a carbon source at pH 10.0. Methane quantities increased within all microcosms supplied with calcium carbonate and hydrogen, in contrast negative controls lacking carbonate and/or hydrogen showed no measurable methanogenesis. The rate of methane generation and hydrogen consumption was influenced by the type of calcium carbonate used, with the surface area of the mineral in question affecting these rates. No CO<sub>2</sub> was detected in the headspace of methanogenic microcosms, however geochemical modelling via PHREEQC suggested that at equilibrium very low amounts of CO<sub>2</sub> would be generated by these carbonates at pH 10.0, although the dominant carbon species present would be HCO<sub>3</sub><sup>-</sup> and CO<sub>3</sub><sup>2-</sup>. The dissolved inorganic carbon species were consumed by the methanogenic population, further indicating the potential for autotrophic growth via consumption of calcium carbonate. All microcosms were dominated by methanogens capable of hydrogenotrophic methanogenesis, including the genera *Methanobacterium* and *Methanoculleus*, although small proportions of the metabolically diverse genus *Methanosarcina* and the strictly acetoclastic genus *Methanosaeta* were detected, indicating the potential for acetoclastic methanogenesis, despite the lack of measurable acetate consumption. Phenolphthalein, SEM and XRD analysis suggested the NRVB underwent carbonation during incubation with CO<sub>2</sub>, signified by the low pH areas formed on the surface, the detection of calcium, carbon and oxygen via EDS and the morphology of the minerals and the XRD patterns. Organic biofilm materials were detected on the surface of the NRVB, suggesting the microorganisms were growing in close association with the carbonate minerals and were capable of attachment to the cement surface, with the formation of eDNA scaffolding possibly improving biofilm attachment. Archaea were detected within the biofilm materials formed on the NRVB surface via FISH, further confirming the growth of methanogens within close association to the calcite minerals.

Calcite has been identified as an important mineral within the near-field of an ILW-GDF, and the data shown here suggests it could provide methanogens with a carbon source for hydrogenotrophic metabolism, so long as molecular hydrogen is available. Alongside methanogenesis, microcosms also showed evidence of homoacetogenesis, signified by the generation of acetate in reactors supplemented with calcite and hydrogen gas. The combination of H<sub>2</sub> and calcite therefore has the potential to provide both hydrogenotrophic and acetoclastic

methanogens with substrate for metabolism, however hydrogenotrophic metabolism was evidently the dominant pathway within this study. Overall this data suggests that inorganic and highly insoluble calcium carbonate is able to support both homoacetogenesis and methanogenesis at pH 10.0, which could have a significant impact on gas generation within the near-field of an ILW-GDF.

# **8.0 Development of Sulphate-reducing and Methanogenic Biofilms on Steel Surfaces under Alkaline Conditions**

## 8.1 Rationale

Microcosms developed from the New Lime site B sediments operating at pH 10.0 under sulphate-reducing conditions and fed with CDP were used as inoculum to develop biofilm on stainless steel surfaces at pH 11.0. Previous work has demonstrated methanogenic activity at pH 11.0 in planktonic culture (24) and biofilm systems (304), however to the authors knowledge sulphate-reduction at pH 11.0 has never been demonstrated under laboratory conditions. Earlier work utilising sediments from site B suggest sulphate reduction above pH 10.0 is not viable in planktonic culture (115), although studies into the alkaline soda lakes have measured sulphate-reducing activity above pH 10.5 (357) and pure cultures of alkaliphilic SRB have demonstrated growth at pH 10.5 (358). The formation of biofilm has been shown to facilitate microbial survival under extreme conditions (125) and could ease the environmental stresses associated with high pH. The generation of sulphide within a GDF has the potential to enhance the corrosion of any steel materials present, such as the steel canisters used to contain the waste, therefore an active sulphate-reducing community could impact the long-term performance of such a facility.

## 8.2 Results and Discussion

### 8.2.1 CDC Biofilm Reactor Bulk Chemistry

CDC biofilm reactors were inoculated under methanogenic (no TEA's) and sulphate-reducing conditions (amended with sulphate) and incubated for 3 months under a two-weekly waste/feed cycle. Under both methanogenic and sulphate-reducing conditions all three forms of ISA showed evidence of microbial degradation compared to abiotic control reactors (Figure 8.2A). ISA first order rate constants are shown in Table 8.1 and remained similar under both conditions tested, suggesting the rate of fermentation was not impeded by the addition of sulphate. The generation of acetate and hydrogen via the degradation of ISA suggests fermentation pathways were active within the reactors as previously reported (24), with no acetate or hydrogen detected in abiotic reactors. The ISA degradation rates observed here were comparable with those reported previously using neutral-pH soils (23) and alkaline sediments (24) in planktonic culture.

Methane was generated in reactors lacking sulphate (Figure 8.2B), with highest quantities detected on day 84 of 0.25 mmoles. However, methanogenesis was inhibited in reactors

amended with sulphate, suggesting the presence of a dissimilatory sulphate-reduction pathway competing for common fermentation end products. The microcosms used as inoculum in this study were operating under sulphate-reducing conditions, suggesting the methanogens were co-existing with SRB and could only be detected in the absence of sulphate. The co-existence of SRB and methanogens has been observed previously (359), however the survival of the methanogens within the inoculating reactors could not be accounted for, with no spore-forming methanogens described in the literature. It is possible that methane was generated at undetectable levels (<1% v/v) within the sulphate-reducing microcosms. Regardless, methane generation rates were inhibited in the presence of sulphate in this study. The fermentation of ISA to acetate and hydrogen has the potential to drive methanogenesis, however the consumption of hydrogen and accumulation of acetate (Figure 8.2BC) within methanogenic reactors suggests the hydrogenotrophic pathway was responsible for the methane generated. Hydrogen was also consumed in sulphate-amended reactors (Figure 8.2B), indicating the presence of a hydrogenotrophic sulphate-reducing community competing for molecular hydrogen with methanogens. Autotrophic and hydrogen-consuming SRB have been identified previously (360, 361).

Acetate provides a potential carbon source for SRB (361) and this could account for the low rates of consumption observed under sulphate-reducing conditions (Figure 8.2C). The generation of acetate via ISA fermentation could also be masking consumption rates further. The competition for substrates between SRB and methanogens has been investigated previously (362-364), with many of these studies suggesting SRB outcompete methanogens for hydrogen and acetate.

Sulphate was removed at a steady state within sulphate-amended reactors, which coincided with the generation of dissolved sulphide, with no sulphate and negligible sulphide concentrations detected in methanogenic reactors (Figure 8.2D). On average 60.7 mg ( $\pm 3.8$ ) of sulphate was lost between days 70-84, which equates to a removal rate of 4.34 mg day<sup>-1</sup> ( $\pm 0.27$ ). Dissolved sulphide concentrations in sulphate amended reactors increased from 46.2 mg/L on day 70 to 49.2 mg/L on day 84. Sulphate showed no signs of degradation within abiotic reactors, suggesting sulphate in the biotic systems was removed via microbial activity. All reactors remained alkaline throughout the testing period, with the lowest pH value recorded at 10.81 and highest at 11.14 (Figure 8.1).

Although previous studies undertaken on the Harper Hill site using acetate and lactate as electron donors suggest sulphate-reduction above pH 10.0 is not viable (115), CDP was used as substrate for this study and therefore could provide a wider range of electron donors, such as hydrogen from fermentation, and allow for sulphate-reduction to take place under the conditions imposed here. Furthermore the products of fermentation are likely to provide electron donors in concentrations more in line with that seen in the natural environment and reduce the potential for substrate inhibition.

**Table 8.1. ISA degradation rate constants.** Average ISA degradation rates under methanogenic and sulphate-reducing conditions at pH 11.0 (n=2).

ISA	Rate (day <sup>-1</sup> )	Standard Deviation
Alpha	$7.7 \times 10^{-2}$	$1.4 \times 10^{-2}$
Beta	$1.0 \times 10^{-1}$	$3.5 \times 10^{-3}$
Xylo	$1.5 \times 10^{-1}$	$1.0 \times 10^{-2}$

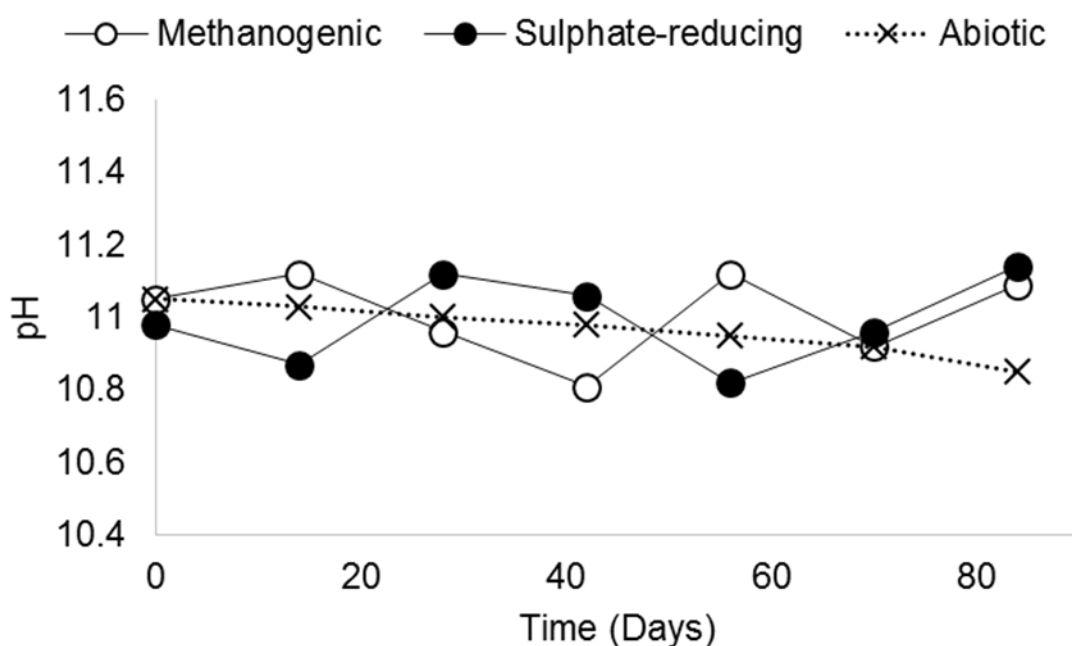


**Figure 8.1. Bulk liquid pH of CDC biofilm reactors.** Shows CDC biofilm reactor bulk pH values under methanogenic and sulphate-reducing conditions, alongside abiotic control reactors.

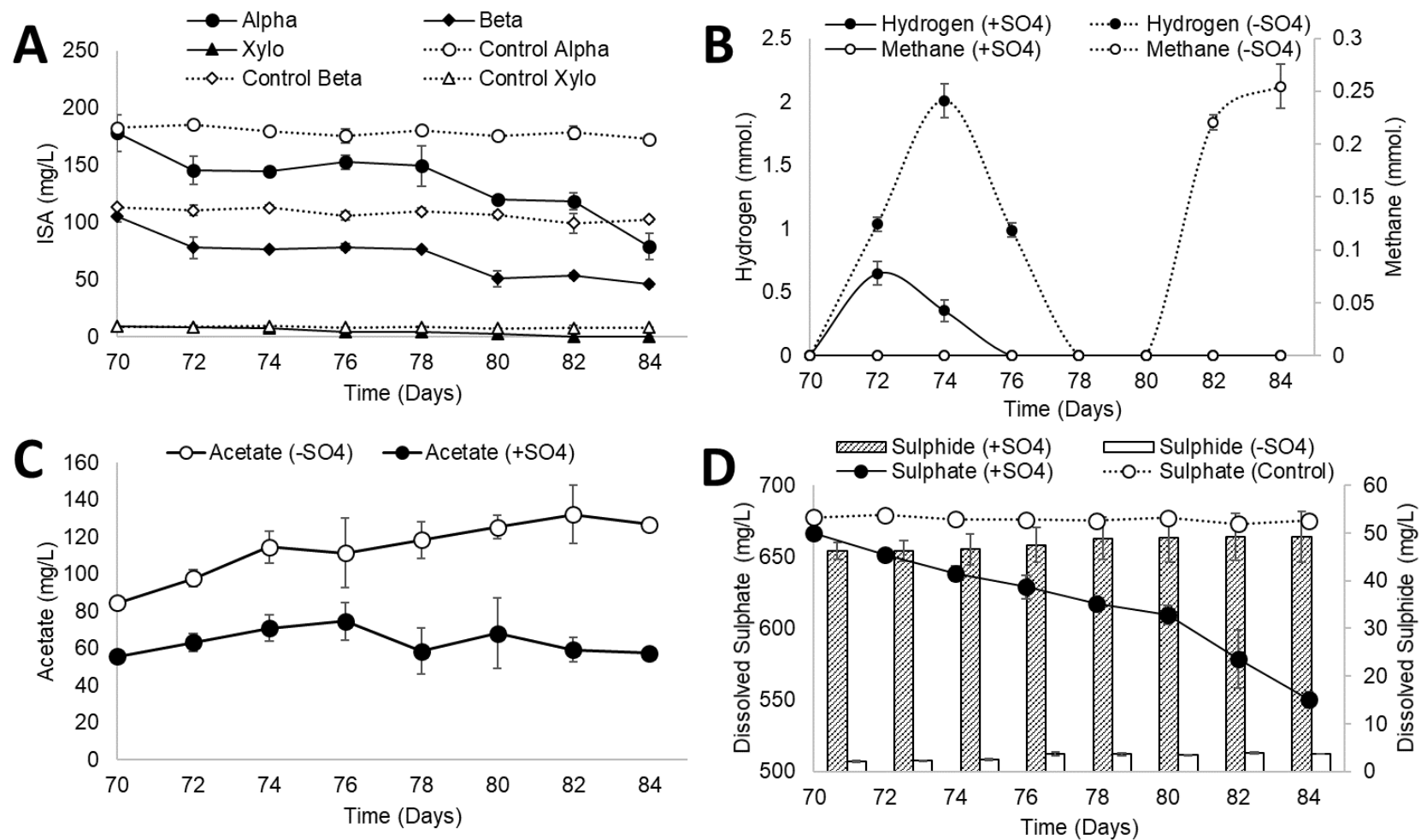


**Figure 8.2. CDC biofilm reactor bulk chemistry under sulphate-reducing and methanogenic conditions at pH 11.0.** Showing ISA concentration (A), headspace gas quantities (B), acetate concentration (C) and dissolved sulphate/sulphide concentration (D) under methanogenic (-SO<sub>4</sub>) and sulphate-reducing (+SO<sub>4</sub>) conditions. The final 2 weeks of the 3-month incubation period are shown. Error bars represent standard deviation (n=2).

## 8.2.2 Biofilm Micro-profiling

### 8.2.2.1 pH Profiles

In order to determine the internal pH of the sulphate-reducing biofilm formed on the steel coupons after 3 months' incubation, triplicate pH profiles were undertaken using a micro-pH electrode (Dia. 10  $\mu\text{m}$ ) connected to a motorised micro-manipulator. The profiling revealed a range of low-pH microsites within the internal surface of the biofilm (Figure 8.3). At the time of sampling the bulk liquid pH within sulphate-reducing reactors and abiotic control reactors was 11.17 ( $\pm 0.02$ ) and 11.06 ( $\pm 0.002$ ) respectively. The significant pH changes observed in the biotic experiments as the electrode neared the steel surface were assumed to be a result of the micro-electrode entering the biofilm matrix, substantiated by the fact that no significant shifts in pH were observed in abiotic controls or in the bulk liquid of the biotic experiments. The pH values within the internal surface of the biofilm fluctuated significantly across the replicate profiles, suggesting the biofilms were heterogeneous. The pH reached a minimum value of 9.70, 10.26 and 10.24 in triplicate profiles, equating to a reduction of 1.47, 0.91 and 0.93 pH units respectively. However the pH did not continually drop at increasing depth through the biofilm, possibly due to external bulk liquid entering the biofilm matrix due to damage caused by the electrode during profiling. Nevertheless, the pH always remained lower in the biofilm compared to the bulk fluid in all replicate profiles. This large drop in pH could be attributed to the generation of metabolic acids, such as acetate, via fermentation, or could be due to the properties of the EPS components (365). Previous work developing biofilms on silicate surfaces using soil bacteria have measured pH changes between the biofilm and bulk fluid as high as 1.2 pH units using micro-electrodes (366). The bacterial species *Burkholderia brasiliensis* has been shown to produce acidic exopolysaccharides (367), indicating a potential route for the development of low pH microsites within the biofilms studied here. The lower pH sites detected in the biofilm offer a niche site for improved microbial activity compared to bulk fluid conditions.

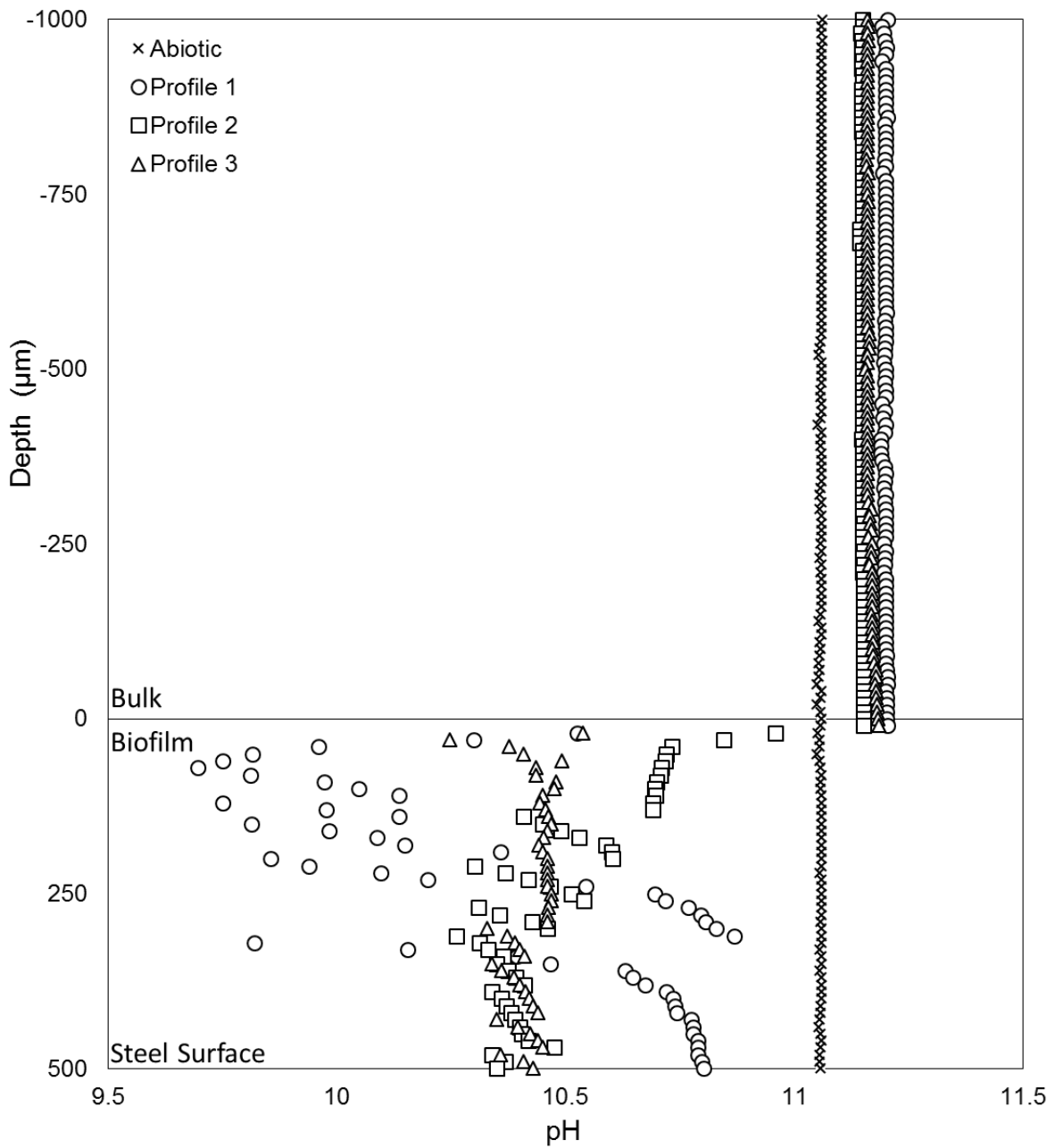
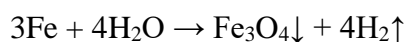


**Figure 8.3. pH profiles of sulphate-reducing biofilm at pH 11.0.** Shows triplicate pH profiles (A-C) in 10 µm increments of the bulk liquid and solid biofilm materials formed on steel surfaces after 3 months incubation under sulphate-reducing conditions. Abiotic control surfaces are also shown.

### 8.2.2.2 H<sub>2</sub> Profiles

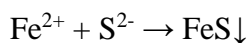
Hydrogen profiles of both sulphate-reducing and methanogenic biofilms were undertaken using a H<sub>2</sub> micro-sensor. Under both conditions no dissolved hydrogen could be detected within the bulk fluid (lower detection limits >1 μM), however H<sub>2</sub> was detected within the internal surface of both the methanogenic and sulphidogenic biofilms (Figure 8.4). Hydrogen concentrations increased sharply within the upper layers of the methanogenic biofilm, reaching highest values of 5.61μM and 21.1μM in duplicate profiles. However H<sub>2</sub> concentrations decreased in the lower layers of the methanogenic biofilm and became undetectable at the steel surface. The detection of H<sub>2</sub> within the biofilm could be a marker for fermentation and suggests the majority of the microbial activity was present within the upper layers of biofilm in the methanogenic systems. In contrast, H<sub>2</sub> concentrations continued to increase at depth within the sulphate-reducing biofilms, with highest concentrations (71.8 μM) detected within close proximity to the steel surface. Previous studies detected comparable hydrogen concentrations within hypersaline microbial mats using micro-sensors (368). The high H<sub>2</sub> concentrations observed at the biofilm/steel interface under sulphate-reducing conditions could be a result of anaerobic corrosion via the following reactions:



SRB are capable of producing hydrogen sulphide via the oxidation of molecular hydrogen:



The generation of sulphide results in the precipitation of free iron to form iron (II) sulphide:



The equilibrium concentration of iron ions can be calculated from the solubility product constants ( $K_{sp}$ ). The production of H<sub>2</sub>S leads to the formation of HS<sup>-</sup> and S<sup>2-</sup> ions in alkali solution resulting in a decrease of free iron due to the precipitation of FeS. The production of FeS results in further dissolution of iron from the passive layer until the equilibrium concentration is reached, resulting in corrosion of the steel surface.

Hydrogen produced via fermentation or anaerobic corrosion appears to diffuse immediately to the headspace of the reactors studied here, since no H<sub>2</sub> could be detected in the bulk liquid phase of the reactors. The production of EPS limited the diffusion of hydrogen and allowed for its detection within the biofilm matrix. It is important to note that the H<sub>2</sub> micro-sensor used in this study is sensitive to H<sub>2</sub>S (368) and therefore sulphide produced in the sulphate-reducing systems could be obscuring the hydrogen profiles measured here. Future work employing the sulphide micro-sensors could corroborate this further.

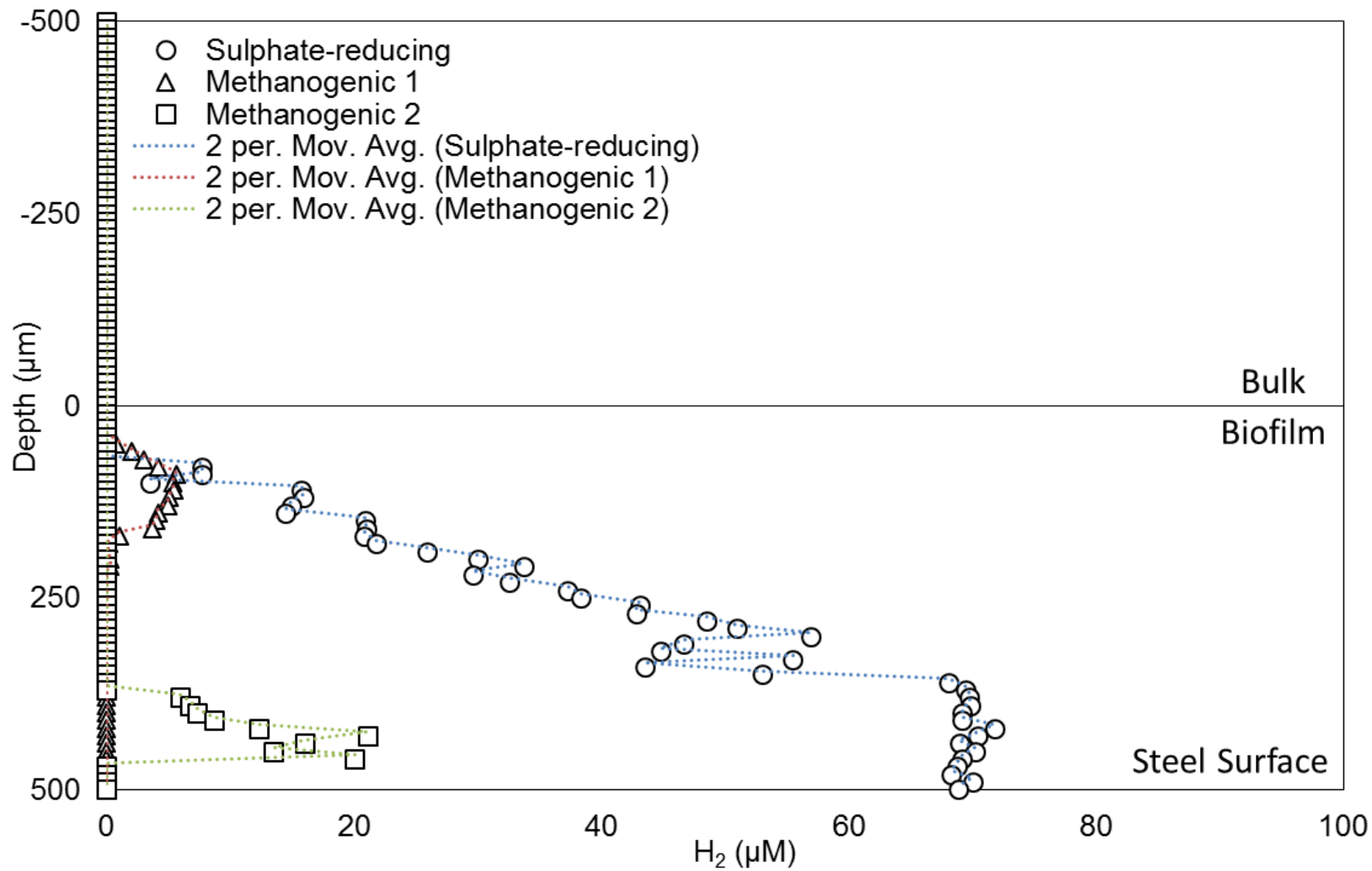


**Figure 8.4.** H<sub>2</sub> profiles of sulphate-reducing and methanogenic biofilm at pH 11.0. Shows sulphate reducing and methanogenic dissolved hydrogen profiles of the bulk liquid and solid biofilm materials formed on steel surfaces after 3 months incubation.

### **8.2.2.3 Redox Profiles**

The reduction potential of bulk liquid and biofilms within sulphate-reducing and methanogenic systems was determined using a redox micro-electrode (Figure 8.5). Both biotic and abiotic profiles revealed the reactors were under chemically reducing conditions, with the average redox potential within the bulk fluid for abiotic, sulphate-reducing and methanogenic systems was -358.6 mV ( $\pm 3.61$  n=100), -377.5 mV ( $\pm 0.76$  n=100) and 378.3 mV ( $\pm 1.53$  n=100) respectively. Within the sulphate-reducing and methanogenic biofilms the average redox was -378.9 mV ( $\pm 0.76$  n=50) and -377.0 mV ( $\pm 1.53$  n=50) respectively, indicating the differences in redox potential between bulk fluid and biofilms was negligible ( $< 2$  mV). The development of chemically reducing conditions is an important factor in anaerobic respiratory processes, with methanogens reportedly requiring a redox potential between -200 mV to -400 mV for growth (372), suggesting the conditions imposed in this study were favourable. The generation of hydrogen via fermentation or through anaerobic corrosion could account for the differences in redox potential between abiotic and biotic systems, with hydrogen acting as a reducing agent.

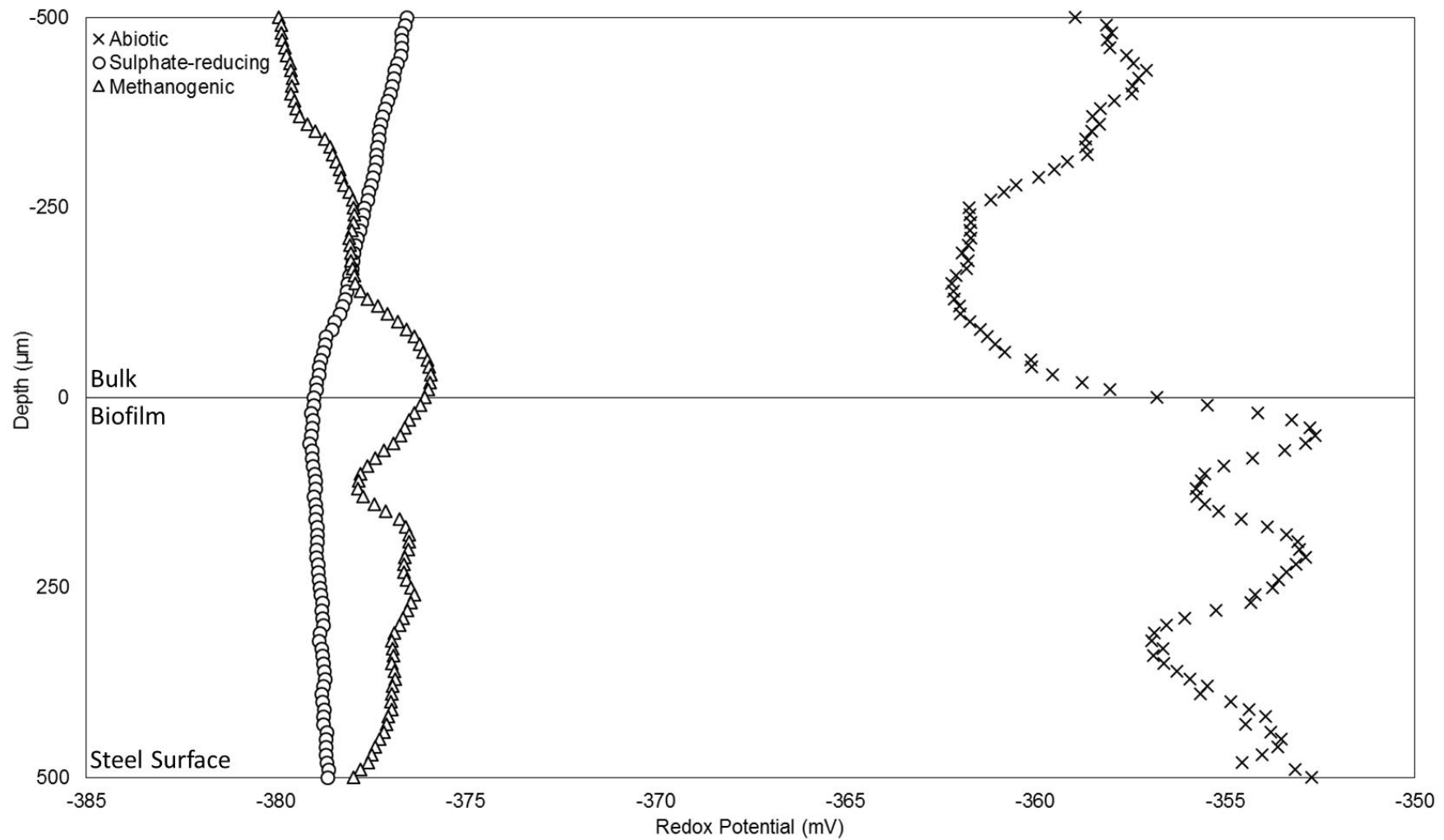


**Figure 8.5. Redox profiles of sulphate-reducing and methanogenic biofilm at pH 11.0.** Shows sulphate reducing and methanogenic redox profiles of bulk liquid and biofilms alongside abiotic controls after incubation for 3 months.

## **8.2.3 Biofilm Characterisation**

### ***8.2.3.1 Scanning Electron Microscopy***

The morphology and coverage of the sulphate-reducing and methanogenic biofilms formed on steel surfaces was investigated via SEM. Under both conditions micrographs revealed cocci and bacilli shaped microbial cells embedded in EPS-like structures (Figures 8.6 and 8.7). The steel coupons were not completely colonised by biofilm and discs retrieved from methanogenic reactors were particularly sparse (Figure 8.7C), potentially suggesting cells were surviving in close proximity to bulk fluid conditions. Based on the SEM images microbial cells were relatively low in number and the EPS appeared to account for the majority of biomass, particularly within the sulphate-reducing experiments (Figure 8.6D). Previous work has shown that microorganisms develop biofilm at a higher rate on grade 304 stainless steel compared to grade 316 (373). The biofilms studied here had a similar appearance to previous work investigating biofilms on carbon steel (374).

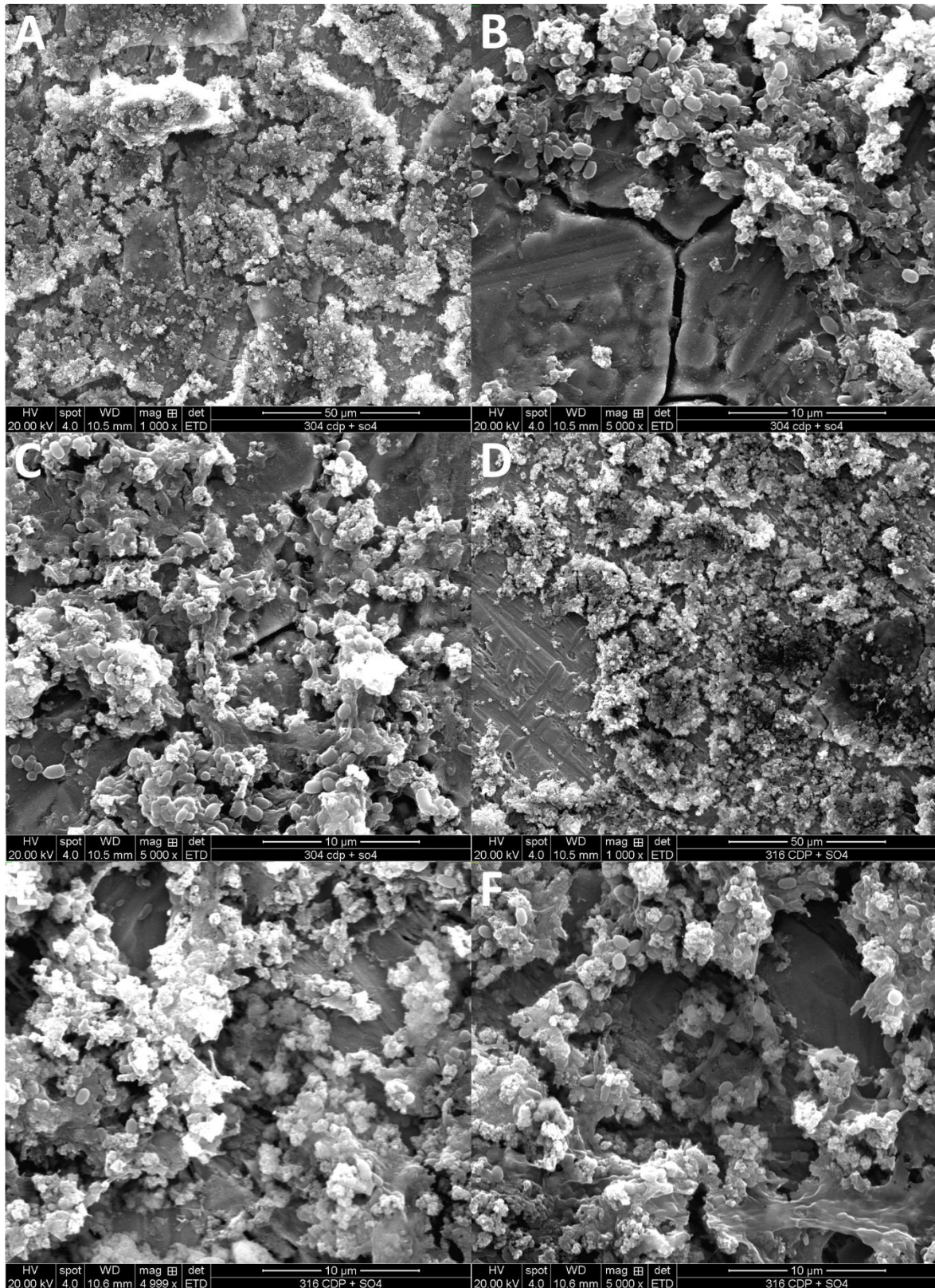


**Figure 8.6. SEM investigation of sulphate-reducing biofilm.** Shows scanning electron micrographs of biofilm formed on grade 304 (A-C) and 316 (D-F) steel surfaces after 3 month incubation period under sulphate-reducing conditions at pH 11.0.

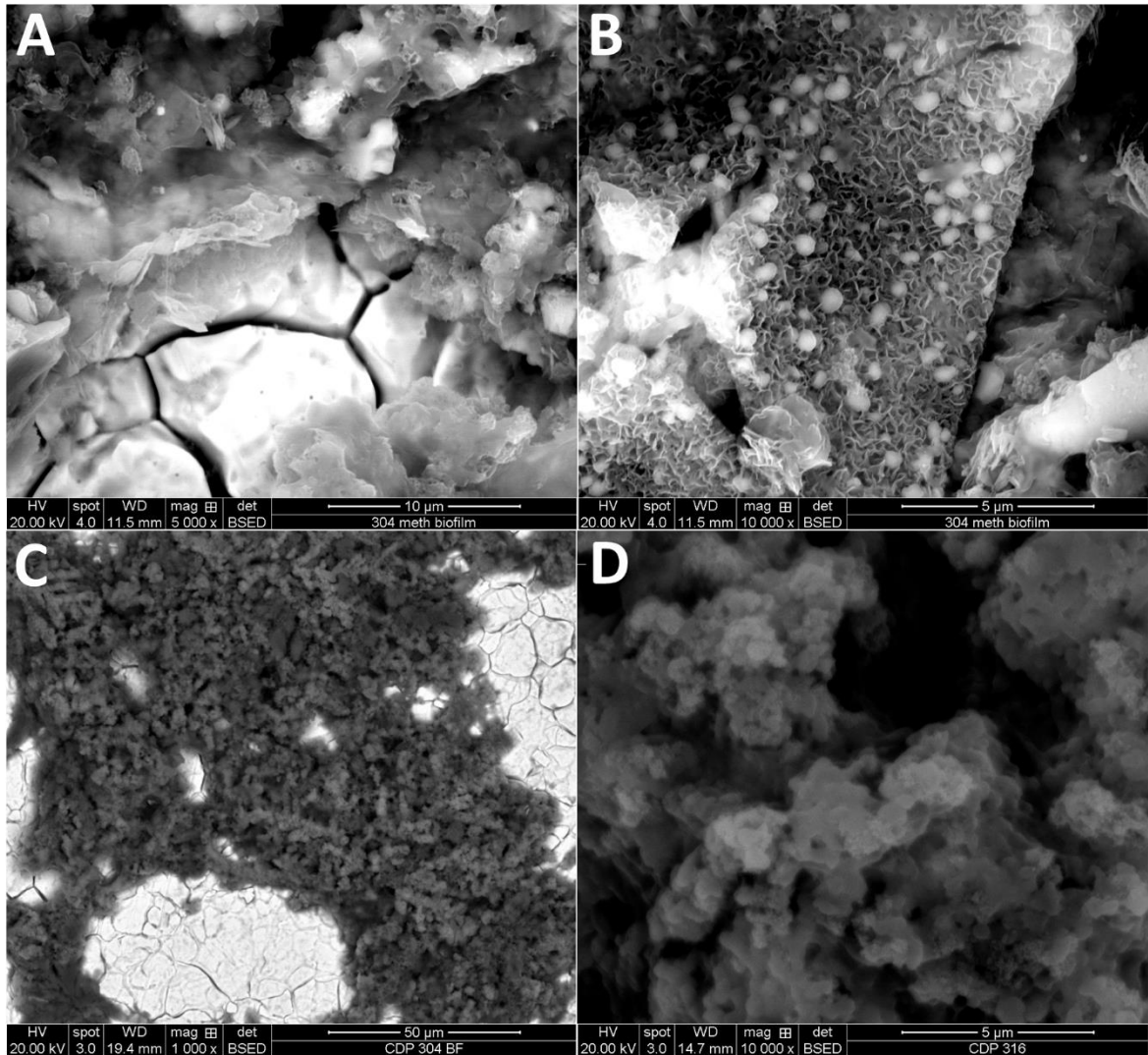


**Figure 8.7. SEM investigation of methanogenic biofilm.** Shows scanning electron micrographs of biofilm formed on grade 304 (A-B) and 316 (C-D) steel surfaces after 3 month incubation period under methanogenic conditions at pH 11.0 ( $\pm 0.2$ ).

### ***8.2.3.2 Confocal Laser Scanning Microscopy***

In order to visualise the individual EPS components, 5-colour CLSM imaging was undertaken and revealed biofilms to be comprised of a range of extracellular polymers, including polysaccharides, proteins, sugars, lipids and eDNA, alongside a cellular component (Figures 8.8 & 8.9). Lipids and protein were the predominant polymers detected within both the sulphate-reducing and methanogenic biofilms (Figure 8.10) which will contribute to their hydrophobicity and limit the diffusion of chemical species. The high lipid content and the buffering capacity of the protein component (375) could account for the lower pH micro-sites detected within the biofilm matrix (Figure 8.3). Polysaccharides were detected predominantly at the interface between the biofilm/steel surface and could be providing cells with a mechanism of adhesion and attachment as shown previously (376). The sulphate-reducing biofilms appeared to be relatively heterogeneous (Figure 8.11), which could account for the variability observed across replicate pH profiles in Section 8.2.2.1. Biofilm matrix proteins have also been shown to provide cells with a mechanism of adhesion (377) and a thin layer of protein was observed on the steel surfaces taken from methanogenic reactors (Figure 8.12). In contrast steel coupons retrieved from sulphate-reducing reactors had a thin layer of polysaccharides coating the surface (Figure 8.13), with these differences likely to be a result of the microbial community composition.

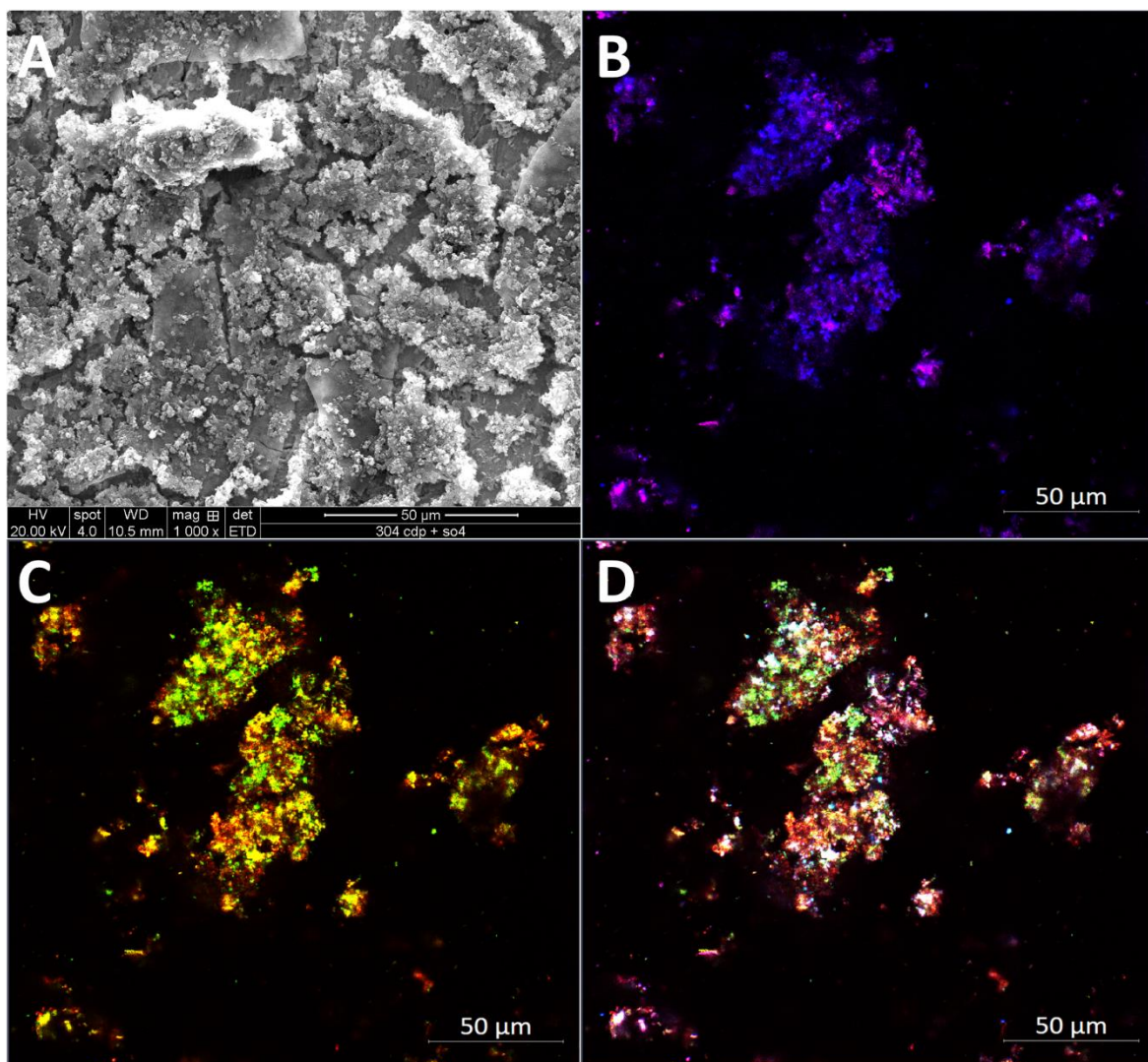


**Figure 8.8. 5-colour CLSM investigation of sulphate-reducing biofilm.** Shows individual EPS components of sulphate-reducing biofilm formed on steel after 3 months incubation, including SEM image (A) and fluorescence imaging (B-D). Polysaccharides (blue), eDNA and cells (pink), lipids (yellow), protein (green) and sugars (red). Images shown are polysaccharides together with eDNA and cells (B). Protein, together with lipids and sugars (C). Combined image (D).

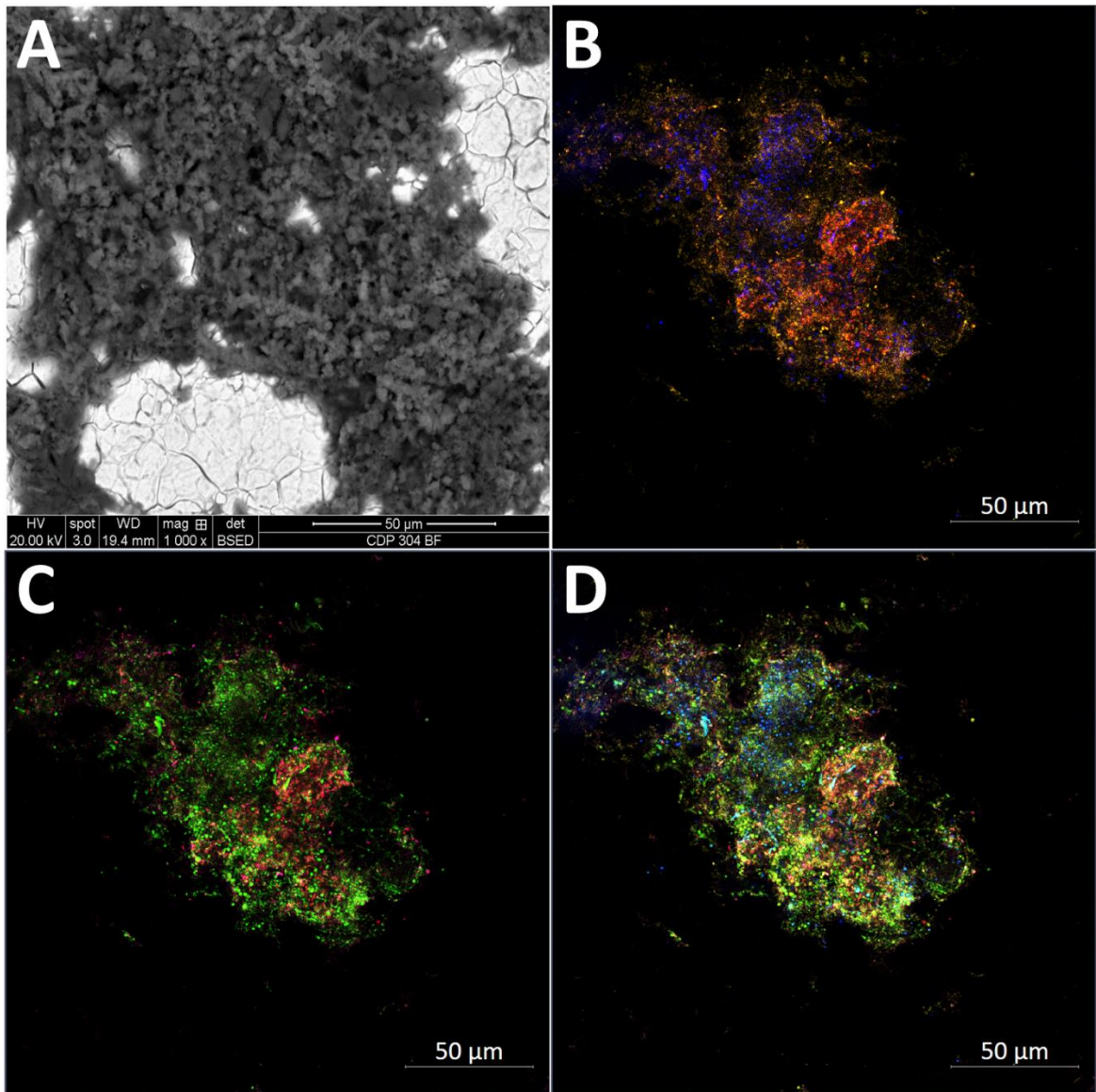


**Figure 8.9. 5-colour CLSM investigation of methanogenic biofilm.** Shows individual EPS components of methanogenic biofilm formed on steel after 3 months incubation, including SEM image (A) and fluorescence imaging (B-D). Polysaccharides (blue), eDNA and cells (pink), lipids (yellow), protein (green) and sugars (red). Images shown are polysaccharides together with sugars and lipids (B). Protein, together with cells and eDNA (C). Combined image (D).

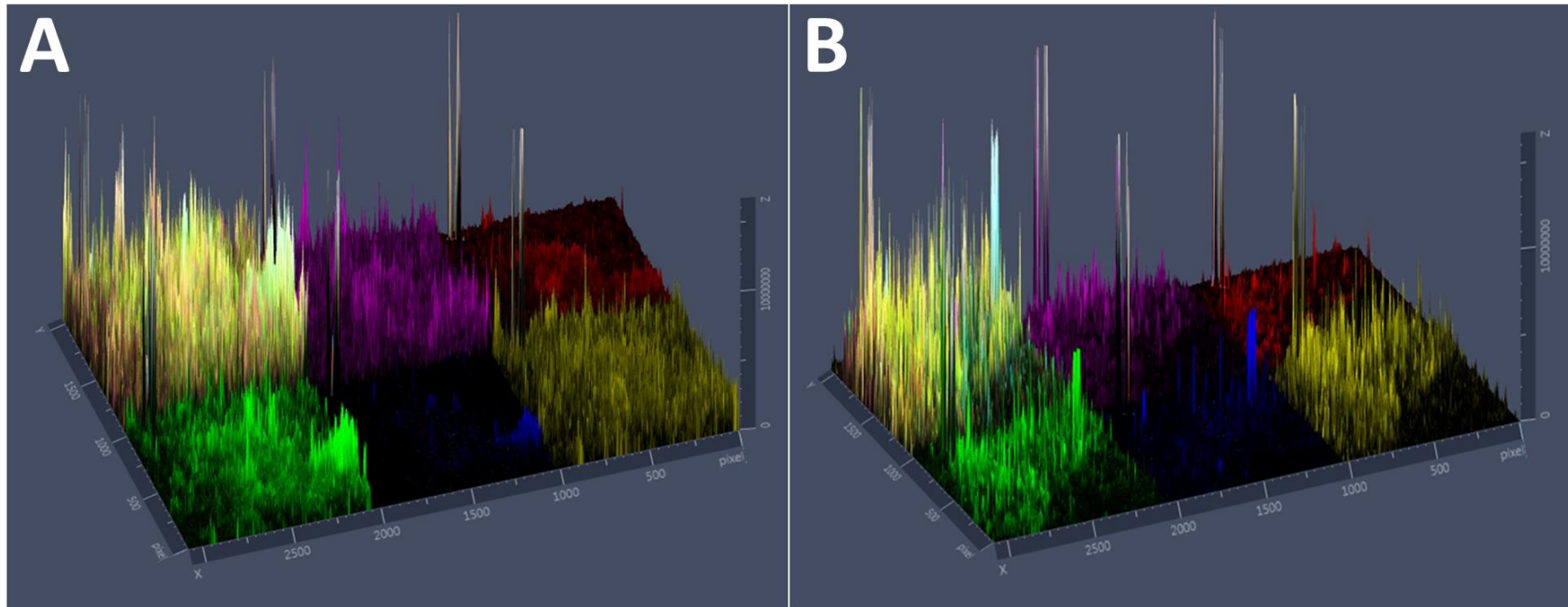


**Figure 8.10. 5-colour CLSM investigation of sulphate-reducing and methanogenic biofilms.** Shows 5-colour 2.5D image of biofilm formed on steel surface after 3 months incubation period under sulphate-reducing (A) and methanogenic (B) conditions at pH 11.0. X and Y axis represents the steel surface and peak height represents distance from the steel surface. Yellow – lipids, blue – polysaccharides, green – protein, red – sugars, pink – cells and eDNA. Combined image is also shown (top left).

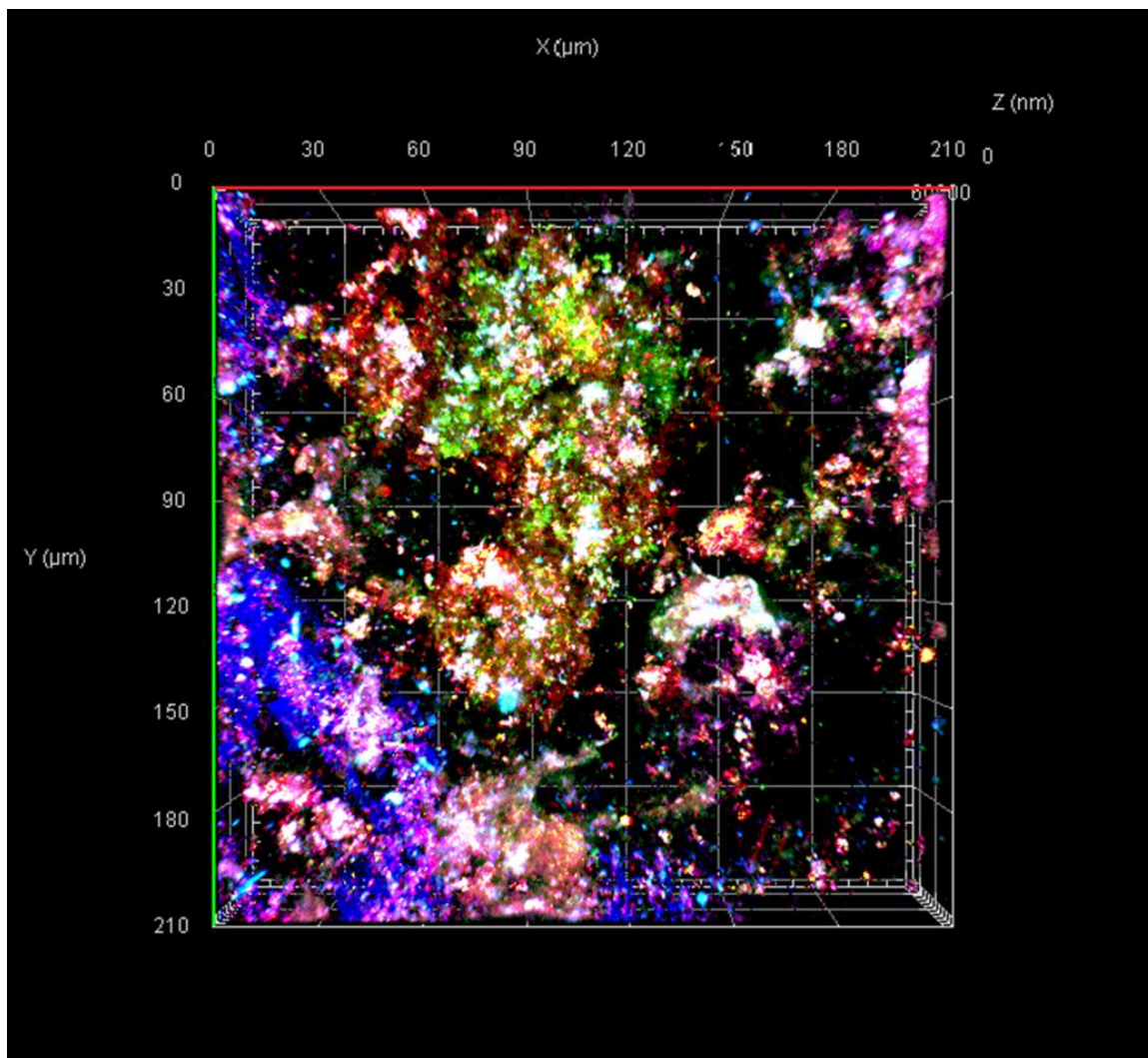


**Figure 8.11. 5-colour CLSM investigation of sulphate-reducing biofilm.** Shows 5-colour Z-stack 3D fluorescence image of biofilm formed on steel surface after incubation for 3 months under sulphate-reducing conditions at pH 11.0. Yellow – lipids, blue – polysaccharides, green – protein, red – sugars, pink – cells and eDNA.

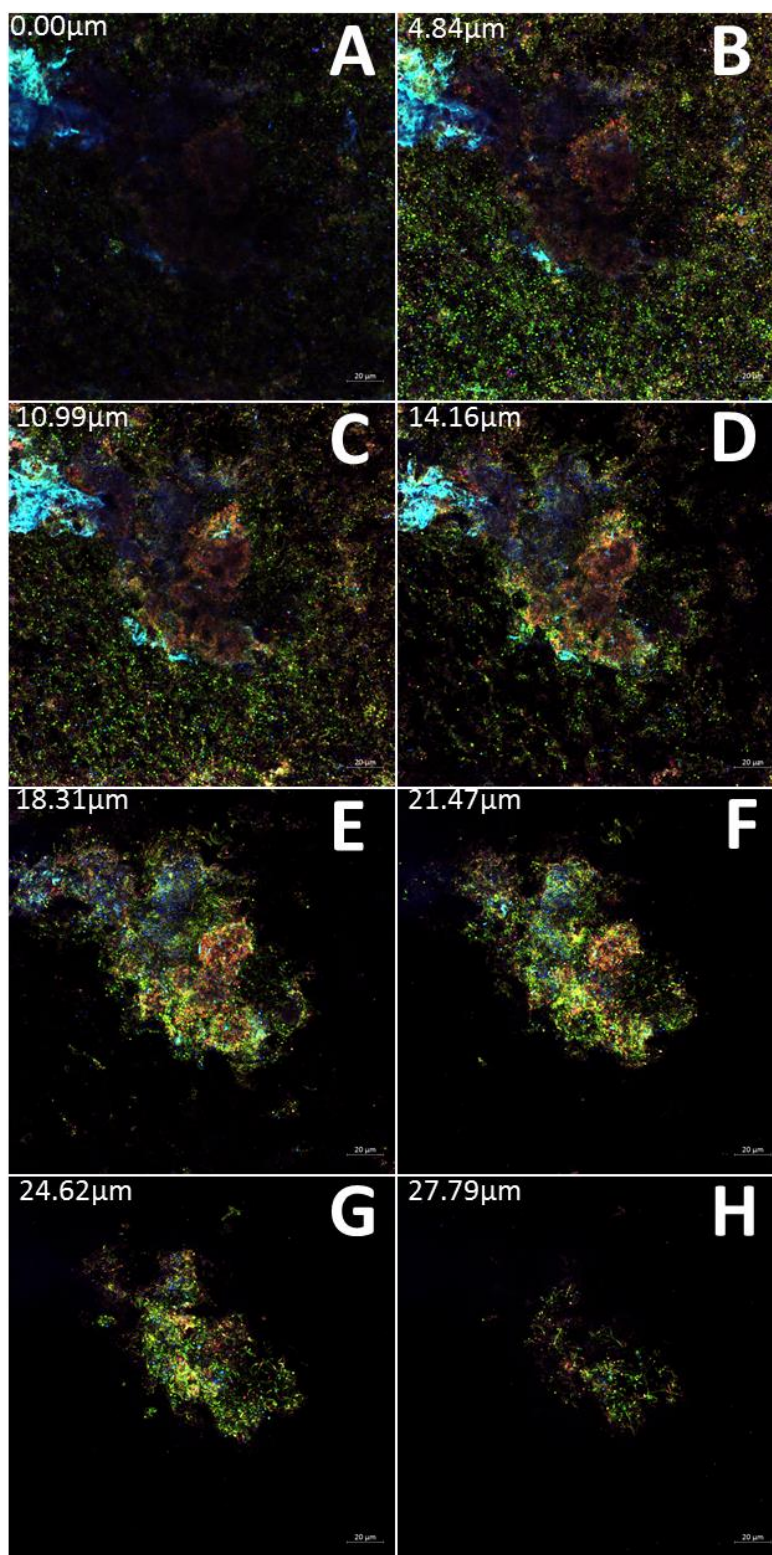


**Figure 8.12. 5-colour CLSM investigation of methanogenic biofilm.** Shows 5-colour z-stack image of biofilm formed on steel surface after 3 month incubation under sulphate-reducing conditions at pH 11.0 ( $\pm 0.2$ ). (A) steel surface, (B-H) increasing height above steel surface. Yellow – lipids, blue – polysaccharides, green – protein, red – sugars, pink – cells and eDNA.

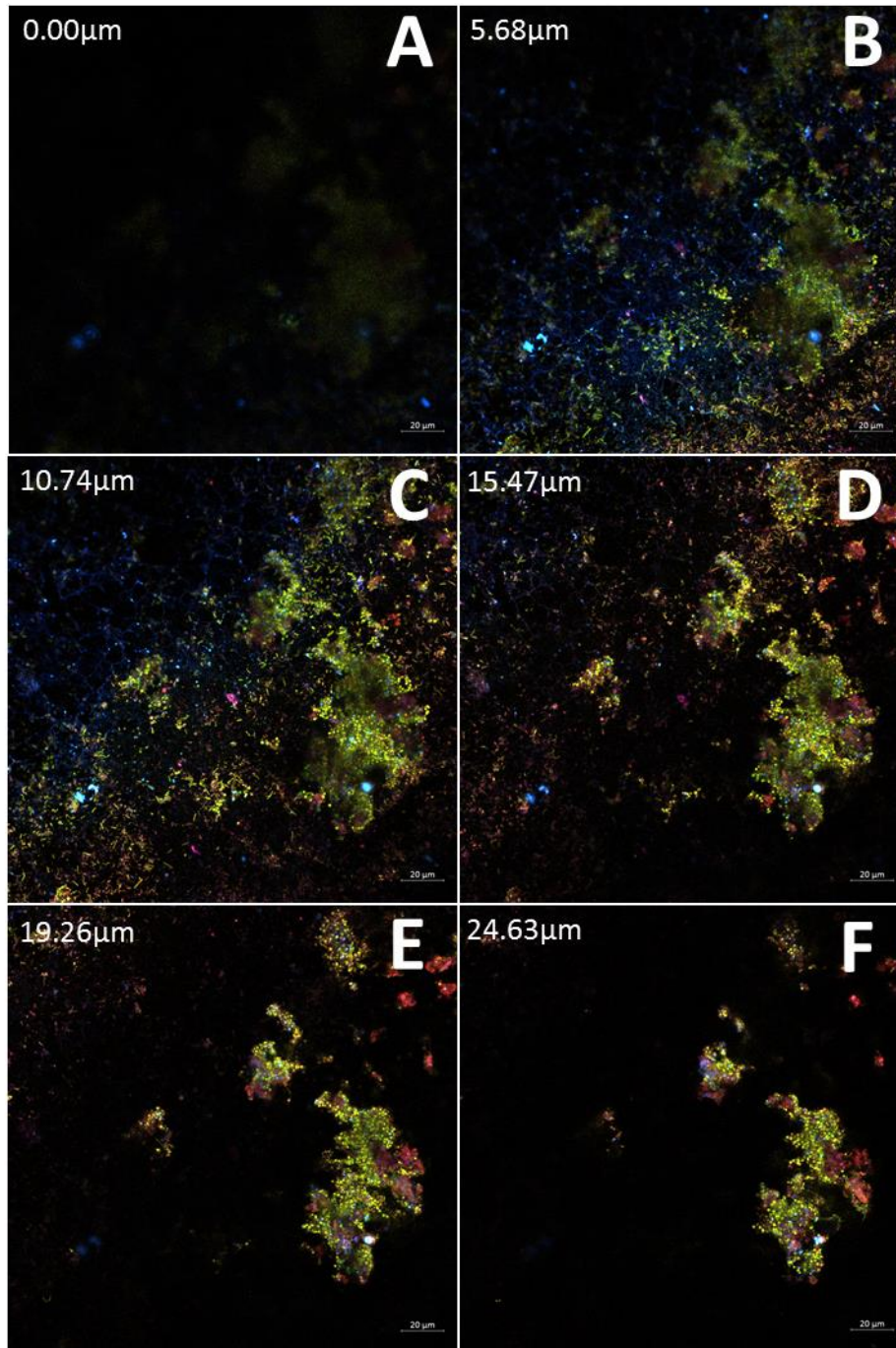


**Figure 8.13. 5-colour CLSM investigation of sulphate-reducing biofilm.** Shows 5-colour Z-stack image of biofilm formed on steel surface after 3 month incubation under methanogenic conditions at pH 11.0 ( $\pm 0.2$ ). (A) steel surface, (B-F) increasing height above steel surface. Yellow – lipids, blue – polysaccharides, green – protein, red – sugars, pink – cells and eDNA.

## 8.2.4 Microbial Community Analysis

### 8.2.4.1 16S rRNA Gene Sequencing

DNA was extracted and sequenced from the bulk liquid of methanogenic and sulphate-reducing systems, along with biofilms formed on grade 304 and 316 steel in order to analyse the microbial community. Members of the Firmicutes and Proteobacteria were the dominant phyla within all communities analysed, however the proportion of reads attributed to these varied across biofilm and bulk microbiomes (Figure 8.14). Bulk liquid communities were similar at the Phylum-level under both methanogenic and sulphate-reducing conditions, with Firmicutes representing 81% and 79% of the total reads respectively. However the proportion of Firmicutes reads reduced significantly in the biofilm community under both conditions and gave way to an increase in Proteobacteria, Bacteroidetes and Actinobacteria (Figure 8.14).

Actinobacteria were only detected within the sulphate-reducing biofilms and represented 13% and 14% of the community on grade 304 and 316 steel respectively, however this phylum was absent from the bulk microbiome, possibly due to the more extreme conditions. Actinobacteria species have demonstrated the ability to generate extracellular polysaccharides previously (378), which could explain the detection of polysaccharides on the steel surfaces under sulphate-reducing conditions explained in Section 8.2.3.2. Actinobacteria have been detected in extreme environments previously (379), however the lack of this phylum within the methanogenic biofilms could only be explained by their tolerance to high sulphide concentrations. Previous work has shown that marine bacteria demonstrate variable responses to high sulphide concentrations (380), which could account for the differences seen between methanogenic and sulphate-reducing communities profiles in this study.

Although SRB are found in several phylogenetic lines, including the Firmicutes (381), Nitrospirae (382), Thermodesulfobacteria (383) and Euryarchaeota (92), all of the SRB identified in this study were members of the Proteobacteria phylum, Deltaproteobacteria class and *Desulfonatronum* genus, suggesting their importance in alkaline systems, with selection pressures possibly resulting in the absence of SRB from other lineages. All identified species within the *Desulfonatronum* genus are alkaliphilic (384-388) and many of these are capable of utilising hydrogen as electron donor (386-388) and have even demonstrated autotrophic growth (384) which verifies the consumption of H<sub>2</sub> within sulphate-reducing reactors and explains the inhibition of methanogenesis. This also confirms the assertion that methanogenesis was

proceeding via the hydrogenotrophic pathway. Furthermore, pure cultures of *Desulfonatronum zhilinae* have demonstrated growth at pH 10.5 (387), eliminating the possibility that sulphate-reduction above pH 10.0 will not be viable within the near-field of an ILW-GDF. A small proportion of 16S rRNA gene reads were attributed to SRB under methanogenic conditions, with 0.14%, 0.51% and 0.16% of reads comprising the 304 biofilm, 316 biofilm and bulk liquid respectively. However the percentage of SRB reads increased significantly in reactors amended with sulphate to 18.0%, 18.4% and 10.1% of the 304 biofilm, 316 biofilm and bulk liquid respectively (Figure 8.15). The detection of SRB within the methanogenic reactors could be attributed to their ability to act as fermenters (389). Furthermore, DNA sequencing does not represent an active community profile and therefore the SRB reads detected within methanogenic reactors could be a result of carry-over from the inoculating reactors. Preliminary attempts to extract RNA from the biofilms in order to generate cDNA and demonstrate an active community profile were unsuccessful. The significant increase in SRB reads under sulphate-reducing conditions does however verify the presence of classical dissimilatory sulphate-reducing pathways in the sulphate-amended reactors.

Methanogens were detected within reactors lacking sulphate and represented 0.17%, 4.39% and 0.12% of the total community in 304 biofilms, 316 biofilms and bulk liquid respectively (Figure 8.15). However using the same primers, no methanogens were detected within sulphate-amended reactor biofilms or bulk liquid, further confirming the absence of methanogenesis in the presence of sulphate. Hydrogenotrophic methanogens dominated the archaeal 16S reads and the strictly acetoclastic genus *Methanosaeta* was absent from the community, which is in line with the bulk chemistry outlined in Section 8.2.1 where acetate concentrations increased and hydrogen was consumed. The metabolically diverse genus *Methanosarcina* was the dominant methanogen within the biofilm formed on grade 316 steel (Figure 8.15), however the strictly hydrogenotrophic *Methanobacterium* dominated the biofilm on grade 304 steel and the bulk liquid microbiome. The large increase in methanogen reads detected within the biofilm formed on grade 316 steel either indicates biofilms were heterogeneous or that grade 316 steel provided a more amenable surface for biofilm formation. Grade 316 stainless steel contains a higher proportion of nickel and molybdenum than grade 304 (390), which could account for the variation seen across biofilm communities in this study. Previous studies have suggested that nickel can enhance biofilm formation (391).

Rarefaction curves (Figure 8.16A) showed that sampling reached saturation and rank abundance curves (Figure 8.16B) indicated a diverse microbial community in both biofilms

and bulk liquid. The number of valid reads and OTU's increased within the bulk liquid under both methanogenic and sulphate-reducing conditions (Table 8.2), with the Shannon index correspondingly revealing an increase in diversity. Goods Coverage values showed that >99% of OTU's were detected, with Ace and Chao1 values also indicating an increase in microbial diversity within the bulk liquid (Table 8.2). Principle components analysis showed that both biofilm and bulk communities under sulphate-reducing conditions clustered closely together (Figure 8.17A), however methanogenic communities were highly dissimilar, with heat-maps suggesting these variations were due to Proteobacteria, Bacteroidetes and Euryarchaeota (Figure 8.17B). Independent t-tests confirmed the variation in communities between methanogenic and sulphate-reducing conditions (Figure S8.1) and between biofilms and bulk phases (Figure S8.2). Independent t-tests revealed Proteobacteria ( $P=0.023$ ), Actinobacteria ( $P=0.017$ ), Synergistetes ( $P=0.016$ ) and Euryarchaeota ( $P=0.016$ ) were significantly different when comparing methanogenic and sulphate-reducing communities, with no differences in Firmicutes ( $P=0.168$ ) and Bacteroidetes ( $P=0.055$ ). The differences between bulk liquid and biofilm communities was due to variation in the phyla Actinobacteria ( $P=0.000$ ) and Bacteroidetes ( $P=0.009$ ).

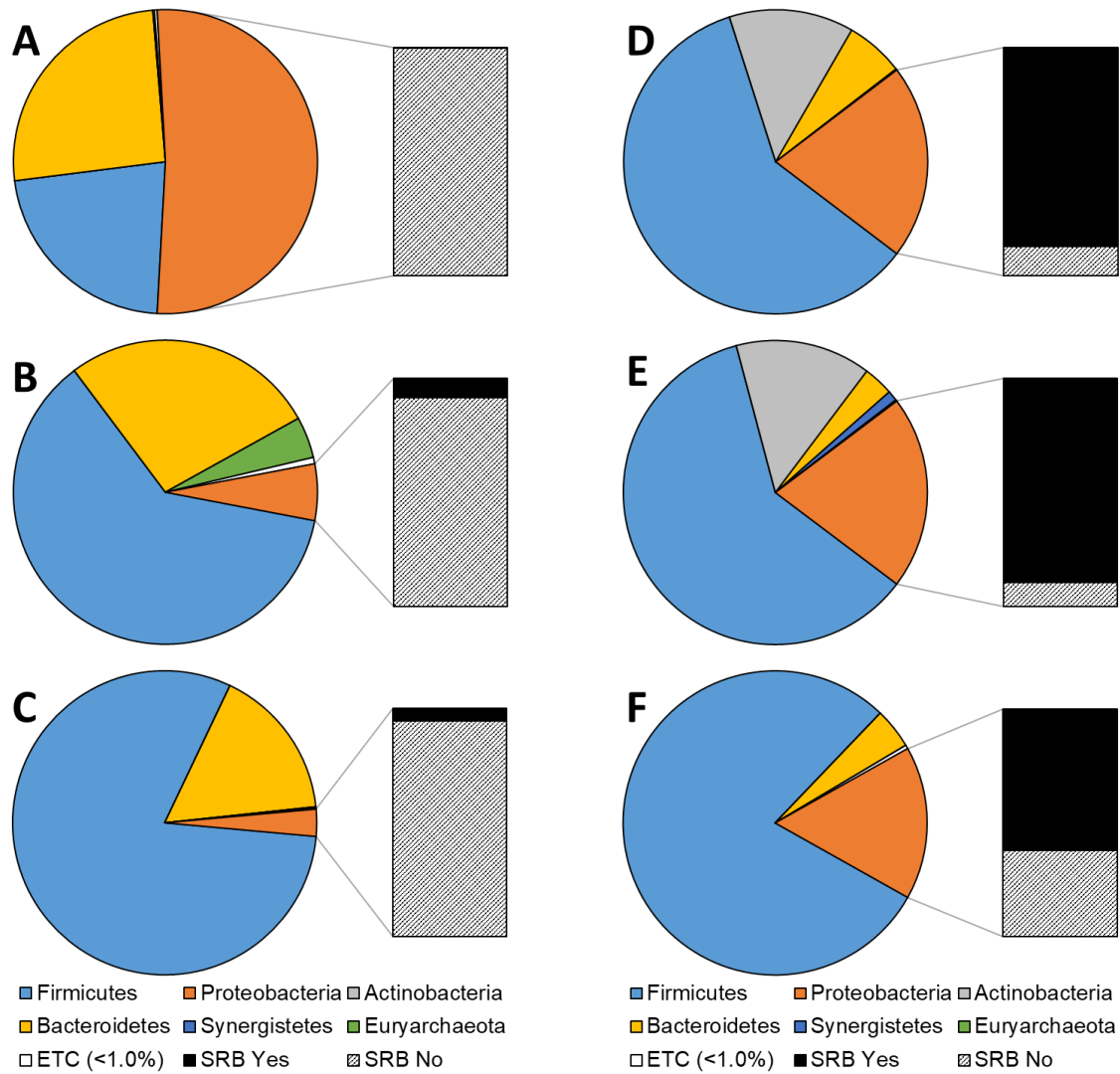


**Figure 8.14 Phylum-level community analysis of methanogenic and sulphate-reducing biofilms and bulk liquid at pH 11.0.** Showing phylum-level composition of methanogenic biofilms on grade 304 steel (A), 316 steel (B) and bulk liquid (C), along with sulphate-reducing biofilms on grade 304 steel (D), 316 steel (E) and bulk liquid (F). ETC group signifies anything representing < 1.0% of the total 16S rRNA gene reads.

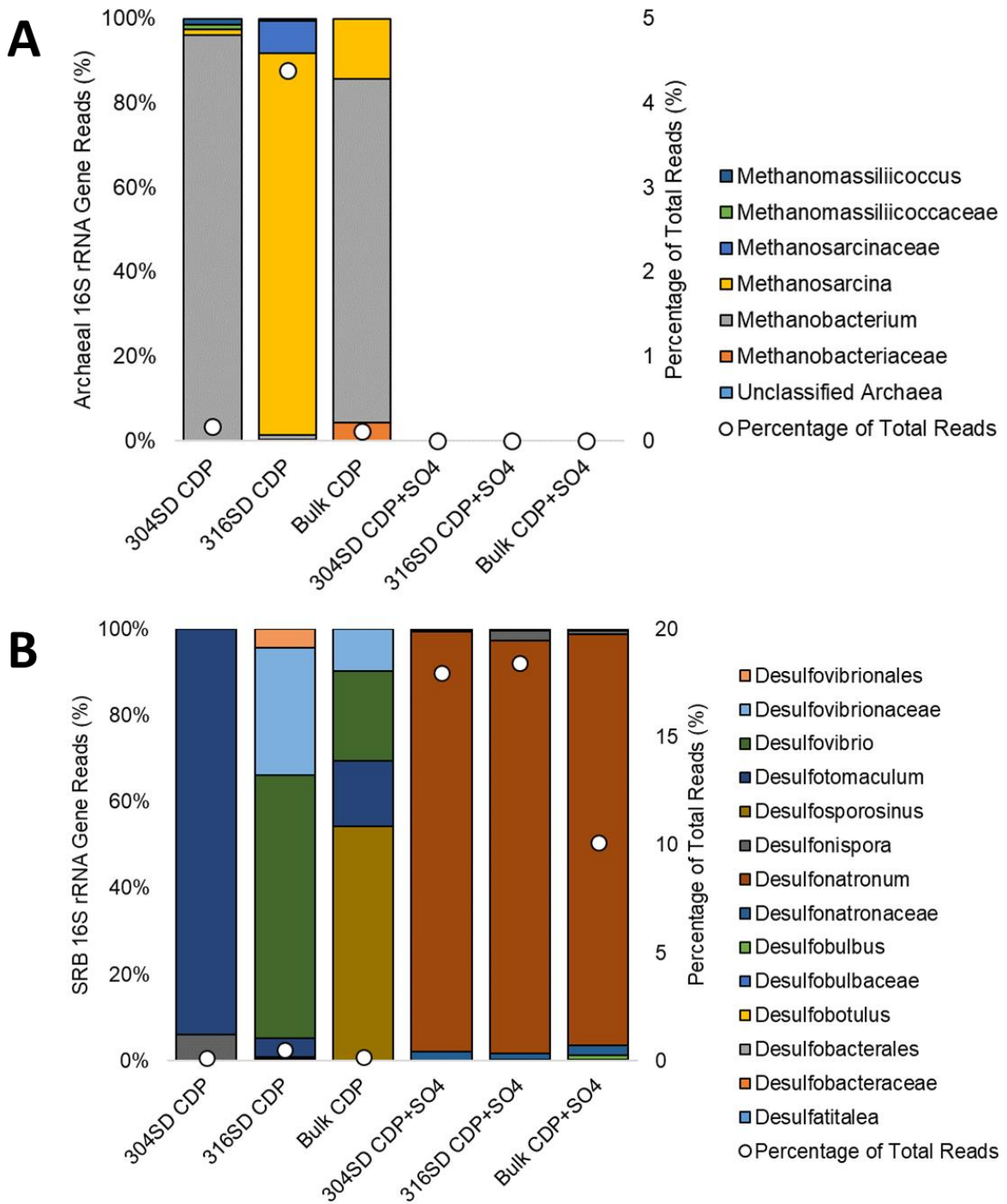


**Figure 8.15. Genus-level community analysis of methanogenic and sulphate-reducing biofilms and bulk liquid at pH 11.0.** Showing genus-level composition of archaea (A) and sulphate-reducing bacteria (B) of biofilms and bulk liquid under methanogenic and sulphate-reducing conditions.

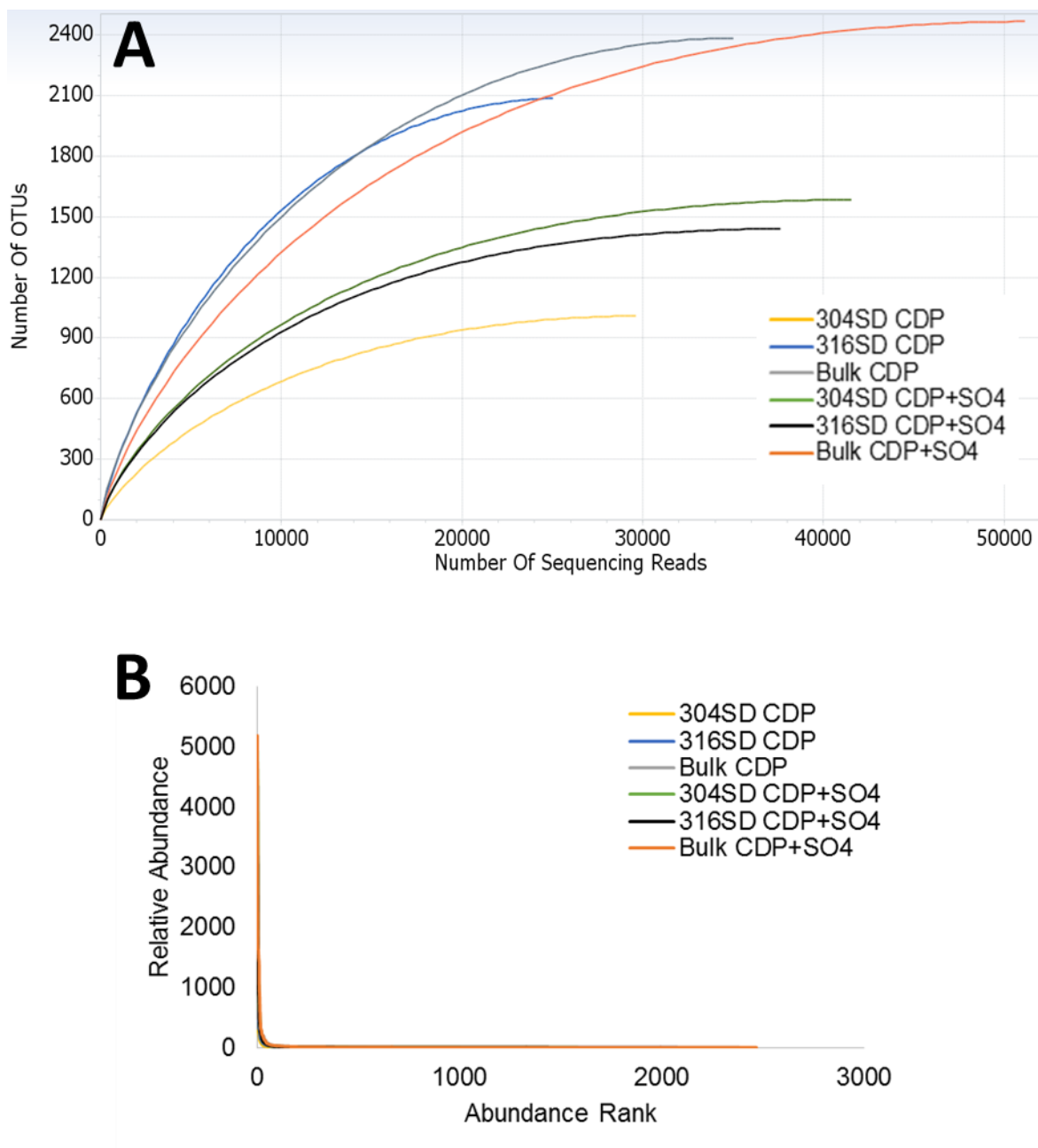


**Figure 8.16. Rarefaction and rank abundance curves of biofilms and bulk communities under sulphate-reducing and methanogenic conditions. (A) Rarefaction curves showed samples reached saturation. (B) Rank abundance indicates microbial communities were diverse.**

**Table 8.2. Alpha diversity statistics of biofilms and bulk communities under sulphate-reducing and methanogenic conditions.** Species richness and biodiversity increased within the bulk liquid community under both methanogenic and sulphate-reducing conditions.

	<b>Valid reads</b>	<b>OTUs</b>	<b>Ace</b>	<b>Chao1</b>	<b>Shannon</b>	<b>Goods Lib. Coverage</b>
<b>304SD CDP</b>	46115	1010	1017.9	1010.4	2.96	99.9
<b>316SD CDP</b>	44709	2087	2109.4	2088.7	4.75	99.7
<b>Bulk CDP</b>	59099	2385	2395.5	2385.3	5.10	99.9
<b>304SD CDP+SO4</b>	40865	1585	1590.4	1585.2	4.10	99.9
<b>316SD CDP+SO4</b>	37086	1441	1447.3	1441.4	3.99	99.9
<b>Bulk CDP+SO4</b>	49824	2467	2476.5	2467.4	4.66	99.9

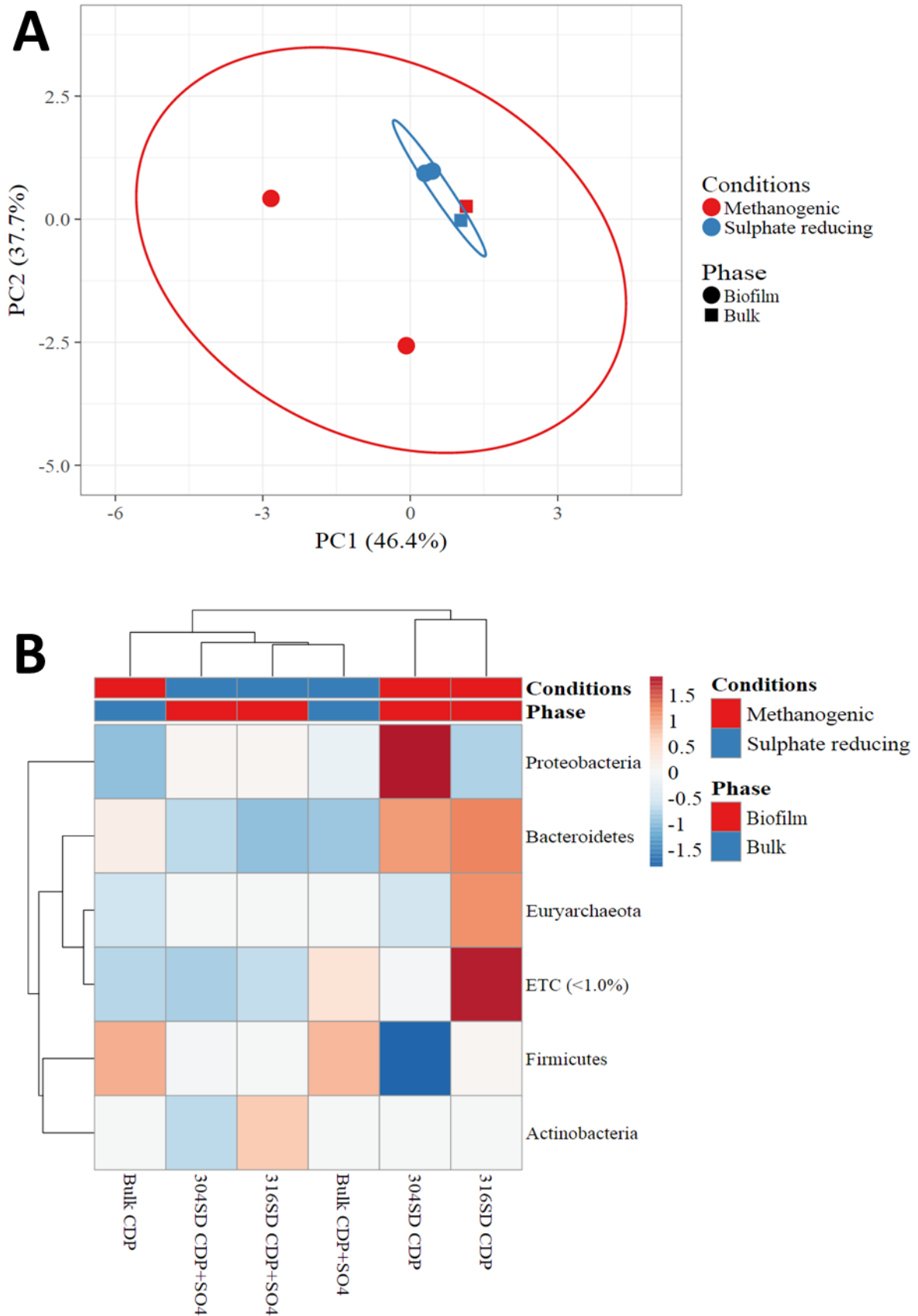


**Figure 8.17. Principle components analysis and heat-map of steel disk biofilm and bulk liquid communities.**

#### 8.2.4.2 Fluorescence In situ Hybridisation

FISH was carried out on sulphate-reducing biofilms to confirm the presence of SRB and to determine the community structure. The probes used to visualise the individual phyla were specific for the Firmicutes, Bacteroidetes and Deltaproteobacteria class, since these lineages were all detected within the sulphate-reducing biofilms as described in Section 8.2.4.1. All SRB's detected in the community analysis were members of the Deltaproteobacteria class and *Desulfonatronum* genus. Furthermore, a general Eubacterial probe was used to visualise the SRB growing in association with the other phyla present. Visualisation of the Deltaproteobacteria revealed rod-shaped cells growing individually and in chains within the biofilm matrix, alongside Eubacteria (Figure 8.16ABC). SRB appeared to be growing in close association with the Firmicutes (Figure 8.17) which are likely candidates for fermentation processes within the biofilm (23). The growth of SRB in close proximity with fermentative species would give them easy access to electron donors (i.e. hydrogen and acetate) for respiration. Furthermore, the detection of fermentative bacteria within the internal biofilm architecture further supports the assumption that acetate production is resulting in the generation of low pH sites mentioned in Section 8.2.2.1 and the SRB were growing in association with these lower pH niches. Interestingly, the Bacteroidetes appeared to be concentrated on the periphery of the biofilm (Figure 8.17), with Proteobacteria and Firmicutes focused within the centre, suggesting a syntrophic community structure was present. Since the majority of SRB were detected within the centre of the biofilm surrounded by dense clusters of cells, this will provide an additional barrier to the more extreme bulk fluid conditions and facilitate their survival at high pH.

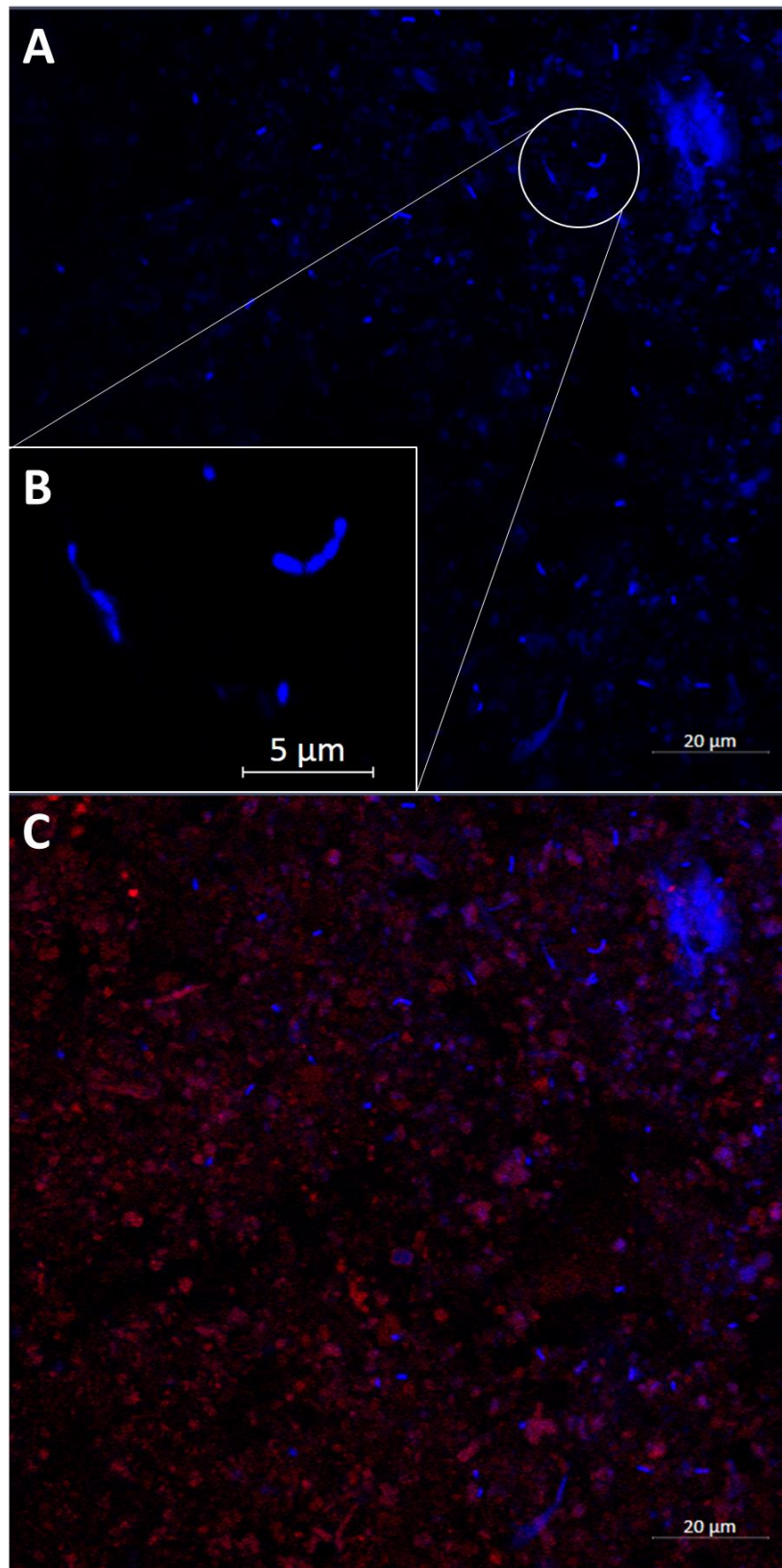


**Figure 8.16. FISH investigation of sulphate-reducing biofilms.** Showing distribution of Deltaproteobacteria (Blue) and Eubacteria (Red) throughout the sulphate-reducing biofilm. (A) Deltaproteobacteria only, (B) zoomed image of rod-shaped Deltaproteobacteria chains, (C) Deltaproteobacteria and Eubacteria together.

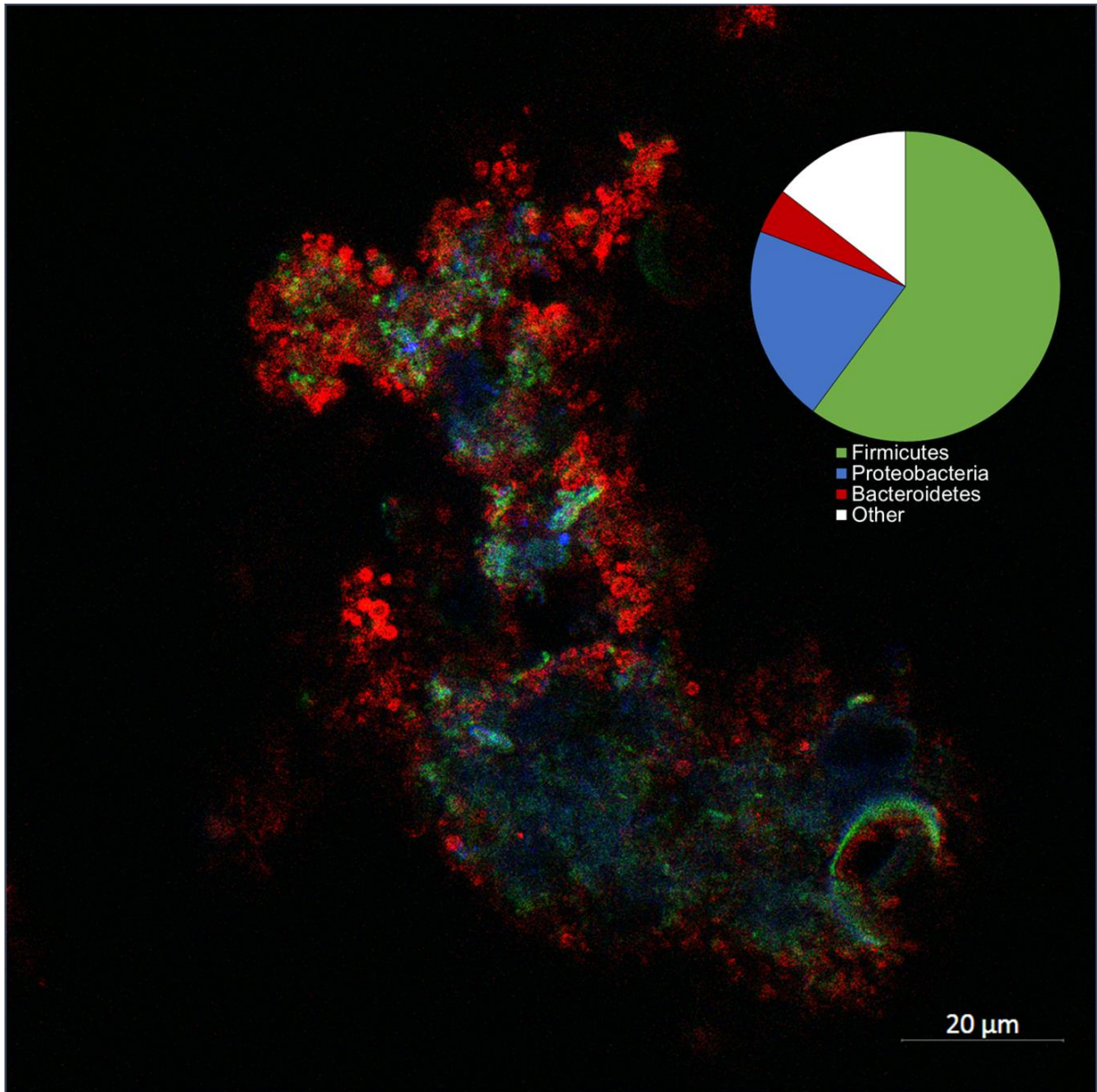


**Figure 8.17. FISH investigation of sulphate-reducing biofilms.** Shows Bacteroidetes (Red), Proteobacteria (Blue) and Firmicutes (Green) within biofilms grown on steel surfaces under sulphate-reducing conditions at pH 11.0.

## 8.2.5 Steel Surface Characterisation

### 8.2.5.1 Scanning Electron Microscopy

The ability of the sulphate-reducing and methanogenic biofilms to corrode grade 304 and 316 steel was analysed. The biofilm materials were removed from the steel coupons via a nitric acid wash for surface characterisation via SEM, with abiotic control disks undergoing the same washing step to eliminate bias. Morphological characterisation of surfaces via SEM revealed significant differences between biotic coupons incubated under sulphate-reducing conditions and abiotic controls (Figure 8.18). Abiotic coupons incubated under the same conditions as biotic experiments had an identical morphology to disks received on shipment (Figure 8.18AB), with smooth surfaces and no evidence of pitting corrosion, suggesting the experimental conditions did not solely impact surface morphology. Abiotic coupons incubated under high sulphide concentrations (10X greater than sulphate-reducing reactors) for the same time period showed evidence of corrosion (Figure 8.18CD), signified by the porous nature of the surface and by the presence of small (dia. <math>< 5 \mu\text{m}</math>) pits. Interestingly, dark pitted areas were also detected on the surfaces of biotic coupons incubated under sulphate-reducing conditions (Figure 8.18EF), however the quantity and diameter of pits was significantly reduced compared to positive controls, presumably due to the difference in sulphide concentration. The pits observed in this study had a similar morphology to previous work investigating MIC of grade 304 and 316 stainless steel using *Bacillus* and *Geobacillus* species as biofilm formers (392). Grade 304 steel appeared to have a larger number of pits compared to 316 steel (Figure 8.18EF), with these differences likely to be a result of the composition of steel. Previous work has demonstrated that steel corrosion resistance increases due to the presence of molybdenum as alloy (393), which could explain the reduced number of pits formed on grade 316 steel compared to grade 304 in this study. The morphology of disks retrieved from methanogenic reactors were comparable with negative controls (Figure S8.3), suggesting the corrosion observed in this study was due to the production of sulphide.

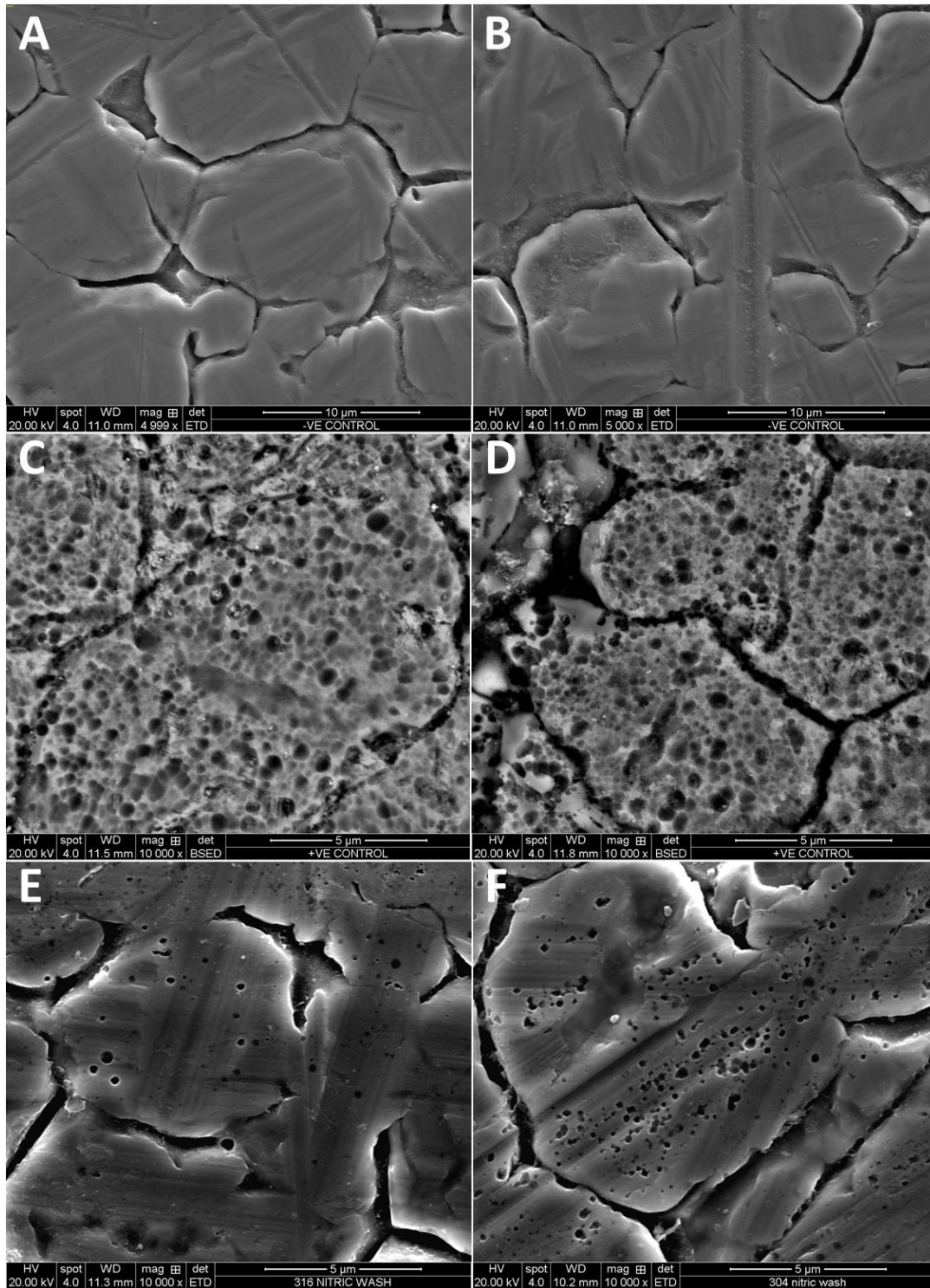


**Figure 8.18. Steel surface characterisation.** Scanning electron micrographs of steel surfaces after incubation under sulphate-reducing at pH 11.0 for 3 months. Shown are negative control abiotic coupons grade 304 (A) and 316 (B), positive control abiotic coupons grade 304 (C) and 316 (D) exposed to high sulphide concentrations and biotic coupons after removal of sulphate-reducing biofilm materials grade 304 (E) and 316 (F).

### **8.2.5.2 Atomic Force Microscopy**

To supplement the surface characterisation, AFM of the steel coupons was undertaken on abiotic controls and disks retrieved from sulphate-reducing reactors. In similar fashion to the SEM images (Figure 8.18), the morphology of negative controls, positive controls and biotic disks were significantly different (Figure 8.19). Negative control surfaces (Figure 8.19AB) had a smooth gentle downward slope compared to positive controls (Figure 8.19CD) which had a rougher surface with a large number of peaks and troughs indicative of pitting corrosion. Biotic surfaces taken from sulphate-reducing reactors were comparable with positive controls and previous work using AFM to detect corrosion pits (109), which validates the SEM imaging undertaken in Section 8.2.5.1. Furthermore the pits detected via AFM had a similar diameter to those detected via SEM ( $<5 \mu\text{m}$ ). Although a number of previous studies have shown that SRB are capable of localised corrosion attack on carbon and stainless steel surfaces under neutral-pH conditions (109, 394, 395), bio-corrosion under alkaline conditions has never been demonstrated. Coupons incubated under methanogenic conditions could not be sampled due to time constraints, however future work could investigate the ability of none-sulphate reducing communities at corroding steel.

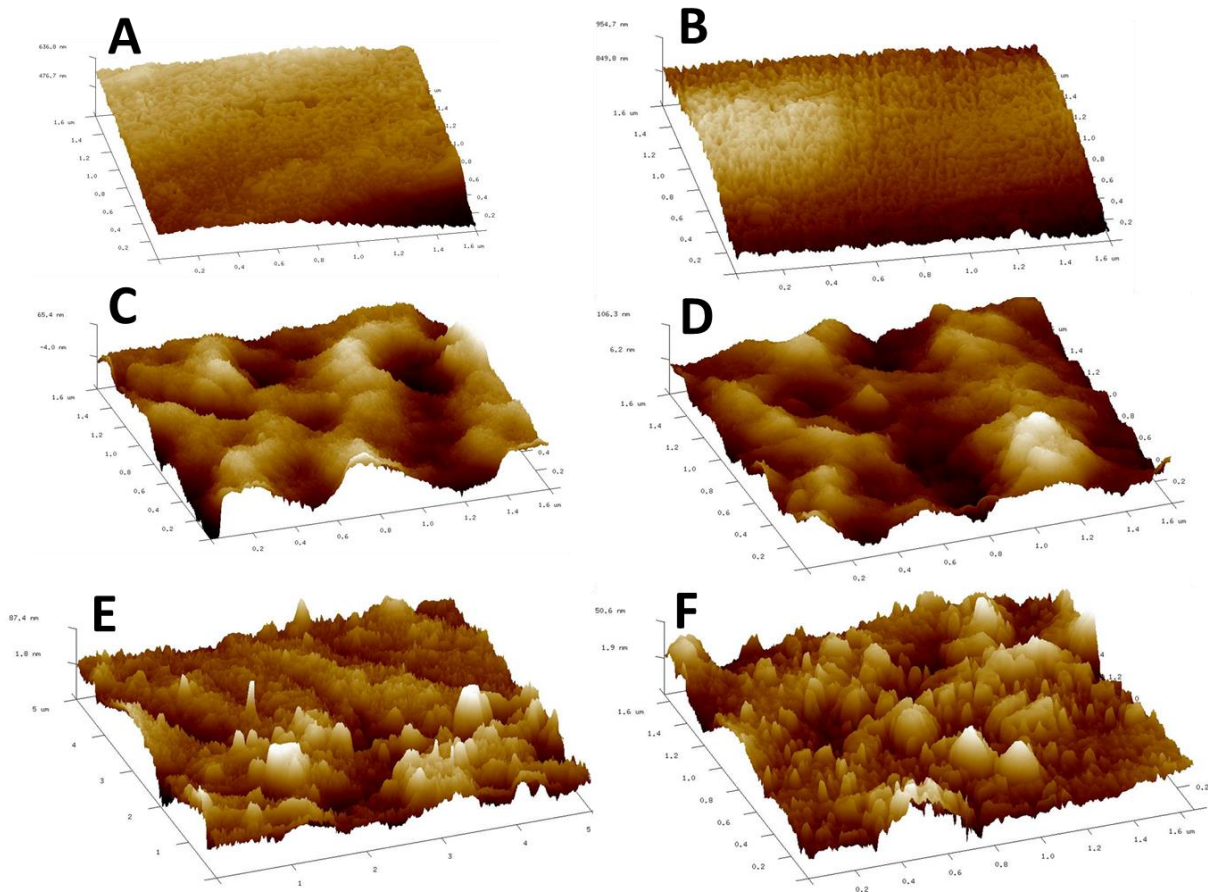


**Figure 8.19. Steel surface characterisation.** Atomic force micrographs of abiotic negative control coupons grade 304 (A) and 316 (B) stainless steel. Grade 304 (C) and 316 (D) positive control steel coupons after incubation under high sulphide concentrations for the same time period as biotic experiments. Biotic steel surfaces after removal of sulphate-reducing biofilms grade 304 (E) and 316 (F).

### 8.2.5.3 Alicona

A high resolution replication material (Microset) was used to replicate the steel surface followed by visualisation via an Alicona 3D metrology instrument. In agreement with the SEM and AFM investigation mentioned in Section 8.2.5.1 and 8.2.5.2, replication of the steel surfaces revealed potential pits on disks removed from sulphate-reducing reactors (Figures 8.20 & 8.21) and positive control coupons (Figures 8.22 & 8.23), however no pitting was discovered on negative controls (Figures 8.24 & 8.25). The surfaces of negative controls did have a gradual downward slope, however this appeared to be the natural slope of the steel surface, with the morphology of pits within positive controls being more characteristic of those observed via SEM and AFM. The largest pits present on grade 304 and 316 disks taken from the sulphate-reducing reactors had a diameter of 8-10  $\mu\text{m}$  and depth of 800-1200nm (Figures 8.20 & 8.21). In contrast pits detected on positive controls were wider ( $\approx 20 \mu\text{m}$ ) and deeper ( $>6 \mu\text{m}$ ) (Figures 8.22 & 8.23). The replicating material used here may be unable to discern the full extent of corrosion, since the diameter of the pits observed via SEM were  $<5 \mu\text{m}$ , therefore only the widest pits will be visible using this technique. The fact that no pits with a diameter of  $>5\mu\text{m}$  could be seen on the SEM images in Section 8.2.5.1 does however raise doubt as to whether pits observed in the Microset replicates were valid. Nevertheless, significant differences were observed between controls and biotic coupons in similar fashion to the SEM and AFM investigations.

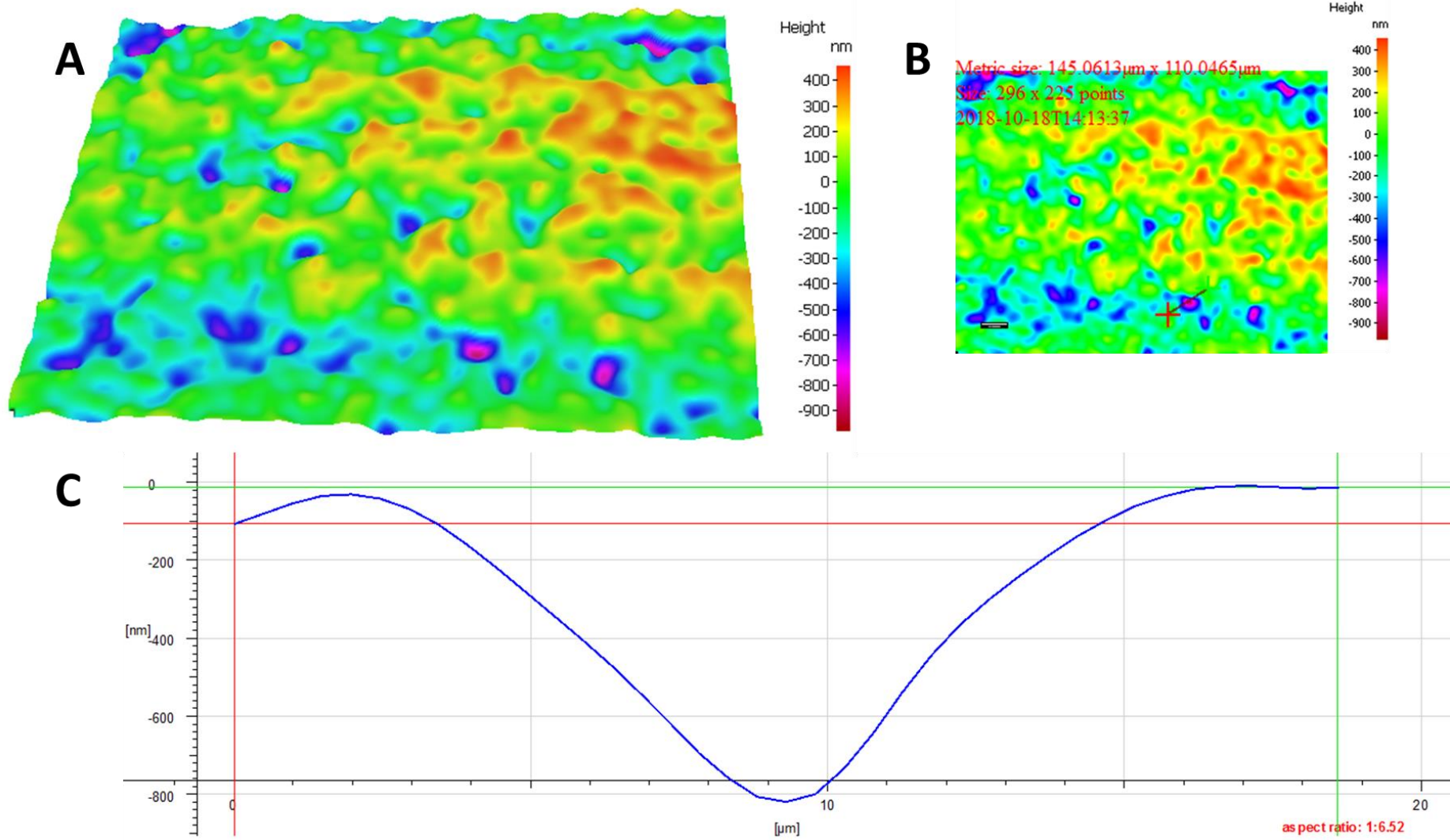


**Figure 8.20. Steel surface characterisation of grade 304 biotic steel surfaces via Alicona.** Grade 304 steel surfaces after removal of sulphate-reducing biofilm materials.

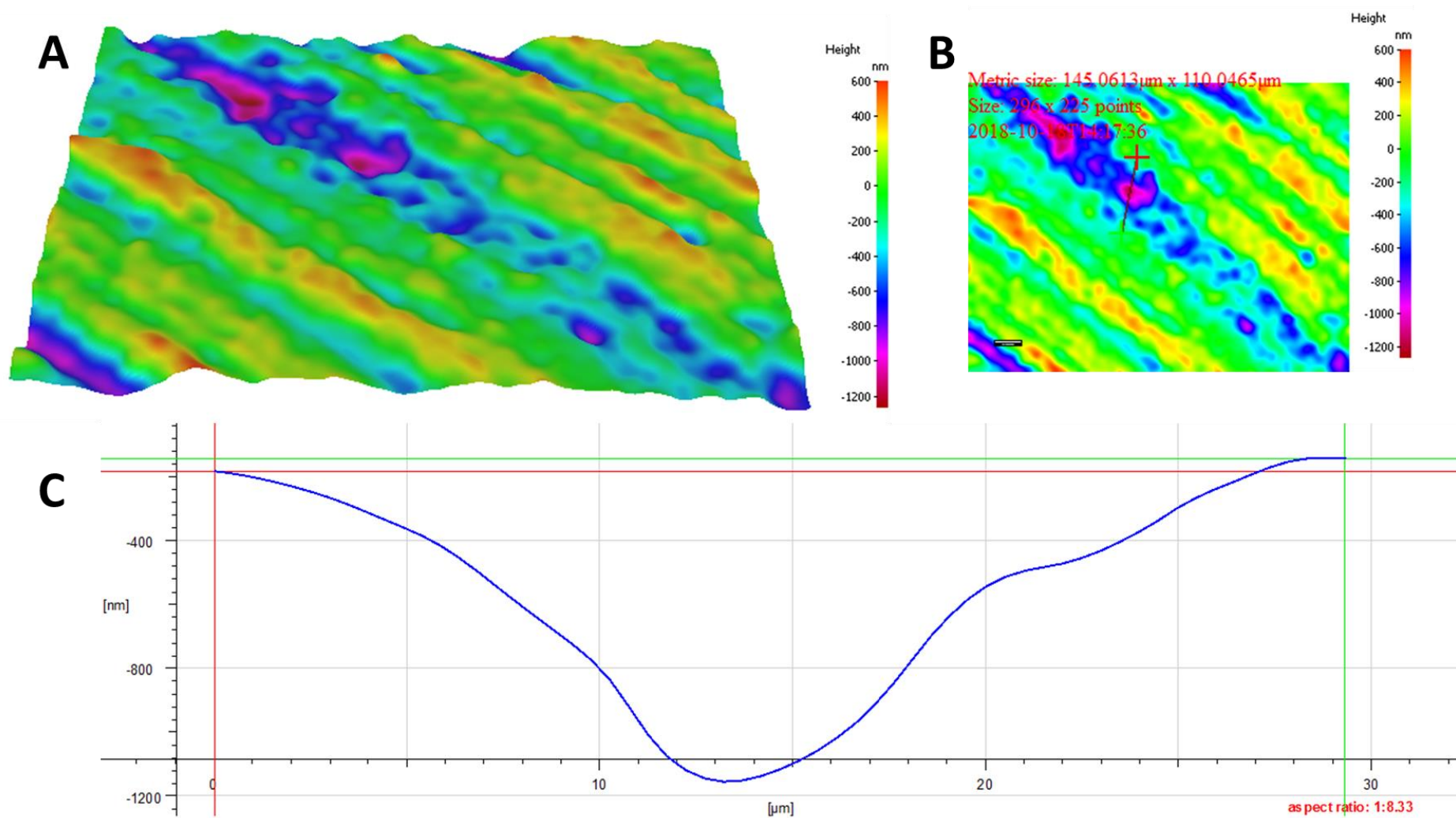


**Figure 8.21. Steel surface characterisation of grade 316 biotic steel surfaces via Alicona.** Grade 316 steel surfaces after removal of sulphate-reducing biofilm materials.

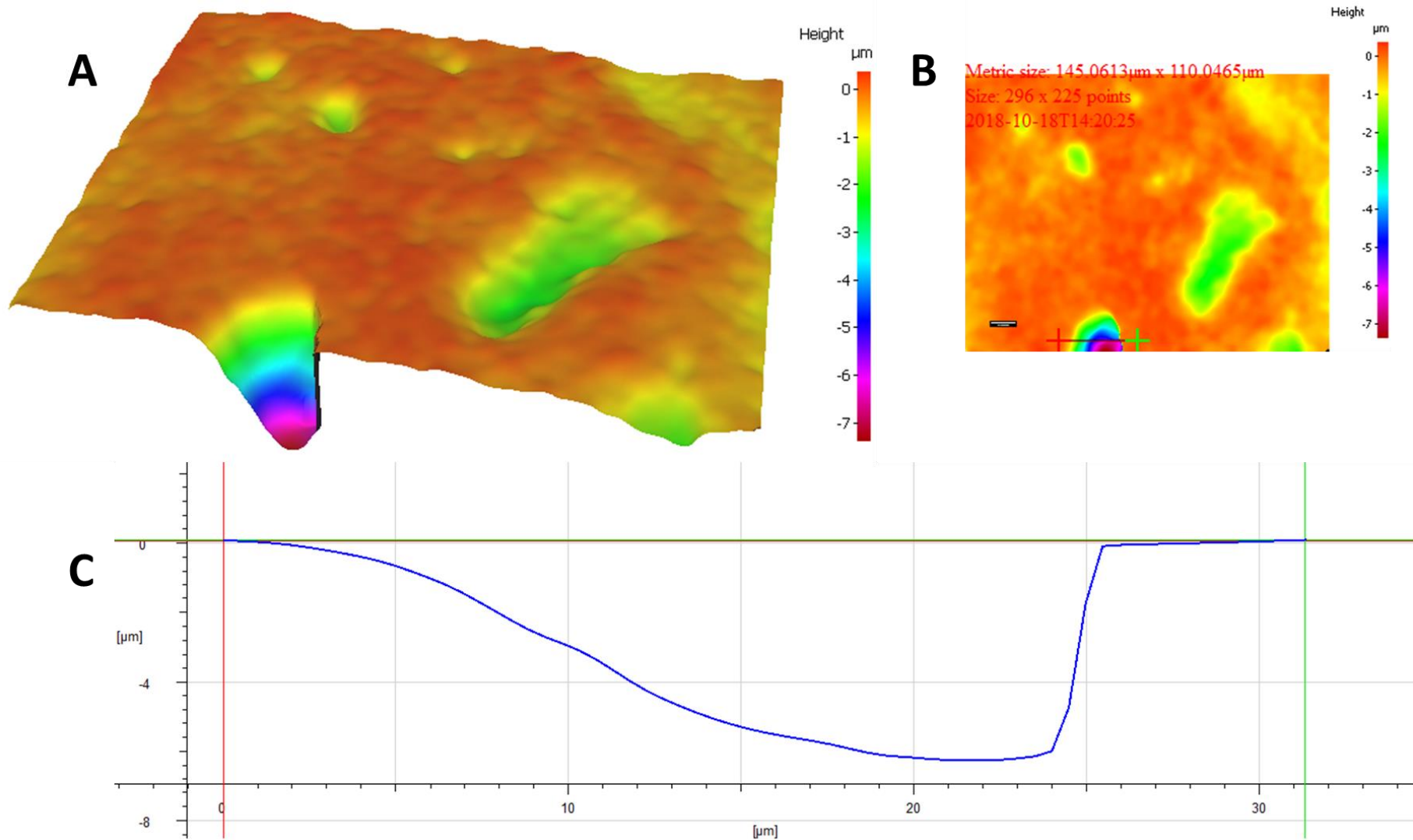


**Figure 8.22. Steel surface characterisation of grade 304 abiotic positive controls via Alicona. Grade 304 positive control steel surfaces**

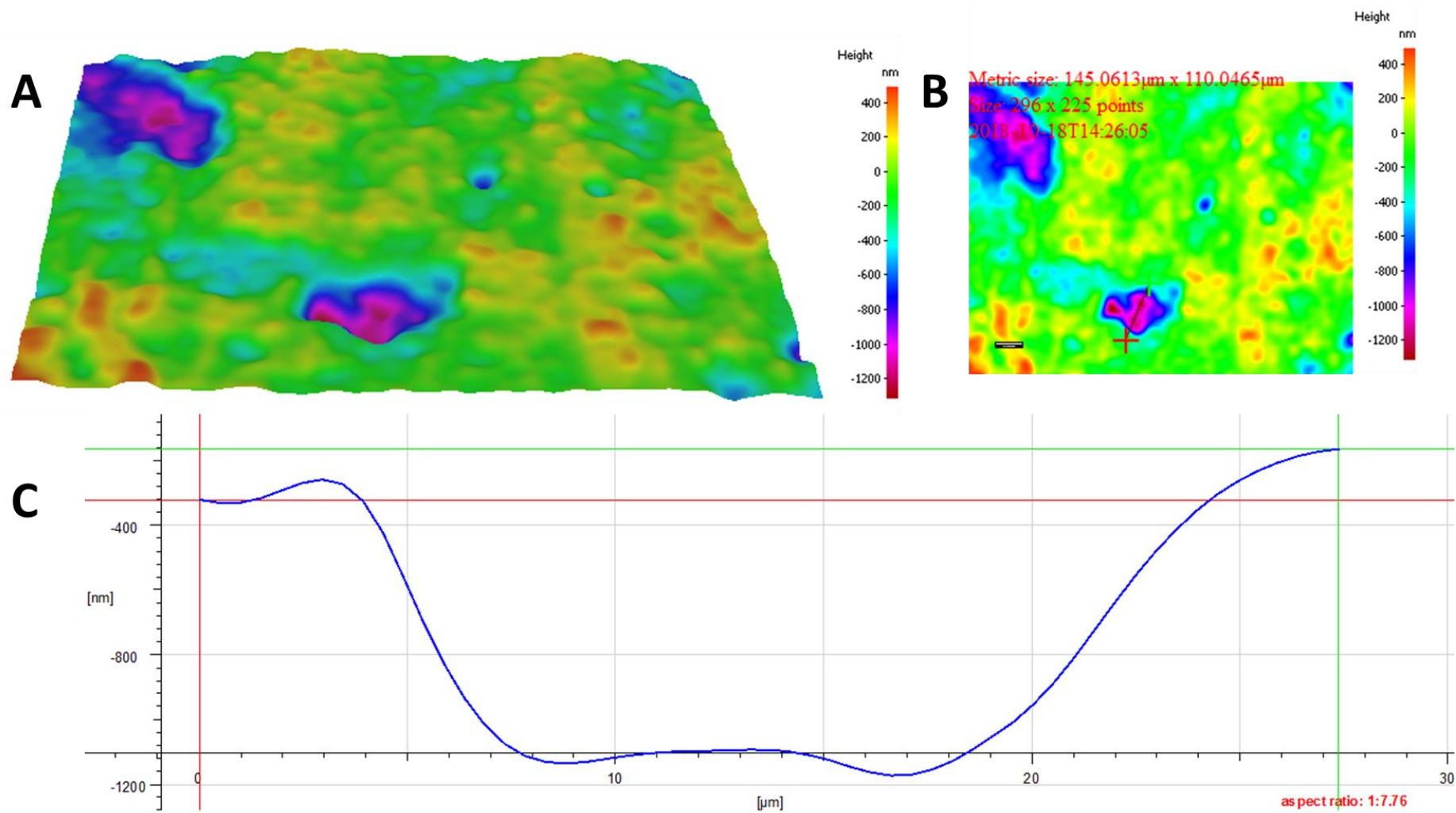


**Figure 8.23. Steel surface characterisation of grade 316 abiotic positive controls via Alicona. Grade 316 positive control steel surfaces**

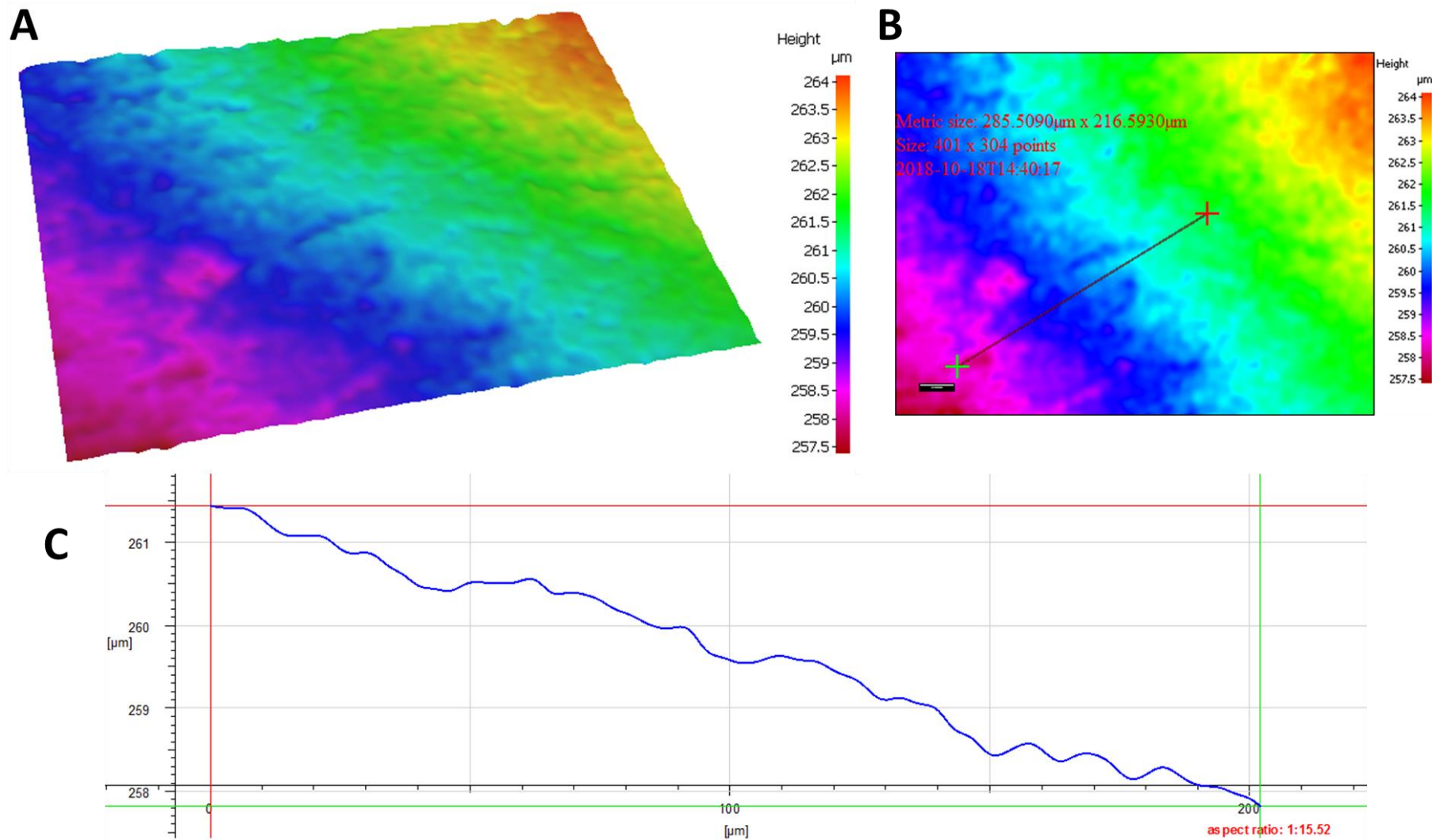


**Figure 8.24. Steel surface characterisation of grade 304 abiotic negative controls via Alicona. Grade 304 negative control steel surfaces**

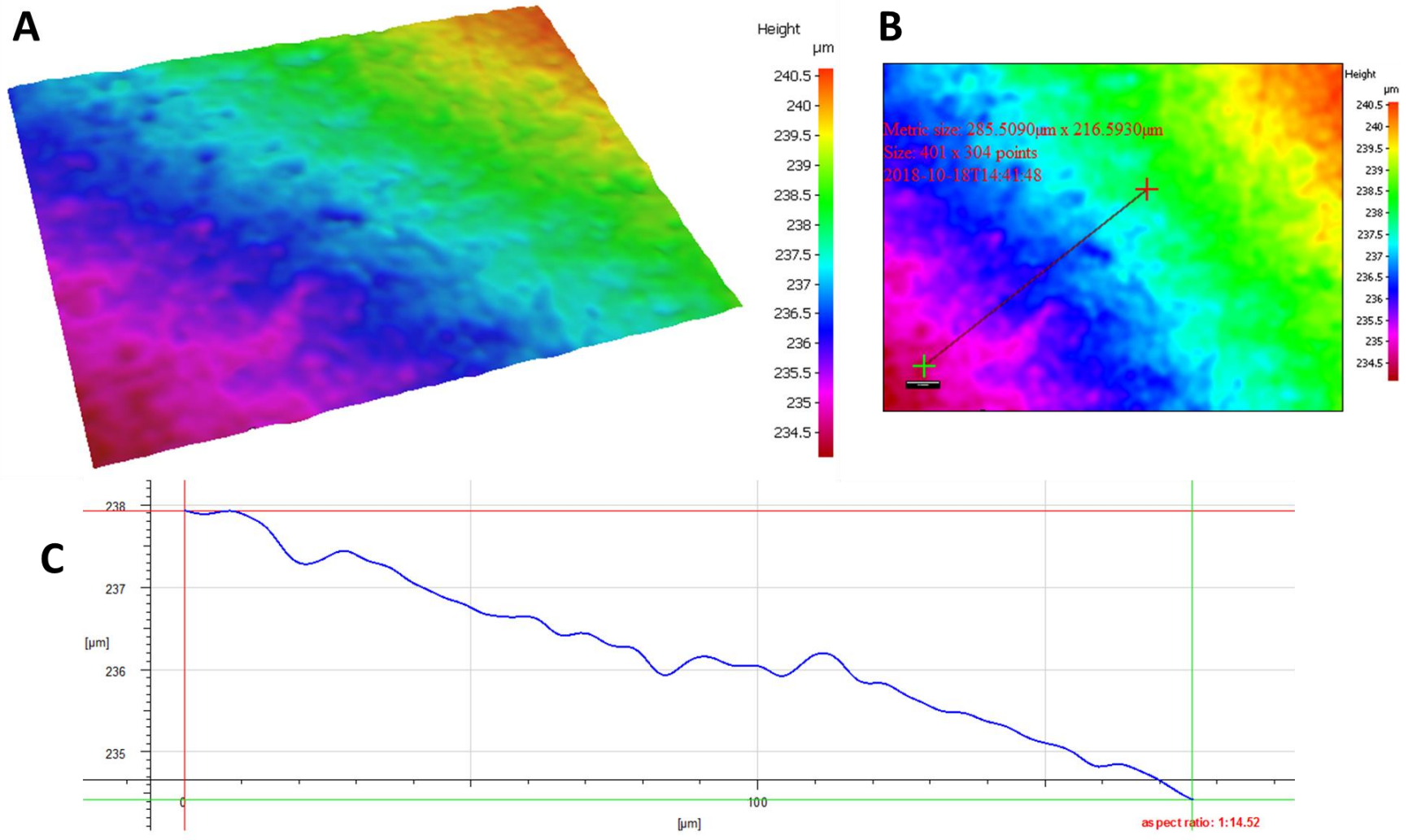


**Figure 8.25. Steel surface characterisation of grade 316 abiotic negative controls via Alicona. Grade 316 negative control steel surfaces**

### 8.3 Conclusions

As biofilms develop and grow over time micro-environments are able to form that have different physical and chemical conditions than that of the bulk fluid phase. The formation of these micro-niches is a result of consumption and production of metabolic products, together with the limited diffusion of chemical species due to the production of EPS. Within the present study microorganisms harvested from an anthropogenic alkaline site in the UK were capable of degrading ISA at pH 11.0 under methanogenic and sulphate-reducing conditions in biofilm systems. The fermentation of ISA provided electron donors (hydrogen and acetate) for downstream anaerobic respiratory processes, including sulphate-reduction and methanogenesis. The addition of sulphate as TEA inhibited methanogenesis and resulted in the generation of sulphide, suggesting dissimilatory pathways were active and SRB were outcompeting methanogens for fermentation end-products. The reduced abundance of SRB detected in the bulk fluid suggests the majority of sulphate-reducing activity was present in the biofilm, where low pH microsites were detected. Only one genus of SRB was detected with any significance, namely the alkaliphilic *Desulfonatronum*, suggesting its importance within alkaline systems. The high concentration of H<sub>2</sub> at the interface between the steel surface and sulphate-reducing biofilm is an indicator of anaerobic corrosion and could provide SRB with a constant source of hydrogen for further metabolism. The high proportion of lipids and protein within the biofilms contributes to their hydrophobicity and allows for the development of low pH micro-niches and H<sub>2</sub> gradients within the biofilm matrix. FISH of the biofilms revealed a syntrophic community structure where SRB were growing in association with fermentative bacteria within the centre of the biofilm, where conditions were more favourable for growth. The morphology of the steel surfaces changed markedly after incubation under sulphate-reducing conditions for 3 months, with surfaces showing evidence of pitting corrosion as detected by SEM, AFM and Alicona. This is the first study to demonstrate bio-corrosion of stainless steel due to sulphate-reduction at pH 11.0 and indicates a potential route for the corrosion of steel surfaces within an ILW-GDF.

## **9.0 Concluding Remarks**

Microorganisms have successfully colonised every environment on earth where water can be found and therefore an ILW-GDF could provide a niche site for a range of specialist organisms. An ILW-GDF is expected to be operational for thousands of years' post-closure and the ability to predict the evolution of such a facility requires extensive research from a wide range of scientific disciplines. One important aspect when trying to predict the evolution of an ILW-GDF over long time-frames is determining the potential for microbial activity. The colonisation of a GDF by microorganisms is possible, either during the facilities construction phase or from the subterranean biosphere via ground-water flowing into the facility (396). The organic carbon sources produced from the alkaline hydrolysis of cellulose represent a potential substrate for microbial activity and the generation of gases from these substrates may impact the performance of a GDF (4, 6, 7) (Figure 9.1). The high bulk pH values of the near-field may inhibit microbial activity by neutrophilic organisms, however a variety of microbial processes have been observed in other alkaline environments, such as soda lakes or legacy lime working sites, suggesting alkaliphilic microbial processes have the potential to develop given time (154, 397). The metabolism of cellulose degradation products by microorganisms under near-field conditions has been extensively studied (22-25), however very few of these studies have provided information regarding the generation of methane or sulphide under ILW-GDF conditions. The data outlined in this thesis could help to better predict the potential for methane generation and sulphide production within an ILW-GDF.

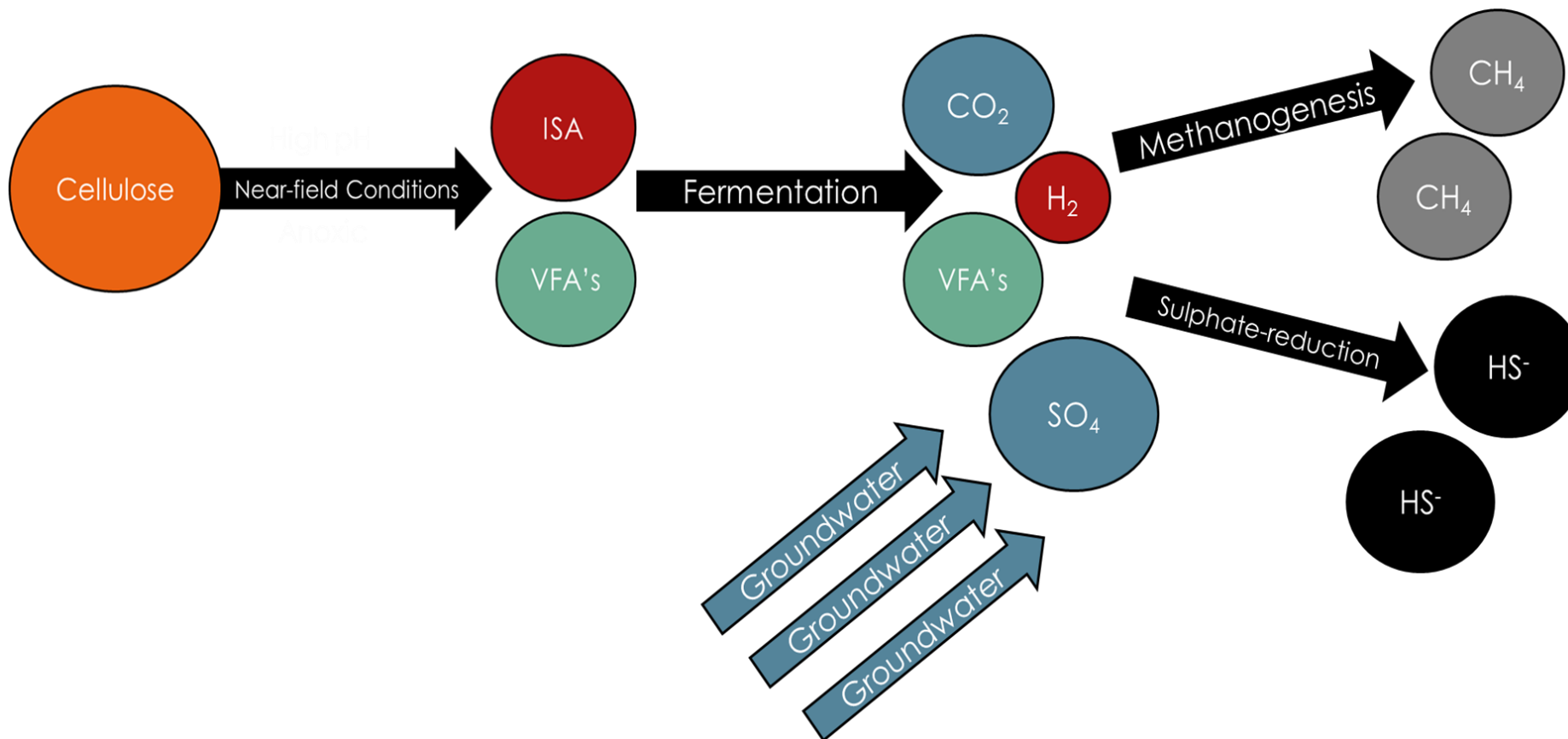


**Figure 9.1. The disposal of cellulose within the near-field of an ILW-GDF will result in the generation of ISA and VFA's through alkaline hydrolysis pathways. The fermentation of these cellulose degradation products provides the substrates for downstream methanogenic and sulphate-reducing processes. Sulphate-rich inflowing ground-water could saturate the facility post-closure, leading to the development of sulphate-reducing and methanogenic conditions within the near-field.**

### **Conclusion 1a: Anthropogenic alkaline sites with analogous conditions to an ILW-GDF harbour active methanogenic and sulphate reducing communities.**

The aim of the first section of work described in Chapter 5 was to characterise the near-surface (~1 m deep) anaerobic microbial communities within a range of anthropogenic alkaline sites that demonstrated bulk pH values similar to those likely to be experienced within an ILW-GDF (pH 11.0 – 13.0). The incubation of cellulose within these sites for 3 months provided a substrate for microbial colonisation and allowed for direct comparisons to be made between the different sampling sites. The extraction of RNA from these extreme environmental samples followed by the generation of cDNA and sequencing of the 16S rRNA gene was employed to provide an active *in situ* community profile, primarily focused on the microbial pathways that result from cellulose degradation, i.e. sulphate-reduction and methanogenesis. The ability of cellulosic materials to provide the substrates for sulphate-reduction and methanogenesis in these environments indicates the potential for these processes to occur within an ILW-GDF.

Not only was biofilm able to form on the incubated cellulose, but a diverse and active microbial population was present, capable of anaerobic processes including cellulose degradation, sulphate reduction and methanogenesis, despite the harsh environmental conditions. Although cellulose is susceptible to alkaline chemical hydrolysis in these sites (24), a significant proportion of the RNA extracted from the incubated samples had 16S sequence homology to cellulose-degrading bacteria, including members of the family *Fibrobacteraceae* and genus *Fibrobacter*, suggesting microbial activity played a significant role in the degradation of cellulose in these environments. The majority of cellulose within an ILW-GDF is expected to degrade through abiotic alkaline hydrolysis pathways (6), however biotic cellulose degradation within the near-field could stimulate downstream methanogenic and sulphate-reducing processes through the production of fermentation end-products. The detection of fermentative *Clostridia* lineages on the cellulose samples, including the genus *Ruminococcus* indicates a further route for cellulose degradation and potentially ISA fermentation *in situ*. *Clostridia* have been identified as potential ISA-degrading bacteria in microcosms employing sediments from some of the lime-contaminated sites studied here (24) and the removal of ISA within an ILW-GDF could influence the mobility of radioelements.

Hydrogen appeared to be an important end-product of cellulose degradation in these sites, evidenced by an archaeal community almost exclusively dependent on hydrogenotrophic methanogenesis, with the genera *Methanoregula*, *Methanoculleus* and *Methanospirillum* dominating. The ubiquitous nature of hydrogen-consuming bacteria of the genus *Hydrogenophaga* throughout these sites further underlines the importance of H<sub>2</sub> within an ILW-GDF. Within the younger sulphate-rich and organic-rich steel slag sites that demonstrated lower bulk pH values (~11.0), dissimilatory sulphate reduction played an important terminal role in the complete mineralisation of organic matter, where acetate-metabolising SRB of the genus *Desulfobacter* were abundant, a process which appeared to be competing with acetoclastic methanogenesis and resulting in a methanogen community dominated by hydrogenotrophic species. This could suggest that an ILW-GDF saturated with sulphate-rich ground-waters could result in a decreased contribution of acetoclastic methanogenesis under alkaline conditions through competition with SRB. It has been theorised that acetate-driven sulphate reduction becomes more favourable under alkaline conditions (398). Even though sulphate was detected in the sites that demonstrated the highest bulk pH values (~13.0), SRB were largely absent from these environments, even though methanogenic archaea were still able to maintain a population under these conditions. This suggests under environmental conditions the upper pH limits is higher for methanogenesis than for sulphate reduction.

Although the active methanogen population on the cellulose samples were strictly hydrogenotrophic, methanogens capable of all three pathways were detected in the sediments of the organic-rich steel slag sites and acetoclastic methanogens dominated the neutral-pH canal sediments, however this was based on DNA (rather than cDNA) sequencing and so does not account for dormant microbial populations. The pH appeared to be an important driver of microbial community composition in these sites, with comparisons between non-contaminated background sediments and contaminated alkaline sediments showing significant differences at the phylum level based on principal components analysis. However, these differences could also be due to factors other than pH, for example organic carbon content appeared to play a small role in shaping the methanogen communities in these environments, where an increase in acetoclastic lineages was observed in the sites with higher organic carbon content ( $R^2 = 0.4247$ ). Fermentative lineages of the phylum Firmicutes tended to increase in abundance within the alkaline-disturbed zones of these sites, potentially due to their ability to form spores

(280), which could be advantageous to their survival within an ILW-GDF. Spore-forming bacteria could be important within the early post-closure period when microbial activity will be limited by bulk pH values of  $>13.0$ . As the pH of the near-field evolves towards more agreeable values (pH 10.0 – 12.5) (Figure 9.2), niche sites may develop that enable dormant populations to become active and result in the colonisation of a GDF.

Overall the data shown in Chapter 5 suggests the products of alkaline and microbial cellulose degradation can support hydrogenotrophic methanogenesis in near-surface sediment communities up to pH  $\sim 13.0$  under environmental conditions. Within sulphate-rich and organic-rich near-surface sediments, these cellulose degradation products can also stimulate sulphate reduction up to pH  $\sim 11.0$  under environmental conditions. This data suggests the upper pH limits for methanogenesis is higher than sulphate reduction under environmental conditions, which reduces the potential for sulphide production within the early post-closure period of an ILW-GDF.

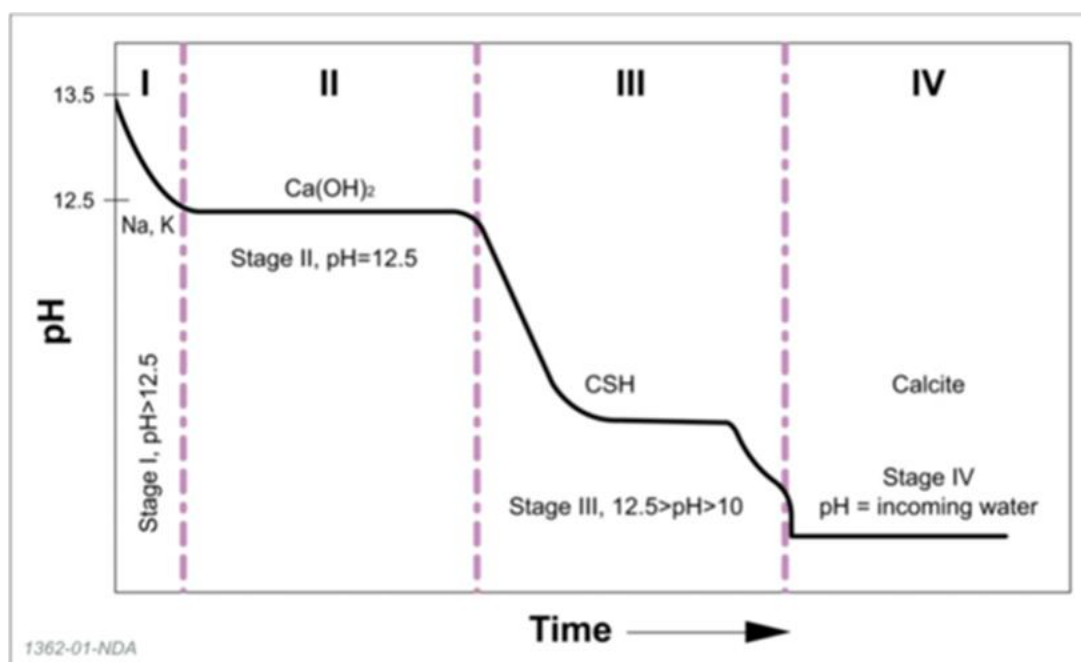


**Figure 9.2. Evolution of pH within the near-field of an ILW-GDF.** Initial pH values of  $>12.5$  are expected within the early post-closure period, however these values are expected to drop to 10.0-12.5 during the late post-closure period. Taken from (6).

## **Conclusion 1b: Microbial activity within anthropogenic alkaline sites is facilitated by the formation of low pH microsites.**

A significant amount of microbial activity was detected within the sampling sites using culture-independent molecular methods, even when bulk pH values of ~13.0 were observed. However, a considerable amount of microbial activity could be ongoing under conditions much milder than this. For example, sediment pH values were always lower than pore-water values and the detection of fermentation end-products (e.g. acetate) within these sites suggests low pH niches could be formed through the production of metabolic acids. A range of EPS materials were detected on the cellulose samples, suggesting biofilm was being formed *in situ* which could be relieving the environmental stresses associated with high pH (112, 125). The dominance of *Pseudomonas* lineages on many of the cellulose samples suggests they were contributing to biofilm formation in these environments, with many strains of this genus capable of EPS production and growth under anaerobic conditions using nitrate as electron acceptor (399, 400). The EPS components were primarily composed of protein and lipid biopolymers, which is likely to be reducing the impact of the high pore-water pH through hydrophobic interactions. The formation of biofilm could negatively impact a GDF not only through facilitating microbial survival, but also through the corrosion of materials and the blocking of pore throats leading to 'bio-clogging' and potential pressurisation issues (401, 402). Therefore, the ability of these alkali-adapted near-surface communities to form biofilm, even when bulk pH values of ~13.0 are observed, underlines their ability to survive under ILW-GDF conditions. Biofilms have been shown to offer microorganisms limited (<2 weeks) survival up to pH 13.0 in recent studies (125), and numerous authors have detected low pH niches within the internal surfaces of biofilms compared with the external environment (366, 403). The upper pH limits for microbial activity can differ greatly between planktonic and biofilm systems and between pure and mixed cultures (112, 404). Therefore, the detection of active sulphate-reducing and methanogenic communities within these sites based on molecular methods does not guarantee their survival within a GDF, where a pH of >12.5 is expected for thousands of years (6). However, if low pH microsites develop within the near-field through the production of biofilm and metabolic acids then the data shown in Chapter 5 suggests a range of microbial processes are available and active under bulk pH values of 13.0, which could have a significant impact on the evolution of an ILW-GDF.

## **Conclusion 2: Hydrogenotrophic methanogenesis dominates under ILW-GDF conditions in mixed culture planktonic systems.**

The next section of work outlined in Chapter 6 aimed to develop acetoclastic and hydrogenotrophic methanogen enrichment cultures under fermentative and non-fermentative conditions over a range of pH values (7.0 – 12.0) using near-surface sediments from the anthropogenic alkaline sites described in Chapter 5. Preliminary experiments utilised neutral-pH canal sediments as a reference for the alkaline sites. Both acetoclastic and hydrogenotrophic enrichment cultures were successfully developed from these ‘Control’ sediments under neutral-pH conditions. These cultures demonstrated high acetate and hydrogen consumption rates and were dominated by the acetate-utilising lineages *Methanosarcina* and hydrogen-consuming *Methanobacterium* genera. However, after gradually increasing the pH of these microcosms through sub-culturing, the rate of acetate consumption decreased significantly at pH 9.0 and became undetectable at pH 10.0, which resulted in a loss of the acetoclastic population (*Methanosarcina*) from the cultures. However, under the same conditions hydrogenotrophic methanogenesis was still able to proceed, with the hydrogen-consuming genus *Methanobacterium* able to maintain an active population up to pH 10.0. Methyl fluoride inhibited methane production rates in pH 7.0 microcosms, however the inhibitor had little effect on pH 10.0 microcosms and suggested ~73 % of the methane formed under neutral-pH conditions was derived from acetate and only ~13 % at pH 10.0. The enrichment cultures developed from the ‘Control’ sediments demonstrated an interesting shift in methanogen community composition and functioning towards hydrogenotrophic methanogenesis at high pH, which could suggest under near-field conditions methane generation within an ILW-GDF will be reliant on the presence of hydrogen and carbon dioxide. A number of other environments were included in the study to determine whether this trend was ubiquitous.

The alkaline sediments retrieved from the ‘New Lime’ sites (B, H and T) were used in the same way as the ‘Control’ sediments, however enrichment cultures were initiated at pH 10.0. Methanogenesis was stimulated in these cultures when supplied with H<sub>2</sub>/CO<sub>2</sub> compared to unamended controls, however at this pH acetoclastic cultures were negative for methane generation and acetate consumption. All of the microcosms developed from the lime sites were dominated by strictly hydrogenotrophic methanogens of the genera *Methanoculleus* and *Methanobacterium*, even when acetate was available. After gradually decreasing the pH of

these microcosms through sub-culturing, low levels of acetate consumption were observed at pH 7.0 and 8.0, which resulted in low methane production rates, however the community was again dominated by hydrogenotrophic *Methanobacterium* species which suggested SAO played a role in these systems. The addition of methyl fluoride had no impact on the ability of these cultures to generate methane at pH 7.0 or 10.0, which confirmed the presence of SAO pathways under neutral-pH conditions. The inhibitor studies suggested 100 % of the methane formed at pH 7.0 and 10.0 was derived from H<sub>2</sub>/CO<sub>2</sub> when employing the 'New Lime' sediments. The alkaline sediments were capable of methanogenesis from H<sub>2</sub>/CO<sub>2</sub> up to pH 11.0, one pH unit higher than the canal sediments, suggesting the populations within these sites have adapted mechanisms to grow under conditions of higher alkalinity. However, no methane production was observed at pH 12.0, suggesting methanogenesis within the early post-closure period of an ILW-GDF will be reliant on the formation of low pH niches if planktonic systems develop. This also suggests the upper pH limits for methanogenesis decreases in planktonic culture compared to under environmental conditions, since methanogen RNA was obtained from the cellulose samples incubated within the sites where bulk pH values of ~13.0 were observed (Chapter 5). Since the growth conditions imposed on these samples were identical to the 'Control' microcosms which were positive for acetoclastic methanogenesis, it would seem acetate-consuming methanogens were absent from the inoculating samples. It is possible the high pH pore-waters of the lime sites are selecting against acetoclastic species, as observed within the microcosms employing the canal sediments. The use of the lime sediments added confidence to the hypothesis that hydrogenotrophic methanogenesis contributes to the majority of methane produced under near-field conditions (Figure 9.3).

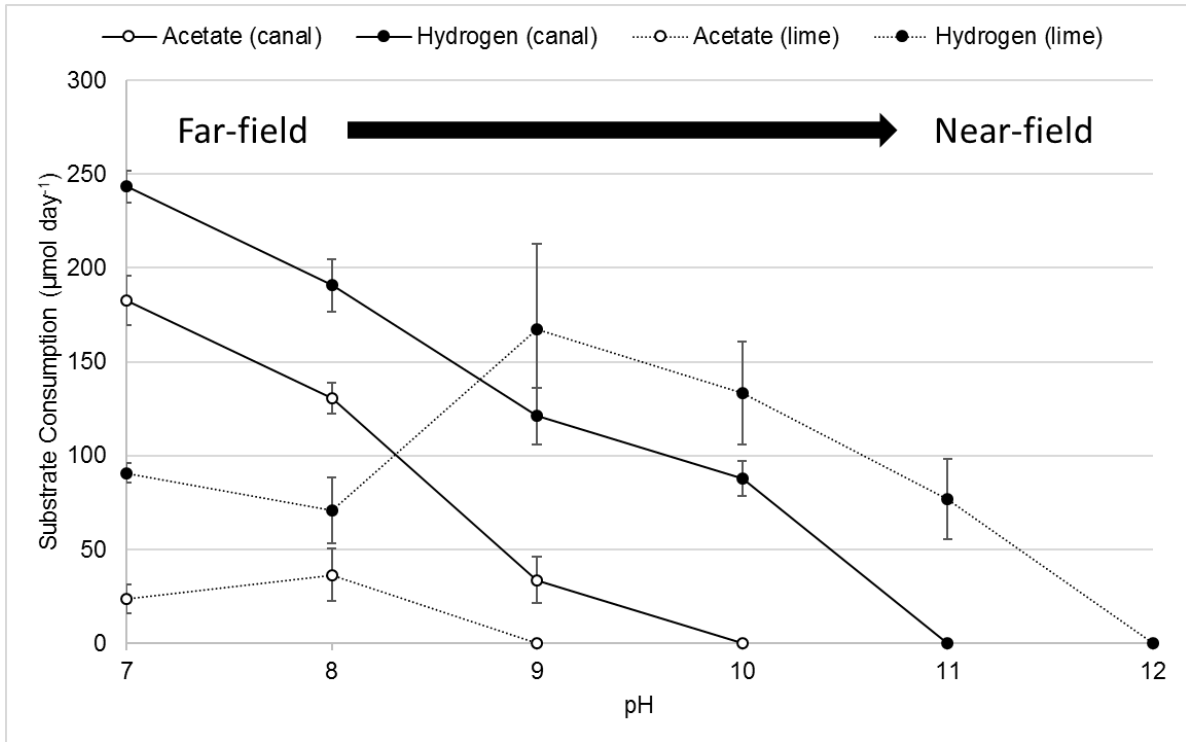


**Figure 9.3. Hydrogen and acetate consumption rates under far-field and near-field conditions when employing canal sediments or alkali-adapted lime sediments.** Under near-field conditions (pH  $\geq 10.0$ ) methane production was reliant on hydrogenotrophic metabolism.

The ‘Old Lime’ (LK) and ‘Steel’ (CW, CS, RC, SC) sediments were used to expand the study further by developing acetoclastic and hydrogenotrophic methanogen enrichments at pH 7.0 and 10.0 to compare the community composition and functioning under far-field and near-field conditions. Again the addition of  $H_2/CO_2$  stimulated methanogenesis in pH 10.0 cultures compared to un-amended controls, with acetate-fed cultures negative for methane production under these conditions. However, high acetate consumption and methane generation rates were observed at pH 7.0, particularly from the ‘Steel’ sediments which led to the development of a community dominated by the acetoclastic genus *Methanosarcina*. However, at pH 10.0 the microcosms were dominated by hydrogenotrophic methanogens of the genera *Methanobacterium* (Steel) and *Methanoculleus* (Old Lime). The ubiquitous nature of the strictly hydrogenotrophic *Methanoculleus* and *Methanobacterium* species within microcosms operating under near-field conditions indicates their importance within an ILW-GDF. Although methanogenesis above pH 11.0 was unable to proceed in planktonic culture using

defined mixed cultures, future work could determine whether the upper pH limits for methanogenesis changes in pure cultures or biofilm systems.

Overall the data shown in Chapter 6 suggests that under the alkaline near-field conditions of an ILW-GDF (pH  $\geq 10.0$ ), biological methane generation will be dependent on the hydrogenotrophic pathway. However, under far-field conditions (neutral-pH) acetoclastic methanogenesis becomes more important. This data could have a significant impact on gas generation modelling studies used to evaluate ILW-GDF performance.

### **Conclusion 3: Calcium carbonate provides a substrate for hydrogenotrophic methanogenesis under ILW-GDF conditions.**

Carbon dioxide speciation is highly dependent on pH and any CO<sub>2</sub> produced within an ILW-GDF is expected to precipitate out of solution as insoluble calcium carbonates through interactions with the cement-based backfill (NRVB) (6). These alkaline carbonation reactions could result in hydrogenotrophic methanogenesis being inaccessible under ILW-GDF conditions through the removal of CO<sub>2</sub> from the liquid and gas phases of the near-field. Methanogenesis from calcium and magnesium carbonates has been demonstrated previously under neutral-pH conditions (236), however the ability of methanogens to access precipitated carbonates under the conditions expected of an ILW-GDF have never been validated. The next section of work discussed in Chapter 7 aimed to determine whether sub-cultures of the methanogenic microcosms developed from the alkaline sediments in Chapter 6 that were operating at pH 10.0 and fed with H<sub>2</sub>/CO<sub>2</sub> as the sole carbon and energy source, were instead able to utilise precipitated forms of calcium carbonate for hydrogenotrophic methanogenesis at this pH. This was achieved by supplying the sub-cultures with either a solid calcium carbonate powder or ground pieces of marble in replace of an external source of CO<sub>2</sub>. To supplement the study, NRVB was prepared in the laboratory and incubated under CO<sub>2</sub> to allow for the carbonation of the materials surface. The pre-carbonated NRVB was also tested as a potential carbon source for hydrogenotrophic metabolism.

All cultures supplied only with H<sub>2</sub> and precipitated carbonates demonstrated methanogenesis compared with un-amended controls lacking either carbonates or H<sub>2</sub>. Hydrogen was actively removed from these microcosms despite the lack of TEA's, albeit at slow rates compared with positive controls where CO<sub>2</sub> was supplied. Highest rates of metabolism were observed in microcosms supplemented with NRVB, which was attributed to the high surface area of this

material, with lowest hydrogen consumption rates coming from marble-amended microcosms. Geochemical modelling suggested under the conditions of these experiments CO<sub>2</sub> availability will be extremely limited after equilibration with calcite (Figure 9.4), however the formation of biofilm materials on the NRVB surfaces could be resulting in increased levels of CO<sub>2</sub> and HCO<sub>3</sub><sup>-</sup> through the production of low pH microsites. Both CO<sub>2</sub> and HCO<sub>3</sub><sup>-</sup> are consumable substrates for autotrophic species (75), although the direct utilisation of CO<sub>3</sub><sup>2-</sup> or CaCO<sub>3</sub> by methanogens has never been authenticated. The detection of archaea within the biofilm materials via FISH suggested the methanogens were growing in close association with the carbonate minerals, which were detected on the NRVB surfaces using SEM, SEM-EDS, XRD and phenolphthalein staining. Alongside hydrogenotrophic methanogenesis, these microcosms also showed evidence of homoacetogenesis, suggesting that methanogens and homoacetogens were competing for hydrogen and calcium carbonate. The archaeal community was dominated by hydrogenotrophic methanogens of the genera *Methanobacterium* and *Methanoculleus*, however within a small number of these microcosms (2 out of 27) the strictly acetoclastic genus *Methanosaeta* was also present in low abundance, suggesting homoacetogenesis was stimulating the production of methane from acetate. This is contrary to the findings in Chapter 6 where acetoclastic lineages were absent from pH 10.0 microcosms, however the lack of carbonate buffers applied to these systems resulted in a significant reduction in pH during the incubation period which could have stimulated the growth of acetate-consuming methanogens. No acetate consumption was detected within these microcosms however, and the discovery of genes for the H<sub>2</sub>/CO<sub>2</sub> pathway in *Methanosaeta* could suggest these organisms were contributing to hydrogenotrophic methane production in these cultures (405). The production of hydrogen from abiotic corrosion processes (6) or from the fermentation of cellulose degradation products (23, 24) (Figure 9.1) and the likely abundance of precipitated carbonates in the near-field (6) suggests all the substrates for hydrogenotrophic methanogenesis will be available during the evolution of an ILW-GDF. Future work could determine whether this process is available at pH 11.0, where the accessibility of CO<sub>2</sub> and HCO<sub>3</sub><sup>-</sup> will be even more restricted and could provide further evidence that methanogens are able to utilise precipitated forms of inorganic carbon directly for ATP synthesis.

Overall the data shown in Chapter 7 suggests methanogens are able to utilise precipitated carbonates for hydrogenotrophic methanogenesis at pH 10.0 in the absence of externally

supplied CO<sub>2</sub>. This could have a significant impact on gas generation within the near-field of an ILW-GDF, where precipitated carbonates will be abundant and CO<sub>2</sub> availability will be limited. This is the first study to demonstrate methane from calcite under alkaline conditions.

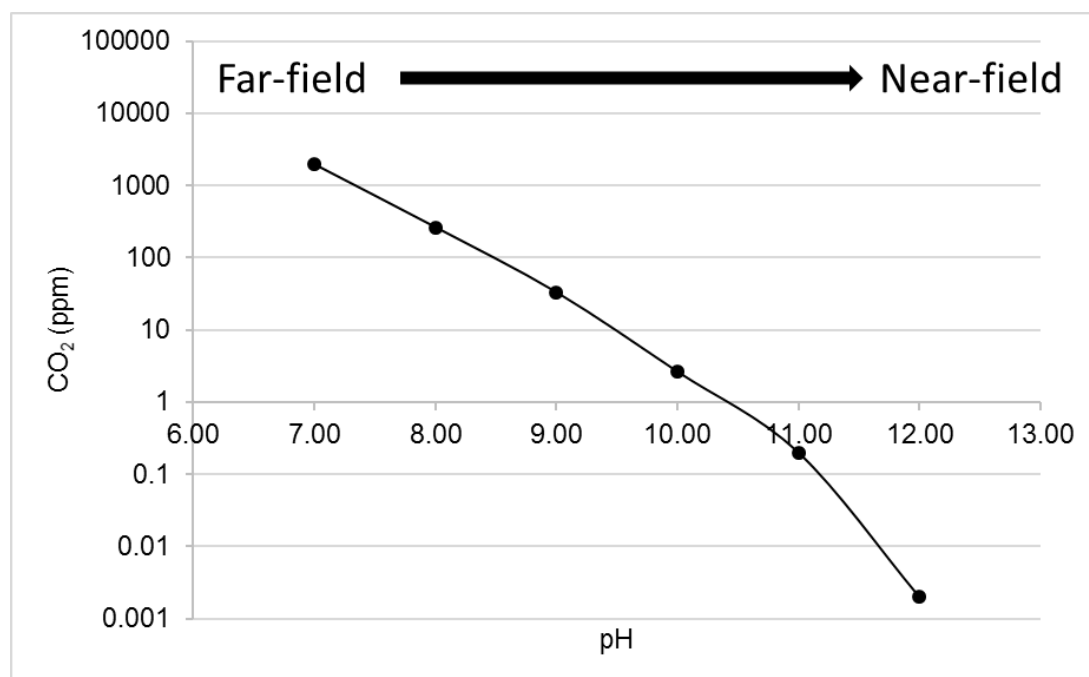


**Figure 9.4. CO<sub>2</sub> availability under far-field and near-field conditions within a closed system as determined through geochemical modelling using PHREEQC.**

#### **Conclusion 4a: Biofilms facilitate sulphate reduction under ILW-GDF conditions.**

Previous studies employing sediments from a proposed ILW-GDF analogue site in Buxton, UK showed little to no sulphate-reducing activity at pH  $\geq 10.0$  in planktonic culture when supplied with acetate, lactate or ISA as electron donors, and it has been theorised that this process is not likely to proceed under near-field conditions (25, 115). However, as discussed previously the upper pH limits for microbial activity can increase with the formation of biofilm (112, 125). The final section of work outlined in Chapter 8 sought to grow methanogenic and sulphate reducing biofilms on stainless steel surfaces within CDC biofilm reactors at pH 11.0 using the products of alkaline cellulose degradation (CDP) as the sole carbon and energy source. The biofilm reactors were seeded with fluid from a microcosm that had been developed previously from the ‘New Lime’ site B sediments which was operating at pH 10.0 under sulphate reducing conditions and fed with CDP. Following a 2-weekly waste/feed cycle for 3

months, biofilm was successfully formed on the steel coupons at pH 11.0 under both methanogenic (CDP only) and sulphate reducing (amended with sulphate) conditions. Under both conditions, all three forms of ISA showed evidence of microbial degradation via fermentation pathways compared to abiotic control reactors, with ISA degradation resulting in the generation of hydrogen and acetate as end-products. Hydrogen was consumed which resulted in the production of methane in reactors lacking sulphate, however methanogenesis was inhibited in reactors amended with sulphate, suggesting dissimilatory sulphate reduction pathways were out-competing methanogenesis for fermentation end-products. This suggests the addition of sulphate as electron acceptor played a role in minimising methanogenesis from CDP and its fermentation end-products and therefore an ILW-GDF saturated with sulphate-rich ground-waters could result in a lower contribution of methane generation.

Consistent with findings in the previous chapters of work, hydrogen was consumed and acetate accumulated in methanogenic reactors and the archaeal bulk liquid community was dominated by hydrogenotrophic methanogens of the genus *Methanobacterium*. However, the metabolically diverse genus *Methanosarcina* appeared to dominate the biofilm communities formed on grade 316 steel, with *Methanobacterium* dominating the grade 304 biofilm. All sulphate reducing biofilms were dominated by the alkaliphilic SRB *Desulfonatronum*, most strains of which have a maximum growth pH of 10.5 in pure culture (406), suggesting biofilm formation was increasing the upper pH limits for this organism. This was substantiated by the development of low pH microsites within the internal biofilm surface as analysed with the use of micro-pH probes (dia. 10 µm), where a difference of between 0.91 – 1.47 pH units was observed between bulk fluid and biofilms. The pH profiles suggested under bulk fluid conditions of pH ~11.0, the internal biofilm pH was between 9.7 - 10.3 at its lowest values. These low pH microsites within the biofilms could also be offering *Methanosarcina* species with improved growth rates as seen in Chapter 6. The detection of fermentative lineages of the phylum Firmicutes within the biofilm matrix via FISH suggested metabolic acids were being produced that resulted in the formation of these lower pH niches. The fact that SRB were growing in close association with the fermenters not only suggests a syntrophic community structure was present, but also that SRB were surviving in close proximity to fermentation end-products and the associated low pH microsites. The detection of Bacteroidetes lineages on the

periphery of these communities could be offering SRB with further protection from the external environment and resulting in their survival under the conditions imposed here.

**Conclusion 4b: Alkaliphilic sulphate-reducing biofilms are capable of corroding stainless steel surfaces under ILW-GDF conditions.**

Although steel materials within an ILW-GDF are predicted to corrode naturally through abiotic processes (6), microbial activity could enhance the rate of these corrosion kinetics and thereby have a significant impact on GDF performance. Especially when considering that an ILW-GDF is required to be operational for extended time frames to ensure long-lived radionuclides, such as carbon-14 (half-life 5,730 years) do not reach the biosphere. The integrity of the engineered barriers (e.g. steel waste canisters) for long time frames is therefore critical to the performance of a GDF. Microscopic techniques (SEM, AFM and Alicona) were used to characterise the steel surfaces after removal of the biofilm materials. The presence of localised corrosion pits on the steel surfaces incubated under sulphate-reducing conditions compared with methanogenic surfaces and negative controls suggested the production of sulphide was facilitating bio-corrosion processes in these systems (Figure 9.5). The detection of high H<sub>2</sub> concentrations at the steel surface using micro-sensors within the sulphate reducing biofilms provides further evidence that anaerobic corrosion processes were ongoing, despite the alkaline conditions imposed.

The data outlined in Chapter 8 is the first report of bio-corrosion due to alkaliphilic *Desulfonatronum* sulphate-reducing biofilms at pH 11.0. A number of studies have demonstrated this process under neutral-pH conditions (109, 110), however the ability of sulphate reducing biofilms to corrode stainless steel at pH 11.0 using only the products of alkaline cellulose degradation as substrate could have important implications on the corrosion of steel materials within the near-field of an ILW-GDF.

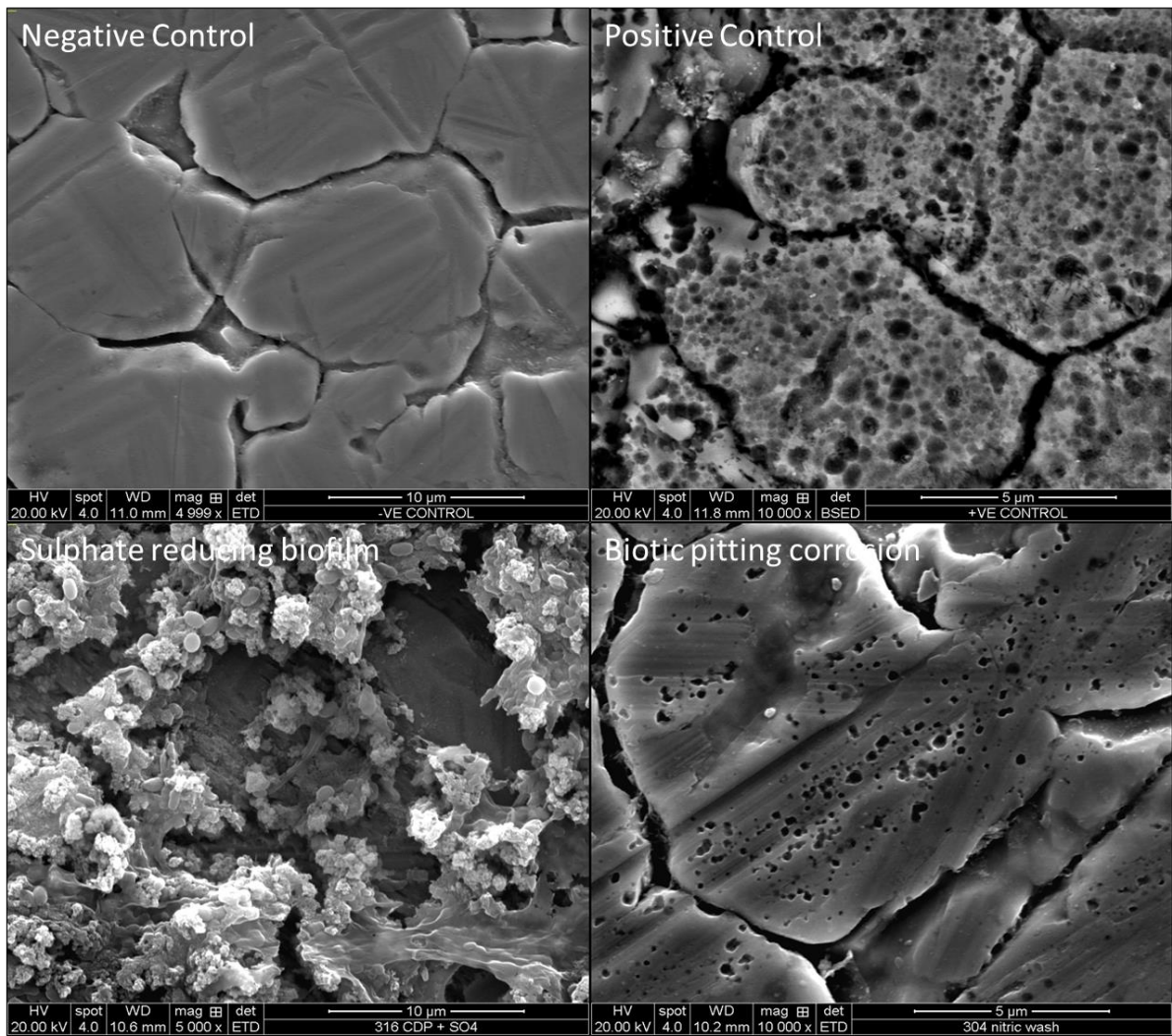


**Figure 9.5. Characterisation of abiotic control stainless steel surfaces, together with biotic surfaces before and after removal of biofilm materials.** The removal of sulphate reducing biofilms revealed the presence of localised pitting corrosion on the stainless steel surfaces compared with negative controls.

## 9.1 Synopsis

- Methanogenic and sulphate-reducing communities were detected via DNA and cDNA sequencing technologies within a range of anthropogenic alkaline sites where pH values of 11.0-13.0 were encountered. This provides evidence that methanogenic and sulphate-reducing microbial processes could be present under the alkaline conditions of an ILW-GDF.
- Methanogen enrichment cultures were developed from the sediments within these alkaline sites, where methanogenesis was capable of proceeding up to pH 11.0 under laboratory conditions when supplied with H<sub>2</sub>/CO<sub>2</sub>. None of these cultures were capable of acetoclastic methanogenesis under alkaline conditions, suggesting acetate-dependent methanogenesis will be unavailable under the alkaline conditions of an ILW-GDF.
- The methanogen enrichment cultures showed evidence of utilising calcium carbonate as a carbon source for hydrogenotrophic methanogenesis at pH 10.0. Calcium carbonate will be readily available within an ILW-GDF and therefore could provide a substrate for methanogens and impact gas generation within the facility.
- Dissimilatory sulphate-reducing biofilms were capable of corroding stainless steel surfaces within 3 months at pH 11.0 using CDP as the sole carbon and energy source. This provides evidence that microbial processes could impact the integrity of stainless steel waste canisters within an ILW-GDF if sulphate is available within the groundwater.

## References

1. N.D.A. High Level Summary UK Radwaste Inventory 2016. 2017.
2. N.D.A. 2010 UK Radioactive Waste Inventory Main Report. Harwell, Didcot, Oxfordshire, UK.: Nuclear Decommissioning Authority (Radioactive Waste Management Directorate); 2011 Report No.: NDA/ST/STY(11)0004.
3. Beadle I, Humphreys PN, Pettit C, Small J. Integrating microbiology into the Drigg post-closure radiological safety assessment. United States: Materials Research Society; 2001.
4. N.D.A. Geological Disposal Disposal System Safety Case Data Report. Harwell, Didcot, Oxfordshire, UK. : Nuclear Decommissioning Authority (Radioactive Waste Management Directorate); 2016.
5. N.D.A. Geological Disposal Generic Disposal System Technical Specification December 2010. Nuclear Decommissioning Authority (Radioactive Waste Management Directorate), Harwell, Didcot, Oxfordshire, UK.; 2010. Report No.: NDA/RWMD/044.
6. N.D.A. Geological Disposal Near-field evolution status report. Nuclear Decommissioning Authority (Radioactive Waste Management Directorate), Harwell, Didcot, Oxfordshire, UK.; 2010. Report No.: NDA/RWMD/033.
7. N.D.A. Geological Disposal An introduction to the generic Disposal System Safety Case. Nuclear Decommissioning Authority (Radioactive Waste Management Directorate), Harwell, Didcot, Oxfordshire, UK. ; 2010.
8. Felipe-Sotelo M, Hinchliff J, Evans N, Warwick P, Read D. Sorption of radionuclides to a cementitious backfill material under near-field conditions 2012.
9. Butcher EJ, Borwick J, Collier N, Williams SJ. Long term leachate evolution during flow-through leaching of a vault backfill (NRVB). *Mineralogical Magazine*. 2012;76(8):3023-31.
10. Libert M, Bildstein O, Esnault L, Jullien M, Sellier R. Molecular hydrogen: An abundant energy source for bacterial activity in nuclear waste repositories. *Physics and Chemistry of the Earth, Parts A/B/C*. 2011;36(17):1616-23.
11. Olszewska A, Miskiewicz A, G Z-K, Lankof L, Pająk L. Multi-barrier system against migration of radionuclides from radioactive waste repository 2015. 557-63 p.
12. Bugg TD, Ahmad M, Hardiman EM, Rahmanpour R. Pathways for degradation of lignin in bacteria and fungi. *Nat Prod Rep*. 2011;28(12):1883-96.
13. Loon LRv, Glaus MA. Experimental and Theoretical Studies on Alkaline Degradation of Cellulose and its Impact on the Sorption of Radionuclides. Switzerland; 1998. Report No.: 1019-0643 Contract No.: PSI--98-07.
14. Knill CJ, Kennedy JF. Degradation of cellulose under alkaline conditions. *Carbohydrate Polymers*. 2003;51(3):281-300.
15. Pavasars I, Hagberg J, Borén H, Allard BJJOP, Environment t. Alkaline Degradation of Cellulose: Mechanisms and Kinetics. 2003;11(2):39-47.
16. Greenfield BF, Holtom GJ, Hurdus MH, O'Kelly N, Pilkington NJ, Rosevear A, et al. The Identification and Degradation of Isosaccharinic Acid, a Cellulose Degradation Product. *MRS Proceedings*. 1994;353:1151.
17. Warwick P, Evans N, Hall T, Vines S. Stability constants of uranium(IV)-alpha-isosaccharinic acid and gluconic acid complexes 2004.
18. Warwick P, Evans N, Hall T, Vines S. Complexation of Ni (II) by  $\alpha$ -isosaccharinic acid and gluconic acid from pH 7 to pH 13 2003.

19. Worthington SRH, Ford DCJEG. High sulfate concentrations in limestone springs: An important factor in conduit initiation? 1995;25(1):9-15.
20. Müller VJEoLS. Bacterial fermentation. 2001.
21. Madigan MT, Gest HJAoM. Growth of a photosynthetic bacterium anaerobically in darkness, supported by “oxidant-dependent” sugar fermentation. 1978;117(2):119-22.
22. Rout SP, Radford J, Laws AP, Sweeney F, Elmekawy A, Gillie LJ, et al. Biodegradation of the alkaline cellulose degradation products generated during radioactive waste disposal. PLoS one. 2014;9(9):e107433-e.
23. Rout SP, Charles CJ, Doulgeris C, McCarthy AJ, Rooks DJ, Loughnane JP, et al. Anoxic Biodegradation of Isosaccharinic Acids at Alkaline pH by Natural Microbial Communities. PLoS ONE. 2015;10(9):e0137682.
24. Rout SP, Charles CJ, Garratt EJ, Laws AP, Gunn J, Humphreys PN. Evidence of the generation of isosaccharinic acids and their subsequent degradation by local microbial consortia within hyper-alkaline contaminated soils, with relevance to intermediate level radioactive waste disposal. PLOS ONE. 2015;10(3).
25. Bassil NM, Bryan N, Lloyd JR. Microbial degradation of isosaccharinic acid at high pH. The ISME journal. 2015;9(2):310-20.
26. Thauer RK. Biochemistry of methanogenesis: a tribute to Marjory Stephenson:1998 Marjory Stephenson Prize Lecture. 1998;144(9):2377-406.
27. Thauer RK, Kaster A-K, Seedorf H, Buckel W, Hedderich R. Methanogenic archaea: ecologically relevant differences in energy conservation. Nature Reviews Microbiology. 2008;6:579.
28. Thauer RK, Kaster A-K, Goenrich M, Schick M, Hiromoto T, Shima S. Hydrogenases from Methanogenic Archaea, Nickel, a Novel Cofactor, and H<sub>2</sub> Storage. 2010;79(1):507-36.
29. Lang K, Schuldes J, Klingl A, Poehlein A, Daniel R, Brune A. New Mode of Energy Metabolism in the Seventh Order of Methanogens as Revealed by Comparative Genome Analysis of “Candidatus Methanoplasma termitum”. Applied and Environmental Microbiology. 2015;81(4):1338-52.
30. Bapteste E, Brochier C, Boucher Y. Higher-level classification of the Archaea: evolution of methanogenesis and methanogens. Archaea (Vancouver, BC). 2005;1(5):353-63.
31. Mach V, Blaser MB, Claus P, Chaudhary PP, Rulík M. Methane production potentials, pathways, and communities of methanogens in vertical sediment profiles of river Sitka. Frontiers in microbiology. 2015;6:506-.
32. Conrad R. Contribution of hydrogen to methane production and control of hydrogen concentrations in methanogenic soils and sediments. FEMS Microbiology Ecology. 1999;28(3):193-202.
33. Conrad R, Schink B, Phelps TJ. Thermodynamics of H<sub>2</sub>-consuming and H<sub>2</sub>-producing metabolic reactions in diverse methanogenic environments under in situ conditions. FEMS Microbiology Letters. 1986;38(6):353-60.
34. Conrad R, Mayer H-P, Wüst M. Temporal change of gas metabolism by hydrogen-syntrophic methanogenic bacterial associations in anoxic paddy soil. 1989;62(4):265-73.
35. Schink B. Energetics of syntrophic cooperation in methanogenic degradation. Microbiology and molecular biology reviews : MMBR. 1997;61(2):262-80.
36. Müller V. Energy conservation in acetogenic bacteria. Applied and environmental microbiology. 2003;69(11):6345-53.
37. Winfrey MR, Zeikus JG. Anaerobic metabolism of immediate methane precursors in Lake Mendota. 1979;37(2):244-53.

38. Kuivila KM, Murray JW, Devol AH, Novelli PC. Methane production, sulfate reduction and competition for substrates in the sediments of Lake Washington. *Geochimica et Cosmochimica Acta*. 1989;53(2):409-16.
39. Rothfuss F, Conrad RJB. Vertical profiles of CH<sub>4</sub> concentrations, dissolved substrates and processes involved in CH<sub>4</sub> production in a flooded Italian rice field. 1992;18(3):137-52.
40. Oremland RS, Marsh LM, Polcin S. Methane production and simultaneous sulphate reduction in anoxic, salt marsh sediments. *Nature*. 1982;296(5853):143-5.
41. Banat IM, Nedwell DB, Balba MT. Stimulation of Methanogenesis by Slurries of Saltmarsh Sediment after the Addition of Molybdate to Inhibit Sulphate-reducing Bacteria. 1983;129(1):123-9.
42. Phelps TJ, Zeikus JG. Influence of pH on Terminal Carbon Metabolism in Anoxic Sediments from a Mildly Acidic Lake. 1984;48(6):1088-95.
43. Chin K-J, Conrad R. Intermediary metabolism in methanogenic paddy soil and the influence of temperature. *FEMS Microbiology Ecology*. 1995;18(2):85-102.
44. Lansdown JM, Quay PD, King SL. CH<sub>4</sub> production via CO<sub>2</sub> reduction in a temperate bog: A source of <sup>13</sup>C-depleted CH<sub>4</sub>. *Geochimica et Cosmochimica Acta*. 1992;56(9):3493-503.
45. Namsaraev BB, Dulov LE, Sokolova EN. Bacterial methane production in the bottom sediments of Lake Baikal 1995.
46. Sandbeck KA, Ward DM. Fate of immediate methane precursors in low-sulfate, hot-spring algal-bacterial mats. *Applied and environmental microbiology*. 1981;41(3):775-82.
47. Gwynfryn Jones J, M. Simon B, Gardener S. Factors Affecting Methanogenesis and Associated Anaerobic Processes in the Sediments of a Stratified Eutrophic Lake 1982. 1-11 p.
48. Deuser WG, Degens ET, Harvey GR, Rubin M. Methane in Lake Kivu: New Data Bearing on Its Origin. 1973;181(4094):51-4.
49. Fournier GP, Gogarten JP. Evolution of Acetoclastic Methanogenesis in *Methanosarcina* via Horizontal Gene Transfer from Cellulolytic Clostridia. *Journal of Bacteriology*. 2008;190(3):1124-7.
50. Lang K, Schuldes J, Klingl A, Poehlein A, Daniel R, Brunea A. New mode of energy metabolism in the seventh order of methanogens as revealed by comparative genome analysis of "Candidatus methanoplasma termitum". *Applied and environmental microbiology*. 2015;81(4):1338-52.
51. Fournier GP, Gogarten JP. Evolution of Acetoclastic Methanogenesis in *Methanosarcina* via Horizontal Gene Transfer from Cellulolytic Clostridia. 2008;190(3):1124-7.
52. Ferry JG. Methane from acetate. 1992;174(17):5489-95.
53. Berger S, Welte C, Deppenmeier U. Acetate activation in *Methanosaeta thermophila*: characterization of the key enzymes pyrophosphatase and acetyl-CoA synthetase. *Archaea* (Vancouver, BC). 2012;2012:315153-.
54. Aceti D, Ferry J. Purification and characterization of acetate kinase from acetate-grown *Methanosarcina thermophila*. Evidence for regulation of synthesis 1988. 15444-8 p.
55. Conklin A, Stensel HD, Ferguson J. Growth Kinetics and Competition Between *Methanosarcina* and *Methanosaeta* in Mesophilic Anaerobic Digestion. 2006;78(5):486-96.
56. Carton M, McHugh S, O'Flaherty V, Mahony T. Methanogenic population structure in a variety of anaerobic bioreactors. *FEMS Microbiology Letters*. 2003;219(2):297-304.
57. Zheng D, Raskin L. Quantification of *Methanosaeta* Species in Anaerobic Bioreactors Using Genus- and Species-Specific Hybridization Probes 2000. 246-62 p.

58. De Vrieze J, Hennebel T, Boon N, Verstraete W. Methanosarcina: The rediscovered methanogen for heavy duty biomethanation. *Bioresource Technology*. 2012;112:1-9.
59. Chen S, Cheng H, Liu J, Hazen TC, Huang V, He QJAM, et al. Unexpected competitiveness of Methanosaeta populations at elevated acetate concentrations in methanogenic treatment of animal wastewater. 2017;101(4):1729-38.
60. Battumur U, Yoon Y, Bae GS, Kim C-H. Isolation and characterization of new Methanosarcina mazei strains KOR-3, -4, -5, and -6 from an anaerobic digester using pig slurry. *Asian-Australasian journal of animal sciences*. 2017;30(8):1198-205.
61. Elbersen MA, Sowers KR. Isolation of an Aceticlastic Strain of Methanosarcina siciliae from Marine Canyon Sediments and Emendation of the Species Description for Methanosarcina siciliae. 1997;47(4):1258-61.
62. Shimizu S, Upadhye R, Ishijima Y, Naganuma T. Methanosarcina horonobensis sp. nov., a methanogenic archaeon isolated from a deep subsurface Miocene formation. 2011;61(10):2503-7.
63. Sowers K, Baron S, Ferry J. Methanosarcina acetivorans sp. nov., an Acetotrophic Methane-Producing Bacterium Isolated from Marine Sediments 1984. 971-8 p.
64. Zinder SH, Mah RA. Isolation and Characterization of a Thermophilic Strain of Methanosarcina Unable to Use H<sub>2</sub>-CO<sub>2</sub> for Methanogenesis. *Applied and environmental microbiology*. 1979;38(5):996-1008.
65. Methanosarcina vacuolata sp. nov. a Vacuolated Methanosarcina. *International Journal of Systematic Bacteriology*. 37(3):281-3
66. Ganzert L, Schirmack J, Alawi M, Mangelsdorf K, Sand W, Hillebrand-Voiculescu A, et al. Methanosarcina spelaei sp. nov., a methanogenic archaeon isolated from a floating biofilm of a subsurface sulphurous lake. 2014;64(10):3478-84.
67. Wagner D, Schirmack J, Ganzert L, Morozova D, Mangelsdorf K. Methanosarcinasoligelidi sp. nov., a desiccation- and freeze-thaw-resistant methanogenic archaeon from a Siberian permafrost-affected soil. 2013;63(8):2986-91.
68. Marvin P. Bryant DRB. Emended Description of Strain MST (DSM 800T), the Type Strain of Methanosarcina barkeri *International Journal of Systematic Bacteriology*. 1987;37(2):169-70
69. Mori K, Iino T, Suzuki K-I, Yamaguchi K, Kamagata Y. Aceticlastic and NaCl- Requiring Methanogen Methanosaeta pelagica sp. nov., Isolated from Marine Tidal Flat Sediment. 2012;78(9):3416-23.
70. Ma K, Liu X, Dong X. Methanosaeta harundinacea sp. nov., a novel acetate-scavenging methanogen isolated from a UASB reactor 2006. 127-31 p.
71. Takeda K, Akada S, Fujita T. Isolation and Characteristics of Methanosaeta in Paddy Field Soils AU - MIZUKAMI, Satomi. *Bioscience, Biotechnology, and Biochemistry*. 2006;70(4):828-35.
72. Zhuang G-C, Heuer VB, Lazar CS, Goldhammer T, Wendt J, Samarkin VA, et al. Relative importance of methylotrophic methanogenesis in sediments of the Western Mediterranean Sea. *Geochimica et Cosmochimica Acta*. 2018;224:171-86.
73. Zhuang G-C, Elling FJ, Nigro LM, Samarkin V, Joye SB, Teske A, et al. Multiple evidence for methylotrophic methanogenesis as the dominant methanogenic pathway in hypersaline sediments from the Orca Basin, Gulf of Mexico. *Geochimica et Cosmochimica Acta*. 2016;187:1-20.

74. Oremland RS, Marsh L, Desmarais DJ. Methanogenesis in big soda lake, Nevada: an alkaline, moderately hypersaline desert lake. *Applied and Environmental Microbiology*. 1982;43(2):462-8.
75. Liu Y, Whitman WB. Metabolic, Phylogenetic, and Ecological Diversity of the Methanogenic Archaea. 2008;1125(1):171-89.
76. Gottschalk G, Thauer RK. The Na<sup>+</sup>-translocating methyltransferase complex from methanogenic archaea. *Biochimica et Biophysica Acta (BBA) - Bioenergetics*. 2001;1505(1):28-36.
77. MÜLLER V, WINNER C, GOTTSCHALK G. Electron-transport-driven sodium extrusion during methanogenesis from formaldehyde and molecular hydrogen by *Methanosarcina barkeri*. 1988;178(2):519-25.
78. Lienard T, Becher B, Marschall M, Bowien S, Gottschalk G. Sodium Ion Translocation by N<sup>5</sup>-Methyltetrahydromethanopterin: Coenzyme M Methyltransferase from *Methanosarcina mazei* Gö1 Reconstituted in Ether Lipid Liposomes. 1996;239(3):857-64.
79. Schlegel K, Leone V, D Faraldo-Gómez J, Müller V. Promiscuous Archaeal ATP Synthase Concurrently Coupled to Na<sup>+</sup> and H<sup>+</sup> Translocation. 2012. 947-52 p.
80. Jasso-Chávez R, Apolinario E, Sowers K, Ferry J. MRPA Functions in Energy Conversion during Acetate-Dependent Growth of *Methanosarcina acetivorans*. 2013.
81. Schlegel K, Müller V. Evolution of Na<sup>+</sup> and H<sup>+</sup> bioenergetics in methanogenic archaea. 2013;41(1):421-6.
82. Blake LI, Tveit A, Øvreås L, Head IM, Gray ND. Response of Methanogens in Arctic Sediments to Temperature and Methanogenic Substrate Availability. *PloS one*. 2015;10(6):e0129733-e.
83. Fuchs A, Lyautey E, Montuelle B, Casper P. Effects of increasing temperatures on methane concentrations and methanogenesis during experimental incubation of sediments from oligo- and mesotrophic lakes: Temperature effects on CH<sub>4</sub>. 2016.
84. Pattnaik P, Mishra SR, Bharati K, Mohanty SR, Sethunathan N, Adhya TK. Influence of salinity on methanogenesis and associated microflora in tropical rice soils. *Microbiological Research*. 2000;155(3):215-20.
85. Ismail SB, Gonzalez P, Jeison D, van Lier JB. Effects of high salinity wastewater on methanogenic sludge bed systems. *Water Science and Technology*. 2008;58(10):1963-70.
86. Yuan Q, Hernández M, Dumont MG, Rui J, Fernández Scavino A, Conrad R. Soil bacterial community mediates the effect of plant material on methanogenic decomposition of soil organic matter. *Soil Biology and Biochemistry*. 2018;116:99-109.
87. Sorokin DY, Abbas B, Geleijnse M, Pimenov NV, Sukhacheva MV, van Loosdrecht MCM. Methanogenesis at extremely haloalkaline conditions in the soda lakes of Kulunda Steppe (Altai, Russia). *FEMS Microbiology Ecology*. 2015;91(4):fiv016-fiv.
88. Jones WJ, Leigh JA, Mayer F, Woese CR, Wolfe RS. *Methanococcus jannaschii* sp. nov., an extremely thermophilic methanogen from a submarine hydrothermal vent. *Archives of Microbiology*. 1983;136(4):254-61.
89. Kurr M, Huber R, König H, Jannasch HW, Fricke H, Trincone A, et al. *Methanopyrus kandleri*, gen. and sp. nov. represents a novel group of hyperthermophilic methanogens, growing at 110°C. *Archives of Microbiology*. 1991;156(4):239-47.
90. Boone DR, Worakit S, Mathrani IM, Mah RA. Alkaliphilic methanogens from high-pH lake sediments. *Systematic and Applied Microbiology*. 1986;7(2):230-4.

91. Zhilina TN, Zavarzina DG, Kevbrin VV, Kolganova TVJM. *Methanocalculus natronophilus* sp. nov., a new alkaliphilic hydrogenotrophic methanogenic archaeon from a soda lake, and proposal of the new family Methanocalculaceae. 2013;82(6):698-706.
92. Muyzer G, Stams AJM. The ecology and biotechnology of sulphate-reducing bacteria. *Nature Reviews Microbiology*. 2008;6:441.
93. Fichtel K, Mathes F, Könneke M, Cypionka H, Engelen B. Isolation of sulfate-reducing bacteria from sediments above the deep-subseafloor aquifer. *Frontiers in microbiology*. 2012;3:65-.
94. Marietou A. Nitrate reduction in sulfate-reducing bacteria. *FEMS Microbiology Letters*. 2016;363(15).
95. Enning D, Venzlaff H, Garrelfs J, Dinh HT, Meyer V, Mayrhofer K, et al. Marine sulfate-reducing bacteria cause serious corrosion of iron under electroconductive biogenic mineral crust. *Environmental microbiology*. 2012;14(7):1772-87.
96. An overview of mechanisms by which sulphate-reducing bacteria influence corrosion of steel in marine environments AU - Videla, Hector A. *Biofouling*. 2000;15(1-3):37-47.
97. Zhang Y, Wang X, Zhen Y, Mi T, He H, Yu Z. Microbial Diversity and Community Structure of Sulfate-Reducing and Sulfur-Oxidizing Bacteria in Sediment Cores from the East China Sea. *Frontiers in microbiology*. 2017;8:2133-.
98. Dowling NJE, Brooks SA, Phelps TJ, White DCJJoIM. Effects of selection and fate of substrates supplied to anaerobic bacteria involved in the corrosion of pipe-line steel. 1992;10(3):207-15.
99. Xu D, Li Y, Song F, Gu T. Laboratory investigation of microbiologically influenced corrosion of C1018 carbon steel by nitrate reducing bacterium *Bacillus licheniformis*. *Corrosion Science*. 2013;77:385-90.
100. Dinh HT, Kuever J, Mußmann M, Hassel AW, Stratmann M, Widdel F. Iron corrosion by novel anaerobic microorganisms. *Nature*. 2004;427:829.
101. Larsen J, Rasmussen K, Pedersen H, Sorensen K, Lundgaard T, Skovhus T. Consortia of MIC Bacteria and Archaea causing Pitting Corrosion in Top Side Oil Production Facilities 2010.
102. Enning D, Garrelfs J. Corrosion of Iron by Sulfate-Reducing Bacteria: New Views of an Old Problem. 2014;80(4):1226-36.
103. Pak KR, Lee HJ, Lee HK, Kim YK, Oh YS, Choi SC. Involvement of Organic Acid During Corrosion of Iron Coupon by *Desulfovibrio desulfuricans* 2003. 937-41 p.
104. Cord-Ruwisch R, Widdel FJAM, *Biotechnology*. Corroding iron as a hydrogen source for sulphate reduction in growing cultures of sulphate-reducing bacteria. 1986;25(2):169-74.
105. Sydow U, Wohland P, Wolke I, Cypionka H. Bioenergetics of the alkaliphilic sulfate-reducing bacterium *Desulfonatovibrio hydrogenovorans*. 2002;148(3):853-60.
106. Newman RC, Webster BJ, Kelly RG. The Electrochemistry of SRB Corrosion and Related Inorganic Phenomena. *ISIJ International*. 1991;31(2):201-9.
107. Newman RC, Rumash K, Webster BJ. The effect of pre-corrosion on the corrosion rate of steel in neutral solutions containing sulphide: relevance to microbially influenced corrosion. *Corrosion Science*. 1992;33(12):1877-84.
108. Heggendorf FL, Fraga AGM, Ferreira DdC, Gonçalves LS, Lione VdOF, Lutterbach MTS. Sulfate-Reducing Bacteria: Biofilm Formation and Corrosive Activity in Endodontic Files. *International journal of dentistry*. 2018;2018:8303450-.
109. Sheng X, Ting Y-P, Pehkonen SO. The influence of sulphate-reducing bacteria biofilm on the corrosion of stainless steel AISI 316. *Corrosion Science*. 2007;49(5):2159-76.

110. Silva de Paula M, Monteiro Machado Gonçalves M, Alves da Cruz Rola M, José Maciel D, Ferreira de Senna L, Lago D. Carbon steel corrosion induced by sulphate-reducing bacteria in artificial seawater: Electrochemical and morphological characterizations 2016. 987-95 p.
111. Sorokin DY, Rusanov II, Pimenov NV, Tourova TP, Abbas B, Muyzer G. Sulfidogenesis under extremely haloalkaline conditions in soda lakes of Kulunda Steppe (Altai, Russia). 2010;73(2):278-90.
112. Nielsen PH, Smidt HD, Frølund B. The effect of alkaline pH conditions on a sulphate reducing consortium from a Danish district heating plant AU - Goeres, D M. Biofouling. 1998;12(4):273-86.
113. Frank YA, Kadnikov VV, Lukina AP, Banks D, Beletsky AV, Mardanov AV, et al. Characterization and Genome Analysis of the First Facultatively Alkaliphilic Thermodesulfovibrio Isolated from the Deep Terrestrial Subsurface. 2016;7(2000).
114. Ryzhmanova Y, Nepomnyashchaya Y, Abashina T, Ariskina E, Troshina O, Vainshtein M, et al. New sulfate-reducing bacteria isolated from Buryatian alkaline brackish lakes: Description of *Desulfonatronum buryatense* sp. nov 2013. 851-9 p.
115. Rizoulis A, Steele HM, Morris K, Lloyd JR. The potential impact of anaerobic microbial metabolism during the geological disposal of intermediate-level waste. Mineralogical Magazine. 2012;76(8):3261-70.
116. Roy Krouse H, Mayer B. Sulphur and Oxygen Isotopes in Sulphate. 2000. p. 195-231.
117. Toran L. Sulfate contamination in groundwater from a carbonate-hosted mine. Journal of Contaminant Hydrology. 1987;2(1):1-29.
118. Jezierski P, Szykiewicz A, Jsunędrysek M-OJW, Air., Pollution S. Natural and Anthropogenic Origin Sulphate in an Mountainous Groundwater System: S and O Isotope Evidences. 2006;173(1):81-101.
119. Chen JM, Huang L, Buglass RL. Sulfate-reducing bacteria AU - Hao, Oliver J. Critical Reviews in Environmental Science and Technology. 1996;26(2):155-87.
120. O'Flaherty V, Mahony T, O'Kennedy R, Colleran E. Effect of pH on growth kinetics and sulphide toxicity thresholds of a range of methanogenic, syntrophic and sulphate-reducing bacteria. Process Biochemistry. 1998;33(5):555-69.
121. Moosa S, Harrison STL. Product inhibition by sulphide species on biological sulphate reduction for the treatment of acid mine drainage. Hydrometallurgy. 2006;83(1):214-22.
122. Sorokin DY, Kuenen JG, Muyzer G. The microbial sulfur cycle at extremely haloalkaline conditions of soda lakes. Frontiers in microbiology. 2011;2:44-.
123. Sturr MG, Guffanti AA, Krulwich TA. Growth and bioenergetics of alkaliphilic *Bacillus firmus* OF4 in continuous culture at high pH. 1994;176(11):3111-6.
124. Sorokin D, Tourova T, C. Schmid M, Wagner M, P Koops H, Kuenen JG, et al. Isolation and properties of obligately chemolithoautotrophic and extremely alkali-tolerant ammonia-oxidizing bacteria from Mongolian soda lakes 2001. 170-7 p.
125. Charles CJ, Rout SP, Patel KA, Akbar S, Laws AP, Jackson BR, et al. Floc Formation Reduces the pH Stress Experienced by Microorganisms Living in Alkaline Environments. Applied and Environmental Microbiology. 2017;83(6).
126. Krulwich TA, Hicks DB, Swartz T, Ito M. Bioenergetic Adaptations That Support Alkaliphily. Physiology and Biochemistry of Extremophiles: American Society of Microbiology; 2007.

127. Aono R, Ito M, Machida T. Contribution of the Cell Wall Component Teichuronopeptide to pH Homeostasis and Alkaliphily in the Alkaliphile *Bacillus lentus* C-125. 1999;181(21):6600-6.
128. A Guffanti A, B Hicks D. Molar growth yields and bioenergetic parameters of extremely alkaliphilic *Bacillus* species in batch cultures, and growth in a chemostat at pH 10.5. 1991. 2375-9 p.
129. Pogoryelov D, R Sudhir P, Kovács L, Gombos Z, Brown I, Garab G. Sodium Dependency of the Photosynthetic Electron Transport in the Alkaliphilic Cyanobacterium *Arthrospira platensis* 2003. 427-37 p.
130. Padan E, Bibi E, Ito M, Krulwich TA. Alkaline pH homeostasis in bacteria: new insights. *Biochimica et biophysica acta*. 2005;1717(2):67-88.
131. Slonczewski JL, Fujisawa M, Dopson M, Krulwich TA. Cytoplasmic pH Measurement and Homeostasis in Bacteria and Archaea. In: Poole RK, editor. *Advances in Microbial Physiology*. 55: Academic Press; 2009. p. 1-317.
132. Krulwich TA, Gilmour R, Hicks DB, Guffanti AA, Ito M. Energetics of Alkaliphilic *Bacillus* Species: Physiology and Molecules. In: Poole RK, editor. *Advances in Microbial Physiology*. 40: Academic Press; 1998. p. 401-38.
133. Enomoto K, Koyama NJCM. Effect of Growth pH on the Phospholipid Contents of the Membranes from Alkaliphilic Bacteria. 1999;39(5):270-3.
134. Krulwich T, Liu J, Morino M, Fujisawa M, Ito M, B. Hicks D. Adaptive Mechanisms of Extreme Alkaliphiles. 2011. p. 119-39.
135. Daae FL, Økland I, Dahle H, Jørgensen SL, Thorseth IH, Pedersen RB. Microbial life associated with low-temperature alteration of ultramafic rocks in the Leka ophiolite complex. 2013;11(4):318-39.
136. Brazelton WJ, Nelson B, Schrenk MO. Metagenomic evidence for  $H_2$  oxidation and  $H_2$  production by serpentinite-hosted subsurface microbial communities. *Frontiers in microbiology*. 2012;2:268-.
137. Rees HC, Grant WD, Jones BE, Heaphy SJE. Diversity of Kenyan soda lake alkaliphiles assessed by molecular methods. 2004;8(1):63-71.
138. Paul Antony C, Kumaresan D, Hunger S, Drake HL, Murrell JC, Shouche YS. Microbiology of Lonar Lake and other soda lakes. *The Isme Journal*. 2012;7:468.
139. Humayoun SB, Bano N, Hollibaugh JT. Depth distribution of microbial diversity in Mono Lake, a meromictic soda lake in California. *Applied and environmental microbiology*. 2003;69(2):1030-42.
140. Foti M, Sorokin DY, Lomans B, Mussman M, Zacharova EE, Pimenov NV, et al. Diversity, Activity, and Abundance of Sulfate-Reducing Bacteria in Saline and Hypersaline Soda Lakes. 2007;73(7):2093-100.
141. Surakasi VP, Ahmad Wani A, Shouche Y, Ranade D. Phylogenetic Analysis of Methanogenic Enrichment Cultures Obtained from Lonar Lake in India: Isolation of *Methanocalculus* sp. and *Methanoculleus* sp. 2007. 697-704 p.
142. Moody JB. Serpentinization: a review. *Lithos*. 1976;9(2):125-38.
143. Rizoulis A, Milodowski AE, Morris K, Lloyd JR. Bacterial Diversity in the Hyperalkaline Allas Springs (Cyprus), a Natural Analogue for Cementitious Radioactive Waste Repository. *Geomicrobiology Journal*. 2016;33(2):73-84.
144. Blank JG, Green SJ, Blake D, Valley JW, Kita NT, Treiman A, et al. An alkaline spring system within the Del Puerto Ophiolite (California, USA): A Mars analog site. *Planetary and Space Science*. 2009;57(5):533-40.

145. Pedersen K, Nilsson E, Arlinger J, Hallbeck L, O'Neill AJE. Distribution, diversity and activity of microorganisms in the hyper-alkaline spring waters of Maqarin in Jordan. 2004;8(2):151-64.
146. Houry HN, Salameh E, Clark ID, Fritz P, Bajjali W, Milodowski AE, et al. A natural analogue of high pH cement pore waters from the Maqarin area of northern Jordan. I: introduction to the site. *Journal of Geochemical Exploration*. 1992;46(1):117-32.
147. T. Burke I, Mortimer R, Palani S, A. Whittleston R, L. Lockwood C, J. Ashley D, et al. Biogeochemical Reduction Processes in a Hyper-Alkaline Leachate Affected Soil Profile 2012.
148. Mayes WM, Jarvis AP, Burke IT, Walton M, Feigl V, Klebercz O, et al. Dispersal and Attenuation of Trace Contaminants Downstream of the Ajka Bauxite Residue (Red Mud) Depository Failure, Hungary. *Environmental Science & Technology*. 2011;45(12):5147-55.
149. Turpeinen R, Kairesalo T, Häggblom MM. Microbial community structure and activity in arsenic-, chromium- and copper-contaminated soils. *FEMS Microbiology Ecology*. 2004;47(1):39-50.
150. Xie Y, Fan J, Zhu W, Amombo E, Lou Y, Chen L, et al. Effect of Heavy Metals Pollution on Soil Microbial Diversity and Bermudagrass Genetic Variation. *Frontiers in plant science*. 2016;7:755-.
151. Hemme CL, Deng Y, Gentry TJ, Fields MW, Wu L, Barua S, et al. Metagenomic insights into evolution of a heavy metal-contaminated groundwater microbial community. *The ISME Journal*. 2010;4:660.
152. Viti C, Pace A, Giovannetti LJCM. Characterization of Cr(VI)-Resistant Bacteria Isolated from Chromium-Contaminated Soil by Tannery Activity. 2003;46(1):0001-5.
153. Hallberg KB. New perspectives in acid mine drainage microbiology. *Hydrometallurgy*. 2010;104(3):448-53.
154. Burke IT, Mortimer RJG, Palaniyandi S, Whittleston RA, Lockwood CL, Ashley DJ, et al. Biogeochemical Reduction Processes in a Hyper-Alkaline Leachate Affected Soil Profile. *Geomicrobiology Journal*. 2012;29(9):769-79.
155. Williamson AJ, Morris K, Shaw S, Byrne JM, Boothman C, Lloyd JR. Microbial Reduction of Fe(III) under Alkaline Conditions Relevant to Geological Disposal. 2013;79(11):3320-6.
156. Bassil NM, Bryan N, Lloyd JR. Microbial degradation of isosaccharinic acid at high pH. *The Isme Journal*. 2014;9:310.
157. Kyeremeh IA, Charles CJ, Rout SP, Laws AP, Humphreys PN. Microbial Community Evolution Is Significantly Impacted by the Use of Calcium Isosaccharinic Acid as an Analogue for the Products of Alkaline Cellulose Degradation. *PloS one*. 2016;11(11):e0165832-e.
158. Flemming H-C, Wingender J. The biofilm matrix. *Nature Reviews Microbiology*. 2010;8:623.
159. ten Cate JMJO. Biofilms, a new approach to the microbiology of dental plaque. 2006;94(1):1-9.
160. Whiteley M, Ott JR, Weaver EA, McLean RJC. Effects of community composition and growth rate on aquifer biofilm bacteria and their susceptibility to betadine disinfection. 2001;3(1):43-52.
161. Meyer-Dombard DAR, Swingley W, Raymond J, Havig J, Shock EL, Summons RE. Hydrothermal ecotones and streamer biofilm communities in the Lower Geyser Basin, Yellowstone National Park. 2011;13(8):2216-31.

162. Hinsla-Leasure SM, Koid C, Tiedje JM, Schultzhous JN. Biofilm Formation by *Psychrobacter arcticus* and the Role of a Large Adhesin in Attachment to Surfaces. 2013;79(13):3967-73.
163. Vlamakis H, Aguilar C, Losick R, Kolter R. Control of cell fate by the formation of an architecturally complex bacterial community. *Genes & development*. 2008;22(7):945-53.
164. Stewart PS. Diffusion in biofilms. *Journal of bacteriology*. 2003;185(5):1485-91.
165. Davey ME, O'Toole GA. Microbial biofilms: from ecology to molecular genetics. *Microbiology and molecular biology reviews : MMBR*. 2000;64(4):847-67.
166. Jiao Y, D'haeseleer P, Dill BD, Shah M, VerBerkmoes NC, Hettich RL, et al. Identification of Biofilm Matrix-Associated Proteins from an Acid Mine Drainage Microbial Community. 2011;77(15):5230-7.
167. O'Toole GA, Kolter R. Flagellar and twitching motility are necessary for *Pseudomonas aeruginosa* biofilm development. 1998;30(2):295-304.
168. Petrova OE, Sauer K. Sticky situations: key components that control bacterial surface attachment. *Journal of bacteriology*. 2012;194(10):2413-25.
169. Hinsla SM, Espinosa-Urgel M, Ramos JL, O'Toole GA. Transition from reversible to irreversible attachment during biofilm formation by *Pseudomonas fluorescens* WCS365 requires an ABC transporter and a large secreted protein. 2003;49(4):905-18.
170. Ono K, Oka R, Toyofuku M, Sakaguchi A, Hamada M, Yoshida S, et al. cAMP signaling affects irreversible attachment during biofilm formation by *Pseudomonas aeruginosa* PAO1. *Microbes and environments*. 2014;29(1):104-6.
171. Das T, Sharma PK, Busscher HJ, van der Mei HC, Krom BP. Role of extracellular DNA in initial bacterial adhesion and surface aggregation. *Applied and environmental microbiology*. 2010;76(10):3405-8.
172. Romání AM, Fund K, Artigas J, Schwartz T, Sabater S, Obst UJME. Relevance of Polymeric Matrix Enzymes During Biofilm Formation. 2008;56(3):427-36.
173. Montanaro L, Poggi A, Visai L, Ravaioli S, Campoccia D, Speziale P, et al. Extracellular DNA in Biofilms. 2011;34(9):824-31.
174. Stewart PS, William Costerton J. Antibiotic resistance of bacteria in biofilms. *The Lancet*. 2001;358(9276):135-8.
175. Zhang X, Bishop PL. Biodegradability of biofilm extracellular polymeric substances. *Chemosphere*. 2003;50(1):63-9.
176. Schorer M, Eisele MJW, Air,., Pollution S. Accumulation of Inorganic and Organic Pollutants by Biofilms in the Aquatic Environment. 1997;99(1):651-9.
177. Flemming H-C, Wingender J. Relevance of microbial extracellular polymeric substances (EPSs) - Part I: Structural and ecological aspects 2001. 1-8 p.
178. Fuqua WC, Winans SC, Greenberg EP. Quorum sensing in bacteria: the LuxR-LuxI family of cell density-responsive transcriptional regulators. *Journal of bacteriology*. 1994;176(2):269-75.
179. Felchner-Zwirello M, Winter J, Gallert C. Interspecies distances between propionic acid degraders and methanogens in syntrophic consortia for optimal hydrogen transfer 2012.
180. McDougald D, Rice SA, Barraud N, Steinberg PD, Kjelleberg S. Should we stay or should we go: mechanisms and ecological consequences for biofilm dispersal. *Nature Reviews Microbiology*. 2011;10:39.
181. and MSR, Giovannoni SJ. The Uncultured Microbial Majority. 2003;57(1):369-94.

182. Meier J, Piva A, Fortin D. Enrichment of sulfate-reducing bacteria and resulting mineral formation in media mimicking pore water metal ion concentrations and pH conditions of acidic pit lakes. 2012;79(1):69-84.
183. Antony CP, Murrell JC, Shouche YS. Molecular diversity of methanogens and identification of *Methanobolus* sp. as active methylotrophic Archaea in Lonar crater lake sediments. 2012;81(1):43-51.
184. Beadle I, Humphreys PN, Pettit C, Small J. Integrating Microbiology into the Drigg Post-Closure Radiological Safety Assessment. MRS Proceedings. 2000;663:665.
185. Ye Q, Roh Y, Carroll SL, Blair B, Zhou J, Zhang CL, et al. Alkaline anaerobic respiration: isolation and characterization of a novel alkaliphilic and metal-reducing bacterium. Applied and environmental microbiology. 2004;70(9):5595-602.
186. Jintoku T, Iwata Y, Nakayama M, Tsuji T, Sakaya N, Mogi K-i, et al. Investigation of Microorganisms in Bentonite Deposits AU - Fukunaga, Sakae. Geomicrobiology Journal. 2005;22(7-8):361-70.
187. Masterson BA, Rivera A, Miranda A, Davis MA, Martin S. Bacterial Growth Dynamics, Limiting Factors, and Community Diversity in a Proposed Geological Nuclear Waste Repository Environment AU - Horn, Joanne M. Geomicrobiology Journal. 2004;21(4):273-86.
188. Hallbeck L, Pedersen K. Characterization of microbial processes in deep aquifers of the Fennoscandian Shield. Applied Geochemistry. 2008;23(7):1796-819.
189. Stewart EJ. Growing Unculturable Bacteria. 2012;194(16):4151-60.
190. Griffiths RI, Whiteley AS, O'Donnell AG, Bailey MJ. Rapid method for coextraction of DNA and RNA from natural environments for analysis of ribosomal DNA- and rRNA-based microbial community composition. Applied and environmental microbiology. 2000;66(12):5488-91.
191. Ariefdjohan MW, Savaiano DA, Nakatsu CH. Comparison of DNA extraction kits for PCR-DGGE analysis of human intestinal microbial communities from fecal specimens. Nutrition journal. 2010;9:23-.
192. Hurt RA, Jr., Robeson MS, 2nd, Shakya M, Moberly JG, Vishnivetskaya TA, Gu B, et al. Improved yield of high molecular weight DNA coincides with increased microbial diversity access from iron oxide cemented sub-surface clay environments. PloS one. 2014;9(7):e102826-e.
193. Saiki R, Gelfand D, Stoffel S, Scharf S, Higuchi R, Horn G, et al. Primer-directed enzymatic amplification of DNA with a thermostable DNA polymerase. 1988;239(4839):487-91.
194. Bartlett JMS, Stirling D. A Short History of the Polymerase Chain Reaction. In: Bartlett JMS, Stirling D, editors. PCR Protocols. Totowa, NJ: Humana Press; 2003. p. 3-6.
195. Brons JK, van Elsas JD. Analysis of bacterial communities in soil by use of denaturing gradient gel electrophoresis and clone libraries, as influenced by different reverse primers. Applied and environmental microbiology. 2008;74(9):2717-27.
196. Yang C, Cao G, Li Y, Zhang X, Ren H, Wang X, et al. Correction: A Constructed Alkaline Consortium and Its Dynamics in Treating Alkaline Black Liquor with Very High Pollution Load 2008.
197. Díez B, Pedrós-Alió C, Marsh TL, Massana R. Application of Denaturing Gradient Gel Electrophoresis (DGGE) To Study the Diversity of Marine Picoeukaryotic Assemblages and Comparison of DGGE with Other Molecular Techniques. 2001;67(7):2942-51.

198. Pedersen K. Investigations of subterranean bacteria in deep crystalline bedrock and their importance for the disposal of nuclear waste. *Canadian Journal of Microbiology*. 1996;42(4):382-91.
199. Rondon MR, August PR, Bettermann AD, Brady SF, Grossman TH, Liles MR, et al. Cloning the soil metagenome: a strategy for accessing the genetic and functional diversity of uncultured microorganisms. *Applied and environmental microbiology*. 2000;66(6):2541-7.
200. Wang GC, Wang Y. Frequency of formation of chimeric molecules as a consequence of PCR coamplification of 16S rRNA genes from mixed bacterial genomes. *Applied and environmental microbiology*. 1997;63(12):4645-50.
201. Speksnijder AGCL, Kowalchuk GA, De Jong S, Kline E, Stephen JR, Laanbroek HJ. Microvariation Artifacts Introduced by PCR and Cloning of Closely Related 16S rRNA Gene Sequences. 2001;67(1):469-72.
202. Cline J, Braman JC, Hogrefe HH. PCR fidelity of pfu DNA polymerase and other thermostable DNA polymerases. *Nucleic acids research*. 1996;24(18):3546-51.
203. Acinas SG, Sarma-Rupavtarm R, Klepac-Ceraj V, Polz MF. PCR-induced sequence artifacts and bias: insights from comparison of two 16S rRNA clone libraries constructed from the same sample. *Applied and environmental microbiology*. 2005;71(12):8966-9.
204. Abubucker S, Segata N, Goll J, Schubert AM, Izard J, Cantarel BL, et al. Metabolic reconstruction for metagenomic data and its application to the human microbiome. *PLoS computational biology*. 2012;8(6):e1002358-e.
205. Handelsman J. Metagenomics: application of genomics to uncultured microorganisms. *Microbiology and molecular biology reviews : MMBR*. 2004;68(4):669-85.
206. Sinai L, Rosenberg A, Smith Y, Segev E, Ben-Yehuda S. The molecular timeline of a reviving bacterial spore. *Molecular cell*. 2015;57(4):695-707.
207. Kambura AK, Mwirichia RK, Kasili RW, Karanja EN, Makonde HM, Boga HI. Bacteria and Archaea diversity within the hot springs of Lake Magadi and Little Magadi in Kenya. *BMC microbiology*. 2016;16(1):136-.
208. Vavourakis CD, Ghai R, Rodriguez-Valera F, Sorokin DY, Tringe SG, Hugenholtz P, et al. Metagenomic Insights into the Uncultured Diversity and Physiology of Microbes in Four Hypersaline Soda Lake Brines. *Frontiers in microbiology*. 2016;7:211-.
209. Narasingarao P, Podell S, Ugalde JA, Brochier-Armanet C, Emerson JB, Brocks JJ, et al. De novo metagenomic assembly reveals abundant novel major lineage of Archaea in hypersaline microbial communities. *The ISME journal*. 2012;6(1):81-93.
210. Parks DH, Rinke C, Chuvochina M, Chaumeil P-A, Woodcroft BJ, Evans PN, et al. Recovery of nearly 8,000 metagenome-assembled genomes substantially expands the tree of life. *Nature Microbiology*. 2017;2(11):1533-42.
211. Chun J, Lee J-H, Jung Y, Kim M, Kim S, Kim BK, et al. EzTaxon: a web-based tool for the identification of prokaryotes based on 16S ribosomal RNA gene sequences. 2007;57(10):2259-61.
212. Cole JR, Wang Q, Fish JA, Chai B, McGarrell DM, Sun Y, et al. Ribosomal Database Project: data and tools for high throughput rRNA analysis. *Nucleic acids research*. 2014;42(Database issue):D633-D42.
213. Quast C, Pruesse E, Yilmaz P, Gerken J, Schweer T, Yarza P, et al. The SILVA ribosomal RNA gene database project: improved data processing and web-based tools. *Nucleic acids research*. 2013;41(Database issue):D590-D6.
214. Johnson M, Zaretskaya I, Raytselis Y, Merezhuk Y, McGinnis S, Madden TL. NCBI BLAST: a better web interface. *Nucleic acids research*. 2008;36(Web Server issue):W5-W9.

215. Edgar RC, Haas BJ, Clemente JC, Quince C, Knight R. UCHIME improves sensitivity and speed of chimera detection. *Bioinformatics* (Oxford, England). 2011;27(16):2194-200.
216. Chao A. Nonparametric Estimation of the Number of Classes in a Population. *Scandinavian Journal of Statistics*. 1984;11(4):265-70.
217. Chazdon R, Colwell R, S. Denslow J, Guariguata M. Statistical methods for estimating species richness of woody regeneration in primary and secondary rain forests of NE Costa Rica. 1998. p. 285-309.
218. Hughes JB, Hellmann JJ, Ricketts TH, Bohannan BJM. Counting the Uncountable: Statistical Approaches to Estimating Microbial Diversity. 2001;67(10):4399-406.
219. Keylock CJ. Simpson diversity and the Shannon–Wiener index as special cases of a generalized entropy. 2005;109(1):203-7.
220. Lozupone CA, Knight R. Species divergence and the measurement of microbial diversity. *FEMS microbiology reviews*. 2008;32(4):557-78.
221. Baum MM, Kainović A, O’Keeffe T, Pandita R, McDonald K, Wu S, et al. Characterization of structures in biofilms formed by a *Pseudomonas fluorescens* isolated from soil. *BMC microbiology*. 2009;9:103-.
222. Wimpenny J, Manz W, Szewzyk U. Heterogeneity in biofilms. *FEMS Microbiology Reviews*. 2000;24(5):661-71.
223. Sandal I, Hong W, Swords WE, Inzana TJ. Characterization and Comparison of Biofilm Development by Pathogenic and Commensal Isolates of *Histophilus somni*. 2007;189(22):8179-85.
224. Dec W, Mosiałek M, Socha R, Jaworska-Kik M, Simka W, Michalska J. The effect of sulphate-reducing bacteria biofilm on passivity and development of pitting on 2205 duplex stainless steel 2016.
225. Reith F, Rogers SL, McPhail DC, Webb D. Biomineralization of Gold: Biofilms on Bacterioform Gold. 2006;313(5784):233-6.
226. Abdullah A, Yahaya N, Md Noor N, Mohd Rasol R. Microbial Corrosion of API 5L X-70 Carbon Steel by ATCC 7757 and Consortium of Sulfate-Reducing Bacteria %J *Journal of Chemistry*. 2014;2014:7.
227. Chicote E, García AM, Moreno DA, Sarró MI, Lorenzo PI, Montero FJJoIM, et al. Isolation and identification of bacteria from spent nuclear fuel pools. 2005;32(4):155-62.
228. Chen M-Y, Lee D-J, Tay J-H, Show K-YJAM, *Biotechnology*. Staining of extracellular polymeric substances and cells in bioaggregates. 2007;75(2):467-74.
229. González-Machado C, Capita R, Riesco-Peláez F, Alonso-Calleja C. Visualization and quantification of the cellular and extracellular components of *Salmonella Agona* biofilms at different stages of development. *PloS one*. 2018;13(7):e0200011-e.
230. Ainsworth TD, Fine M, Blackall LL, Hoegh-Guldberg O. Fluorescence in situ hybridization and spectral imaging of coral-associated bacterial communities. *Applied and environmental microbiology*. 2006;72(4):3016-20.
231. Wagner D, Kobabe S, Pfeiffer E-M. Characterisation of microbial community composition of a Siberian tundra soil by fluorescence in situ hybridisation. *FEMS Microbiology Ecology*. 2004;50(1):13-23.
232. Takai K, Moser DP, Onstott TC, Spoelstra N, Pfiffner SM, Dohnalkova A, et al. *Alkaliphilus transvaalensis* gen. nov., sp. nov., an extremely alkaliphilic bacterium isolated from a deep South African gold mine. 2001;51(4):1245-56.

233. S Roadcap G, Sanford R, Jin Q, Pardinas J, M Bethke C. Extremely Alkaline (pH > 12) Ground Water Hosts Diverse Microbial Community 2006. 511-7 p.
234. Metcalfe R, Crawford MB, Bath AH, Littleboy AK, Degnan PJ, Richards HG. Characteristics of deep groundwater flow in a basin marginal setting at Sellafield, Northwest England: 36Cl and halide evidence. *Applied Geochemistry*. 2007;22(1):128-51.
235. Suzuki S, Kuenen JG, Schipper K, van der Velde S, Ishii Si, Wu A, et al. Physiological and genomic features of highly alkaliphilic hydrogen-utilizing Betaproteobacteria from a continental serpentinizing site. *Nature Communications*. 2014;5:3900.
236. Kral TA, Birch W, Lavender LE, Virden BT. Potential use of highly insoluble carbonates as carbon sources by methanogens in the subsurface of Mars. *Planetary and Space Science*. 2014;101:181-5.
237. B.S.I. BS ISO 14853:2005 Plastics. Determination of the ultimate anaerobic biodegradation of plastic materials in an aqueous system. Method by measurement of biogas production. London: British Standards Institute; 2005.
238. Almond M, Shaw PB, Humphreys PN, Chadha MJ, Niemelä K, Laws AP. Behaviour of xyloisosaccharinic acid and xyloisosaccharino-1,4-lactone in aqueous solutions at varying pHs. *Carbohydrate Research*. 2012;363:51-7.
239. Shaw PB, Robinson GF, Rice CR, Humphreys PN, Laws AP. A robust method for the synthesis and isolation of  $\beta$ -gluco-isosaccharinic acid ((2R,4S)-2,4,5-trihydroxy-2-(hydroxymethyl)pentanoic acid) from cellulose and measurement of its aqueous pKa. *Carbohydrate Research*. 2012;349:6-11.
240. B.S.I. BS ISO10390:2005 Soil quality. Determination of pH. London: British Standards Institute; 2005.
241. Brück WM, Brück TB, Self WT, Reed JK, Nitecki SS, McCarthy PJ. Comparison of the anaerobic microbiota of deep-water *Geodia* spp. and sandy sediments in the Straits of Florida. *The Isme Journal*. 2010;4:686.
242. Manz W, Amann R, Ludwig W, Vancanneyt M, Schleifer K-H. Application of a suite of 16S rRNA-specific oligonucleotide probes designed to investigate bacteria of the phylum cytophaga-flavobacter-bacteroides in the natural environment. 1996;142(5):1097-106.
243. Lückner S, Steger D, Kjeldsen KU, MacGregor BJ, Wagner M, Loy A. Improved 16S rRNA-targeted probe set for analysis of sulfate-reducing bacteria by fluorescence in situ hybridization. *Journal of Microbiological Methods*. 2007;69(3):523-8.
244. Castillo M, Skene G, Roca M, Anguita M, Badiola I, Duncan SH, et al. Application of 16S rRNA gene-targeted fluorescence in situ hybridization and restriction fragment length polymorphism to study porcine microbiota along the gastrointestinal tract in response to different sources of dietary fibre. 2007;59(1):138-46.
245. Takahashi S, Tomita J, Nishioka K, Hisada T, Nishijima M. Development of a Prokaryotic Universal Primer for Simultaneous Analysis of Bacteria and Archaea Using Next-Generation Sequencing. *PLOS ONE*. 2014;9(8):e105592.
246. Cheng YF, Mao SY, Liu JX, Zhu WY. Molecular diversity analysis of rumen methanogenic Archaea from goat in eastern China by DGGE methods using different primer pairs. 2009;48(5):585-92.
247. Cytryn E, Minz D, Oremland RS, Cohen Y. Distribution and diversity of archaea corresponding to the limnological cycle of a hypersaline stratified lake (Solar lake, Sinai, Egypt). *Applied and environmental microbiology*. 2000;66(8):3269-76.

248. Masella AP, Bartram AK, Truszkowski JM, Brown DG, Neufeld JDJBB. PANDAseq: paired-end assembler for illumina sequences. 2012;13(1):31.
249. Huang Y, Niu B, Gao Y, Fu L, Li W. CD-HIT Suite: a web server for clustering and comparing biological sequences. *Bioinformatics (Oxford, England)*. 2010;26(5):680-2.
250. Metsalu T, Vilo J. ClustVis: a web tool for visualizing clustering of multivariate data using Principal Component Analysis and heatmap. *Nucleic Acids Research*. 2015;43(W1):W566-W70.
251. Janssen PH, Frenzel P. Inhibition of methanogenesis by methyl fluoride: studies of pure and defined mixed cultures of anaerobic bacteria and archaea. 1997;63(11):4552-7.
252. Angel R, Claus P, Conrad R. Methanogenic archaea are globally ubiquitous in aerated soils and become active under wet anoxic conditions. *The Isme Journal*. 2011;6:847.
253. Avery GB, Martens CS. Controls on the stable carbon isotopic composition of biogenic methane produced in a tidal freshwater estuarine sediment. *Geochimica et Cosmochimica Acta*. 1999;63(7):1075-82.
254. Chang C-F, Chen J-W. The experimental investigation of concrete carbonation depth. *Cement and Concrete Research*. 2006;36(9):1760-7.
255. Brito EMS, Piñón-Castillo HA, Guyoneaud R, Caretta CA, Gutiérrez-Corona JF, Duran R, et al. Bacterial biodiversity from anthropogenic extreme environments: a hyper-alkaline and hyper-saline industrial residue contaminated by chromium and iron. *Applied Microbiology and Biotechnology*. 2013;97(1):369-78.
256. Leboulanger C, Agogué H, Bernard C, Bouvy M, Carré C, Cellamare M, et al. Microbial Diversity and Cyanobacterial Production in Dziani Dzaha Crater Lake, a Unique Tropical Thalassohaline Environment. *PLOS ONE*. 2017;12(1):e0168879.
257. Aguirre-Garrido JF, Ramírez-Saad HC, Toro N, Martínez-Abarca F. Bacterial Diversity in the Soda Saline Crater Lake from Isabel Island, Mexico. *Microbial Ecology*. 2016;71(1):68-77.
258. White R. Aspects of the Management of the Remains of Limestone Industries in the Yorkshire Dales. *Industrial Archaeology Review*. 2006;28(2):107-15.
259. Gomes HI, Mayes WM, Rogerson M, Stewart DI, Burke IT. Alkaline residues and the environment: a review of impacts, management practices and opportunities. *Journal of Cleaner Production*. 2016;112:3571-82.
260. Williams R. *Lime Kilns and Lime Burning*. UK: Bloomsbury Publishing; 2008.
261. Johnson D. The Archaeology and Technology of Early-Modern Lime Burning in the Yorkshire Dales: Developing a Clamp Kiln Model. *Industrial Archaeology Review*. 2008;30(2):127-43.
262. A E Milodowski RPS, D I Stewart. The Harpur Hill Site: its geology, evolutionary history and a catalogue of materials present. 2013. Report No.: CR/13/104.
263. N.D.A. Geological Disposal: Near-Field Evolution Status Report. 2010. Report No.: NDA/RWMD/033.
264. Wu X, Wu L, Liu Y, Zhang P, Li Q, Zhou J, et al. Microbial Interactions With Dissolved Organic Matter Drive Carbon Dynamics and Community Succession. *Frontiers in microbiology*. 2018;9:1234-.
265. Li D, Sharp JO, Saikaly PE, Ali S, Alidina M, Alarawi MS, et al. Dissolved Organic Carbon Influences Microbial Community Composition and Diversity in Managed Aquifer Recharge Systems. *Applied and Environmental Microbiology*. 2012;78(19):6819-28.
266. Mayes W, Younger P, Aumônier J. Hydrogeochemistry of Alkaline Steel Slag Leachates in the UK2008. 35-50 p.

267. Gryndler M, Rohlenová J, Kopecký J, Matucha M. Chloride concentration affects soil microbial community. *Chemosphere*. 2008;71(7):1401-8.
268. Gadd GM, Griffiths AJ. Microorganisms and heavy metal toxicity. *Microbial Ecology*. 1977;4(4):303-17.
269. Deocampo D, F Jones B. *Geochemistry of Saline Lakes*. 2014. p. 437-69.
270. Lüneberg K, Schneider D, Siebe C, Daniel R. Drylands soil bacterial community is affected by land use change and different irrigation practices in the Mezquital Valley, Mexico. *Scientific Reports*. 2018;8(1):1413.
271. Azarbad H, Niklinska M, Gestel C, van Straalen NM, Röling W, Laskowski R. Microbial community structure and functioning along metal pollution gradients 2013.
272. Simon Gaisford VK, Peter Haines. *Principles of Thermal Analysis and Calorimetry: 2nd Edition*. illustrated ed: Royal Society of Chemistry; 2016. 268 pages p.
273. Plante AF, Fernández JM, Leifeld J. Application of thermal analysis techniques in soil science. *Geoderma*. 2009;153(1):1-10.
274. Goulding KWT. Soil acidification and the importance of liming agricultural soils with particular reference to the United Kingdom. *Soil use and management*. 2016;32(3):390-9.
275. Magdziarz A, Werle S. Analysis of the combustion and pyrolysis of dried sewage sludge by TGA and MS. *Waste Management*. 2014;34(1):174-9.
276. De Mandal S, Chatterjee R, Kumar NS. Dominant bacterial phyla in caves and their predicted functional roles in C and N cycle. *BMC microbiology*. 2017;17(1):90-.
277. Wang YF, Zhu HW, Wang Y, Zhang XL, Tam NFY. Diversity and Dynamics of Microbial Community Structure in Different Mangrove, Marine and Freshwater Sediments During Anaerobic Debromination of PBDEs. 2018;9(952).
278. Zheng B, Wang L, Liu L. Bacterial community structure and its regulating factors in the intertidal sediment along the Liaodong Bay of Bohai Sea, China. *Microbiological Research*. 2014;169(7):585-92.
279. Kalwasińska A, Felföldi T, Szabó A, Deja-Sikora E, Kosobucki P, Walczak M. Microbial communities associated with the anthropogenic, highly alkaline environment of a saline soda lime, Poland. *Antonie van Leeuwenhoek*. 2017;110(7):945-62.
280. Galperin MY. Genome Diversity of Spore-Forming Firmicutes. *Microbiology spectrum*. 2013;1(2):TBS-0015-2012.
281. Vekeman B, Kerckhof F-M, Cremers G, de Vos P, Vandamme P, Boon N, et al. New *Methyloceanibacter* diversity from North Sea sediments includes methanotroph containing solely the soluble methane monooxygenase. 2016;18(12):4523-36.
282. Mantri S, Chinthlagiri MR, Gundlapally SRJAoM. Description of *Hydrogenophaga laconesensis* sp. nov. isolated from tube well water. 2016;198(7):637-44.
283. Miyazaki M, Koide O, Kobayashi T, Mori K, Shimamura S, Nunoura T, et al. *Geofilum rubicundum* gen. nov., sp. nov., isolated from deep seafloor sediment. 2012;62(5):1075-80.
284. Salah ZB, Charles CJ, Humphreys PN, Laws AP, Rout SP. Genomic Insights Into A Novel, Alkalitolerant Nitrogen Fixing Bacteria, *Azonexus* sp. Strain ZS02. *Journal of genomics*. 2019;7:1-6.
285. Sucharita K, Sasikala C, Park SC, Baik KS, Seong CN, Ramana CV. *Shewanella chilikensis* sp. nov., a moderately alkaliphilic gammaproteobacterium isolated from a lagoon. 2009;59(12):3111-5.

286. Kalyuzhnaya MG, Bowerman S, Lara JC, Lidstrom ME, Chistoserdova L. *Methylotenera mobilis* gen. nov., sp. nov., an obligately methylamine-utilizing bacterium within the family Methylophilaceae. 2006;56(12):2819-23.
287. Barton L, Fardeau M-L, Fauque G. Hydrogen Sulfide: A Toxic Gas Produced by Dissimilatory Sulfate and Sulfur Reduction and Consumed by Microbial Oxidation 2014. 237-77 p.
288. Dias M, Salvado JC, Monperrus M, Caumette P, Amouroux D, Duran R, et al. Characterization of *Desulfomicrobium salsuginis* sp. nov. and *Desulfomicrobium aestuarii* sp. nov., two new sulfate-reducing bacteria isolated from the Adour estuary (French Atlantic coast) with specific mercury methylation potentials. *Systematic and Applied Microbiology*. 2008;31(1):30-7.
289. Rosnes JT, Torsvik T, Lien T. Spore-forming thermophilic sulfate-reducing bacteria isolated from North Sea oil field waters. 1991:Medium: X; Size: Pages: 2302-7.
290. Campbell LL, Postgate JR. Classification of the spore-forming sulfate-reducing bacteria. *Bacteriological reviews*. 1965;29(3):359-63.
291. de Rezende JR, Hubert CRJ, Røy H, Kjeldsen KU, Jørgensen BB. Estimating the Abundance of Endospores of Sulfate-Reducing Bacteria in Environmental Samples by Inducing Germination and Exponential Growth. *Geomicrobiology Journal*. 2017;34(4):338-45.
292. Kwon MJ, O'Loughlin EJ, Boyanov MI, Brulc JM, Johnston ER, Kemner KM, et al. Impact of Organic Carbon Electron Donors on Microbial Community Development under Iron- and Sulfate-Reducing Conditions. *PloS one*. 2016;11(1):e0146689-e.
293. Dissimilatory sulphate reduction with acetate as electron donor. 1982;298(1093):467-71.
294. Smith RL, Klug MJ. Electron donors utilized by sulfate-reducing bacteria in eutrophic lake sediments. *Applied and environmental microbiology*. 1981;42(1):116-21.
295. Lennon JT, Jones SE. Microbial seed banks: the ecological and evolutionary implications of dormancy. *Nature Reviews Microbiology*. 2011;9:119.
296. Ransom-Jones E, Jones DL, McCarthy AJ, McDonald JEJME. The Fibrobacteres: an Important Phylum of Cellulose-Degrading Bacteria. 2012;63(2):267-81.
297. Anandkumar B, George RP, Maruthamuthu S, Palaniswamy N, Dayal RK. Corrosion behavior of SRB *Desulfobulbus propionicus* isolated from an Indian petroleum refinery on mild steel. 2012;63(4):355-62.
298. Widdel F. New types of acetate-oxidizing, sulfate-reducing *Desulfobacter* species, *D. hydrogenophilus* sp. nov., *D. latus* sp. nov., and *D. curvatus* sp. nov. *Archives of Microbiology*. 1987;148(4):286-91.
299. Kitano Y, Oomori TJJotOSoJ. The coprecipitation of uranium with calcium carbonate. 1971;27(1):34-42.
300. Purser G, Milodowski AE, Harrington JF, Rochelle CA, Butcher A, Wagner D. Modification to the Flow Properties of Repository Cement as a Result of Carbonation. *Procedia Earth and Planetary Science*. 2013;7:701-4.
301. Schmitt J, Flemming HC. Water binding in biofilms. *Water Science and Technology*. 1999;39(7):77-82.
302. Cruz LF, Cobine PA, De La Fuente L. Calcium increases *Xylella fastidiosa* surface attachment, biofilm formation, and twitching motility. *Applied and environmental microbiology*. 2012;78(5):1321-31.

303. Doulgeris C, Humphreys P, Rout S. An approach to modelling the impact of <sup>14</sup>C release from reactor graphite in a geological disposal facility 2015. 1495-503 p.
304. Charles C, Rout S, Garratt E, Patel K, Laws A, Humphreys P. The enrichment of an alkaliphilic biofilm consortia capable of the anaerobic degradation of isosaccharinic acid from cellulosic materials incubated within an anthropogenic, hyperalkaline environment. *FEMS microbiology ecology*. 2015:fiv085.
305. Karakashev D, Batstone DJ, Trably E, Angelidaki I. Acetate Oxidation Is the Dominant Methanogenic Pathway from Acetate in the Absence of Methanosaetaceae. 2006;72(7):5138-41.
306. Whitman WB, Bowen TL, Boone DR. The Methanogenic Bacteria. In: Dworkin M, Falkow S, Rosenberg E, Schleifer K-H, Stackebrandt E, editors. *The Prokaryotes: Volume 3: Archaea Bacteria: Firmicutes, Actinomycetes*. New York, NY: Springer New York; 2006. p. 165-207.
307. von Klein D, Arab H, Völker H, Thomm MJE. *Methanosarcina baltica*, sp. nov., a novel methanogen isolated from the Gotland Deep of the Baltic Sea. 2002;6(2):103-10.
308. Mukhopadhyay B, Purwantini E, Conway de Macario E, Daniels LJCM. Characterization of a *Methanosarcina* strain isolated from goat feces, and that grows on H<sub>2</sub>-CO<sub>2</sub> only after adaptation. 1991;23(3):165-73.
309. Asakawa S, Akagawa-Matsushita M, Morii H, Koga Y, Hayano K. Characterization of *Methanosarcina mazei* TMA isolated from a paddy field soil 1995. 34-8 p.
310. J Cairó J, Clarens M, Touzel J-P, Bardulet M, M París J. *Methanosarcina mazei* JC2, a new methanogenic strain isolated from lake sediments, that does not use H<sub>2</sub>/CO<sub>2</sub> 1992. 21-31 p.
311. Lyimo TJ, Pol A, Op den Camp HJ, Harhangi HR, Vogels GD. *Methanosarcina semesiae* sp. nov., a dimethylsulfide-utilizing methanogen from mangrove sediment. 2000;50(1):171-8.
312. WORAKIT S, BOONE DR, MAH RA, ABDEL-SAMIE M-E, EL-HALWAGI MM. *Methanobacterium alcaliphilum* sp. nov., an H<sub>2</sub>-Utilizing Methanogen That Grows at High pH Values. 1986;36(3):380-2.
313. Battumur U, Yoon Y-M, Kim C-H. Isolation and Characterization of a New *Methanobacterium formicicum* KOR-1 from an Anaerobic Digester Using Pig Slurry. *Asian-Australasian journal of animal sciences*. 2016;29(4):586-93.
314. Joulain C, Patel B, Ollivier B, L Garcia J, Roger P. *Methanobacterium oryzae* sp. nov., a novel methanogenic rod isolated from a Philippines ricefield 2000. 525-8 p.
315. Shlimon AG, Friedrich MW, Niemann H, Ramsing NB, Finster K. *Methanobacterium aarhusense* sp. nov., a novel methanogen isolated from a marine sediment (Aarhus Bay, Denmark). 2004;54(3):759-63.
316. Shimizu S, Ueno A, Tamamura S, Naganuma T, Kaneko K. *Methanoculleus horonobensis* sp. nov., a methanogenic archaeon isolated from a deep diatomaceous shale formation. 2013;63(11):4320-3.
317. Cheng L, Qiu T-L, Li X, Wang W-D, Deng Y, Yin X-B, et al. Isolation and characterization of *Methanoculleus receptaculi* sp. nov. from Shengli oil field, China. *FEMS Microbiology Letters*. 2008;285(1):65-71.
318. Tian J, Wang Y, Dong X. *Methanoculleus hydrogenitrophicus* sp. nov., a methanogenic archaeon isolated from wetland soil. 2010;60(9):2165-9.
319. Dianou D, Miyaki T, Asakawa S, Morii H, Nagaoka K, Oyaizu H, et al. *Methanoculleus chikugoensis* sp. nov., a novel methanogenic archaeon isolated from paddy

- field soil in Japan, and DNA-DNA hybridization among *Methanoculleus* species. 2001;51(5):1663-9.
320. Hattori S. Syntrophic Acetate-Oxidizing Microbes in Methanogenic Environments. *Microbes and Environments*. 2008;23(2):118-27.
321. Ye R, Jin Q, Bohannon B, Keller JK, McAllister SA, Bridgham SD. pH controls over anaerobic carbon mineralization, the efficiency of methane production, and methanogenic pathways in peatlands across an ombrotrophic–minerotrophic gradient. *Soil Biology and Biochemistry*. 2012;54:36-47.
322. Welte C, Kröninger L, Deppenmeier U. Experimental evidence of an acetate transporter protein and characterization of acetate activation in aceticlastic methanogenesis of *Methanosarcina mazei*. *FEMS Microbiology Letters*. 2014;359(2):147-53.
323. Welte C, Deppenmeier U. Bioenergetics and anaerobic respiratory chains of aceticlastic methanogens. *Biochimica et Biophysica Acta (BBA) - Bioenergetics*. 2014;1837(7):1130-47.
324. Mathrani IM, Boone DR, Mah RA, Fox GE, Lau PP. *Methanohalophilus zhilinae* sp. nov., an Alkaliphilic, Halophilic, Methylotrophic Methanogen. 1988;38(2):139-42.
325. Jetten MSM, Stams AJM, Zehnder AJB. Methanogenesis from acetate: a comparison of the acetate metabolism in *Methanotrix soehngenii* and *Methanosarcina* spp. *FEMS Microbiology Reviews*. 1992;8(3-4):181-97.
326. Daebeler A, Gansen M, Frenzel P. Methyl fluoride affects methanogenesis rather than community composition of methanogenic archaea in a rice field soil. *PloS one*. 2013;8(1):e53656-e.
327. Conrad R, Klose M. How specific is the inhibition by methyl fluoride of acetoclastic methanogenesis in anoxic rice field soil? *FEMS Microbiology Ecology*. 1999;30(1):47-56.
328. M. Maestrojuan G, R. Boone D. Characterization of *Methanosarcina barkeri* MST and 227, *Methanosarcina mazei* S-6T, and *Methanosarcina vacuolata* Z-76IT1991.
329. Dridi B, Fardeau M-L, Ollivier B, Raoult D, Drancourt M. *Methanomassiliicoccus luminyensis* gen. nov., sp. nov., a methanogenic archaeon isolated from human faeces. 2012;62(8):1902-7.
330. Ye R, Jin Q, Bohannon B, Keller JK, Bridgham SD. Homoacetogenesis: A potentially underappreciated carbon pathway in peatlands. *Soil Biology and Biochemistry*. 2014;68:385-91.
331. Ellis DE, Lutz EJ, Odom JM, Buchanan RJ, Bartlett CL, Lee MD, et al. Bioaugmentation for Accelerated In Situ Anaerobic Bioremediation. *Environmental Science & Technology*. 2000;34(11):2254-60.
332. Hoehler TM, Albert DB, Alperin MJ, Martens CS. Acetogenesis from CO<sub>2</sub> in an anoxic marine sediment. 1999;44(3):662-7.
333. Liu F, Conrad R. Chemolithotrophic acetogenic H<sub>2</sub>/CO<sub>2</sub> utilization in Italian rice field soil. *The Isme Journal*. 2011;5:1526.
334. Nozhevnikova AN, Kotsyurbenko OR, Simankova MV. Acetogenesis at Low Temperature. In: Drake HL, editor. *Acetogenesis*. Boston, MA: Springer US; 1994. p. 416-31.
335. Morgan-Sagastume F, Pratt S, Karlsson A, Cirne D, Lant P, Werker A. Production of volatile fatty acids by fermentation of waste activated sludge pre-treated in full-scale thermal hydrolysis plants. *Bioresource Technology*. 2011;102(3):3089-97.
336. Ma K, Liu X, Dong X. *Methanobacterium beijingense* sp. nov., a novel methanogen isolated from anaerobic digesters. 2005;55(1):325-9.

337. König H. Isolation and characterization of *Methanobacterium uliginosum* sp. nov. from a marshy soil. *Canadian Journal of Microbiology*. 1984;30(12):1477-81.
338. Blotevogel K-H, Fischer U, Mocha M, Janssen SJAoM. *Methanobacterium thermoalcaliphilum* spec. nov., a new moderately alkaliphilic and thermophilic autotrophic methanogen. 1985;142(3):211-7.
339. Ferry JG. Fundamentals of methanogenic pathways that are key to the biomethanation of complex biomass. *Current opinion in biotechnology*. 2011;22(3):351-7.
340. Lackner N, Hintersonleitner A, Wagner AO, Illmer P. Hydrogenotrophic Methanogenesis and Autotrophic Growth of *Methanosarcina thermophila* %J *Archaea*. 2018;2018:7.
341. Cheng L, Qiu T-L, Li X, Wang W-D, Deng Y, Yin X-B, et al. Isolation and characterization of *Methanoculleus receptaculi* sp. nov. from Shengli oil field, China. 2008;285(1):65-71.
342. Lai M-C, Lin C-C, Yu P-H, Huang Y-F, Chen S-C. *Methanocalculus chunghsingensis* sp. nov., isolated from an estuary and a marine fishpond in Taiwan. 2004;54(1):183-9.
343. Sorokin DY, Abbas B, Merkel AY, Rijpstra WIC, Damsté JSS, Sukhacheva MV, et al. *Methanosalsum natronophilum* sp. nov., and *Methanocalculus alkaliphilus* sp. nov., haloalkaliphilic methanogens from hypersaline soda lakes. 2015;65(10):3739-45.
344. Wintsche B, Glaser K, Sträuber H, Centler F, Liebetrau J, Harms H, et al. Trace Elements Induce Predominance among Methanogenic Activity in Anaerobic Digestion. *Frontiers in microbiology*. 2016;7:2034-.
345. Glass JB, Orphan VJ. Trace metal requirements for microbial enzymes involved in the production and consumption of methane and nitrous oxide. *Frontiers in microbiology*. 2012;3:61-.
346. Yang G-C, Zhou L, Mbadinga SM, Liu J-F, Yang S-Z, Gu J-D, et al. Formate-Dependent Microbial Conversion of CO<sub>2</sub> and the Dominant Pathways of Methanogenesis in Production Water of High-temperature Oil Reservoirs Amended with Bicarbonate. *Frontiers in microbiology*. 2016;7:365-.
347. Rotaru A-E, Shrestha PM, Liu F, Shrestha M, Shrestha D, Embree M, et al. A new model for electron flow during anaerobic digestion: direct interspecies electron transfer to *Methanosaeta* for the reduction of carbon dioxide to methane. *Energy & Environmental Science*. 2014;7(1):408-15.
348. Yoo K, Lee S-H, Hwang S-H, Ahn J-W. Effect of CO<sub>2</sub> Carbonation on the Chemical Properties of Waste Cement: CEC and the Heavy Metal Adsorption Ability 2011. 1679-84 p.
349. Žigovečki Gobac Ž, Posilović H, Bermanec V. Identification of biogenetic calcite and aragonite using SEM 2009. 201-6 p.
350. Philips J, Rabaey K, Lovley DR, Vargas M. Biofilm Formation by *Clostridium ljungdahlii* Is Induced by Sodium Chloride Stress: Experimental Evaluation and Transcriptome Analysis. *PloS one*. 2017;12(1):e0170406-e.
351. Bang C, Ehlers C, Orell A, Prasse D, Spinner M, Gorb SN, et al. Biofilm formation of mucosa-associated methanoarchaeal strains. *Frontiers in microbiology*. 2014;5:353-.
352. Tang L, Schramm A, Neu TR, Revsbech NP, Meyer RL. Extracellular DNA in adhesion and biofilm formation of four environmental isolates: a quantitative study. *FEMS Microbiology Ecology*. 2013;86(3):394-403.
353. Watanabe M, Sasaki K, Nakashimada Y, Kakizono T, Noparatnaraporn N, Nishio NJAM, et al. Growth and flocculation of a marine photosynthetic bacterium *Rhodovulum* sp. 1998;50(6):682-91.

354. Whitchurch CB, Tolker-Nielsen T, Ragas PC, Mattick JS. Extracellular DNA Required for Bacterial Biofilm Formation. 2002;295(5559):1487-.
355. Wilton M, Charron-Mazenod L, Moore R, Lewenza S. Extracellular DNA Acidifies Biofilms and Induces Aminoglycoside Resistance in *Pseudomonas aeruginosa*. 2016;60(1):544-53.
356. Chen S, Dong X. *Proteiniphilum acetatigenes* gen. nov., sp. nov., from a UASB reactor treating brewery wastewater. 2005;55(6):2257-61.
357. Sorokin DY, Rusanov II, Pimenov NV, Tourova TP, Abbas B, Muyzer G. Sulfidogenesis under extremely haloalkaline conditions in soda lakes of Kulunda Steppe (Altai, Russia). *FEMS Microbiology Ecology*. 2010;73(2):278-90.
358. Ryzhmanova Y, Nepomnyashchaya Y, Abashina T, Ariskina E, Troshina O, Vainshtein M, et al. New sulfate-reducing bacteria isolated from Buryatian alkaline brackish lakes: description of *Desulfonatronum buryatense* sp. nov. *Extremophiles*. 2013;17(5):851-9.
359. Raskin L, Rittmann BE, Stahl DA. Competition and coexistence of sulfate-reducing and methanogenic populations in anaerobic biofilms. *Applied and Environmental Microbiology*. 1996;62(10):3847-57.
360. Brysch K, Schneider C, Fuchs G, Widdel F. Lithoautotrophic growth of sulfate-reducing bacteria, and description of *Desulfobacterium autotrophicum* gen. nov., sp. nov. *Archives of Microbiology*. 1987;148(4):264-74.
361. Pikuta E, Lysenko A, Suzina N, Osipov G, Kuznetsov B, Tourova T, et al. *Desulfotomaculum alkaliphilum* sp. nov., a new alkaliphilic, moderately thermophilic, sulfate-reducing bacterium. *International Journal of Systematic and Evolutionary Microbiology*. 2000;50(1):25-33.
362. Dar SA, Kleerebezem R, Stams AJM, Kuenen JG, Muyzer G. Competition and coexistence of sulfate-reducing bacteria, acetogens and methanogens in a lab-scale anaerobic bioreactor as affected by changing substrate to sulfate ratio. *Applied Microbiology and Biotechnology*. 2008;78(6):1045-55.
363. Oremland RS, Polcin S. Methanogenesis and Sulfate Reduction: Competitive and Noncompetitive Substrates in Estuarine Sediments. *Applied and Environmental Microbiology*. 1982;44(6):1270-6.
364. Ozuolmez D, Na H, Lever M, Kjeldsen K, Jørgensen B, Plugge C. Methanogenic archaea and sulfate reducing bacteria co-cultured on acetate: teamwork or coexistence? *Frontiers in Microbiology*. 2015;6(492).
365. Jiao Y, D'haeseleer P, Dill BD, Shah M, VerBerkmoes NC, Hettich RL, et al. Identification of Biofilm Matrix-Associated Proteins from an Acid Mine Drainage Microbial Community. *Applied and Environmental Microbiology*. 2011;77(15):5230-7.
366. Liermann LJ, Barnes AS, Kalinowski BE, Zhou X, Brantley SL. Microenvironments of pH in biofilms grown on dissolving silicate surfaces. *Chemical Geology*. 2000;171(1):1-16.
367. Mattos KA, Jones C, Heise N, Previato JO, Mendonça-Previato L. Structure of an acidic exopolysaccharide produced by the diazotrophic endophytic bacterium *Burkholderia brasiliensis*. *European Journal of Biochemistry*. 2001;268(11):3174-9.
368. Nielsen M, Revsbech NP, Kühl M. Microsensor measurements of hydrogen gas dynamics in cyanobacterial microbial mats. *Frontiers in Microbiology*. 2015;6(726).
369. Masaaki Kaneko NM, Ai Fujiwara, Masafumi Yamamoto. Evaluation of Gas Generation Rate by Metal Corrosion in the Reducing Environment The Radioactive Waste Management Funding and Research Center 2004

370. Stams AJM, Elferink SJWHO, Westermann P. Metabolic Interactions Between Methanogenic Consortia and Anaerobic Respiring Bacteria. In: Ahring BK, Angelidaki I, de Macario EC, Gavala HN, Hofman-Bang J, Macario AJL, et al., editors. Biomethanation I. Berlin, Heidelberg: Springer Berlin Heidelberg; 2003. p. 31-56.
371. Kiilerich B, van de Ven W, Nielsen A, Vollertsen J. Sulfide Precipitation in Wastewater at Short Timescales. *Water*. 2017;9(9):670.
372. Reeburgh WS. Rates of Biogeochemical Processes in Anoxic Sediments. *Annual Review of Earth and Planetary Sciences*. 1983;11(1):269-98.
373. Percival SL, Beech IB, Edyvean RGJ, Knapp JS, Wales DS. Biofilm Development on 304 and 316 Stainless Steels in a Potable Water System. *Water and Environment Journal*. 1997;11(4):289-94.
374. Rajala P, Carpén L, Vepsäläinen M, Raulio M, Sohlberg E, Bomberg M. Microbially induced corrosion of carbon steel in deep groundwater environment. *Frontiers in Microbiology*. 2015;6(647).
375. Holma B, Hegg PO. pH- and protein-dependent buffer capacity and viscosity of respiratory mucus. Their interrelationships and influence of health. *Science of The Total Environment*. 1989;84:71-82.
376. Limoli DH, Jones CJ, Wozniak DJ. Bacterial Extracellular Polysaccharides in Biofilm Formation and Function. *Microbiology Spectrum*. 2015;3(3).
377. Fong JNC, Yildiz FH. Biofilm Matrix Proteins. *Microbiology spectrum*. 2015;3(2):10.1128/microbiolspec.MB-0004-2014.
378. Manivasagan P, Sivasankar P, Venkatesan J, Senthilkumar K, Sivakumar K, Kim S-K. Production and characterization of an extracellular polysaccharide from *Streptomyces violaceus* MM72. *International Journal of Biological Macromolecules*. 2013;59:29-38.
379. Zenova GM, Manucharova NA, Zvyagintsev DG. Extremophilic and extremotolerant actinomycetes in different soil types. *Eurasian Soil Science*. 2011;44(4):417-36.
380. Mirzoyan N, Schreier HJ. Effect of sulfide on growth of marine bacteria. *Archives of Microbiology*. 2014;196(4):279-87.
381. Sánchez-Andrea I, Stams AJM, Amils R, Sanz JL. Enrichment and isolation of acidophilic sulfate-reducing bacteria from Tinto River sediments. *Environmental Microbiology Reports*. 2013;5(5):672-8.
382. Frank YA, Kadnikov VV, Lukina AP, Banks D, Beletsky AV, Mardanov AV, et al. Characterization and Genome Analysis of the First Facultatively Alkaliphilic *Thermodesulfobacterium* Isolated from the Deep Terrestrial Subsurface. *Frontiers in Microbiology*. 2016;7:2000.
383. Jeanthon C, apos, Haridon S, Cueff V, Banta A, Reysenbach A-L, et al. *Thermodesulfobacterium hydrogenophilum* sp. nov., a thermophilic, chemolithoautotrophic, sulfate-reducing bacterium isolated from a deep-sea hydrothermal vent at Guaymas Basin, and emendation of the genus *Thermodesulfobacterium*. *International Journal of Systematic and Evolutionary Microbiology*. 2002;52(3):765-72.
384. Pikuta EV, Hoover RB, Bej AK, Marsic D, Whitman WB, Cleland D, et al. *Desulfonatronum thiodismutans* sp. nov., a novel alkaliphilic, sulfate-reducing bacterium capable of lithoautotrophic growth. *International Journal of Systematic and Evolutionary Microbiology*. 2003;53(5):1327-32.
385. Pérez Bernal MF, Souza Brito EM, Bartoli M, Aubé J, Fardeau M-L, Cuevas Rodriguez G, et al. *Desulfonatronum parangueonense* sp. nov., a sulfate-reducing bacterium

- isolated from sediment of an alkaline crater lake. *International Journal of Systematic and Evolutionary Microbiology*. 2017;67(12):4999-5005.
386. Zhilina TN, Zavarzina DG, Kuever J, Lysenko AM, Zavarzin GA. *Desulfonatronum cooperativum* sp. nov., a novel hydrogenotrophic, alkaliphilic, sulfate-reducing bacterium, from a syntrophic culture growing on acetate. *International Journal of Systematic and Evolutionary Microbiology*. 2005;55(3):1001-6.
387. Zakharyuk AG, Kozyreva LP, Khijniak TV, Namsaraev BB, Shcherbakova VA. *Desulfonatronum zhilinae* sp. nov., a novel haloalkaliphilic sulfate-reducing bacterium from soda Lake Alginskoe, Trans-Baikal Region, Russia. *Extremophiles*. 2015;19(3):673-80.
388. Pikuta E, Zhilina TN, Zavarzin GA, Kostrikina NA, Osipov G, Rainey F. *Desulfonatronum lacustre* gen. nov., sp. nov.: A new alkaliphilic sulfate-reducing bacterium utilizing ethanol1998. 105-13 p.
389. Martins M, Pereira IAC. Sulfate-reducing bacteria as new microorganisms for biological hydrogen production. *International Journal of Hydrogen Energy*. 2013;38(28):12294-301.
390. Panahi H, Eslami A, Golozar MA. Corrosion and stress corrosion cracking initiation of grade 304 and 316 stainless steels in activated Methyl Diethanol Amine (aMDEA) solution. *Journal of Natural Gas Science and Engineering*. 2018;55:106-12.
391. Ogawa A, Noda M, Kanematsu H, Sano K. Application of bacterial 16S rRNA gene analysis to a comparison of the degree of biofilm formation on the surface of metal coated glasses2015. 61-5 p.
392. Gupta S, Anand S. Induction of pitting corrosion on stainless steel (grades 304 and 316) used in dairy industry by biofilms of common sporeformers. *International Journal of Dairy Technology*. 2018;71(2):519-31.
393. Pardo A, Merino MC, Coy AE, Viejo F, Arrabal R, Matykina E. Effect of Mo and Mn additions on the corrosion behaviour of AISI 304 and 316 stainless steels in H<sub>2</sub>SO<sub>4</sub>. *Corrosion Science*. 2008;50(3):780-94.
394. Javed MA, Stoddart PR, Wade SA. Corrosion of carbon steel by sulphate reducing bacteria: Initial attachment and the role of ferrous ions. *Corrosion Science*. 2015;93:48-57.
395. Guan F, Zhai X, Duan J, Zhang M, Hou B. Influence of Sulfate-Reducing Bacteria on the Corrosion Behavior of High Strength Steel EQ70 under Cathodic Polarization. *PloS one*. 2016;11(9):e0162315-e.
396. Humphreys P, West J, Metcalfe R. *Microbial Effects on Repository Performance*2010.
397. Duckworth AW, Grant WD, Jones BE, van Steenberg R. Phylogenetic diversity of soda lake alkaliphiles. *FEMS Microbiology Ecology*. 1996;19(3):181-91.
398. M. Bethke C, Sanford R, Kirk M, Jin Q, Flynn T. The Thermodynamic ladder in Geomicrobiology2011. 183-210 p.
399. Rasamiravaka T, Labtani Q, Duez P, El Jaziri M. The formation of biofilms by *Pseudomonas aeruginosa*: a review of the natural and synthetic compounds interfering with control mechanisms. *BioMed research international*. 2015;2015:759348-.
400. Toyofuku M, Uchiyama H, Nomura N. Social Behaviours under Anaerobic Conditions in *Pseudomonas aeruginosa*. *International journal of microbiology*. 2012;2012:405191-.
401. Vigneron A, Alsop EB, Chambers B, Lomans BP, Head IM, Tsesmetzis N. *Complementary Microorganisms in Highly Corrosive Biofilms from an Offshore Oil Production Facility*. 2016;82(8):2545-54.

402. Taylor S, Milly P, Jaffe P. Biofilm Growth and the Related Changes in the Physical Properties of a Porous Medium: 2. Permeability 1990.
403. Babauta JT, Nguyen HD, Harrington TD, Renslow R, Beyenal H. pH, redox potential and local biofilm potential microenvironments within *Geobacter sulfurreducens* biofilms and their roles in electron transfer. *Biotechnology and bioengineering*. 2012;109(10):2651-62.
404. Sorokin DY. Is there a limit for high-pH life? 2005;55(4):1405-6.
405. Smith K, Ingram-Smith C. Methanosaeta, the Forgotten Methanogen? 2007. 150-5 p.
406. Pikuta E, Hoover R, Marsic D, Whitman W, Cleland D, Krader P, et al. *Desulfonatronum paiuteum* sp. nov.: A New Alkaliphilic, Sulfate-Reducing Bacterium, Isolated from Soda Mono Lake, California 2002.



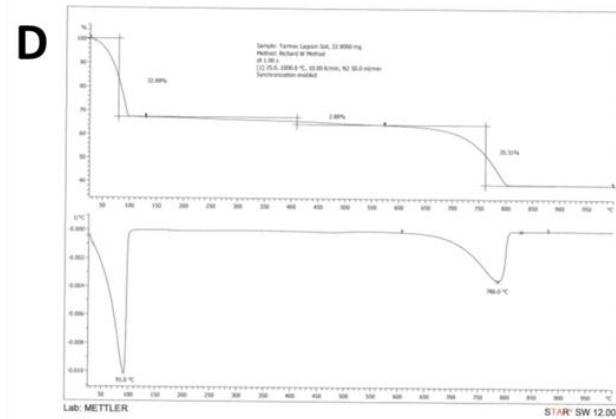
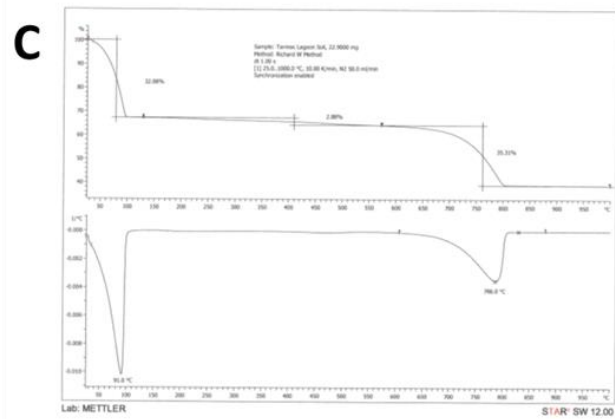
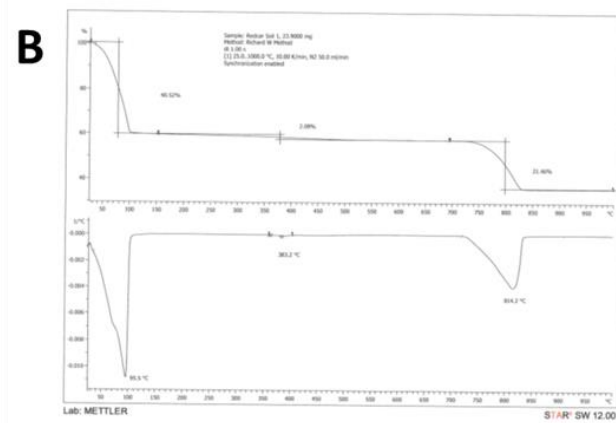
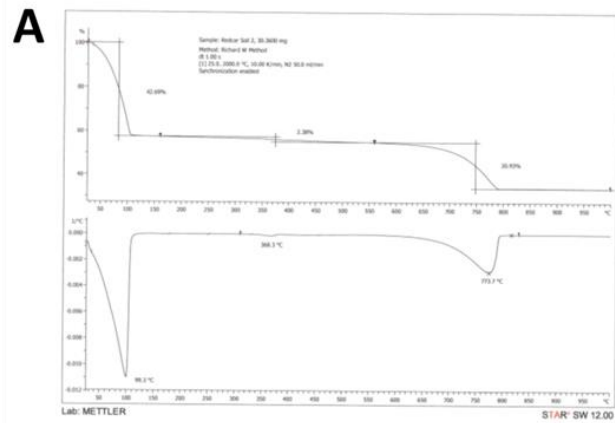


**Figure S5.2. Thermal analysis of sediment samples from anthropogenic alkaline sites. [A-B] Site RC thermograms, [C-D] Site T thermograms.**

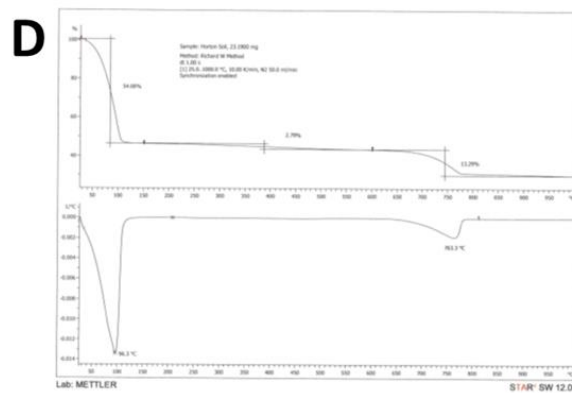
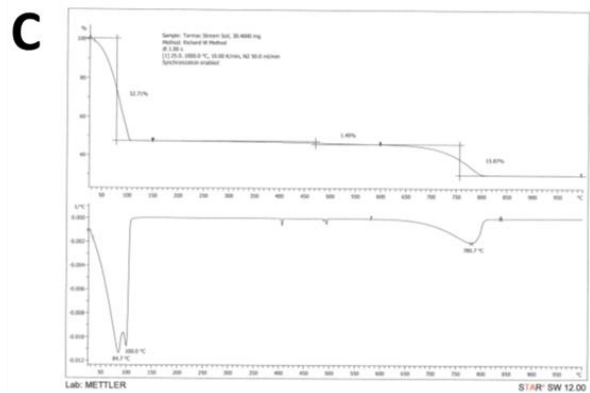
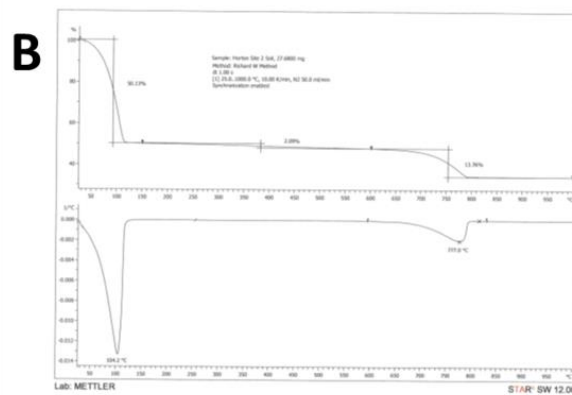
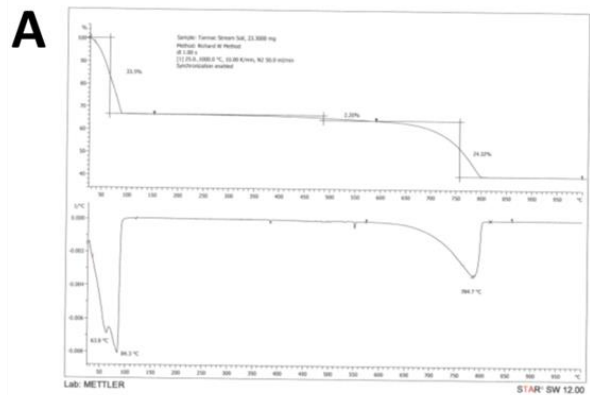


**Figure S5.3. Thermal analysis of sediment samples from anthropogenic alkaline sites. [A and C] Site T thermograms, [B and D] Site H thermograms.**

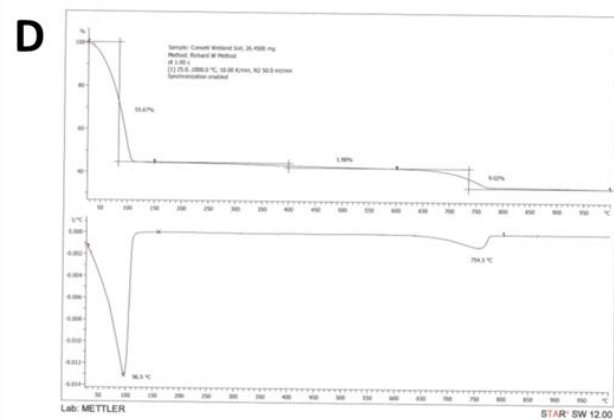
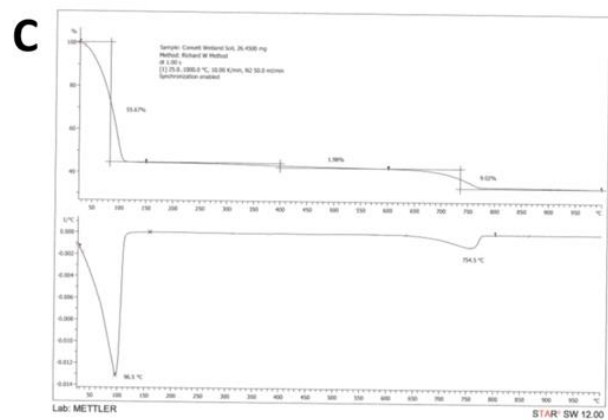
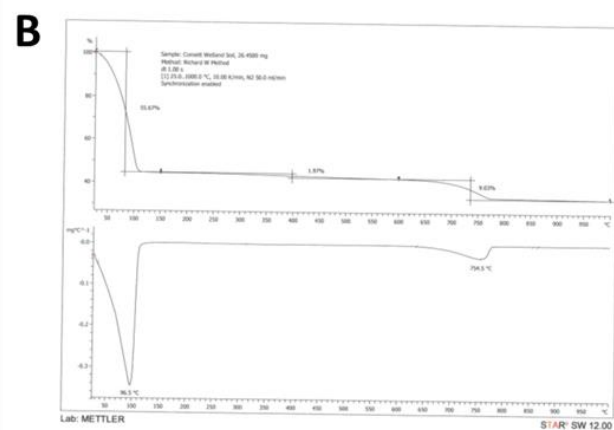
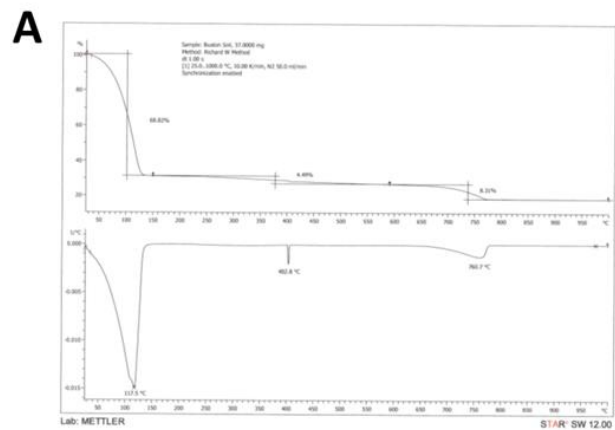


**Figure S5.4. Thermal analysis of sediment samples from anthropogenic alkaline sites. [A] Site B thermograms, [B-D] Site CW thermograms.**

**Table S5.1. Dominant genus-level taxon within alkaline contaminated sediments from the New Lime site B.**

<b>Site B</b>	
<b><u>Genus/Taxon ID</u></b>	<b><u>16S rRNA Gene Reads (%)</u></b>
Terrimicrobium	2.63267
Bradyrhizobium	1.81118
FM253654_g	1.67223
Mycobacterium	1.50403
Bradyrhizobiaceae_uc	1.50403
CP015136_f_uc	1.38946
Mesorhizobium	1.36753
GQ396871_g	1.3334
AF370880_g	1.32121
Sphingomonas	1.23589
Methyloceanibacter	1.22858
Ilumatobacter	1.20664
Gaiella	1.03357

**Table S5.2. Dominant genus-level taxon within alkaline contaminated sediments from the New Lime site H.**

<b>Site H</b>	
<b><u>Genus/Taxon ID</u></b>	<b><u>16S rRNA Gene Reads (%)</u></b>
Geofilum	20.59095
ML635J-40_f_uc	10.59146
Hydrogenophaga	3.9183
Flavobacterium	3.80811
Marinilabiliaceae_uc	3.67741
Bacteroidales_uc_g	2.6011
ASKU_g	1.93737
Rhodocyclaceae_uc	1.8938
Paludibacter	1.84255
FJ439862_g	1.76567
Ruminococcaceae_uc	1.71698
Comamonadaceae_uc	1.69904
Azonexus	1.56835
JN398066_g	1.48634
CP011215_f_uc	1.41971
AB237727_g	1.34539
Flavitalea	1.31208
EU801574_g	1.26852

Mobilitalea	1.26595
Fusibacter	1.20701
Porphyromonadaceae_uc	1.09682

**Table S5.3. Dominant genus-level taxon within alkaline contaminated sediments from the New Lime site T.**

Site T	
<u>Genus/Taxon ID</u>	<u>16S rRNA Gene Reads (%)</u>
CP015136_f_uc	2.29861
Cytophagaceae_uc	1.66093
EU786132_f_uc	1.51857
HQ190410_g	1.42069
EU786132_g	1.37917
Mycobacterium	1.2279
AF370880_g	1.07664
Bradyrhizobiaceae_uc	1.05884
Sphingosinicella	1.03808
Polyangiaceae_uc	1.01732

**Table S5.4. Dominant genus-level taxon within alkaline contaminated sediments from the Steel site CW.**

Site CW	
<u>Genus/Taxon ID</u>	<u>16S rRNA Gene Reads (%)</u>
Pseudomonas	9.16922
Hydrogenophaga	4.21544
Thiobacillus	3.84626
Exiguobacterium	3.83482
Flavobacterium	3.63449
Arthrobacter	3.43416
Algoriphagus	3.41413
Rhizobium	3.38265
Cavicella	3.17088
Proteiniclasticum	2.67865
Rheinheimera	2.23793
Rhodiferax	2.17211
GU454901_g	1.60261
Paenisporosarcina	1.34219
AB237727_g	1.23058
Intrasporangium	1.15045

Aeromonas	1.02166
GQ396959_g	1.01022

**Table S5.5. Dominant genus-level taxon within alkaline contaminated sediments from the Steel site CS.**

<b>Site CS</b>	
<b><u>Genus/Taxon ID</u></b>	<b><u>16S rRNA Gene Reads (%)</u></b>
Silanimonas	8.14716
Hydrogenophaga	5.55251
Malikia	5.5107
Rhodobacter	3.23483
GQ396871_g	2.51104
AM778010_g	1.96232
Tabrizicola	1.84213
AP014683_g	1.74022
AB237727_g	1.70887
HM141892_g	1.6357
ML635J-40_f_uc	1.48415
Georgfuchsia	1.36396
Methylothera	1.3117
Aquiflexum	1.19412
AM777983_g	1.1497
DQ395705_g	1.11311
Novosphingobium	1.09482
AY093455_g	1.0295
Porticoccus	1.00076

**Table S5.6. Dominant genus-level taxon within alkaline contaminated sediments from the Steel site RC.**

<b>Site RC</b>	
<b><u>Genus/Taxon ID</u></b>	<b><u>16S rRNA Gene Reads (%)</u></b>
Shewanella	10.73175
Rhizobium	9.35791
Clostridium	5.33689
Pseudomonas	4.7746
Methylobacter	4.55046
Herbaspirillum	4.11957
Bacillus	3.81041
Actinotalea	2.94282

AB533980_f_uc	2.80757
GQ396959_g	2.43271
Paenibacillus	2.1506
Psychrobacillus	2.00761
Sulfuricella	1.75835
Paenisporosarcina	1.47045
Ferribacterium	1.44533
Accumulibacter	1.35644
AJ229237_g	1.25597
Ercella	1.25017
Marinilabiliaceae_uc	1.21539
EF632712_g	1.19607
EU181507_f_uc	1.11878
EF559174_g	1.09945

**Table S5.7. Dominant genus-level taxon within alkaline contaminated sediments from the Steel site SC.**

<b>Site SC</b>	
<b><u>Genus/Taxon ID</u></b>	<b><u>16S rRNA Gene Reads (%)</u></b>
Thiobacillus	11.71736
Rhodocyclaceae_uc	7.26494
Dethiobacter	5.79378
AB237727_g	4.50435
Azospira	3.9981
Pseudomonas	3.8856
Lentimicrobium	3.38367
BBZD_g	3.2279
Azoarcus	3.19761
Desulfuromonas_g2	2.82549
Hydrogenophaga	2.37982
ML635J-40_f_uc	1.72645
Thiobacillus_f_uc	1.58366
Prolixibacteraceae_uc	1.31106
Comamonadaceae_uc	1.28943
DQ677001_g	1.28078
Desulfomicrobium	1.2202
HQ183936_g	1.19856

**ANOVA – Background soils – Control vs New Lime vs Old Lime vs Steel**

		Sum of Squares	df	Mean Square	F	Sig.
Proteobacteria	Between Groups	643.439	3	214.480	11.273	.000
	Within Groups	380.535	20	19.027		
	Total	1023.974	23			
Firmicutes	Between Groups	63.438	3	21.146	72.865	.000
	Within Groups	5.804	20	.290		
	Total	69.242	23			
Bacteroidetes	Between Groups	231.104	3	77.035	8.005	.001
	Within Groups	192.457	20	9.623		
	Total	423.561	23			
Actinobacteria	Between Groups	863.459	3	287.820	26.405	.000
	Within Groups	218.003	20	10.900		
	Total	1081.462	23			
Euryarchaeota	Between Groups	.218	3	.073	1.852	.170
	Within Groups	.783	20	.039		
	Total	1.001	23			
Acidobacteria	Between Groups	276.956	3	92.319	10.078	.000
	Within Groups	183.215	20	9.161		
	Total	460.171	23			
Fibrobacteres	Between Groups	.082	3	.027	.214	.886
	Within Groups	2.561	20	.128		
	Total	2.643	23			
Verrucomicrobia	Between Groups	22.272	3	7.424	4.868	.011

	Within Groups	30.502	20	1.525		
	Total	52.774	23			
Chlorobi	Between Groups	3.682	3	1.227	3.382	.038
	Within Groups	7.258	20	.363		
	Total	10.941	23			
Chloroflexi	Between Groups	63.276	3	21.092	8.327	.001
	Within Groups	50.658	20	2.533		
	Total	113.934	23			
Gemmatimonadetes	Between Groups	3.436	3	1.145	.991	.417
	Within Groups	23.104	20	1.155		
	Total	26.540	23			
Latescibacteria	Between Groups	22.256	3	7.419	11.153	.000
	Within Groups	13.303	20	.665		
	Total	35.559	23			
Lentisphaerae	Between Groups	.000	3	.000	.	.
	Within Groups	.000	20	.000		
	Total	.000	23			
Nitrospirae	Between Groups	1.895	3	.632	.239	.868
	Within Groups	52.960	20	2.648		
	Total	54.855	23			
Omnitrophica	Between Groups	.000	3	.000	.	.
	Within Groups	.000	20	.000		
	Total	.000	23			
Parcubacteria	Between Groups	2.938	3	.979	1.823	.175

	Within Groups	10.745	20	.537		
	Total	13.683	23			
Planctomycetes	Between Groups	20.943	3	6.981	3.897	.024
	Within Groups	35.824	20	1.791		
	Total	56.767	23			
Saccharibacteria	Between Groups	.000	3	.000	.	.
	Within Groups	.000	20	.000		
	Total	.000	23			
Spirochaetes	Between Groups	2.363	3	.788	4.891	.010
	Within Groups	3.222	20	.161		
	Total	5.585	23			

**Figure S5.5. ANOVA of background soils at Phylum taxonomic level.** Comparing Control, New Lime, Old Lime and Steel background soil communities at the Phylum level.

**ANOVA – Contaminated soils – New Lime vs Old Lime vs Steel**

		Sum of Squares	df	Mean Square	F	Sig.
Proteobacteria	Between Groups	452.253	2	226.126	2.191	.138
	Within Groups	2064.607	20	103.230		
	Total	2516.860	22			
Firmicutes	Between Groups	1144.742	2	572.371	2.325	.124
	Within Groups	4923.320	20	246.166		
	Total	6068.062	22			
Bacteroidetes	Between Groups	689.714	2	344.857	3.209	.062
	Within Groups	2149.228	20	107.461		
	Total	2838.941	22			
Actinobacteria	Between Groups	138.816	2	69.408	1.638	.219
	Within Groups	847.451	20	42.373		
	Total	986.266	22			
Euryarchaeota	Between Groups	4.530	2	2.265	.646	.535
	Within Groups	70.112	20	3.506		
	Total	74.642	22			
Acidobacteria	Between Groups	155.780	2	77.890	6.985	.005
	Within Groups	223.014	20	11.151		
	Total	378.794	22			
Fibrobacteres	Between Groups	.837	2	.418	4.348	.027
	Within Groups	1.924	20	.096		
	Total	2.761	22			
Verrucomicrobia	Between Groups	18.215	2	9.108	1.953	.168

	Within Groups	93.264	20	4.663		
	Total	111.480	22			
Synergistetes	Between Groups	.000	2	.000	.	.
	Within Groups	.000	20	.000		
	Total	.000	22			
Aminicenantes	Between Groups	.000	2	.000	.	.
	Within Groups	.000	20	.000		
	Total	.000	22			
Bacillariophyta	Between Groups	.621	2	.311	.248	.782
	Within Groups	25.012	20	1.251		
	Total	25.634	22			
Bathyarchaeota	Between Groups	.035	2	.017	.248	.782
	Within Groups	1.391	20	.070		
	Total	1.425	22			
Chlamydiae	Between Groups	.066	2	.033	.248	.782
	Within Groups	2.641	20	.132		
	Total	2.706	22			
Chlorobi	Between Groups	.509	2	.255	.484	.623
	Within Groups	10.519	20	.526		
	Total	11.028	22			
Chloroflexi	Between Groups	2.226	2	1.113	.167	.847
	Within Groups	133.073	20	6.654		
	Total	135.299	22			
Cyanobacteria	Between Groups	.479	2	.239	.248	.782

	Within Groups	19.261	20	.963		
	Total	19.740	22			
Deinococcus	Between Groups	.416	2	.208	.424	.660
	Within Groups	9.802	20	.490		
	Total	10.218	22			
Fusobacteria	Between Groups	.144	2	.072	.248	.782
	Within Groups	5.788	20	.289		
	Total	5.932	22			
Gemmatimonadetes	Between Groups	12.936	2	6.468	4.394	.026
	Within Groups	29.440	20	1.472		
	Total	42.376	22			
Latescibacteria	Between Groups	.607	2	.304	1.957	.167
	Within Groups	3.103	20	.155		
	Total	3.710	22			
Nitrospirae	Between Groups	.614	2	.307	.764	.479
	Within Groups	8.031	20	.402		
	Total	8.645	22			
Omnitrophica	Between Groups	.034	2	.017	.248	.782
	Within Groups	1.352	20	.068		
	Total	1.385	22			
Parcubacteria	Between Groups	13.043	2	6.521	1.012	.382
	Within Groups	128.940	20	6.447		
	Total	141.982	22			
Planctomycetes	Between Groups	20.999	2	10.500	3.513	.049

	Within Groups	59.773	20	2.989		
	Total	80.772	22			
Saccharibacteria	Between Groups	.417	2	.209	.215	.809
	Within Groups	19.429	20	.971		
	Total	19.847	22			
Spirochaetes	Between Groups	4.433	2	2.216	1.027	.376
	Within Groups	43.155	20	2.158		
	Total	47.587	22			
Tenericutes	Between Groups	.152	2	.076	.534	.594
	Within Groups	2.839	20	.142		
	Total	2.991	22			
TM6	Between Groups	.854	2	.427	1.115	.347
	Within Groups	7.656	20	.383		
	Total	8.510	22			

**Figure S5.6. ANOVA of contaminated soils at Phylum taxonomic level.** Comparing Control, New Lime, Old Lime and Steel contaminated soil communities at the Phylum level.

### Independent Samples Test – Cotton – New Lime vs Steel

		Levene's Test for Equality of Variances		t-test for Equality of Means				
		F	Sig.	t	df	Sig. (2-tailed)	Mean Difference	Std. Error Difference
Proteobacteria	Equal variances assumed	4.373	.058	-.122	12	.905	-2.705	22.087
	Equal variances not assumed			-.145	4.164	.892	-2.705	18.692
Firmicutes	Equal variances assumed	1.053	.325	1.198	12	.254	10.122	8.452
	Equal variances not assumed			.937	2.510	.430	10.122	10.808
Bacteroidetes	Equal variances assumed	7.111	.021	-1.525	12	.153	-9.500	6.230
	Equal variances not assumed			-2.738	11.983	.018	-9.500	3.469
Actinobacteria	Equal variances assumed	.113	.743	.587	12	.568	1.835	3.123
	Equal variances not assumed			.515	2.758	.645	1.835	3.564
Euryarchaeota	Equal variances assumed	2.210	.163	-.666	12	.518	-1.527	2.292
	Equal variances not assumed			-1.314	10.000	.218	-1.527	1.162
Acidobacteria	Equal variances assumed	13.255	.003	4.020	12	.002	6.579	1.637
	Equal variances not assumed			1.948	2.025	.189	6.579	3.377
Fibrobacteres	Equal variances assumed	5.279	.040	-1.287	12	.222	-6.684	5.193
	Equal variances not assumed			-2.262	11.778	.043	-6.684	2.955
Verrucomicrobia	Equal variances assumed	3.327	.093	-.730	12	.479	-1.880	2.576
	Equal variances not assumed			-1.184	9.828	.264	-1.880	1.588
Synergistetes	Equal variances assumed	1.270	.282	-.507	12	.621	-.223	.441
	Equal variances not assumed			-1.000	10.000	.341	-.223	.223
Chlorobi	Equal variances assumed	2.882	.115	-.712	12	.490	-.271	.380
	Equal variances not assumed			-1.405	10.000	.190	-.271	.193

Chloroflexi	Equal variances assumed	.507	.490	.001	12	1.000	.001	1.541
	Equal variances not assumed			.001	11.902	.999	.001	.868
Cloacamonas	Equal variances assumed	1.270	.282	-.507	12	.621	-.093	.183
	Equal variances not assumed			-1.000	10.000	.341	-.093	.093
Cyanobacteria	Equal variances assumed	.904	.360	-.391	12	.703	-.623	1.595
	Equal variances not assumed			-.599	8.258	.565	-.623	1.040
DQ833500	Equal variances assumed	.411	.533	-.208	12	.839	-.492	2.366
	Equal variances not assumed			-.357	11.350	.728	-.492	1.378
Lentisphaerae	Equal variances assumed	3.470	.087	-.834	12	.421	-2.436	2.922
	Equal variances not assumed			-1.644	10.000	.131	-2.436	1.482
Parcubacteria	Equal variances assumed	1.270	.282	-.507	12	.621	-.308	.607
	Equal variances not assumed			-1.000	10.000	.341	-.308	.308
Planctomycetes	Equal variances assumed	47.831	.000	3.028	12	.011	2.336	.772
	Equal variances not assumed			1.395	2.000	.298	2.336	1.675
Spirochaetes	Equal variances assumed	2.529	.138	-.776	12	.453	-.633	.816
	Equal variances not assumed			-1.531	10.000	.157	-.633	.414
Streptophyta	Equal variances assumed	69.868	.000	2.514	12	.027	3.907	1.554
	Equal variances not assumed			1.158	2.000	.367	3.907	3.374

**Figure S5.7. Independent samples t-test of cotton communities at Phylum taxonomic level.** Comparing New Lime and Steel cotton communities at the Phylum level.

**Table S5.8. Alpha-diversity statistics of background soil samples.**

<b>Site</b>	<b>Valid reads</b>	<b>OTUs</b>	<b>Ace</b>	<b>Chao1</b>	<b>Shannon</b>	<b>Goods Lib. Coverage</b>
<b>C1</b>	13956	2871	3133.9	2970.6	7.22	96.59
<b>C2</b>	15479	2928	3297.6	3100.7	7.19	96.21
<b>C3</b>	9182	1797	2172.9	1996.3	6.60	94.70
<b>C4</b>	15470	2862	3124.3	2972.2	7.16	96.91
<b>B1</b>	59995	5069	5331.8	5152.9	7.33	98.90
<b>B2</b>	8310	1219	1524.9	1381.1	6.56	90.95
<b>B3</b>	45908	5010	5223.6	5061.9	7.51	98.74
<b>B4</b>	54004	5150	5453.1	5254.6	7.44	98.66
<b>H1</b>	37966	4778	5057.1	4854.0	7.49	98.10
<b>H2</b>	48477	4324	4601.6	4425.1	7.07	98.71
<b>H3</b>	48115	5288	5551.2	5365.6	7.49	98.61
<b>H4</b>	39413	4426	4667.8	4495.1	7.37	98.34
<b>T1</b>	29888	3772	4002.8	3844.8	7.27	97.96
<b>T2</b>	43674	4759	5005.9	4822.6	7.40	98.61
<b>T3</b>	36236	4603	4856.8	4671.8	7.50	98.16
<b>T4</b>	30593	4377	4634.8	4456.5	7.55	97.72
<b>T5</b>	51633	5221	5532.2	5318.5	7.45	98.55
<b>T6</b>	40495	4205	4499.6	4306.9	7.07	98.31
<b>LK1</b>	13799	2150	2891.4	2637.9	6.64	93.07
<b>LK2</b>	14875	2103	2727.0	2506.8	6.58	94.28
<b>CW</b>	138910	16150	16273.2	16162.6	8.35	99.69
<b>CS</b>	123256	10830	10952.4	10847.5	7.90	99.68
<b>RC</b>	117368	10406	10528.3	10425.6	7.77	99.65
<b>SC</b>	39885	4462	4916.2	4639.4	7.44	97.22

**Table S5.9. Alpha-diversity statistics of contaminated soil samples.**

<b>Site</b>	<b>Valid reads</b>	<b>OTUs</b>	<b>Ace</b>	<b>Chao1</b>	<b>Shannon</b>	<b>Goods Lib. Coverage</b>
<b>C1</b>	17635	3928	4126.8	3980.7	7.55	97.49
<b>C2</b>	22405	4679	4802.0	4704.8	7.69	98.48
<b>C3</b>	21910	4764	4912.6	4796.7	7.76	98.25
<b>C4</b>	13527	3026	3179.5	3069.8	7.34	97.41
<b>B</b>	41023	3446	3831.3	3578.5	7.12	96.40
<b>H</b>	39022	1675	1722.9	1682.6	4.81	99.52
<b>T</b>	33716	2845	3147.7	2951.7	7.26	95.42
<b>LK1</b>	42343	3445	3737.2	3530.8	6.98	96.97
<b>LK2</b>	42756	3348	3648.9	3446.9	6.97	96.91
<b>LK3</b>	40253	3353	3573.4	3410.6	7.16	97.49
<b>LK4</b>	42465	514	523.7	515.1	2.09	99.91
<b>LK5</b>	58163	641	645.7	641.2	1.93	99.96
<b>CW1U</b>	65666	4062	4158.3	4078.3	6.29	99.53
<b>CW1L</b>	34870	1977	2086.8	2031.1	5.65	99.31
<b>CW2</b>	48119	2041	2150.2	2095.7	5.45	99.50
<b>CW3</b>	63485	6865	7024.8	6888.7	7.55	99.11
<b>CS1</b>	62779	5012	5215.3	5062.4	6.40	99.01
<b>CS2</b>	38259	2039	2174.7	2106.3	5.69	99.28
<b>CS3</b>	53569	3450	3809.6	3601.4	5.60	98.56
<b>RC1U</b>	57452	1472	1593.6	1530.7	4.76	99.62
<b>RC1L</b>	93041	2027	2138.5	2082.1	4.59	99.74
<b>RC2U</b>	78931	1799	1894.8	1839.1	4.76	99.74
<b>RC2L</b>	51753	1488	1611.3	1535.2	4.62	99.50
<b>RC3</b>	37820	1152	1230.6	1192.7	4.83	99.59
<b>SC1</b>	23045	2060	2098.2	2066.6	5.40	99.46
<b>SC2</b>	44327	2263	2345.2	2279.7	5.49	99.43
<b>SC3</b>	25676	2975	3015.1	2979.1	6.25	99.48

pH 7								
	0	2	4	6	8	10	12	14
	2.127533	2.29559	2.665077	3.039333	2.753278	2.967819	2.824791	3.396901
	1.93683	2.544696	2.489869	2.705602	2.324195	2.657926	2.395709	3.06317
average	<b>2.032181</b>	<b>2.420143</b>	<b>2.577473</b>	<b>2.872467</b>	<b>2.538737</b>	<b>2.812872</b>	<b>2.61025</b>	<b>3.230036</b>
stdev	<b>0.134848</b>	<b>0.176145</b>	<b>0.123891</b>	<b>0.235983</b>	<b>0.303407</b>	<b>0.219127</b>	<b>0.303407</b>	<b>0.235983</b>
stderr	<b>0.095352</b>	<b>0.124553</b>	<b>0.087604</b>	<b>0.166865</b>	<b>0.214541</b>	<b>0.154946</b>	<b>0.214541</b>	<b>0.166865</b>
pH 8								
	0	2	4	6	8	10	12	14
	1.831943	2.179976	3.022646	3.556615	4.189511	4.557807	4.308701	4.707986
	1.924911	2.545888	2.878427	3.11323	3.556615	3.737783	3.556615	3.718713
	1.680572	1.8236	2.133492	2.526818	2.443385	2.848629	2.443385	2.50298
	1.764005	1.728248	1.859356	2.133492	2.193087	2.216925	2.312277	2.228844
average	<b>1.800358</b>	<b>2.069428</b>	<b>2.47348</b>	<b>2.832539</b>	<b>3.09565</b>	<b>3.340286</b>	<b>3.155244</b>	<b>3.289631</b>
stdev	<b>0.103572</b>	<b>0.372411</b>	<b>0.565186</b>	<b>0.628545</b>	<b>0.939697</b>	<b>1.023723</b>	<b>0.950245</b>	<b>1.145997</b>
stderr	<b>0.051786</b>	<b>0.186206</b>	<b>0.282593</b>	<b>0.314272</b>	<b>0.469848</b>	<b>0.511862</b>	<b>0.475123</b>	<b>0.572999</b>
pH 9								
	0	2	4	6	8	10	12	14
	1.730632	1.924911	1.885578	2.092968	2.222884	2.210965	2.188319	2.27056
	1.624553	1.781883	1.637664	1.831943	2.308701	2.289631	2.282479	2.179976
	1.573302	1.799762	1.871275	2.121573	2.27652	2.550656	2.491061	2.586412
	1.537545	1.692491	1.740167	2.205006	2.181168	2.264601	2.336114	2.38379
	1.573302	1.620977	1.966627	2.121573	2.526818	2.943981	3.432658	3.587604
	1.656734	1.692491	2.038141	2.085816	2.789035	3.194279	3.730632	3.694875
average	<b>1.616011</b>	<b>1.752086</b>	<b>1.856575</b>	<b>2.07648</b>	<b>2.384188</b>	<b>2.575685</b>	<b>2.743544</b>	<b>2.78387</b>
stdev	<b>0.070249</b>	<b>0.107072</b>	<b>0.146702</b>	<b>0.127077</b>	<b>0.231849</b>	<b>0.407565</b>	<b>0.663298</b>	<b>0.678697</b>
stderr	<b>0.028679</b>	<b>0.043712</b>	<b>0.059891</b>	<b>0.051879</b>	<b>0.094652</b>	<b>0.166388</b>	<b>0.27079</b>	<b>0.277077</b>
pH 10								
	0	2	4	6	8	10	12	14
	1.340882	1.381406	1.57211	1.818832	1.353993	1.617402	1.702026	1.674613
	1.448153	1.47199	1.462455	1.942789	1.444577	1.769964	1.793802	2.038141
	1.462455	1.448153	1.680572	1.632896	1.418355	1.680572	1.8236	1.918951
	1.417163	1.464839	1.8236	1.895113	1.764005	1.632896	1.692491	1.871275
	1.382598	1.418355	1.692491	1.620977	1.537545	1.728248	1.799762	1.883194
	1.442193	1.489869	1.775924	1.871275	1.442193	1.620977	1.752086	1.728248
average	<b>1.415574</b>	<b>1.445769</b>	<b>1.667859</b>	<b>1.796981</b>	<b>1.493445</b>	<b>1.67501</b>	<b>1.760628</b>	<b>1.852404</b>
stdev	<b>0.046123</b>	<b>0.039739</b>	<b>0.13271</b>	<b>0.137687</b>	<b>0.145085</b>	<b>0.063077</b>	<b>0.054309</b>	<b>0.132102</b>
stderr	<b>0.01883</b>	<b>0.016223</b>	<b>0.054179</b>	<b>0.05621</b>	<b>0.059231</b>	<b>0.025751</b>	<b>0.022171</b>	<b>0.053931</b>
pH 11								
	0	2	4	6	8	10	12	14
	1.581645	1.810489	1.464839	1.448153	1.901073	1.969011	2.346841	2.096544
	1.686532	1.700834	1.580453	1.555423	1.711561	1.691299	2.056019	1.934446
average	<b>1.634088</b>	<b>1.755662</b>	<b>1.522646</b>	<b>1.501788</b>	<b>1.806317</b>	<b>1.830155</b>	<b>2.20143</b>	<b>2.015495</b>
stdev	<b>0.074166</b>	<b>0.077537</b>	<b>0.081751</b>	<b>0.075852</b>	<b>0.134005</b>	<b>0.196372</b>	<b>0.205642</b>	<b>0.11462</b>
stderr	<b>0.052443</b>	<b>0.054827</b>	<b>0.057807</b>	<b>0.053635</b>	<b>0.094756</b>	<b>0.138856</b>	<b>0.145411</b>	<b>0.081049</b>

Figure S6.1. Acetate quantities within pH 7.0-11.0 CDP-fed microcosms employing the lime sediments (B, H, T).

pH 7	0	2	4	6	8	10	12	14
AUC1	11.67	10.59	6.39	3.12	0	0	0	0
AUC2	11.35	10.36	6.12	2.89	0	0	0	0
mM1	1.390942	1.262217	0.761621	0.371871	0	0	0	0
mM2	1.352801	1.234803	0.72944	0.344458	0	0	0	0
average	1.371871	1.24851	0.74553	0.358164	0	0	0	0
stdev	0.02697	0.019384	0.022756	0.019384	0	0	0	0
sterr	0.01907	0.013707	0.016091	0.013707	0	0	0	0
pH 8	0	2	4	6	8	10	12	14
AUC1	10.63	10.75	8.52	6.35	4.27	3.29	0	0
AUC2	11.12	10.85	8.27	5.86	3.95	2.58	0	0
mM1	1.266985	1.281287	1.015495	0.756853	0.508939	0.392133	0	0
mM2	1.325387	1.293206	0.985697	0.698451	0.470799	0.307509	0	0
average	1.296186	1.287247	1.000596	0.727652	0.489869	0.349821	0	0
stdev	0.041297	0.008428	0.02107	0.041297	0.02697	0.059839	0	0
sterr	0.029201	0.005959	0.014899	0.029201	0.01907	0.042312	0	0
pH 9	0	2	4	6	8	10	12	14
AUC1	10.87	11.24	13.29	10.47	8.59	5.27	3.19	2.92
AUC2	9.89	10.89	12.55	10.23	6.32	3.26	0	0
mM1	1.29559	1.33969	1.584029	1.247914	1.023838	0.628129	0.380215	0.348033
mM2	1.178784	1.297974	1.495828	1.219309	0.753278	0.388558	0	0
average	1.237187	1.318832	1.539928	1.233611	0.888558	0.508343	0.190107	0.174017
stdev	0.082594	0.029498	0.062367	0.020227	0.191315	0.169402	0.268852	0.246097
sterr	0.058403	0.020858	0.0441	0.014303	0.13528	0.119785	0.190107	0.174017
pH 10	0	2	4	6	8	10	12	14
AUC1	12.59	13.69	17.85	22.39	21.47	28.36	27.63	27.75
AUC2	13.12	12.85	19.26	27.41	25.96	22.54	23.47	25.69
mM1	1.500596	1.631704	2.127533	2.668653	2.558999	3.380215	3.293206	3.307509
mM2	1.563766	1.531585	2.29559	3.266985	3.09416	2.686532	2.797378	3.061979
average	1.532181	1.581645	2.211561	2.967819	2.826579	3.033373	3.045292	3.184744
stdev	0.044668	0.070795	0.118834	0.423084	0.378416	0.490508	0.350604	0.173616
sterr	0.031585	0.05006	0.084029	0.299166	0.26758	0.346841	0.247914	0.122765

**Figure S6.2. Acetate quantities within pH 7.0-10.0 CDP-fed microcosms employing the control sediments.**

pH 7													
Sample	Ribonic	alpha	adjustmer	Alpha (mg/L)	Alpha (mg)	beta	adjustment	beta (mg/L)	beta (mg)	Xylo	adjustment	Xylo (mg/L)	Xylo (mg)
T0	45.05	7.29	6.829874	156.2006674	7.81003337	6.82	6.38953936	146.1301168	7.306506	1.4	1.31163565	29.9973847	1.499869
T0	49.12	6.95	7.099594	162.3692274	8.11846137	5.86	5.98613289	136.9041256	6.845206	1.6	1.63443901	37.379966	1.868998
T2	43.62	5.5	4.98929	114.1061132	5.70530566	4.8	4.35428928	99.58351697	4.979176	1.1	0.99785796	22.8212226	1.141061
T2	45.17	4.9	4.602953	105.2705112	5.26352556	5.1	4.79082874	109.5672668	5.478363	0.92	0.86422793	19.7650756	0.988254
T4	47.85	1.25	1.243891	28.44805092	1.42240255	2.9	2.88582718	65.99947813	3.299974	1.14	1.13442862	25.9446224	1.297231
T4	48.25	0.98	0.983363	22.48971515	1.12448576	2.5	2.50857856	57.37172233	2.868586	1.05	1.05360299	24.0961234	1.204806
T6	49.26	0	0	0	0	0	0	0	0	0.96	0.98345846	22.491903	1.124595
T6	51.2	0	0	0	0	0	0	0	0	0.85	0.90506395	20.699004	1.03495
T8	51.26	0	0	0	0	0	0	0	0	0.63	0.67159821	15.3595932	0.76798
T8	52.03	0	0	0	0	0	0	0	0	0.55	0.59512322	13.6105939	0.68053
T10	49.85	0	0	0	0	0	0	0	0	0	0	0	0
T10	47.52	0	0	0	0	0	0	0	0	0	0	0	0
T12	45.23	0	0	0	0	0	0	0	0	0	0	0	0
T12	46.25	0	0	0	0	0	0	0	0	0	0	0	0
T14	43.12	0	0	0	0	0	0	0	0	0	0	0	0
T14	47.52	0	0	0	0	0	0	0	0	0	0	0	0
pH 8													
Sample	Ribonic	alpha	adjustmer	Alpha (mg/L)	Alpha (mg)	beta	adjustment	beta (mg/L)	beta (mg)	Xylo	adjustment	Xylo (mg/L)	Xylo (mg)
T0	51.02	6.95	7.374212	168.6497961	8.4324898	5.25	5.57044816	127.397328	6.369866	1.2	1.27324529	29.1193892	1.455969
T0	49.51	6.42	6.610257	151.1779723	7.55889861	5.57	5.73506707	131.1621971	6.55811	1.15	1.18408027	27.0801664	1.354008
T2	45.02	6.15	5.757991	131.6864736	6.58432368	5.52	5.16814807	118.1966397	5.909832	1.29	1.20777373	27.6220408	1.381102
T2	46.12	6.29	6.032958	137.9750327	6.89875163	5.63	5.39992929	123.4975253	6.174876	1.22	1.17014454	26.7614531	1.338073
T4	48.79	2.21	2.242402	51.28420804	2.5642104	3.65	3.70351461	84.7001626	4.235008	1.26	1.27847354	29.2389602	1.461948
T4	51.12	1.95	2.073079	47.41175352	2.37058768	2.98	3.16808984	72.45488487	3.622744	1.18	1.25447853	28.6901893	1.434509
T6	52.05	1.2	1.29895	29.70725618	1.48536281	0	0	0	0	0	0	0	0
T6	51.07	0.99	1.051457	24.04703934	1.20235197	0	0	0	0	0	0	0	0
T8	50.89	0.85	0.899584	20.57367798	1.0286839	0	0	0	0	0	0	0	0
T8	45.12	0.77	0.722521	16.52419752	0.82620988	0	0	0	0	0	0	0	0
T10	47.89	0	0	0	0	0	0	0	0	0	0	0	0
T10	46.21	0	0	0	0	0	0	0	0	0	0	0	0
T12	46.85	0	0	0	0	0	0	0	0	0	0	0	0
T12	46.14	0	0	0	0	0	0	0	0	0	0	0	0
T14	49.59	0	0	0	0	0	0	0	0	0	0	0	0
T14	47.52	0	0	0	0	0	0	0	0	0	0	0	0
pH 9													
Sample	Ribonic	alpha	adjustmer	Alpha (mg/L)	Alpha (mg)	beta	adjustment	beta (mg/L)	beta (mg)	Xylo	adjustment	Xylo (mg/L)	Xylo (mg)
T0	45.25	5.95	5.599199	128.0548733	6.40274366	4.86	4.57346366	104.5960814	5.229804	0.69	0.64931891	14.8500609	0.742503
T0	49.36	6.36	6.528639	149.3113521	7.4655676	5.23	5.3686763	122.7827628	6.139138	1.05	1.07784132	24.6504591	1.232523
T2	47.24	5.14	5.049675	115.4871249	5.77435624	4.26	4.18513882	95.7150101	4.785751	0.78	0.76629302	17.5252835	0.876264
T2	51.05	4.15	4.405896	100.7637692	5.03818846	5.04	5.35077467	122.3733487	6.118667	1.12	1.18906104	27.1940775	1.359704
T4	52.13	3.82	4.141346	94.71344846	4.73567242	4.05	4.39069356	100.4160906	5.020805	0.52	0.56374337	12.8929302	0.644647
T4	53.74	3.36	3.75515	85.88108073	4.29405404	3.54	3.95631902	90.48185291	4.524093	0.85	0.94996361	21.7258686	1.086293
T6	49.86	1.96	2.032351	46.48029834	2.32401492	1.26	1.30651139	29.88019179	1.49401	0.36	0.37328897	8.53719765	0.42686
T6	53.62	1.12	1.248922	28.56310351	1.42815518	1.98	2.20791515	50.49548657	2.524774	0.63	0.70251846	16.0667454	0.803337
T8	51.24	0.81	0.863147	19.74034331	0.98701717	0.95	1.01233323	23.1522545	1.157613	0.41	0.43690132	9.99202563	0.499601
T8	47.21	1.09	1.070165	24.47490754	1.22374538	1.26	1.23707185	28.29209496	1.414605	0.52	0.51053759	11.6761027	0.583805
T10	41.25	0.51	0.437506	10.00586618	0.50029331	0	0	0	0	0	0	0	0
T10	43.25	0.36	0.323802	7.405411122	0.37027056	0	0	0	0	0	0	0	0
T12	49.85	0	0	0	0	0	0	0	0	0	0	0	0
T12	47.63	0	0	0	0	0	0	0	0	0	0	0	0
T14	51.45	0	0	0	0	0	0	0	0	0	0	0	0
T14	50.02	0	0	0	0	0	0	0	0	0	0	0	0
pH 10													
Sample	Ribonic	alpha	adjustmer	Alpha (mg/L)	Alpha (mg)	beta	adjustment	beta (mg/L)	beta (mg)	Xylo	adjustment	Xylo (mg/L)	Xylo (mg)
T0	48.32	5.15	5.175169	118.3572092	5.91786046	4.56	4.58228554	104.7978396	5.239892	0.65	0.65317667	14.9382885	0.746914
T0	49.52	5.37	5.530257	126.4781438	6.32390719	4.12	4.2429531	97.03723508	4.851862	0.85	0.87536654	20.0198179	1.000991
T2	53.63	5.26	5.866565	134.1695931	6.70847965	4.36	4.86278049	111.2128186	5.560641	0.74	0.8253343	18.8755701	0.94
T2	51.21	5.31	5.655092	129.3331509	6.46665755	4.27	4.54750338	104.0023643	5.200118	0.92	0.97978996	22.4080036	1.1
T4	45.12	5.12	4.804292	109.8751835	5.49375918	4.12	3.86595404	88.41518673	4.420759	0.77	0.72252054	16.5241975	0.8
T4	43.75	5.61	5.104242	116.7351055	5.83675527	3.97	3.61209317	82.6093349	4.130467	0.82	0.74607466	17.0628853	0.85
T6	39.69	5.59	4.614061	105.5245401	5.27622701	4.25	3.50800665	80.22885431	4.011443	0.62	0.51175626	11.703974	0.58
T6	42.23	5.36	4.707347	107.658031	5.38290155	3.69	3.24069252	74.11532358	3.705766	0.79	0.6938068	15.8675083	0.79
T8	47.52	5.45	5.385962	123.1780985	6.15890493	4.05	4.00241239	91.53601818	4.576801	0.65	0.64236248	14.6909659	0.73
T8	48.1	5.94	5.941853	135.8914344	6.79457172	3.96	3.96123531	90.59428959	4.529714	0.77	0.7702402	17.6155563	0.88
T10	45.2	4.76	4.47441	102.330701	5.11653505	4.59	4.31460955	98.67603306	4.933802	0.55	0.51700114	11.8239255	0.59
T10	42.35	5.85	5.152282	117.8337888	5.89168944	3.48	3.06494749	70.09599746	3.5048	0.62	0.54605386	12.4883674	0.62
T12	49.68	4.98	5.145189	117.6715547	5.88357773	3.67	3.79173547	86.7177923	4.33589	0.51	0.52691692	12.0507014	0.60
T12	51.24	5.21	5.551844	126.9718379	6.34859189	4	4.26245191	97.48317686	4.874159	0.65	0.69264844	15.8410162	0.79
T14	57.36	3.96	4.723835	108.0351029	5.40175515	3.05	3.63830716	83.20885453	4.160443	0.39	0.46522616	10.6398207	0.53
T14	55.04	4.85	5.551503	126.9640377	6.34820188	4.36	4.99062909	114.1367432	5.706837	0.55	0.62955184	14.3979837	0.71

ICA (mM/l)

Figure S6.3. ISA concentrations within CDP-fed microcosms employing the control sediments between pH 7-10.

pH 7													
Sample	Ribonic	alpha	adjustmer	Alpha (mg/L)	Alpha (mg)	beta	adjustment	beta (mg/L)	beta (mg)	Xylo	adjustment	Xylo (mg/L)	Xylo (mg)
T0	45.36	5.74	5.414711	123.8355963	6.191779815	5.12	4.82984715	110.459626	5.522981	0.96	0.90559634	20.7111799	1.035559
T0	49.85	5.96	6.178767	141.3097031	7.065485154	5.36	5.55674327	127.083894	6.354195	1.12	1.16111053	26.5548435	3.27742
T2	45.12	5.15	4.832443	110.5189834	5.525949171	5.11	4.79490902	109.6605835	5.483029	0.95	0.89142144	20.3869969	1.01935
T2	46.25	5.29	5.088125	116.3664996	5.81832498	5.26	5.05927004	115.7065762	5.785329	0.89	0.85603619	19.5777287	0.978886
T4	49.35	4.96	5.090486	116.4204825	5.821024126	5.05	5.18285328	118.532951	5.926648	0.86	0.88262452	20.1858095	1.00929
T4	51.25	4.25	4.529739	103.5960893	5.179804464	4.11	4.38052407	100.1835122	5.009176	0.74	0.7887075	18.0379073	0.901895
T6	52.16	4.15	4.501695	102.954715	5.147735752	4.05	4.39322034	100.4738785	5.023694	0.62	0.67254237	15.3811863	0.769059
T6	44.16	3.82	3.508188	80.23299221	4.011649611	3.24	2.97553083	68.05101957	3.402551	0.42	0.38571696	8.82142846	0.441071
T8	39.69	4.25	3.508007	80.22885431	4.011442716	3.65	3.01275866	68.90242782	3.445121	0.65	0.53651866	12.2702954	0.613515
T8	41.15	4.89	4.184746	95.70602087	4.785301044	3.95	3.38031611	77.30854447	3.865427	0.39	0.33375273	7.63299553	0.38165
T10	42.36	4.12	3.629473	83.0681094	4.150340547	3.62	3.18900281	72.93316884	3.646658	0.39	0.3435666	7.85744084	0.392872
T10	49.86	3.05	3.162587	72.32903569	3.616451784	2.89	2.99668088	68.53472562	3.426736	0.42	0.43550398	9.9606393	0.498003
T12	45.24	3.81	3.584577	81.98004142	4.099002071	2.85	2.68137673	61.32365303	3.066183	0.36	0.33870002	7.74614565	0.387307
T12	48.27	2.96	2.971388	67.95627597	3.397813798	2.27	2.27873349	52.11511704	2.605756	0.51	0.51196215	11.7086827	0.585434
T14	45.12	2.85	2.674264	61.16099082	3.058049541	2.92	2.73994801	62.66319059	3.13316	0.41	0.38471873	8.79859868	0.43993
T14	49.86	2.21	2.291579	52.40890782	2.620445391	2.15	2.22936467	50.98604155	2.549302	0.32	0.33181242	7.58862014	0.379431
pH 8													
Sample	Ribonic	alpha	adjustmer	Alpha (mg/L)	Alpha (mg)	beta	adjustment	beta (mg/L)	beta (mg)	Xylo	adjustment	Xylo (mg/L)	Xylo (mg)
T0	47.36	5.27	5.190542	118.7087879	5.935439393	4.52	4.45184985	101.8147478	5.090737	1.22	1.20160549	27.4809718	3.74049
T0	48.25	5.95	5.970417	136.5446991	6.827234957	4.86	4.87667672	111.5306282	5.576531	0.89	0.89305397	20.4243331	1.021217
T2	49.63	5.19	5.356758	122.5101847	6.125509233	4.41	4.55169596	104.0982494	5.204912	1.15	1.18695019	27.145802	1.35729
T2	49.21	5.51	5.638912	128.9631182	6.448155909	4.51	4.61551627	105.578336	5.277892	0.96	0.98246023	22.4690732	1.23454
T4	41.23	5.56	4.767366	109.0306718	5.451533588	4.12	3.53265259	80.79251216	4.039626	0.95	0.81456795	18.6293414	0.931467
T4	39.68	6.13	5.058059	115.6891685	5.784458423	5.16	4.25805969	97.38272581	4.869136	1.15	0.94898617	21.7035145	1.085176
T6	45.21	5.55	5.218166	119.3405546	5.967027728	4.89	4.59762712	105.1487048	5.257435	0.94	0.88379744	20.2126345	1.016632
T6	49.63	4.59	4.737479	108.3471575	5.417357877	4.05	4.18012894	95.60043312	4.780022	0.81	0.83602579	19.1200866	0.956004
T8	51.24	4.96	5.28544	120.8791393	6.043956965	3.95	4.20917126	96.26463715	4.813232	0.79	0.81843245	19.2529274	0.962466
T8	50.29	4.32	4.518099	103.3298845	5.166494225	3.25	3.39003296	77.3660292	3.88683	0.66	0.69026519	15.7865101	0.789326
T10	45.12	4.92	4.616625	105.5831842	5.279159208	3.56	3.34048456	76.39758853	3.819879	0.63	0.59115317	13.519798	0.67599
T10	49.68	4.81	4.96955	113.6546542	5.682732711	3.69	3.81239888	87.19036883	4.359518	0.75	0.77487772	17.7216197	0.886081
T12	45.12	5.04	4.729225	108.1583838	5.407919188	3.67	3.44370178	78.75818818	3.937909	0.69	0.64745543	14.8073978	0.74037
T12	49.36	4.85	4.9786	113.8616443	5.693082213	3.96	4.06500156	92.96744562	4.648372	0.57	0.58511386	13.3816778	0.669084
T14	44.22	4.51	4.147493	94.85404188	4.742702094	3.61	3.31983363	75.92529738	3.796265	0.55	0.50579183	11.5675661	0.578378
T14	41.37	5.25	4.516845	103.3012046	5.165060229	4.05	3.48442342	79.68950067	3.984475	0.72	0.61945305	14.1670223	0.708351
pH 9													
Sample	Ribonic	alpha	adjustmer	Alpha (mg/L)	Alpha (mg)	beta	adjustment	beta (mg/L)	beta (mg)	Xylo	adjustment	Xylo (mg/L)	Xylo (mg)
T0	48.52	6.12	6.175364	141.2318916	7.061594578	4.98	5.02055147	114.9239902	5.7462	0.96	0.96868462	22.1540222	1.107701
T0	47.31	5.97	5.87378	134.3345858	6.716729291	4.85	4.77183113	109.1327875	5.456639	1.24	1.22001456	27.901991	1.3951
T2	43.69	6.52	5.924068	135.4846837	6.774234187	5.79	5.26079027	120.3153863	6.015769	1.15	1.04488926	23.8968384	1.194842
T2	41.75	6.45	5.600239	128.0786543	6.403932716	5.25	4.5583342	104.2500675	5.212503	1.25	1.08531767	24.8214466	1.241072
T4	45.25	5.95	5.99199	128.0548733	6.402743664	4.89	4.60169492	105.2417362	5.262087	1.27	1.19512322	27.3327209	1.366636
T4	49.63	6.27	6.471459	148.0036335	7.400181675	5.27	5.43932827	124.3985883	6.219929	1.14	1.17662889	26.9097515	1.345488
T6	51.02	5.96	6.323785	144.6262999	7.231314996	5.05	5.35824062	122.5440964	6.127205	1.22	1.29446605	29.6047124	1.480236
T6	52.12	5.52	5.983205	136.8371582	6.841857909	4.25	4.60663409	105.3546961	5.267735	0.95	1.02971821	23.5498732	1.177494
T8	54.12	5.68	6.392879	146.2065017	7.310325073	4.52	5.08729126	116.3474272	5.817371	0.99	1.1425185	25.4831574	1.274159
T8	53.69	5.12	5.71681	130.7446499	6.537232494	4.1	4.57791411	104.6978642	5.234893	0.89	0.99374233	22.7270973	1.136355
T10	44.12	5.59	5.129059	117.3026634	5.865133171	4.27	3.91790371	89.60328673	4.480164	0.98	0.89919102	20.5646888	1.028234
T10	49.56	5.94	6.122209	140.0162056	7.000810279	5.12	5.27705521	120.6873691	6.034368	1.09	1.12343535	25.6932094	1.28466
T12	48.2	5.15	5.162317	118.0632757	5.903163786	4.12	4.12985338	94.45062057	4.722531	1.05	1.0525118	24.1071533	1.203558
T12	39.65	6.63	5.466975	125.0308782	6.251543909	5.24	4.3208069	98.81776797	4.940888	0.86	0.70914006	16.2181833	0.810909
T14	42.14	5.67	4.968988	113.6418125	5.682090623	4.36	3.8209504	87.38594398	4.369297	0.99	0.86760112	19.8422102	0.92111
T14	48.25	5.21	5.227878	119.5626693	5.978133467	2.95	2.9601227	67.69863235	3.384932	1.04	1.04356868	23.8666365	1.193332
pH 10													
Sample	Ribonic	alpha	adjustmer	Alpha (mg/L)	Alpha (mg)	beta	adjustment	beta (mg/L)	beta (mg)	Xylo	adjustment	Xylo (mg/L)	Xylo (mg)
T0	45.12	5.86	5.498663	125.7555811	6.287779056	4.95	4.64477488	106.2269841	5.311349	1.12	1.05093896	24.0351964	1.20176
T0	49.36	6.36	6.528639	149.3113521	7.465567603	5.27	5.40973692	123.7218279	6.186091	1.2	1.23181865	28.1719532	1.408598
T2	48.75	5.97	6.052563	138.4243001	6.821170005	5.19	5.26177602	120.3379307	6.016897	1.05	1.06452116	24.3458241	1.217291
T2	49.23	5.59	5.723109	130.8887153	6.544435766	4.89	5.00644068	114.4983574	5.724918	0.95	0.9726214	22.2440572	1.122203
T4	39.65	5.84	4.815556	110.1327796	5.506638978	4.88	4.02395758	92.02876101	4.601438	0.96	0.79159821	18.405186	0.905201
T4	43.27	6.57	5.912112	135.2112495	6.760562476	5.27	4.74228762	108.457121	5.422856	1.12	1.0078486	23.0497107	1.152486
T6	49.63	6.52	6.729492	153.9048948	7.69524474	5.29	5.45997088	124.8706892	6.243534	1.01	1.04245191	23.8410957	1.192055
T6	51.24	5.24	5.583812	127.7029617	6.385148084	4.51	4.80591453	109.9122819	5.495614	0.84	0.8951149	18.4714671	1.023573
T8	47.5	5.36	5.29479	121.0929783	6.054648914	4.49	4.43537486	101.4379613	5.071898	0.82	0.81002932	18.5254183	0.926271
T8	45.59	6.12	5.80245	132.7032551	6.635162754	4.98	4.72160133	107.9840213	5.399201	0.93	0.88174483	20.1656907	1.008285
T10	49.61	5.53	5.705382	130.4832964	6.524164821	4.27	4.40542165	100.7529251	5.037646	0.82	0.84600603	19.3483369	0.967417
T10	46.35	5.12	4.93526	112.8704511	5.643522557	3.98	3.83639389	87.73913976	4.386957	0.62	0.5976292	13.6679062	0.683395
T12	45.17	4.36	4.095689	93.66927122	4.683463561	4.42	4.15205158	94.95829789	4.747915	0.81	0.76089633	17.40186	0.870093
T12	49.63	5.12	5.284509	120.8578315	6.042891575	4.58	4.72715816	108.1111071	5.405555	0.96	0.99084538	22.6608434	1.133042
T14	47.25	4.65	4.569252	104.4997682	5.224988411	4.39	4.31376729	98.65677043	4.932839	0.71	0.69767079	15.9558786	0.797794
T14	41.36	5	4.300717	98.35831857	4.917915928	4.27	3.67281273	83.99800406	4.1999	0.69	0.59349901	13.573448	0.678672
pH 11													
Sample	Ribonic	alpha	adjustmer	Alpha (mg/L)	Alpha (mg)	beta	adjustment	beta (mg/L)	beta (mg)	Xylo	adjustment	Xylo (mg/L)	Xylo (mg)
T0	43.16	6.32	5.672688	129.7355734	6.486778672	4.85	4.35324945	99.55973594	4.9778				

pH 9													
Sample	Ribonic	alpha	adjustment	Alpha (mg/L)	Alpha (mg)	beta	adjustment	beta (mg/L)	beta (mg)	Xylo	adjustment	Xylo (mg/L)	Xylo (mg)
T0	47.35	5.75	5.662108766	129.4936253	6.474681264	4.32	4.253966934	97.28912369	4.864456	0.95	0.93547884	21.39459896	1.06973
T0	46.12	6.32	6.061732349	138.6331012	6.931655059	3.98	3.817356764	87.30375675	4.365188	0.81	0.776899241	17.76784999	0.888392
T2	48.95	6.31	6.42351045	146.9070429	7.345352144	3.85	3.919257565	89.63424962	4.481712	0.82	0.834750962	19.09093109	0.954547
T2	43.12	5.78	5.183188104	118.5406084	5.927030422	3.15	2.824747842	64.60258073	3.230129	0.74	0.663591557	15.17647928	0.758824
T4	44.25	5.86	5.392638037	123.3307727	6.166538636	3.52	3.239263804	74.08264845	3.704132	0.66	0.607361963	13.89049659	0.694525
T4	45.91	5.74	5.480366019	125.3371302	6.266856511	3.19	3.045708641	69.65600094	3.4828	0.71	0.677884995	15.50337325	0.775169
T6	49.63	5.75	5.934750962	135.72901	6.7864505	3.05	3.147998336	71.99538791	3.599769	0.61	0.629599667	14.39907758	0.719954
T6	50.85	4.36	4.610710201	105.4479177	5.272395884	2.84	3.003306644	68.68625831	3.434313	0.51	0.539326193	12.33450413	0.616725
T8	52.75	5.56	6.0994073	139.4947353	6.974736763	2.25	2.468285328	56.45020762	2.82251	0.45	0.493657066	11.29004152	0.564502
T8	53.15	4.24	4.686617448	107.1839325	5.359196625	1.98	2.188561922	50.05287414	2.502644	0.41	0.453187065	10.36448404	0.518224
T10	49.26	4.12	4.220675886	96.5277504	4.82638752	1.89	1.936183841	44.28093404	2.214047	0.39	0.399529999	9.137335597	0.456867
T10	43.17	3.89	3.492384319	79.8715682	3.99357841	1.74	1.562146199	35.72661405	1.786331	0.45	0.404003327	9.239641565	0.461982
T12	48.25	3.57	3.582250182	81.92681948	4.096340974	1.69	1.695799106	38.78328429	1.939164	0	0	0	0
T12	47.12	3.31	3.24357284	74.18119702	3.709059851	1.51	1.479696371	33.84096903	1.692048	0	0	0	0
T14	44.31	2.97	2.736834772	62.59199021	3.12959951	1.45	1.336165124	30.55837906	1.527919	0	0	0	0
T14	45.51	2.25	2.129510242	48.70234974	2.435117487	1.42	1.343957575	30.73659406	1.53683	0	0	0	0
pH 10													
Sample	Ribonic	alpha	adjustment	Alpha (mg/L)	Alpha (mg)	beta	adjustment	beta (mg/L)	beta (mg)	Xylo	adjustment	Xylo (mg/L)	Xylo (mg)
T0	49.36	5.59	5.738221899	131.2343487	6.561717437	4.85	4.978600395	113.8616443	5.693082	0.95	0.975189768	22.3027963	1.11514
T0	45.36	5.74	5.414711448	123.8355963	6.191779815	4.36	4.11291671	94.06327524	4.703164	0.98	0.92446293	21.14266278	1.057133
T2	50.25	5.69	5.94618904	135.9906013	6.799530063	4.45	4.65035874	106.3546882	5.317734	0.99	1.034574192	23.66983062	1.183047
T2	47.25	5.71	5.610845378	128.3212208	6.416061038	4.21	4.136893002	94.61161811	4.730581	0.89	0.874545076	20.00103091	1.000052
T4	45.36	5.66	5.339245087	122.1096647	6.105483233	4.32	4.075183529	93.20030941	4.660015	0.96	0.90559634	20.71117987	1.035559
T4	49.62	5.85	6.036747426	138.0616907	6.903084536	4.59	4.736524904	108.3253266	5.416266	1.05	1.083518769	24.78030346	1.239015
T6	39.69	5.95	4.911209317	112.320396	5.616019802	4.36	3.598802121	82.30536584	4.115268	0.98	0.808905064	18.49982994	0.924991
T6	50.25	6.12	6.395549548	146.2675711	7.313378557	4.61	4.817562649	110.1786769	5.508934	1.05	1.097275658	25.09492642	1.254746
T8	45.36	5.88	5.546777581	126.8559767	6.342798835	4.41	4.160083186	95.14198253	4.757099	0.98	0.92446293	21.14266278	1.057133
T8	47.17	6.05	5.934875741	135.7318637	6.786593186	4.39	4.306463554	98.48973251	4.924487	0.95	0.931922637	21.31326786	1.065663
T10	41.25	6	5.147135281	117.7160728	5.885803638	4.45	3.817458667	87.30608729	4.365304	0.89	0.763491733	17.46121746	0.873061
T10	45.02	6.25	5.851616928	133.8277171	6.691385853	4.59	4.297427472	98.28307541	4.914154	0.96	0.89880836	20.55593734	1.027797
T12	43.62	5.59	5.070932723	115.9733041	5.798665207	4.32	3.918860351	89.62516527	4.481258	0.88	0.798286368	18.25697811	0.912849
T12	41.25	5.69	4.881199958	111.6340757	5.581703783	4.51	3.86893002	88.48324802	4.424162	0.79	0.677706145	15.49928291	0.774964
T14	44.49	5.24	4.848239576	110.8802647	5.544013237	3.67	3.395618176	77.65850603	3.882925	0.47	0.434861183	9.945367257	0.497268
T14	44.91	4.47	4.174850785	95.47972064	4.773986032	3.37	3.147482583	71.98359252	3.59918	0.39	0.364248726	8.330445425	0.416522
pH 11													
Sample	Ribonic	alpha	adjustment	Alpha (mg/L)	Alpha (mg)	beta	adjustment	beta (mg/L)	beta (mg)	Xylo	adjustment	Xylo (mg/L)	Xylo (mg)
T0	43.12	6.98	6.259282521	143.1511154	7.15755577	3.38	3.030999272	69.31959456	3.46598	0.85	0.762233545	17.43244242	0.871622
T0	45.96	6.85	6.547280857	149.7376983	7.486884913	3.42	3.268861391	74.75955154	3.737978	0.92	0.87934283	20.11075656	1.005538
T2	47.84	6.57	6.536524904	149.4917073	7.474585367	3.33	3.31303317	75.76976948	3.788488	0.82	0.815821982	18.65802131	0.932901
T2	43.12	6.32	5.667430592	129.6153366	6.480766829	3.05	2.735073308	62.55170515	3.127585	0.75	0.67255901	15.38156684	0.769078
T4	43.69	6.85	6.223905584	142.3420374	7.117101868	3.4	3.089237808	70.6515222	3.532576	0.8	0.726879484	16.62388758	0.831194
T4	43.33	6.74	6.073499012	138.9022073	6.945110363	3.38	3.045760632	69.65718999	3.482859	0.85	0.765945721	17.51734068	0.875867
T6	47.21	6.32	6.204995321	141.9095556	7.095477782	3.28	3.220314027	73.64926306	3.682463	0.82	0.805078507	18.41231576	0.920616
T6	40.21	6.12	5.117712384	117.0431649	5.852158244	3.05	2.550493917	58.33033544	2.916517	0.69	0.576996985	13.1960431	0.659802
T8	45.2	6.33	5.950213164	136.0826338	6.804131691	3.35	3.149006967	72.0184555	3.600923	0.72	0.676801497	15.47859342	0.77393
T8	49.61	6.41	6.613291047	151.2473653	7.562368264	2.95	3.043558282	69.60682178	3.480341	0.66	0.680931683	15.57305165	0.778653
T10	45.27	6.42	6.044159301	138.2312019	6.911560093	2.87	2.701983987	61.79494538	3.089747	0.75	0.706093376	16.14850489	0.807425
T10	41.02	6.51	5.553503171	127.0097924	6.350489619	3.39	2.891916398	66.13873981	3.306937	0.69	0.588620152	13.46186739	0.673093
T12	47.86	5.98	5.952018301	136.1239177	6.806195884	3.05	3.035728398	69.42775066	3.471388	0.65	0.646958511	14.79607801	0.739804
T12	50.25	5.12	5.350525112	122.3676412	6.11838206	2.12	2.215451804	50.66785144	2.533393	0.55	0.57476344	13.14496146	0.657248
T14	51.29	5.32	5.674592908	129.7791403	6.488957014	2.59	2.762630758	63.18194987	3.159097	0.39	0.415994593	9.513884343	0.475694
T14	49.85	4.86	5.03839035	115.2290532	5.761452659	1.95	2.021576375	46.23387936	2.311694	0.45	0.466517625	10.66935678	0.533468

**Figure S6.4. ISA concentrations within CDP-fed microcosms employing the site-H sediments between pH 9-11.**

pH 7													
Sample	Ribonic	alpha	adjustment	Alpha (mg/L)	Alpha (mg)	beta	adjustment	beta (mg/L)	beta (mg)	Xylo	adjustment	Xylo (mg/L)	Xylo (mg)
T0	44.59	6.36	5.897731101	134.8823579	6.744117897	4.52	4.191469273	95.85978898	4.792989	0.95	0.8809504	20.14752202	1.007376
T0	49.69	6.21	6.417279817	146.764547	7.338227349	4.82	4.980883852	113.9138674	5.695693	1.15	1.188385151	27.17861981	1.358931
T2	48.25	5.54	5.559010086	127.1357367	6.356786834	4.63	4.645887491	106.2524298	5.312621	0.99	0.993397109	22.71920204	1.13596
T2	47.52	5.12	5.059839867	115.7196082	5.785980408	4.25	4.20006239	96.05631537	4.802816	0.96	0.948719975	21.69742653	1.084871
T4	41.26	4.58	3.929932411	89.87838562	4.493919281	3.96	3.397932827	77.71144259	3.885572	0.9	0.772257461	17.6616915	0.883085
T4	49.35	4.89	5.018644068	114.7774515	5.738872576	4.05	4.1565457	95.06107948	4.753054	1.06	1.087886035	24.88018377	1.244009
T6	48.25	4.12	4.134137465	94.5485984	4.72742992	3.82	3.833108038	87.66399172	4.3832	0.85	0.85291671	19.50638559	0.975319
T6	42.28	3.85	3.385213684	77.4205531	3.871027655	3.62	3.182980139	72.79542914	3.639771	0.77	0.677042737	15.48411062	0.774206
T8	47.21	3.12	3.063225538	70.05661608	3.502830804	3.14	3.082861599	70.50569695	3.525285	0.66	0.647990018	14.81966879	0.740983
T8	41.24	2.75	2.358531767	53.94012045	2.697006022	2.86	2.452873037	56.09772527	2.804886	0.59	0.50601227	11.57260766	0.578663
T10	45.69	0	0	0	0	2.26	2.147434751	49.11228704	2.455614	0.58	0.551111573	12.60403827	0.630202
T10	49.63	0	0	0	0	2.15	2.219080794	50.75084721	2.537542	0.55	0.567671831	12.98277487	0.649139
T12	45.52	0	0	0	0	0	0	0	0	0.36	0.340796506	7.794088192	0.389704
T12	51.24	0	0	0	0	0	0	0	0	0.47	0.500838099	11.45427328	0.572714
T14	52.36	0	0	0	0	0	0	0	0	0	0	0	0
T14	51.24	0	0	0	0	0	0	0	0	0	0	0	0
pH 8													
Sample	Ribonic	alpha	adjustment	Alpha (mg/L)	Alpha (mg)	beta	adjustment	beta (mg/L)	beta (mg)	Xylo	adjustment	Xylo (mg/L)	Xylo (mg)
T0	42.24	6.32	5.551768743	126.9701256	6.348506281	5.15	4.52398877	103.4645802	5.173229	1.05	0.922366642	21.09472024	1.054736
T0	43.12	6.54	5.864714568	134.1272628	6.706363142	5.62	5.039708849	115.2592075	5.76296	1.25	1.120931683	25.63594473	1.281797
T2	45.96	6.33	6.050260996	138.3707489	6.918537446	5.52	5.276056982	120.6645393	6.033227	1.28	1.223433503	27.98018303	1.399009
T2	44.27	6.05	5.57000104	127.3871021	6.369355106	5.17	4.75981907	108.8580691	5.442903	1.22	1.123206821	25.68797762	1.284399
T4	48.95	5.85	5.95523552	136.1974962	6.809874809	4.85	4.937246543	112.9158729	5.645794	0.98	0.997629198	22.81599081	1.1408
T4	46.32	5.24	5.047661433	115.4410848	5.77205424	4.59	4.451202025	101.1211029	5.056055	0.78	0.75136945	17.18397827	0.859199
T6	48.75	4.36	4.42029739	101.0931364	5.054656821	4.05	4.106010119	93.90532168	4.695266	0.79	0.800925445	18.31733435	0.915867
T6	44.21	4.12	3.787983779	86.63199037	4.331599518	4.19	3.852342726	88.10389311	4.405195	0.69	0.634395342	14.50875567	0.725438
T8	49.58	3.65	3.763481335	86.0716143	4.303580715	4.32	4.454312156	101.8710613	5.093553	0.39	0.402125403	9.196693034	0.459835
T8	44.1	3.28	3.008173027	68.7975535	3.439877675	4.07	3.732702506	85.36769596	4.268385	0.21	0.192596444	4.404721413	0.220236
T10	47.96	3.25	3.241551419	74.13496671	3.706748335	3.86	3.849965686	88.04952969	4.402476	0	0	0	0
T10	49.67	3.15	3.253831756	74.41582061	3.720791031	3.69	3.811631486	87.17281843	4.358641	0	0	0	0
T12	42.31	2.84	2.98916502	57.15074905	2.857537452	3.15	2.771685557	63.38903503	3.169452	0	0	0	0
T12	43.51	2.89	2.615033794	59.80637609	2.990318804	2.98	2.696470833	61.66885839	3.083443	0	0	0	0
T14	47.16	2.25	2.206717271	50.46809083	2.523404541	2.51	2.461715712	56.2999591	2.814998	0	0	0	0
T14	48.25	2.19	2.197514818	50.25762876	2.512881438	2.29	2.29785796	52.55249765	2.627625	0	0	0	0
pH 9													
Sample	Ribonic	alpha	adjustment	Alpha (mg/L)	Alpha (mg)	beta	adjustment	beta (mg/L)	beta (mg)	Xylo	adjustment	Xylo (mg/L)	Xylo (mg)
T0	50.25	6.2	6.479151503	148.1795655	7.408978276	4.95	5.172870958	118.3046531	5.915233	0.95	0.992773214	22.70493343	1.135247
T0	51.39	5.85	6.25208485	142.9865031	7.149325157	4.81	5.140603099	117.5666804	5.878334	0.98	1.047357804	23.95329454	1.197665
T2	52.47	5.82	6.350741395	145.2427992	7.26213996	4.62	5.04131018	115.2958303	5.764792	0.89	0.971161485	22.21066861	1.110533
T2	55.21	5.74	6.590525112	150.7267035	7.536335176	4.51	5.178269731	118.4281242	5.921406	0.87	0.998912343	22.8453366	1.142267
T4	49.86	5.63	5.837824685	133.5122855	6.675614277	4.21	4.365407092	99.83778368	4.991889	0.69	0.715470521	16.36292617	0.818148
T4	43.12	5.74	5.147318291	117.7202582	5.886012911	4.63	4.151930956	94.95553929	4.747777	0.95	0.851908079	19.483318	0.974166
T6	42.85	5.73	5.106176562	116.7793382	5.838966909	4.95	4.411094936	100.8826744	5.044134	0.75	0.668347718	15.28525369	0.764263
T6	41.96	5.95	5.192097328	118.7443643	5.937218213	5.02	4.380559426	100.1843208	5.009216	0.82	0.715549548	16.36476953	0.818238
T8	48.57	6.15	6.212030779	142.0704581	7.103522903	5	5.050431528	115.5044375	5.775222	0.74	0.747463866	17.09465674	0.854733
T8	46.36	5.85	5.640137257	128.9911322	6.449556612	4.59	4.425338463	101.2084268	5.060421	0.59	0.568834356	13.00936205	0.605468
T10	49.85	5.82	6.033627951	137.9903476	6.899517382	4.36	4.520037434	103.3742123	5.168711	0.69	0.715327025	16.35968039	0.817984
T10	42.36	5.51	4.853979411	111.011536	5.505768	4.12	3.629472809	83.00681094	4.150341	0.58	0.510945201	11.68542484	0.584271
T12	48.71	5.59	5.662657793	129.5061817	6.475309083	4.1	4.153291047	94.98664487	4.749332	0.51	0.516628886	11.81541192	0.590771
T12	47.58	5.14	5.086018509	116.3183192	5.815915962	3.69	3.651246751	83.5047856	4.175239	0.48	0.474958927	10.86241114	0.543121
T14	47.25	5.12	5.031090777	115.0621104	5.753105519	3.52	3.458874909	79.10520089	3.95526	0.45	0.442185713	10.1128808	0.505644
T14	41.36	5.35	4.601767703	105.2434009	5.262170043	3.33	2.864277841	65.50664017	3.275332	0.39	0.335455963	7.671948848	0.383597
pH 10													
Sample	Ribonic	alpha	adjustment	Alpha (mg/L)	Alpha (mg)	beta	adjustment	beta (mg/L)	beta (mg)	Xylo	adjustment	Xylo (mg/L)	Xylo (mg)
T0	46.29	5.98	5.756768223	131.6585071	6.582925355	5.29	5.092525736	116.4671409	5.823357	0.99	0.953043569	21.79630803	1.089815
T0	43.27	6.49	5.840122699	133.5648416	6.67824208	6.21	5.588160549	127.8024139	6.390121	0.96	0.86387023	19.75689491	0.987845
T2	45.49	6.43	6.082992617	139.119328	6.955966401	6.14	5.808643028	132.8448949	6.642245	1.05	0.99333472	22.71777518	1.135889
T2	48.52	5.53	5.580027035	127.6163988	6.380819938	5.29	5.33785588	122.0778932	6.103895	0.92	0.928322762	21.23093795	1.061547
T4	41.06	6.47	5.247624	126.3524848	6.317624242	6.05	5.166122491	118.1503143	5.907516	0.95	0.811209317	18.55252869	0.977676
T4	42.39	6.78	5.977003223	136.6953282	6.834766408	6.59	5.809506083	132.8646331	6.643232	0.92	0.811038785	18.5486286	0.974286
T6	49.69	5.73	5.921258189	135.4204274	6.771021371	6.15	6.355277113	145.346532	7.267327	0.96	0.992043257	22.68823915	1.107696
T6	41.23	5.69	4.878833316	111.5799501	5.578997503	5.09	4.364369346	99.81405022	4.990703	0.85	0.728823958	16.66835809	0.818238
T8	40.29	5.78	4.843011334	110.7606937	5.538034687	5.29	4.432444629	101.3709464	5.068547	0.93	0.797238848	17.8213573	0.854733
T8	45.57	6.23	5.904150983	135.029182	6.7514591	5.57	5.278671103	120.7243248	6.036216	0.96	0.909788915	20.80706496	1.061547
T10	41.28	5.82	4.996352293	114.2676339	5.713381696	5.35	4.592866798	105.0398353	5.251992	0.82	0.703953416	16.09956354	0.818238
T10	44.29	5.69	5.240929604	119.8611688	5.993058438	5.19	4.780390974	109.3285529	5.466428	0.75	0.690807944	15.79892383	0.818238
T12	47.85	5.52	5.493022772	125.6265928	6.281329642	5.26	5.234293439	119.7093983	5.98547	0.75	0.746334616	17.06883055	0.818238
T12	41.96	5.39	4.703429344	107.5684241	5.378421205	4.86	4.240940002	96.99119502	4.84956	0.63	0.549751482	12.57293269	0.630202
T14	45.25	5.57	5.241603411	119.8765789	5.993828943	4.38	4.121763544	94.2656042	4.71328	0.32	0.30113341	6.886984782	0.383597
T14	50.27	4.39	4.589483207	104.9624518	5.248122592	4.26	4.453575959	101.8542243	5.092711	0.42	0.439084954	10.04196578	0.505644

Figure S6.5. ISA concentrations within CDP-fed microcosms employing the site-T sediments between pH 7-10.

pH 7 Volu	0	2	4	6	8	10	12	14
C1	0	0.005471	0.016351	0.028762	0.039079	0.094696	0.093321	0.104075
C2	0	0.006128	0.01238	0.02376	0.030013	0.088756	0.082441	0.113392
Ph 7 Mole	0	2	4	6	8	10	12	14
C1	0	2.24E-05	6.68E-05	0.000118	0.00016	0.000387	0.000381	0.000425
C2	0	2.5E-05	5.06E-05	9.71E-05	0.000123	0.000363	0.000337	0.000463
Ph 7 mMo	0	2	4	6	8	10	12	14
C1	0	0.022362	0.066832	0.117563	0.159732	0.387062	0.381439	0.425397
C2	0	0.025046	0.050603	0.097117	0.122674	0.362783	0.33697	0.463477
AVERAGE	0	0.023704	0.058717	0.10734	0.141203	0.374922	0.359205	0.444437
STDEV	0	0.001898	0.011475	0.014457	0.026204	0.017168	0.031445	0.026927
STERR	0	0.001342	0.008114	0.010223	0.018529	0.01214	0.022235	0.01904
rate/day1	0.030386							
rate/day2	0.033106							
average	0.031746							
stdev	0.001923							
pH 8 Volu	0	2	4	6	8	10	12	14
C1	0	0.004252	0.013349	0.038516	0.026668	0.04802	0.068654	0.085067
C2	0	0.008566	0.009223	0.030106	0.040548	0.039454	0.098604	0.099073
Ph 8 Mole	0	2	4	6	8	10	12	14
C1	0	1.74E-05	5.46E-05	0.000157	0.000109	0.000196	0.000281	0.000348
C2	0	3.5E-05	3.77E-05	0.000123	0.000166	0.000161	0.000403	0.000405
Ph 8 mMo	0	2	4	6	8	10	12	14
C1	0	0.017379	0.054564	0.157432	0.109001	0.196278	0.280617	0.347704
C2	0	0.035013	0.037697	0.123057	0.165738	0.161265	0.403035	0.404952
AVERAGE	0	0.026196	0.046131	0.140244	0.137369	0.178772	0.341826	0.376328
STDEV	0	0.012469	0.011927	0.024306	0.040119	0.024758	0.086563	0.04048
STERR	0	0.008817	0.008434	0.017187	0.028368	0.017507	0.061209	0.028624
rate/day1	0.024836							
rate/day2	0.028925							
average	0.026881							
stdev	0.002891							
pH 9 Volu	0	2	4	6	8	10	12	14
C1	0	0	0	0	0	0.009316	0.030826	0.048302
C2	0	0	0	0	0.004283	0.017601	0.040142	0.067341
Ph 9 Mole	0	2	4	6	8	10	12	14
C1	0	0	0	0	0	3.81E-05	0.000126	0.000197
C2	0	0	0	0	1.75E-05	7.19E-05	0.000164	0.000275
Ph 9 mMo	0	2	4	6	8	10	12	14
C1	0	0	0	0	0	0.03808	0.125996	0.197428
C2	0	0	0	0	0.017507	0.071943	0.164076	0.27525
AVERAGE	0	0	0	0	0.008753	0.055012	0.145036	0.236339
STDEV	0	0	0	0	0.012379	0.023945	0.026927	0.055028
STERR	0	0	0	0	0.008753	0.016932	0.01904	0.038911
rate/day1	0.014102							
rate/day2	0.019661							
average	0.016881							
stdev	0.003931							
pH 10 Volu	0	2	4	6	8	10	12	14
C1	0	0	0	0	0	0.004877	0.012255	0.039485
C2	0	0	0	0	0	0.007316	0.005846	0.035171
Ph 10 Mole	0	2	4	6	8	10	12	14
C1	0	0	0	0	0	1.99E-05	5.01E-05	0.000161
C2	0	0	0	0	0	2.99E-05	2.39E-05	0.000144
Ph 10 mM	0	2	4	6	8	10	12	14
C1	0	0	0	0	0	0.019935	0.050092	0.161393
C2	0	0	0	0	0	0.029902	0.023896	0.143759
AVERAGE	0	0	0	0	0	0.024918	0.036994	0.152576
STDEV	0	0	0	0	0	0.007048	0.018523	0.012469
STERR	0	0	0	0	0	0.004984	0.013098	0.008817
rate/day1	0.011528							
rate/day2	0.010268							
average	0.010898							
stdev	0.000891							

**Figure S6.6. Methane quantities within CDP-fed microcosms employing the control sediments between pH 7-10.**

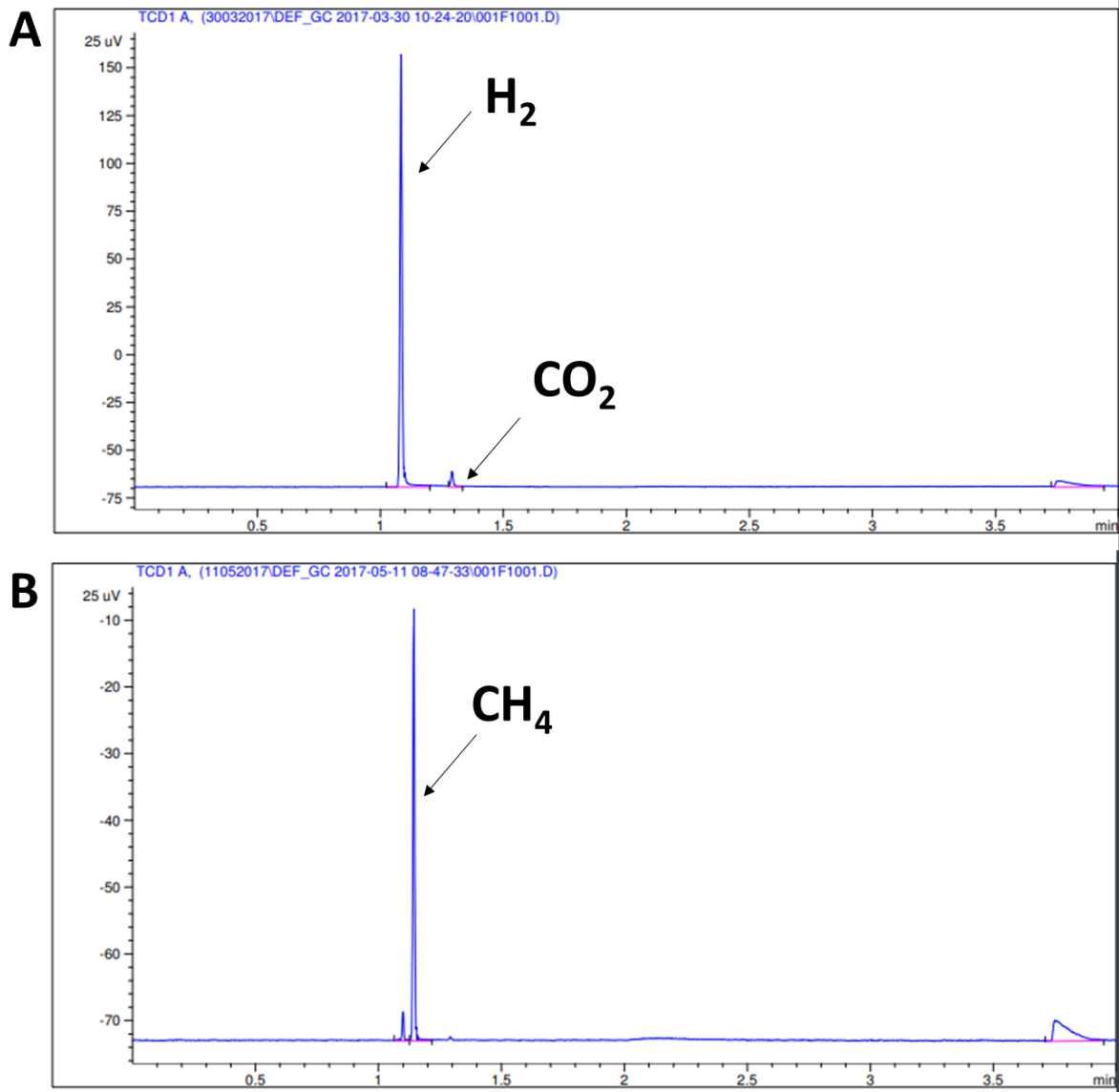


**Figure S6.7. Raw chromatogram output from GC-TCD showing retention times for different gases. [A]  $\text{H}_2/\text{CO}_2$ -fed microcosms begin with hydrogen gas and carbon dioxide in the headspace, [B] following the incubation hydrogen is consumed and is replaced with methane.**

**Independent Samples Test – Methanogens vs SRB**

		Levene's Test for Equality of Variances		t-test for Equality of Means						
		F	Sig.	t	df	Sig. (2-tailed)	Mean Difference	Std. Error Difference	95% Confidence Interval of the Difference	
									Lower	Upper
Firmicutes	Equal variances assumed	2.827	.168	-.632	4	.561	-11.606	18.350	-62.553	39.341
	Equal variances not assumed			-.632	2.523	.580	-11.606	18.350	-76.782	53.570
Proteobacteria	Equal variances assumed	12.728	.023	.065	4	.951	1.037	15.860	-42.997	45.072
	Equal variances not assumed			.065	2.033	.954	1.037	15.860	-66.145	68.219
Actinobacteria	Equal variances assumed	15.276	.017	-1.995	4	.117	-9.227	4.626	-22.070	3.616
	Equal variances not assumed			-1.995	2.000	.184	-9.227	4.626	-29.130	10.676
Bacteroidetes	Equal variances assumed	7.158	.055	5.227	4	.006	18.457	3.531	8.654	28.261
	Equal variances not assumed			5.227	2.264	.026	18.457	3.531	4.844	32.070
Synergistetes	Equal variances assumed	16.000	.016	-1.000	4	.374	-.366	.366	-1.381	.650
	Equal variances not assumed			-1.000	2.000	.423	-.366	.366	-1.940	1.208
Euryarchaeota	Equal variances assumed	15.986	.016	1.101	4	.333	1.554	1.412	-2.365	5.473
	Equal variances not assumed			1.101	2.000	.386	1.554	1.412	-4.519	7.628
ETC	Equal variances assumed	1.619	.272	.807	4	.465	.150	.186	-.366	.666
	Equal variances not assumed			.807	3.041	.478	.150	.186	-.437	.737

**Figure S8.1. Independent samples t-test output comparing differences between communities under methanogenic and sulphate-reducing conditions at the phylum-level.**

Independent Samples Test – Biofilms vs Bulk											
		Levene's Test for Equality of Variances		t-test for Equality of Means							
		F	Sig.	t	df	Sig. (2-tailed)	Mean Difference	Std. Error Difference	95% Confidence Interval of the Difference		
									Lower	Upper	
Firmicutes	Equal variances assumed	3.538	.133	-1.986	4	.118	-28.765	14.485	-68.983	11.453	
	Equal variances not assumed			-2.970	3.042	.058	-28.765	9.685	-59.348	1.818	
Proteobacteria	Equal variances assumed	.638	.469	1.009	4	.370	15.162	15.027	-26.560	56.883	
	Equal variances not assumed			1.291	3.879	.268	15.162	11.743	-17.847	48.170	
Actinobacteria	Equal variances assumed	379.765	.000	1.153	4	.313	6.920	6.004	-9.749	23.589	
	Equal variances not assumed			1.729	3.000	.182	6.920	4.002	-5.817	19.658	
Bacteroidetes	Equal variances assumed	22.496	.009	.521	4	.630	5.286	10.142	-22.872	33.444	
	Equal variances not assumed			.609	3.165	.584	5.286	8.683	-21.553	32.125	
Synergistetes	Equal variances assumed	4.000	.116	.667	4	.541	.274	.412	-.868	1.417	
	Equal variances not assumed			1.000	3.000	.391	.274	.274	-.599	1.148	
Euryarchaeota	Equal variances assumed	3.693	.127	.664	4	.543	1.077	1.622	-3.427	5.580	
	Equal variances not assumed			.995	3.018	.393	1.077	1.083	-2.357	4.511	
ETC	Equal variances assumed	.294	.617	.217	4	.839	.046	.211	-.541	.633	
	Equal variances not assumed			.250	3.042	.818	.046	.184	-.534	.625	

**Figure S8.2. Independent samples t-test output comparing differences between bulk and biofilm communities at the phylum-level.**

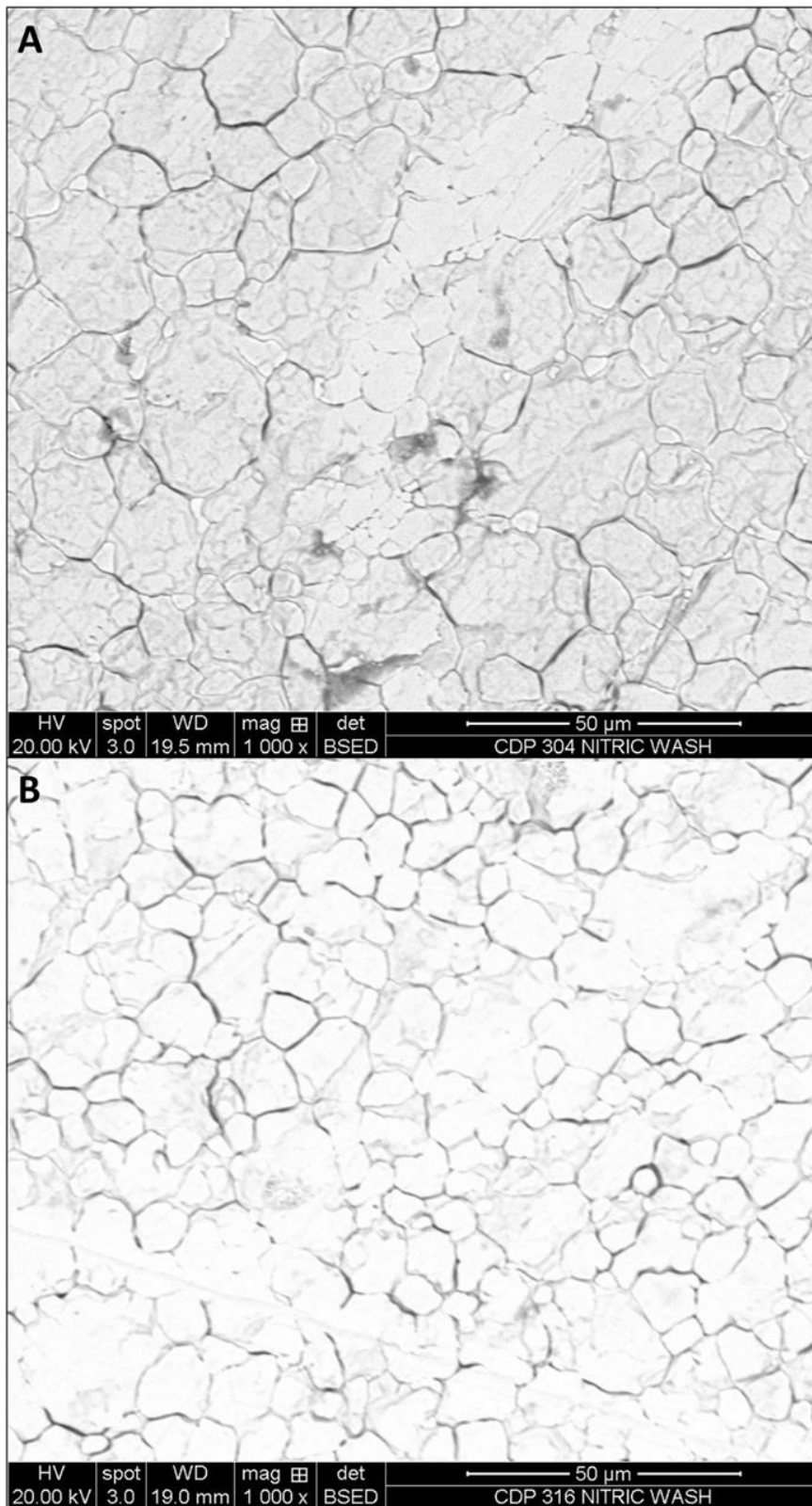


**Figure S8.3. SEM investigation of steel surfaces incubated under methanogenic conditions.** Shows steel surfaces after removal of methanogenic biofilms incubated for 3 months at pH 11.0.

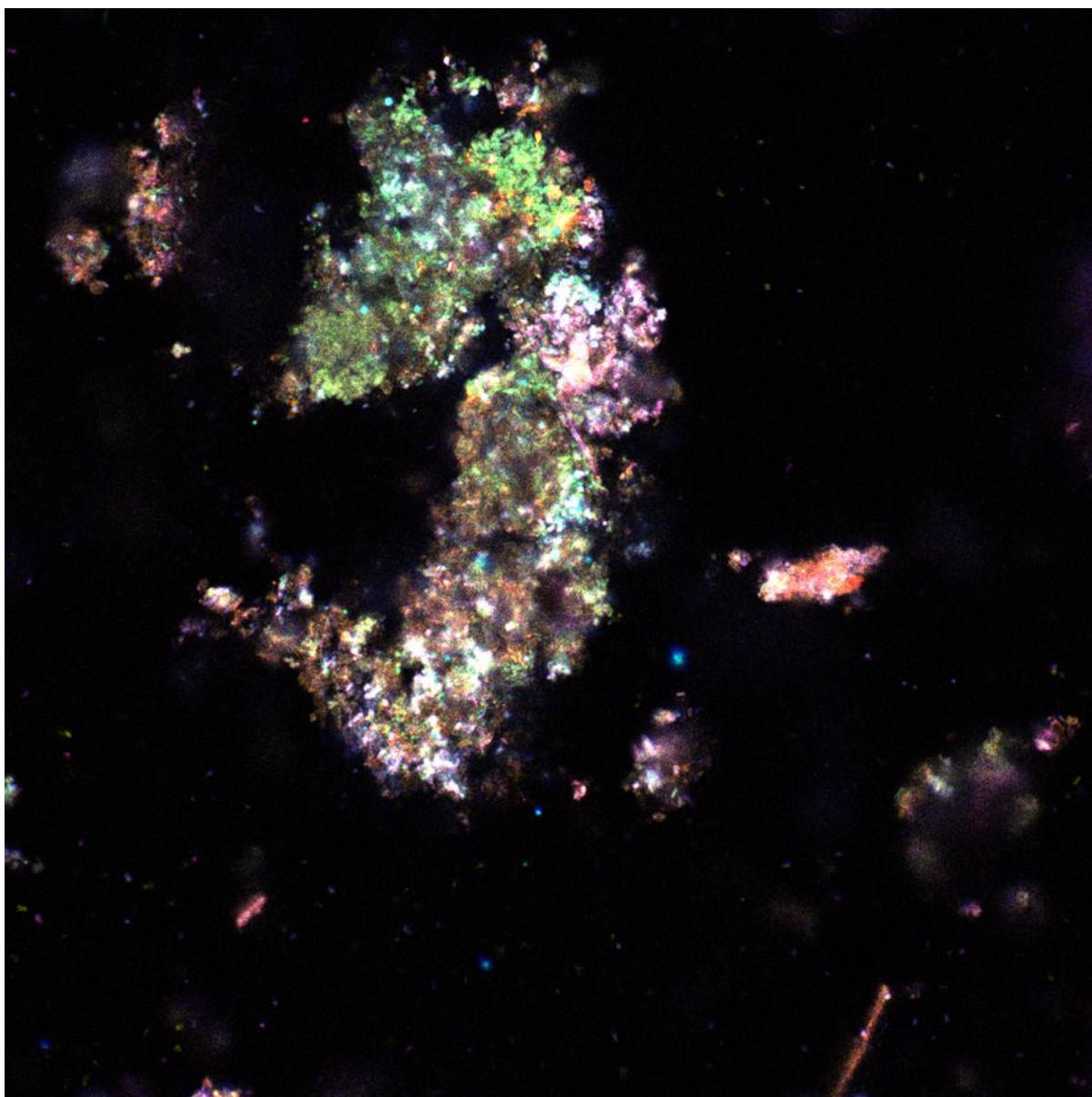


**Figure S8.4. 5-colour CLSM investigation of sulphate-reducing biofilm.** Visualisation of individual EPS components that comprise the sulphate-reducing biofilm formed on steel surface after 3 months incubation. The combined top-down image is shown. Colours represent protein (Green), lipids (Yellow), sugars (Red), polysaccharides (Blue) and eDNA with cells (Pink).

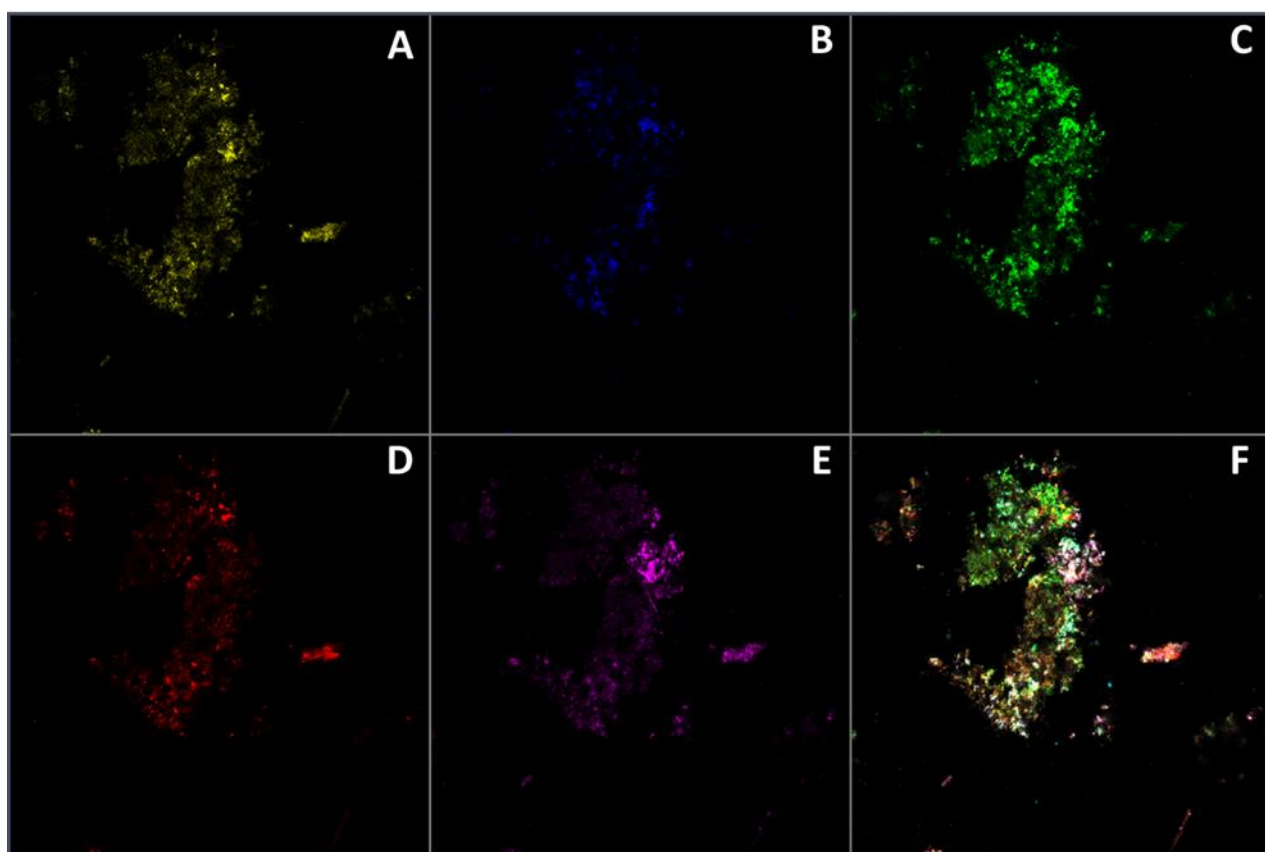


**Figure S8.5. 5-colour CLSM investigation of sulphate-reducing biofilm.** Visualisation of individual EPS components that comprise the sulphate-reducing biofilm formed on steel surface after 3 months incubation. The split view image is shown. (A) Lipids, (B) Polysaccharides, (C) Protein, (D) Sugars, (E) eDNA and cells, (F) Combined image.

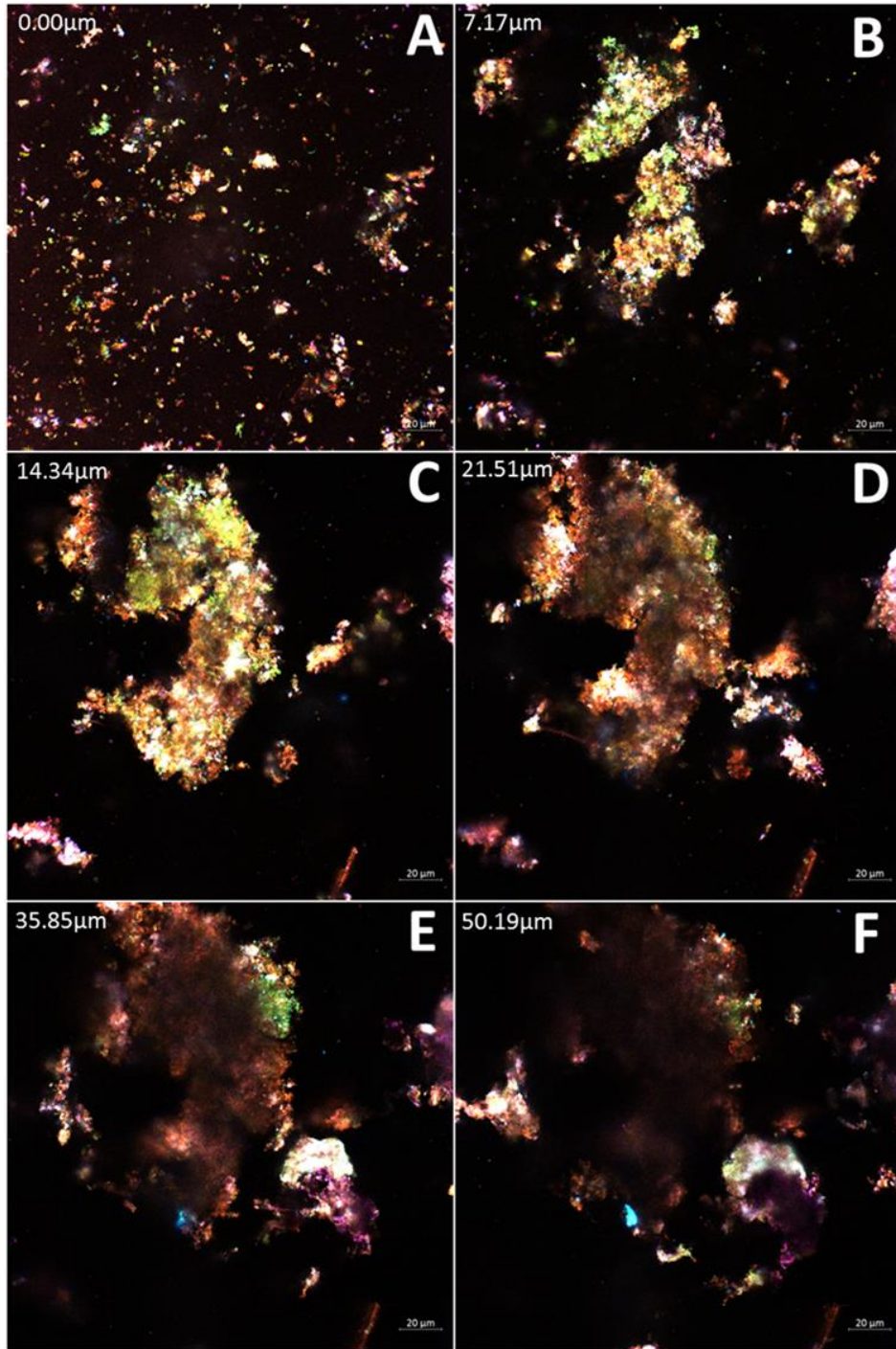


**Figure S8.6. 5-colour CLSM investigation of sulphate-reducing biofilm.** Visualisation of individual EPS components that comprise the sulphate-reducing biofilm formed on steel surface after 3 months incubation. (A) steel surface, (B-H) increasing height above steel surface. Yellow – lipids, blue – polysaccharides, green – protein, red – sugars, pink – cells and eDNA.

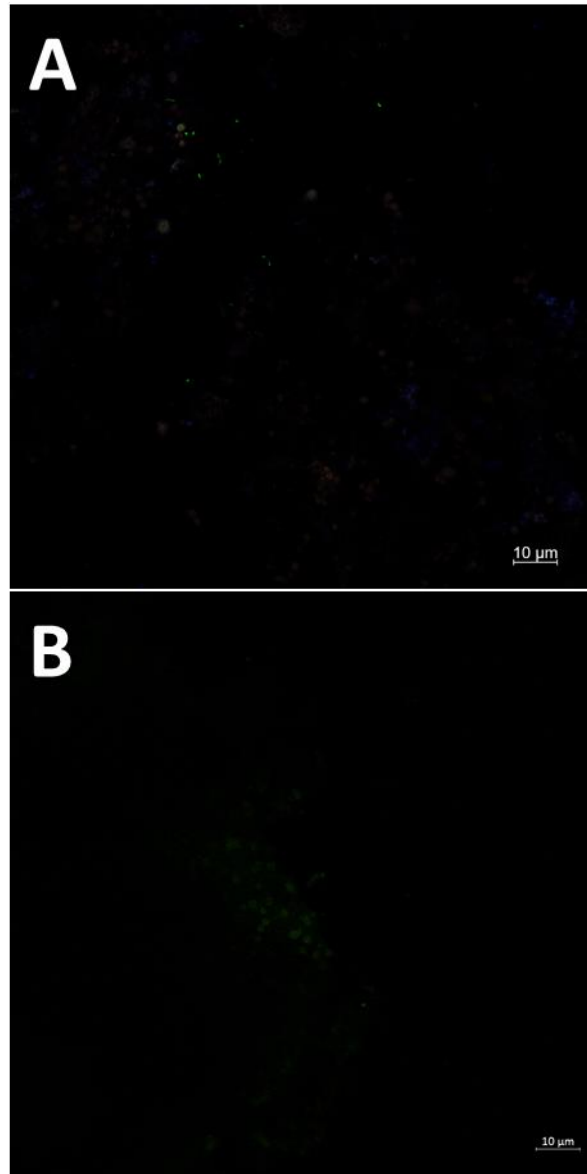


**Figure S8.7. 5-colour CLSM investigation of auto-fluorescent controls.** Visualisation of individual EPS components on biofilms not exposed to stains for auto-fluorescence testing.

**Table S8.1. Micro-electrode pH profiles of sulphate-reducing biofilms and abiotic controls.**

Abiotic			Profile 1			Profile 2			Profile 3		
dept h	pH	std	dept h	pH	std	dept h	pH	std	dept h	pH	std
-1000	11.06 22	0.0041 42	-1000	11.203 6	0.0045 83	-1000	11.148 7	0.0045 83	-1000	11.16	7.11E-15
-990	11.06	3.55E-15	-990	11.191 6	8.88E-15	-990	11.149	8.88E-15	-990	11.162	0.004
-980	11.06	3.55E-15	-980	11.195 4	8.88E-15	-980	11.145	8.88E-15	-980	11.161	0.003
-970	11.06 22	0.0041 42	-970	11.198 8	0.004	-970	11.148	0.004	-970	11.161 6	0.0048 99
-960	11.06	3.55E-15	-960	11.202 2	8.88E-15	-960	11.15	8.88E-15	-960	11.16	0
-950	11.06	3.55E-15	-950	11.2	0.0032 5	-950	11.148 12	0.0032 5	-950	11.16	0
-940	11.06	3.55E-15	-940	11.191	0.0014	-940	11.149 8	0.0014	-940	11.16	0
-930	11.06	3.55E-15	-930	11.199	0.0071 67	-930	11.147 08	0.0071 67	-930	11.16	0
-920	11.06	3.55E-15	-920	11.2	0.0032 5	-920	11.148 8	0.0032 5	-920	11.16	0
-910	11.06	3.55E-15	-910	11.199	0.0023 75	-910	11.149 4	0.0023 75	-910	11.16	0
-900	11.06	3.55E-15	-900	11.2	3.55E-15	-900	11.147	3.55E-15	-900	11.16	0
-890	11.06	3.55E-15	-890	11.2	0.003	-890	11.147 1	0.003	-890	11.16	0
-880	11.06	3.55E-15	-880	11.2	0.0041 42	-880	11.147 8	0.0041 42	-880	11.16	0
-870	11.06	3.55E-15	-870	11.2	0.0045 83	-870	11.147	0.0045 83	-870	11.16	0
-860	11.06	3.55E-15	-860	11.204 2	0.0047 37	-860	11.146 6	0.0047 37	-860	11.16	0

-850	11.06	3.55E-15	-850	11.1984	0.004142	-850	11.1478	0.004142	-850	11.16	0
-840	11.06	3.55E-15	-840	11.2	0.004737	-840	11.1466	0.004737	-840	11.16	0
-830	11.06	3.55E-15	-830	11.199	8.88E-15	-830	11.149	8.88E-15	-830	11.16	0
-820	11.06	3.55E-15	-820	11.2	8.88E-15	-820	11.149	8.88E-15	-820	11.16	0
-810	11.0594	0.002375	-810	11.199	8.88E-15	-810	11.149	8.88E-15	-810	11.16	0
-800	11.06	3.55E-15	-800	11.1978	8.88E-15	-800	11.149	8.88E-15	-800	11.159	0.003
-790	11.06	3.55E-15	-790	11.2	8.88E-15	-790	11.149	8.88E-15	-790	11.1578	0.004142
-780	11.06	3.55E-15	-780	11.1928	8.88E-15	-780	11.149	8.88E-15	-780	11.16383	0.004583
-770	11.06	3.55E-15	-770	11.199	8.88E-15	-770	11.149	8.88E-15	-770	11.16098	0.001498
-760	11.06	3.55E-15	-760	11.2	8.88E-15	-760	11.149	8.88E-15	-760	11.16	0
-750	11.06	3.55E-15	-750	11.2	8.88E-15	-750	11.149	8.88E-15	-750	11.16	0
-740	11.06	3.55E-15	-740	11.2	8.88E-15	-740	11.149	8.88E-15	-740	11.162	0.004
-730	11.06	3.55E-15	-730	11.2	8.88E-15	-730	11.149	8.88E-15	-730	11.16	0
-720	11.06	3.55E-15	-720	11.2	8.88E-15	-720	11.149	8.88E-15	-720	11.16	0
-710	11.06	3.55E-15	-710	11.2	0.003	-710	11.149	0.003	-710	11.16	0
-700	11.06	3.55E-15	-700	11.2	0.004583	-700	11.143	0.004583	-700	11.16	0
-690	11.06	3.55E-15	-690	11.199	0.003	-690	11.1441	0.003	-690	11.16	0
-680	11.06	3.55E-15	-680	11.2	0.00196	-680	11.14404	0.00196	-680	11.16	0

-670	11.06	3.55E-15	-670	11.2	8.88E-15	-670	11.15	8.88E-15	-670	11.16	0
-660	11.06	3.55E-15	-660	11.2	0.003	-660	11.149	0.003	-660	11.16	0
-650	11.06	3.55E-15	-650	11.2	0.00325	-650	11.1488	0.00325	-650	11.16	0
-640	11.06	3.55E-15	-640	11.2	8.88E-15	-640	11.15	8.88E-15	-640	11.16	0
-630	11.0592	0.002713	-630	11.2	8.88E-15	-630	11.15	8.88E-15	-630	11.16	0
-620	11.06	3.55E-15	-620	11.2	8.88E-15	-620	11.15	8.88E-15	-620	11.16	0
-610	11.06	3.55E-15	-610	11.2	8.88E-15	-610	11.15	8.88E-15	-610	11.16	0
-600	11.06	3.55E-15	-600	11.2	8.88E-15	-600	11.15	8.88E-15	-600	11.16	0
-590	11.06	3.55E-15	-590	11.199	8.88E-15	-590	11.15	8.88E-15	-590	11.16	0
-580	11.06	3.55E-15	-580	11.2014	8.88E-15	-580	11.15	8.88E-15	-580	11.16	0
-570	11.06	3.55E-15	-570	11.1976	8.88E-15	-570	11.15	8.88E-15	-570	11.16	0
-560	11.06	3.55E-15	-560	11.199	8.88E-15	-560	11.15	8.88E-15	-560	11.16	0
-550	11.06	3.55E-15	-550	11.2	8.88E-15	-550	11.15	8.88E-15	-550	11.164	0.004899
-540	11.0572	0.00449	-540	11.2	8.88E-15	-540	11.15	8.88E-15	-540	11.164	0.004899
-530	11.0558	0.004936	-530	11.1972	0.003	-530	11.149	0.003	-530	11.1634	0.004737
-520	11.0524	0.004271	-520	11.197	8.88E-15	-520	11.15	8.88E-15	-520	11.16	0
-510	11.059	0.003	-510	11.196	0.002375	-510	11.1494	0.002375	-510	11.1594	0.002375
-500	11.0594	0.002375	-500	11.2	8.88E-15	-500	11.15	8.88E-15	-500	11.1554	0.004984

-490	11.06	3.55E-15	-490	11.2	8.88E-15	-490	11.15	8.88E-15	-490	11.16	0
-480	11.0596	0.00196	-480	11.198	8.88E-15	-480	11.15	8.88E-15	-480	11.16	0
-470	11.057	0.004583	-470	11.1992	8.88E-15	-470	11.15	8.88E-15	-470	11.16	0
-460	11.0584	0.003666	-460	11.2	8.88E-15	-460	11.15	8.88E-15	-460	11.16	0
-450	11.06	3.55E-15	-450	11.1922	8.88E-15	-450	11.15	8.88E-15	-450	11.16	0
-440	11.059	0.003	-440	11.197	8.88E-15	-440	11.15	8.88E-15	-440	11.16	0
-430	11.058	0.004	-430	11.1932	8.88E-15	-430	11.15	8.88E-15	-430	11.16	0
-420	11.0518	0.003842	-420	11.199	8.88E-15	-420	11.15	8.88E-15	-420	11.16	0
-410	11.06	3.55E-15	-410	11.1978	0.003	-410	11.149	0.003	-410	11.16	0
-400	11.0578	0.004142	-400	11.19	0.003842	-400	11.1482	0.003842	-400	11.16	0
-390	11.058	0.004	-390	11.19	8.88E-15	-390	11.15	8.88E-15	-390	11.16	0
-380	11.06	3.55E-15	-380	11.19	8.88E-15	-380	11.15	8.88E-15	-380	11.16	0
-370	11.06	3.55E-15	-370	11.1922	8.88E-15	-370	11.15	8.88E-15	-370	11.16	0
-360	11.06	3.55E-15	-360	11.1988	8.88E-15	-360	11.15	8.88E-15	-360	11.16	0
-350	11.06	3.55E-15	-350	11.2	8.88E-15	-350	11.15	8.88E-15	-350	11.16	0
-340	11.06	3.55E-15	-340	11.197	8.88E-15	-340	11.15	8.88E-15	-340	11.16	0
-330	11.058	0.004	-330	11.1964	8.88E-15	-330	11.15	8.88E-15	-330	11.16	0
-320	11.0564	0.0048	-320	11.2	8.88E-15	-320	11.15	8.88E-15	-320	11.16	0

-310	11.06	3.55E-15	-310	11.1988	8.88E-15	-310	11.15	8.88E-15	-310	11.1618	0.003842
-300	11.0548	0.004996	-300	11.2	8.88E-15	-300	11.15	8.88E-15	-300	11.1678	0.004142
-290	11.06	3.55E-15	-290	11.2	8.88E-15	-290	11.15	8.88E-15	-290	11.164	0.004899
-280	11.06	3.55E-15	-280	11.2	0.008718	-280	11.152	0.008718	-280	11.1658	0.004936
-270	11.06	3.55E-15	-270	11.1994	8.88E-15	-270	11.15	8.88E-15	-270	11.1682	0.003842
-260	11.06	3.55E-15	-260	11.1992	8.88E-15	-260	11.15	8.88E-15	-260	11.1618	0.003842
-250	11.0578	0.004142	-250	11.1954	0.004737	-250	11.14957	0.004737	-250	11.17	0
-240	11.06	3.55E-15	-240	11.2	0.003	-240	11.151	0.003	-240	11.169	0.003
-230	11.0558	0.004936	-230	11.1972	0.00196	-230	11.1504	0.00196	-230	11.1684	0.003666
-220	11.06	3.55E-15	-220	11.1982	0.003	-220	11.151	0.003	-220	11.1642	0.004936
-210	11.057	0.004583	-210	11.1958	0.004984	-210	11.15054	0.004984	-210	11.17	0
-200	11.06	3.55E-15	-200	11.2	0.00325	-200	11.1512	0.00325	-200	11.17	0
-190	11.06	3.55E-15	-190	11.2	0.004936	-190	11.15158	0.004936	-190	11.17	0
-180	11.06	3.55E-15	-180	11.2	0.004	-180	11.152	0.004	-180	11.17	0
-170	11.06	3.55E-15	-170	11.2	0.004936	-170	11.15158	0.004936	-170	11.17	0
-160	11.0592	0.002713	-160	11.2	0.003	-160	11.1509	0.003	-160	11.17	0
-150	11.0568	0.004665	-150	11.2	0.004737	-150	11.15134	0.004737	-150	11.168	0.006
-140	11.0528	0.00449	-140	11.2	0.003842	-140	11.1518	0.003842	-140	11.17	0

-130	11.06	3.55E-15	-130	11.2	0.002713	-130	11.15092	0.002713	-130	11.17	0
-120	11.06	3.55E-15	-120	11.2	0.004899	-120	11.1516	0.004899	-120	11.17	0
-110	11.0546	0.004984	-110	11.2	0.003	-110	11.1509	0.003	-110	11.172	0.004
-100	11.0582	0.003842	-100	11.2	0.003666	-100	11.1516	0.003666	-100	11.17	0
-90	11.0556	0.004964	-90	11.201	0.004737	-90	11.15134	0.004737	-90	11.172	0.004
-80	11.053	0.004583	-80	11.2	0.0048	-80	11.15136	0.0048	-80	11.1752	0.004996
-70	11.0562	0.004854	-70	11.201	0.004	-70	11.152	0.004	-70	11.18	5.33E-15
-60	11.0528	0.00449	-60	11.2038	0.004665	-60	11.15168	0.004665	-60	11.1786	0.00347
-50	11.05	3.55E-15	-50	11.205	0.004	-50	11.1518	0.004	-50	11.1762	0.004854
-40	11.0588	0.00325	-40	11.1996	7.11E-15	-40	11.151	7.11E-15	-40	11.179	0.003
-30	11.057	0.004583	-30	11.20218	7.11E-15	-30	11.151	7.11E-15	-30	11.18	5.33E-15
-20	11.05	3.55E-15	-20	11.20237	0.003	-20	11.1509	0.003	-20	11.18071	0.039322
-10	11.0582	0.003842	-10	11.20256	0.003	-10	11.1509	0.003	-10	11.18165	0.007181
0	11.0588	0.00325	0	11.203	3.55E-15	0	11.15098	3.55E-15	0	11.18333	0.0048
10	11.0578	0.004142	10	11.20323	0.004984	10	11.15092	0.004984	10	11.18442	0.004386
20	11.0512	0.00325	20	10.5246	0.004854	20	10.96	0.004854	20	10.5376	0.009724
30	11.0548	0.004996	30	10.29874	1.24E-14	30	10.8454	1.24E-14	30	10.2462	0.004899
40	11.0546	0.004984	40	9.959853	0.00347	40	10.7338	0.00347	40	10.3764	0.004854

50	11.05	3.55E-15	50	9.8164	5.33E-15	50	10.72	5.33E-15	50	10.4074	7.11E-15
60	11.0562	0.004854	60	9.7512	0.004	60	10.7186	0.004	60	10.4912	0.004964
70	11.0572	0.00449	70	9.6972	3.55E-15	70	10.71	3.55E-15	70	10.436	5.33E-15
80	11.0592	0.002713	80	9.8124	0.004996	80	10.708	0.004996	80	10.4362	0.004996
90	11.057	0.004583	90	9.9732	0.004737	90	10.7	0.004737	90	10.48	0.00449
100	11.0578	0.004142	100	10.0474	3.55E-15	100	10.6952	3.55E-15	100	10.4756	0.004
110	11.06	3.55E-15	110	10.1366	3.55E-15	110	10.6966	3.55E-15	110	10.45	0.003842
120	11.06	3.55E-15	120	9.7504	0.005016	120	10.69	0.005016	120	10.4448	7.11E-15
130	11.06	3.55E-15	130	9.9772	0.005657	130	10.69	0.005657	130	10.4572	0.004665
140	11.06	3.55E-15	140	10.137	0.0044	140	10.4078	0.0044	140	10.462	0.002713
150	11.06	3.55E-15	150	9.813	1.24E-14	150	10.45	1.24E-14	150	10.4682	5.33E-15
160	11.06	3.55E-15	160	9.983	0.00325	160	10.4908	0.00325	160	10.46	0.005276
170	11.06	3.55E-15	170	10.0868	8.88E-15	170	10.53	8.88E-15	170	10.4532	7.11E-15
180	11.06	3.55E-15	180	10.1486	0.0048	180	10.5888	0.0048	180	10.4408	7.11E-15
190	11.06	3.55E-15	190	10.3586	0.006096	190	10.6	0.006096	190	10.45	7.11E-15
200	11.06	3.55E-15	200	9.8548	0.003842	200	10.6036	0.003842	200	10.4596	0.00196
210	11.059	0.003	210	9.9398	0.003	210	10.3022	0.003	210	10.46	1.24E-14
220	11.0548	0.004996	220	10.0968	0.004899	220	10.3682	0.004899	220	10.46	0.003842

230	11.06	3.55E-15	230	10.1984	0.004899	230	10.419	0.004899	230	10.46	0.012073
240	11.06	3.55E-15	240	10.5436	7.11E-15	240	10.466	7.11E-15	240	10.4604	7.11E-15
250	11.06	3.55E-15	250	10.6952	0	250	10.514	0	250	10.47	0.002713
260	11.06	3.55E-15	260	10.7178	0.005142	260	10.54	0.005142	260	10.4682	0.003
270	11.06	3.55E-15	270	10.7678	0.0048	270	10.31	0.0048	270	10.4632	0.004271
280	11.06	3.55E-15	280	10.7956	7.11E-15	280	10.3566	7.11E-15	280	10.46	8.88E-15
290	11.0566	0.004737	290	10.8052	0.00347	290	10.4264	0.00347	290	10.4608	8.88E-15
300	11.0588	0.00325	300	10.8298	0.00347	300	10.46	0.00347	300	10.329	0.003
310	11.06	3.55E-15	310	10.869	0.00325	310	10.2614	0.00325	310	10.3724	0.003
320	11.0592	0.002713	320	9.8196	0.0048	320	10.3114	0.0048	320	10.39	0.003
330	11.0548	0.004996	330	10.154	8.88E-15	330	10.3312	8.88E-15	330	10.4	0.004386
340	11.06	3.55E-15	340	10.394	0.004854	340	10.3636	0.004854	340	10.411	8.88E-15
350	11.0596	0.00196	350	10.4676	0.002375	350	10.35	0.002375	350	10.339	0.003842
360	11.056	0.004899	360	10.6294	1.07E-14	360	10.3738	1.07E-14	360	10.361	5.33E-15
370	11.06	3.55E-15	370	10.6474	0.003842	370	10.3906	0.003842	370	10.3874	5.33E-15
380	11.06	3.55E-15	380	10.674	8.88E-15	380	10.41	8.88E-15	380	10.4	0.0014
390	11.059	0.003	390	10.7198	3.55E-15	390	10.3382	3.55E-15	390	10.4118	0.003
400	11.06	3.55E-15	400	10.735	0.003	400	10.36	0.003	400	10.42	0.004964

410	11.05 82	0.0038 42	410	10.74	8.88E- 15	410	10.37	8.88E- 15	410	10.43	0.0041 42
420	11.05 7	0.0045 83	420	10.743	8.88E- 15	420	10.381	8.88E- 15	420	10.439 8	0
430	11.05 64	0.0048	430	10.774	0.0048 99	430	10.39	0.0048 99	430	10.349	5.33E- 15
440	11.05 28	0.0044 9	440	10.779	0.0027 13	440	10.4	0.0027 13	440	10.395 6	0.007
450	11.05 68	0.0046 65	450	10.78	0.0049 84	450	10.404	0.0049 84	450	10.422 2	0.0032 5
460	11.05 92	0.0027 13	460	10.790 2	0.003	460	10.419 2	0.003	460	10.44	5.33E- 15
470	11.05 78	0.0041 42	470	10.79	0.0038 42	470	10.474 6	0.0038 42	470	10.45	0.0048 54
480	11.05 5	0.005	480	10.79	8.88E- 15	480	10.339	8.88E- 15	480	10.359	0.0069 17
490	11.05 58	0.0049 36	490	10.796 8	8.88E- 15	490	10.368 2	8.88E- 15	490	10.408 8	5.33E- 15
500	11.05 8	0.004	500	10.802 2	0.0049 84	500	10.35	0.0049 84	500	10.43	0.0045 83

**Table S8.2. Micro-electrode hydrogen profiles of methanogenic and sulphate reducing biofilms**

Sulphate-reducing		Methanogenic 1		Methanogenic 2	
Depth	H2	Depth	H2	Depth	H2
-500	0	-500	0	-500	0
-490	0	-490	0	-490	0
-480	0	-480	0	-480	0
-470	0	-470	0	-470	0
-460	0	-460	0	-460	0
-450	0	-450	0	-450	0
-440	0	-440	0	-440	0
-430	0	-430	0	-430	0
-420	0	-420	0	-420	0
-410	0	-410	0	-410	0
-400	0	-400	0	-400	0
-390	0	-390	0	-390	0

-380	0	-380	0	-380	0
-370	0	-370	0	-370	0
-360	0	-360	0	-360	0
-350	0	-350	0	-350	0
-340	0	-340	0	-340	0
-330	0	-330	0	-330	0
-320	0	-320	0	-320	0
-310	0	-310	0	-310	0
-300	0	-300	0	-300	0
-290	0	-290	0	-290	0
-280	0	-280	0	-280	0
-270	0	-270	0	-270	0
-260	0	-260	0	-260	0
-250	0	-250	0	-250	0
-240	0	-240	0	-240	0
-230	0	-230	0	-230	0
-220	0	-220	0	-220	0
-210	0	-210	0	-210	0
-200	0	-200	0	-200	0
-190	0	-190	0	-190	0
-180	0	-180	0	-180	0
-170	0	-170	0	-170	0
-160	0	-160	0	-160	0
-150	0	-150	0	-150	0
-140	0	-140	0	-140	0
-130	0	-130	0	-130	0
-120	0	-120	0	-120	0
-110	0	-110	0	-110	0
-100	0	-100	0	-100	0
-90	0	-90	0	-90	0
-80	0	-80	0	-80	0
-70	0	-70	0	-70	0
-60	0	-60	0	-60	0
-50	0	-50	0	-50	0
-40	0	-40	0	-40	0
-30	0	-30	0	-30	0
-20	0	-20	0	-20	0
-10	0	-10	0	-10	0
0	0	0	0	0	0
10	0	10	0	10	0
20	0	20	0	20	0
30	0	30	0	30	0

40	0	40	0	40	0
50	0	50	0.7868	50	0
60	0	60	2.0042	60	0
70	0	70	2.9876	70	0
80	7.6814	80	4.1244	80	0
90	7.736	90	5.6064	90	0
100	3.4396	100	5.3592	100	0
110	15.748	110	5.4362	110	0
120	15.8672	120	5.0754	120	0
130	14.9168	130	4.9444	130	0
140	14.4578	140	4.1642	140	0
150	20.8912	150	3.9894	150	0
160	20.992	160	3.683	160	0
170	20.8548	170	1.0202	170	0
180	21.741	180	0.1082	180	0
190	25.9114	190	0.0858	190	0
200	29.9834	200	0.2154	200	0
210	33.7264	210	0.2714	210	0
220	29.5994	220	0	220	0
230	32.5606	230	0	230	0
240	37.2584	240	0	240	0
250	38.3178	250	0	250	0
260	43.0898	260	0	260	0
270	42.8102	270	0	270	0
280	48.5446	280	0	280	0
290	50.9812	290	0	290	0
300	56.932	300	0	300	0
310	46.6878	310	0	310	0
320	44.7664	320	0	320	0
330	55.4828	330	0	330	0
340	43.4936	340	0	340	0
350	53.015	350	0	350	0
360	68.0732	360	0	360	0
370	69.4234	370	0	370	0
380	69.7724	380	0	380	5.9148
390	69.8428	390	0	390	6.7474
400	69.1862	400	0	400	7.3484
410	69.2014	410	0	410	8.6388
420	71.7788	420	0	420	12.3122
430	70.4318	430	0	430	21.0736
440	68.9336	440	0	440	16.0024
450	70.2326	450	0	450	13.4896

460	69.1842	460	0	460	20.0468
470	68.7222	470	0	470	0
480	68.2934	480	0	480	0
490	69.996	490	0	490	0
500	68.8428	500	0	500	0

**Table S8.3. Micro-electrode redox profiles of sulphate reducing and methanogenic biofilms together with abiotic controls.**

Abiotic		Sulphate-reducing		Methanogenic	
Depth	Redox	Depth	Redox	Depth	Redox
-500	-358.945	-500	-376.561	-500	-379.929
-490	-358.127	-490	-376.602	-490	-379.859
-480	-357.991	-480	-376.694	-480	-379.85
-470	-358.111	-470	-376.709	-470	-379.836
-460	-358.022	-460	-376.706	-460	-379.77
-450	-357.593	-450	-376.723	-450	-379.721
-440	-357.421	-440	-376.812	-440	-379.626
-430	-357.081	-430	-376.882	-430	-379.612
-420	-357.282	-420	-376.901	-420	-379.56
-410	-357.446	-410	-376.962	-410	-379.585
-400	-357.452	-400	-376.991	-400	-379.598
-390	-357.915	-390	-377.062	-390	-379.518
-380	-358.278	-380	-377.138	-380	-379.475
-370	-358.487	-370	-377.2	-370	-379.387
-360	-358.308	-360	-377.247	-360	-379.166
-350	-358.503	-350	-377.301	-350	-378.958
-340	-358.669	-340	-377.295	-340	-378.707
-330	-358.686	-330	-377.339	-330	-378.576
-320	-358.636	-320	-377.365	-320	-378.505
-310	-359.147	-310	-377.365	-310	-378.429
-300	-359.501	-300	-377.412	-300	-378.336
-290	-359.905	-290	-377.451	-290	-378.288
-280	-360.517	-280	-377.503	-280	-378.219
-270	-360.829	-270	-377.579	-270	-378.079
-260	-361.167	-260	-377.603	-260	-377.989
-250	-361.741	-250	-377.692	-250	-377.969
-240	-361.722	-240	-377.702	-240	-377.941
-230	-361.707	-230	-377.757	-230	-377.957
-220	-361.713	-220	-377.809	-220	-378.008
-210	-361.697	-210	-377.859	-210	-378.081
-200	-361.775	-200	-377.903	-200	-378.054

-190	-361.935	-190	-377.955	-190	-378.026
-180	-361.766	-180	-377.985	-180	-378.031
-170	-361.809	-170	-378.007	-170	-377.973
-160	-362.082	-160	-378.074	-160	-377.929
-150	-362.196	-150	-378.131	-150	-377.909
-140	-362.163	-140	-378.147	-140	-377.766
-130	-362.124	-130	-378.181	-130	-377.593
-120	-361.998	-120	-378.258	-120	-377.329
-110	-361.979	-110	-378.336	-110	-377.076
-100	-361.728	-100	-378.458	-100	-376.799
-90	-361.436	-90	-378.539	-90	-376.564
-80	-361.27	-80	-378.682	-80	-376.349
-70	-361.056	-70	-378.706	-70	-376.211
-60	-360.805	-60	-378.768	-60	-376.125
-50	-360.122	-50	-378.84	-50	-376.011
-40	-360.102	-40	-378.881	-40	-375.959
-30	-359.543	-30	-378.876	-30	-375.93
-20	-358.775	-20	-378.948	-20	-375.945
-10	-358.042	-10	-378.943	-10	-375.984
0	-356.786	0	-379.007	0	-376.078
10	-355.457	10	-379.002	10	-376.202
20	-354.132	20	-379.08	20	-376.365
30	-353.237	30	-379.043	30	-376.502
40	-352.761	40	-379.063	40	-376.605
50	-352.62	50	-379.074	50	-376.722
60	-352.874	60	-379.122	60	-376.915
70	-353.44	70	-379.061	70	-377.161
80	-354.27	80	-379.055	80	-377.397
90	-355.042	90	-379.035	90	-377.59
100	-355.531	100	-378.987	100	-377.785
110	-355.622	110	-378.959	110	-377.824
120	-355.775	120	-378.973	120	-377.834
130	-355.743	130	-379.005	130	-377.697
140	-355.539	140	-378.96	140	-377.403
150	-355.164	150	-378.948	150	-377.12
160	-354.582	160	-378.975	160	-376.739
170	-353.898	170	-378.921	170	-376.583
180	-353.373	180	-378.92	180	-376.487
190	-353.089	190	-378.926	190	-376.485
200	-353.029	200	-378.934	200	-376.506
210	-352.878	210	-378.94	210	-376.606
220	-353.12	220	-378.892	220	-376.634

230	-353.389	230	-378.905	230	-376.625
240	-353.581	240	-378.885	240	-376.565
250	-353.757	250	-378.855	250	-376.444
260	-354.217	260	-378.822	260	-376.364
270	-354.33	270	-378.787	270	-376.454
280	-355.24	280	-378.799	280	-376.545
290	-356.063	290	-378.785	290	-376.659
300	-356.549	300	-378.77	300	-376.754
310	-356.864	310	-378.86	310	-376.879
320	-356.938	320	-378.883	320	-376.958
330	-356.641	330	-378.804	330	-376.935
340	-356.892	340	-378.787	340	-376.906
350	-356.623	350	-378.759	350	-376.947
360	-356.26	360	-378.743	360	-376.879
370	-355.929	370	-378.713	370	-376.867
380	-355.464	380	-378.768	380	-376.924
390	-355.656	390	-378.81	390	-376.961
400	-354.839	400	-378.792	400	-376.965
410	-354.377	410	-378.749	410	-376.962
420	-353.932	420	-378.758	420	-377.032
430	-354.466	430	-378.772	430	-377.088
440	-353.803	440	-378.677	440	-377.158
450	-353.521	450	-378.699	450	-377.266
460	-353.621	460	-378.682	460	-377.384
470	-354.029	470	-378.687	470	-377.479
480	-354.558	480	-378.659	480	-377.573
490	-353.158	490	-378.634	490	-377.782
500	-352.72	500	-378.656	500	-377.965